SHORT PAPERS IN—

Analytical methods
Floods
Geochemistry
Geomorphology
Geophysics
Glacial Geology
Ground water
Hydrologic instrumentation
Isotope studies
Mineralogy
Petrology
Paleontology
Rock mechanics
Storage and retrieval of geologic data
Stratigraphy
Structural geology
Surface water
Topographic studies

GEOLOGICAL SURVEY RESEARCH 1969

Chapter C

GEOLOGICAL SURVEY PROFESSIONAL PAPER 650–C

GEOLOGICAL SURVEY RESEARCH 1969

Chapter C

GEOLOGICAL SURVEY PROFESSIONAL PAPER 650–C

Scientific notes and summaries of investigations in geology, hydrology, and related fields

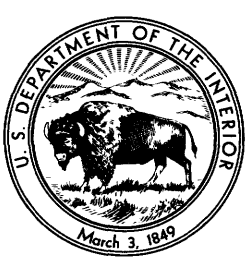

UNITED STATES GOVERNMENT PRINTING OFFICE, WASHINGTON: 1969

UNITED STATES DEPARTMENT OF THE INTERIOR

WALTER J. HICKEL, Secretary

GEOLOGICAL SURVEY

William T. Pecora, Director

For sale by the Superintendent of Documents, U.S. Government Printing Office
Washington, D.C. 20402 – Price $3.00

CONTENTS

GEOLOGIC STUDIES

HYDROLOGIC STUDIES

GEOLOGICAL SURVEY RESEARCH 1969

This collection of 38 short papers is the second published chapter of "Geological Survey Research 1969." The papers report on scientific and economic results of current work by members of the Geologic, Topographic, and Water Resources Divisions of the U.S. Geological Survey.

Chapter A, to be published later in the year, will present a summary of significant results of work done during fiscal year 1969, together with lists of investigations in progress, reports published, cooperating agencies, and Geological Survey offices.

"Geological Survey Research 1969" is the tenth volume of the annual series Geological Survey Research. The nine volumes already published are listed below, with their series designations.

Geological Survey Research 1960—Prof. Paper 400
Geological Survey Research 1961—Prof. Paper 424
Geological Survey Research 1962—Prof. Paper 450
Geological Survey Research 1963—Prof. Paper 475
Geological Survey Research 1964—Prof. Paper 501
Geological Survey Research 1965—Prof. Paper 525
Geological Survey Research 1966—Prof. Paper 550
Geological Survey Research 1967—Prof. Paper 575
Geological Survey Research 1968—Prof. Paper 600

METAMORPHIC CHANGES ACROSS PART OF THE CAROLINA SLATE BELT–CHARLOTTE BELT BOUNDARY, NORTH CAROLINA AND VIRGINIA

By OTHMAR T. TOBISCH [1] and LYNN GLOVER III,
Santa Cruz, Calif., Beltsville, Md.

Work done in part in cooperation with the North Carolina Department of Conservation and Development, Division of Mineral Resources

Abstract.—Five distinct metamorphic zones are developed along the boundary between the Carolina slate belt and Charlotte belt in parts of North Carolina and Virginia. Each zone is defined by index minerals and characteristic mineral assemblages in rocks of at least three different bulk chemical compositions. The metamorphic zones form a progressive sequence across the boundary between the two belts and are correlated with regional metamorphic facies ranging from greenschist to upper amphibolite. Investigation of anorthite content of plagioclase by X-ray diffraction has shown that the plagioclase in the lower grade zones is probably a peristerite, which is absent from the higher grade zones where plagioclase is more calcic than An_{20}. On the basis of field and laboratory evidence, it is concluded that a metamorphic gradient is one of several factors that define the boundary between the two geological belts in this part of the southern Appalachians.

The southern Piedmont geologic province has been divided into several narrow lithologic belts, which roughly parallel the general northeast trend of the Piedmont province (King, 1955). These belts from northwest to southeast are the Brevard zone, the Inner Piedmont, Kings Mountain, and Charlotte belts, and the Carolina slate belt (fig. 1).

The area of this study is on the North Carolina-Virginia State line (fig. 1), and covers approximately 35 square miles in a narrow strip across the boundary between the Carolina slate belt and Charlotte belt. The eastern half of the area was mapped in detail by Laney (1917), who established that the slate-belt rocks are of lower metamorphic grade than the rocks of the Charlotte belt, and who interpreted this break as an unconformity, with younger slate-belt rocks overlying older Charlotte belt rocks. Most workers recognize the metamorphic difference between to two belts, but the nature of the change across the two belts has never been examined in detail. The work discussed in this report, part of a larger investigation, was undertaken to determine if the metamorphic change noted by Laney (1917) was sharp (for example, fault controlled) or gradational. We have concluded that it is gradational.

Acknowledgments.—We wish to thank B. A. Morgan III, D. W. Rankin, George W. Fisher, and J. C. Reed, Jr., for helpful criticism and valuable assistance during the investigation. Most of the petrographic work was done by Tobisch, and most of the X-ray work was done by Glover.

GEOLOGIC SETTING

The term "Carolina slate belt" has been entrenched in the geologic literature for many decades, even though it was realized more than half a century ago that much of the rock in the belt was not slate (Overstreet and Bell, 1965, p. 18–19). In general, the belt consists of a thick sequence of volcaniclastic and nonvolcanic(?) epiclastic rocks that have been metamorphosed to greenschist facies.

The Charlotte belt, in the type area of Charlotte, N.C., consists largely of metamorphosed but weakly foliated granodiorite and dioritic plutons (King, 1955). In the area under consideration (fig. 1), however, it consists of highly deformed, interlayered felsic and mafic gneiss and minor amounts of pelitic schist that range in metamorphic grade from low to high amphibolite facies. At least part of the felsic and mafic gneisses, which make up the bulk of the Charlotte belt in this area, are orthogneiss. Some gneisses are probably meta-

[1] Department of Geology, University of California, Santa Cruz, Calif. 95060

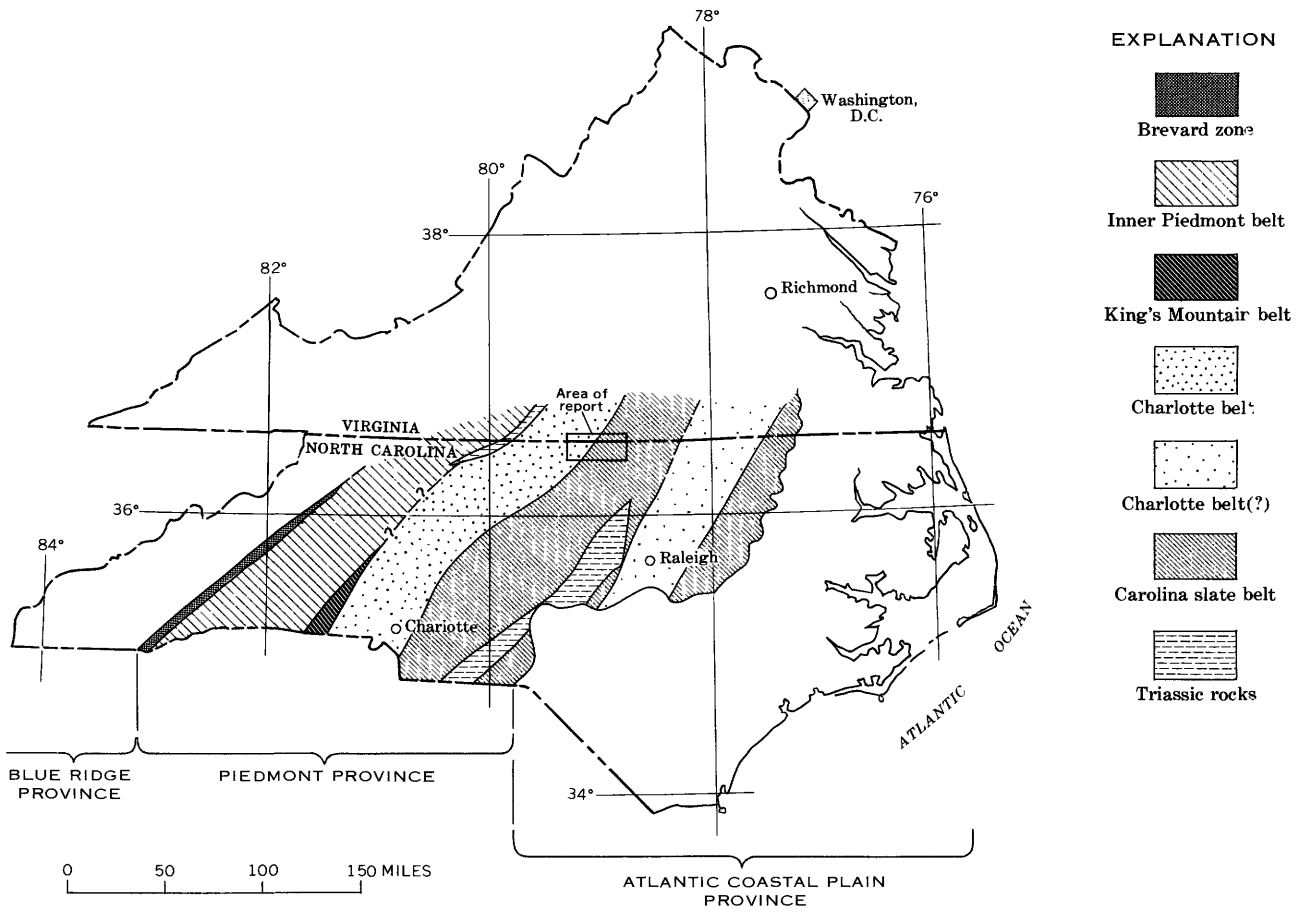

FIGURE 1.—Map showing locality of this study and the general distribution of geologic provinces and geologic belts within parts of North Carolina and Virginia.

volcaniclastic(?) and (or) metaepiclastic layered rocks. The relatively high metamorphic grade and intense deformation of the rocks in this area, coupled with poor exposure, has rendered the distinction between orthogneiss and paragneiss exceedingly difficult.

OUTLINE OF STRUCTURE AND STRATIGRAPHIC SUCCESSION

In the area studied, the only large-scale structure known at present is the Virgilina synclinorium (Laney, 1917), whose axial trace lies just outside the eastern edge of the area covered by figure 2. Minor structural elements in the Carolina slate belt are bedding, early (slaty) cleavage, later (strain-slip) cleavage, intersection of the above planar surfaces, and elongated lapilli and chlorite blebs. Bedding and early (slaty) cleavage are usually parallel or subparallel in the Carolina slate belt of figure 2. Minor structural elements in the Charlotte belt are compositional layering, schistosity, intersection of layering and schistosity, and mineral alinement. Later (strain-slip) cleavage is virtually parallel to early cleavage, and the later cleavage surface is not well developed within the Charlotte belt of figure 2. Small folds are found locally in both belts. These minor structures, while essential in understanding the structural history of the rocks, do not affect the geometry of the gross stratigraphic succession. For the purposes of this discussion, therefore, map units A–E shown in figure 2 may be considered a layered sequence, dipping to the southeast.

METAMORPHIC ZONES

Paralleling the general trend of the stratigraphy or compositional layering in the Charlotte belt and Carolina slate belt is a sequence of five metamorphic zones that are defined by characteristic mineral assemblages and the successive appearance of different index minerals. The southeasternmost appearance of each index mineral is shown on figure 2 by an isograd, most of which separate zones of different metamorphic grade. However, the kyanite-chloritoid "isograd," which lies within the garnet zone, probably represents a compositional boundary, rather than a change in metamorphic grade (Turner and Verhoogen, 1960, p. 539); similarly, the first appearance of hornblende occurs within the garnet zone, and is probably compositionally

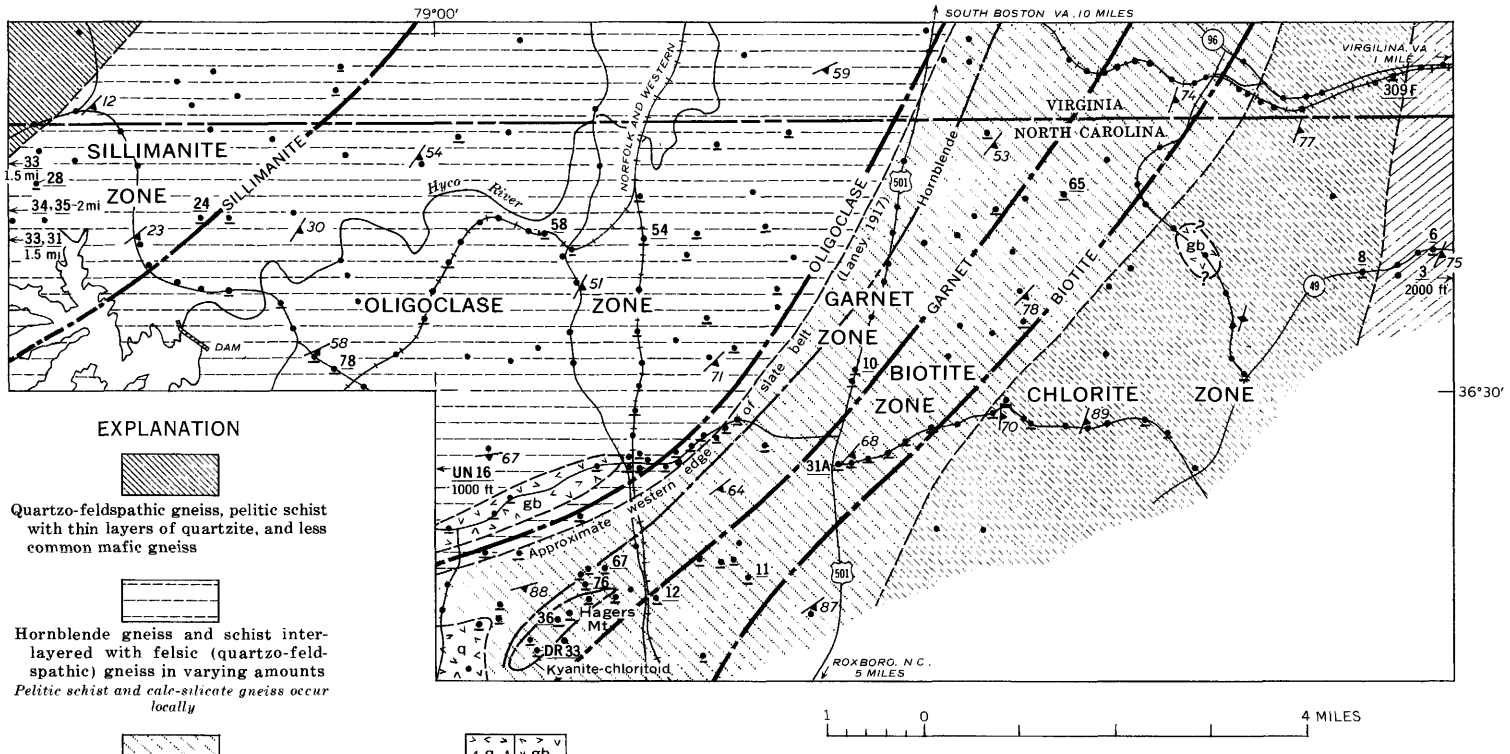

EXPLANATION

Quartzo-feldspathic gneiss, pelitic schist with thin layers of quartzite, and less common mafic gneiss

Hornblende gneiss and schist interlayered with felsic (quartzo-feldspathic) gneiss in varying amounts

Pelitic schist and calc-silicate gneiss occur locally

In large part Hyco Quartz Porphyry of Laney (1917)

Chiefly metamorphosed felsic pyroclastic rocks ranging from tuff to lapilli tuff. Metamorphosed mudstone and intermediate and mafic volcaniclastic rocks are common in southeastern outcrops of this unit

Aaron Slate of Laney (1917)

Metamorphosed mudstone, argillite and some medium to fine-grained feldspathic sandstone (reworked tuff?) with intercalations of mafic, intermediate and felsic volcaniclastic rocks. Quartzite pebble conglomerate near base of unit

Virgilina greenstone of Laney (1917)

Chiefly metamorphosed mafic, pyroxene-crystal-rich volcaniclastic rocks. Coarse tuffs, lapilli tuffs, and tuff-breccia are common

Foliated to unfoliated intrusive rocks

q, *quartz-diorite to quartz-monzonite;* gb, *gabbro*

Isograd showing new mineral appearance

Heavy where zone boundary

Contact

Specimen locality

Thin-section locality

67

Sample locality for partial mineral composition

67

Strike and dip of bedding or foliation (slate belt) or compositional layering (Charlotte belt)

FIGURE 2.—Simplified geologic map of an area along the North Carolina-Virginia border, showing distribution of mineral zones and other data.

controlled, in part. The heavy isograds on figure 2 form the boundaries of the metamorphic zones. The distribution of index and other important minerals within the metamorphic zones are shown in figure 3.

Rocks of at least three different general bulk chemical compositions are represented in each of the zones. Typical mineral assemblages from these zones are listed in table 1 along with the corresponding index mineral (metamorphic zone name), and we have correlated the zones with metamorphic facies (Turner and Verhoogen, 1960; Fyfe and Turner, 1966). Recently, Lambert (1965) has criticized the applicability of some aspects of the

TABLE 1.—*Typical mineral assemblages of selected rock types from part of the Carolina slate belt–Charlotte belt boundary area, North Carolina and Virginia*

Metamorphic facies (Turner and Verhoogen, 1960; Fyfe and Turner, 1966)	Index mineral and zone	Rock type and mineral assemblages [1]
Greenschist facies	Chlorite zone	Pelitic: Muscovite-chlorite-quartz-(epidote). Muscovite-chlorite-epidote-quartz-albite-(magnetite). Quartzo-feldspathic: Quartz-albite-muscovite-chlorite-epidote-(magnetite). Mafic: Chlorite-muscovite-epidote-quartz-albite-(magnetite). Muscovite-stilpnomelane-quartz-albite-(magnetite-hematite).[2] Tremolite/actinolite-epidote-(chlorite-quartz-magnetite).
	Biotite zone	Pelitic: Biotite-chlorite-muscovite-quartz-albite-(epidote-magnetite). Quartzo-feldspathic: Quartz-albite-biotite-chlorite-(epidote). Quartz-albite-(K feldspar-biotite-muscovite-epidote). Quartz-albite-muscovite-(epidote-tourmaline-magnetite). Mafic: Epidote-chlorite-muscovite-quartz-albite-(sphene-magnetite). Chlorite-epidote-albite-(biotite-tremolite/actinolite/sphene-magnetite).
Greenschist-amphibolite transition facies	Garnet zone	Pelitic: [3] Kyanite-chloritoid-muscovite-paragonite-quartz. Chloritoid-muscovite-quartz-magnetite-(hematite-pyrite). Kyanite-quartz-oligoclase(An_{15})-muscovite-paragonite-(chloritoid-magnetite). Quartzo-feldspathic: Quartz-albite-K feldspar-biotite-muscovite-(epidote-garnet-magnetite). Quartz-albite-muscovite-biotite-(epidote-garnet-magnetite-hematite). Mafic: Hornblende-chlorite-epidote-(biotite-sphene-quartz-magnetite-pyrite). Chlorite-epidote-albite-(quartz-biotite-muscovite-magnetite).
Amphibolite facies, Lower	Oligoclase zone	Pelitic: Biotite-muscovite-oligoclase/andesine-quartz-(epidote-garnet-magnetite-pyrite). Quartzo-feldspathic: Quartz-andesine-biotite-(muscovite-epidote-magnetite). Quartz-oligoclase-K feldspar-muscovite-(biotite-epidote-sphene). Quartz-oligoclase-K feldspar-hornblende-biotite-(epidote-magnetite-pyrite). Mafic: Hornblende-labradorite-epidote-chlorite-(magnetite-pyrite). Hornblende-andesine-quartz-epidote-(sphene-magnetite). Hornblende-andesine-biotite-(epidote-chlorite-quartz-magnetite). Calcareous: Epidote-quartz-andesine-(magnetite). Tremolite-zoisite-quartz-sphene-(magnetite).
Amphibolite facies, Upper	Sillimanite zone	Pelitic: Muscovite-biotite-quartz-sillimanite. Biotite-andesine-quartz-K feldspar-(sillimanite-garnet-muscovite-pyrite). Quartzo-feldspathic: Quartz-(sillimanite-muscovite-biotite-hematite). Quartz-sillimanite-(muscovite-magnetite). Quartz-oligoclase-K feldspar-biotite-(muscovite-epidote-magnetite-pyrite). Quartz-andesine-biotite-(epidote-sphene-magnetite-pyrite). Mafic: Clinopyroxene-hornblende-labradorite/bytownite-quartz-(magnetite). Clinopyroxene-hornblende-andesine-quartz-(epidote-sphene-scapolite-magnetite). Calcareous: Clinopyroxene-scapolite-tremolite-(quartz-zoisite-calcite-sphene-pyrite).

[1] Accessory minerals are in parentheses.
[2] Biotite, as distinct from stilpnomelane, has been noted in two specimens from within the chlorite zone.
[3] Kyanite and chloritoid are restricted to the immediate vicinity of Hagers Mountain (fig. 2).

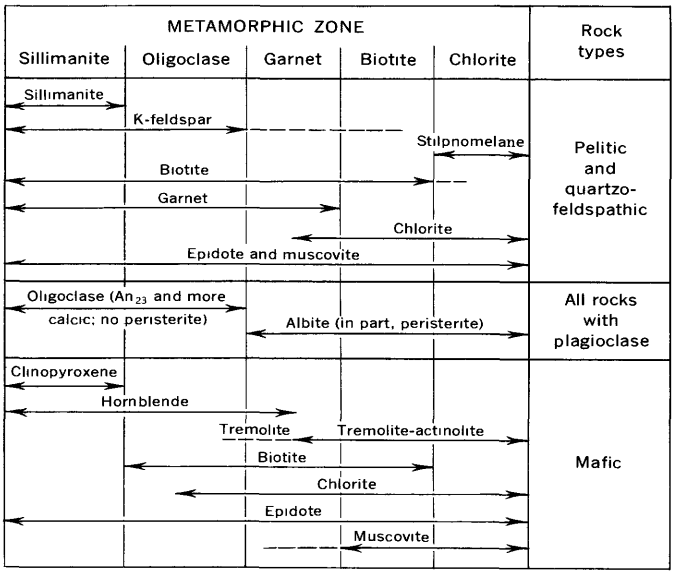

FIGURE 3.—Schematic graph showing distribution of index and other important minerals within the metamorphic zones. Dashed lines indicate that occurrence of mineral is uncommon or rare.

metamorphic facies concept, and subsequently Fyfe and Turner (1966) suggested that the definition of metamorphic facies be modified to exclude any inference of temperature-pressure and equilibrium conditions. We welcome this pragmatic apprach and wish to emphasize that we are using metamorphic zones (and in part, metamorphic facies) as mappable units, which are characterized by a finite group of metamorphic mineral assemblages from rocks of several different bulk chemical compositions.

X-RAY DIFFRACTION DATA

We selected a number of rock samples from each zone to establish the possible presence of paragonite and to verify the anorthite content of plagioclase that had been determined optically. Paragonite was detected in only two samples (from the garnet zone at Hagers Mountain; see also Espenshade and Potter, 1960; Zen, 1961). Basal spacing of the mica in these and other specimens is shown in table 2. The restriction of paragonite, kyanite, and chloritoid to rocks at Hagars Mountain suggests that these three minerals are present in this part of the garnet zone largely as a result of an unusual bulk rock composition at that locality.

In our investigation of plagioclase composition, we selected 20 samples across the 5 metamorphic zones for X-ray powder diffraction analysis. In sodic plagioclase

TABLE 2.—*Mineralogy, anorthite content of plagioclase, and basal spacing of muscovite and a paragonite from selected rock samples from parts of the Carolina slate belt–Charlotte belt boundary area, North Carolina and Virginia*

Zone	Sample number	Minerals [1]																					Anorthite content of plagioclase (mol percent)			$d_{(002)}$ spacing (angstroms)	
		Quartz	Plagioclase	K feldspar	Hornblende	Tremolite/actinolite	Clinopyroxene	Epidote	Chlorite	Biotite	Muscovite	Paragonite	Garnet	Scapolite	Kyanite	Sillimanite	Chloritoid	Sphene	Calcite	Magnetite	Hematite	Pyrite	Leucoxene	Flat stage	Universal stage	X-ray	Muscovite	Paragonite
Chlorite	3	1	1					1	2															9		0 and 15		
	6	1	1					3	1											3						0		
	8	1	1					3	1	3	1									3				5		0 and 12		
	309F	1	1					1	1		1									3				9		0 and 15	9.9570	
Biotite	11	1	1					3	1	1													3			[2](0–3)		
	12		1			3		2	1	3								3		3				12		0 and 18		
	31A	2	1					1	1	2								3		3						0		
	65	1	1	3				3		3	1													7		(0–3) and 15	9.9870	
Garnet	DR–33	1	1								1	1			3		3			3						15	9.8930	9.6195
	36	1									1	1			1		1						3				9.8810	9.6195
	67	2	1					3	2	2	3									3				8	7	3 and 14	9.9695	
	76	2	1					1	2	3										3						(0–2)		
	10	1	1	2				3		3	1		[3]3							3	3			5				
Oligoclase	UN–16	1	[4]1		1			3	2	3										3		3		58		50		
	54	1	1	1				3		3	1									3				26		22	9.9595	
	58	2	3		1			2	1	3																24		
	78	1	1	2				3		3	1									3				25		22		
Sillimanite	24	1	1	1						2	2			[5]1				3	3	3		3				29	9.9630	
	28	3				2	1	2																				
	30	2	1		1		2	2						3				3		3				37		35		
	31	2	1					3		1								3		3		3		30		29		
	33	1									3					2				3							9.9590	
	34	3	1	3		3	3																	33		29		
	35	1	1		1					1			3					3		3				41	38	52		

[1] 1, principal (>10 percent); 2, minor (<10>5 percent); 3, accessory (<5 percent).
[2] (0–3) indicates X-ray peaks were broad.
[3] Garnet: a=11.63A; n=1.795±0.005.
[4] Plagioclase: core=58 percent, rim=49 percent anorthite content.
[5] Scapolite: ϵ=1.555±0.002; ω=1.585±0.002; meionite content=68 mol percent.

(An_0–An_{70}), we used the formula (2θ $1\bar{3}1 - 2\theta$ 131) and curve of Smith and Yoder (1956, p. 641), and for the more calcic plagioclase (An_{20}–An_{70}) the formula (2θ $131 + 2\theta$ $220 - 4\theta$ $1\bar{3}1$) and curve of Smith and Gay (1958, p. 749). The samples were crushed and processed on the Franz magnetic separator. The nonmagnetic fraction, containing 75–85 percent plagioclase, 15–25 percent quartz, 2–5 percent sericite, and trace amounts of chlorite and epidote, was then prepared in the normal manner for X-ray diffraction analysis. Samples were run using CuK_α radiation, Ni filter, and 0.50° per minute scan speed. The results are shown in figures 4, 5, and table 2.

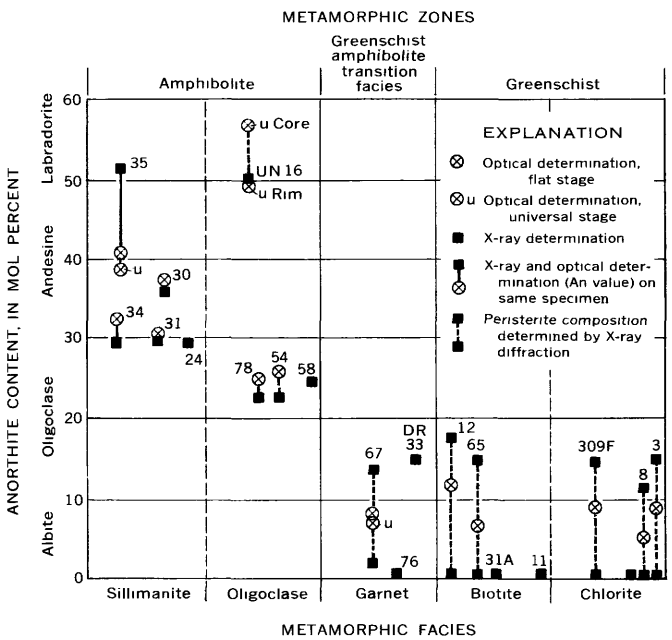

FIGURE 4.—Diagram showing relation between metamorphic zones and anorthite content of plagioclase as determined by X-ray diffraction and optical methods (see text). Numbers indicate sample number. Universal stage determinations by twin law method of Turner (1947) using curves of Slemmons (1962). The curve of Smith and Gay (1958) gives An content in weight percent; An values determined using this curve have been converted to mol percent.

In the low grade rocks east of the oligoclase isograd, X-ray diffraction patterns showed that the plagioclase is predominantly albite (An_{0-3}, which is several anorthite percent below that which was determined optically (table 2 and fig. 4). More than half the samples, however, showed a second diffraction peak of approximately the same intensity as, and very close to, the albite ($1\bar{3}3$) peak (fig. 5, samples 209F and 65). Impurities (for example, muscovite, chlorite, and potassic feldspar) probably did not cause this peak. Such impurities are in small amounts and also occur in plagioclase from the oligoclase and sillimanite zones whose samples show only one ($1\bar{3}1$) peak (fig. 5).

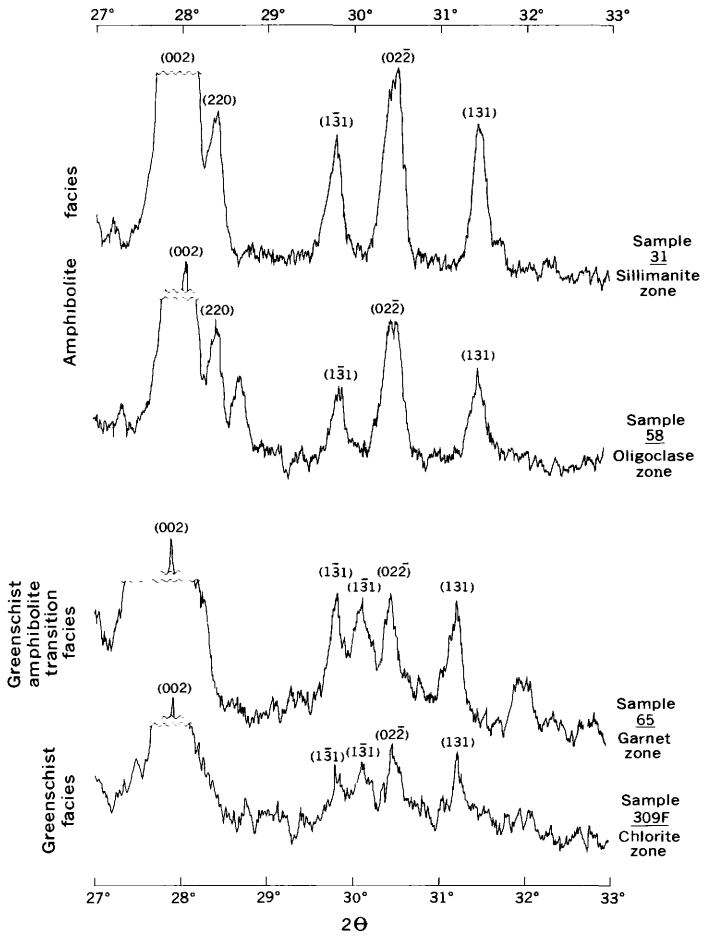

FIGURE 5.—X-ray diffraction patterns showing two ($1\bar{3}1$) peaks which indicate peristerite in greenschist and greenschist-amphibolite transition facies. A single ($1\bar{3}1$) peak in amphibolite facies rocks indicates absence of peristerite.

Tentatively, therefore, we have taken the peak at about 29.85° 2θ to be a second ($1\bar{3}1$) peak of plagioclase. Assuming that the (131) peak for the second plagioclase is unresolved from the (131) peak for An_{0-3}, the anorthite content is consistently about An_{15-18}. This second plagioclase could not be found optically, and in fact anorthite determinations on the plagioclase by flat stage (maximum extinction in plane {010} and universal stage (twin law method of Turner, 1947, using the curves of Slemmons, 1962) consistently yielded values which fell roughly midway between the two values determined by X-ray diffraction work (fig. 4 and table 2). We suggest that the two plagioclases are present on a submicroscopic scale, and that the optics average the two "end members" (that is, An_{0-3} and An_{15-18}), yielding an apparent median value (that is An_{5-9}). We tentatively conclude, therefore, that the plagioclase is a peristerite, consisting of two phases, An_{0-3} and An_{15-18}. These results are in contrast to the findings of other workers who have shown that

plagioclase in the range An_2—An_{18} unmixes into two phases of An_{0-1} and An_{25-28} (for example, Laves, 1954; Brown, 1962; Crawford, 1966). More detailed analysis of the plagioclase by X-ray, electron microscopy, and electron-probe techniques is underway in order to substantiate the presence of peristerite in the lower grade rocks, and to determine the exact nature of the two phases in the peristerite.

Above the oligoclase isograd (oligoclase and sillimanite zones), X-ray diffraction patterns show only one $(1\bar{3}1)$ peak for plagioclase (fig. 5). Our interpretation is that at higher metamorphic grades, the plagioclase is homogeneous. Optical and X-ray determinations of anorthite content generally agree within at least 4 An percent (fig. 4 and table 2). Plagioclase from felsic rocks is in the range An_{22-33}, whereas in mafic rocks it is in the range An_{35-38} or more calcic. Where plagioclase is zoned (sample UN–16, fig. 4 and table 2), the X-ray determination appears to favor the rim composition. In one sample (sample 35, fig. 4, table 2), the X-ray determination yields an anorthite content considerably higher than the flat-stage and universal-stage determinations, which are very close to each other. Within the range An_{37-55}, however, the curve of Smith and Gay (1958, fig. 1) is nearly flat, and small errors in the ordinate $(2\theta\ (131)+2\theta\ (220)-4\theta\ (1\bar{3}1))$ lead to large errors in the abscissa (An percent). The An value determined by X-ray analysis in sample 35 is, therefore, considered to have a large margin of error; that value obtained optically, is probably more reliable.

Figure 4 illustrates the well-defined break in anorthite content of plagioclase between the garnet and oligoclase zones. In the field, however, the break is a zone about 0.3 mile in width and contains rocks which yield both albite and more calcic plagioclase.

CONCLUSIONS

From field mapping and laboratory work, we have delineated 5 metamorphic zones which parallel the contact of the 2 geologic belts, and have correlated these zones with the metamorphic facies (Turner and Verhoogen, 1960). The metamorphic grade shows a progressive increase from east to west. Our present evidence indicates that a metamorphic gradient ranging from greenschist facies in the east to upper amphibolite facies in the west is one of several factors which defines the boundary between the Carolina slate belt and Charlotte belt in this part of the Piedmont geologic province.

REFERENCES

Brown, W. L. 1962, Peristerite unmixing in the plagioclases and metamorphic facies series: Norsk Geol. Tidssk., v. 42, pt. 2, p. 354–382.

Crawford, M. L., 1966, Composition of plagioclase and associated minerals in some schists from Vermont, U.S.A., and South Westland, New Zealand, with inferences about peristerite solvus: Contr. Mineralogy and Petrology, v. 13, no. 3, p. 269–294.

Espenshade, G. H., and Potter, D. B., 1960, Kyanite, sillimanite, and andalusite deposits of the southeastern States: U.S. Geol. Survey Prof. Paper 336, 121 p.

Fyfe, W. S., and Turner, F. J., 1966, Reappraisal of the metamorphic facies concept: Contr. Mineralogy and Petrology, v. 12, no. 4, p. 354–364.

King, P. B., 1955, Geologic section across the southern Appalachians; an outline of the geology in the segment in Tennessee, North Carolina, and South Carolina, *in* Russell, R. J., ed., Guides to southeastern geology: New York, Geol. Soc. America, p. 332–373.

Lambert, R. St. J., 1965, The metamorphic facies concept: Mineralog. Mag., v. 34, p. 283–291.

Laney, F. B., 1917, The geology and ore deposits of the Virgilina district of Virginia and North Carolina: North Carolina Geol. and Econ. Survey Bull. 26, p. 1–176.

Laves, Fritz, 1954, The coexistence of two plagioclases in the oligoclase compositional range: Jour. Geology, v. 62, no. 4, p. 409–411.

Overstreet, W. C., and Bell, Henry III, 1965, The crystalline rocks of South Carolina: U.S. Geol. Survey Bull. 1183, p. 126.

Slemmons, D. B., 1962, Determination of volcanic and plutonic plagioclases using a three- or four-axis universal stage—Revision of Turner method: Geol. Soc. America Spec. Paper 69, 64 p.

Smith, J. R., and Yoder, H. S., Jr., 1956, Variations in X-ray powder diffraction patterns of plagioclase feldspars: Am. Mineralogist, v. 41, nos. 7–8, p. 632–647.

Smith, J. V., and Gay, P., 1958, The powder patterns and lattice parameters of plagioclase feldspars, II: Mineralog. Mag., v. 31, no. 240, p. 744–762.

Turner, F. J., 1947, Determination of plagioclase with the four-axis universal stage: Am. Mineralogist, v. 32, nos. 7–8, p. 389–410.

Turner, F. J., and Verhoogen, Jean, 1960, Igneous and metamorphic petrology, 2d ed.: New York, McGraw-Hill, 694 p.

Zen, E-an, 1961, Mineralogy and petrology of the system Al_2O_3–SiO_2–H_2O in some pyrophyllite deposits of North Carolina: Am. Mineralogist, v. 46, nos. 1–2, p. 52–66.

POSSIBLE FISSURE VENT FOR A PLIOCENE ASH-FLOW TUFF, BUZZARD CREEK AREA, HARNEY COUNTY, OREGON

By GEORGE W. WALKER, Menlo Park, Calif.

Abstract.—Steeply inclined foliation and lineation, manifested by flattened and stretched pumice fragments, indicate nearly vertical laminar flowage in a restricted area of a large-volume Pliocene ash-flow tuff. The orientation of these structures and their presence in only the basal part of the ash flow in a small area are suggestive of fissure vents related to a northwest-trending graben, although some of the structures could have formed during compaction-welding and flowage away from underlying topographic highs.

A complex northwest-trending graben may be the site of a fissure vent that was the source of all or part of a large volume of Pliocene ash-flow tuff in southeast Oregon. Locally the tuff has unusually steeply inclined foliation and well-marked lineation along margins of the graben. The graben is spatially and probably genetically related to the Brothers fault zone. Interpretation of the structures and study of their relation to the ash-flow tuff suggest local venting, although compaction, welding, and draping of the ash flow over preexisting fault scarps and some turbulent flowage may account for some of the unusual structures.

The graben was first recognized as a possible vent area during reconnaissance geologic mapping of a large region in southeast Oregon underlain chiefly by ash-flow tuffs and less extensive basalt flows and tuffaceous sedimentary rocks. The graben that contains the possible vent bounds parts of Buzzard Creek (lat 43°08′ N.; long 119°23′ W.), about 16 kilometers west-southwest of Harney Lake, Harney County, and lies mostly in the northern part of T. 28 S., R. 28 E., Willamette meridian.

Prior to the present study no geologic mapping had been done in the Buzzard Creek area, although Piper, Robinson, and Park (1939) summarize the geology of most of Harney Basin east of the area, and Walker and Swanson (1968a) briefly describe the geology adjacent to Harney Lake.

GEOLOGY OF BUZZARD CREEK AREA

In a regional sense, the Buzzard Creek area is part of Harney Basin, a large physiographic and structural depression developed in widespread Pliocene and Pleistocene volcanic and continental sedimentary rocks. Conspicuous among these rocks is a highly pumiceous, mostly welded rhyolitic ash-flow tuff of middle Pliocene age that represents the youngest of several ash-flow sheets of the Danforth Formation and, according to Campbell, Conel, Rogers, and Whitfield (1958) is possibly equivalent to the pumiceous ash-flow tuff of the Rattlesnake Formation in the John Day Basin 150 km north of Buzzard Creek. This tuff covers more than 7,700 sq km (3,000 sq miles) in Harney Basin alone—mostly to the south, west, and north of the Buzzard Creek area—and ranges from about 6 meters to more than 120 m in thickness, the average being about 25 m. The total volume of ash-flow tuff must be more than 180 cu km.

Most of the bedrock outcrops in the area are of the pumiceous ash-flow tuff (fig. 1). However, a scoriaceous diktytaxitic olivine basalt of probable Pliocene age crops out in several places at the base of a fault scarp in the northwest corner of the Buzzard Creek area and is more widely exposed in fault scarps farther to the west. The tuff overlies the olivine basalt in the Buzzard Creek area, but in nearby areas it rests on Pliocene tuffaceous sedimentary rocks or, locally, on Pliocene ash-flow tuffs traceable over large parts of Harney Basin. Poorly consolidated surficial deposits of alluvium and slopewash along Buzzard Creek are derived largely from erosion and redeposition of the poorly indurated upper part of the pumiceous tuff. This upper zone apparently was never very thick and was almost completely stripped from upland surfaces by erosion.

U.S. GEOL. SURVEY PROF. PAPER 650–C, PAGES C8–C17

Northwest-trending high-angle normal faults, and a few trending north and northeast, all with small to moderate displacements, break the tuff sheet into a number of separate blocks, some of which have steep faces as much as 80 m high. An irregular, moderately complex northwest-trending graben, bounded by some of these faults and locally by minor broken monoclinal warps, transects the area. The faults lie in the northwest-trending Brothers fault zone, which is characterized at the surface by closely spaced en echelon normal faults with displacements of as much as 100 m. The zone of en echelon faults is exposed for nearly 250 km through south-central Oregon (Walker and King, 1969), and many basaltic and rhyolitic vents of Pliocene and Pleistocene age occur throughout its length.

In adjacent parts of Harney Basin, distribution of rock units indicates that faulting and basin collapse were virtually concurrent with eruption of the ash flows. However, continuity and relatively little variation in thickness of certain ash flows, such as the one discussed in this paper, over very large parts of the basin indicate that eruption and spreading of the flows were largely undisturbed by concurrent faulting or high fault scarps.

PUMICEOUS ASH-FLOW TUFF AWAY FROM POSSIBLE VENT AREA

Away from its possible vent area on Buzzard Creek, the pumiceous ash-flow tuff is composed predominantly of vitroclastic debris and minor amounts of mineral grains and rock fragments. The tuff sheet is zoned into several distinct lithologic layers (fig. 2), that result from differential compaction, vapor-phase crystallization, and, in places, from minor laminar flowage. Local complexities of zonation suggest that two or more lobes of lithologically identical material may have been superimposed in places, but throughout most of its outcrop area the sheet appears to be composed of a single flow that cooled as a single unit, according to the general pattern outlined by Smith (1960) and Ross and Smith (1961).

In most places, the ash-flow tuff is mottled and streaked in shades of light gray and medium dark gray. The upper and lower parts of the cooling unit are pinkish gray or light brown. Before devitrification and vapor-phase crystallization more than 98 percent of the tuff was composed of glass. This glass was in the form of shards (mostly less than 1 mm in length) and of pumice lapilli and blocks, later flattened into lensoid disks as much as 25 cm in diameter. The glass is mostly colorless to pinkish or yellowish brown and has a refractive index of 1.500 ± 0.005, indicating a silica content of about 70 percent (Huber and Rinehart, 1966). Phenocrysts of sanidine ($2V(-) \approx 20$–$30°$), quartz, a pleochroic bright-green clinopyroxene ($2V(+) \approx 60$–$70°$) with reddish hematized margins (probably aegirine-augite), plagioclase, and less abundant magnetite, colorless to light-amber clinopyroxene, and oxyhornblende make up about 1 percent of the tuff. Rounded mostly equidimensional fragments of andesite or basalt, highly eutaxitic pieces of older welded tuff, perlitic glass, flow-banded rhyolite, and indurated sedimentary rocks constitute less than 1 percent of the ash-flow tuff; most of these rocks fragments are less than 1 cm in diameter. A strong eutaxitic texture is discernible except in the thin basal nonwelded zone and in an internal zone that is so thoroughly crystallized and pockmarked by abundant lithophysae that welding textures are obliterated.

The general zoning characteristics of the cooling unit in areas at some distance from the possible vent area are shown in figure 2. Thickness and degree of compaction and welding of individual zones vary only slightly throughout Harney Basin. The basal zone, exposed in only a few places, is about a meter thick and is not welded. Pumice fragments in it are mostly less than 1 cm in diameter and show virtually no compaction. This nonwelded zone grades upward within a few centimeters into moderately dense vitrophyre about 1.5 m thick.

The vitrophyre, which also is poorly exposed, is composed mostly of compressed shards and pumice lumps; these exhibit little evidence of stretching, although slight stretching of pumice fragments and devitrification of glass is recognizable near the top of the zone. Some completely collapsed pumice lumps now form lenses of dense dark-gray glass in a less-indurated pinkish-brown vitrophyre.

In a few places the vitrophyre is overlain by a layer about 2 m thick that is characterized by strong compaction, nearly complete crystallization, many lithophysae, and only slight stretching of pumice fragments. Completely crystallized ash-flow tuff forms a zone about 6 to 10 m thick above the 2-m layer or, where it is missing, the vitrophyre. The completely crystallized tuff has a high degree of compaction, some stretched pumice fragments, a few lithophysae and many lensoid miarolitic cavities, and widely spaced columnar joints. The lensoid cavities and flattened pumice fragments give rocks of the zone a pronounced nearly horizontal foliation. Crystallization products form a fine intergrowth of alkali feldspar and cristobalite in fairly dense rock, and many of the miarolitic cavities also are lined with these minerals.

The zone of crystallized tuff grades upward into a zone of tuff that is also completely crystallized, owing to vapor-phase alteration, but is distinguished from the

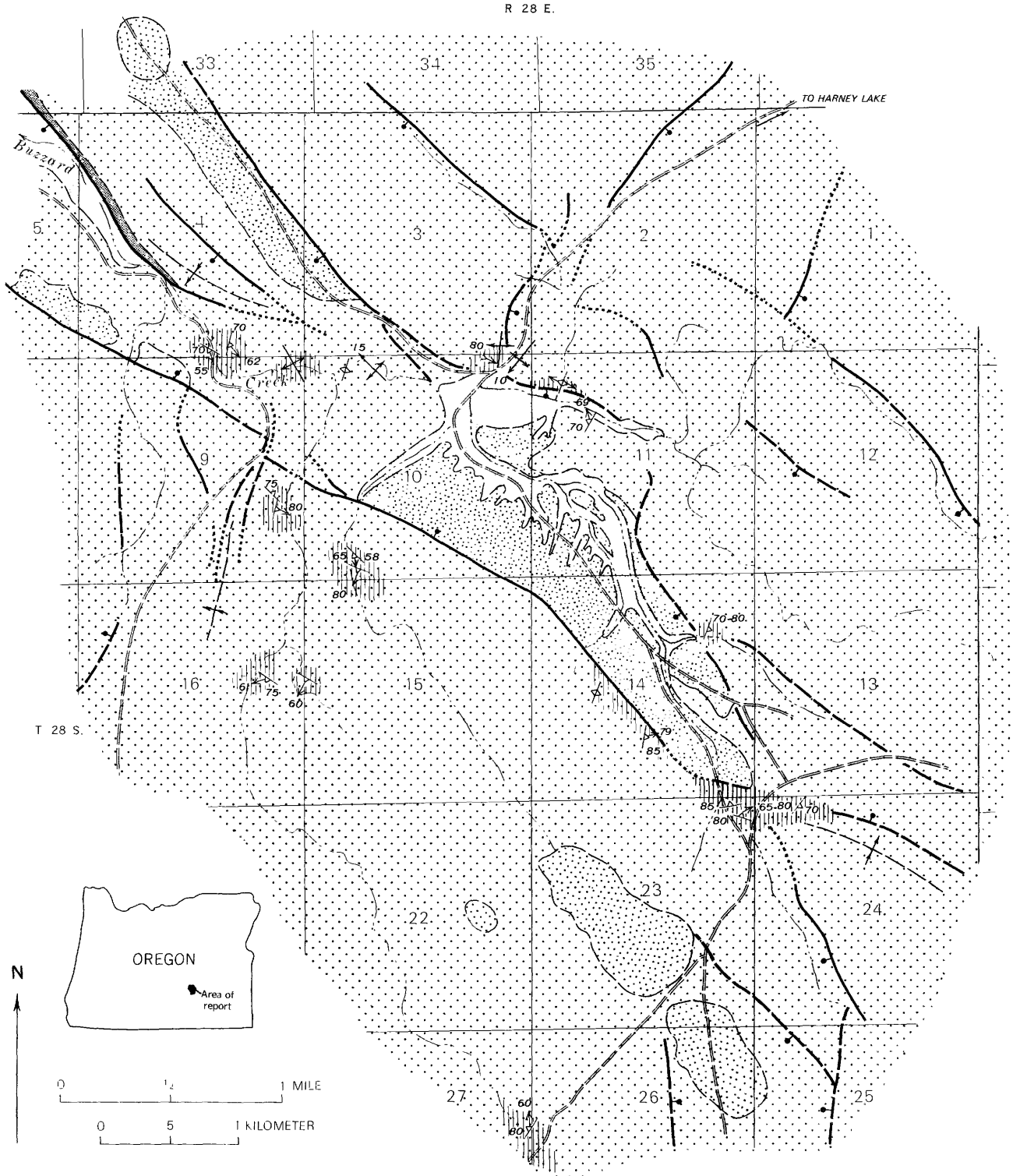
R 28 E.
T 28 S.
TO HARNEY LAKE
Buzzard
33
34
35
5
4
3
2
1
9
10
11
12
16
15
14
13
22
23
24
27
26
25
OREGON
Area of report
N
0 1/2 1 MILE
0 5 1 KILOMETER

FIGURE 1.

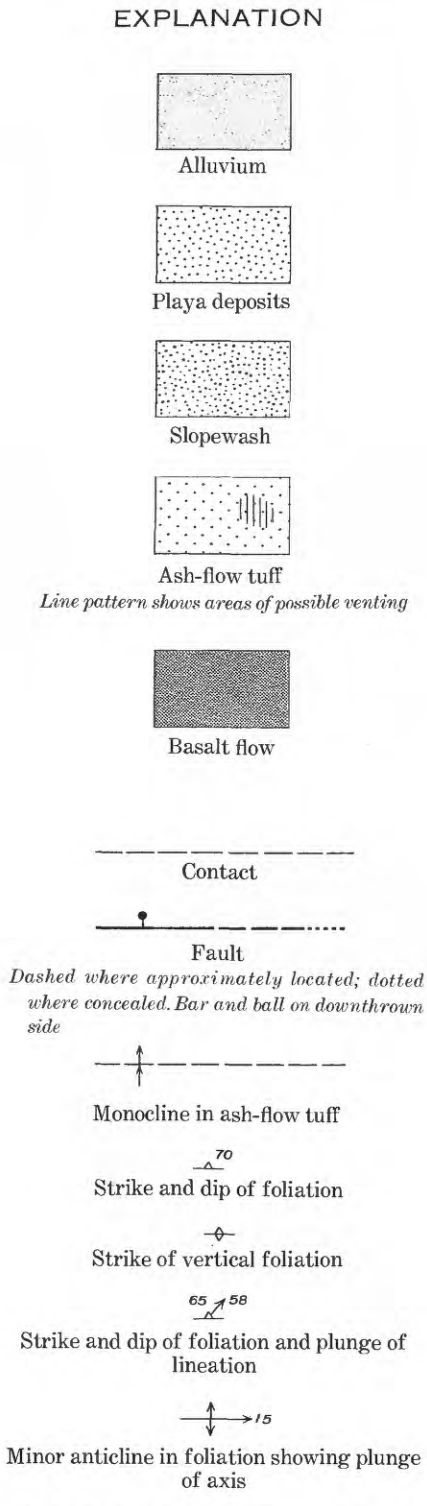

FIGURE 1.—Geologic sketch map of Buzzard Creek area, showing faults, minor folds, and orientation of some flowage structures in ash-flow tuff.

337-735 O—69——2

underlying zone by abundant spherical gas pockets and concentrically banded lithophysae less than 2.5 cm in diameter; tuff in this zone is neither foliated nor jointed. Primary eutaxitic texture is almost completely destroyed, and the vapor-phase zone is now composed almost entirely of secondary alkali feldspar and some cristobalite. This tuff characteristically weathers to rounded, more or less structureless outcrops. The zone is 3 to 15 m thick in the Buzzard Creek area and as much as 60 m thick in adjoining areas.

The vapor-phase zone grades upward within a few tens of centimeters into a zone commonly 1.5 to 3 m thick of pinkish-gray ash-flow tuff in which pumice fragments and shards are only moderately compacted. Crystallization of glass throughout most of this zone has created a dense stony rock that is highly resistant to erosion and, as a result, forms ledges at the top of most fault scarps (see figs. 2, 3, and 4). Nonwelded and noncompacted ash-flow tuff above the stony zone has been removed by erosion throughout the Buzzard Creek area, though it is present elsewhere. The oxidized nature of minerals in the stony zone suggests that this upper, poorly indurated part of the ash-flow was never very thick.

STRUCTURES OF PUMICEOUS ASH-FLOW TUFF IN POSSIBLE VENT AREA

The structures that suggest local venting of the pumiceous ash-flow tuff from steep fissurelike conduits in the Buzzard Creek area include (1) steeply inclined compaction foliation, (2) asymmetric folds of several different shapes and sizes, and (3) stretched and lineated pumice fragments in the plane of foliation that point to laminar flowage. Similar laminar flowage structures have been described in several recent papers (Schmincke and Swanson, 1967; Hoover, 1964; Walker and Swanson, 1968b). However, these structures occur in nearly horizontal ash-flow tuff sheets rather than in nearly vertical fissurelike conduits, but whether the mechanisms involved in their formation are precisely comparable remains to be proved.

The individual pumice fragments, where distorted only by compaction, are lensoid disks commonly a few millimeters to a few centimeters thick, though locally they are flattened into paper-thin sheets many tens of centimeters in diameter. The highly flattened pumice fragments produce a moderately to well-defined foliation in many outcrops of the tuff. The strongly foliated

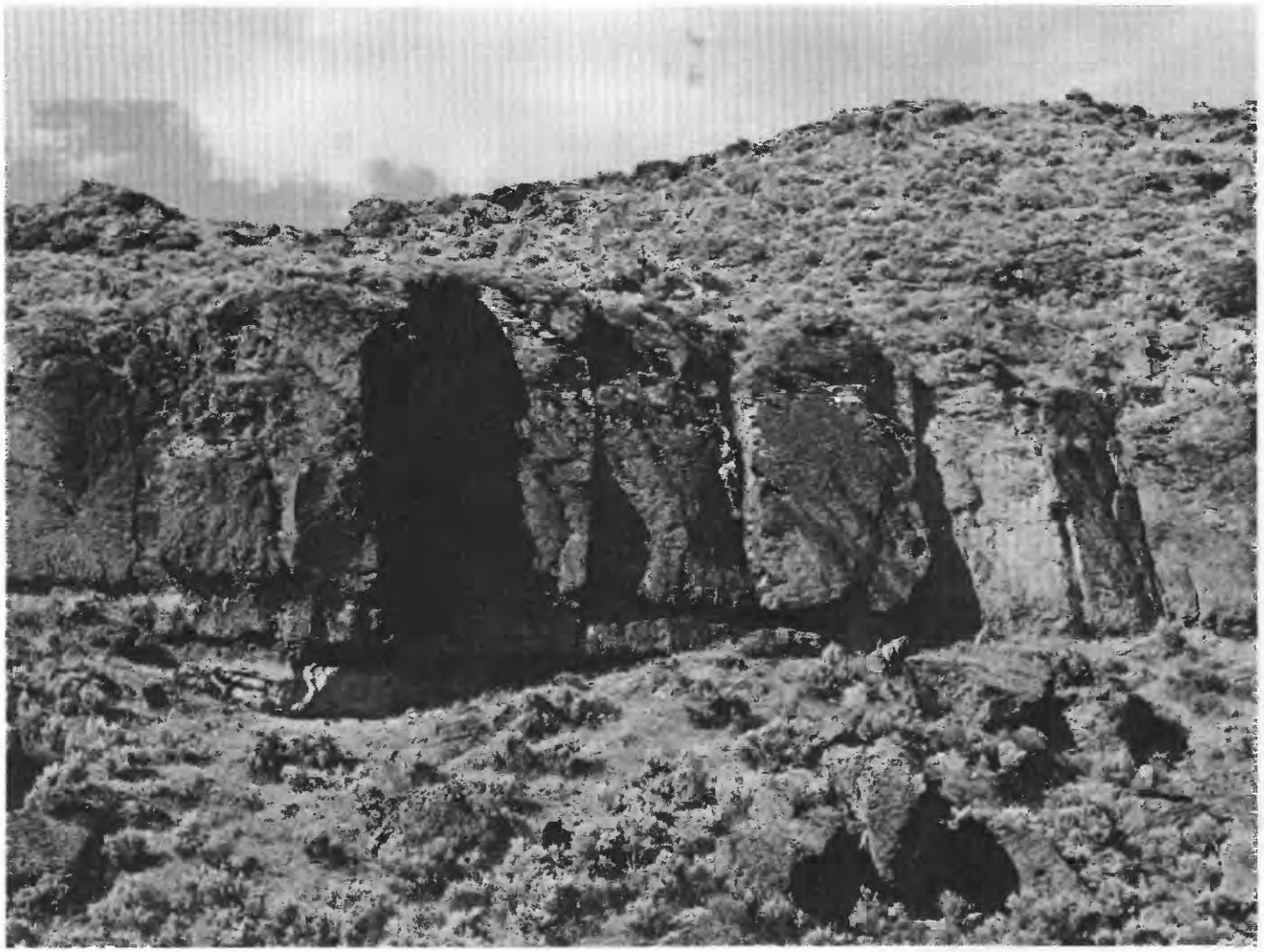

FIGURE 2.—Single cooling unit of flat-lying ash-flow tuff exposed on north wall of Buzzard Creek west of possible vent area. A light-colored air-fall tuff at the base is overlain by 1.5 m of dark vitrophyre. A 2-m-thick layer of lithophysal tuff overlies the vitrophyre; it grades upward into thick crystallized ash-flow tuff (vertical wall) containing both lithophysae and nearly horizontal foliation. Some thin layers near base of wall show many stretched pumice fragments. Slope above wall is underlain by lithophysal ash-flow tuff that is capped by a 2- to 3-m-thick resistant ledge of stony, partly crystallized ash-flow tuff showing the original, highly pumiceous character of ash flow. Total thickness of tuff about 24 m.

tuff also has conspicuous sheet jointing (figs. 3 and 4) that parallels the foliation. Where pronounced laminar flowage has occurred in addition to compaction, the flattened pumice fragments are also stretched as much as 20 to 30 times their width. The elongation of these fragments imparts a distinct lineation to the tuff, although the actual direction of movement cannot be determined from the lineation.

Macroscopic and microscopic folds that involve flattened pumice fragments and matrix shards, and some very large folds with amplitudes of many meters that also involve foliation and sheet jointing, characterize the lower parts of the pumiceous ash-flow tuff in the area of possible venting. However, at a distance from the possible vent, comparable folds appear to be lacking. Most of the folds are open asymmetric flexures, similar to those described by Schmincke and Swanson (1967, p. 655), with amplitudes that range from a fraction of a millimeter to several tens of meters (figs. 3 and 5). The folds occur as high in the ash-flow tuff as the vapor-phase lithophysal zone and may have extended into that zone before vapor-phase crystallization and ensuing development of abundant lithophysae obliterated them. Axes of the larger folds have randomly oriented bearings and plunge at angles ranging from zero to as much as 20°. No systematic study has been made of the microscopic folds, although the axes of many of them seem to be alined at right angles to the stretched and elongated pumice fragments. None of the larger folds are isoclinal, although some microscopic folds in highly compacted and sheared tuff have tight isoclinal bends near phenocrysts or rock fragments.

None of these structures by itself indicates local venting; each is known to occur in flat-lying and

FIGURE 3.—Asymmetric anticlinal fold in foliation of ash-flow tuff, looking about N. 10° W. Flexure trends N. 30° W.; northeast limb is steeper. Rounded outcrops and lower parts of spires consist of lithophysal ash-flow tuff; spires are capped by layer of crystallized, stony, pumiceous tuff.

gently dipping ash-flow sheets at some distance from postulated sources (Schmincke and Swanson, 1967; Walker and Swanson, 1968b). However, the orientations of these structures, their restriction to a very small part of the total outcrop area of the tuff, their relation to the faults bounding the northwest-trending graben, and the restriction of steeply inclined flowage structures to the lower part of the ash-flow sheet with apparent crosscutting of the basal vitrophyre in one place may suggest local fissurelike vents.

ORIENTATION OF FLOWAGE STRUCTURES

The structural features associated with laminar flowage of the pumiceous ash-flow tuff in the Buzzard Creek area are most numerous near the base of the tuff, where they indicate movement in a nearly vertical plane. Their relation to the basal nonwelded tuff and overlying vitrophyre is not well established because the exposures are poor; but in one place, on the

FIGURE 4.—Exposures of a simple cooling unit of ash-flow tuff on north wall of Buzzard Creek. One of possible fissure zones is marked by steep foliation in center of picture. Lineation (not visible) in plane of foliation has steep but erratic plunge. Ledge at skyline is composed of crystallized, stony, pumiceous ash-flow tuff underlain by rounded outcrops of lithophysal tuff. Plane of foliation and lineation in intermediate ledge becomes horizontal above fissure zone. To west (left), zone of horizontal foliation merges with other lithologic parts of ash-flow tuff.

FIGURE 5.—Slightly asymmetric anticlinal fold defined by foliation in ash-flow tuff, looking northwest. Axis of fold bears N. 45° W. and plunges 15°–20° NW. Rounded outcrops are lithophysal ash-flow tuff.

west wall of the south fork of Buzzard Creek (in sec. 16), highly stretched and laminated tuff with contorted and nearly vertical foliation and lineation seems to cut across the vitrophyre in a zone several meters wide. These structural features possibly represent a fissure. The foliation and lineation become nearly horizontal at the top of the ash-flow sheet (fig. 6). Elsewhere in the Buzzard Creek area, steep foliation is present in many outcrops a few tens of centimeters to several meters above the vitrophyre. In many of these outcrops the foliation has a northwest trend (fig. 1) and a lineation in the foliation plane that also is steep. Most foliation planes are inclined at angles greater than 80°, and the lineation commonly plunges more than 60°. A typical exposure of steep foliation and lineation in the basal part of the ash-flow tuff is shown in figure 7. Some of these flowage structures change orientation in a distance of 3 to 10 m from a steep inclination low in

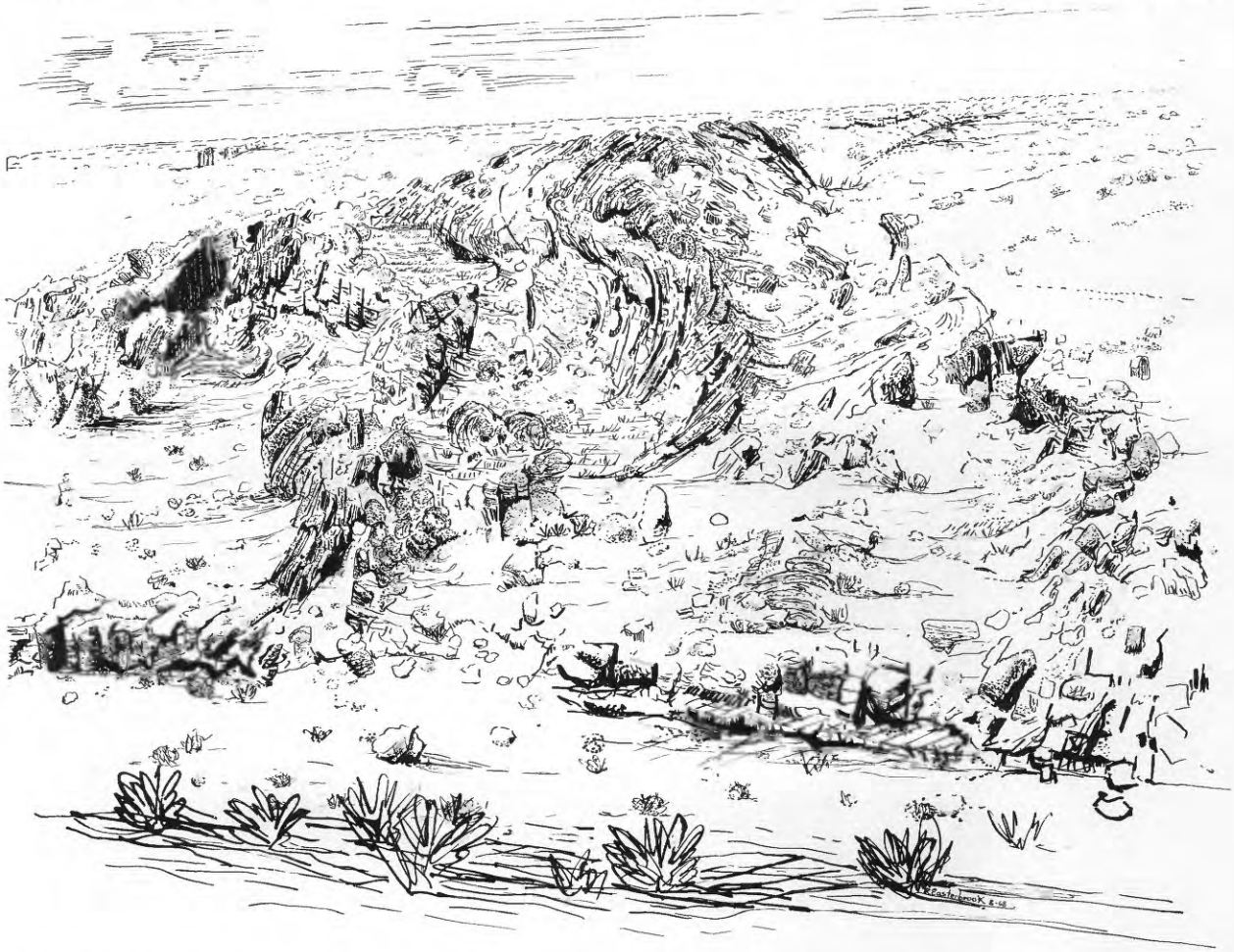

FIGURE 6.—Exposures on west wall of south fork of Buzzard Creek, showing strongly foliated and contorted, bulbous masses of ash-flow tuff. Foliated tuff appears to cut basal ledge-forming vitrophyre, projects through lithophysal zone that is characterized by heavy outcrops shown in central part of drawing, and extends up to thin stony zone of ash-flow tuff near skyline. Lineation, in the plane of foliation, is nearly vertical in the lower outcrops. Sketch made by Robin Easterbrook from photograph.

FIGURE 7.—Lineated and foliated ash-flow tuff in eastern part of Buzzard Creek area. Lineation plunges 65°–80° eastward (right) and results mostly from stretched pumice fragments, some of which are now elongate cavities lined with vapor-phase crystals of alkali feldspar and cristobalite.

the tuff into a nearly horizontal attitude in the upper part of the flat-lying tuff (fig. 4).

The steeply inclined laminar flowage structures in the tuff apparently are restricted to an area of a few square kilometers near Buzzard Creek, whereas the total outcrop area of the tuff is more than 7,700 sq km. At a distance from the postulated vent area on Buzzard Creek, laminar flowage structures in the pumiceous tuff are rare, and, in the few places where they have been recognized, all are horizontal or nearly so.

The seeming localization of steep laminar flowage structures on and near faults and monoclinal warps related to the northwest-trending graben may be

fortuitous and only a result of more abundant exposures along the fault scarps. However, the localization may be real because many contemporaneous fault scarps in neighboring areas expose normal, nearly flat-lying ash-flow tuff.

Were the faults the actual conduits for the ash flow, or did they form scarps and associated monoclinal warps that caused local steep viscous flowage as the tuff draped over them during static compaction? In all outcrops examined, the foliation flattens upward (for example, figs. 3 and 4) but not downward; if draping were the cause, the resulting foliation should flatten downward as well, at and near the base of the preexisting scarps. No evidence for such draping has been recognized. Also, if compaction draping over scarps had been important, similar steep flowage structures should be present, at least locally, throughout the total outcrop area of the tuff since it is broken by many faults apparently contemporaneous with those in the Buzzard Creek area. No such structures have been recognized. Thus, the steeply inclined laminar flowage structures seem to strengthen the argument in favor of nearly vertical movement of particulate material through steep conduits along faults related to the northwest-trending Brothers fault zone.

Although the laminar flowage structures can be interpreted as being primary and as being related to local venting rather than to draping over existing fault scarps and warps, they afford little precise data on the mechanism of venting and probably typify only the end stages of the whole eruptive sequence. The possible vent area on Buzzard Creek may also be only one of several fissure zones from which the ash flow emerged; the others may have been buried by the widespread ash-flow sheet. For these reasons the following discussion is necessarily speculative.

CONCLUSIONS

If the steeply inclined laminar flowage structures resulted from local venting, they formed during the time that viscous particulate material was either driven by expanding gases through the narrow fissure zones or slumped back into these zones as a result of withdrawal of magma. Vesiculation and fragmentation of the silicic magma occurred at some unknown depth below any zones now exposed, but the rising inhomogeneous magma retained a high degree of fluidity, and individual pumice fragments remained highly plastic, both in the conduits and in the ash flow at considerable distance from the possible vents. The fluidity of these silicic particles is shown by dense welding in some parts of the tuff and probably indicates comparatively high emplacement temperatures; a temperature close to the liquidus is also suggested by the paucity of crystals and crystal fragments in the ash-flow tuff. Low viscosity may have been related to a high volatile content of the erupting magma, as suggested by the thick and widespread zones of vapor-phase crystallization, or to its anhydrous chemical composition. However, none of the chemical factors reported by Schmincke and Swanson (1967) and Walker and Swanson (1968b) that may affect viscosity in silicic magmas has been recognized in the ash-flow tuff on Buzzard Creek.

The earliest eruptions that resulted in noncompacted air-fall tuff at the base of the ash flow may have been comparatively violent, inasmuch as pumice lapilli were apparently ejected with enough force to permit cooling and consequent loss of plasticity before they were deposited and buried beneath the overriding ash flow. All other particulate material in the widespread pumiceous ash-flow sheet is thought to have erupted rapidly and relatively nonviolently, because there is no evidence of explosive activity in the possible vent area and the particles are densely welded. Turbulent flowage probably characterized this main stage of eruption, during which the ash flow rapidly spread over large parts of western Harney Basin. Flattening and stretching of pumice fragments to form distinct flowage structures in the ash-flow tuff took place during the end stages of deflation after turbulent flowage had ceased; examples of this type of flowage structures have been described by Schmincke and Swanson (1967) for other ash-flow tuffs.

The strongly foliated and lineated tuff in the possible conduits is not typical of the main venting stage in which tremendous volumes of ash-flow tuff erupted and moved turbulently over large areas, but instead probably denotes a largely degassed end stage of magma eruption characterized by laminar flowage in a slowly moving magma column that may have been rising or, as a result of magma withdrawal, sinking. Flattening and elongation of individual pumice fragments in what are thought to be conduits was not the normal compaction, flattening, and stretching recognized in many ash-flow tuffs (Ross and Smith, 1961; Schmincke and Swanson, 1967; Walker and Swanson, 1968b) that is due partly to the weight and tangential movement of overlying tuff. It must be related largely to shearing stresses resulting from laminar movement of viscous material through the confining fissure zones. Exsolution of dissolved gases was probably still tending to expand individual pumice fragments in the slowly moving magma stream; the still-plastic fragments were flattened and stretched in planes of laminar flow. The dilated walls of the fissure zones probably tended to relax and return to their preeruption position during this end stage of eruption, creating compressional stresses that also aided in flattening the fragments of pumice.

REFERENCES

Campbell, Ian, Conel, J. E., Rogers, J. J. W., and Whitfield, J. M., 1958, Possible correlation of Rattlesnake and Danforth formations of eastern Oregon [abs.]: Geol. Soc. America Bull., v. 69, no. 12, pt. 2, p. 1678.

Hoover, D. L., 1964, Flow structures in a welded tuff, Nye County, Nevada [abs.]: Geol. Soc. America Spec. Paper 76, p. 83.

Huber, N. K., and Rinehart, C. D., 1966, Some relationships between the refractive index of fused glass beads and the petrologic affinity of volcanic rocks suites: Geol. Soc. America Bull., v. 77, no. 1, p. 101–110.

Piper, A. M., Robinson, T. W., Jr., and Park, C. F., Jr., 1939, Geology and ground-water resources of the Harney Basin, Oregon, with a statement on precipitation and tree growth, by Lorne Theodore Jessup: U.S. Geol. Survey Water-Supply Paper 841, 189 p.

Ross, C. S., and Smith, R. L., 1961, Ash-flow tuffs—their origin, geologic relations, and identification: U.S. Geol. Survey Prof. Paper 366, 81 p.

Schmincke, Hans-Ulrich, and Swanson, D. A., 1967, Laminar viscous flowage structures in ash-flow tuffs from Gran Canaria, Canary Islands: Jour. Geology, v. 75, no. 6, p. 641–663.

Smith, R. L., 1960, Zones and zonal variations in welded ash flows: U.S. Geol. Survey Prof. Paper 354–F, p. 149–159.

Walker, G. W., and King, P. B., 1969, Geologic map of Oregon: U.S. Geol. Survey Misc. Geol. Inv. I–595, scale 1:2,000,000. [In press]

Walker, G. W., and Swanson, D. A., 1968a, Summary report on the geology and mineral resources of the Harney Lake and Malheur Lake areas of the Malheur National Wildlife Refuge, north-central Harney County, Oregon: U.S. Geol. Survey Bull. 1260–L, p. L1–L17.

——— 1968b, Laminar flowage in a Pliocene soda rhyolite ash-flow tuff, Lake and Harney Counties, Oregon, *in* Geological Survey Research 1968: U.S. Geol. Survey Prof. Paper 600–B, p. B37–B47.

PETROGRAPHY AND HEAVY MINERALS OF THREE GROUPS OF RHYOLITIC LAVAS, PAHUTE MESA, NEVADA TEST SITE

By K. A. SARGENT, Denver, Colo.

Work done in cooperation with the U.S. Atomic Energy Commission

Abstract.—Three groups of Tertiary rhyolitic lavas closely related to known volcanic centers occur on Pahute Mesa in the northern part of the Nevada Test Site. The lavas are useful stratigraphic markers in thick volcanic sections inasmuch as they can be identified and correlated by means of petrography and heavy minerals. Diagnostic nonopaque heavy-mineral assemblages for the three groups are (1) rhyolitic lavas of Quartet Dome—clinopyroxene, olivine, and amphibole, (2) upper rhyolitic lavas of Area 20—biotite and allanite, and (3) lower rhyolitic lavas of Scrugham Peak quadrangle—biotite, sphene, hornblende, and (or) clinopyroxene.

This paper briefly describes three groups of Tertiary rhyolitic lava flows occurring at Pahute Mesa, in the northern part of the Nevada Test Site (fig. 1). The lavas are from oldest to youngest:

Group I. Rhyolitic lavas of Quartet Dome; peralkaline rhyolites that are genetically related to the Silent Canyon volcanic center (Noble and others, 1968; Orkild and others, 1968).

Group II. Upper rhyolitic lavas of Area 20; known to occur only within the Silent Canyon volcanic center and exposed only on Pahute Mesa. Only the upper flows in this calc-alkalic group are discussed in this report.

Group III. Lower rhyolitic lavas of the Scrugham Peak quadrangle; calc-alkalic flows probably extruded from concentric ring-fracture zone on the north side of the Timber Mountain caldera complex (Christiansen and others, 1965). Only the three oldest of five flows in this group are discussed here. They are well exposed on the south face of Pahute Mesa.

The lava flows serve as useful stratigraphic markers in the thick volcanic section penetrated by deep drilling, particularly in areas where ash-flow tuff marker beds are absent. In this report emphasis is placed on the description of major nonopaque heavy-mineral analyses and thin-section petrography, inasmuch as these were the best methods of rhyolite identification.

Acknowledgments.—The writer is indebted to D. R. Miller, R. P. Snyder, John Cook, and J. D. Kibler for their aid in heavy mineral separation; and to F. M. Byers, Jr., and W. D. Quinlivan for modal analyses.

DESCRIPTION OF THE RHYOLITIC LAVAS

Rhyolitic lavas of Quartet Dome

The rhyolitic lavas of Quartet Dome crop out along a broad arcuate zone on the east side of the Silent Canyon volcanic center (fig. 2). The lavas were extruded in late Miocene time from numerous vents close to the main caldera collapse zone of the Silent Canyon center and along concentric ring fracture zones east of the main collapse. Most of the rhyolites studied in the field are endogenous domes which are as much as 1,000 feet high and 1 mile in diameter, and whose external shapes are much like huge beehives. The exterior two-thirds of the flows is coarsely flow layered and vesicular and locally contains thin (generally less than 10 feet thick) black vitrophyres. Zones of flow brecciation as much as 40 feet thick locally occur along outer contacts of the flows. The inner one-third of thick flows is generally dense and jointed.

The rhyolitic lavas of Quartet Dome contain 20–35 percent phenocrysts consisting mainly of quartz (25–30 percent of total phenocrysts), sanidine or anorthoclase (65–70 percent), and mafic minerals (<5 percent) consisting of sparse augite and aegirine-augite, some hypersthene, hornblende, fayalitic olivine, and opaque iron oxides. Phenocrysts are as large as 3 millimeters and are generally euhedral. The groundmass is glassy to microcrystalline and consists mainly of alkali feldspar, less common silica minerals, and sodic-rich py-

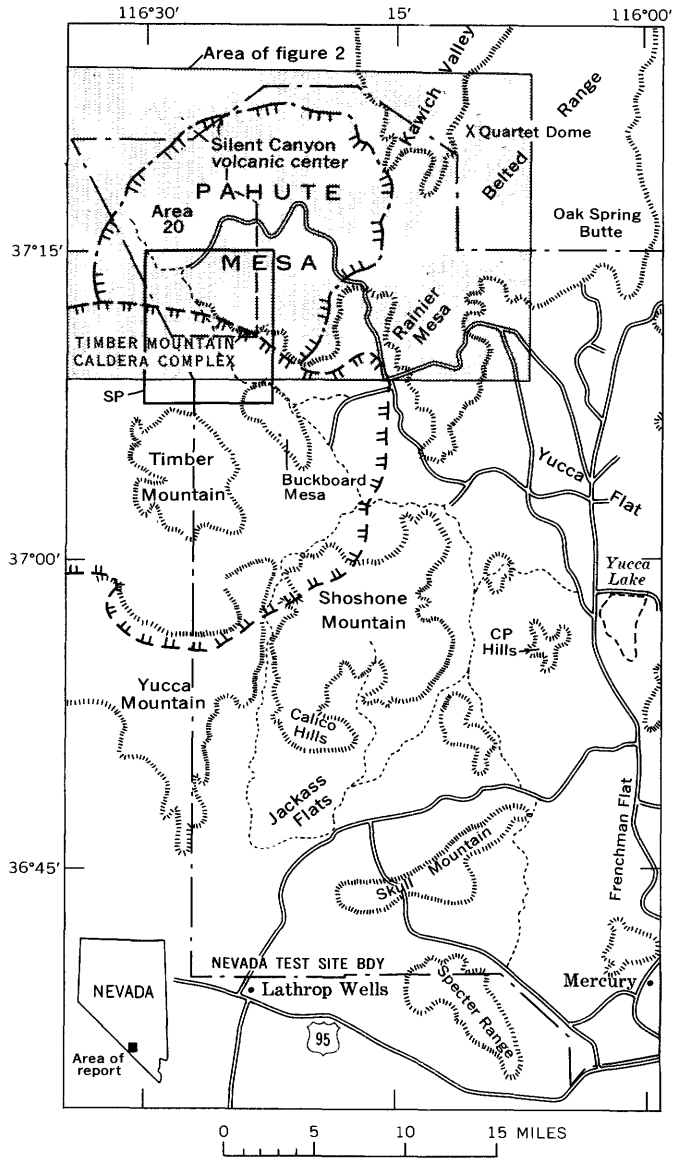

FIGURE 1.—Index map of the Nevada Test Site, showing Pahute Mesa area, generalized topographic features, and caldera outlines (hachured). SP, Scrugham Peak quadrangle.

roxene (aegirine, especially near the tops of the flows). In the lower part of the central zone of the flows, where slow cooling allowed reaction of minerals with volatiles and water vapor, sodic amphiboles and iron oxide pseudomorphs after clinopyroxene and iddingsite after olivine may occur. Throughout the flows, bimodal zircon is invariably present and consists of a small clear variety and a larger pink variety, both with a length-to-breadth ratio of 2:1. Apatite and allanite are common accessory minerals. Biotite occurs rarely, probably as a xenocrystic mineral.

Chemically the lavas are peralkaline and are distinctly different in major- and minor-element content from calc-alkaline suites. Chemical analyses representative of the crystalline zone are given in table 1. Specimens 1 and 4 are from a cooling zone in the upper third of this type of flow. Specimens 2 and 3 are representative of the central crystalline zone containing sodic amphibole. They differ from calc-alkalic flows in having a higher Na+K: Al ratio and higher Fe+Ti+Mn contents, at given silica contents.

TABLE 1.—*Chemical analyses of the crystalline zone of rhyolitic lavas of Quartet Dome, Nevada Test Site, Nev.*

[Major oxides in weight percent, recalculated without H_2O, F, Cl, and CO_2. Analyses by P. L. D. Elmore, S. D. Botts, G. W. Chloe, Lowell Artis, and H. Smith, U.S. Geological Survey]

Specimen No.	1	2	3	4
Serial No.	D700987W	D700988W	D700919W	161331
SiO_2	75. 67	76. 13	75. 97	77. 97
Al_2O_3	12. 26	12. 17	12. 29	10. 66
Fe_2O_3	2. 21	2. 11	2. 02	2. 21
FeO	. 08	. 16	. 28	. 20
MgO	. 35	. 40	. 30	. 10
CaO	. 07	. 19	. 06	. 16
Na_2O	4. 62	4. 22	4. 53	4. 02
K_2O	4. 52	4. 43	4. 33	4. 43
TiO_2	. 11	. 10	. 11	. 16
P_2O_5	. 00	. 00	. 00	. 02
MnO	. 10	. 08	. 13	. 06
Total	99. 99	99. 99	100. 02	99. 99

The nonopaque heavy-mineral assemblage is distinctive and, therefore, useful for correlation purposes. Assemblages from various vertical lithologic zones in the domal flow rhyolites are presented in figure 3 and table 2. The percentages of heavy minerals are fairly consistent throughout the flow with the exception of the central crystalline zone. An apparent relative increase in zircon in the central zone results from the difficulty in identification of altered clinopyroxene and olivine. The diagnostic assemblage is clinopyroxene, olivine, hornblende (or sodic amphibole), and pink and clear zircon.

Upper rhyolitic lavas of Area 20

The upper rhyolitic lavas of Area 20 are limited in areal extent to the caldera formed by the collapse of the Silent Canyon volcanic center (Orkild and others, 1968). The rhyolites crop out locally near the center of the Silent Canyon caldera and have been penetrated in several drill holes on Pahute Mesa (fig. 2). Stratigraphically these flows occur above the Belted Range Tuff (Sargent and others, 1965) of late Miocene age and below the Paintbrush Tuff (Orkild, 1965) of late Miocene age.

Like the rhyolitic lavas of Quartet Dome, the upper rhyolitic lavas of Area 20 appear to be steep-sided

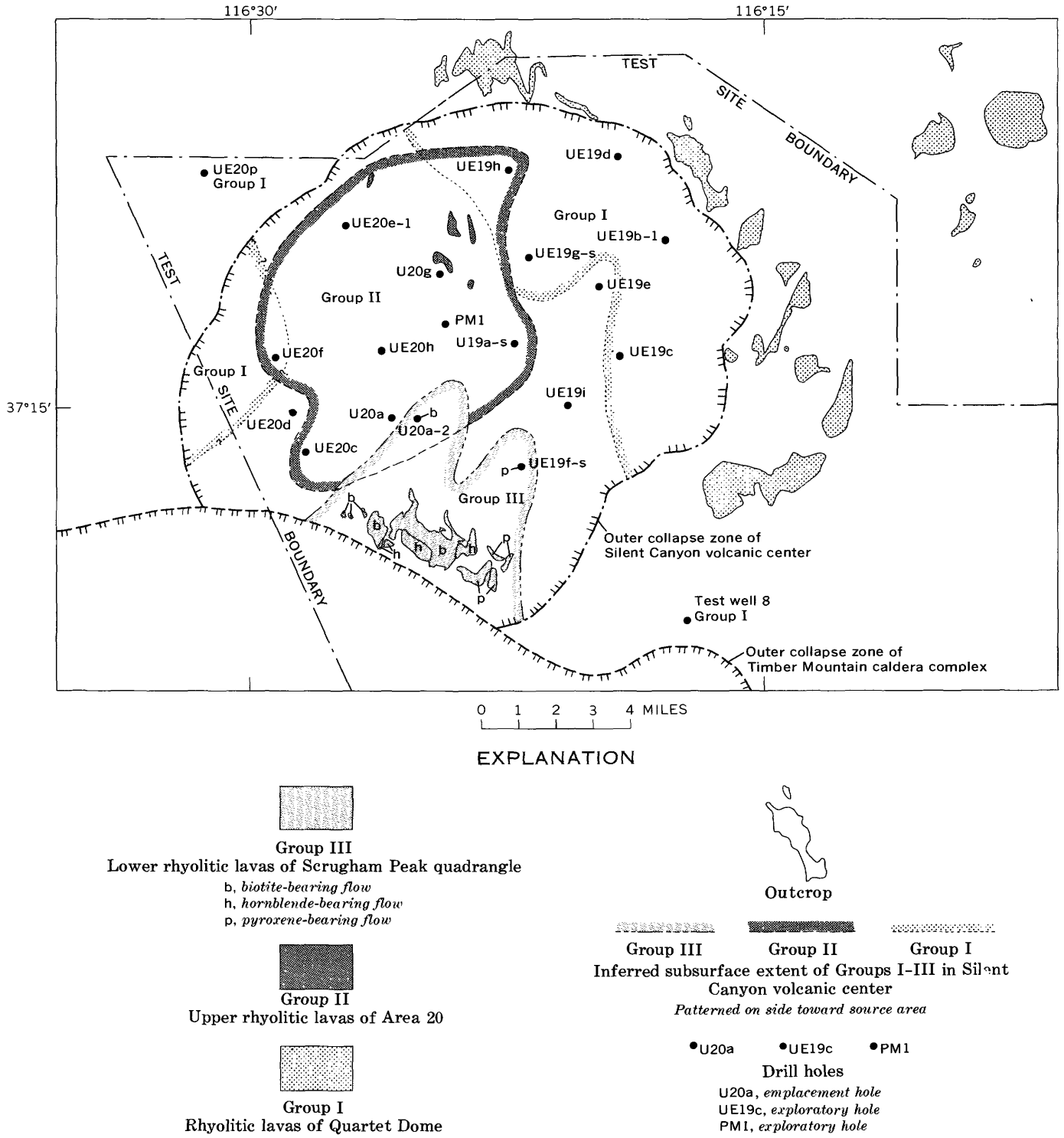

FIGURE 2.—Map of northern part of Nevada Test Site, showing caldera outlines, area of outcrop of lavas, their inferred subsurface extent in Silent Canyon caldera, and subsurface drill-hole control at Pahute Mesa.

TABLE 2.—*Heavy-mineral assemblages of the rhyolitic lavas of Quartet Dome, Nevada Test Site, Nev., based on 137 samples of 13 flows*

[Tr., trace]

Major cooling zonation	Heavy minerals, in volume percent of total nonopaque heavy minerals, averaged by zones								Total nonopaque heavy minerals in samples, in volume percent (approx)
	Clino-pyroxene	Olivine [1]	Amphi-bole	Zircon	Allanite	Biotite	Apatite	Hyper-sthene	
Upper vitrophyre	85	6	1.0	8	Tr.	----	Tr.	±Tr.	0.16
Crystalline zone:									
Upper intermediate part	86	5	1.0	8	----	----	±Tr.	----	.18
Lower intermediate part	65	20	7.0	8	----	----	----	----	.18
Central part	20	10	56.0	14	Tr.	----	Tr.	----	.28
Basal vitrophyre	77	16	1.5	5	0.5	Tr.	Tr.	±Tr.	.30
Basal breccia	82	8	4.0	4	Tr.	2	Tr.	±Tr.	.30

[1] Includes iddingsite.

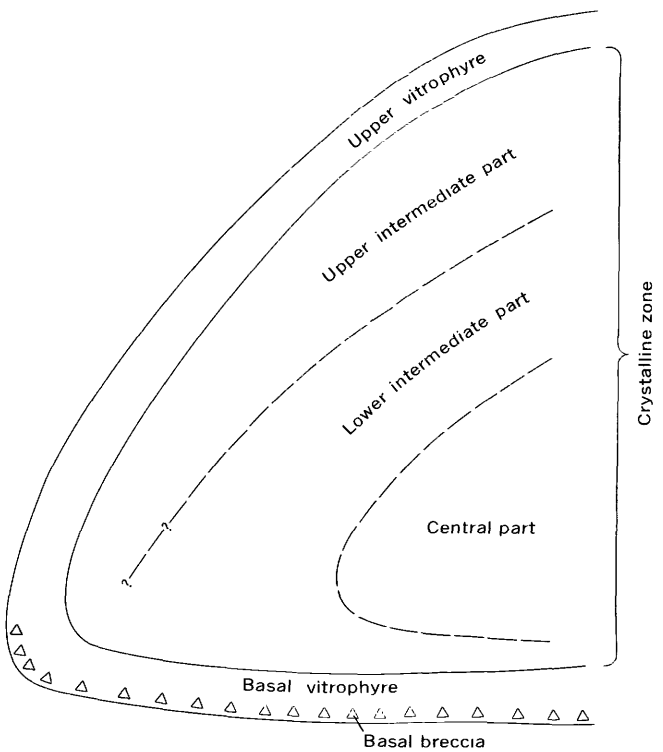

FIGURE 3.—Diagrammatic cross section of rhyolitic lavas on Pahute Mesa, showing major cooling zonations.

domes over which ash-flow tuffs and bedded tuffs thin or pinch out. Individual flows may be as much as 1,200 feet thick, but most flows are 400–500 feet thick. The areal extent of individual flows seems to be somewhat greater than that of the flows of Quartet Dome, possibly owing to a lower initial viscosity and possibly because the Area 20 flows issued from linear fissures, whereas the Quartet Dome flows came from central vents.

Vitrophyres of this group of rhyolitic lavas are light gray where vesicular, dark gray to black where dense, and grayish brown to reddish gray where partly devitrified. Commonly, thick zones of flow breccia exist at the base and thick zones of vesiculated lava exist at the tops of the flows. Generally, the interiors are conspicuously flow layered. The phenocryst content is low (3–10 percent) and consists of alkali-feldspar (40–60 percent of the total phenocrysts), quartz (30–40 percent), plagioclase (5–15 percent), conspicuous biotite (<1 percent), allanite (<1 percent), and trace amounts of zircon, apatite, and clinopyroxene.

Table 3 contains chemical analyses of the upper rhyolites of Area 20. Specimens 1, 2, and 3 are representative of the upper vitrophyre, crystalline zone, and basal vitrophyre, respectively, of lava flow 1. (See fig. 3 and table 4.) Specimen 4 is an upper Area 20 rhyolite whose position is not known with respect to the lava flows shown in table 4.

TABLE 3.—*Chemical analyses of the upper rhyolitic lavas of Area 20, Nevada Test Site, Nev.*

Major oxides, in weight percent, recalculated without H_2O, F, Cl, and CO_2. Analyses 1, 2, and 3 by P. L. D. Elmore, S. D. Botts, G. W. Chloe, and Lowell Artis; analysis 4 by C. L. Parker, U.S. Geological Survey]

Specimen No.	[1] 1	[2] 2	[1] 3	[2] 4
Serial No.	D700994W	D700965W	D700980W	D700851
SiO_2	76.96	79.23	77.10	78.55
Al_2O_3	12.64	11.13	13.00	11.64
Fe_2O_3	.67	.60	.47	.83
FeO	.33	.12	.38	.09
MgO	.10	.10	.16	.05
CaO	.52	.25	.79	.43
Na_2O	3.70	1.82	4.09	2.78
K_2O	4.93	6.68	3.88	5.50
TiO_2	.06	.04	.06	.07
P_2O_5	.00	.00	.00	.01
MnO	.08	.03	.06	.05
Total	99.99	100.00	99.99	100.00

[1] Vitric.
[2] Crystalline.

Nonopaque heavy-mineral analyses from three flows of the upper Area 20 rhyolites show similar assemblages with different ratios of the two diagnostic minerals, biotite and allanite (table 4). Several of these analyses are based on separates from carefully picked drill cut-

TABLE 4.—*Heavy-mineral assemblages of the upper rhyolitic lavas of Area 20, Nevada Test Site, Nev., based on 76 samples*

[Each flow approximately 500 feet thick]

Major cooling zonation	Heavy minerals, in volume percent of total nonopaque heavy minerals, averaged by zones					Total nonopaque heavy minerals in samples, in volume percent (approx)
	Biotite	Allanite	Clinopyroxene	Zircon	Apatite	
Lava flow 3:						
Upper vitrophyre	97.0	2.0	0	1.0	0	0.15
Crystalline zone	96.5	2.0	0	1.5	0	.20
Basal vitrophyre	94.4	3.8	0	1.8	0	.11
Lava flow 2:						
Upper vitrophyre	54.0	40.6	0	4.8	.4	.06
Crystalline zone	60.0	33.0	2.0	5.0	0	.05
Basal vitrophyre	73.0	19.5	.5	6.5	.5	.05
Lava flow 1:						
Upper vitrophyre	87.6	4.3	2.7	4.7	.7	.20
Crystalline zone	80.6	16.2	.6	2.6	0	.20
Basal vitrophyre	81.3	16.0	0	2.7	0	.24

tings, and if some contamination exists it must be very minor.

Remanent heat, pressure, and circulating solutions seem to have had little effect on the heavy mineral assemblages of this group of flows other than local oxidation of the biotite. Samples from all parts of the flows seem to maintain virtually the same assemblage and ratios between heavy minerals.

Lower rhyolitic lavas of Scrugham Peak quadrangle

The lower rhyolitic lavas of Scrugham Peak quadrangle are exposed along the south face of Pahute Mesa north of the Timber Mountain caldera complex (figs. 1 and 2), where they are interlayered with Paintbrush Tuff (Byers and Cummings, 1967). The flows, from youngest to oldest, are informally called biotite-bearing, hornblende-bearing, and pyroxene-bearing rhyolite flows of Scrugham Peak quadrangle. Of these three flows, two are below and one above the Tiva Canyon Member of Paintbrush Tuff (Orkild, 1965). Like the flows of Area 20, the three Scrugham Peak flows may be as much as 1,000 feet thick in places, but in most outcrops they are less than 600 feet thick. All the flows have a brecciated vitric envelope, which is dark gray to black and dense at the base (basal vitrophyre) and light gray and vesiculated at the top (upper vitrophyre). Within the brecciated envelope, an unbrecciated vitrophyre as much as 50 feet thick encloses a thick crystalline zone (fig. 3). The crystalline zone, which constitutes the bulk of the flow, is generally light gray to reddish gray and massive to flow banded. Locally, lithophysae as much as 4 inches in diameter are common between flow layers.

The flows contain 5–11 percent phenocrysts, primarily alkali feldspar and plagioclase, with minor biotite, hornblende, and (or) clinopyroxene (table 5). Sphene, apatite, zircon, and opaque oxides are present in all flows. Five chemical analyses of the vitrophyres from the three flows (table 6) show the consistency of the chemistry. Lesser amounts of CaO, MgO, and total iron in the hornblende-bearing flow have been directly related to phenocryst content (F. M. Byers, Jr., oral commun., 1966).

The three flows of Scrugham Peak quadrangle have similar but not identical nonopaque heavy-mineral assemblages (table 7). All the flows contain biotite, sphene, allanite, and apatite. Nonopaque heavy-mineral examination shows that the presence of small but persistent amounts of clinopyroxene characterize the pyroxene-bearing flow, a high percentage of hornblende distinguishes the hornblende-bearing flow, and a relatively high percentage of biotite with very minor or no hornblende or clinopyroxene distinguishes the biotite-bearing flow. Slow cooling and residual volatiles in the centers of the flows caused oxidation of the biotite and resulted in an apparent decrease in its percentage that is similar to the clinopyroxene and olivine decrease in the flows of Quartet Dome.

SAMPLING AND SEPARATION PROCEDURE FOR HEAVY-MINERAL ANALYSES

To determine whether the heavy-mineral assemblages in each of the rhyolitic lavas on Pahute Mesa were consistent enough to be used as criteria for correlating a flow in one area with a flow in another, samples were taken from various lithologic zones of exposed flows. Heavy-mineral assemblages of the vitric zones, especially the basal vitrophyres, proved most consistent for correlation in this study. Samples taken at various vertical and lateral positions in the interior of flows showed that all similar zones of crystallization of related

TABLE 5.—*Average modal analyses of three rhyolitic lavas of Scrugham Peak quadrangle, Nevada Test Site, Nev.*

[Modified from Byers and Cummings (1967); Tr., trace]

Rhyolite flows and thickness	Phenocrysts in rock (volume percent)	Phenocrysts, in percent of total phenocrysts									
		Alkali feldspar	Plagioclase	Biotite	Hornblende	Clinopyroxene	Opaque oxide	Sphene	Zircon	Allanite	Apatite
Biotite bearing (0 to ±1,000 ft)	11	46	45	5.0	0.01	0.02	2	1	Tr.	Tr.	Tr.
Hornblende bearing (0 to ±400 ft)	5	79	18	.1	2.0	0.0	1	1	Tr.	Tr.	Tr.
Pyroxene bearing (0 to ±980 ft)	10	62	30	4.0	0.0	.4	2	1	Tr.	Tr.	Tr.

TABLE 6.—*Chemical analyses of vitrophyres of rhyolitic lavas of Scrugham Peak quadrangle, Nevada Test Site, Nev.*

[Major oxides in weight percent, recalculated without H_2O, F, Cl, and CO_2. Analyses by P. L. D. Elmore, S. D. Botts, G. W. Chloe, Lowell Artis, and H. Smith, U.S. Geological Survey]

Rhyolite flow	Pyroxene bearing	Hornblende bearing		Biotite bearing	
Cooling zone	Upper vitrophyre	Basal vitrophyre	Upper vitrophyre	Basal vitrophyre	Upper vitrophyre
Laboratory No.	160678	161148	161149	161147	161146
SiO_2	74.28	75.93	75.43	74.68	75.41
Al_2O_3	14.11	13.90	14.14	14.09	13.57
Fe_2O_3	.78	.61	.66	.81	.82
FeO	.43	.33	.26	.38	.38
MgO	.28	.04	.16	.27	.18
CaO	.53	.46	.31	.58	.60
Na_2O	3.73	3.63	3.56	3.91	3.63
K_2O	5.50	4.98	5.34	5.04	5.18
TiO_2	.24	.04	.04	.15	.17
P_2O_5	.03	.00	.00	.00	.00
MnO	.09	.08	.08	.08	.07
Total	100.00	100.00	99.98	99.99	100.01

flows had similar assemblages and that most had the same relative percentages of heavy minerals.

In this study, the samples were crushed to pass 60-mesh screen, washed to remove rock powder, and dried. A 50-cubic-centimeter sample was split from the bulk crushed rock and placed in a separatory funnel with bromoform (specific gravity $2.85 \pm .01$). The heavy separate was cleaned with acetone, dried, and measured in a small-diameter graduated metric cylinder. The magnetic portion was removed with a strong hand magnet, and the remainder was measured and calculated to percentage of total rock. The nonmagnetic heavy separate was then split to the desired amount and mounted in index oil $n=1.54$ for identification and grain counting under the petrographic microscope.

Volumetric measurements of heavy minerals were used so that direct comparison with thin-section modal analyses could be made. The percentages of the major nonopaque accessory minerals from thin-section modes (5,000–10,000 points) were found to compare closely with the percentages of the major nonopaque heavy minerals, especially those from vitric samples (F. M. Byers, Jr., oral commun., 1966). This is rather surprising because (1) only about 70 percent of the total heavy minerals are assumed to be recovered (Lee and Dodge, 1964, p. 1663) and (2) the volume measurements are subject to error because of inadequate control of compaction of crushed sample in the measuring container.

SUMMARY AND CONCLUSIONS

Three distinct groups of rhyolitic lavas occur on Pahute Mesa; each is related to its own volcanic episode and each is petrographically distinctive. They are: rhyolitic lavas of Quartet Dome, rhyolitic lavas of Area 20, and rhyolitic lavas of Scrugham Peak quadrangle.

The rhyolitic lavas of Quartet Dome are genetically related to the peralkaline rocks of the Silent Canyon volcanic center. They are distinctive, both mineralogically and chemically, and can be readily distinguished from the more abundant calc-alkalic rhyolites and quartz latites of the rest of the Nevada Test Site. The lavas of Quartet Dome constitute about 10 percent of the total volume of volcanic rock extruded from this center. They seem to have been extruded from central vents along arcuate zones concentric about the caldera collapse zone, and flowed into and out of the caldera area. The lavas contain a nonopaque heavy-mineral suite characterized by clinopyroxene, olivine, and amphibole.

The rhyolitic lavas of Area 20 belong to a calc-alkaline suite of tuffs and lavas that are largely confined in areal extent to the preexisting Silent Canyon volcanic depression. The chemistry of the tuffs and rhyolites of Area 20 is not distinctive, and is similar to that of the rhyolitic lavas of Scrugham Peak quadrangle or any other calc-alkaline suite occurring on the Test Site.

TABLE 7.—*Heavy-mineral assemblages of three rhyolitic lavas of Scrugham Peak quadrangle, Nevada Test Site, Nev., based on 29 samples*

Major cooling zonation	Heavy minerals, in volume percent of total nonopaque heavy minerals, averaged by zones							Total nonopaque heavy minerals in samples, in volume percent (approx)
	Biotite	Sphene	Hornblende	Clinopyroxene	Allanite	Zircon	Apatite	
Biotite-bearing flow:								
Upper vitrophyre	51.2	28.2	2.8	0.15	2.6	1.3	1.3	0.45
Crystalline zone	43.5	33.5	.5	0	8.0	12.0	2.5	.84
Basal vitrophyre	56.5	35.7	2.5	.17	2.3	1.5	1.4	.53
Hornblende-bearing flow:								
Upper vitrophyre	2.2	36.2	58.4	0	.8	1.8	.4	.10
Crystalline zone	No samples							
Basal vitrophyre	3.1	24.1	59.7	0	.8	1.1	1.2	.20
Pyroxene-bearing flow:								
Upper vitrophyre	64.9	20.0	0	7.9	3.8	2.8	.54	.37
Crystalline zone	51.2	30.7	0	6.5	4.5	6.6	.4	.60
Basal vitrophyre	58.0	25.4	0	13.4	1.6	1.6	0	.16

The nonopaque heavy-mineral suite, consisting largely of biotite and allanite, is diagnostic, however.

The rhyolitic lavas of Scrugham Peak quadrangle were extruded later than the rhyolites of Area 20, from vents at or very close to the area of outcrop on the south face of Pahute Mesa. The lavas probably flowed northward from a ring-fracture zone of the Timber Mountain caldera complex. They can be distinguished petrographically by a nonopaque heavy-mineral suite consisting of biotite, sphene, hornblende, and (or) clinopyroxene.

Investigation of the chemistry, thin-section petrography, and nonopaque heavy-mineral analyses indicated that the lavas could be distinguished most expeditiously by the latter two methods. Moreover, certain lithologic zones, namely the basal vitrophyres, contained the best preserved and most consistent mineral assemblages for correlation and distinction of each group. Distinction of the three groups of lavas aided in subsurface correlation of Pahute Mesa drill holes and helped in piecing together the geologic history of the area.

REFERENCES

Byers, F. M., Jr., and Cummings, David, 1967, Geologic map of the Scrugham Peak quadrangle, Nye County, Nevada: U.S. Geol. Survey Geol. Quad. Map GQ–695.

Christiansen, R. L., Lipman, P. W., Orkild, P. P., and Byers, F. M., Jr., 1965, Structure of the Timber Mountain caldera, southern Nevada, and its relation to basin-range structure, *in* Geological Survey Research 1965: U.S. Geol. Survey Prof. Paper 525–B, p. B43–B48.

Lee, D. E., and Dodge, F. C. W., 1964, Accessory minerals in some granitic rocks in California and Nevada as a function of calcium content: Am. Mineralogist, v. 49, nos. 11–12, p. 1660–1669.

Noble, D. C., Sargent, K. A., Mehnert, H. H., Ekren, E. B., and Byers, F. M., Jr., 1968, Silent Canyon volcanic center, *in* Eckel, E. B., ed., Nevada Test Site: Geol. Soc. America Mem. 110, p. 65–76.

Orkild, P. P., 1965, Paintbrush Tuff and Timber Mountain Tuff of Nye County, Nevada, *in* Cohee, G. V., and West, W. S., Changes in stratigraphic nomenclature by the U.S. Geological Survey, 1964: U.S. Geol. Survey Bull. 1224-A, p. A44–A51.

Orkild, P. P., Byers, F. M., Jr., Hoover, D. L., and Sargent, K. A., 1968, Subsurface geology of Silent Canyon caldera, Nevada Test Site, Nevada, *in* Eckel, E. B., ed., Nevada Test Site: Geol. Soc. America Mem. 110, p. 77–86.

Sargent, K. A., Noble, D. C., and Ekren, E. B., 1965, Belted Range Tuff of Nye and Lincoln Counties, Nevada, *in* Cohee, G. V., and West, W. S., Changes in stratigraphic nomenclature by the U.S. Geological Survey, 1964: U.S. Geol. Survey Bull. 1224-A, p. A32–A36.

DISTRIBUTION OF NONOPAQUE HEAVY MINERALS IN MIOCENE AND PLIOCENE ROCKS OF CENTRAL WYOMING AND PARTS OF ADJACENT STATES

By N. M. DENSON, Denver, Colo.

Abstract.—Miocene and Pliocene rocks in central Wyoming and the northern High Plains of western Nebraska and northeastern Colorado contain two distinct assemblages of nonopaque heavy minerals. A plutonic assemblage is characterized by blue-green hornblende, garnet, epidote, zircon, tourmaline, actinolite, sphene, and gray-green biotite; it generally constitutes more than 46 percent of the nonopaque heavy minerals in upper Miocene and Pliocene rocks (Ogallala and South Pass Formations), and Miocene North Park Formation. A volcanic assemblage is characterized by green-brown hornblende and oxyhornblende, augite, hypersthene, and red-brown biotite; it generally constitutes 70–90 percent of the nonopaque heavy minerals in lower Miocene rocks (Arikaree Formation). These heavy-mineral assemblages reliably reflect Cenozoic volcanism and tectonism and are distinct enough to correlate the formations in one area with those in another.

Throughout central Wyoming and adjacent areas Miocene and Pliocene rocks comprise two readily recognizable lithogenetic units that have been mapped discontinuously eastward from South Pass at the southeast end of the Wind River Range through the Granite Mountains and Shirley Basin-Bates Hole areas of central Wyoming, along the north and east flanks of the Laramie Mountains of central Wyoming, and into western Nebraska and northeastern Colorado. These rocks have a maximum thickness of about 2,800 feet. The lower unit (Arikaree Formation and equivalents) is chiefly very fine grained tuffaceous sandstone overlain by an upper unit (Ogallala Formation and equivalents) of medium- to coarse-grained sandstone and conglomerate. Beds of volcanic ash and limestone occur throughout the sequence. The Miocene rocks in most areas overlie rocks of Oligocene age with only slight disconformity, but in a few areas they unconformably overlie the truncated edges of rocks ranging in age from Eocene to Precambrian. In some areas the Miocene and Pliocene rocks have been tilted and faulted along high-angle faults with stratigraphic displacements of at least 2,000 feet. In general, however, the Miocene and Pliocene rocks away from the major mountain uplifts dip very gently, the low dips probably representing original surfaces of deposition.

The courses of most of the present-day major streams that drain the intermontane basins of central Wyoming and the High Plains were established by streams flowing on a surface of late Miocene (and Pliocene) age. Present-day erosion is largely exhuming an ancient antecedent drainage pattern developed prior to Miocene deposition.

During the course of mapping middle and upper Tertiary formations from western Nebraska and northeastern Colorado into central Wyoming, 550 representative samples of Miocene and Pliocene rocks from 54 measured sections were collected for heavy-mineral analysis. A study of the nonopaque mineral grains from the very fine grained sand fractions of these samples revealed that differences in the nonopaque heavy-mineral assemblages are useful in correlating Miocene and Pliocene rocks in adjacent areas and that the nonopaque heavy minerals reliably reflect Cenozoic volcanism and tectonism.

Only the nonopaque heavy minerals in the very fine sand-size fraction (0.062–0.125 mm) were studied. Comparisons between the various groups of samples are, therefore, for heavy minerals from the same size range. The mineral ratios of the nonopaque assemblages were established by counting 100 grains or more per sample after most of the magnetite, ilmenite, ferruginous and clay aggregates, leucoxene, and pyrite had been removed. Sample preparation, techniques of study, and interpretations placed on the heavy-mineral analyses are described by Sato and Denson (1967) and hence are not described here.

Samples of vitric tuff and volcanic ash of Miocene and Pliocene age from the northern High Plains and the intermontane basins of central Wyoming were also

U.S. GEOL. SURVEY PROF. PAPER 650–C, PAGES C25–C32

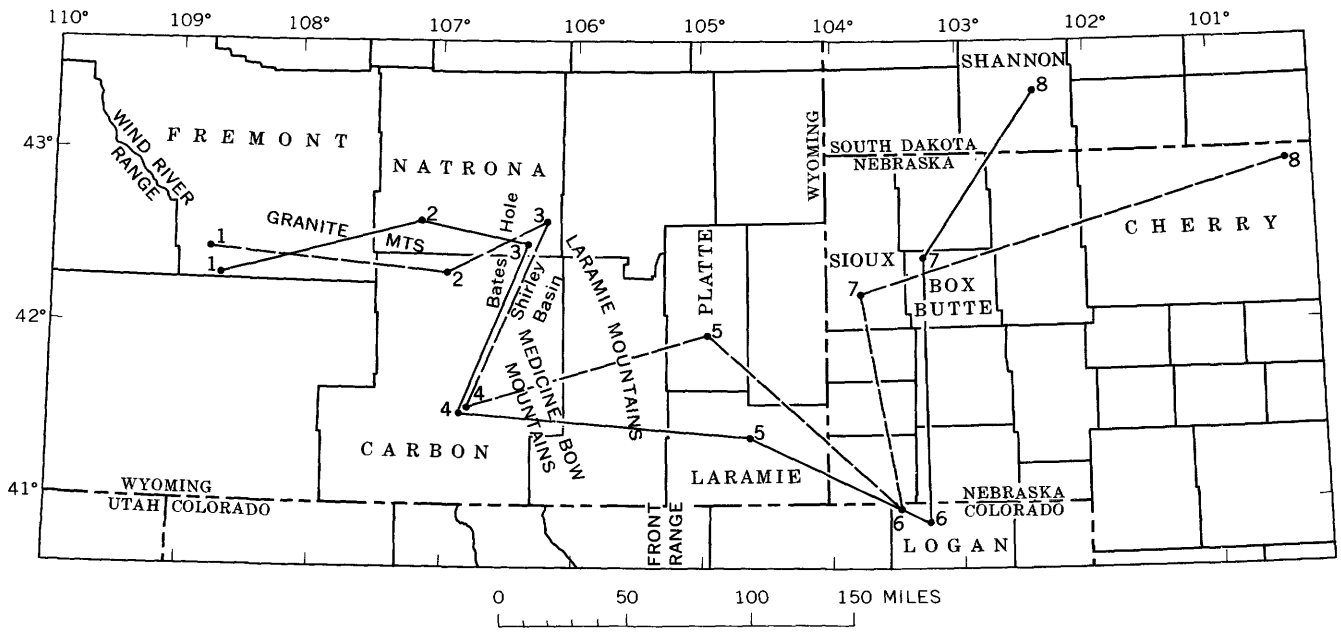

FIGURE 1.—Index map showing locations of stratigraphic sections where samples of Miocene and Pliocene rocks were collected for heavy-mineral analysis. Dashed line indicates Pliocene and upper Miocene rocks; solid line, lower Miocene rocks. (See table 1 for names and precise locations of sections.)

studied to help in establishing which heavy-mineral assemblages are largely of volcanic origin. Samples from terraces deposited by streams draining only Precambrian igneous and metamorphic terranes in the Front Range of Colorado, the Medicine Bow, Laramie, Wind River, and Granite Mountains in Wyoming, and the Black Hills of South Dakota were studied to establish which heavy-mineral assemblages were derived largely from the cores of the major mountain ranges.

The present study of the heavy-mineral assemblages from the Miocene and Pliocene stratigraphic sequence reveals that most of the lower half of the sequence is of volcanic derivation, whereas most of the upper half is locally derived clastic material.

Acknowledgments.—The author is indebted to Robert F. Gantnier, Philip G. Hanna, Thomas D. Hessin, and David E. Schieck for making size analyses and preparing more than 550 slides of heavy minerals from Miocene and Pliocene sedimentary rocks and 45 slides from samples of terrace deposits taken along present-day streams that drain only Precambrian metamorphic and igneous terranes in Colorado, Wyoming, and South Dakota. Laura W. McGrew supplied information on the Wheatland area and loaned rock samples from several wells. Peter M. Banks assisted with the field mapping and helped collect representative samples from measured stratigraphic sections. Mineral counts on all samples were made by W. A. Chisholm and Yoshiaki Sato. The interpretation and organization of the field and laboratory data were the responsibility of the author.

SELECTION OF REPRESENTATIVE DATA

Sixteen stratigraphic sections were selected to portray the most significant lithologic and mineralogic variations of Miocene and Pliocene rocks within an area about 400 miles long and 200 miles wide and to illustrate clearly the twofold lithic subdivision of these rocks. The locations of the sections selected are given in figure 1 and table 1. Heavy-mineral analyses of the 178 samples from these sections are shown graphically on figure 3.

The following publications describe the diagnostic faunas of the Miocene and Pliocene sequence from which most of the samples were collected: Black (1961), Cook and Cook (1933), Elias (1942), Galbreath (1953), L. W. McGrew (1963), P. O. McGrew (1951), Lugn (1939), Moore (1959), Rachou (1951), Rich (1962), Schultz and Falkenbach (1949), Schultz and Stout (1955), Stecher, Schultz, and Tanner (1962), Van Houten (1964), Voorhies (1965), Wilson (1960), and Wood, Chaney, Clark, Colbert, Jepsen, Reeside, and Stock (1941).

STRATIGRAPHIC AND AGE RELATIONSHIPS

In general, after Darton's (1898) pioneering stratigraphic work, Miocene stratigraphy in the region covered by this report was interpreted locally and the

TABLE 1.—*Locations of stratigraphic sections from which samples were collected from Miocene and Pliocene rocks for heavy-mineral analysis*

Stratigraphic section (fig. 1)	Name of section	Locality			
		County	Section	Township (north)	Range (west)
UPPER MIOCENE AND PLIOCENE					
Wyoming					
1	South Pass (Wind River Range)	Fremont		28, 29	99, 100
2	Buzzard Ranch (Granite Mountains)	Carbon	11, 16	27	85
3	Bates Hole and vicinity	Natrona		31	78
4	Saratoga Valley	Carbon	11, 13	18	84
5	Wheatland (southeast Wyoming)	Platte	13, 24	23	68
Colorado					
6	Kennesaw Point (northeast Colorado)	Logan	27	12	55
Nebraska					
7	Sheep Creek (Nebraska panhandle)	Sioux	29, 32	26	55
8	Valentine (northwest Nebraska)	Cherry	10, 22	34	27
LOWER MIOCENE					
Wyoming					
1	Continental Peak (Wind River Range)	Fremont	24	27	100
2	Beulah Lake (Granite Mountains)	Natrona	32	31	86
3	Twin Buttes	do	7	29	79
4	Pick Ranch	Carbon	9, 17	18	84
5	Cheyenne (southeast Wyoming) [1]	Laramie	3	16	65
Colorado					
6	Martin Canyon (northeast Colorado)	Logan	27	11	53
Nebraska					
7	Marsland (Nebraska panhandle)	Box Butte	8, 17, 20	28	51
South Dakota					
8	Big Badlands (south-central South Dakota)	Shannon	20	39	43

[1] Drill cuttings.

interpretation was based largely on paleontology. Little emphasis was placed on persistent lithologic characteristics from basin to basin. Rocks in many areas did not yield diagnostic fossils, and a systematic petrographic study was not coordinated with regional mapping. It is not surprising, therefore, that correlations and age assignments are in dispute.

Heavy-mineral, faunal, and field relations indicate to the author that the Miocene (and Pliocene) of central Wyoming and adjacent areas can be divided into two units. The lower unit referred to the Arikaree Formation and equivalents by Sato and Denson (1967, p. C42, fig. 4) is predominantly windblown buff and tan fine- to medium-grained generally poorly bedded tuffaceous sandstone that contains abundant tiny rounded grains of bluish-gray magnetite. Lateral persistence in lithology and the general absence of coarse detritus and locally derived debris from the adjacent highlands are outstanding characteristics of rocks assigned to the lower unit. The upper unit referred to as the Ogallala Formation and equivalents by Sato and Denson (1967, p. C42, fig. 4) is mostly sandstone, algallike limestone, siltstone, and claystone which grade mountainward into fanlike deposits of coarse-grained sandstone, conglomerate, and gravel. The basal contact of the upper unit becomes a pronounced unconformity near the mountains, but near some of the basin centers in central Wyoming it appears conformable.

Miocene and Pliocene rocks were correlated from the southeast end of the Wind River Range of western Wyoming eastward to the Big Badlands-Valentine

area of south-central South Dakota and northwestern Nebraska, a distance of about 400 miles. The major rock units (formations) have been mapped over wide areas and thus are known to have lithologic continuity. Some of the stratigraphic units are useful cartographic units in some areas, but areal mapping and heavy-mineral studies clearly indicate that they do not have regional lithologic significance. They are differentiated largely on faunal rather than lithologic criteria. Lithologic samples collected from the Marsland Formation (top of lower Miocene), for example, cannot be distinquished on the basis of nonopaque heavy-mineral assemblages from samples collected from the Harrison Sandstone, which is in the middle part of lower Miocene, or from the Monroe Creek and Gering Sandstones, which are in the lower part of lower Miocene. Yet, slight color differences and the presence in some areas of an unconformity at the base of the Marsland make it possible to differentiate the Marsland locally from the underlying rocks of Arikaree age. Similarly, lithologic samples from the Miocene Runningwater Formation of Cook (1965) and Sheep Creek Formation and the Pliocene Valentine Formation of Schultz and Stout (1961) cannot be distinguished from one another on the basis of nonopaque heavy-mineral assemblages. Locally, however, slight color differences and bedding characteristics permit these units to be recognized individually and mapped separately.

The Trail Creek, Box Butte, and Sand Canyon local faunas and the Spoon Butte Beds of Peterson (1909) refer to specific local areas where the vertebrate faunas from Miocene and Pliocene strata may be quite distinct and distinguishable from one another. Because the rocks containing the faunas cannot be separated from one another on the basis of lithologic criteria, these terms are principally biostratigraphic or faunal designations useful only in establishing the chronology of the rocks containing the faunas.

The position of the Miocene-Pliocene boundary in the northern High Plains of western Nebraska and southeastern Wyoming has long been debated. As of this date no agreement among vertebrate paleontologists has been reached. Some vertebrate paleontologists (for example, Wood and others, 1941, p. 27) consider the oldest of several local faunas of the Ogallala to be of latest Miocene age, whereas others (for example, Schultz and Falkenbach, 1949, p. 80, 83) believe that all the Ogallala is Pliocene. Lewis (1964, p. D22) has also outlined these differences in correlation.

Regardless of the position of the Miocene-Pliocene boundary in the stratigraphic sequence, it is significant that the rocks unconformably overlying the Arikaree comprise a single lithogenetic unit whose members can be differentiated chiefly on the basis of vertebrate faunas. Within this widespread deposit of locally derived detritus there are undoubtedly numerous diastems, local unconformities, and a wide variation in lithologies both laterally and vertically. Such variations, however, have little regional importance and can be used only locally in conjunction with vertebrate evidence to differentiate the various members. The Miocene-Pliocene faunal boundary, therefore, probably has little bearing on the depositional history of the upper Cenozoic rocks in central Wyoming, western Nebraska, and northern Colorado.

Recent isotope age determinations and their bearing on the Miocene-Pliocene boundary in Europe (Funnell, 1964) may cause a reevaluation of the temporal divisions of the Miocene and Pliocene rocks and their associated faunas in America. For example, the 12- to 13-million-year age for this boundary in America as dated by Evernden, Curtis, Obradovich, and Kistler (1961, p. 85) and by Kulp (1961, p. 1109, 1111) is not in agreement with the 7-million-year age for the Miocene-Pliocene boundary on Elba Island, Italy. If the younger age for this boundary is used in America perhaps rocks much higher stratigraphically than the Valentine Formation and its lateral equivalents may be of late Miocene age.

PHYSICAL CHARACTERISTICS

The lower Miocene rocks are mostly well-sorted moderately calcareous tuffaceous sandstone containing a relatively large percentage of very fine grained heavy minerals, whereas the upper Miocene (and Pliocene) rocks in marked contrast show a significantly larger average grain-size distribution accompanied by noticeably less uniform distribution of the sand-size fractions. As shown graphically in figure 3, these poorly sorted upper Miocene (and Pliocene) rocks are moderately calcareous but contain relatively small percentages of very fine grained heavy minerals.

In central Wyoming the Ogallala and its equivalents can be readily distinguished in hand specimen from the underlying Arikaree by the ubiquitous occurrence of needlelike glass shards in calcareous, sandy, or siliceous beds. In southeastern Wyoming, northeastern Colorado, or western Nebraska, however, the Ogallala and equivalents can be differentiated in the field from the Arikaree and equivalents only by their very irregular bedding, very poor sizing, and general lack of needle-shaped crystals of hornblende and augite.

HEAVY MINERALS

The sedimentary rocks described and designated as of Arikaree and Ogallala age in this report contain two distinct assemblages of nonopaque heavy minerals: (1) plutonic minerals—those derived largely from the

weathering of Precambrian metamorphic and plutonic rocks and their sedimentary cover, and (2) volcanic minerals—those that are largely the products of explosive volcanic eruptions. The plutonic minerals are generally rounded to subrounded because they were transported by water, whereas the volcanic minerals are generally angular to subangular because they were distributed largely through the atmosphere.

An average of the nonopaque heavy-mineral assemblages from 46 samples collected from terrace deposits of streams draining only Precambrian terrane in six of the major mountain uplifts of northern Colorado, Wyoming, and South Dakota clearly shows that the plutonic assemblage is characterized by the abundance of blue-green hornblende, garnet, epidote, zircon, tourmaline, actinolite, sphene, and biotite (gray-green). (See fig. 2*A*; abbreviations used in illustration are explained in table 2.) Similarly, an average of 22 samples of vitric tuff and volcanic ash from the Miocene and Pliocene rocks of the middle Rocky Mountains and High Plains areas indicates that the volcanic assemblage is characterized by green-brown hornblende and oxyhornblende (red), augite, hypersthene, and red-brown biotite. (See fig. 2*B*.)

TABLE 2.—*Abbreviations used in figures 2 and 3*

MINERALS

Actinolite	Act	Pyroxene	Pyr
Amphibole	Amp	Hypersthene	Hyp
Hornblende	Hbl	Sillimanite	Sil
Apatite	Apa	Sphene	Sph
Biotite	Bio	Staurolite	Sta
Chlorite	Chl	Tourmaline	Tou
Epidote	Epi	Zircon	Zir
Garnet	Gar	Zoisite	Zoi
Kyanite	Kya		

COLORS

Blue	Bl	Green	Gr
Brown	Br	Red	Rd

A small proportion of some minerals, such as sphene and zircon, which are interpreted in figure 3 as plutonic, may be of volcanic origin. Conversely, a small proportion of the green-brown hornblende and augite interpreted in figure 3 as volcanic may be plutonic. However, the percentages are too small, as indicated in figures 2*A* and 2*B*, to affect the interpretations placed upon the ratio of volcanic minerals to plutonic minerals in any particular sample group. A closer assessment of the small proportions of these minerals seems, to the author, neither practical nor possible.

Figure 3 shows graphically the abundance of the volcanic assemblage—green-brown hornblende and pyroxene (augite and hypersthene) in the very fine grained sandstone which makes up most of the lower Miocene Arikaree Formation. This abundance is in marked contrast to the relatively low percentages of these minerals in the overlying rocks assigned on lithologic

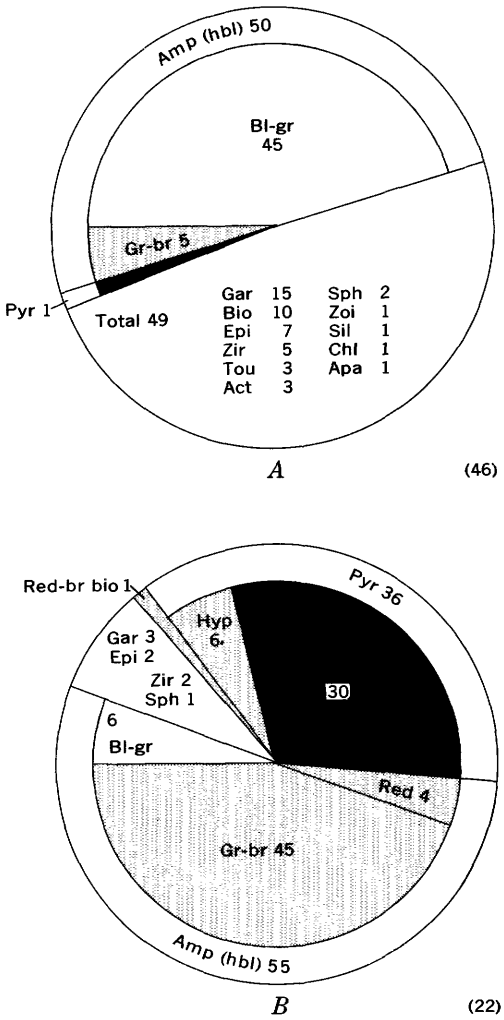

FIGURE 2.—Average percentages of nonopaque heavy minerals in the very fine sand fractions. White, mostly plutonic and metamorphic minerals; stippled, mostly volcanic minerals; black, augite. Numbers in parentheses are number of samples studied. Abbreviations are explained in table 2. *A*, samples from deposits of streams draining Precambrian igneous and metamorphic rocks in selected areas in Colorado, Wyoming, and South Dakota. *B*, samples of vitric tuff and volcanic ash from Miocene and Pliocene rocks in the intermontane basins of central Wyoming and the northern High Plains.

and faunal evidence to the upper Miocene and Pliocene Ogallala and South Pass Formations and Miocene North Park Formation. A striking similarity exists between the relative proportions of the nonopaque heavy minerals in the lower Miocene sedimentary rocks of the Arikaree Formation and those in the vitric tuff and volcanic ash (fig. 2*B*), further suggesting their volcanic affinities.

In contrast, the nonopaque heavy-mineral assemblage in the upper Miocene and Pliocene rocks is chiefly

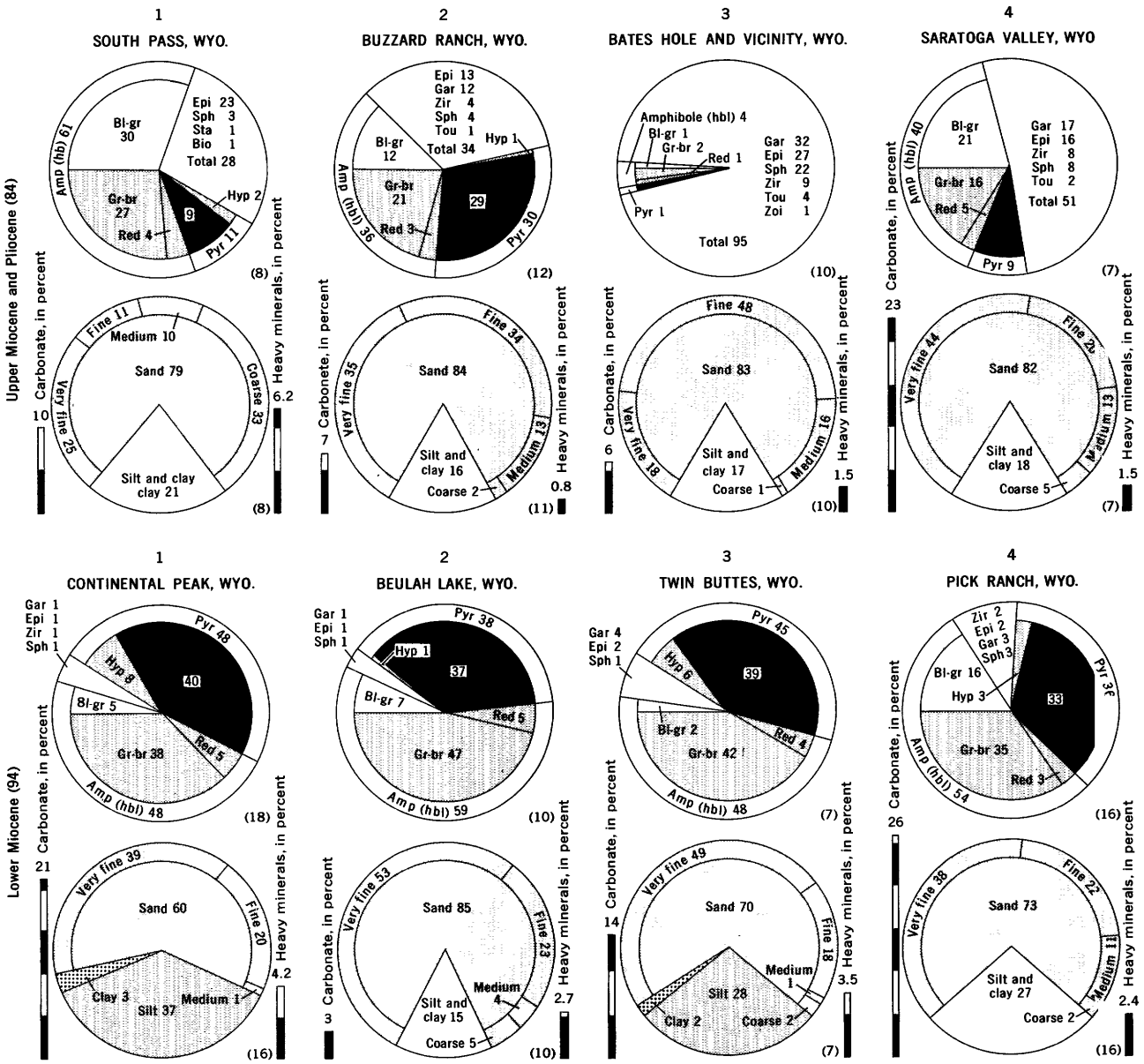

FIGURE 3.—Average percentages of very fine grained nonopaque heavy minerals (upper circle of each pair), grain-size analyses (lower circle of each pair), and carbonate content for grab samples of lower Miocene (Arikaree, Gering, Monroe Creek, Harrison, and Marsland Formations and equivalents) and upper Miocene and Pliocene rocks (Ogallala and South Pass Formations and equivalents) from central Wyoming and the northern High Plains. White, mostly plutonic and metamorphic minerals; stippled, mostly volcanic minerals; black, augite. Total of very fine grained nonopaque minerals equals 100 percent. Numbers within circles and at top of bar scales (carbonate at left of circles, heavy minerals at right) are percentages; numbers in parentheses are number of samples studied. Asterisk (*) indicates carbonate analyses not made.

blue-green hornblende, garnet, and epidote. These minerals are largely the product of weathering of the Precambrian highlands and reflect tectonism and uplift. The very low percentage of plutonic minerals in the Arikaree Formation may indicate that by the end of Oligocene time most of the mountains were blanketed by lower and middle Tertiary sediments or reduced to low relief. Thus the cores of the mountains could not contribute significantly to the lower Miocene deposits.

CONCLUSIONS

The Miocene and Pliocene rocks of central Wyoming and parts of adjacent States can be divided on the basis of lithology and faunal data into (a) a lower highly tuffaceous unit (Arikaree Formation and its equivalents), which contains a diagnostic assemblage of nonopaque heavy minerals of volcanic origin, and (b) an upper locally derived detrital unit (Ogallala Formation and its equivalents), whose volcanic con-

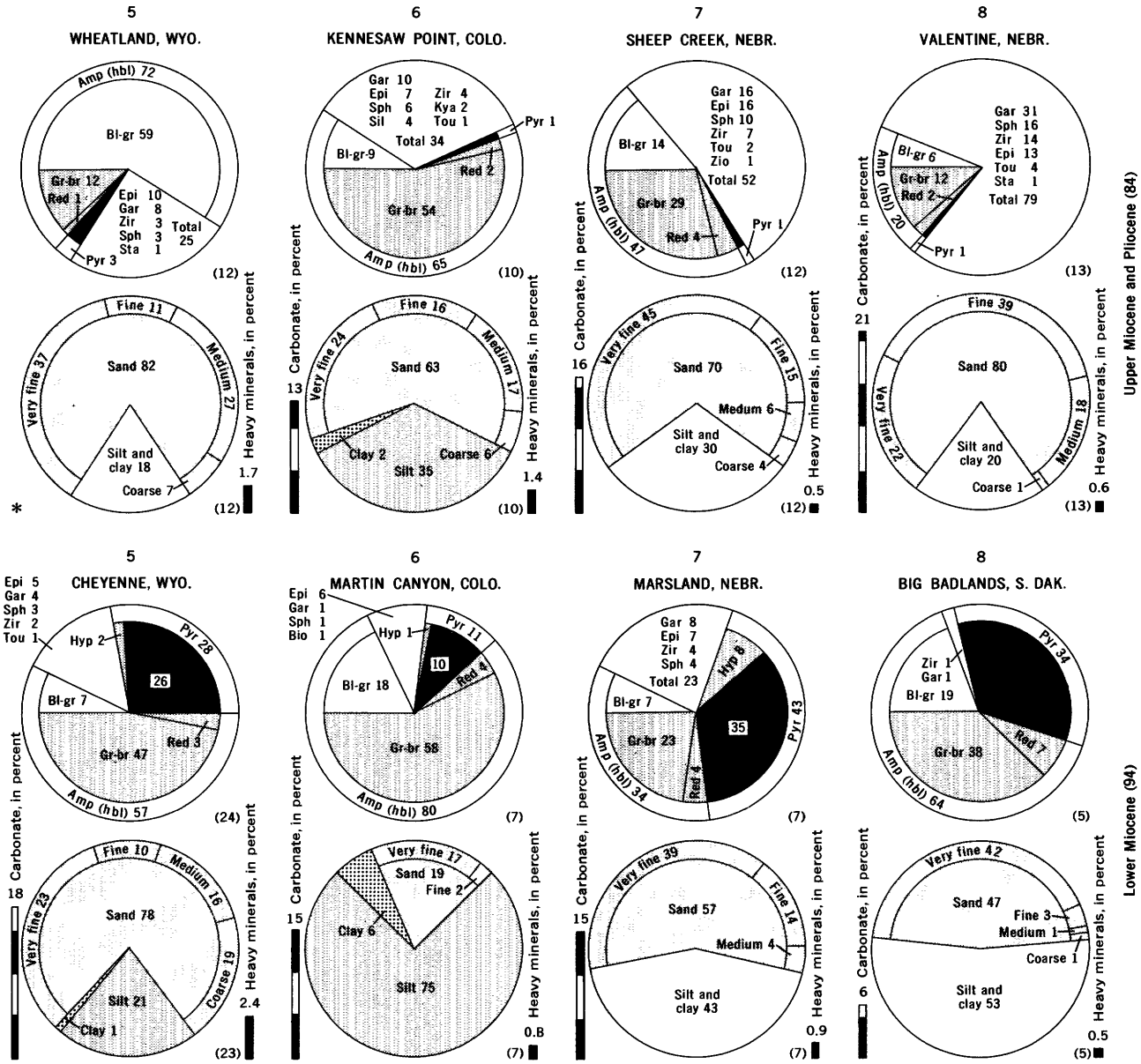

FIGURE 3.

stituents are minor and probably have been derived for the most part from the reworking of older Tertiary rocks. The rocks of the lower unit are well sorted and contain a relatively large percentage of very fine grained heavy minerals, whereas the rocks of the upper unit show a significantly larger grain-size distribution, contain a relatively small percentage of very fine grained heavy minerals, and have a much less uniform distribution of grain size within the sand-size fractions.

The term "middle Miocene" or Hemingford Group of Lugn (1938) has no rock-stratigraphic meaning in the twofold lithic subdivision of Miocene rocks emphasized by this study. Similarly, faunas designated only as Hemingford or of Hemingfordian provincial age of Wood, Chaney, Clark, Colbert, Jepsen, Reeside, and Stock (1941) cannot be fixed with respect to the unconformity between Ogallala and Arikaree Formations or their equivalents, because the rocks containing the Sheep Creek fauna are lithologically allied to the Ogallala, whereas those containing the Marsland fauna are lithologically allied to the Arikaree.

The lack of a significant lithologic break within the Ogallala in the northern High Plains makes it uncertain where to place the series boundary in the stratigraphic sequence described in this report. Irrespective of the position of this boundary, the rocks overlying the Arikaree constitute a single lithogenetic

unit. The boundary, therefore, seems to have little bearing on the depositional history of the Cenozoic rocks herein described.

A westerly source for the volcanic heavy minerals making up the Arikaree Formation is suggested by the noticeably higher percentages of volcanic minerals in nonopaque heavy-mineral concentrates from samples from the western part of the region as compared with percentages of volcanic minerals in concentrates from samples from the eastern part. This conclusion is also corroborated, as shown in figure 3, by a corresponding, but erratic, increase in the average size of the mineral grains in the samples collected in the west as compared with those collected in the east.

Tectonism and uplift of regional significance during late Miocene are suggested by marked increases in the percentages of nonopaque heavy minerals of plutonic and metamorphic derivation accompanied by a noticeably less uniform distribution of the sand-size fractions. The greater frequency of conglomerate and coarse-grained sandstone throughout the Ogallala and equivalents confirms this interpretation.

Nonopaque heavy minerals in the sedimentary rocks of Miocene and Pliocene age in central Wyoming and adjacent States reliably reflect volcanism and tectonism and are distinctive enough to be used in correlating a formation in one area with a formation in another.

REFERENCES

Black, C. C., 1961, New rodents from the early Miocene deposits of Sixty-Six Mountain, Wyoming: Breviora, no. 146, 7 p.

Cook, H. J., 1965, Runningwater Formation, middle Miocene of Nebraska: Am. Mus. Novitates, no. 2227, 8 p., 3 figs.

Cook, H. J., and Cook, M. C., 1933, Faunal lists of the Tertiary Vertebrata of Nebraska and adjacent areas, with preface by G. E. Condra: Nebraska Geol. Survey Paper 5, 58 p.

Darton, N. H., 1898, Preliminary report on the geology and water resources of Nebraska west of the one hundred and third meridian: U.S. Geol. Survey 19th Ann. Rept., pt. 4, p. 719–785.

Elias, M. K., 1942, Tertiary prairie grasses and other herbs from the High Plains: Geol. Soc. America Spec. Paper 41, 176 p., pls. 1–17.

Evernden, J. F., Curtis, G. H., Obradovich, John, and Kistler, R. W., 1961, On the evaluation of glauconite and illite for dating sedimentary rocks by the potassium-argon method: Geochim. et Cosmochim. Acta, v. 23, p. 78–99.

Funnell, B. M., 1964, The Tertiary period, p. 179–193 *in* Harland, W. B., Smith, A. G., and Wilcock, Bruce, eds., The Phanerozoic time-scale—A symposium dedicated to Professor Arthur Holmes: Geol. Soc. London Quart. Jour., supp., v. 120s, 458 p.

Galbreath, E. C., 1953, A contribution to the Tertiary geology and paleontology of northeastern Colorado: Kansas Univ. Paleont. Contr. 13, Vertebrata, art. 4, 119 p., 2 pls., 26 figs.

Kulp, J. L., 1961, Geologic time scale: Science, v. 133, no. 3459, p. 1105–1114.

Lewis, G. E., 1964, Miocene vertebrates of the Barstow Formation in southern California: Art. 125 *in* U.S. Geol. Survey Prof. Paper 475–D, p. D18–D23.

Lugn, A. L., 1938, The Nebraska State Geological Survey and the "Valentine problem": Am. Jour. Sci., 5th ser., v. 36, no. 213, p. 220–227.

——— 1939, Classification of the Tertiary system in Nebraska: Geol. Soc. America Bull., v. 50, no. 8, p. 1245–1275, 1 pl.

McGrew, L. W., 1963, Geology of the Fort Laramie area, Platte and Goshen Counties, Wyoming: U.S. Geol. Survey Bull. 1141–F, p. F1–F39.

McGrew, P. O., 1951, Tertiary stratigraphy and paleontology of south-central Wyoming, *in* Wyoming Geol. Assoc. Guidebook 6th Ann. Field Conf., South-Central Wyoming, 1951: p. 54–57.

Moore, F. E., 1959, The geomorphic evolution of the east flank of the Laramie Range, Colorado and Wyoming: Wyoming Univ. unpub. Ph. D. thesis, 123 p. [abs., Wyoming Univ. Pub., v. 23, no. 5, p. 105–106, 1959].

Peterson, O. A., 1909, A revision of the Entelodontidae: Carnegie Mus. Mem. 4, p. 41–156.

Rachou, J. F., 1951, Tertiary stratigraphy of the Rattlesnake Hills, central Wyoming: Wyoming Univ. unpub. M.A. thesis, 70 p. [abs., Geol. Soc. America Bull., v. 62, no. 12, pt. 2, p. 1541, 1951].

Rich, E. I., 1962, Reconnaissance geology of Hiland-Clarkson Hill area, Natrona County, Wyoming: U.S. Geol. Survey Bull. 1107–G, p. 447–540.

Sato, Yoshiaki, and Denson, N. M., 1967, Volcanism and tectonism as reflected by the distribution of nonopaque heavy minerals in some Tertiary rocks of Wyoming and adjacent States, *in* Geological Survey Research 1967: U.S. Geol. Survey Prof. Paper 575–C, p. C42–C54.

Schultz, C. B., and Falkenbach, C. H., 1949, Promerycochoerinae, a new family of oreodonts: Am. Mus. Nat. History Bull., v. 93, art. 3, p. 69–198, figs. 1–26, 8 tables, 6 charts.

Schultz, C. B., and Stout, T. M., 1955, Classification of Oligocene sediments in Nebraska—A guide for the stratigraphic collecting of fossil mammals: Nebraska Univ. State Mus. Bull., v. 4, no. 2, p. 17–52, figs. 1–12.

——— 1961, Field conference on the Tertiary and Pleistocene of western Nebraska, Guidebook, 9th field conference of Society of Vertebrate Paleontology: Nebraska Univ. State Mus. Spec. Pub. 2, 55 p.

Stecher, R. M., Schultz, C. B., and Tanner, L. G., 1962, A middle Miocene rhinoceros quarry in Morrill County, Nebraska (with notes on hip disease in *Diceratherium*): Nebraska Univ. State Mus. Bull., v. 4, no. 7, p. 101–111, figs. 1–6.

Van Houten, F. B., 1964, Tertiary geology of the Beaver Rim area, Fremont and Natrona Counties, Wyoming: U.S. Geol. Survey Bull. 1164, 99 p. [1965].

Voorhies, M. R., 1965, The Carnivora of the Trail Creek fauna: Wyoming Univ. Contr. Geology, v. 4, no. 1, p. 21–25.

Wilson, R. W., 1960, Early Miocene rodents and insectivores from northeastern Colorado: Kansas Univ. Paleont. Contr. 24, Vertebrata, art. 7, 92 p., 131 figs.

Wood, H. E., 2d, Chaney, R. W., Clark, John, Colbert, E. H., Jepsen, G. L., Reeside, J. B., Jr., and Stock, Chester, 1941, Nomenclature and correlation of the North American continental Tertiary: Geol. Soc. America Bull., v. 52, no. 1, p. 1–48.

PRELIMINARY REPORT ON ELECTRON MICROSCOPIC EXAMINATION OF SURFACE TEXTURES OF QUARTZ SAND GRAINS FROM THE BERING SHELF

By MILES L. SILBERMAN, Menlo Park, Calif.

Abstract.—The surface textures of quartz sand grains from a dredge haul taken from a submerged ridge, 40 km north of St. Lawrence Island in the Bering Sea, were examined at magnifications of × 4,000 to × 13,000 using the electron microscope. The surface patterns, although etched by chemical solution, indicate that the deposit is of glacial origin and may have been modified by some marine reworking. This confirms the nature of the deposit inferred from other geologic features.

Examination by Krinsley and Takahashi (1962a, b, c) of the surface textures of quartz sand grains from South Africa, Australia, England, Long Island, and North Africa, at magnification of × 2,000 to × 20,000, using the electron microscope, has shown that the textures of grains collected from different modern sedimentary environments are distinct and characteristic. Thus, it is possible to distinguish a characteristic texture for aeolian, littoral, and glacial sand grains. Krinsley and others (1964) showed that when sand is eroded from a deposit formed in one environment and subjected to the conditions of a new environment, the texture characteristic of the new environment is progressively superimposed upon, and finally replaces, that characteristic of the old environment. However, the old texture or textures can be recognized as relicts for a considerable distance of transportation, even in a high-energy environment.

Hamilton and Krinsley (1967) showed that, under certain circumstances, relict textures can be retained for long periods of geologic time; for example, they found glacial textures in South African and Australian Permian tillites.

Acknowledgments.—I wish to express my appreciation to Michael Carr, U.S. Geological Survey, for instruction in the use of the microscrope and aid in taking many of the photographs.

THEORY

The surface textures of the sand grains are related to the physical and chemical properties in the environment of deposition. During transportation and deposition, physical factors are dominant; however, in the post-depositional environment, chemical factors may become dominant and result in removal of the texture by solution or by deposition. Although no rigorous theory has been worked out to explain the textures, physical factors, such as fluid medium viscosity and velocity and relative size and velocity of impacting particles, must be important. The features on the surface of quartz sand from glacial, aeolian, and littoral environments have been duplicated experimentally.

PRESENT APPLICATION

Although subaerial sediments of several types have been studied, little attention has been given, up to the present, to the surface of sediments submerged beneath the sea. As part of the U.S. Geological Survey's Heavy Metals program, studies have been recently initiated to assess the mineral-resource potential of the continental shelves of the United States. Detrital deposits of heavy metals are likely to be associated with relict sediments on the sea bottom, and, consequently, new criteria are needed to assist in the recognition of relict sediments such as beach deposits, alluvium, and glacial drift based on material recovered in bottom samples. The results reported here are part of a pilot study made to establish the usefulness of electron microscopic study of surface textures of sand grains recovered in bottom samples.

The material studied was recovered during the joint U.S. Geological Survey-University of Washington cruise of the RV *Thomas G. Thompson* to the Bering Sea

U.S. GEOL. SURVEY PROF. PAPER 650–C, PAGES C33–C37

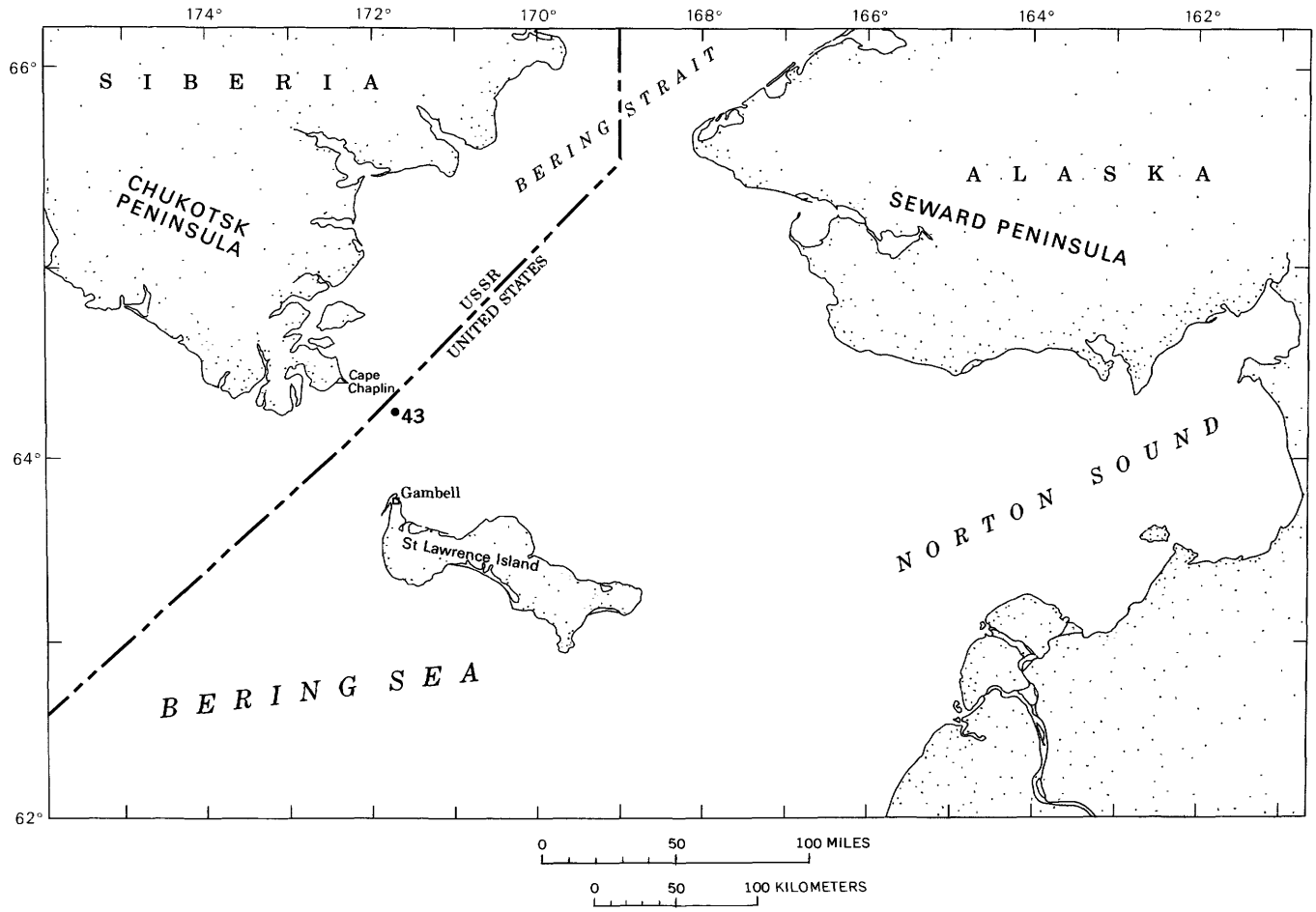

FIGURE 1.—Location map for station 43.

in 1967. The specimen is part of a chain-dredge haul recovered at lat 64°55.5′ N., long 171°39′ W., about 40 km north of Gambell at the northwestern tip of St. Lawrence Island and about 25 km east of Cape Chaplin, Siberia (fig. 1). The dredge haul sampled coarse bottom sediments on a low knoll believed to be the crest of a glacial moraine of pre-Wisconsin age (Creager and McManus, 3967, p. 27); the water depth is 46.6 meters.

Several kilograms of pebbles, cobbles, and boulders were recovered. The rock fragments are rough and irregular in shape, and many are faceted. One argillite pebble appears to bear glacial striae, according to D. M. Hopkins, U.S. Geological Survey (deck notes, July 29, 1967). Most of the fine material was washed through the apertures in the chain dredge, but some coarse, poorly sorted sand was recovered, and some silt and clay adhered to the surfaces of the pebbles. High-resolution seismic profile lines studied by Hopkins and Muriel Grim (University of Washington) show a subsurface reflector of rugged microrelief reaching the surface at the sample station. Although the shapes of the pebbles and the seismic profiling records point strongly to the possibility that glacial drift is present at the sea bottom at the sample station, evidence of a more definitive nature was needed. Consequently, I undertook a study of the surface textures of quartz sand grains from this dredge haul in order to determine the feasibility of electron microscopy for resolution of the problem.

TEXTURES CHARACTERISTIC OF GLACIAL DEPOSITS

The following textures are found on the surface of quartz sand grains from glacial deposits, as summarized by Hamilton and Krinsley (1967) and Krinsley and Funnell (1965):

1. Very high surface relief compared with that of grains from other environments. Where the texture has a worn appearance, fluvial action is probable.
2. Large-scale (15–40 microns) arc-shaped or conchoidal breakage patterns, possibly caused by grinding together of particles of different size.
3. Semiparallel striations, or step patterns, possibly caused by dragging of sharp edges of one surface along another, or by shearing action.

4. Large-sized polygonal breakage patterns, usually with subsidiary conchoidal patterns surrounding them. This feature may be caused by pressure-induced chipping or flaking.

5. Patterns of long prism shape, possibly caused by cleavage or recrystallization.

6. Irregular small-scale indentations, commonly associated with conchoidal patterns caused by grinding.

Such textures as summarized above were found by electron photomicroscopy of sand grains from the Bering Sea. Figure 2 shows the high relief characteristic of the glacial surface texture and a large polygonal breakage pattern with some subdued semiparallel steps. The surface appears worn and rounded. The background consists of very small-scale lines and branching lines characteristic of chemical etching or solution. A number of small V-shaped patterns represent sublittoral action and may indicate some reworking of the sediment by marine processes.

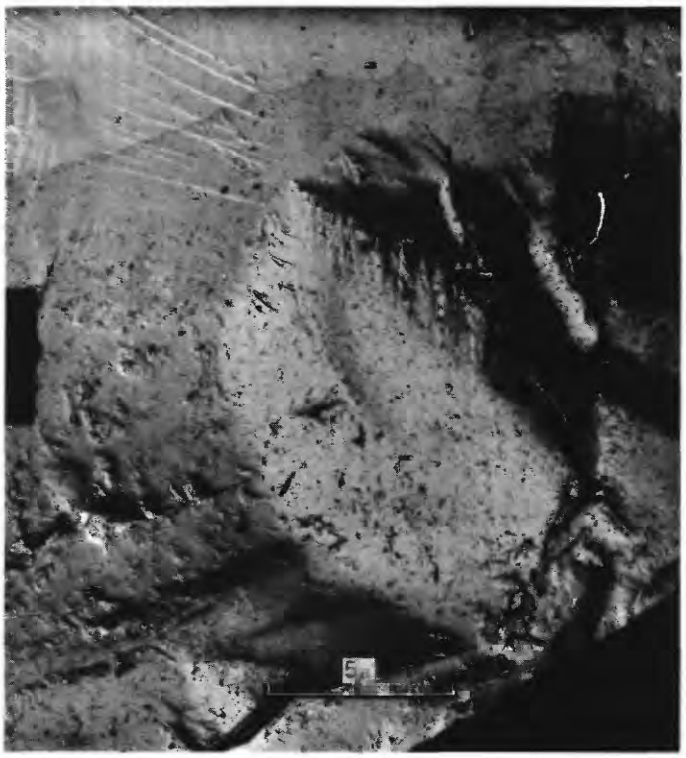

FIGURE 2.—Surface texture of sand grain from station 43, north of St. Lawrence Island, Bering Sea, showing high relief, large-scale polygonal breakage patterns (right), semiparallel steps (lower and upper left), V's(?) (to left), and chemical etching (upper left).

Figure 3 shows a large (about 30-micron) conchoidal breakage pattern, with superimposed small irregular indentations. The linear etching pattern is again visible.

Figure 4 shows the semiparallel step pattern and speckled background probably related to etching.

FIGURE 3.—Surface texture of sand grain from station 43, north of St. Lawrence Island, Bering Sea. Conchoidal fracture pattern with superimposed irregular indentations. Note linear, textured etching pattern.

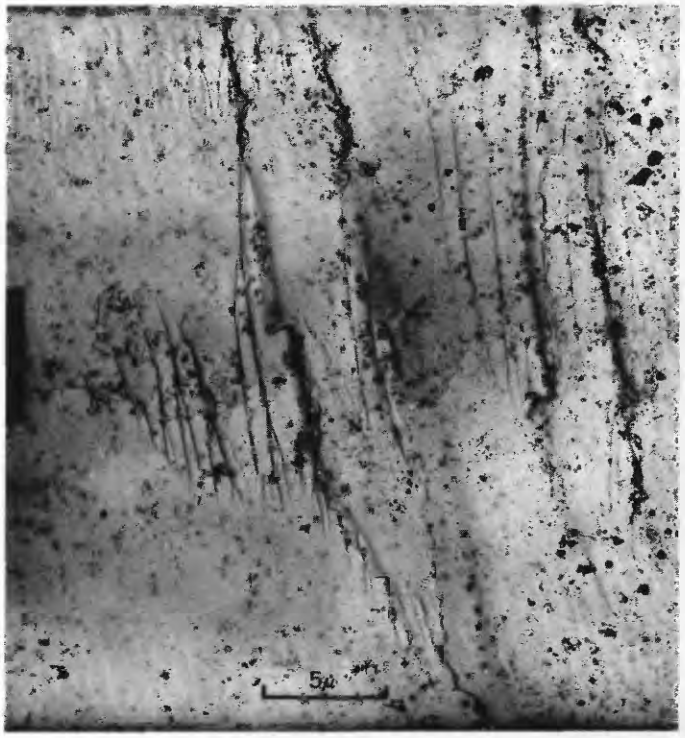

FIGURE 4.—Surface texture of sand grain from station 43, north of St. Lawrence Island, Bering Sea, showing semiparallel step pattern. Speckled pattern of background due to etching.

Figure 5 shows a surface pattern that is smooth and almost featureless, consisting of low undulating ridges that may be relict blocky breakage patterns. This pattern is similar to the pattern described by Krinsley and Funnell (1965) as characteristic of glaciofluvial action on deposits from Norfolk, England.

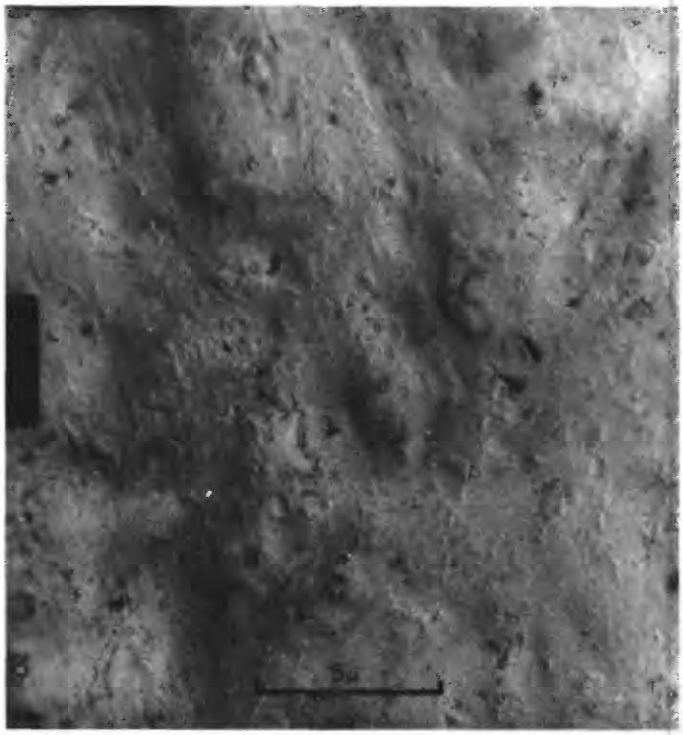

FIGURE 5.—Surface texture of sand grain from station 43, north of St. Lawrence Island, Bering Sea. Note featureless, undulating surface, relict glacial(?) features.

The sand-grain specimen shown on figure 6 for comparison with Bering Sea sand-grain surface textures was collected approximately 250 feet from an outcrop of the Pleistocene Montauk Till Member of the Manhasset Formation. The surface shows large polygonal breakage patterns and surrounding conchoical patterns.

The surface of a sand grain taken from an outcrop of the Montauk Till Member of the Manhasset Formation, figure 7, has a large (20–30 microns) conchoidal fracture pattern.

FIGURE 6.—Surface texture of sand grain from beach below till outcrop at Montauk Point, Long Island, showing large polygonal breakage patterns and conchoidal fracture patterns.

FIGURE 7.—Surface texture of sand grain from till at Montauk Point, Long Island, showing large conchoidal fracture pattern.

DISCUSSION

Figures 6 and 7 show glacial features that are fresher and sharper than the Bering Shelf samples. They lack the textured background and rounding of the glacial features that are characteristic of chemical etching of the surface. The fact that chemical attack of the surface features is indicated suggests that the deposit from which the sample was taken has been in place for a considerable period of time. Although no actual estimate of the time is possible, in general most Wisconsin material that has been examined does not show etching. This suggests that the Bering Shelf deposits are at least pre-Wisconsin in origin.

Regional geological and geophysical considerations suggest that the sediments sampled by dredge haul 73 may consist of glacial drift of pre-Wisconsin age. If this is true, the sediments have probably been reworked by

waves and bottom currents on several occasions, and they have been exposed to submarine weathering as well. On the basis of my very limited sampling and analysis of the surface textures of a few grains from dredge haul 73, it can be stated with assurance that there is a component of glacial origin in the material recovered in dredge haul 73. The presence of a few small V patterns may record some marine reworking of the sample, and more of these features may have been removed by solution. The extensive solution etching in itself suggests, as I have indicated, that the deposits are of pre-Wisconsin age. Thus, the history suggested for the sediments at station 43 in the northern Bering Sea based on study of surface textures is consistent with, and supports, the geologic history inferred by Creager and McManus (1967).

It would be desirable to examine more samples from this area, and from other areas in the Bering Shelf, as the technique appears to be useful in working out the environmental history of sediments now largely inaccessible by direct observational means.

REFERENCES

Creager, J. S., and McManus, D. A., 1967, Geology of the floor of Bering and Chukchi Seas—American studies, *in* Hopkins, D. M., ed., The Bering Land Bridge: Stanford, Calif., Stanford Univ. Press, p. 7–31.

Hamilton, Warren, and Krinsley, David, 1967, Upper Paleozoic glacial deposits of South Africa and southern Australia: Geol. Soc. America Bull., v. 78, no. 6, p. 783–799.

Krinsley, D. H., and Funnell, B. M., 1965, Environmental history of quartz sand grains from the Lower and Middle Pleistocene of Norfolk, England: Geol. Soc. London Quart. Jour., v. 121, p. 435–461.

Krinsley, D. H., and Takahashi, Taro, 1962a, Surface textures of sand grains—An application of electron microscopy: Science, v. 135, no. 3507, p. 923–925.

——— 1962b, Surface textures of sand grains—An application of electron microscopy—Glaciation: Science, v. 138, no. 3546, p. 1262–1264.

——— 1962c, Applications of electron microscopy to geology: New York Acad. Sci. Trans., ser. 2, v. 25, no. 1, p. 3–22.

Krinsley, D. H., Takahashi, Taro, Silberman, M. L., and Newman, W. S., 1964, Transportation of sand grains along the Atlantic shore of Long Island, New York—An application of electron microscopy: Marine Geology, v. 2, nos. 1–2, p. 100–120.

DISTRIBUTION OF LANTHANIDES IN MINERALS

By JOHN W. ADAMS, Denver, Colo.

Abstract.—Fractionation of the lanthanide group of elements by natural processes is well demonstrated in rare-earth-bearing minerals, where variation in the relative abundance of these elements is found not only between individual species, but also in the same species in different deposits. Several mechanisms, such as ionic-radii differences, basicity, and accommodation in crystal lattices, may contribute to fractionation.

The increased interest in the geochemistry of the rare earths and improvements in analytical methods in recent years have resulted in many additional data on the distribution of these elements in terrestrial materials and meteorites. Among terrestrial materials, minerals have received much attention, and well over a thousand analyses may be found in the literature, largely Russian, in which all detectable lanthanide elements are reported, not only for strictly rare-earth minerals, but also for many species in which the rare earths are only vicarious constituents. The present paper has been modified from a talk given at the Seventh Rare-Earth Research Conference, Coronado, Calif., Oct. 28–30, 1968.

The variations in the lanthanide assemblage found in minerals show that effective fractionation of the group has taken place through geologic processes, but before discussing the fractionation it would be well to consider the basic pattern of distribution for these elements—the fundamental relationships that existed prior to fractionation.

PRIMORDIAL LANTHANIDE DISTRIBUTION

Some investigators suggest that the primordial lanthanide distribution, undisturbed by geologic processes, is to be found in chondritic meteorites (R. A. Schmitt, quoted in Haskin and Frey, 1966, p. 301). The average lanthanide content of 20 meteorites analyzed by Schmitt (Haskin and Frey, 1966, p. 302) is shown in figure 1*A*. This graph and the others that follow are plotted in the form suggested by Semenov and Barinskii (1958) in which odd-even pairs of elements are arranged in order of increasing atomic number along the abscissa, and abundance in atomic percent is plotted along the ordinate. The upper curve connects elements of even atomic number, the lower, their odd-numbered neighbors.

If the meteorite distribution pattern does represent primordial relationships, then fractionation has taken place during the development of crustal rocks. Some basic rocks, such as basalts from the mid-Atlantic ridge analyzed by Frey and Haskin (1964), show patterns very close to that of chondritic meteorites, whereas patterns of acidic rocks, such as granites, differ appreciably. Which distribution pattern approximates the average for the earth's crust, or, more properly, for the continental crust? One answer appears to be provided by the rare-earth distribution found in sedimentary rocks, such as shales, which are composed largely of material derived from the weathering of various other types of rock, so that in effect they represent a crude composite sample. Early X-ray analyses by Minami (1935) and more recent activation analyses by Haskin and coworkers (Haskin and Gehl, 1962; Haskin and Frey, 1966) have shown that the relative amounts of the rare earths in sedimentary rocks vary only slightly, and that their average distribution pattern is probably characteristic of crustal materials. Thus, as a distribution pattern with which to compare lanthanide distribution in minerals, the abundance data of Haskin and Haskin (196°) for a composite of North American shales (fig. 1*B*) seem best suited.

As shown in figure 1*B*, the pattern for the shales differs from that of meteorites chiefly in the greater relative abundance of the light rare earths and the generally lower relative abundance of the heavy elements. This difference could have resulted from a very early fractionation process by which some of the lanthanides of small ionic radius (that is, the heavier elements) were entrapped into the structures of ferromagnesian minerals that make up much of the deep-

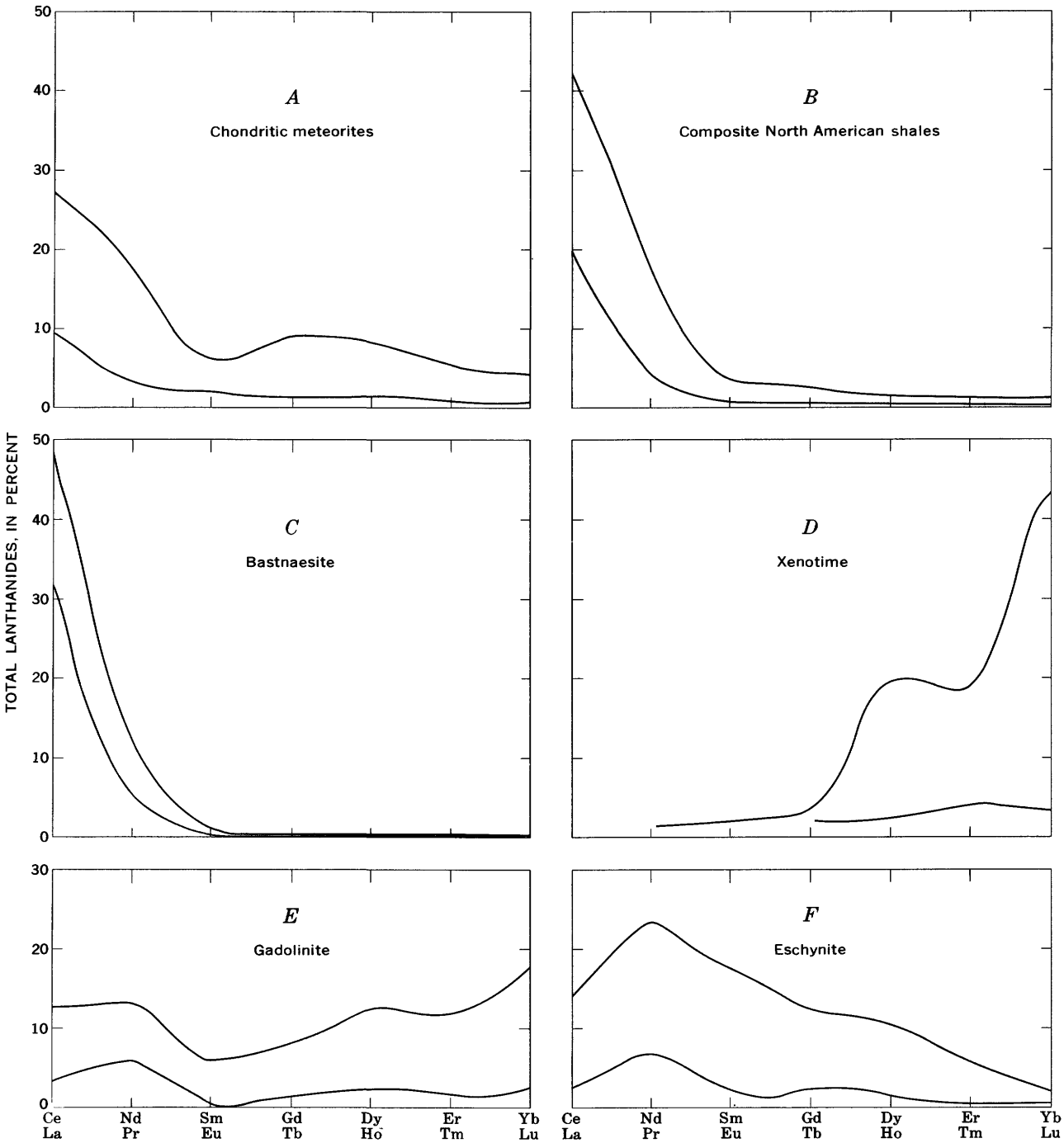

FIGURE 1.—Distribution of lanthanides in *A*, average of 20 chondritic meteorites; *B*, composite North American shales; *C*, bastnaesite from California; *D*, xenotime from Nigeria; *E*, gadolinite from Sweden; and *F*, eschynite from the U.S.S.R.

seated mafic rocks; the lanthanides with larger radii were excluded from these early-formed minerals and became constituents of the less mafic and more siliceous differentiates that characterize the upper parts of the crust.

Additional fractionation may have taken place during the evolution of various rock types through changes in chemistry that accompanied the further differentiation of the magmas in the upper crust. The effect of host rock composition has been well demonstrated in recent work by Lee and Bastron (1967), who, through a study of allanite and monazite from a series of related granitic rocks, showed that the rare earths became progressively enriched in the light elements lanthanum, cerium, and

praseodymium with increase in the calcium content of the rocks. Late-stage derivatives of igneous rocks, such as pegmatites and hydrothermal veins, probably were enriched in complexing agents that could have markedly affected the solubility relations of the rare earths. Thus, in the evolution of the crust, considerable fractionation may have taken place prior to the crystallization of the various rare-earth minerals; if so, the rare-earth composition of their particular host melt or solution may have been the most important factor in determining what minerals formed and what lanthanide assemblage resulted.

DISTRIBUTION OF LANTHANIDES IN SELECTED MINERALS

The rare-earth minerals are customarily divided into three broad classes on the basis of their rare-earth assemblage: (1) cerium-selective minerals, or those containing largely the cerium group, (2) the yttrium-selective minerals, in which the yttrium group is dominant, and (3) complex minerals, in which both the cerium and yttrium groups are well represented. The first class is well exemplified by the distribution pattern for a bastnaesite (Kruesi and Duker, 1965) (fig. 1*C*). For the second class, an ytterbium-rich xenotime (Jefford, 1962) (fig. 1*D*) is a good example, and for the third class, a gadolinite (Semenov and Barinskii, 1958) is commonly used (fig. 1*E*).

The bastnaesite pattern has a cerium maximum and a general lanthanide distribution not too dissimilar from the crustal pattern. Xenotime, on the other hand, shows marked fractionation, with a maximum for ytterbium. Between these extremes are minerals whose analyses show maximum values for the even-atomic-numbered lanthanides, neodymium, gadolinium, dysprosium, erbium, and possibly samarium.

Figure 1*F* shows one such example, the distribution of lanthanides in a sample of eschynite from an alkalic pegmatite in the U.S.S.R. (Semenov and Barinskii, 1958). Eschynite is a multiple oxide of rare earths, titanium, and niobium, that in most samples shows a cerium maximum. In this eschynite, however, neodymium is the most abundant even-numbered lanthanide, and its odd-numbered neighbor, praseodymium, shows a parallel relationship on the curve for odd-numbered elements.

Preferential enrichment in samarium appears to be very rare, but a possible example is shown in figure 2*A*,

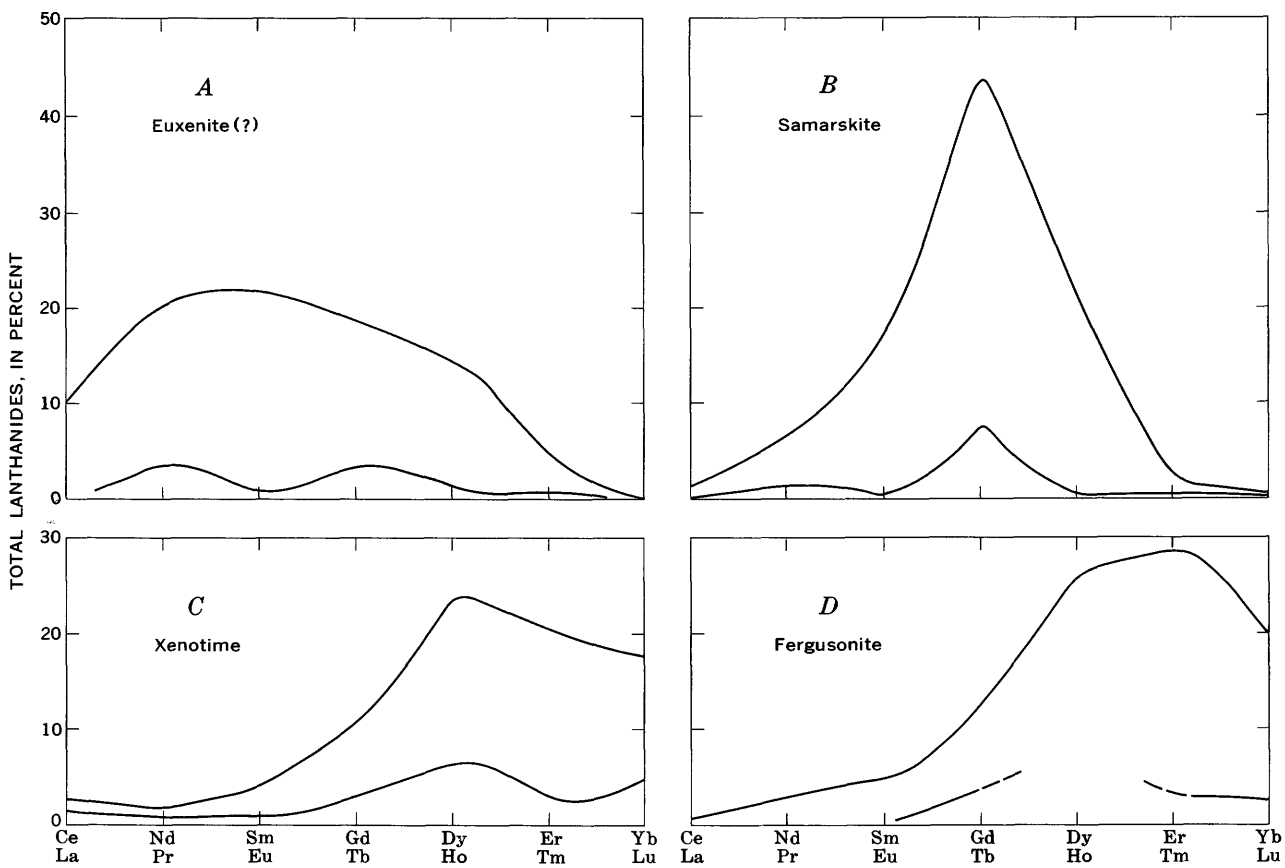

FIGURE 2.—Distribution of lanthanides in *A*, euxenite(?) from Arizona; *B*, samarskite from North Carolina; *C*, xenotime from the U.S.S.R.; and *D*, fergusonite from Norway.

which represents the analysis (Shaw, 1959) of a so-called euxenite concentrate from Arizona. The mineral is probably what was later identified by Heinrich (1960) as yttrotantalite.

Gadolinium maxima are not uncommon. Figure 2*B* is a probable samarskite from North Carolina analyzed by Butler (1958).

Dysprosium enrichment is found in many rare-earth minerals, notably some xenotimes and minerals of the multiple-oxide type. The example shown (fig. 2*C*) is a xenotime from the U.S.S.R. (Zhirov and others, 1961).

Erbium, like samarium, is found only rarely as the dominant lanthanide, generally being subordinate to ytterbium or dysprosium. One of eleven fergusonites analyzed by Butler and Hall (1960) showed an erbium maximum (fig. 2*D*), the others having either ytterbium, dysprosium, or gadolinium as their most abundant lanthanide.

Minerals of selective yttrium group composition commonly show a maximum for ytterbium. This is well illustrated by thortveitite, a scandium-yttrium silicate from Norway, analyzed by R. G. Havens, U.S. Geological Survey (fig. 3*A*); its lanthanide distribution is probably as close to the ultimate fractionation of the group as will be found in minerals.

Lanthanum is predominant in only a few minerals. One of the most interesting of these minerals is davidite, a complex uranium-lanthanum-cerium-iron titanate, in which lanthanum exceeds cerium in nearly all samples, including those from granitic pegmatites. Other minerals showing predominance of lanthanum among the lanthanides include lamprophyllite, a sodium-strontium-titanium silicate, and innelite, a sodium-barium-titanium silicate. In the latter two, the accumulation of lanthanum is due partly to the environment (alkalic pegmatites) and partly to the large ionic radius of the main cation (strontium, barium) which favored substitution of lanthanum.

FACTORS AFFECTING LANTHANIDE DISTRIBUTION

The causes of different lanthanide distributions in minerals are controversial. Some researchers, notably E. I. Semenov (1957; 1958), consider that crystallochemical factors exert the most control on what ions are admitted to any particular structure, and they relate the selectivity of lanthanide content to the coordination number of the rare earths for that mineral. Minerals in which the rare earths have high coordination numbers (10, 11, or 12) are, expectably, selective cerium-group species; those with low coordination, such as 6, have a selective yttrium-group assemblage, and intermediate coordination values favor a mixed assemblage. It is not too clear how the coordination state

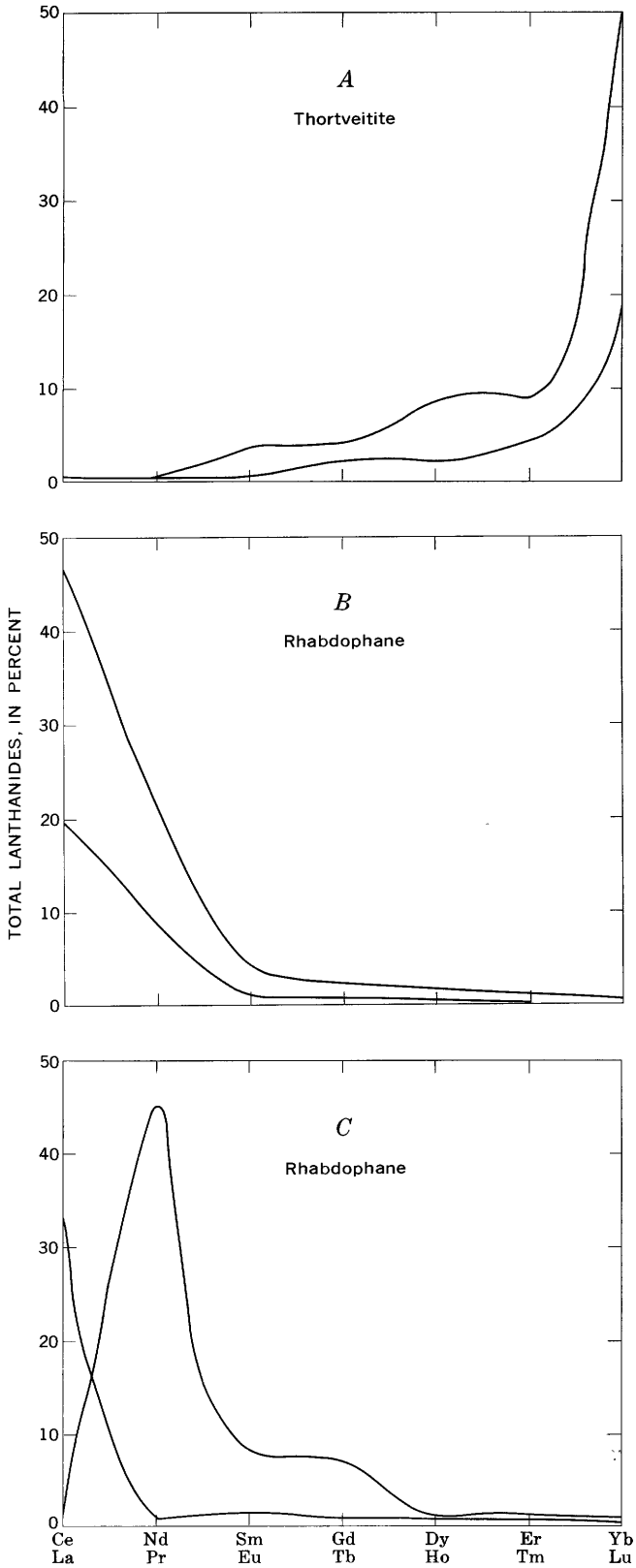

FIGURE 3.—Distribution of lanthanides in *A*, thortveitite from Norway; *B*, rhabdophane from the Ukraine; and *C*, rhabdophane from Connecticut.

controls selectivity in strictly rare-earth minerals, but a theory has been proposed by A. P. Khomyakov (1963) to explain the variations in the rare-earth assemblages found in isomorphous replacement of calcium, which is the displaced element in minerals like apatite, fluorite, and sphene. Khomyakov suggested that changes in the effective ionic radii with changes in coordination are not uniform throughout the periodic table, and hence the change in the radius of calcium is disproportionate to that of the rare earths. His data indicate that in 6-coordination, calcium has a radius comparable to those of yttrium and the heavy rare earths, but in 12-coordination, it has a radius equal to that of praseodymium and therefore would be replaced preferentially by the light rare earths.

The many discrepancies to be found in a strictly crystallochemical approach are pointed out by Borodin (1962), who favors control by the relative basicity of the lanthanides whereby the differences between the high basicity of yttrium and the first four lanthanides, lanthanum, cerium, praseodymium and neodymium, are very much larger than between yttrium and the remaining lanthanides. The middle six lanthanides, samarium to holmium, have basicities more comparable to the last four elements, erbium to lutetium. The basicity control proposal of Borodin is supported by the composition characteristics of some minerals such as bastnaesite, in which the four most basic lanthanides are dominant to the relative exclusion of the remaining ten elements of the group, whereas in other minerals only the last ten elements are commonly well represented. Normally, yttrium has a low basicity, close to that of holmium; however, an anomalously high basicity, comparable to that of the first four lanthanides, has been reported by Moeller and Kremers (1945, p. 108–109, 150) and is believed to be due to concentration effects. This behavior, Borodin suggests, may explain the large amounts of yttrium found in some minerals that otherwise are dominated by highly basic lanthanides of the cerium group.

In a study of Brazilian rare-earth deposits, Murata and coworkers (Murata and others, 1958) found that monazite crystallized earlier than xenotime, in reverse order to the experimentally determined solubility characteristics of rare-earth phosphates (Carron and others, 1958). To explain this apparently anomalous paragenetic sequence, which is common to many other rare-earth deposits, Murata suggested that the rare earths were present as complexes, in which case the more basic cerium group, by reason of its lower stabilities, would be the first to precipitate. This view is strongly supported by Mineyev (1963), who believes that the rare earths are transported in the form of complexes with fluoride, carbonate, phosphate, or other ligands and that their fractionation has resulted from the stability differences of the complexes under changing conditions.

Ionic radius difference is considered by Neumann and coworkers (Neumann and others, 1966) to be the major factor in the fractionation of the rare earths. This is probably the best general conclusion that can be made at this time, inasmuch as radii differences are fundamentally involved in basicity and coordination effects, as well as in isomorphous replacement.

Another mechanism that can contribute to the fractionation of the lanthanides is a change in oxidation state. The common deficiency of europium in minerals is attributed to its ready reduction to divalency during geologic processes; the resulting increase in ionic radius and decrease in charge then exclude europium from structural sites available to its trivalent former associates, and facilitate its entry into other minerals, notably feldspars, where it follows barium and strontium in substituting for potassium (Goldschmidt, 1954, p. 244, 317; Taylor and others, 1968). Geologic environments may be sufficiently oxidizing to convert Ce^{+3} to Ce^{+4} as demonstrated by the existence of the rare mineral cerianite, which is largely CeO_2, and by the occurrence of cerium-deficient examples of the cerium-group phosphate, rhabdophane. Rhabdophane normally has a distribution pattern like that shown in figure 3*B*, which represents a rhabdophane from the Ukraine (Semenov and Barinskii, 1958). Figure 3*C* shows another rhabdophane, this one from Salisbury, Conn. (Hildebrand and others, 1957), in which cerium is virtually absent. As rhabdophane appears to be most commonly a secondary mineral, the fractionation of cerium from the other lanthanides would most reasonably take place by oxidation during the transition period between the destruction of the primary mineral and the formation of the rhabdophane. Another cerium-deficient rhabdophane has recently been found in a highly oxidized mineralized zone in Idaho (Adams, 1968) but the complete analysis is not yet available.

SUMMARY AND CONCLUSIONS

All the factors that have been mentioned—ionic radius differences, crystal structure, stability of complexes, basicity differences, and oxidation states—are probably involved in lanthanide fractionation in geologic processes. The development and composition of any particular rare-earth mineral in a deposit will be governed fundamentally, however, by the total chemistry of the melt or solution as well as by existing temperature and pressure conditions. Included in the total chemistry will be a rare-earth assemblage, whose distribution pattern will differ from that of average

crustal abundance to the extent that the rare earths have been fractionated by earlier processes. For example, the selective cerium-group assemblage that characterizes deposits in carbonatites, such as at Mountain Pass, Calif., must result from fractionation that has removed most of the yttrium group prior to the emplacement of the deposits.

Even though this study has been concerned primarily with the distribution of the lanthanides, the role of yttrium should be mentioned. The ionic radius of trivalent yttrium is very close to those of the heavy lanthanides, so that where the magnitude of the radius is important in determining the rare-earth assemblage of a mineral, yttrium will be best accommodated in structures that favor the other members of its group, and in these minerals it is commonly the most abundant rare earth.

For some cerium-group minerals, like bastnaesite, the yttrium content is very low, again suggesting crystallochemical control, but in this case by a lattice that favors large ions and for the most part excludes the smaller ones.

There is, however, a large and quantitatively important group of minerals whose lanthanide assemblage is generally dominated by cerium-group elements but which may contain yttrium in amounts greatly in excess of any other heavy rare earth that may be present. Though including chiefly minerals in which rare earths are substituting for calcium in the crystal structure, the group includes some primarily rare-earth minerals such as monazite. These minerals apparently have structures that can accommodate rare-earth ions of any size, and thus their composition will reflect the available rare-earth assemblage more closely than minerals having more rigid crystallochemical requirements. The distribution pattern in atomic percent for all the rare earths in a composite of North American shales (Haskin and Haskin, 1968) (fig. 4A) is remarkably similar to those of an apatite (fig. 4*B*) (Lindberg and Ingram, 1964) and allanite (Lee and Bastron, 1967) (fig. 4*C*) in regard to the relation of yttrium to the lanthanides. Such minerals, by reason of their tolerance for all the rare earths, may therefore be valuable guides to changes in rare-earth composition that have taken place during the development of the rocks in which they are found.

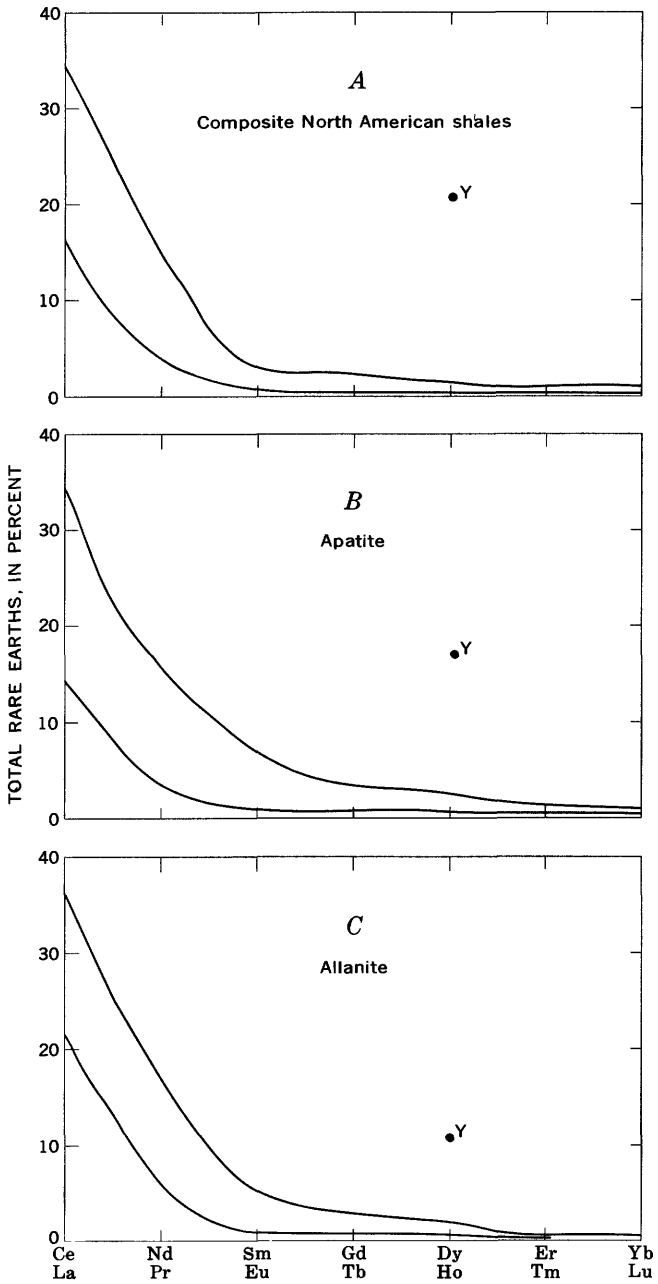

FIGURE 4.—Distribution of rare earths in *A*, composite North American shales; *B*, apatite from New York; and *C*, allanite from Nevada. The relationship of yttrium (Y) to the other rare earths is indicated.

REFERENCES

Adams, J. W., 1968, Rhabdophane from a rare-earth occurrence, Valley County, Idaho, *in* Geological Survey Research 1968: U.S. Geol. Survey Prof. Paper 600-B, p. B48–B51.

Borodin, L. S., 1962, Some basic problems of the geochemistry of the rare earths: Trudy Inst. Mineral., Geokhim., i Kristallokhim. Redkhim. Elementov, v. 9, p. 94–124 [In Russian].

Butler, J. R., 1958, Rare earths in some niobate-tantalates: Mineralog. Mag., v. 31, p. 763–780.

Butler, J. R., and Hall, R. A., 1960, Chemical variations in members of the fergusonite-formanite series: Mineralog. Mag., v. 32, p. 392–407.

Carron, M. K., Naeser, C. R., Rose, H. J., Jr., and Hildebrand, F. A., 1958, Fractional precipitation of rare earths with phosphoric acid: U.S. Geol. Survey Bull. 1036-N, p. 253–275.

Frey, F. A., and Haskin, Larry, 1964, Rare earths in oceanic basalts: Jour. Geophys. Research, v. 69, p. 775–780.

337-735 O—69——4

Goldschmidt, V. M., 1954, Geochemistry: Oxford, Oxford Univ. Press, 730 p.

Haskin, L. A., and Frey, F. A., 1966, Dispersed and not-so-rare earths: Science, v. 152, no. 3720, p. 299–314.

Haskin, L. A., and Gehl, M. A., 1962, The rare-earth distribution in sediments: Jour. Geophys. Research, v. 67, p. 2537–2541.

Haskin, L. A., and Haskin, M. A., 1968, Rare-earth elements in the Skaergaard intrusion: Geochim. et Cosmochim. Acta, v. 32, p. 433–447.

Heinrich, E. W., 1960, Some rare-earth mineral deposits in Mohave County, Arizona: Arizona Bur. Mines, Min. Tech. Ser. 51, Bull. 167, 22 p.

Hildebrand, F. A., Carron, M. K., and Rose, H. J., Jr., 1957, Re-examination of rhabdophane (scovillite) from Salisbury, Connecticut [abs.]: Geol. Soc. America Bull., v. 68, no. 12, pt. 2, p. 1744–1745.

Jefford, Godfrey, 1962, Xenotime from Rayfield, Northern Nigeria: Am. Mineralogist, v. 47, p. 1467–1473.

Khomyakov, A. P., 1963, Relation between content and composition of rare earths in minerals: Geokhimiya 1963, no. 2, p. 115–121 [In Russian]; translation in Geochemistry 1963, no. 2, p. 125–132.

Kruesi, P. R., and Duker, George, 1965, Production of rare-earth chlorides from bastnaesite: Jour. Metals, v. 17, no. 8, p. 847–849.

Lee, D. E., and Bastron, Harry, 1967, Fractionation of rare-earth elements in allanite and monazite as related to geology of the Mt. Wheeler mine area, Nevada: Geochim. et Cosmochim. Acta, v. 31, no. 3, p. 339–356.

Lindberg, M. L., and Ingram, Blanche, 1964, Rare-earth silication apatite from the Adirondack Mountains, New York, *in* Geological Survey Research 1964: U.S. Geol. Survey Prof. Paper 501-B, p. B64–B65.

Minami, E., 1935, Gehalte an seltenen Erden europäischen und japanischen Tonschiefern: Nachr. Gesell. Wiss. Göttingen, Math. Phys. Klasse, Fachgr. IV, Geol. u. Mineral., v. 1, p. 155–170.

Mineyev, D. A., 1963, Geochemical differentiation of the rare earths: Geokhimiya 1963, no. 12, p. 1082–1100 [In Russian]; translation in Geochemistry 1963, no. 12, p. 1129–1149.

Moeller, Therald, and Kremers, H. E., 1945, Basicity characteristics of scandium, yttrium and the rare earth elements: Chem. Reviews, v. 37, p. 97–159.

Murata, K. J., Dutra, C. V., Teixeira da Costa, M., and Branco, J. J. R., 1958, Composition of monazites from pegmatites in eastern Minas Gerais, Brazil: Geochim. et Cosmochim. Acta, v. 16, p. 1–14.

Neumann, Henrich, Jensen, B. B., and Brunfelt, A. O., 1966, Distribution patterns of rare earths in minerals: Norsk Geol. Tidsskr., v. 46, p. 141–179.

Semenov, E. I., 1957, Isomorphism and camouflage of rare earths: Geokhimiya 1957, no. 7, p. 626–637 [In Russian]; translation in Geochemistry 1957, no. 7, p. 735–748.

——— 1958, Relation between composition of rare earths and composition and structure of minerals: Geokhimiya 1958, no. 5, p. 452–461 [In Russian]; translation in Geochemistry 1958, no. 5, p. 574–586.

Semenov, E. I., and Barinskii, R. L., 1958, The composition characteristics of the rare earths in minerals: Geokhimiya 1958, no. 4, p. 314–333 [In Russian]; translation in Geochemistry 1958, no. 4, p. 398–419.

Shaw, V. E., 1959, Extraction of yttrium and rare-earth elements from Arizona euxenite concentrate: U.S. Bur. Mines Rept. Inv. 5544, 9 p.

Taylor, S. R., Ewart, A., and Capp, A. C., 1968, Leucogranites and rhyolites—trace element evidence for fractional crystallization and partial melting: Lithos, v. 1, no. 2, p. 179–186.

Zhirov, K. K., Bandurkin, G. A., and Lavrent'yev, Yu. G., 1961, Geochemistry of rare-earth elements in pegmatites of northern Karelia: Geokhimiya 1961, no. 11, p. 995–1004 [In Russian]; translation in Geochemistry 1961, no. 11, p. 1107–1118.

PHENGITIC MICAS FROM THE CAMBRIAN PROSPECT MOUNTAIN QUARTZITE OF EASTERN NEVADA

By DONALD E. LEE and RICHARD E. VAN LOENEN, Denver, Colo.

Abstract.—Four samples of Cambrian Prospect Mountain Quartzite collected from the southern and central Snake Range of eastern Nevada contain phengitic micas of very similar composition, indicating that these quartzites recrystallized under conditions of low-grade greenschist facies metamorphism.

Four phengitic micas were recovered from samples of Cambrian Prospect Mountain Quartzite during study of low-grade regional metamorphism in the southern part of the Snake Range of eastern Nevada (fig. 1). This paper presents analytical data for these phengites and for a biotite that coexists with one of them.

The phengite-bearing quartzites sampled are part of a Paleozoic miogeosynclinal sequence of sedimentary rocks, and the samples were collected just west of the Cretaceous Sevier orogenic belt of Nevada and Utah (Armstrong, 1968). Three of these samples were collected within a few miles of each other in or near an area mapped by Drewes (1958) and by Whitebread, Griggs, Rogers, and Mytton (1969). The fourth sample was collected north of Sacramento Pass, some 17–22 miles northeast of the other three.

MICA AND ROCK ANALYSIS

The micas analyzed (table 1) were recovered from the respective quartzite samples after grinding the rock to −150 mesh. The final purification of each of the phengites was effected by repeated centrifuging to obtain a concentrate having a narrow range of specific gravity. Thus, the specific gravity listed in table 1 as 2.89 ± 0.01 indicates that the phengite fraction analyzed had been centrifuged at 2.88 and 2.90. However, the biotite (sample 418–DL–67) in table 1 is not so homogeneous, and so while the 3.00 specific gravity listed is a good bulk figure, the actual range of individual grains is 2.97–3.03.

Thin sections of the rocks indicate that the micas formed from argillaceous materials deposited with the original sandstone, as shown by textural relations in figure 2. Moreover, the behavior of each of these phengites during centrifuging indicates a very narrow range of specific gravity and thus of chemical composition, which one would not expect if the mica in the rock were detrital.

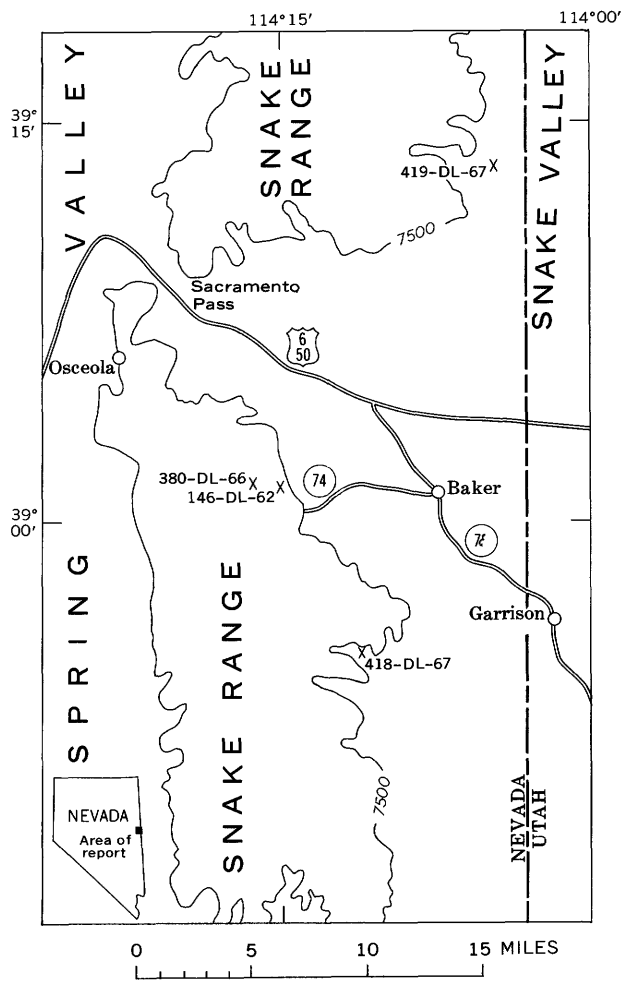

FIGURE 1.—Index map showing sample localities.

TABLE 1.—*Analytical data for four phengitic micas and one biotite recovered from Prospect Mountain Quartzite*

[Chemical analyses by Elaine L. Munson. Optical properties measured in sodium light. Each $2V$ listed for phengite is an average of 5 grains measured on a universal stage. Determination of specific gravity and cell parameters as described in text. Semiquantitative spectrographic analyses by Harriet Neiman; results are based on their identity with geometric brackets whose boundaries are 1.2, 0.83, 0.56, 0.38, 0.26, 0.18, 0.12, and so forth, and are reported arbitrarily as midpoints of these brackets, 1., 0.7, 0.5, 0.3, 0.2, 0.15, 0.1, respectively. The precision of a reported value is approximately plus or minus one bracket at 68-percent or two brackets at 95-percent confidence. 0, below limit of spectrographic detection]

Mica	Phengitic micas				Biotite
Sample No.	146-DL-62	380-DL-66	419-DL-67	418-DL-67	418-DL-67
Chemical analyses (weight percent)					
SiO_2	46.38	46.55	46.82	46.34	37.64
Al_2O_3	27.72	29.04	29.73	27.26	15.63
Fe_2O_3	5.77	5.26	4.93	5.90	12.44
FeO	1.26	1.20	1.12	1.48	8.51
MgO	1.84	1.42	1.14	1.92	8.77
CaO	.00	.00	.00	.00	.28
Na_2O	.32	.24	.23	.24	.23
K_2O	10.80	10.94	10.86	10.80	8.75
H_2O+	4.01	4.11	4.10	4.18	3.85
H_2O-	.07	.05	.06	.06	.27
TiO_2	1.22	.73	.67	1.53	3.16
P_2O_5	.00	.00	.00	.03	.12
MnO	.02	.01	.05	.02	.14
Cl	.00	.00	.00	.01	.02
F	.24	.04	.03	.05	.19
Subtotal	99.65	99.69	99.74	99.82	100.00
Less O	.10	.02	.01	.02	.08
Total	99.55	99.67	99.73	99.80	99.92
Optical properties and specific gravity					
$\alpha(\pm 0.003)$	1.576	1.577	1.577	1.578	1.603
$\beta(\pm 0.003)$	1.611	1.610	1.611	1.615	1.664
$\gamma(\pm 0.003)$	1.614	1.613	1.613	1.617	1.664
$2V_\alpha$	29°	28°	26°	33°	0–15° (est)
Specific gravity (± 0.01)	2.89	2.89	2.89	2.89	3.00 (avg)
Cell parameters					
$a(\pm 0.004)$	5.209	5.204	5.202	5.209	----
$b(\pm 0.008)$	9.048	9.036	9.034	9.062	----
$c(\pm 0.009)$	20.007	20.019	20.028	20.016	----
Volume (± 0.9)	938.3	936.7	936.4	940.1	----
$\beta(\pm 3.9')$	95°43.3′	95°46.5′	95°47.4′	95°46.1′	----
Structural type	$2M_1$	$2M_1$	$2M_1$	$2M_1$	----
Numbers of ions on basis of 24 (O, OH, F, Cl)					
Si	6.365 } 8.00	6.363 } 8.00	6.373 } 8.00	6.352 } 8.00	5.600 } 8.00
Al	1.635	1.637	1.627	1.648	2.400
Al	2.849 } 4.09	3.041 } 4.08	3.142 } 4.08	2.756 } 4.09	.340 } 5.12
Ti	.126	.075	.069	.158	.354
Fe^{+3}	.596	.541	.505	.609	1.393
Fe^{+2}	.145	.137	.128	.170	1.066
Mn	.002	.001	.006	.002	.018
Mg	.376	.289	.231	.392	1.945
Ca	---- } 1.98	---- } 1.97	---- } 1.95	---- } 1.95	.045 } 1.77
Na	.085	.064	.061	.064	.066
K	1.891	1.908	1.886	1.888	1.661
Cl	---- } 3.78	---- } 3.76	---- } 3.74	---- } 3.84	.005 } 3.92
F	.104	.017	.013	.022	.089
OH	3.671	3.747	3.723	3.822	3.821

TABLE 1.—*Analytical data for four phengitic micas and one biotite recovered from Prospect Mountain Quartzite*—continued

Mica	Phengitic micas				Biotite
Sample No.	146-DL-62	380-DL-66	419-DL-67	418-DL-67	418-DL-67
	Semiquantitative spectrographic analyses (weight percent)				
B	0	0	0.0020	0	0
Ba	.2000	.1500	.1000	.1000	.0300
Be	.0010	.0002	.0003	.0005	.0002
Co	.0010	.0015	.0007	.0007	.0070
Cr	.0070	.0070	.0050	.0100	.0070
Cu	.0050	.0003	.0200	.0003	.0020
Ga	.0070	.0050	.0050	.0070	.0030
Nb	0	.0010	.0010	0	0
Ni	.0015	.0020	.0015	.0010	.0150
Pb	0	0	0	0	.0030
Sc	.0020	.0010	.0007	.0020	.0007
Sr	.0020	.0015	.0020	.0010	.0015
V	.0300	.0050	.0050	.0100	.0500
Y	0	0	0	0	.0010
Yb	.0002	0	0	.0002	.0002
Zr	.0020	.0050	.0015	.0030	.0030

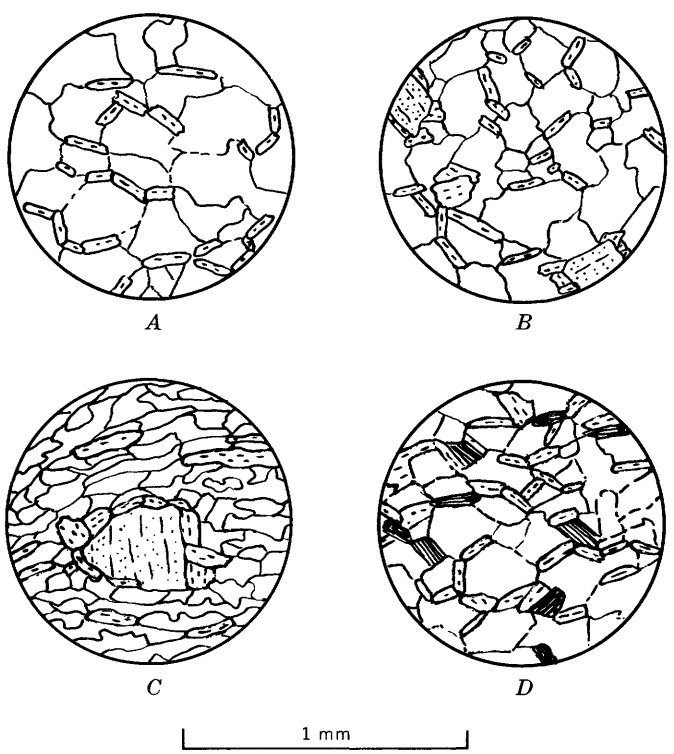

FIGURE 2.—Quartzites from which analyzed micas were recovered. *A*, sample 146-DL-62: quartz and muscovite. *B*, sample 380-DL-66: quartz, two plagioclase grains (stippled and showing cleavage), and muscovite. *C*, sample 419-DL-67: large grain of orthoclase with quartz and muscovite. *D*, sample 418-DL-67: quartz, muscovite, and biotite.

The analyses of these phengites (table 1) are almost identical, despite the fact that they were recovered from quartzites collected miles apart, quartzites that themselves show a considerable range of composition (table 2). Optical properties, specific gravities, and minor-element contents also are very similar (table 1). These phengites are so homogeneous and well crystallized that we were able to calculate rather precise unit-cell parameters by least-squares refinement of powder diffractometer data (table 1), using an internal standard of CaF_2 and a self-indexing program developed by Evans, Appleman, and Handwerker (1963).

DISCUSSION

Phengitic micas, being high in silica, low in alumina, and containing several percent $MgO+FeO+Fe_2O_3$, represent a solid solution between muscovite and celadonite. Recent studies have shown that phengites are stable under conditions of high pressure and relatively low temperature. In Scotland's Moine Series rocks of the greenschist facies, Lambert (1959) found that white micas change from phengitic to muscovitic compositions as metamorphic grade increases. Ernst (1963) showed that phengites are widespread in blueschist facies rocks, where they are associated with such relatively high-pressure, low-temperature minerals as lawsonite, jadeitic pyroxene, and metamorphic aragonite. Velde's (1965, p. 909) discussion is especially pertinent to the present results. He showed that formation of phengite from argillaceous materials is likely during metamorphism of normal sediments, where temperature is low and pressure is high ($P_{H_2O}=P_{Total}$), and where detrital K-feldspar is present. Detrital K-feldspar is present in all of the rocks in table 2, although sample 146-DL-62 contains only a very few grains.

The phengite of sample 418-DL-67 probably represents the limit of solid solution of celadonite in muscovite, given the conditions under which these quartzites were recrystallized, for it is the only phengite described here that is present with coexisting biotite. Ernst (1963, p. 1366) emphasized that the apparent incompatibility of muscovite with biotite in low-grade greenschist

TABLE 2.—*Analytical data for quartzites from which micas were recovered*

[Chemical analyses by Elaine L. Munson. Spectrographic analyses by G. W. Sears, Jr. Precision of spectrographic method explained in table 1. 0, below limit of detection]

Sample No.	146-DL-62	380-DL-66	419-DL-67	418-DL-67
Chemical analyses (weight percent)				
SiO_2	96.53	90.74	91.14	85.74
Al_2O_3	1.30	4.85	4.55	6.65
Fe_2O_3	.55	.72	.47	1.26
FeO	.18	.24	.12	.46
MgO	.09	.23	.07	.49
CaO	.00	.00	.00	.02
Na_2O	.08	.08	.17	.17
K_2O	.41	2.25	2.78	3.62
H_2O+	.14	.47	.24	.60
H_2O-	.02	.03	.02	.02
TiO_2	.45	.10	.06	.65
P_2O_5	.02	.01	.03	.07
MnO	.00	.01	.02	.01
CO_2	.01	.00	.01	.01
Cl	.00	.00	.00	.00
F	.02	.01	.01	.02
Subtotal	99.80	99.74	99.69	99.79
Less O	.01	.00	.00	.01
Total	99.79	99.74	99.69	99.78
Semiquantitative spectrographic analyses (weight percent)				
Ba	0.0300	0.0700	0.0700	0.0700
Co	0	.0005	.0003	.0005
Cr	.0003	.0015	.0003	.0010
Cu	.0005	.0005	.0003	.0100
Ga	0	.0007	.0005	.0010
Mo	.0005	0	0	0
Ni	0	.0007	.0005	.0010
Pb	0	0	0	.0015
Sc	0	0	0	.0005
Sr	0	.0015	.0030	.0030
V	.0010	0	0	.0070
Y	.0010	0	0	.0015
Yb	.0002	0	0	.0003
Zr	.0500	.0070	.0070	.0700

assemblages probably results not from lack of stability of biotite itself but from the increased compositional range of dioctahedral micas. He pointed out that the presence of biotite with phengite under these conditions may represent either (1) conditions transitional between higher and lower grade portions of the greenschist facies, or (2) $K_2O+MgO+FeO$-rich bulk compositions. Compared to the other quartzites in table 2, sample 418–DL–67 is relatively rich in $K_2O+MgO+FeO$, and it probably is an example of the second condition. We note, however, that Velde (1965, fig. 7B) did not show biotite and phengite as a stable pair in his high-pressure, low-temperature phase diagram, but he did show this pair as stable in his (relatively) high-pressure, high-temperature phase diagram.

Regional metamorphism in the eastern Great Basin has been recognized by previous workers. Drewes (1958, p. 226) considers regional metamorphism to be one possible explanation for the recrystallized Cambrian Pole Canyon Limestone present in the southern Snake Range. Misch and Hazzard (1962), Armstrong and Hansen (1966), and Drewes (1967) discussed this metamorphism in some detail. The phengite analyses in table 1 seem to indicate that the metamorphism was low grade in the area sampled. We are currently obtaining isotopic age dates for the analyzed micas in table 1 in an effort to better understand this metamorphism.

REFERENCES

Armstrong, R. L., 1968, Sevier orogenic belt in Nevada and Utah: Geol. Soc. America Bull., v. 79, no. 4, p. 429–458.

Armstrong, R. L., and Hansen, Edward, 1966, Cordilleran infrastructure in the eastern Great Basin: Am. Jour. Sci., v. 264, no. 2, p. 112–127.

Drewes, H. D., 1958, Structural geology of the southern Snake Range, Nevada: Geol. Soc. America Bull., v. 69, no. 2, p. 221–239.

——— 1967, Geology of the Connors Pass quadrangle, Schell Creek Range, east-central Nevada: U.S. Geol. Survey Prof. Paper 557, 93 p.

Ernst, W. G., 1963, Significance of phengitic micas from low-grade schists: Am. Mineralogist, v. 48, nos. 11–12, p. 1357–1373.

Evans, H. T., Jr., Appleman, D. E., and Handwerker, D. S., 1963, The least squares refinement of crystal unit cells with powder diffraction data by an automatic computer indexing method [abs.]: Am. Cryst. Assoc. Ann. Mtg., 1963, Program and Abs., no. E-10, p. 42–43.

Lambert, R. St. J., 1959, The mineralogy and metamorphism of the Moine schists of the Morar and Knoydart districts of Inverness-shire: Royal Soc. Edinburgh Trans., v. 63, pt. 3, p. 553–588.

Misch, Peter, and Hazzard, J. C., 1962, Stratigraphy and metamorphism of Late Precambrian rocks in central northeastern Nevada and adjacent Utah: Am. Assoc. Petroleum Geologists Bull., v. 46, no. 3, pt. 1, p. 289–343.

Velde, Bruce, 1965, Phengite micas—Synthesis, stability, and natural occurrence: Am. Jour. Sci., v. 263, no. 10, p. 886–913.

Whitebread, D. H., Griggs, A. B., Rogers, W. B., and Mytton, J. W., 1969, Geologic map of the Wheeler Peak and Garrison quadrangles, White Pine County, Nevada, and Milford County, Utah: U.S. Geol. Survey Misc. Geol. Inv. Map I-578 [In press].

AN OCCURRENCE OF PERMIAN MANGANESE NODULES NEAR DILLON, MONTANA

By R. A. GULBRANDSEN and D. W. REESER,
Menlo Park, Calif., Hawaii Volcano National Park

Abstract.—Concentrically ringed manganese nodules, similar in form to many found on modern ocean and sea floors, occur in a very fine grained argillaceous sandstone bed of the Permian Park City Formation near Dillon, Mont. They are enriched in many rare elements and contain as much as 2.5 percent zinc, 1.3 percent nickel, and 0.22 percent cobalt. The manganese minerals are chalcophanite and todorokite. The nodules probably formed in a shallow marine oxidizing environment on the western side of the Permian sedimentary basin. The occurrence of an appreciable amount of fluorite in the bed suggests that the water was saline.

A review of manganese-iron accumulations in the marine environment by Manheim (1965) shows that they are widely distributed on modern ocean and sea floors, are of great variety in form, and contain unusual amounts of many rare elements in large-abundance ranges. It is the concentrically ringed nodules that have received the most attention, probably due largely to Mero's (1960) stimulating assessment of the economic potential of the nodules and such associated elements as nickel, cobalt, and copper. Present-day abundance of the nodules is a puzzling contrast to their apparent rarity in the geologic column. The only well-documented occurrence is in the Cretaceous rocks of parts of Indonesia (Molengraaff, 1916, 1921; Audley-Charles, 1965). The nodules described here in Permian rock of Montana are considered to represent another ancient occurrence.

The Permian manganese nodules (iron-poor) that occur in the Park City Formation represent a mode of rare-element enrichment in the Permian rocks of the northern Rocky Mountains not previously described. Only one other occurrence of rare-element enrichment associated with manganese (non-nodular) is known. This is in a thin mudstone near the base of the Meade Peak Phosphatic Shale Member of the Phosphoria Formation at Trail Canyon, Idaho (McKelvey and others, 1953, p. 29, bed P–3), shown by X-ray spectrographic analysis to contain approximately 2 percent manganese, 1 percent zinc, and 0.3 percent nickel. Zinc and nickel, the most abundant rare elements in the manganese nodules, are among those elements enriched in the vanadiferous zone of the Meade Peak in western Wyoming and southeastern Idaho (Love, 1961; McKelvey, 1950; Davidson and Lakin, 1961). The organic-matter- and sulfide-rich vanadiferous mudstone represents a depositional environment, however, that contrasts sharply with the strongly oxidizing one required for the formation of the manganese nodules. Although many rare elements are enriched in both modes of occurrence, some of their magnitudes of enrichment are markedly different.

GEOLOGIC SETTING

The Permian manganese nodules occur in a very fine grained argillaceous sandstone bed of the Franson Tongue of the Park City Formation at Sheep Creek, about 15 miles southwest of Dillon, Mont. (see index map, fig. 1). The Permian section at Sheep Creek was measured, described, and sampled by members of the U.S. Geological Survey as part of an investigation of the Permian phosphate deposits in the Western States, and a spectrographic analysis of a group of the manganese nodules was reported by Swanson and others (1953, sample ERC–388, p. 18). The Franson Tongue is 100.4 feet thick at Sheep Creek, where it consists of interbedded chert, dolomite, and sandstone (Cressman and Swanson, 1964, p. 434–436). The nodule-bearing bed, 2.3 feet thick, occurs near the top of the Franson (fig. 2). The black nodules are enclosed by a dusky-yellowish-orange sandstone matrix that is similar in appearance to both overlying and underlying sandstone beds. About 3 feet above the nodule-bearing bed lies the base of the Retort Phosphatic Shale Member of the Phosphoria Formation. This unit is not only rich

U.S. GEOL. SURVEY PROF. PAPER 650–C, PAGES C49–C57

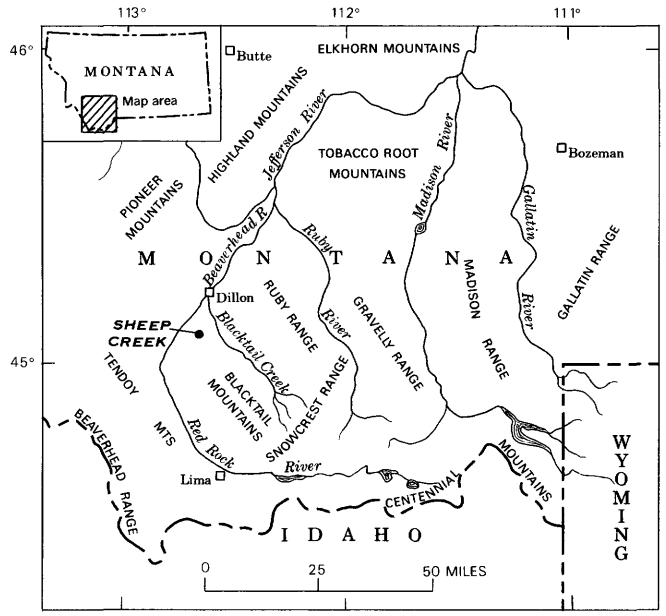

FIGURE 1.—Index map showing location of Sheep Creek manganese nodule occurrence.

in phosphate but contains much oil—one bed as much as 9.7 percent oil (Swanson and others, 1953, p. 23).

The manganese nodules exposed in a bulldozer trench at Sheep Creek have not been recognized at any other locality; the nearest locality containing the interval exposed at Sheep Creek is about 5 miles to the west. Cressman and Swanson (1964), in a detailed study of the origin of the Permian rocks in southwestern Montana, show the Sheep Creek section to be located on the western side of the sedimentation basin but on the eastern edge of the sand facies whose constituents were derived from a northwestern source. They conclude that during deposition of the Franson, which was characterized by the formation of dolomite, the sea was warmer and more saline than normal. The sand of the Franson is considered to have accumulated at depths of less than 50 meters.

Weaver (1955), in a petrographic study of some of the Permian rocks below the Retort Phosphatic Shale Member, including those of the Franson at Sheep Creek, considers the source of the detritus to be chiefly older sediments. He found that kaolinite was the principal clay mineral in the detrital rocks at Sheep Creek, and at another locality about 30 miles to the south, constituting as much as 20 percent of some rocks. At a locality about 25 miles northwest of Sheep Creek, however, illite is more abundant than kaolinite. Weaver found two occurrences of montmorillonite, one in an insoluble residue of carbonate rock at a locality south of Sheep Creek, the other in some small veins in dolomite at Sheep Creek near the base of the Franson Tongue. Three clay layers described by Swanson and

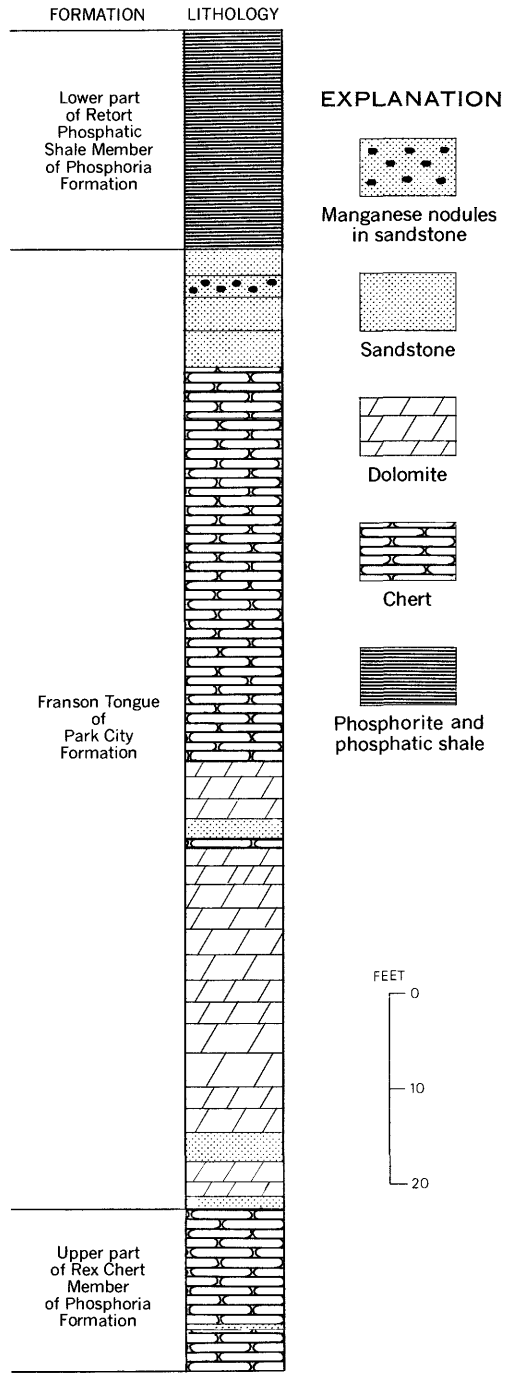

FIGURE 2.—Part of Permian stratigraphic section at Sheep Creek, Mont. Data from Cressman and Swanson (1964, p. 434–436).

others (1953, p. 18) within a chert bed about 50 feet below the top of the Franson at Sheep Creek appear to contain significantly more montmorillonite than kaolinite. Semiquantitative spectrographic analyses (Swanson and others, 1953, p. 21, 22) indicate also that the layers may be enriched in manganese, nickel, and zinc. It is possible that these layers are partly of

bentonitic origin and are an indication of the Permian volcanism that occurred west of here. No montmorillonite is present in the manganese-nodule-bearing bed or adjacent ones, however, and the significance of these layers is not known.

THE MANGANESE NODULE BED

The manganese nodules are most abundant in the upper part of the very fine grained sandstone bed in which they are found. They occur in a variety of shapes, but tend to be spherical (see fig. 3). The common size is about 2–4 centimeters in diameter, the range about 0.5 to 8 cm. There are compound nodules (see fig. 4) that well illustrate the growth of the nodules outward from a nuclear area. Note in the section of the compound nodule (fig. 4) that the inner growth rings define two discrete nodules and that the outer ones are continuous around both. Nearly all nodules show well-defined growth rings, but in some the rings are diffuse. No nuclear material that is foreign to other parts of the nodules has been discovered, and qualitative X-ray spectrographic analyses of inner and outer parts of the nodules reveal no marked compositional differences. The surfaces of the nodules are irregular, pustulate—some with marked protuberances. Although attention is devoted here to the nodules, all of the manganese is not in this form. Some is lightly and irregularly disseminated in the sandstone and in streaks that parallel the bedding.

Mineral composition

The nodules are composed of two manganese minerals, chalcophanite and todorokite, plus quartz, dolomite, fluorite, kaolinite, apatite, goethite, and trace amounts of muscovite-illite. Except for the manganese minerals, the mineral suite is the same as that of the host rock or matrix for the nodules. Quartz appears to be the most abundant mineral, although the combined manganese minerals may be greater in some nodules. Dolomite is a major constituent in some nodules. Fluorite, kaolinite, and apatite are consistently present in small amounts. Goethite, although in small amount, appears to provide the dusky-yellowish-orange coloration of the matrix rock. Fluorite is irregularly distributed as microcrystalline aggregates; its significance is discussed later in the paper.

Because the regular constituents of the matrix rock are incorporated in the manganese nodules, the nodules must have developed either contemporaneously with sedimentation or at some later time. The bedding, which is poorly developed, provides no clue in this regard.

Efforts to separate and concentrate todorokite were not successful, and the mineral is identified solely on the basis of its principal X-ray peaks of about 9.6 angstroms and 4.8 angstroms. Chalcophanite, however, was found to make up the residue, along with fluorite, after treatment of a portion of a nodule with concentrated HF. X-ray data shown in table 1 were obtained from this sample. The main peaks of chalcophanite are discernible on all X-ray patterns of the nodules but characteristically are of small intensity. The todorokite peaks are barely evident on most patterns but are relatively strong on some. A protuberance on one nodule showed the strongest todorokite peaks. On the basis of X-ray intensities, therefore, chalcophanite is the predominant manganese mineral in the nodules; however, possible differences in crystallinity or ordering of the phases makes any estimate of relative magnitudes somewhat tenuous.

TABLE 1.—*X-ray diffraction data of chalcophanite*

[ND, not determined]

Montana[1]		Sterling Hill, Franklin, N.J.[2]			
d (measured)	*I*	*d* (measured)	*I*	*d* (calculated)	*hkl*
6. 96	100	6. 96	10	6. 95	001
6. 26	15	6. 23	1	6. 22	010
4. 08	25	4. 08	5	4. 07	011
3. 51	35	3. 50	6	3. 51	$\bar{1}12$
3. 47	25			3. 47	002
3. 31	15	3. 32	1	3. 31	$\bar{1}21$
([3])		3. 23	½	3. 22	$\bar{2}21$
2. 76	15	2. 77	2	2. 76	$\bar{2}22$
2. 70	5	2. 71	½	2. 71	012
2. 56	15	2. 57	4	2. 57	021
				2. 55	$\bar{1}22$
2. 45	60	2. 46	2	2. 45	$\bar{1}30$
2. 41	25	2. 41	2	2. 42	$\bar{1}13$
2. 40	25			2. 40	$\bar{2}31$
2. 23	50	2. 24	5	2. 23	$\bar{1}31$
2. 12	5	2. 13	2	2. 12	$\bar{2}32$
ND		1. 986	½	1. 985	013
([3])		1. 900	3	1. 898	$\bar{1}32$
ND		1. 849	1	1. 842	$\bar{3}33$, 031
1. 794	10	1. 795	2	1. 801	$\bar{3}41$
				1. 790	$\bar{2}33$
ND		1. 750	½		
ND		1. 715	½		
([3])		1. 668	1		
1. 593	20	1. 597	4		

[1] Cu radiation, λ=1.5418 A. CaF_2 internal standard.
[2] Data from Berry and Thompson (1962, p. 206).
[3] Obscured by CaF_2 peak.

Although Palache and others (1944, p. 739) show chalcophanite to be principally a hydrated oxide of zinc and tetravalent manganese, recent reports (Hewett

FIGURE 3.—Permian manganese nodules. Light spots on nodules are bits of rock matrix.

and Radtke, 1967; Radtke and others, 1967) of new occurrences indicate that many elements may replace zinc. Radtke and others (1967) have named one silver-rich variety, aurorite, that contains only 0.25 percent ZnO. They derived a general formula for aurorite, $(R)R'_3O_7 \cdot 3H_2O$, that is in agreement with Wadsley's (1953) structural analysis of chalcophanite and the formula $ZnMn_3O_7 \cdot 3H_2O$. In the mineral series, therefore, the data indicate that R represents Zn, Mn^{+2}, Ag, Ba, Ca, Mg, K, Pb, and Cu; and R′ includes Mn^{+4}, Fe^{+3}, Al, and Si. Not only is the number of elements that appear to be able to fit in the R position large but the range in ionic radii is unusual—0.69 A for Mg to 1.34 A for Ba.

Because chalcophanite probably is the principal manganese mineral of the nodules described here, the chemical analysis of two nodules, table 2, provides some information about the mineral's composition. The elements concentrated in the nodules along with manganese, as contrasted with the matrix rock (analysis 3), are Zn, Ni, Cd, Co, Tl, Cu, and Mo. That they are associated with the chalcophanite was shown by a qualitative X-ray spectrographic analysis of the chalcophanite-fluorite concentrate, referred to above, in which the proportions relative to Mn appear to be approximately the same as in a similar analysis of the whole sample. If all these elements are indeed in chalcophanite, the number and range of ionic sizes of elements in the mineral are both extended beyond the above list. The principal constituents, in addition to Mn^{+4} and H_2O, appear to be Zn, Mn^{+2}, Ni, Cd, and Co. The other major constituents in the analyses are adequately accounted for by other mineral phases.

Since attempts to concentrate todorokite were unsuccessful, direct evidence of its composition in this occurrence is lacking. Much recent data however, on the composition of todorokite is available. Like chalcophanite, todorokite is basically a hydrated tetravalent manganese oxide. It even appears to have a zinc analog, woodruffite (Frondel, 1953). Todorokite also apparently may contain about the same large and varied suite of elements (Hewett and Fleischer, 1960; Straczek and others, 1960; Frondel and others, 1960; Levinson, 1960; Larson, 1962; Radtke and others, 1967). The difference between the two minerals seems to be in the cation proportions and amounts of H_2O. At present there is no agreement among the workers on the specific composition and structure of todorokite. The composition of todorokite in the nodules described here, therefore, is probably similar to chalcophanite, the elements available in this occurrence being distributed between two different yet similar structures.

Unlike chalcophanite, which has not previously been identified in marine manganese nodules, todorokite is a widespread component of modern nodules and possibly the principal one (Straczek and others, 1960, p. 1176; Hewett and others, 1963, p. 38; Manheim, 1965, p. 248; Meylan and Goodell, 1967, p. 149). Both minerals appear to be of primary formation in the Permian nodules. They are of secondary formation in occurrences in some manganese deposits of other origins (Hewett and Fleischer, 1960, p. 11, 13).

FIGURE 4.—Sawed halves of Permian manganese nodules, showing concentric growth rings. Note compound nodule on right side of photograph.

Chemical composition

Manganese nodules are possibly most noted for their contents of nickel, copper, and cobalt. The chemical analyses of the Permian nodules, table 2, reveal this characteristic, although the amount of copper is unusually low relative to the amounts of nickel and cobalt and in comparison with Manheim's estimated averages of the amounts in deep-ocean nodules shown in table 2. Nickel, on the other hand, is unusually high in Permian nodule 1. The individual amounts of these three elements, of nickel especially, tend to characterize the marine manganese nodules, as shown by the data of Hewett and others (1963) in comparison with other geologic environments of manganese deposition—supergene oxides, hypogene vein oxides, hot-spring apron oxides, and stratified oxides.

The amounts of zinc in the Permian nodules are the highest so far reported—about 3 to 4 times greater than the maximum of 0.6 percent Zn found by Riley and Sinhaseni (1958, p. 477) in a Pacific nodule. Cadmium, similar geochemically to zinc, is also high, and both are above expected amounts in the matrix rock. The reason for this is not known; no other zinc mineral has been recognized, even among the heavy accessory minerals of the matrix rock.

The amount of iron shown in Manheim's average nodule (table 2) is about the same magnitude as manganese, whereas the amounts in the Permian nodules are extremely low, near the minimum of 0.8 reduced weight percent found by Mero (1962, table 2, p. 762) in Pacific nodules. The amounts present are apparently due to background sedimentation as indicated by the amount in the matrix rock (analysis 3 in table 2). This suggests that the separation of iron from manganese in solution occurred elsewhere, owing to the greater ease of oxidizing the ferrous ion than manganese ion (Krauskopf, 1957), and because only manganese was available for oxidation and fixation in the nodules of this locality.

Vanadium and molybdenum are moderately concentrated in the nodules as compared with the matrix

TABLE 2.—*Chemical composition, in weight percent, of manganese nodules and matrix rock*

	Deep ocean average nodule [1]	Permian nodule 1 [2]	Permian nodule 1 [2]	Permian matrix 3 [3]
Oxides				
SiO_2	16.2	38.5	49.8	----
Al_2O_3	4.6	5.6	3.5	5.7
TiO_2	.94	.08	.10	.08
Fe_2O_3(total)	16.7	.61	.55	1.4
MnO(total)	24.5	18.69	7.47	.04
CaO	2.2	14.0	13.8	4.2
MgO	2.3	.23	4.2	.12
K_2O	.82	----	----	----
Na_2O	2.8	.07	.04	.04
P_2O_5	.44	2.1	1.9	4.6
CO_2	.61	.93	9.3	----
H_2O+	----	5.8	4.1	----
H_2O-	----	2.6	1.1	----
O(excess)	5.0	3.42	1.20	----
Ignition loss	25	----	----	----
Elements				
F	----	6.4	3.1	----
Zn	0.04–0.4	2.5	1.4	.15
Ni	.58	1.3	.68	.007
Co	.28	.22	.08	.0015
As	----	.04	.06	----
B	.01	.0015	.0015	.002.
Ba	.15	.01	.03	.01
Cd	.001	.12	.05	.015
Cr	.001	.007	.01	.01
Cu	.40	.02	.015	.002
Mo	.038	.007	.005	.0015
Sc	.001	.001	.0007	.0015
Sr	.06	.01	.01	.01
Te	----	.0001	.0001	----
Tl	.01	.1	.03	0
V	.044	.07	.07	.02
Y	.013	.002	.003	.005
Yb	.0025	.0003	.0003	.0005
Zr	.040	.007	.015	.02

[1] Data from Manheim (1965, p. 245 and 247).
[2] SiO_2, Al_2O_3, Fe_2O_3, MgO of nodule 2, CaO, H_2O+, H_2O-, TiO_2, P_2O_5, CO_2, F, Ni, As, and Zn analyses by Lois Schlocker, A. C. Bettiga, and W. W. Brannock. MnO and excess O analyses by S. Neil. Cd, Co, and MgO of nodule 1 are quantitative spectrographic analyses by R. E. Mays. Te analyses by H. M. Nakagawa. Other elements are semiquantitative spectrographic analyses by Chris Heropoulos.
[3] Semiquantitative spectrographic analyses by Chris Heropoulos.

rock and are among those elements expected in this mode of occurrence.

Arsenic, for which few data have been reported, is present in the Permian nodules in amounts about 30 to 45 times greater than in average shale (Turekian and Wedepohl, 1961). Sevast'yanov (1967) has reported arsenic contents of manganese-iron concretions, oxidized sediment, and reduced sediment in the Black Sea as 380–910 parts per million, 26–61 ppm, and 3–26 ppm, respectively. The amounts in the Permian nodules (table 2) agree well with Sevast'yanov's values, and his range for reduced sediments includes the value of 13 ppm as given by Turekian and Wedepohl (1961) for average shale. Sevast'yanov attributes the enrichment of arsenic in the oxidized sediment and in the nodules to its polyvalent character, where, like manganese, its higher valent ion is readily formed and fixed in an oxidizing environment.

Thallium is enriched in the Permian nodules about 3 to 11 times more than Manheim's average nodule (table 2), which itself is a significant concentration as compared with the 1.4 ppm of shale (Turekian and Wedepohl, 1961). Little is known about thallium, but because it is readily adsorbed by clays (Krauskopf, 1955, p. 453), its concentration in the nodules may be due to the well-known adsorption capability of manganese.

Rare earths, including yttrium, are frequently enriched in manganese nodules by an order of magnitude over their abundance in marine sediment (Ehrlich, 1968, p. 18, 67) and also show a distribution pattern characterized by an enrichment of cerium. The value Manheim gives for yttrium in table 2 is representative of this total rare-earth enrichment. The values for yttrium in the Permian nodules are well below Manheim's and, in comparison with the amount in the matrix rock, indicate no enrichment. This is substantiated by the complete determination (shown in table 3) of

TABLE 3.—*Rare-earth content of a Permian nodule from the Permian Park City Formation near Dillon, Mont.*[1]

Element	*Content (ppm)*
La	12.7
Ce	11
Pr	3.37
Nd	11.5
Sm	2.52
Eu	.58
Tb	.38
Dy	2.12
Ho	.59
Tm	.172
Yb	.92
Y	18.9

[1] Data from Ehrlich (1968, p. 67), who also reported the following (p. 69): Mn (6.4 percent), Ca (9.4 percent), C as CO_2 (17 percent), P (1.1 percent), and Fe (0.30 percent)

the rare earths in one of these Permian nodules (6.4 percent Mn) by Ehrlich (1968, p. 67). Of special interest is Ehrlich's finding that the distribution pattern of the rare earths in the Permian nodule indicates a cerium depletion, rather than enrichment, similar to what he found for phosphorite material and to what is shown for marine apatite by Altschuler and others (1967). It seems likely, therefore, that the rare-earth content of the Permian nodules and matrix rock is mostly due to the apatite common to both, and perhaps the rare earths, as a whole, have been preferentially taken up by the apatite, which makes up a greater part of the total rock than the manganese minerals do.

Tellurium is reported by Lakin and others (1963, p. 1568–1569) to be present in a group of 12 nodules from the Pacific and Indian Oceans in amounts ranging from 5 to 125 ppm. They note the possibility of an association of these unusual amounts of tellurium with volcanic emanations. The determinations of 1 ppm for the Permian nodules fall somewhat below the lowest

value given by Lakin and others, but still represent an appreciable concentration over the 0.01–ppm value given for average clays and shales by Vinogradov (1962).

SIGNIFICANCE OF FLUORITE

The presence of a significant amount of fluorite in the nodule bed is of particular interest. Hewett and Fleischer (1960, p. 6) note that fluorite is generally considered to be of hydrothermal and hypogene origin in its association with many manganese deposits. Few data of the occurrence here can be interpreted to support this mode of origin. On the other hand, Kazakov and Sokolova (1950) cite many occurrences of sedimentary fluorite in evaporitic sequences of dolomite, dolomitized limestones, and gypsum and anhydrite; and their experimental work supports this mode of origin. Occurrences in the Permian rocks of the northern Rocky Mountain region provide additional examples of sedimentary origins.

Fluorite is widespread in very small amounts in some phosphorites of the Phosphoria Formation, but it is secondary in these occurrences and apparently is the product of a diagenetic reorganization of apatite. Rare occurrences in Permian carbonate rocks of Wyoming have been noted by Sheldon (1963, p. 144) and Gulbrandsen (1960, p. 114). Of most significance, however, is a remarkable occurrence in a Permian carbonate rock sequence in the northern part of the Big Horn Basin of Wyoming that is reported by DeKoster (1960, p. 53–55). He found 12–15 percent fluorite in a dolomitic limestone. Of special importance is the facies change he shows eastward from the carbonate sequence to one within 20 miles that is dominated by gypsum. A possible interpretation of this spatial relationship of fluorite and gypsum is that the fluorite was precipitated from saline waters at a stage of evaporation shortly preceding that at which gypsum is formed. If this were so, the position within an evaporite sequence for the formation of fluorite, as predicted by Kazakov and Sokolova (1950) on the basis of experimental work, is further affirmed. Their data indicate that this could occur at a stage where sea water was concentrated 3 to 4 times. Fluorite could precipitate at an earlier stage of sea-water concentration if an extra supply of fluorine were possible, such as from the dissolution of pyroclastic material in in sea water or from volcanic gases. Mansfield (1940), of course, indicated Permian volcanism as an extra source for fluorine as an aid in forming apatite of the Phosphoria Formation. An association of volcanism and phosphorite formation does appear to exist (Gulbrandsen, 1969), but its significance is not yet clear.

A primary sedimentary origin for the fluorite in the nodule bed is considered plausible and is not inconsistent with any other features. It probably indicates, however, a more saline environment for the formation of manganese nodules than any known so far.

SUMMARY

The manganese nodules described here are considered to have formed virtually syngenetically with their enclosing sediments in a shallow marine environment. The features of this single occurrence in Permian rock in Montana are not identical in all aspects with any known occurrence on the modern sea or ocean floors, but none of the many and broadly ranging characteristics of modern deposits appear to uniquely define a marine origin. An epigenetic hypogene origin in which manganese and associated elements would have been transported by hydrothermal solutions laterally along bedding into this depositional site cannot be disproved, but it is an origin for which positive evidence is meager.

Features of this deposit that appear particularly significant in a concept of marine origin are the following:

1. Both manganese minerals, chalcophanite and todorokite, appear to be of primary formation in this occurrence.
2. The high nickel content of one of these nodules (analysis 1 of table 2) is especially characteristic, although not unique, of many nodules of marine origin.
3. The occurrence of manganese in the form of discrete nodules that tend to a spherical shape and show concentric growth rings is a common feature of marine deposits and not characteristic of deposits of other origins.

The features of this occurrence of manganese nodules do not provide any conclusive information as to the source of the manganese and associated elements. An association with Permian volcanism is possible, but the wide distribution of modern nodules, as shown by Manheim (1965), including areas remote from any possible volcanic effects, indicates that the ocean itself, and the supply of elements from the continents, is a sufficient source. The deposition of manganese, therefore, seems to be principally dependent upon a special environment, one that is strongly oxidizing and can can raise Mn^{+2} to higher valent forms that are precipitated as oxides. Most of the many elements associated with the manganese are probably adsorbed by the manganese oxides by processes that are poorly understood.

The presence of fluorite in the nodule bed places definite restraints upon a marine origin for the nodules as it requires a marked concentration of sea water beyond that indicated by any other characteristics of

the Permian rocks in the region. The presence of dolomite is compatible in this respect, but probably does not require highly saline waters for its formation. If the Permian sea were somehow enriched in fluorine, a lesser degree of concentration would be required for the formation of fluorite. The subsequent formation of large amounts of apatite in this sea is consistent with a condition of fluorine enrichment, though not required.

It is possible, however, that the conditions under which the manganese nodules were formed are barely perceived at our present state of knowledge of the marine environment. This is forcefully illustrated by the recent discoveries of sedimentary iron and heavy-metal deposits in the Red Sea that appear to be derived from existing hot brines of heretofore unknown compositions (Miller and others, 1966).

REFERENCES

Altschuler, Z. S., Berman, Sol, and Cuttitta, Frank, 1967, Rare earths in phosphorites—Geochemistry and potential recovery, *in* Geological Survey Research 1967: U.S. Geol. Survey Prof. Paper 575–B, p. B1–B9.

Audley-Charles, M. G., 1965, A geochemical study of Cretaceous ferromanganiferous sedimentary rocks from Timor: Geochim. et Cosmochim. Acta, v. 29, no. 11, p. 1153–1173.

Berry, L. G., and Thompson, R. M., 1962, X-ray powder data for ore minerals—The Peacock atlas: Geol. Soc. America Mem. 85, 281 p.

Cressman, E. R., and Swanson, R. W., 1964, Stratigraphy and petrology of the Permian rocks of southwestern Montana: U.S. Geol. Survey Prof. Paper 313–C, p. 275–569.

Davidson, D. F., and Lakin, H. W., 1961, Metal content of some black shales of the western United States: Art. 267 *in* U.S. Geol. Survey Prof. Paper 424–C, p. C329–C331.

DeKoster, G. R., 1960, Petrology of the (Permian) Phosphoria Formation carbonates, eastern Big Horn Basin, Wyoming: Iowa State Univ. Sci. and Technology, Ames, M. A. thesis, 112 p.

Ehrlich, A. M., 1968, Rare earth abundances in manganese nodules: Massachusetts Inst. Technology, Cambridge, Ph. D. thesis, 220 p.

Frondel, Clifford, 1953, New manganese oxides—hydrohausmannite and woodruffite [N.J.]: Am. Mineralogist, v. 38, nos. 9–10, p. 761–769.

Frondel, Clifford, Marvin, U. B., and Ito, Jun, 1960, New occurrences of todorokite: Am. Mineralogist, v. 45, nos. 11–12, p. 1167–1173.

Gulbrandsen, R. A., 1960, Petrology of the Meade Peak phosphatic shale member of the Phosphoria formation at Coal Canyon, Wyoming: U.S. Geol. Survey Bull. 1111–C, p. 71–146.

——— 1969, Physical and chemical factors in the formation of marine apatite: Econ. Geology, v. 64, no. 4.

Hewett, D. F., and Fleischer, Michael, 1960, Deposits of the manganese oxides: Econ. Geology, v. 55, no. 1, pt. 1, p. 1–55.

Hewett, D. F., Fleischer, Michael, and Conklin, Nancy, 1963, Deposits of the manganese oxides—supplement: Econ. Geology, v. 58, no. 1, p. 1–51.

Hewett, D. F., and Radtke, A. S., 1967, Silver-bearing black calcite in western mining districts: Econ. Geology, v. 62, no. 1, p. 1–21.

Kazakov, A. V., and Sokolova, E. I., 1950, Florapatitovaya sistema ravnovesii v usloviyakh obrazovaniya osadochnykh porod [Conditions of the formation of fluorite in sedimentary rocks]: Akad. Nauk SSSR, Inst. Geol. Nauk Trudy, vyp. 114, Geol. Ser., no. 40, p. 22–64. [Translation by V. L. Skitsky, 1951, U.S. Geol. Survey Trace Elements Inv. Rept. 386, p. 1–76]

Krauskopf, K. B., 1955, Sedimentary deposits of rare metals: Econ. Geology, 50th Anniversary Volume, p. 411–463.

——— 1957, Separation of manganese from iron in sedimentary processes: Geochim. et Cosmochim. Acta, v. 12, nos. 1–2, p. 61–84.

Lakin, H. W., Thompson, C. E., and Davidson, D. F., 1963, Tellurium content of marine manganese oxides and other manganese oxides: Science, v. 142, no. 3599, p. 1568–1569.

Larson, L. T., 1962, Zinc-bearing todorokite from Philipsburg, Montana: Am. Mineralogist, v. 47, nos. 1–2, p. 59–66.

Levinson, A. A., 1960, Second occurrence of todorokite: Am. Mineralogist, v. 45, nos. 7–8, p. 802–807.

Love, J. D., 1961, Vanadium and associated elements in the Phosphoria formation in the Afton area, western Wyoming: Art. 250 *in* U.S. Geol. Survey Prof. Paper 424–C, p. C279–C282.

Manheim, F. T., 1965, Manganses-iron accumulations in the shallow marine environment, *in* Symposium on marine geochemistry: Rhode Island Univ. Narragansett Marine Lab. Occasional Pub. 3, p. 217–276.

Mansfield, G. R., 1940, The rôle of fluorine in phosphate deposition: Am. Jour. Science, v. 238, p. 863–879.

McKelvey, V. E., 1950, Potential by-product elements in the Phosphoria Formation of the western states: U.S. Geol. Survey Trace Elements Inv. Rept. 131, 10 p.

McKelvey, V. E., Armstrong, F. C., Gulbrandsen, R. A., and Campbell, R. M., 1953, Stratigraphic sections of the Phosphoria formation in Idaho, 1947–48, pt. 2: U.S. Geol. Survey Circ. 301, p. 58.

Mero, J. L., 1960, Minerals on the ocean floor: Sci. American, v. 203, no. 6, p. 64–72.

——— 1962, Ocean-floor manganese nodules: Econ. Geology, v. 57, no. 5, p. 747–767.

Meylan, M., and Goodell, H. G., 1967, Mineralogy of manganese nodules from the southern oceans: Geol. Soc. America, 80th Ann. Mtg., New Orleans 1967, Program, p. 149.

Miller, A. R., Densmore, C. D., Degens, E. T., Hathaway, J. C., Manheim, F. T., McFarlin, P. F., Pocklington, R., and Jokela, A., 1966, Hot brines and recent iron deposits in deeps of the Red Sea: Geochim. et Cosmochim. Acta, v. 30, no. 3, p. 341–360.

Molengraaf, G. A. F., 1916, On the occurrence of nodules of manganese in Mesozoic deep-sea deposits from Borneo, Timor, and Rotti, their significance and mode of formation: Acad. Sci. Amsterdam, Proc. v. 18, p. 415–340.

Molengraaf, G. A. F., and Beaufort, L. F. de, 1921, On manganese nodules in Mesozoic deep-sea deposits of Dutch Timor: Acad. Sci. Amsterdam, Proc. v. 23, p. 997–1012.

Palache, Charles, Berman, Harry, and Frondel, Clifford, 1944, Elements, sulphides, sulfosalts, oxides, v. 1 *of* The system of mineralogy of James Dwight Dana and Edward Salisbury Dana, 7th ed.: New York, John Wiley and Sons, Inc., 834 p.

Radtke, A. S., Taylor, C. M., and Hewett, D. F., 1967, Aurorite, argentian todorokite, and hydrous silver-bearing lead manganese oxide: Econ. Geology, v. 62, no. 2, p. 186–206.

Riley, J. P., and Sinhaseni, Prapas, 1958, Chemical composition of three manganese nodules from the Pacific Ocean: Jour. Marine Research, v. 17, p. 466–482.

Sevast'yanov, V. F., 1967, Redistribution of arsenic during formation of iron-manganese concretions in Black Sea sediment: Acad. Sci. USSR Doklady, Earth Sci. sect., v. 176, p. 180–182. [English translation]

Sheldon, R. P., 1963, Physical stratigraphy and mineral resources of Permian rocks in western Wyoming: U.S. Geol. Survey Prof. Paper 313–B, p. 49–273.

Straczek, J. A., Horen, Arthur, Ross, Malcolm, and Warshaw, C. M., 1960, Studies of manganese oxides—[pt.] 4, Todorokite: Am. Mineralogist, v. 45, nos. 11–12, p. 1174–1184.

Swanson, R. W., Lowell, W. R., Cressman, E. R., and Bostwick, D. A., 1953, Stratigraphic sections of the Phosphoria Formation in Montana: U.S. Geol. Survey Circ. 209, 31 p.

Turekian, K. K., and Wedepohl, K. H., 1961, Distribution of the elements in some major units of the earth's crust: Geol. Soc. America Bull., v. 72, no. 2, p. 175–192.

Vinogradov, A. P., 1962, Average contents of chemical elements in the principal types of igneous rocks of the earth's crust: Geochemistry (Geokhimiya), no. 7, p. 641–664.

Wadsley, A. D., 1953, Interstitial atoms in the layer structure $ZnMn_3O_73{\cdot}H_2O$ (chalcophanite): Nature, v. 172, no. 4389, p. 1103–1104.

Weaver, C. E., 1955, Mineralogy and petrology of the rocks near the Quadrant-Phosphoria boundary in southwest Montana: Jour. Sed. Petrology, v. 25, no. 3, p. 163–193.

FAUNAL EVIDENCE FOR AN UNCONFORMITY BETWEEN THE PALEOCENE BRIGHTSEAT AND AQUIA FORMATIONS (MARYLAND AND VIRGINIA)

By JOSEPH E. HAZEL, Washington, D.C.

Abstract.—It has recently been suggested that the lower Danian Brightseat Formation is conformable with the overlying Aquia Formation. Data from a study of the Brightseat and Aquia ostracodes and foraminifers oppose such an interpretation and indicate that a disconformity equivalent to the middle Paleocene *Globorotalia uncinata-Globigerina spiralis* and *Globorotalia pusilla pusilla-Globorotalia angulata* zones is present.

The contact relationship between the oldest exposed Tertiary formation in the Maryland-Virginia region, the Brightseat Formation, and the overlying Aquia Formation has been the subject of some dispute. Bennett and Collins (1952), who proposed the Brightseat as a formation, and Cooke (1952) consider the Brightseat-Aquia contact a disconformity, mainly on lithologic and stratigraphic evidence. On the other hand, more recently, Nogan (1964) in a faunal study and Drobnyk (1965) on sedimentological grounds consider the contact to be transitional. Because of its importance in regional paleogeographic studies, this problem should be resolved.

DISTRIBUTION AND STRATIGRAPHIC RELATIONSHIPS

The Brightseat Formation crops out (figs. 1, 2) only in a few areas in Maryland and Virginia near the District of Columbia. The contact with the overlying Aquia Formation is best seen at a locality in Cabin Branch (loc. 34, this report; Hazel, 1968) in western Prince Georges County, Md. This is the only known locality where both the lower beds of the Aquia and the Brightseat are fossiliferous, a part of the section evidently not seen by Clark and Martin before publication in 1901 of their classic report on the Eocene deposits of Maryland and Virginia. The contact is also well exposed along nearby Addison Road (loc. 33, this report; Hazel, 1968), but the sands of the Aquia are oxidized down to the contact.

South of the District of Columbia, the Brightseat-Aquia contact was exposed in roadcuts during recent construction along Maryland State Highway 210 (figs. 1, 2, loc. *A*); here, however, both formations are,

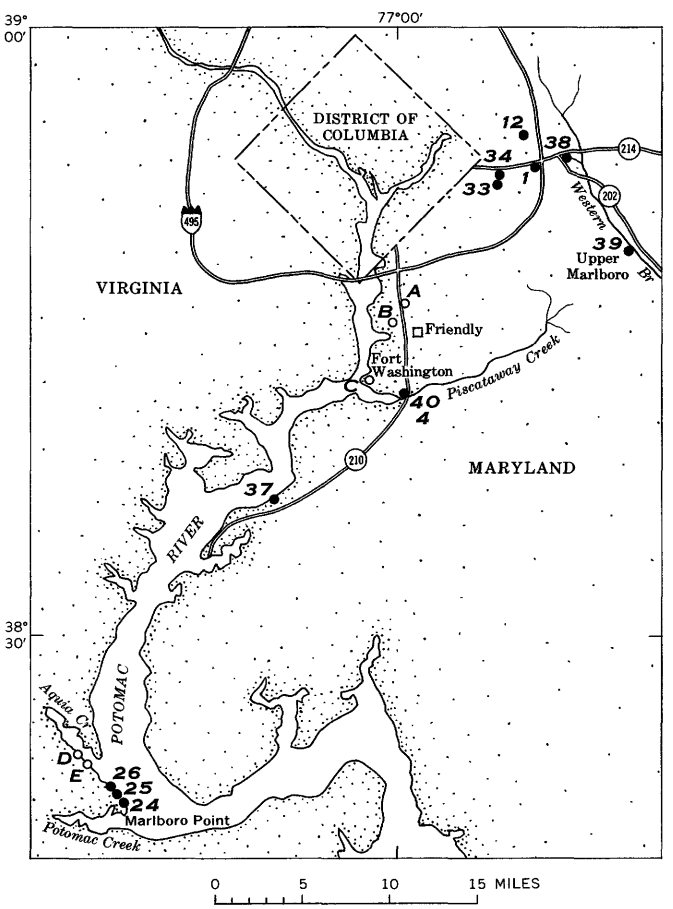

FIGURE 1.—Map showing location of microfossiliferous localities (black dots) used in constructing figure 3. Open circles show location of other localities mentioned in the text. The Brightseat Formation crops out at localities *12*, *33*, *34*, *38*, *A*, *D*, and *E*. It is microfossiliferous only at the numbered localities. At localities *12*, *33*, *34*, *38*, and *A*, the Brightseat overlies the Upper Cretaceous Monmouth Formation. At localities *D* and *E*, the Brightseat overlies the Lower Cretaceous Patapsco Formation. The Aquia Formation is in contact with the Cretaceous at localities *B* (not seen), *C*, and *37*. At the first two it overlies the Monmouth and at the last the Patapsco.

deeply weathered and, except for molds and casts, are unfossiliferous. At Fort Washington and Friendly, Md. (figs. 1, 2, loc. *B*, *C*), the Aquia disconformably overlies the Monmouth Formation of Late Cretaceous age which in this area disconformably overlies the Lower Cretaceous Patapsco Formation (Darton, 1951; Cooke, 1952). At Glymont Wharf, Md. (figs. 1, 2, loc. *37*), the Aquia rests directly on the Patapsco Formation. Along Aquia Creek in Stafford County, Va., sands lithologically similar to those of the Brightseat in the type area, but without fossils, overlie the Patapsco Formation and are overlain by weathered Aquia sands (figs. 1, 2, loc. *D*, *E*). Clark and Martin (1901) probably saw what is now called Brightseat at these localities but included it in their unfossiliferous "zone" 1 of the Aquia (Hazel, 1968).

The stratigraphic relationships of the Aquia to the Brightseat suggest that in places the Brightseat may have been eroded away before deposition of the Aquia, a point already made by Cooke (1952).

Other, mainly physical, phenomena which are commonly characteristic of Coastal Plain disconformities are associated with the Brightseat-Aquia contact in Cabin Branch and along adjacent Addison Road. A concentration of phosphatic material is found near the boundary between the two formations, particularly in the basal shell bed of the Aquia. This includes phosphatic pebbles, shark teeth, and, particularly at the Addison Road locality (loc. 33, this report; Hazel, 1968), phosphatized internal molds of bivalves (see also Cooke, 1952, p. 20). There are many worn, green mollusk shell fragments in the lowermost Aquia; some of these may be of Cretaceous origin. Rounded to subangular quartz pebbles similar to those in the Lower Cretaceous Patapsco Formation also occur in the basal Aquia.

MICROFAUNAL RELATIONSHIPS

Nogan (1964), in his study of the Brightseat and Aquia Foraminiferida, points out that the Cabin

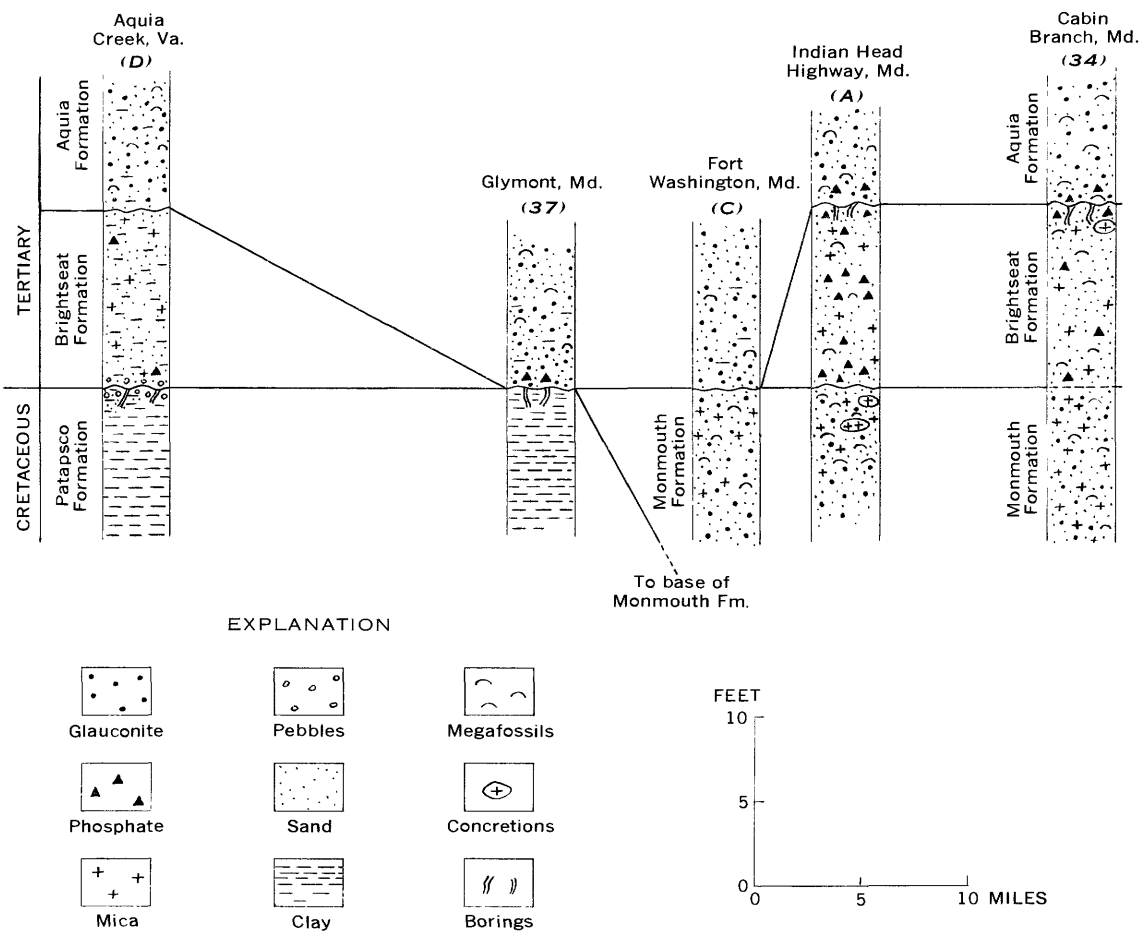

FIGURE 2.—Stratigraphic relationships of the Brightseat and Aquia Formations from Aquia Creek, Va., to western Prince Georges County, Md. See figure 1 for location of sections; datum is the Cretaceous-Tertiary contact.

337-735 O—69——5

Branch section contains beds stratigraphically below those sampled in the type area by Shifflett (1948) and Loeblich and Tappan (1957a, b) in their work on the Aquia foraminifers. Nogan sampled across the Brightseat-Aquia contact and concluded (1964, p. 11) that "the planktonic fauna of the basal portion of the Aquia Formation is * * * transitional to those [sic] of the Brightseat and the overlying sections of the Aquia." This is based principally on his finding *Globorotalia compressa* and the cosmopolitan lower Danian planktonic *Globoconusa daubjergensis* with keeled globorotaliids in the lower 2 feet of the Aquia. Nogan excludes the possibility of reworking of Brightseat elements into the basal Aquia because the specimens are well preserved and "because many of the benthonic species of the Brightseat are not found in the basal part of the Aquia" (Nogan, 1964, p. 11–12). The quoted statement tends to contravene rather than corroborate Nogan's conclusions. Drobnyk (1965), influenced by Nogan's work, considers the physical evidence for an unconformity as inconclusive.

Figure 3 gives the ranges within the planktonic foraminifer zonal scheme advocated by Berggren (1965) of 16 of the better known planktonic species in the Brightseat and Aquia Formations. Figure 4 shows the distribution of these planktonic species and 44 of the more commonly occurring ostracode species

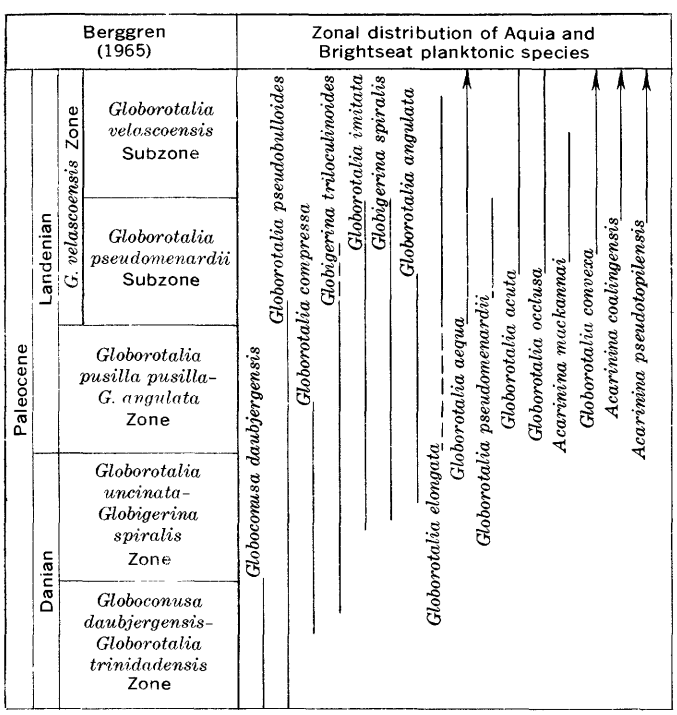

FIGURE 3.—Distribution of some well-known Brightseat and Aquia planktonic foraminifer species in the zones used by Berggren (1965). Range data mainly from Loeblich and Tappan (1957a, b) and Berggren (1965, 1968).

in the Brightseat Formation and the Piscataway Member and lower part of Paspotansa Member of the Aquia Formation. The position of the "zones" of Clark and Martin (1901) are also shown. Ostracode ranges are based on Hazel (1968), Schmidt (1948), and faunal and physical correlation of the localities shown (see "Localities" section). Foraminifer ranges are based on occurrences given by Shifflett (1948; also see Loeblich and Tappan, 1957b, p. 1128), Loeblich and Tappan (1957a), Nogan (1964), and Hermann Duque-Caro and W. A. Berggren (written communs., 1968).

The contrast between the Brightseat and Aquia ostracode assemblages is striking. Only four species cross the boundary between the two formations. In my opinion, a change of this magnitude would be unlikely between transitional arenaceous units with a similar generic composition. A more gradual change, such as that shown by ostracode assemblages in the Paleocene of the Gulf Coast, where there is a fairly steady addition and subtraction of species through the Clayton, Porters Creek, Naheola, and Nanafalia Formations, should be expected.

The ostracode species *Phractocytheridea aquia* (Schmidt), *Hermanites bassleri* (Ulrich), *Hazelina pauca* (Schmidt), *Opimocythere marylandica* (Ulrich), and *O.* cf. *O. betzi* (Jennings) occur in the lower Aquia (fig. 4). They seem to have evolved from *Phractocytheridea ruginosa* (Alexander), *Hermanites hadropleurus* Hazel, *Hazelina alexanderi* Hazel, *Opimocythere elonga* Hazel, and *O. browni* Hazel, respectively, which occur in the Brightseat. In each case, the morphologic change between the progenitor and descendant is greater than I would expect if the two formations were transitional.

In addition, some of the Aquia ostracode species such as *Paracaudites?* n. sp. 1, *Clithrocytheridea pyeatti* (Howe and Garrett), *C. jessupensis* (Howe and Garrett), *Haplocytheridea leei* (Howe and Garrett), and *Opimocythere nanafaliana* (Howe and Garrett), which occur on the Gulf Coast, have not been found stratigraphically below the Nanafalia Formation or its equivalents. The Nanafalia contains planktonic foraminifers of the *Globorotalia pseudomendardii* subzone of the *Globorotalia velascoensis* zone (Loeblich and Tappan, 1957a, b; Berggren, 1965). The Brightseat Formation is correlative with the upper Clayton Formation of the Gulf Coast; it is placed in the *Globoconusa daubjergensis-Globorotalia trinidadensis* zone (Hazel, 1968), which is two zones below the Nanafalia.

One sample taken from within 1 foot of the base of the Aquia at Cabin Branch contains a fragment of *Bythocypris parilis* Ulrich, a rare Brightseat and com-

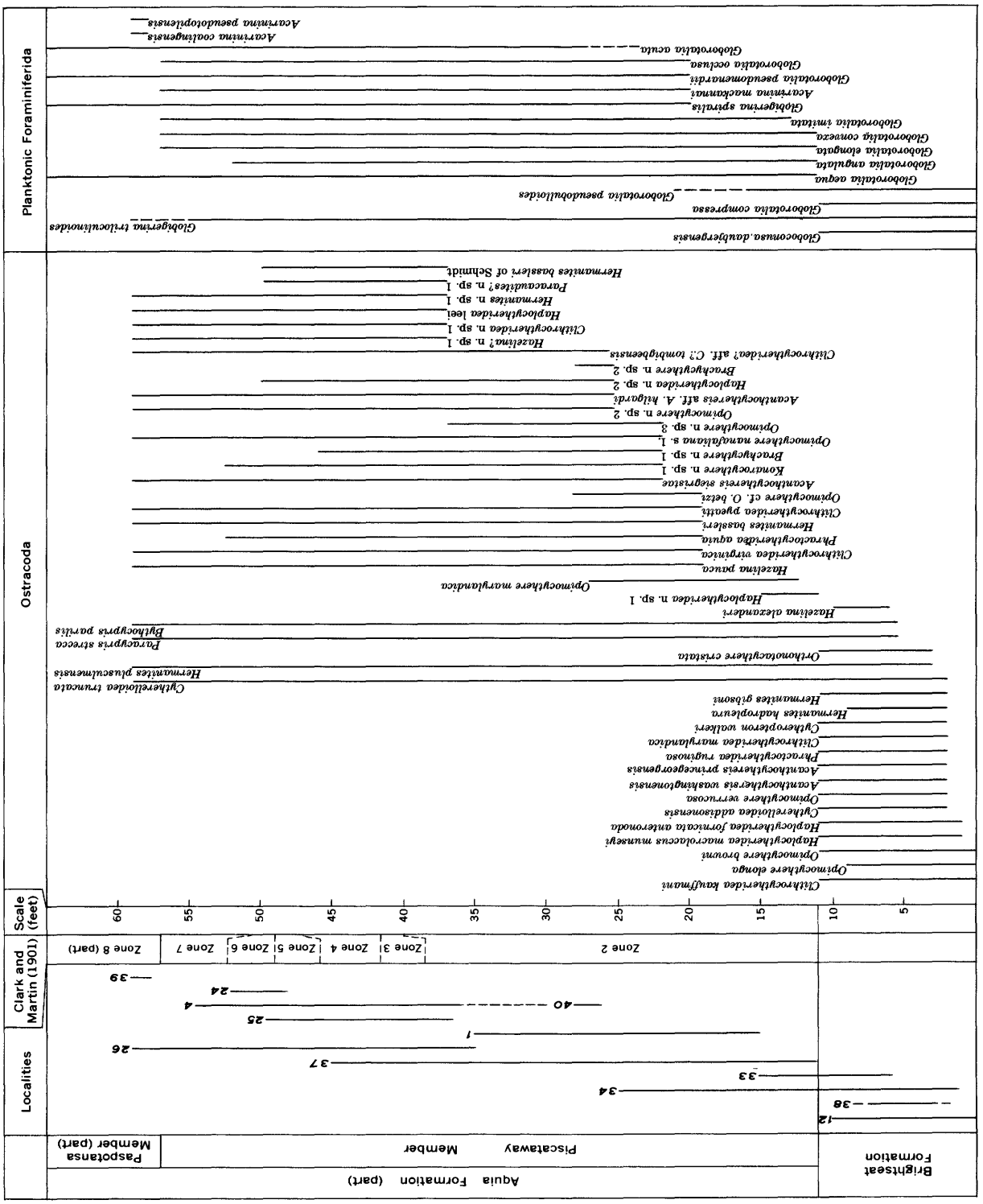

FIGURE 4.—Distribution of 44 species of ostracodes and 16 species of planktonic foraminifers in the Brightseat and Aquia Formations. The positions of the "zones" of Clark and Martin (1901) in the type area of the Aquia Formation are given. For purposes of presentation, their zone 2 is considered to be equivalent to the Aquia below zone 3 and above the Brightseat. Lithologically, these zones are difficult if not impossible to recognize north of Charles County, Md. Composite section compiled by correlating localities shown by faunal and physical criteria. Ostracode data original and from Schmidt (1948) and Hazel (1968). Foraminifer data from Shiffett (1948), Loeblich and Tappan (1957a, b), Nogan (1964), and, for some occurrences at locality 24, Hermann Duque-Caro (written commun., 1968), and locality 39, W. A. Berggren (written commun., 1968). See also "Localities" section and table 1.

mon Aquia form, and specimens of seven species of Cretaceous ostracodes known to occur in the Maestrichtian Monmouth Formation, which underlies the Brightseat, or its equivalents. The species are *Cythereis communis* Israelsky, *Brachycythere rhomboidalis* (Berry), *Nigeria arachoides* (Berry), *"Haplocytheridea" minutus* (Berry), *Clithrocytheridea? fabaformis* (Berry), *Haplocytheridea pinochii* of Schmidt (1948), and *Haplocytheridea plummeri* of Schmidt (1948). The presence of these Cretaceous specimens in the basal Aquia suggests that subaerial or perhaps subaqueous exposures of the Monmouth Formation were present to the west at the beginning of Aquia deposition and that the Brightseat had been eroded away before deposition of the basal Aquia. This assumes, of course, that the Brightseat shoreline was west of the Cabin Branch area. As the Brightseat at Cabin Branch has been interpreted on faunal and sedimentological grounds to represent deposition at middle shelf depths (Nogan, 1964; Drobynk, 1965), this is a reasonable assumption.

The Brightseat Formation contains four globigerinid or globorotaliid planktonic species, *Globoconusa daubjergensis, Globigerina triloculinoides, Globorotalia pseudobulloides*, and *G. compressa* (Nogan, 1964; Hazel, 1968). In a sample from the basal Aquia at locality 34 (sample 34–4, table 1) *Globorotalia elongata, G. angulata*, and *G. pseudobulloides* were found, and Nogan (1964) from this level and locality reports these species plus *G. convexa, G. aequa, Globigerina triloculinoides, Globorotalia compressa*, and *Globoconusa daubjergensis*. Nogan uses the presence of the last two species and the keeled globorotaliids *G. aequa* and *G. angulata* to indicate that the basal beds of the Aquia occupy a transitional position. The foraminifer data, as well as those from the ostracodes and physical relationships outlined above, indicate that this conclusion is incorrect.

Globoconusa daubjergensis is not known to occur higher than the zone named for it (fig. 3). Keeled globorotaliids are not known to occur lower than the upper part of the *Globorotalia uncinata-Globigerina spiralis* zone. Further, *Globorotalia aequa* and *G. convexa*, and possibly *G. elongata*, first appear in the *Globorotalia pseudomenardii* subzone of the *Globorotalia velascoensis* zone. *Globorotalia pseudobulloides* is not known to occur higher than the lower part of the *Globorotalia pseudomenardii* subzone.

The foraminifer and ostracode data indicate that not only is there an unconformity between the Brightseat and Aquia but that the middle two of the four Paleocene planktonic zones apparently are absent. These conclusions are entirely consistent with the physical evidence. Nogan's specimens of *Globoconusa daubjergensis* and *Globorotalia compressa* in the Aquia must be the result of natural or laboratory contamination.

The entire Piscataway Member seems referrable to the *Globorotalia pseudomenardii* subzone. The presence of *Globigerina spiralis* (=*G.* of *G. ouachitaensis* of Shifflett, 1948), *G. triloculinoides*, and *Globorotalia pseudomenardii* (=*G. membranacea* of Shifflett, 1948) in the lower Paspotansa Member (zone 8 of Clark and Martin, 1901; see Shifflett, 1948, fig. 4; Loeblich and Tappan, (957b, p. 1128) indicates that it too should be placed in the *Globorotalia pseudomenardii* zone. *Acarinina pseudotopiliensis* and *A. coalingensis* also have been identified from one sample (sample 39–1) from the lower Paspotansa. Their presence suggests that the lower part of the Paspotansa Member in the Upper Marlboro, Md., area is as young as the upper part of the *Globorotalia pseudomenardii* subzone.

The *Globorotalia pseudomenardii* subzone can be recognized by the planktonic species, which are most common in the middle of the Piscataway Member, and locally, at least, by a large and characteristic assemblage of ostracodes, many of which are as yet undescribed. Species of the genus *Opimocythere* are distinctively abundant (see Hazel, 1968). Ten species of this genus have been identified from the Aquia. Particularly useful in the relatively unmicrofossiliferous lower beds of the Aquia is *Opimocythere marylandica* (Ulrich) (not Schmidt, 1948, which is a new species). *Opimocythere marylandica* appears 5 feet above the base of the Aquia in Cabin Branch (loc. 34) and it was found an estimated 10–15 feet above the base of the Aquia at Piscataway Creek (loc. 40). A single somewhat primitive specimen of *O. marylandica* was found 3 feet above the base of the Aquia at Glymont (loc. 37). The species seems restricted to the lower part of the Piscataway Member. *Opimocythere* cf. *O. betzi* (Jennings), a distinctive undescribed quadrate *Opimocythere*, and other brachycytherids are useful in identifying the middle part of the Piscataway Member. *Paracaudites*? n. sp. 1, *Hermanites* n. sp. 2 (=*Cythereis bassleri* of Schmidt, 1948), abundant *Konarocythere* n. sp. 1 (=*Cytheropteron* cf. *C. midwayensis* of Schmidt, 1948), and *Haplocytheridea* n. sp. 2 (a large form similar to *H. leei* (Howe and Garrett)) characterize the upper part of the Piscataway Member. The assemblage of the lower Paspotansa Member is similar to that of the Piscataway Member, but several of the species common in the lower intervals are absent (fig. 4). Collections from the upper part of the Paspotansa Member have not been studied as yet.

TABLE 1.—*Distribution by sample of ostracode and foraminifer species identified from the localities of figure 4*

[See Hazel (1968) for Brightseat ostracodes from localities 12, 33, and 34. See Nogan (1964), Shifflett (1948) and Loeblich and Tappan (1957a, b) for more complete foraminifer data]

Species \ Samples	34-2	34-3	34-4	34-8	1-1	1-3	1-6	1-7	1-8	37-1	40-1	40-2	4-1	4-2	4-3	4-4	25-1	25-2	25-3	25-4	25-5	26-1	26-2	26-3	24-1	39-1
Ostracoda																										
Acanthocythereis aff. A. hilgardi (Howe and Garrett)									X				X		X						X					
siegristae (Schmidt)				X		X		X	X			X	X	X	X		X	X	X	X	X			X	X	X
aff. A. washingtonensis Hazel							X					X														
Bairdoppilata sp. 1								X																		
Brachycythere n. sp. 1	?			X		X		X					X		X											
n. sp. 2		?	?			X			X																	
Bythocypris parilis Ulrich	X			X	X	X		X	X				X		X	X				X	X		X	X	X	X
Clithrocytheridea n. sp. 1													X													X
n. sp. 2																X										
sp							X																			
jessupensis (Howe and Garrett)								X																		
pyeatli (Howe and Garrett)							X						X		X											X
rugata Schmidt									X																	
virginica Schmidt	X	?					X						X		X						X			X	X	X
Clithrocytheridea? aff. *C.? tombigbeensis* (Steph.)													X		X											X
sp							X																			
Cushmanidea longissima (Schmidt)								X	X				X		X											X
mayeri (Howe and Garrett)								X	X				X													
n. sp. 1													X													
Cyamocytheridea malkinae (Schmidt)							X															X	X			
Cytherella spp		X		X			X					X	X		X				X	X	X			X	X	X
Cytherelloidea truncata Schmidt								X					X		X					X	X			X	X	X
Cytheromorpha n. sp. 1													X		X											
n. sp. 2																									X	
Cytheropteron sp									X																	
Eucythere triordinis Schmidt	X							X																		
Haplocytheridea aff. *H. fornicata* (Alexander)						X			X																	
leei (Howe and Garrett)													X			X				X	X		X	X	X	X
n. sp. 1		X	X																							
n. sp. 2									X				X		X			X		X	X			X	X	
sp							X																			
Hazelina pauca (Schmidt)							X	X					X		X											X
Hazelina? n. sp. 1													X													X
Hermanites basseri (Ulrich)							X	X	X				X		X									X		X
bassleri of Schmidt													X		X						X				X	
plusculmensis (Schmidt)						X	X	X	X		X	X	X		X						X					X
reticulolirus (Schmidt)															X											
n. sp. 1													X		X						X			X	X	X
Konarocythere n. sp. 1				X				X	X				X		X		X		X	X	X		X	X	X	
Loxoconcha aff. *L. corrugata* Alexander						X			X						X						X					
aff. *L. nuda* (Alexander)																					X			X		
sp. of Schmidt									X																	
sp. 1																										X
sp. 2																								X		
Opimocythere cf. *O. betzi* (Jennings)				X		X	X	X	X																	
marylandica (Ulrich)	X	X					X	X	X	X	X	X														
marylandica of Schmidt				X			X	X														X				
nanafaliana (Howe and Garrett) s.l.				X		X		X					X		X						X			X		X
n. sp. 1													X		X											
n. sp. 2									X				X	X	X		X	X		X	X			X	X	X
n. sp. 3	X			X		X		X	X				X													
n. sp. 4													X		X											
n. sp. 5					X																					
n. sp. 6													X		X											X
Paracaudites? n. sp. 1													X		X						X			X	X	
Paracypris strecca Schmidt				X									X		X						X		X	X	X	
Phractocytheridea aquia (Schmidt)	X			X		X	X	X	X		X	X	X		X		X	X	X	X	X		X		X	
n. sp. 1															X										X	
Foraminiferida																										
Globorotalia elongata (Glaessner)			X																							
angulata (White)	X		X																							
pseudobulloides (Plummer)		?	X																							
Globigernia spiralis Bolli	X																									
cf. *G. triloculinoides* Plummer																										X
Acarinina mackannai (White)																										X
coalingensis (Cushman and Hanna)																										X
pseudotopilensis Subbotina																										X

SUMMARY

The Brightseat Formation is placed in the upper part of the *Globoconusa daubjergensis-Globorotalia trinidadensis* zone (fig. 5). It is overlain disconformably by the Aquia Formation, the basal beds of which are dated as lower *Globorotalia pseudomenardii* subzone of the *Globorotalia velascoensis* zone. The entire Piscataway Member of the Aquia and at least the lower part of the Paspotansa Member are also referred to the *Globorotalia pseudomenardii* subzone. The disconformity between the Brightseat and Aquia represents the *Globorotalia uncinata-Globigerina spiralis* and *Globorotalia pusilla pusilla-G. angulata* zones. Assuming a duration of about 9 million years for the Paleocene (63 m.y. ago for the top of the Cretaceous from Kulp, 1961; and about 54 m.y. ago for the top of the Paleocene from Harland and others, 1964), and assuming that the three planktonic zones of the lower and middle Paleocene and the two subzones of the *Globorotalia velascoensis* zone of the upper Paleocene are of approximately equal duration, then the Brightseat-Aquia disconformity represents about 3.6 m.y., a time period approximately equivalent to that represented by the exposed Aquia.

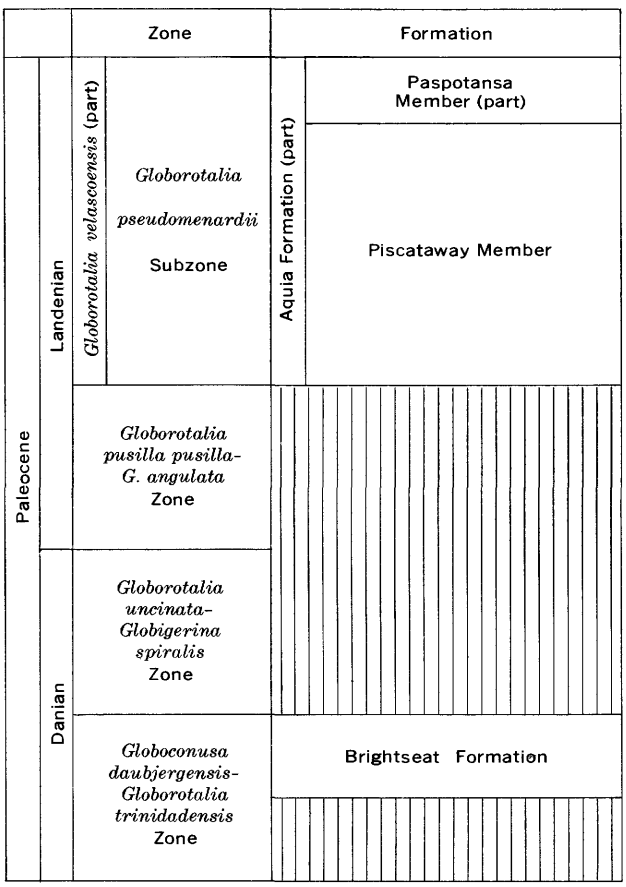

FIGURE 5.—Biostratigraphic position of the Brightseat and Aquia Formations.

LOCALITIES

Descriptions and lists of Brightseat ostracode species for localities *12*, *33*, and *34* of figure 4 can be found in Hazel (1968). Species found in samples from the Aquia localities described below are listed in table 1.

Locality 1. Roadcut 500 yards south of center of the Central Avenue (Maryland Route 214) interchange with Interstate Route 495, on the west side, Prince Georges County, Md. (USGS Cenozoic loc. 24597).

Unit and description	*Thickness (feet)*
Aquia Formation, Piscataway Member	
14. Sand, glauconitic, macrofossiliferous	3.0
13. Sand, partly indurated, glauconitic, macrofossiliferous	1.0
12. Sand, glauconitic	.5
11. Sand, indurated, glauconitic, macrofossiliferous	1.0
10. Sand, glauconitic; zone of concretions at base (sample 1–3)	2.0
9. Sand, glauconitic	.5
8. Sand, glauconitic, indurated, macrofossiliferous	.5
7. Sand, glauconitic (sample 1–8)	.5
6. Sand, glauconitic, very macrofossiliferous	2.0
5. Sand, glauconitic (sample 1–7)	1.5
4. Sand, glauconitic, macrofossiliferous	1.0
3. Sand, glauconitic, argillaceous, very macrofossiliferous (sample 1–6)	2.0
2. Sand, glauconitic, very macrofossiliferous	.5
1. Sand, glauconitic	2.0
Total exposed	18.0

Locality 4. Immediately west of Indian Head Highway (Maryland Route 210, Prince Georges County, Md.) bridges over Piscataway Creek, north bank (see also Nogan, 1964, p. 8). (USGS Cenozoic loc. 24598).

Unit and description	*Thickness (feet)*
Aquia Formation, Piscataway Member	
4. Sand glauconitic, weathered; many *Turritella* (sample 4–6 ft above base)	+10
3. Sand, indurated, glauconitic, macrofossiliferous	2
2. Sand, glauconitic, slightly weathered, macrofossiliferous (sample 4–1 taken 0.5 ft above unit 1; 4–2 is 7 ft above 4–1; 4–3 is 1 ft below unit 3	10
1. Sand, indurated, glauconitic	+1
Total exposed	+23

Locality 24. West bank of Potomac River, Stafford County, Va., 0.75 mile north of Marlboro Point (entrance to Potomac Creek). On U.S. Geological Survey Passapatanzy quadrangle, 1:24,000, 1946, the map point is just east of the "d" in Stafford. (USGS Cenozoic loc. 24599).

Unit and description	*Thickness (feet)*
Aquia Formation, Piscataway Member	
2. Sand, glauconitic, very macrofossiliferous (sample 24–1)	3
1. Sand, indurated, glauconitic	2
Total exposed	5

Locality 25. 0.5 mile upstream from locality 24. (USGS Cenozoic loc. 24600).

Unit and description	*Thickness (feet)*
Aquia Formation, Piscataway Member	
4. Sand, indurated, glauconitic	2.0
3. Sand, glauconitic, very macrofossiliferous (sample 25–3 in lower 0.5 ft; 25–4 is 3 ft below unit 25–5 4; is 0.5 ft below unit 4)	6.0
2. Sand, partly indurated, glauconitic	2.0
1. Sand, glauconitic, very argillaceous in lower part (sample 25–1 in lower 0.5 ft; 25–2 in upper 0.5 ft)	3.5
Total exposed	13.5

Locality 26. 1.0 mile upstream from locality 24 (USGS Cenozoic loc. 24601)

Unit and description	*Thickness (feet)*
Aquia Formation, Piscataway Member	
5. Sand, glauconitic, macrofossiliferous (sample 26–3 is 4 ft above unit 4; 26–2 is 1 ft above unit 4)	+9
4. Sand, indurated, glauconitic, macrofossiliferous	2
3. Sand, glauconitic, macrofossiliferous	6
2. Sand, glauconitic, laterally discontinuously indurated	1
1. Sand, glauconitic, argillaceous (sample 26–1)	10
Total exposed	+28

Locality 37. About 40 feet of Aquia Formation underlain by the Lower Cretaceous Patapsco Formation exposed on east bank of Potomac River 0.37 mile upstream from Glymont Wharf, Charles County, Md. (=locality 1 of Clark and Martin, 1901, p. 68, and locality F of Schmidt, 1948, p. 399). One fossiliferous sample (37–1) collected 3 feet above the base of the Aquia. (USGS Cenozoic loc. 24604)

Locality 38. Brightseat Formation. Two-foot-thick outcrop of argillaceous sand (sample 38–1), ¼ mile southeast of Kettering Road between Maryland Routes 202 and 214 in streambed (tributary to Western Branch), 100 yards west of sanitation plant west of Robert M. Watkins Regional State Park. Collected by Warren Blow. (USGS Cenozoic loc. 24602) The following ostracode species have been identified from sample 38–1: *Cytherella* sp., *Bairdoppilata* sp., *Brachycythere plena* Alexander, *Cytherelloidea truncata* Schmidt, *Opimocythere elonga* Hazel, *Opimocythere browni* Hazel, *Haplocytheridea macrolaccus munseyi* (Hazel), *Haplocytheridea fornicata anteronoda* (Hazel), *Cytherelloidea? addisonensis* Hazel, *Opimocythere verrucosa* (Harris and Jobe). *Acanthocythereis washingtonensis* Hazel, *Phractocytheridea ruginosa* (Alexander), *Clithrocytheridea marylandica* Hazel, *Hermanites hadropleurus* Hazel, and *Hazelina alexanderi* Hazel.

Locality 39. Outcrop of Paspotansa Member of the Aquia Formation (equivalent to the indurated ledge of Clark and Martin, 1901, p. 72) in roadcut on east side of Valley Lane just south of Church Street below Trinity Episcopal Church, Upper Marlboro, Md. (sample 39–1). Collected by A. H. Cheetham, O. B. Nye, E. Voigt, and R. Scolaro. (USGS Cenozoic loc. 24603)

Locality 40. Underlies locality 4 at the same location. The Aquia was exposed during excavation of a ditch for a sewer line in March of 1967. Two samples, 40–1 and 40–2, respectively, were collected by Charles Buddenhagen from just above and just below a 1-foot indurated bed exposed in the ditch that paralleled the north bank of Piscataway Creek. The indurated bed is 4–5 feet below March water level and about 20 feet stratigraphically below the distinctive 2-foot indurated bed (unit 3) of locality 4. (USGS Cenozoic loc. 24631)

REFERENCES

Bennett, R. R., and Collins, G. G., 1952, Brightseat Formation, a new name for sediments of Paleocene age in Maryland: Washington Acad. Sci. Jour., v. 42, no. 4, p. 114–116.

Berggren, W. A., 1965, Some problems of Paleocene-lower Eocene planktonic foraminiferal correlations: Micropaleontology, v. 11, no. 3, p. 228–300.

——— 1968, Phylogenetic and taxonomic problems of some Tertiary planktonic Foraminifera lineages: Tulane Studies in Geology, v. 6, no. 1, p. 1–22.

Clark, W. B., and Martin, G. C., 1901, The Eocene deposits of Maryland: Maryland Geol. Survey, Eocene [volume], p. 21–92.

Cooke, C. W., 1952, Sedimentary deposits of Prince Georges County and the District of Columbia, *in* Geology and water resources of Prince Georges County: Maryland Dept. Geology, Mines, and Water Resources, Bull. 10, p. 1–53.

Darton, N. H., 1951, Structural relations of Cretaceous and Tertiary Formations in part of Maryland and Virginia: Geol. Soc. America Bull., v. 62, no. 7, p. 745–780.

Drobnyk, J. W., 1965, Petrology of the Paleocene-Eocene Aquia Formation of Virginia, Maryland, and Delaware: Jour. Sed. Petrology, v. 35, no. 3, p. 626–642.

Harland, W. B., Smith, A. G., and Wilcock, Bruce, ed., 1964, The Phanerozoic time-scale; a symposium: Geol. Soc. London Quart. Jour., supp., v. 120s, 458 p.

Hazel, J. E., 1968, Ostracodes from the Brightseat Formation (Danian) of Maryland: Jour. Paleontology, v. 42, no. 1, p. 100–142.

Kulp, J. L., 1961, Geologic time scale: Science, v. 133, no. 3459, p. 1105–1114.

Loeblich, A. R., Jr., and Tappan, H. N., 1957a, Planktonic Foraminifera of Paleocene and early Eocene age from the Gulf and Atlantic Coastal Plains: U.S. Natl. Mus. Bull. 215, p. 173–198.

——— 1957b, Correlation of the Gulf and Atlantic Coastal Plain Paleocene and lower Eocene formations by means of planktonic Foraminifera: Jour. Paleontology, v. 31, no. 6, p. 1109–1137.

Nogan, D. S., 1964, Foraminifera, stratigraphy, and paleoecology of the Aquia Formation of Maryland and Virginia: Cushman Found. Foram. Research Spec. Pub. 7, 50 p.

Schmidt, R. A. M., 1948, Ostracoda from the Upper Cretaceous and lower Eocene of Maryland, Delaware, and Virginia: Jour. Paleontology, v. 22, no. 4, p. 389–431.

Shifflett, F. E., 1948, Eocene stratigraphy and Foraminifera of the Aquia Formation: Maryland Dept. Geology, Mines, and Water Resources Bull. 3, 93 p.

LATERAL MIGRATIONS OF THE ARKANSAS RIVER DURING THE QUATERNARY—FOWLER, COLORADO, TO THE COLORADO-KANSAS STATE LINE

By JOSEPH A. SHARPS, Denver, Colo.

Abstract.—Former positions of the Arkansas River between Fowler, Colo., and the Colorado-Kansas State line at given times during the Quaternary have been determined from the positions of terraces cut at those times. Lateral migration of the river during Quaternary time was probably caused by the introduction of a greater volume of sediment into the channel from one side than from the other. Gravel deposited by the Arkansas River differs from tributary gravel in composition and grain size.

During the summers of 1966 and 1967, terrace gravels were mapped along a 115-mile reach of the Arkansas River that extends from 1 mile east of Fowler, Colo., to the Colorado-Kansas State line. The work was part of a project involving the geologic mapping of the Lamar 1:250,000 quadrangle in southeastern Colorado.

This report shows how the modern broad valley of the Arkansas River evolved through Quaternary time and how the migrations of the river produced the present pattern of gravel outcrops.

A detailed geomorphic history is not given, because the processes and events that constitute each geomorphic cycle are virtually the same in this area as are those described by Scott (1963) in relation to the South Platte River near Denver, Colo. The chief difference between the two areas is that here deposits of Nussbaum Alluvium (of early Nebraskan age) are widespread, whereas in the area described by Scott the Nussbaum is absent. For the definition of the term "geomorphic cycle" as used here, and for a description of the processes and events constituting a geomorphic cycle, the reader is referred to Scott (1963).

In each geomorphic cycle, the ancestral Arkansas River cut a strath or broad valley, and contemporaneously deposited gravel on its floor. At the same time, tributaries to the ancestral Arkansas River also cut straths and deposited gravel on their floors. The straths cut by the tributaries were graded to the strath cut by the main stream. Throughout Pleistocene time the Arkansas River progressively deepened its valley, forming a series of strath terraces. Each successively younger terrace is lower than the preceding terrace. Because of this progressive deepening of the valley, gravel that covered terraces along the Arkansas River and its tributaries could be eroded only in the succeeding geomorphic cycle by streams cutting down to a new and lower level. Principal streams in later times could neither erode this older gravel nor add to it, because the older gravel was above the levels of these streams. The fine-grained alluvium and colluvium that commonly cover older alluvial deposits of both the Arkansas River and its tributaries were deposited not by the principal streams but by small local ephemeral streams.

Prior to the first geomorphic cycle, the Ogallala Formation covered much of the Lamar 1:250,000 quadrangle. Its surface was more than 500 feet higher than that of the modern Arkansas River (Soister, 1967, fig. 5). At the beginning of Quaternary time, the Ogallala Formation in the area may have been already partly removed by erosion. During the earliest known geomorphic cycle in Quaternary time, erosion either continued or was initiated and the Ogallala Formation was removed from most of the area, the underlying bedrock was dissected, and the Nussbaum Alluvium was deposited. During this time, the earliest valley that can be regarded as a progenitor of the Arkansas River valley was cut by the ancestral Arkansas River. This initial geomorphic cycle was followed by five more geomorphic cycles during the Pleistocene. These cycles are represented by five ages of terrace gravel deposited on successively lower terraces.

During downcutting, the Arkansas River also moved laterally. Since early Nebraskan time, the Arkansas River between Fowler and La Junta, Colo., has mi-

U.S. GEOL. SURVEY PROF. PAPER 650–C, PAGES C66–C70

grated northward as much as 7 miles, and between La Junta and Kansas it has migrated southward as much as 9 miles.

The terrace deposits that have been mapped are the Nussbaum Alluvium of Pleistocene (early Nebraskan) age, the Rocky Flats Alluvium of Nebraskan or Aftonian age, the Verdos Alluvium of Kansan or Yarmouth age, the Slocum Alluvium of Illinoian or Sangamon age, the Louviers Alluvium of Bull Lake age, and the Broadway Alluvium of Pinedale age. All these units are mainly composed of sand and fine to coarse gravel and, because they are similar lithologically, are difficult to differentiate except by elevation above stream level.

Gravel deposits of Bull Lake or later age can be differentiated from gravel deposits of earlier age by the thickness of the caliche coating on the component pebbles. Deposits of Bull Lake or later age are characterized by a caliche coating that is rarely more than a thirty-second of an inch thick. The coating on pebbles in deposits of earlier age may be as much as half an inch thick. The thickness of the caliche coating cannot be used to determine the respective ages of the several pre-Bull Lake units, because additional variables other than age (such as the level of the water table in the past, the concentration of calcium carbonate in the ground water, and the amount of calcium carbonate in the underlying bedrock) introduce too much uncertainty into these determinations.

Gravel deposited by the Arkansas River can be differentiated from gravel deposited by its tributary streams. The Arkansas River gravel is generally composed of a greater proportion of durable igneous and metamorphic rocks, and, in most places, these rocks constitute almost 100 percent of a deposit. The tributary gravel is generally composed of a greater proportion of sedimentary rocks than is present in the deposits of the Arkansas River. These rocks may make up as much as 10 percent of a tributary deposit. Another difference between gravel deposited by the Arkansas River and gravel deposited by the tributaries is that the average grain size is smaller in the tributary deposits. A larger proportion of the gravel in the tributary deposits has been derived from older alluvial deposits. Part of the Nussbaum Alluvium has been reworked from the Ogallala Formation, and part of the Rocky Flats Alluvium has been reworked from the Nussbaum Alluvium. Additional abrasion during this reworking has reduced the grain size.

In the following discussion of the individual units, all deposits are considered to have been deposited by the Arkansas River, unless it is otherwise stated.

DISCUSSION OF THE TERRACE DEPOSITS

Nussbaum Alluvium

During early Nebraskan time, the Nussbaum Alluvium was deposited widely over the area by the Arkansas River and by its tributaries. All but a few remnants of the Nussbaum Alluvium deposited by the Arkansas River have since been removed by erosion. Two of these remnants lie near the west end of the area (fig. 1); one is 6 miles southwest of Manzanola, and one is 6 miles south of Vroman. Several exposures of Nussbaum Alluvium, also of Arkansas River origin, lie in the northeast part of the area. North of the western two-thirds of the area, Nussbaum Alluvium deposited by tributary streams is widespread. From this scant evidence, the approximate course of the river during early Nebraskan time has been inferred. The deposits show that west of Rocky Ford it was as much as 7 miles south of its present position. Between Rocky Ford and the west end of John Martin Reservoir, the approximate course has been inferred from southward projection of the gradient of the tributary gravels north of the area to the levels of points on the interpolated gradient of the main stream. The river apparently ran to the north of its present position along that section. About 4 miles north of John Martin Reservoir, bluffs of the Fort Hays Limestone Member of the Niobrara Formation stand higher than the interpolated gradient of the Nussbaum Alluvium, so in the area north of the reservoir the course was south of these bluffs. From a few miles northeast of the east end of the reservoir to the State line, the course of the early Nebraskan river can be traced from remnants of Nussbaum gravel. Just east of the reservoir the river swung to the north and followed a course to the State line that was as much as 9 miles north of its present position.

The upper surface of the Nussbaum Alluvium is about 375–410 feet above the river at the west end of the area and about 300–355 feet above at the east end.

Rocky Flats Alluvium

The presence of Rocky Flats Alluvium of Nebraskan or Aftonian age on the bluffs south of the river between Fowler and Rocky Ford shows that the river was then 3–5 miles south of its present position along that reach. Another small deposit lies on the north side of the river 4 miles north of La Junta. Its position shows that between Rocky Ford and La Junta the river swung to the north. Between La Junta and Lamar no mainstream deposits were found, but 16–23 miles north of Las Animas, north of the area shown in figure 1, there is a 7-mile-long tributary deposit. By the southward

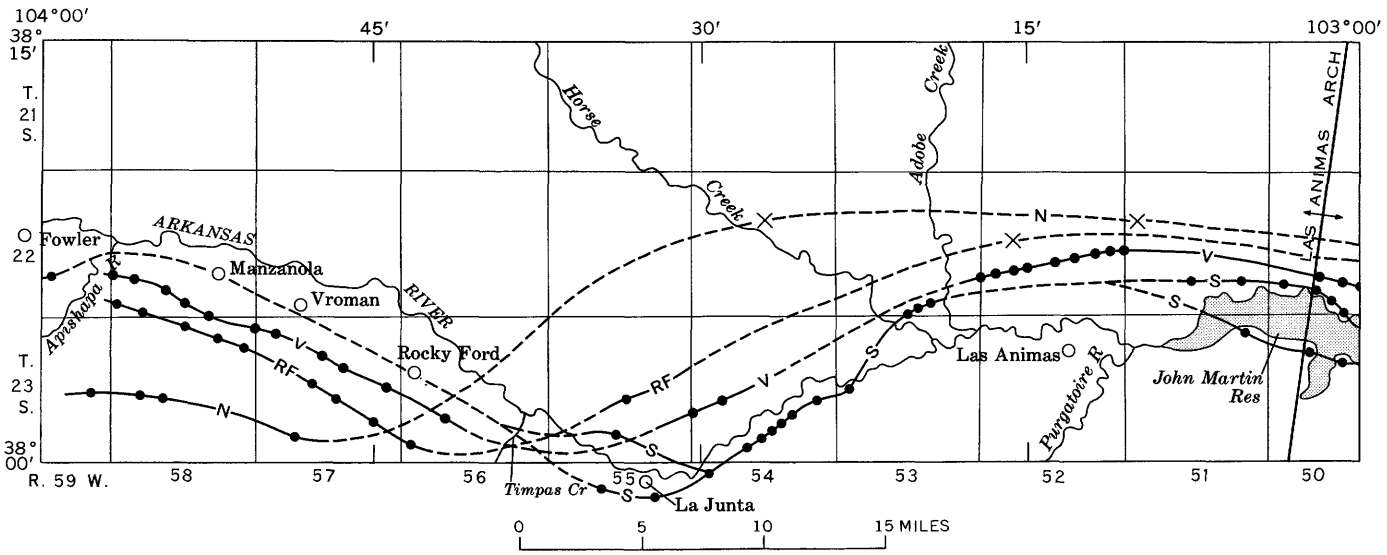

FIGURE 1.—Map of part of Arkansas River valley, showing positions of the Arkansas River in early Nebraskan, Nebraskan or Aftonian, Kansan or Yarmouth, and Illinoian or Sangamon times. Position during Bull Lake and Pinedale times, known from location of deposits of Louviers and Broadway Alluviums, is not shown because the river was in approximately the same position then as now.

projection of the gradient of this deposit to the level of a point on the interpolated gradient of the main stream, the approximate position of the main stream is inferred to have been about 4 miles north of Las Animas. In the area north of John Martin Reservoir, the river was south of bluffs of the Fort Hays Limestone Member. Between the reservoir and Lamar it probably followed a course to the north of its present position, provided that it flowed in a reasonably straight line. From Lamar to the State line deposits are discontinuous and show that the river was 4–9 miles north of its present position.

The Rocky Flats Alluvium is 240–340 feet above the river near the west end of the area and 210–285 feet above near the east end.

Verdos Alluvium

Relatively closely spaced remnants of Verdos Alluvium of Kansan or Yarmouth age are present from Fowler, Colo., to Kansas. Their positions show that, during Kansan or Yarmouth time, the river was 2–3 miles south of its present position between Fowler and Rocky Ford, and 2–6 miles north between La Junta and the State line.

The Verdos Alluvium is 130–180 feet above the river at the west end of the area, and 120–180 feet above the river at the east end.

Slocum Alluvium

Slocum Alluvium of Illinoian or Sangamon age is not as prevalent in the west quarter of the area as is the Verdos Alluvium; however, one deposit lies 2 miles south of the present channel, south of Fowler. The next nearest deposits to the east are near La Junta on both the north and the south sides of the river.

Probably the Slocum Alluvium was initially present between Fowler and La Junta but was subsequently removed during Bull Lake time. At about the end of Illinoian or Sangamon time, the river was downcutting across a barrier formed by the competent Fort Hays Limestone Member of the Niobrara Formation near La Junta. The dip of the beds in that area is to the northwest, so the dip has a gentle upstream, or westward, component. Because of this dip, earlier downcutting had caused this limestone barrier to migrate upstream to the vicinity of La Junta by Bull Lake time. The elevation of the top of this barrier near La Junta remained stable enough during Bull Lake time to control a temporary base level which slowed downcutting upstream from La Junta. This caused the river to meander widely over the less resistant rocks upstream from the barrier and to remove the Slocum Alluvium from the reach between Fowler and La Junta.

From La Junta to just west of the mouth of Horse Creek the river was slightly to the south of its present position, as indicated by remnants of Slocum Alluvium. Gravel terraces a mile north of the present channel between Horse Creek and Adobe Creek show that the river swung to the north near the mouth of Horse Creek. From Adobe Creek to John Martin Reservoir no Slocum deposits were found.

The Slocum Alluvium is absent between Adobe Creek and the reservoir because of post-Sangamon erosion. At the end of Illinoian or Sangamon time the river had cut down to the top of the competent Dakota Sandstone at

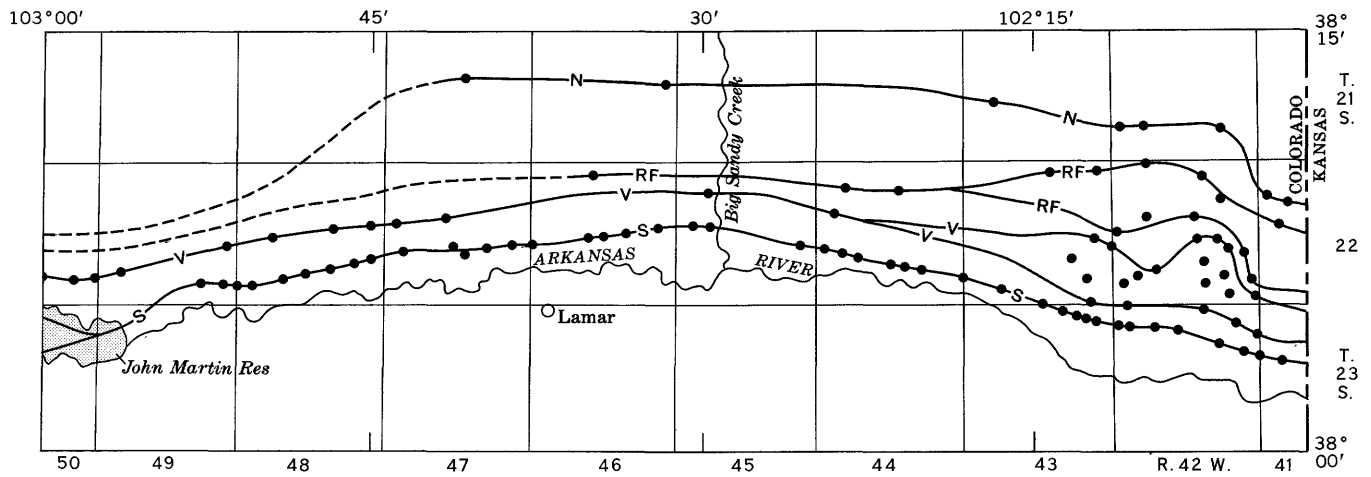

EXPLANATION

Lines are dashed where less accurately located

N

Position in early Nebraskan time as determined from deposits of Nussbaum Alluvium

RF

Position in Nebraskan or Aftonian time as determined from deposits of Rocky Flats Alluvium

Shown by double line where permitted by width of terrace

V

Position in Kansan or Yarmouth time as determined from deposits in Verdos Alluvium

Shown as double line where permitted by width of terrace

S

Position in Illinoian or Sangamon time as determined from deposits of Slocum Alluvium

• • • •

Positions of points located on gravel deposits

×

Point located by extrapolating gradient of tributary gravel north of area to where its elevation is at the level of the correlative gradient of the main stream

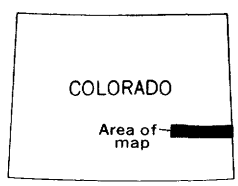

FIGURE 1 (CON.).

the crest of the Las Animas arch in the vicinity of John Martin Reservoir. Since that time the elevation of the top of this sandstone has controlled a temporary base level which has slowed downcutting upstream from the arch. The slowing of downcutting has caused the river to meander widely along the section between Adobe Creek and the arch. This meandering removed the Slocum Alluvium from that section of the stream.

Slocum Alluvium is present both north and south of John Martin Reservoir, and from there to Kansas closely spaced remnants lie 1–3 miles north of the river.

The Slocum Alluvium is 80–110 feet above the river at the west end of the area, and its height above the river gradually decreases to 65–100 feet at the east end.

Louviers Alluvium

The presence of discontinuous deposits of Louviers Alluvium of Bull Lake age north of the river from Fowler to La Junta indicates that the stream flowed slightly north of its present position along most of this segment during that time. East of La Junta, deposits of Louviers Alluvium are uncommon; apparently the river has migrated very little since Bull Lake time and deposits of that age have been removed by erosion. A fairly large remnant south of Las Animas was deposited by the Purgatoire River.

The Louviers Alluvium is 50–70 feet above the river near Fowler and grades to 30–55 feet above the river near the State line.

Broadway Alluvium

Broadway Alluvium of Pinedale age forms an almost continuous terrace on the south side of the river from Fowler to La Junta. From La Junta to the mouth of Horse Creek it lies on the north side. From Horse Creek to Big Sandy Creek it is on both the north and the south sides. East of Big Sandy Creek, deposits are less common, probably because the elevation of the Broadway Alluvium in relation to the river is lower to the east, so the post-Pinedale river could more easily remove it.

The river during post-Pinedale time has migrated slightly northward between Fowler and La Junta. Between La Junta and the mouth of Horse Creek it has migrated slightly southward. From Horse Creek to the State line it occupies virtually the same position now as it did in Pinedale time.

The Broadway Alluvium is 20–50 feet above the river in the west part of the area, and, where found in the east part of the area, it is 15–40 feet above the river.

MIGRATION OF THE RIVER AND CAUSE OF THE MIGRATION

Along the reach between Fowler and La Junta, the Arkansas River migrated northward as much as 7 miles between early Nebraskan time and Bull Lake time. Since Bull Lake time there has been only a slight shifting back and forth along this reach. Along the reach between La Junta and Kansas, the river has apparently migrated southward throughout the Quaternary, and in places it has moved as much as 9 miles since early Nebraskan time.

Migration of the river northward or southward across its valley probably resulted from greater discharge of unconsolidated sediment into the river channel from one side of the valley than from the other. Those streams that discharge a large volume of sediment build alluvial fans at their junctions with the river. The river generally cannot remove the alluvium in the fans as rapidly as it is deposited, so it takes a course around the toes of the fans. In so doing, it cuts into bedrock along the opposite wall of the valley and gradually moves away from the growing fan.

Along the reach of the river between Fowler and La Junta, two tributaries, the Apishapa River and Timpas Creek, apparently supplied a greater volume of sediment from the south than was supplied from the north by the small ephemeral streams on the north side of the river. In this reach, alluvial fans were built on the south side of the river by these two larger tributaries, and the river migrated northward. Such fans of unconsolidated sediment are generally short-lived, and none is now present at the mouth of either the Apishapa River or Timpas Creek. Their presence in earlier times is inferred from what is known concerning deposition by modern tributary streams carrying large volumes of sediment.

Along the reach of the river between La Junta and Kansas, the tributaries from the north are long and flow over unconsolidated deposits. The tributaries from the south are shorter and flow over bedrock. Because of these differences, the tributaries from the north supplied a greater volume of sediment to the river than did the tributaries from the south, and the river migrated southward.

REFERENCES

Scott, G. R., 1963, Quaternary geology and geomorphic history of the Kassler quadrangle, Colorado: U.S. Geol. Survey Prof. Paper 421–A, p. 1–70.

Soister, P. E., 1967, Relation of Nussbaum Alluvium (Pleistocene) to the Ogallala Formation (Pliocene) and to the Platte-Arkansas divide, southern Denver basin, Colorado; *in* Geological Survey Research 1967: U.S. Geol. Survey Prof. Paper 575–D, p. D39–D46.

GLACIAL DRAINAGE DIVIDE IN THE SKAGIT VALLEY, WASHINGTON

By PAUL L. WEIS, Spokane, Wash.

Abstract.—Major valleys in the western part of the North Cascades primitive area have been intensely glaciated and characteristically have U-shaped cross sections, steep walls, flat floors, and relatively gentle gradients. A notable exception is the Skagit Valley, which has a segment about 7 miles long with a steep gradient and the V-shaped cross section characteristic of stream erosion. The valley upstream and downstream from the V-shaped gorge has the typical U-shaped cross section of a glaciated valley. This anomalous section of the Skagit Valley may best be explained by the hypothesis that it was a drainage divide during late Pleistocene time and was occupied by relatively stagnant ice.

At the Canadian border the Cascade Range has a width of about 100 miles—enough to produce a considerable difference in climate between its eastern and western parts. The western part now receives more than four times as much precipitation as the eastern part. This difference apparently existed in late Pleistocene time as well. Glacial erosion was clearly more extensive in the western part of the range. Large, vigorous glaciers occupied all the major valleys, carving them into deep, steep-sided troughs with gentle gradients and pronounced U-shaped cross sections.

The Skagit River is the master stream for much of the western part of the northern Cascades. Like other large valleys in the area, it has a gentle gradient and a pronounced U-shaped cross section throughout most of its course. The 7-mile section of V-shaped gorge between Ross Dam and Newhalem (fig. 1) is in striking contrast. This V-shaped segment of the valley was occupied by ice, as shown by the smoothed walls and broad expanses of bare rock, but obviously, glacial erosion was insignificant compared with the rest of the valley and with other valleys in the same area (fig. 2).

Ice must have occupied the anomalous part of the Skagit Valley for approximately the same length of time as it did those parts of the valley upstream and downstream from the gorge. The gorge is cut at nearly right angles to the strike of resistant gneissic rocks, but that in itself does not account for the shape of the valley. The valleys of Little Beaver, Luna, McMillan, and McAllister Creeks also lie at right angles to the strike of the same metamorphic rock unit, and all four are well-developed U-shaped troughs. The most plausible explanation for the anomaly seems to be that that part of the Skagit Valley was a drainage divide during the late Pleistocene and that the U-shaped

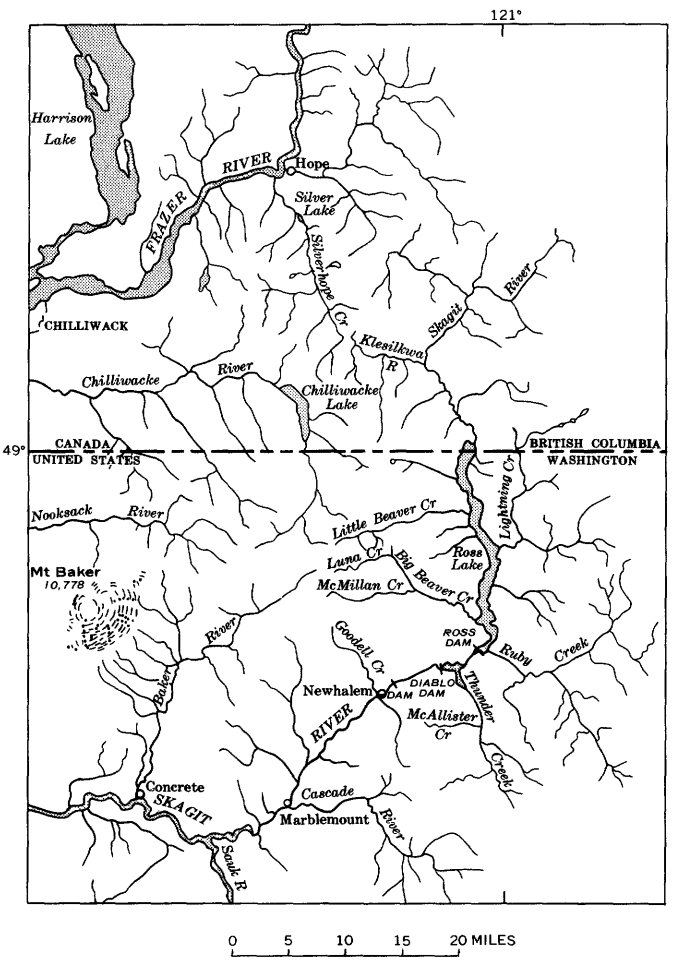

FIGURE 1.—Map of the Skagit River drainage basin and adjacent drainages in northwestern Washington and southwestern British Columbia.

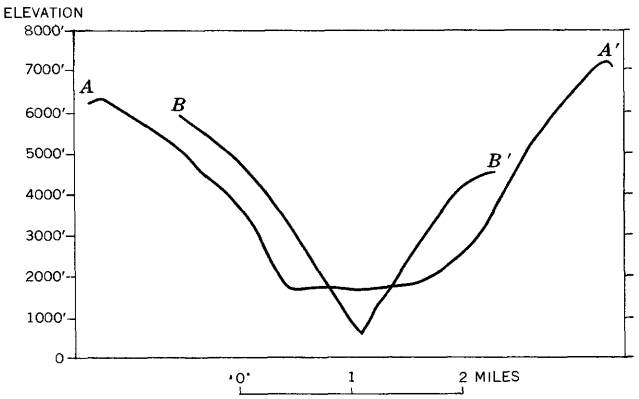

FIGURE 2.—Profiles of Skagit Valley; view upstream. *A–A'*, British Columbia, 7 miles upstream from the United States-Canada boundary. *B–B'*, 1½ miles upstream from Newhalem, Wash. Vertical exaggeration ×2.

sections above and below were occupied by relatively fast-flowing streams of ice, whereas the intervening section was occupied by ice that moved much more slowly.

To examine this hypothesis more fully, it is necessary to consider the drainage of a considerably larger area, including parts of Washington and British Columbia (fig. 1).

SKAGIT VALLEY

The Skagit River heads in British Columbia about 25 miles north of the United States-Canada boundary (Manning Park and Skagit East Half 1:50,000 maps, British Columbia). It flows irregularly southwestward for a considerable distance in a valley that has the typical U-shaped cross section indicative of glacial erosion, but which has a floor less than half a mile wide. About 10 miles north of the international boundary, the Skagit enters a much broader southeast-trending trench and is joined by the Klesilkwa River, which heads in the trench about 6 miles to the northwest. At the point where the two streams join, the floor of the trench is about 1.2 miles wide (fig. 3).

The Skagit continues southeastward to the north border of Washington, meandering along the flat swampy floor of the trench. In this part of its course, the average gradient is less than 20 feet per mile. Where it enters Washington, the river flows into the upper end of Ross Lake, an 18-mile-long artificial lake formed by Ross Dam. Ross Lake occupies the southern extension of the trench in Washington, and has an average width of more than a mile. The gradient of the valley floor beneath most of Ross Lake is less than 20 feet per mile.

At Ross Dam the Skagit begins a bend to the west, and the character of its valley changes drastically. From the mouth of Ruby Creek to the base of Ross Dam, a distance of about a mile, the valley shape

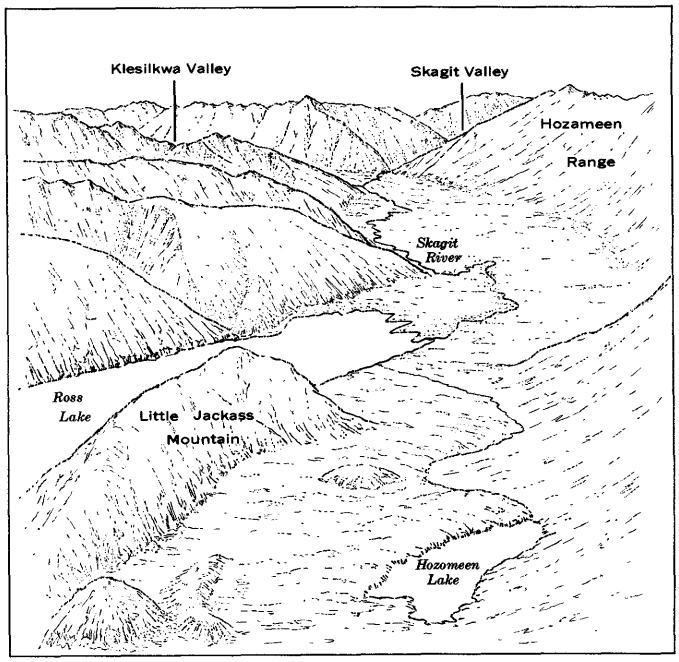

FIGURE 3.—Sketch of the Skagit Valley north of the United States-Canada boundary (from a photograph). View is to the northwest.

changes from a broad flat-bottomed U to a sharp V. The V-shaped segment of the valley is about 7 miles long, extending roughly from Ross Dam to Newhalem (fig. 4). For a large part of this distance, the valley walls maintain a remarkably uniform slope of nearly 40° through a vertical distance of more than 5,000 feet. From the base of Ross Dam to the center of Newhalem, the river drops from about 1,230 feet above

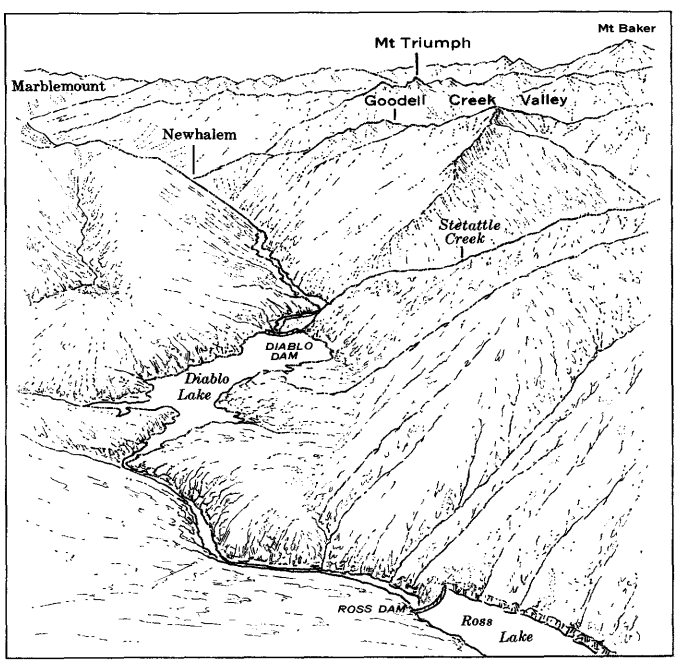

FIGURE 4.—Sketch of the Skagit Valley downstream from Ross Dam (from a photograph). View is to the southwest.

sea level to about 500 feet, an average gradient of more than 100 feet per mile.

The V-shaped gorge of the Skagit was occupied by ice at least 4,000–4,500 feet thick. The valley walls are smooth and show extensive areas of bare rock. Glacial erosion was apparently slight, however, consisting mostly of the removal of soil and weathered rock and smoothing of prominent spurs and irregularities. Erosion was not great enough to form the U-shaped cross section characteristic of intensely glaciated valleys. The river has clearly incised itself a few tens of feet to a few hundred feet in the bottom of the postglacial gorge, but most of this part of the Skagit Valley must be virtually unchanged from its preglacial form.

Downstream from Newhalem the Skagit Valley again assumes its U-shaped cross section and more gentle gradient. A mile southwest of Newhalem the valley floor is nearly three-fourths of a mile across. It is somewhat narrower in places to the west but maintains a substantial width of flat floor to Marblemount, where it broadens to 1½ miles. The gradient in the 14 miles from Newhalem to Marblemount is less than 15 feet per mile.

KLESILKWA VALLEY

The Klesilkwa River heads in a swamp at an elevation of less than 1,900 feet, about 6 miles northwest of its junction with the Skagit (Skagit East Half and West Half 1:50,000 maps, British Columbia). In that 6 miles the floor of the trench narrows somewhat, from a width of more than a mile on the south to about half a mile at the swampy headwaters. The northwest end of the swamp is the headwaters of another stream, the northwesterly flowing Silverhope Creek.

SILVERHOPE VALLEY

Silverhope Creek flows north-northwest to join the Fraser River at Hope, British Columbia (fig. 1) (Skagit West Half and Hope West Half 1:50,000 maps, British Columbia). Silverhope Creek is about 16 miles long. From its head to the outlet of Silver Lake, 12 miles downstream, the width of the flat-bottomed trench decreases only slightly, from slightly more than to slightly less than half a mile. The gradient of Silverhope Creek in this 12-mile section is about 50 feet per mile. From the outlet of Silver Lake, the creek cascades 4 miles to the Fraser in a precipitous gorge with a gradient of more than 200 feet per mile.

FRASER VALLEY

North of Hope, British Columbia, the Fraser River flows almost due south in a valley generally less than 1 mile wide (Hope West Half 1:50,000 map, British Columbia). At Hope the river turns abruptly west and the valley widens to a mile or more. The river continues west and southwest to the west front of the Cascade Range, emptying into Puget Sound at Vancouver.

In late Pleistocene time the Fraser Valley was occupied by a glacier estimated to be at least 7,500 feet thick (Armstrong and Brown, 1954, p. 352). At that time the lower Fraser Valley was depressed at least 750 feet, and possibly as much as 1,500 feet, by the weight of the ice. Armstrong and Brown (1954, p. 361) describe marine shells in deposits that now lie 575 feet above present sea level, and deltaic sands and gravels that may be in part marine are now found as much as 1,200 feet above present sea level. Armstrong and Brown (1954, p. 362) consider 1,500 feet as the maximum distance above present-day sea level at which marine deposits may now be found.

CONCLUSIONS

The divide between the present-day Skagit-Klesilkwa drainage and Silverhope Creek is only 1,900 feet above sea level. In Pleistocene time it may have stood from as little as 400 to as much as 1,400 feet above the present sea level, thus making an unusually low divide between the two drainages. The top of the Fraser glacier must have stood more than 5,000 feet above the Klesilkwa-Silverhope divide, though its southern margin was probably some distance to the north. Ice in the trench between the head of Klesilkwa River and Ross Dam was also at least 5,000 feet thick at approximately the same time. It seems entirely feasible that the ice in the trench now occupied by the Klesilkwa River and that part of the Skagit from Ross Dam to the mouth of the Klesilkwa was a northwest-flowing glacier that joined the Fraser glacier near Hope. West of Newhalem the glacier in the Skagit Valley must have flowed west. This seems the only plausible explanation for the lack of intense glacial erosion in the V-shaped section of the Skagit Valley between Ross Dam and Newhalem.

Additional features worthy of note were seen in the course of this investigation, but time did not permit their study. The V-shaped gorge of the Skagit, with an inner, vertical-walled canyon in places, indicates as much as 300 feet of post-Pleistocene erosion by the Skagit. It would take only about 600 feet of uplift of the bed of the Skagit a few miles upstream from Ross Dam to reverse the whole Skagit drainage above that point and cause it to flow northwestward across the Silverhope-Klesilkwa divide. The Skagit Valley between the mouth of the Klesilkwa and the international boundary is unusually flat. The implication is clear—a sizable lake may have existed in that part of the valley immediately following deglaciation and may have been drained only

when stream erosion in the Skagit gorge lowered its outlet.

Rowland W. Tabor (written commun., 1968) has suggested that the narrow Skagit gorge may have been a stream divide in preglacial time, and that glacial erosion, particularly in the area between Ross Dam and Diablo Dam, may have lowered the divide enough to make stream capture possible. If Fraser ice blocked Silverhope Creek after the Skagit Valley was deglaciated, it would account for both the existence of a late Pleistocene lake and a cause for its overflow and gorge-cutting to the southwest, making reversal of the drainage possible.

REFERENCE

Armstrong, J. E., and Brown, W. L., 1954, Late Wisconsin marine drift and associated sediments of the lower Fraser Valley, British Columbia, Canada: Geol. Soc. America Bull., v. 65, no. 4, p. 349–364.

FAULT SCARP EXPOSURES IN THE SAINT CHARLES AND NORTONVILLE QUADRANGLES, WESTERN KENTUCKY

By JAMES E. PALMER, Madisonville, Ky.

Work done in cooperation with the Kentucky Geological Survey

Abstract.—Many fault scarps exposed by strip mining operations provide an opportunity to observe features of faults not commonly seen, but weathering and erosion rapidly destroy the features. The fault scarps are in a region of relatively intensive faulting south of the Rough Creek fault zone, and east of the Illinois-Kentucky fluorspar district. Data from more than 20 excellent exposures indicate that the faults dip from 51° to 90°, and are remarkably straight over considerable distances, with only local irregular variations. Extensive slickensided surfaces showing only vertical movement, limited brecciation, and the development of fault slices were noted at several exposures.

Normal or gravity type faults have been recognized and mapped in the western Kentucky coal field for more than 50 years. Many faults in the Saint Charles and Nortonville quadrangles have been exposed by recent strip mining operations. Because the faults are exceptionally well exposed and the exposures are being rapidly destroyed by weathering and erosion, their locations and characteristics are reported here.

Faults of the two quadrangles are part of a much larger number in western Kentucky which have considerable importance in mineral exploration and development, and in certain construction work. Since little is known of the origin of the several fault systems, it is desirable to record their details while observation is possible in order to work out the structural history of western Kentucky. The exposures were noted during a cooperative geologic mapping program of the Kentucky Geological Survey and the U.S. Geological Survey. The area discussed covers about 120 square miles south of Madisonville in western Kentucky (fig. 1).

The faults are located in a region of relatively intensive faulting, bounded on the north by the Rough Creek fault zone and on the west by faults of the Illinois-Kentucky fluorspar district (fig. 1). Eight major normal faults and many minor faults which strike generally

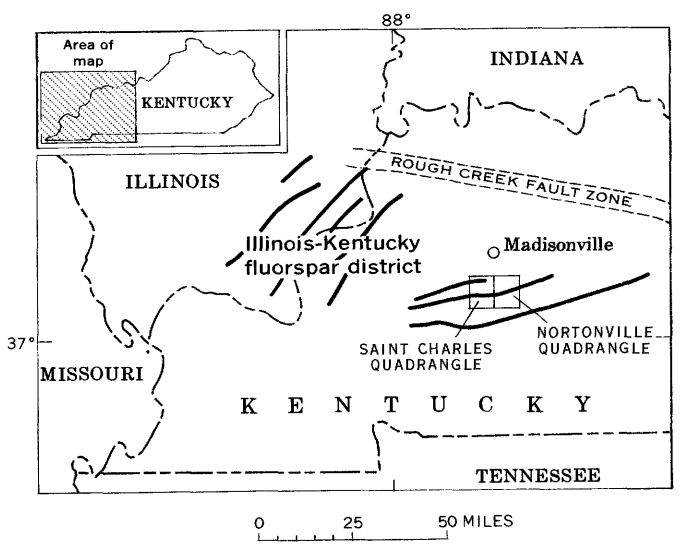

FIGURE 1.—Index map showing location of Saint Charles and Nortonville 7½-minute quadrangles, Rough Creek fault zone, and Illinois-Kentucky fluorspar district. Trends of a few faults in and near the quadrangles are shown.

northeastward have been mapped in the two quadrangles (fig. 2). Surface strata are of Middle and Late Pennsylvanian age and include several major coal beds which have been mined both at the surface and underground. Data from a large number of drill holes, several underground mine maps, and a relatively large number of surface exposures make it possible to accurately locate the faults.

GENERAL CHARACTERISTICS

Faults of the western Kentucky coal field have been considered to be nearly vertical, but at more than 20 exposures in the two quadrangles the faults dip from 54° to 90° (table 1). The average dip is about 72°, and only one vertical fault was observed.

U.S. GEOL. SURVEY PROF. PAPER 650-C, PAGES C75-C78

337-735 O—69——6

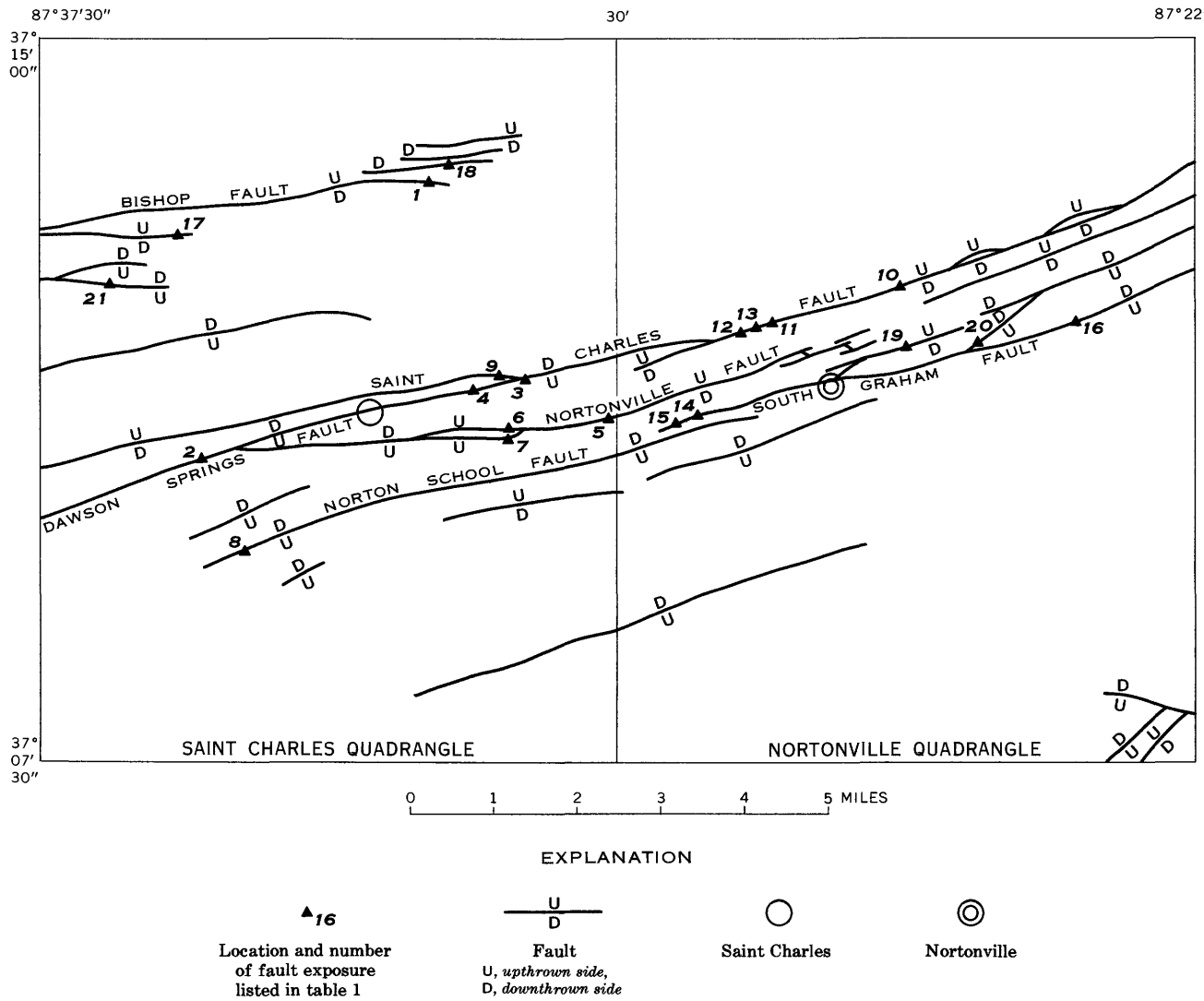

FIGURE 2.—Map of the Saint Charles and Nortonville quadrangles, Kentucky, showing locations of faults and fault exposures discussed in this report. Fault traces compiled from Palmer (1967, 1968).

Oil test holes drilled near the Bishop and Saint Charles faults reached the faults at considerable depths. The Saint Charles fault, where exposed by stripping, dips 67° S. (fig. 3). From the surface to the point it was crossed at a depth of 1,510 feet, the fault has an average dip of 65°. The Bishop fault has an average dip of 74° from the surface to the point where it was crossed at a depth of 1,070 feet.

No published reports of the area are known in which the throw of faults at considerable depths is compared with throw measured at the surface. The two oil test holes discussed above provide the opportunity for such comparisons. Outcrop and test-hole data show the throw of the Saint Charles fault to be 235 feet at the surface, and 185 feet, which is 50 feet less, at a depth of 1,510 feet. Outcrop and test-hole data indicate a throw of 310 feet for the Bishop fault at the surface near the western boundary of the Saint Charles quadrangle. At a depth of 1,070 feet the throw is only 240 feet, or 70 feet less than the surface displacement.

Fault planes in the two quadrangles are sharply defined where exposed, with only limited associated fractures in adjacent rock. Brecciated zones are not common, and where present are usually no more than 1 or 2 feet wide. Drag folding is slight along most faults.

Only vertical movement is indicated by the exposed slickensided surfaces. The uniformity and smoothness of the grooves and the absence of separate superimposed layers of slickensides suggest the likelihood of only one generation of movement.

Examination of fault scarps exposed by strip mining and data from maps of underground mine works indicate that the fault traces are straight or very gently curving over considerable distances. A scarp of the Saint Charles fault, about 1½ miles east of Saint Charles (fig. 4, p. C78), is almost perfectly straight for about 800 feet. A scarp of

TABLE 1.—*Fault and fault-scarp exposures in the Saint Charles and Nortonville quadrangles, Kentucky*

[Locations of faults and fault-scarp exposures listed here are shown by corresponding numbers on figure 2]

Name of fault	Strike and dip	Description
1. Bishop	N. 69° W.; 85° S.	Large scarp, partly exposed by strip mining.
2. Dawson Springs	N. 80° E.; 53° N.	Small natural exposure, slickensided sandstone.
3. do	N. 85° E.; 75° S.	Small natural exposure, slickensided sandstone bluff.
4. do	N. 80° E.; 68° N.	Small exposure in strip pit, strongly slickensided sandstone.
5. Nortonville	N. 80° E.; 59° S.	Small natural exposure, slickensided sandstone bluff.
6. do	N. 79° W.; 75° S.	Small exposure in strip pit, slickensided sandstone.
7. do	N. 87° E.; Vertical	Do.
8. Norton School	N. 72° E.; 80° N.	Large fault scarp partly exposed over distance of 3,000 feet in strip pit.
9. Saint Charles	East; 80° S.	Large fault scarp, well exposed over distance of 800 feet in strip pit.
10. do	N. 73° E.; 68° S.	Good exposure in cut on U.S. Highway 41 Bypass.
11. do	N. 62° E.; 67° S.	Good exposure in strip pit, slickensided sandstone.
12. do	N. 80° E.; 64° S.	Do.
13. do	N. 70° E.; 71° S.	Good exposure in strip pit, strongly slickensided sandstone.
14. South Graham	N. 80° E.; 63° N.	Large fault scarp exposure, slickensided sandstone in strip pit.
15. do	N. 78° E.; 62° N.	Good exposure in strip pit.
16. do	N. 70° E.; 85° N.	Small exposure at south side of State Route 813.
17. Unnamed	N. 83° E.; 70° S.	Small exposure in strip pit, slickensided sandstone.
18. do	N. 84° E.; 75° N.	Small exposure in strip pit.
19. Unnamed	N. 75° E.; 51° S.	Fair exposure in cut on U.S. Highway 41 Bypass.
20. do	N. 65° E.; 85° N.	Small exposure in strip pit.
21. do	N. 88° W.; 85° N.	Good exposure in strip pit.

FIGURE 3.—Slickensided sandstone scarp of Saint Charles fault exposed by strip mining. Fault strikes N. 62° E. and dips 67° S. Throw is 235 feet. Fault plane here has an average dip of 65° to a depth of 1,510 feet. (Location 11 in table 1 and fig. 2.)

the Norton School fault, where it has been exposed by strip mining near its western end in the Saint Charles quadrangle, is nearly straight over a distance of about 3,000 feet. However, local irregularities in strike along the faults are relatively common, as shown by the slickensided sandstone scarp of the South Graham fault exposed by strip mining about 1½ miles southwest of Nortonville (fig. 5, p. C78).

Three locations were recognized in the two quadrangles where small slices have developed along fault planes, displaced with respect to both the upthrown and downthrown sides of the main fault. One such small slice occurs along the Saint Charles fault about 1½ miles east of Saint Charles (fig. 4). Two other larger slices along the strike of the Saint Charles fault in the eastern part of the Nortonville quadrangle (fig. 2) are mapped largely on drill-hole data.

The faults discussed here are part of a greater number exposed by strip mining in the western Kentucky coal field. These many exposures provide unusually precise

FIGURE 4.—Slickensided sandstone scarp of Saint Charles fault exposed by strip mining. The scarp is nearly straight over a distance of about 800 feet. Strike is eastward, and fault plane dips 80° S. Throw is 60 feet. (Location 9 in table 1 and fig. 2.)

data which should be significant in formulating the structural history of western Kentucky.

REFERENCES

Palmer, J. E., 1967, Geologic map of the Saint Charles quadrangle, Hopkins and Christian Counties, Kentucky: U.S. Geol. Survey Geol. Quad. Map GQ–674.

——— 1968, Geologic map of the Nortonville quadrangle, Hopkins and Christian Counties, Kentucky: U.S. Geol. Survey Geol. Quad. Map GQ-762.

FIGURE 5.—Slickensided sandstone scarp of South Graham fault, showing local irregular variation in strike. General strike is N. 80° E., and dip is 63° N. Throw is 85 feet. (Location 14 in table 1 and fig. 2.)

HAWAIIAN SEISMIC EVENTS DURING 1967

By ROBERT Y. KOYANAGI, Hawaiian Volcano Observatory

Abstract.—Several tens of thousands of earthquakes were recorded in Hawaii during 1967; of those, 551 with a magnitude of from 2.0 to 4.6 were located. Of the 140 earthquakes felt by residents, 11 were felt over the entire island.

Hawaiian earthquake locations for 1967, determined by the U.S. Geological Survey's Hawaiian Volcano Observatory, are graphically presented in this report. It is the sixth of a series of reports (Koyanagi, 1964; Koyanagi and Endo, 1965; Koyanagi and Okamura, 1966; Koyanagi, 1968; Koyanagi, 1969) presenting the locations and other data on a selected group of earthquakes during each calendar year.

Earthquakes having a magnitude of 2.0 or greater beneath the five volcanoes of the island of Hawaii (fig. 1) and offshore along the Hawaiian Ridge from lat 18° to 23° N. and long 154° to 161° W. are plotted in figures 2 and 3. The earthquakes are divided into 3 depth groups (less than 10, 10–20, and 20–60 kilometers) (fig. 4) and 2 magnitude groups (2.0–3.5, and greater than 3.5).

Methods of locating earthquakes and evaluating probable accuracy remain unchanged throughout the series of reports. (Eaton, 1962, p. 16–18.) P-wave arrivals and S–P values are applied to Hawaiian seismic-wave traveltime curves. Earthquakes with a magnitude of 2.5 or greater beneath the island of Hawaii are generally located within a 5-km sphere of error, although errors as great as 10 km may be expected from earthquakes located offshore.

During the year, several new seismic stations were added to the existing network on the island of Hawaii. These are omitted from figure 1 and located as follows:

	North latitude	*West longitude*
Mauna Loa (2)	19°27.6′	155°20.7′
Kealakomo	19°18.5′	155°09.6′
Cone Peak	19°23.7′	155°19.7′
Kipuka Nene	19°20.1′	155°17.4′
Outlet	19°23.4′	155°16.8′

CHRONOLOGY OF KEY 1967 SEISMIC EVENTS

Many seismic "events" of considerable significance are made up of swarms of earthquakes smaller than the magnitude cutoff of 2.0 used in selecting the events for plotting. The following paragraphs describe such events and add other notes that put the seismic events of the year into perspective.

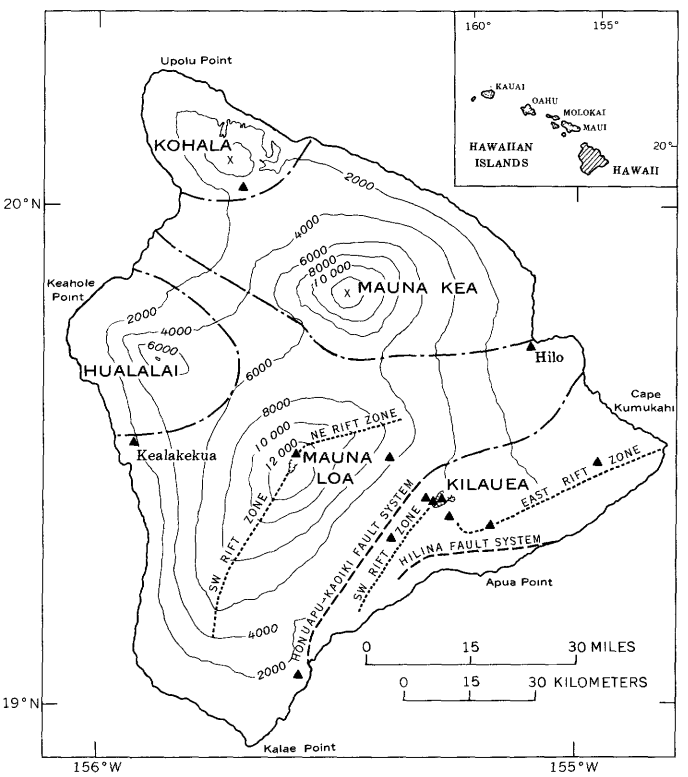

FIGURE 1.—Map of the island of Hawaii, showing the five volcanoes and their principal structural features. Dot-and-dash lines are boundaries of volcanic systems. Location of seismograph stations is indicated by closed triangles. Contour interval is 2,000 feet, and datum is mean sea level.

During the first quarter, on January 6–7, Hawaiian Volcano Observatory seismographs recorded a flurry of nearly a hundred deep Kilauea earthquakes. The largest event of this episode registered a magnitude of 3.9, and was felt islandwide. Throughout most of the quarter, increased activity prevailed along the east rift zone of Kilauea. Upper east rift earthquakes averaged 20 per day, and in the second half of January, nearly 200 earth-

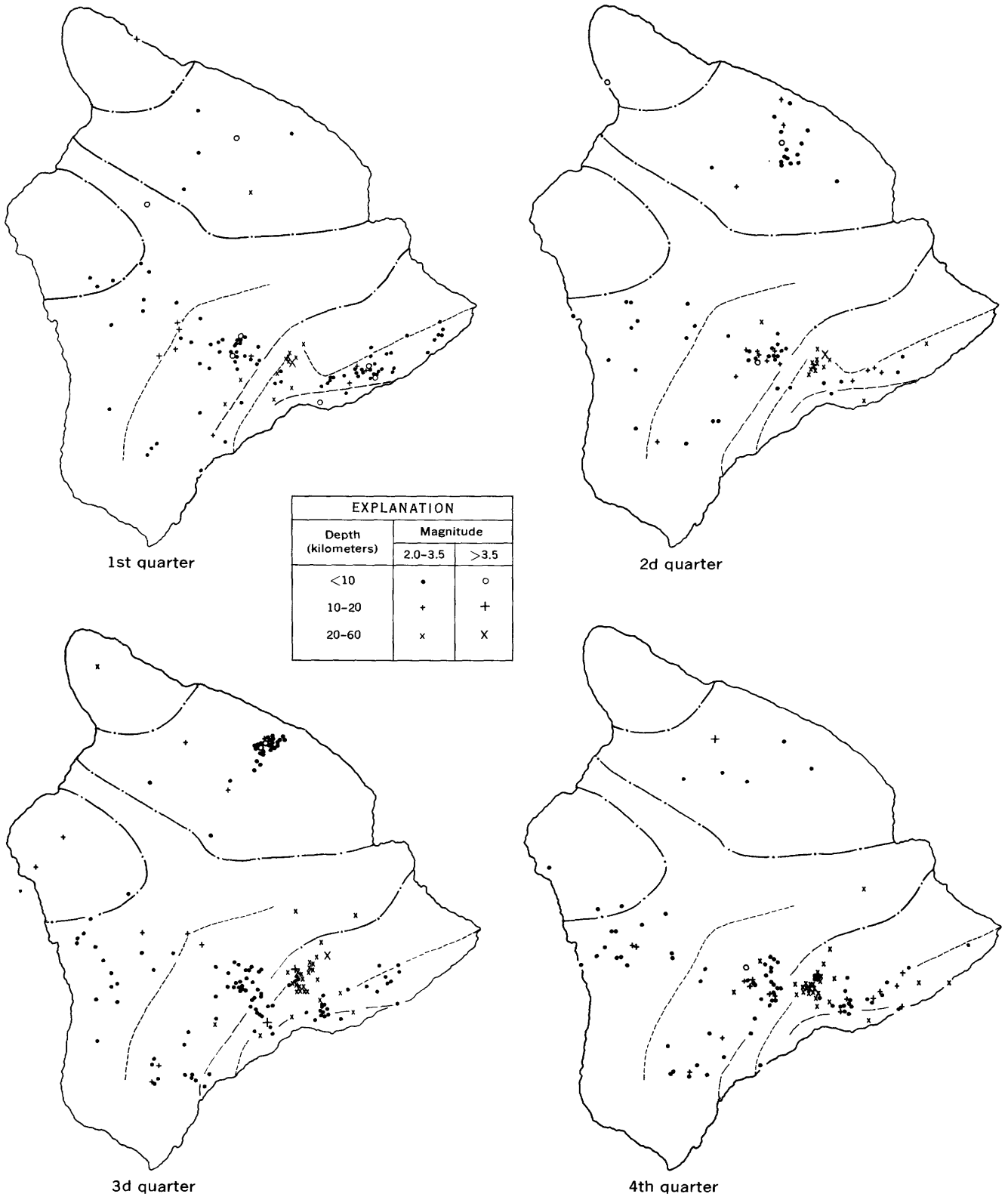

FIGURE 2.—Plot of epicenters of earthquakes having a magnitude of 2.0 or greater beneath the island of Hawaii during each quarter of 1967. Dot-and-dash lines are boundaries of volcanic systems, long-dashed lines are fault systems, and short-dashed lines are rift zones. Geographic names are shown in figure 1.

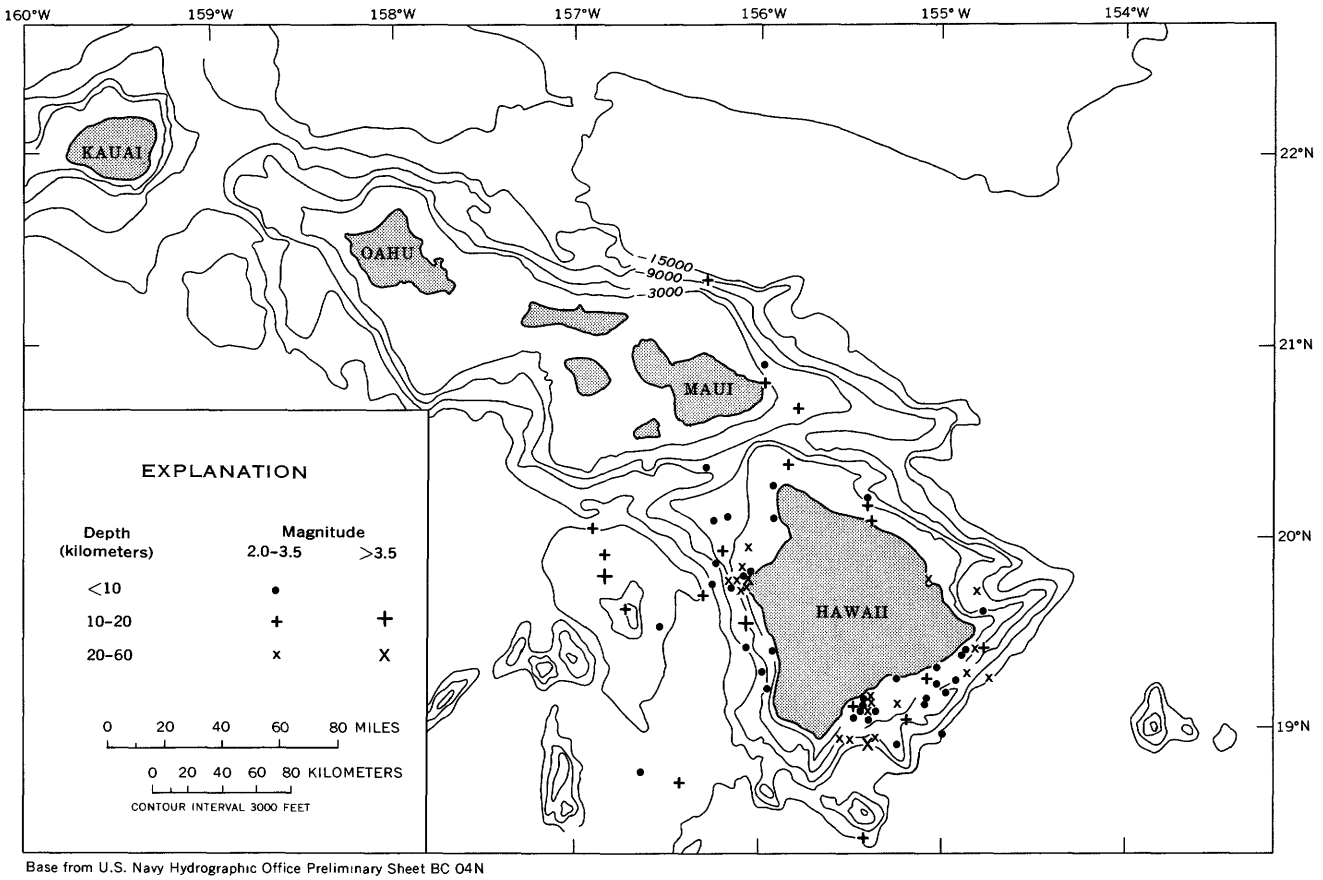

FIGURE 3.—Map of the Hawaiian Islands, showing epicenters of earthquakes having a magnitude of 2.0 or greater that occurred off the island of Hawaii during 1967.

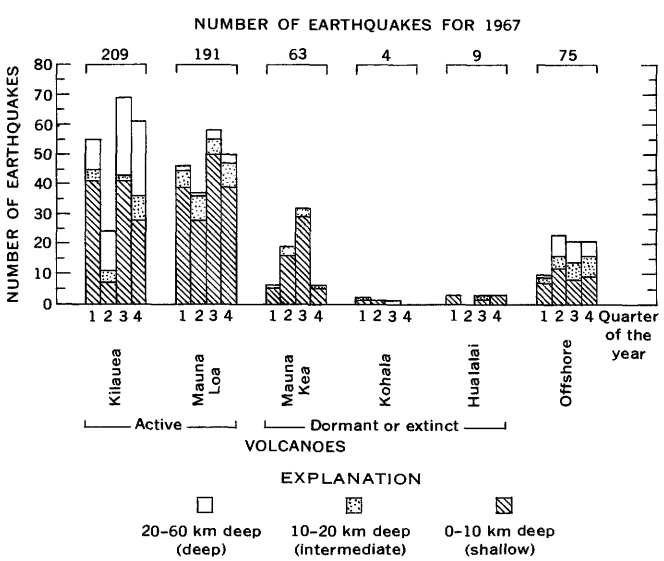

FIGURE 4.—Geographic location and the distribution, with depth, of earthquakes having a magnitude of 2.0 or greater that occurred in the Hawaiian Islands during 1967.

quakes occurred in shallow zones along the eastern part of the rift. Several of these events were felt locally. An earthquake with a magnitude of 4.6 and 8 kilometers beneath the Kaoiki scarp, which was felt islandwide on January 23 at $16^h/59^m$, proved to be the largest event of the year.[1]

Several flurries of shallow Kilauea caldera earthquakes were recorded during the second quarter. Also, from the last week of May and continuing into September, earthquake activity was noted beneath the northeast flank of Mauna Kea. Nearly a dozen shocks were felt by residents on the coastal slopes of Mauna Kea.

Starting in September and extending through October, increased levels of Kilauean seismic activity were recorded. The daily number of earthquakes generally ran high for deep and shallow sources beneath the caldera and for sources beneath the southwest and, to a lesser extent, southeast flanks. With the exception of a relatively few large earthquakes, however, most of the seismic activity described above consisted of small earthquakes with a magnitude less than 2.0.

The summit eruption of Kilauea started on the morning of November 5 and continued into the following year. Observatory seismographs traced the seismic pat-

[1] Times are in hours and minutes, Hawaiian standard time.

terns of the erupting volcano as they recorded earthquakes and harmonic tremor.

SUMMARY

Of several tens of thousands of earthquakes recorded in Hawaii during 1967, 551 had a magnitude of 2.0 or greater. Among the larger events, 443 had magnitudes of 2.0 to 2.9, 98 had magnitudes of 3.0 to 3.9, and 10 had magnitudes of 4.0 to 4.6. As in previous years, the largest concentrations of earthquakes were beneath the active volcanoes Mauna Loa and Kilauea. Most of the events originated from shallow sources (less than 10 km) beneath active structures, and a moderate number of deep Kilauean earthquakes originated from a source about 30 km beneath the summit area.

Some 140 shocks were felt by Hawaii residents during the year. Eleven of these which ranged in magnitude from 3.9 to 4.6, were perceptible over the entire island.

REFERENCES

Eaton, J. P., 1962, Crustal structures and volcanism in Hawaii, *in* Macdonald, G. A., and Kuno, Hisashi, eds., The crust of the Pacific Basin: Am. Geophys. Union Geophys. Mon. 6 (Natl. Acad. Sci.—Natl. Research Council Pub. 1035), p. 13–39.

Koyanagi, R. Y., 1964, Hawaiian seismic events during 1962: Art. 144 *in* U.S. Geological Survey Prof. Paper 475–D, p. D112–D117.

——— 1968, Hawaiian seismic events during 1965, *in* Geological Survey Research 1968: U.S. Geol. Survey Prof. Paper 600–B, p. B95–B98.

——— 1969, Hawaiian seismic events during 1966, *in* Geological Survey Research 1969: U.S. Geol. Survey Prof. Paper 650–B, p. B113–B116.

Koyanagi, R. Y., and Endo, E. T., 1965, Hawaiian seismic events during 1963, *in* Geological Survey Research 1965: U.S. Geol. Survey Prof. Paper 525–B, p. B13–B16.

Koyanagi, R. Y., and Okamura, A. T., 1966, Hawaiian seismic events during 1964, *in* Geological Survey Research 1966: U.S. Geol. Survey Prof. Paper 550–C, p. C129–C132.

ELECTRICAL SOUNDING PROFILE EAST OF THE JORDAN NARROWS, UTAH

By ADEL A. R. ZOHDY and DALLAS B. JACKSON, Denver, Colo.

Work done in cooperation with the Utah Department of Natural Resources, Water Rights Division

Abstract.—In October 1967, the U.S. Geological Survey made a profile of electrical soundings east of the Jordan Narrows, south of Salt Lake City, Utah, to explore the possible existence of a buried stream channel that may be contributing large amounts of ground water to the Jordan Valley. The electrical soundings were made using the Schlumberger electrode array, and the technique of making pairs of crossed soundings provided valuable information on the phenomenon of electrical lateral pseudoanisotropy which reflected the complexity of the bedrock surface. The probable presence of a system of step faults in the bedrock was determined from the analysis of the electrical sounding curves. It was also possible to correlate several geoelectric layers across the profile and to evaluate their thicknesses, resistivities, and horizontal extent. Although the electrical soundings did not confirm the presence of a buried stream channel in the area, the sounding data did illustrate the dependency of electrical sounding curves on the azimuth of the sounding line when the sounding is made over horizontally inhomogeneous media.

Seventeen vertical electrical soundings using the Schlumberger electrode configuration were made along a northeast–southwest traverse extending from the foot of the east Traverse Mountains southwestward to near the Jordan Narrows. The geoelectrical survey was made by the U.S. Geological Survey in cooperation with the Utah Department of Natural Resources, Water Rights Division, to investigate the possible existence of a buried stream channel which may be contributing substantial amounts of ground water to the Jordan Valley. The locations of the electrical sounding stations and the orientation of the sounding lines are shown in figure 1. Interpretation of the sounding curves was made using albums of theoretical curves for horizontally stratified media in conjunction with the auxiliary point diagrams (Compagnie Générale de Géophysique, 1963; Orellana and Mooney, 1966; Zohdy, 1965), as well as sets of theoretical curves for media with both vertical and horizontal boundaries (Berdichevskii and others, 1966; Kunetz, 1955). Five pairs of crossed soundings (Vedrintsev, 1961) were made to study the phenomenon of electrical lateral pseudoanistropy (Zohdy, unpub. data). A pair of crossed soundings is made at a given station by expanding the sounding lines along two perpendicular directions from a common center. The five pairs of crossed soundings proved useful in avoiding grossly erroneous interpretation which may have resulted if only one sounding had been made at each sounding station.

GEOLOGIC SETTING

The Jordan Narrows lies in a topographic constriction, about 2 miles wide, between the east and west Traverse Mountains (fig. 1). The valley it occupies is filled with alluvial, colluvial, and lacustrine deposits of Tertiary to Holocene age. The east and west Traverse Mountains are composed of highly faulted quartzite and sandy limestone of the Oquirrh Formation of late Carboniferous (Pennsylvanian) age. Overlying the Oquirrh Formation on the east flank of the west Traverse Mountains is a series of lava flows of Tertiary age that extend out into the valley beneath the valley fill. These lavas were extruded on an irregular topographic surface and in some places their thickness exceeds 570 feet (Pitcher, 1957; Ted Arnow, written commun., 1968). Whether or not these flows extend across the valley beneath the valley fill to form the bedrock (and perhaps the electrical basement) beneath the Jordan Narrows is not known.

Previous geophysical surveys indicate that the area occupies a saddle between gravity lows to the north and south. These lows were interpreted as grabens (the Jordan Valley graben and Utah Valley graben) by

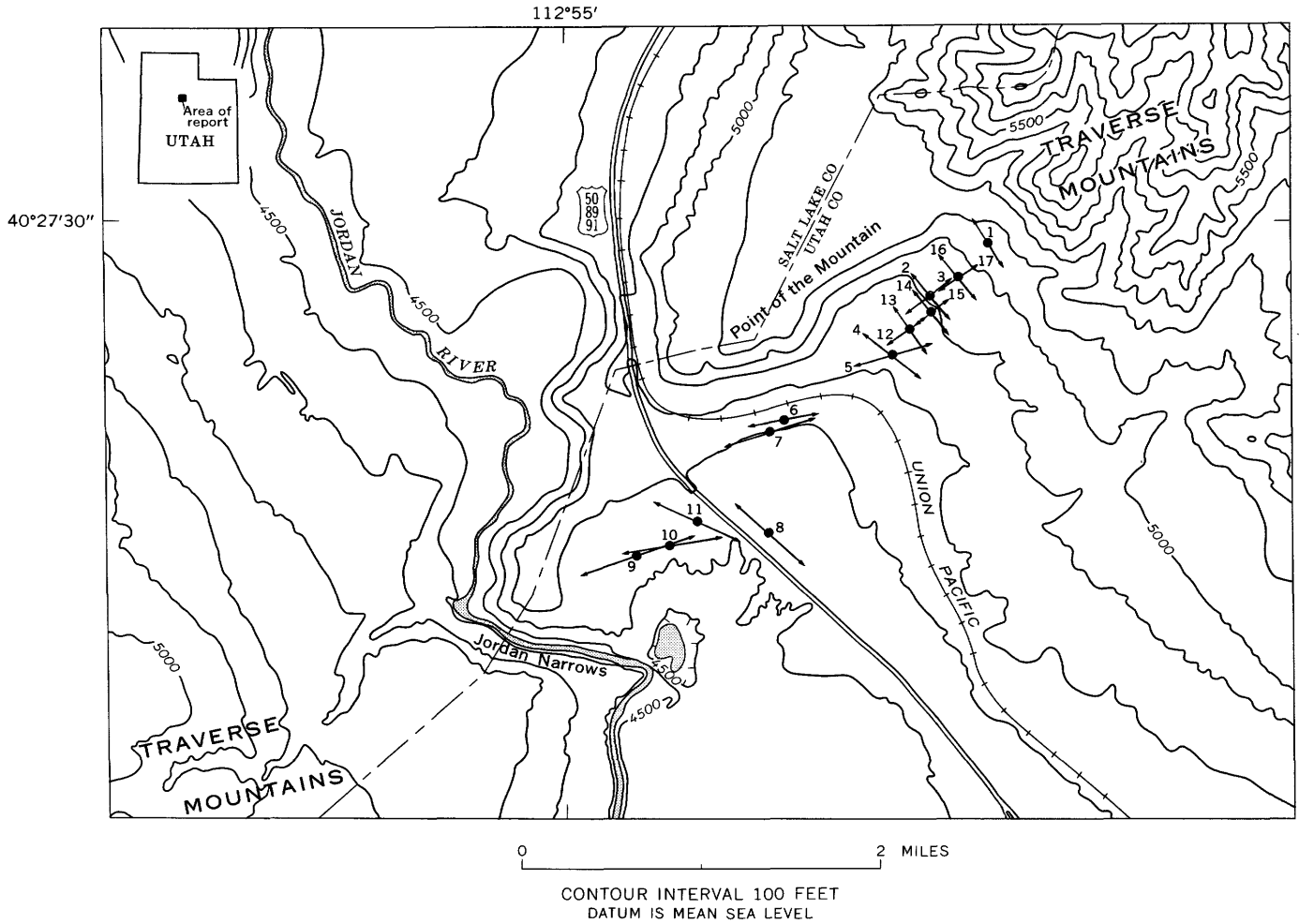

FIGURE 1.—Index map showing location of the electrical sounding stations, Jordan Narrows, Utah. Base from U.S. Geological Survey, Jordan Narrows quadrangle, 1951, 1:24,000.

Cook and Berg (1961). Cook and Berg (1961) believe that the rocks of the saddle area between the Jordan Valley and Utah Valley grabens were downfaulted relative to the adjoining mountain blocks. On the west side of the Jordan Narrows area this supposition is supported by a mapped fault (not shown on fig. 1) with downward displacement to the east along the foot of the west Traverse Mountains (Pitcher, 1957). Although no fault displacements have been measured along the foot of the east Traverse Mountains on the east side of the Jordan Narrows, several zones of brecciation, as well as evidence from the resistivity survey, suggest that faulting has definitely occurred there.

VERTICAL ELECTRICAL SOUNDINGS

Seventeen vertical electrical soundings (VES) were made at 12 sounding stations. At five sounding stations pairs of crossed soundings were made. On the basis of the interpretation of the VES curves, two electrically equivalent cross sections were prepared (fig. 2). The two sections are almost identical except for the middle parts, which are primarily based on alternate interpretations of VES 7. Because of the lack of geologic information from drill holes and the absence of other soundings in the immediate vicinity of VES 7—data from VES 6 were unreliable—either one of the two interpretations is theoretically possible. The interpreted distribution of the layering hinges on the true resistivity value (700 ohm-meters in one section and 1,100 ohm-m in the other) of the second high-resistivity (gravel?) layer. The top cross section is based on the minimum possible value of resistivity (700 ohm-m) for this layer, which in turn yields the maximum thickness for it. Theoretically, no maximum value of resistivity can be assigned to this layer for obtaining a minimum thickness, but, by assuming a value of about 1,100 ohm-m to be the maximum probable resistivity (on the basis of practical experience), it was possible to construct the lower cross section.

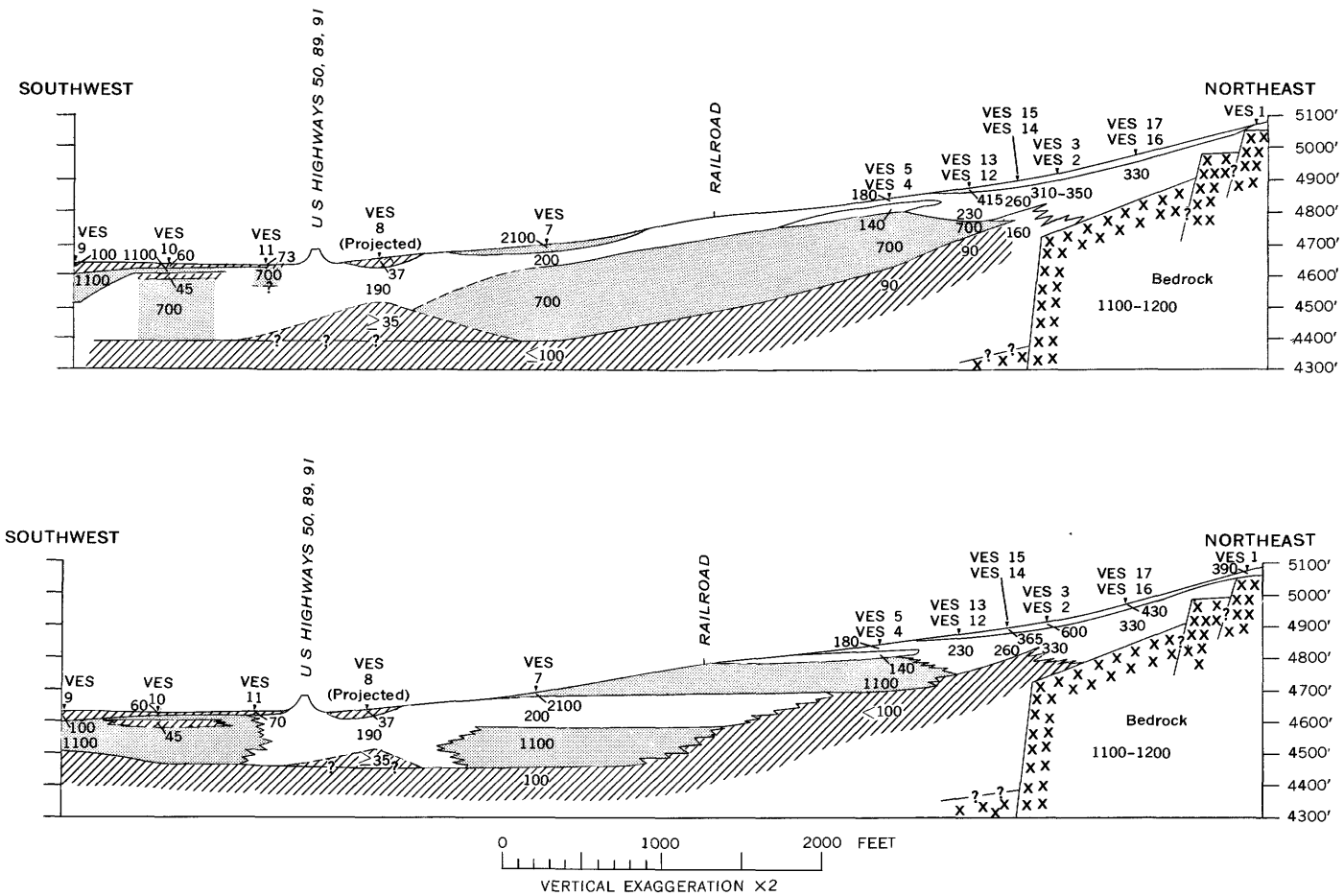

FIGURE 2.—Two equivalent cross sections based on different interpretations of vertical electrical sounding (VES) curves. Numbers designate possible values, in ohm-meters, of true resistivity. Line pattern, low resistivity; stipple, high resistivity. Location of sounding stations shown on figure 1.

The curves of VES 1, 2, 3, 16, and 17 indicate the presence of a high-resistivity bedrock at depths ranging from 15 to 170 feet, as indicated by the rising right-hand branches of the curves. The angle of inclination formed by these rising branches and the abscissa axis is less than 45°, indicating that the basement rocks have a finite resistivity of about 1,200 ohm-m. The absence of these rising branches at large electrode spacings on all subsequent sounding curves to the southwest of VES 2 and 3, and the strong effect of lateral pseudoanisotropy[1] (Zohdy, unpub. data) on crossed sounding curves southwest of VES 2 and VES 3 (for example, VES 12 and 13) indicate the probable presence of a major steeply dipping fault between the pairs of crossed soundings VES 2 and 3 and VES 14 and 15. Analysis of the sounding data, from northeast to southwest, follows:

VES 1.—This sounding was made near the foot of the east Traverse Mountains with the electrode array oriented northwest, virtually parallel to the topographic contours. The VES curve (fig. 3) indicates the presence of a thin, near-surface, coarse-grained alluvial layer having a resistivity of about 390 ohm-m and a thickness of about 15 feet. An underlying layer having a much higher resistivity (1,100–1,200 ohm-m) probably represents a weathered (Paleozoic?) metamorphic basement. The sounding curve also indicates that a more resistive layer (2,200(?) ohm-m) occurs at a depth of about 85 feet and that a conductive layer probably occurs at a maximum depth of about 400 feet. Neither the 2,200-ohm-m layer nor the possible underlying conductor is shown on figure 2. This lowest conductive layer may or may not exist, because the resistivity measurements at large electrode spacings might have been affected by rough topography in the vicinity of this sounding.

VES 16 and VES 17.—VES 16 and VES 17 are crossed soundings, made at the same station with the

[1] Lateral pseudoanisotropy is defined here as the effect of a horizontal inhomogeneity (in a geoelectric section comprised of individually homogeneous and isotropic layers) which makes sounding curves obtained at the same sounding station (with variable azimuth sounding lines) depart from one another and resemble curves obtained over a horizontally homogeneous but anisotropic medium.

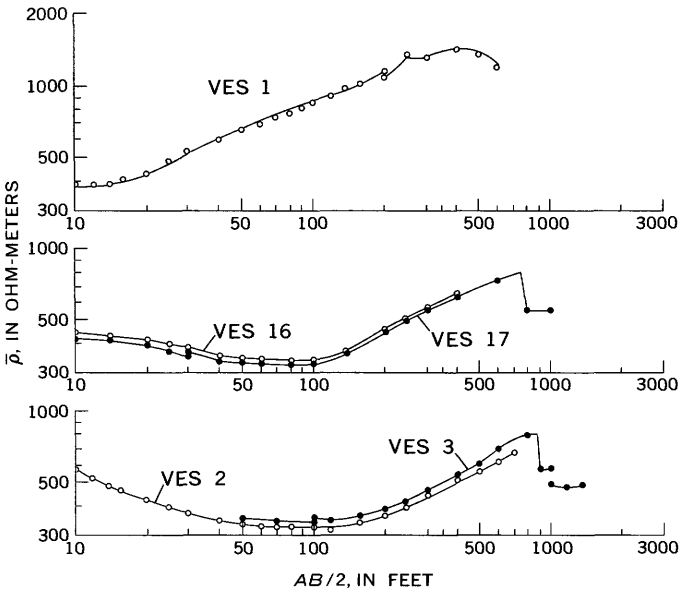

FIGURE 3.—Vertical electrical sounding curves VES 1, 16 and 17, and 2 and 3 where $\bar{\rho}$ is apparent resistivity and $\frac{AB}{2}$ is half the distance between current electrodes. VES 2 and 3, and VES 16 and 17 are pairs of crossed soundings.

electrode arrays oriented almost at right angles. The striking similarity and coincidence of the resulting VES curves (fig. 3) demonstrate the dominance of horizontal stratification and the absence of lateral pseudoanisotropy (relative percentage differences in apparent resistivity values are less than 2 percent). Both curves indicate a thin alluvial cover of 430-ohm-m resistivity to a depth of 9.5 feet, alluvial material of 330-ohm-m resistivity to a depth of 130 feet, and basement rocks of 1,100–1,200-ohm-m resistivity. Sounding VES 16 was expanded to the northwest and southeast to $\frac{AB}{2}$ (half the distance between current electrodes)=400 feet only, but VES 17 was expanded to the northeast and southwest to $\frac{AB}{2}$=1,000 feet. At $\frac{AB}{2}\approx$750 feet a sharp discontinuity is observed on the curve of VES 17. This discontinuity is probably caused by the crossing of one of the current electrodes over a highly resistive ridgelike structure (Kunetz, 1955). The existence and the position of the easternmost fault shown (fig. 2) were inferred on the basis of this discontinuity.

VES 2 and VES 3.—VES 2 and VES 3 are crossed soundings, made with the electrode arrays oriented northwest-southeast and northeast-southwest. The two VES curves (fig. 3) are similar but they separate from one another in a manner prescribed theoretically for a highly resistive bedrock dipping slightly toward the southwest. The curves are interpreted as follows:

Depth (feet)	Probable lithology	Resistivity (ohm-m)
0–3	Sand and gravel	780
3–9	do	500
9–170	do	310–340
>170	Basement rocks	>1, 000

On the curve of VES 3, a sharp discontinuity is observed at $\frac{AB}{2}\approx$900 feet. (Compare with VES 17.) The discontinuity indicates the presence of a second fault offsetting the bedrock (fig. 2) at about 900 feet from the center of VES 3.

VES 14 and VES 15.—The curves of the crossed soundings VES 14 and VES 15 (fig. 4) were obtained from measurements made at a station which is only about 200 feet southwest of the crossed soundings VES 2 and VES 3. Despite the proximity of these two sounding stations, no direct indication of the presence of the highly resistive bedrock was observed on VES 14 and VES 15 curves nor on any of the sounding curves obtained at stations southwest of this locality. Furthermore, the resistivity of the second alluvial layer decreased from about 330 ohm-m at VES 2 and VES 3 to 260 ohm-m at VES 14 and VES 15; this decrease may indicate that faulting in the basement rocks extends into the alluvium and brings into contact two types of alluvial deposits with contrasting electrical properties. The minimum depth to basement at this locality is estimated to be about 500 feet. The two sounding curves display lateral pseudoanisotropy, especially for electrode spacings of $\frac{AB}{2}$>300 feet.

VES 12 and VES 13.—The curves for crossed soundings VES 12 and VES 13 (fig. 4) portray, far more clearly than the curves of VES 14 and VES 15, the presence of a strong lateral discontinuity in the electrical properties of the rocks at depth, especially at electrode spacings of $\frac{AB}{2}$>300 feet. The horizontal discontinuity in electrical properties at depth is the result of a high-angle major fault located between the pairs of crossed soundings VES 2 and 3 and VES 14 and 15. The electrode array for VES 12 (oriented northeast-southwest) was expanded at approximately right angles to the strike of this major fault, whereas for VES 13 the electrode array was expanded approximately parallel to the fault plane. Both VES curves indicate the presence of a fairly uniform layer of alluvium (230 ohm-m) underlain by a conductive layer (water-saturated) as indicated by the descending right-hand branches of the curves. The depth to this conductive zone according to VES 12 (if strict horizontal homogeneity and stratification are assumed) is about 600 to 700 feet. However, an independent interpretation of VES 13 (if strict horizontal homogeneity

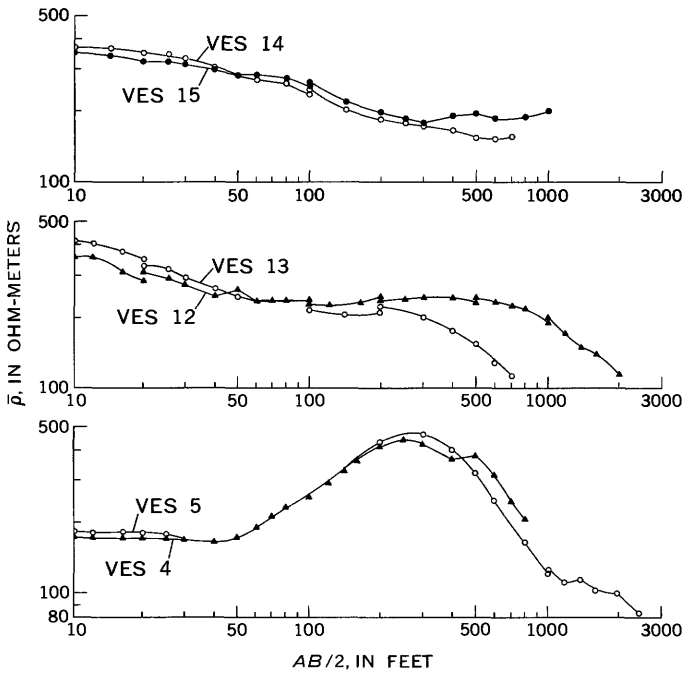

FIGURE 4.—Paired curves of VES 14 and 15, 12 and 13, and 4 and 5. The divergence of the curves of VES 12 and 13 at $\frac{AB}{2} > 300$ feet illustrates the phenomenon of lateral pseudo-anistropy.

and stratification are assumed) results in a depth of only 250 to 300 feet. That is, the depth to the conductive layer according to VES 12 is about twice as large as indicated by VES 13. In reality both interpretations are inaccurate, and the depth to the conductive horizon is probably shallower than indicated by either interpretation. The semiquantitative method described by Fomina (1962) was used to arrive at this conclusion.

VES 4 and VES 5.—The pair of crossed sounding curves VES 4 and VES 5 indicates the presence of a shallow high-resistivity (1,100 ohm-m) layer at a depth of about 36 feet. This layer was not detected on any of the soundings already discussed and it probably pinches out abruptly at least on one end of the sounding line. This is indicated by the sharpness of the maximum on VES 5 (Alfano, 1959). The determination of the thickness of this layer is not unique because of the principle of equivalence (Kalenov, 1957). Its maximum thickness, however, is estimated to be about 175 feet, as determined from its minimum possible resistivity of about 700 ohm-m. It is more likely that this layer has a much higher resistivity. A value of 1,100 ohm-m indicates a thickness of about 100 feet. This gravel(?) layer is underlain by a thick, more conductive layer (water-saturated unconsolidated sediments?) whose resistivity is less than 100 ohm-m.

VES 7.—At least five distinct layers can be seen on the curve of VES 7 (fig. 5). One interpretation of the curve is as follows:

Layer	Depth (feet)	Probable lithology	Resistivity (ohm-m)
1[1]	0–5. 5	Gravel	420
2	5. 5–21	Cemented coarse gravel	2, 100
3	21–76	Sand and gravel	200
4	76–300	Coarse gravel	700
5	>300	Silt(?)	≤100

[1] Layer 1 is not shown in figure 2.

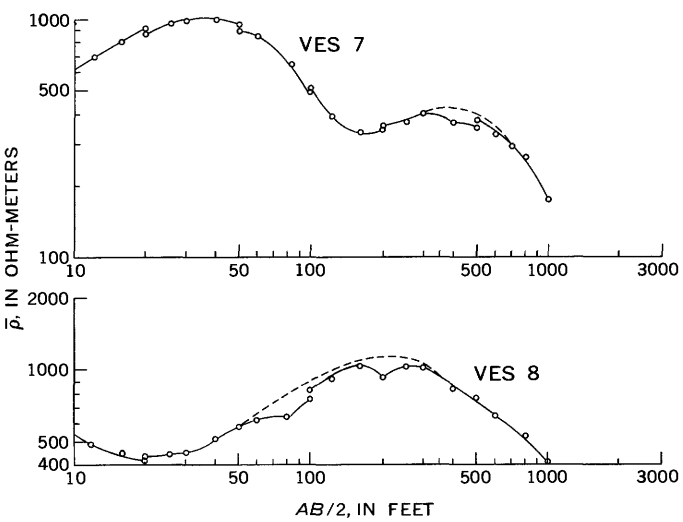

FIGURE 5.—Vertical electrical sounding curves VES 7 and VES 8.

A second interpretation changes only the thickness of the third layer and the thickness and resistivity (and consequently the inferred lithology) of the fourth layer, as follows:

Layer	Depth (feet)	Probable lithology	Resistivity (ohm-m)
3	21–110	Sand and gravel	200
4	110–240	Cemented gravel (?)	1, 100
5	>240	Silt(?)	≤100

If there is a buried channel then the second high-resistivity layer (layer 4) may be part of the fill in the buried channel.

VES 8.—The center of VES 8 does not fall on the profile of the other soundings (fig. 1); its interpretation is projected onto the cross section shown in figure 2. The VES curve (fig. 5) indicates 27 feet of clayey sediments (37 ohm-m) underlain by sand and gravel (190 ohm-m) to a depth of about 130 feet, and an underlying thick conductive layer of 35 ohm-m or less (Salt Lake(?) Formation). There is no evidence that the deep high-resistivity layer observed at VES 7 is present beneath VES 8.

VES 9, VES 10, and VES 11.—Soundings VES 9, VES 10, and VES 11 were made southwest of U.S. Highway 89 and 91. VES 11 (fig. 6) is highly distorted by

lateral heterogeneities at $\frac{AB}{2}$ spacings greater than 100 feet. Nevertheless, useful information can be extracted from it, especially when the curve is correlated with VES curves 9 and 10 (fig. 6). The curve for VES 10 indicates the presence of at least five geoelectric layers, whereas the curve of VES 9 seems to represent only four layers. The third layer of VES 9 and the second and fourth layers of VES 10 correlate fairly well with one another. Both have a resistivity of about 1,100 ohm-m and possibly may correlate, across VES 8, to the 1,100-ohm-m layer at VES 7 (fig. 2).

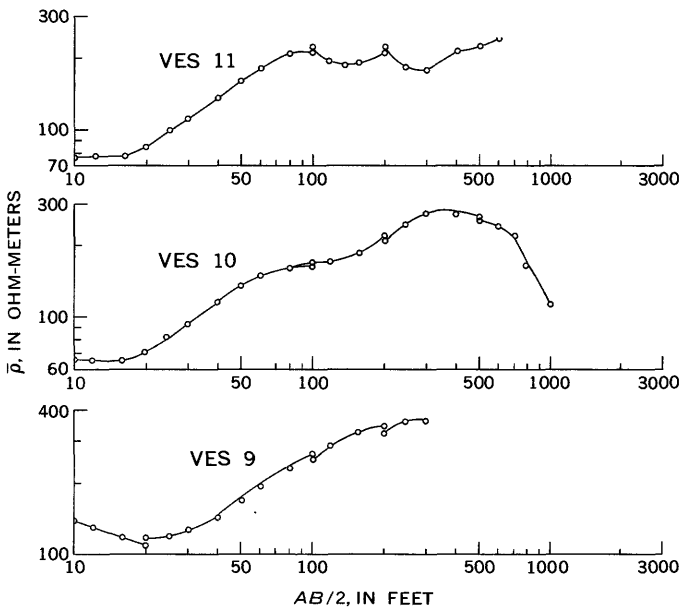

FIGURE 6.—Vertical electrical sounding curves VES 11, VES 10, and VES 9.

SUMMARY AND CONCLUSIONS

Several layers with contrasting electrical properties were recognized in the section, or profile, of electrical soundings (fig. 2). In the northeast end of the profile the bedrock is represented by high-resistivity (1,100 ohm-m) rocks of Paleozoic age, whereas in the middle part and southwestern end of the profile the bedrock is represented by moderately conductive (<100 ohm-m) rocks of Tertiary(?) age (Salt Lake(?) Formation).

Geoelectrical evidence demonstrating the presence of high-resistivity gravel(?) deposits beneath VES 7 below a depth ranging from 76 to 110 feet and extending to a depth ranging from 240 to 300 feet was determined from a double interpretation of the curve of VES 7. Whether these gravel(?) deposits are part of a buried stream channel could not be ascertained from the interpretation of VES 7 alone. The drilling of a test well in the vicinity of VES 7 to a depth of about 300 feet would be valuable for the evaluation of the geoelectrical parameters beneath VES 7, in particular, and throughout the section, in general. Geological data on layer thicknesses and lithologies would help in reducing the domain of the principle of equivalence.

The pairs of curves obtained from crossed soundings determined the location of a major fault in the high-resistivity bedrock. They also illustrate the dependency of electrical sounding curves on the azimuth of the sounding line when the sounding is made over horizontally inhomogeneous media.

REFERENCES

Alfano, Luigi, 1959, Introduction to the interpretation of resistivity measurements for complicated structural conditions: Geophys. Prosp. [Netherlands], v. 7, p. 311–366.

Berdichevskii, M. N., Krolenko, N. G., and Vedrintsev, G. A., 1966, Album of sets of curves [English translation], *in* Dipole methods for measuring earth conductivity: New York, Plenum Press, 1966, p. 179–302.

Compagnie Générale de Géophysique, 1963, Master curves for electrical sounding: The Hague, European Assoc. Exploration Geophysicists, 12 p., 36 p. of theoretical curves.

Cook, K. L., and Berg, J. W., Jr., 1961, Regional gravity survey along the central and southern Wasatch Front, Utah: U.S. Geol. Survey Prof. Paper 316–E, p. 75–89.

Fomina, V. I., 1962, Allowance for the influence of vertical and inclined surfaces of separation when interpreting electrical probings [English translation], chap. II *in* Rast, Nicholas, ed., Applied Geophysics U.S.S.R.: New York, Pergamon Press, p. 271–297.

Kalenov, E. N., 1957, Interpretation of vertical electrical sounding curves [In Russian]: Moscow, Gostoptekhizdat, 472 p.

Kunetz, Géza, 1955, Einfluss vertikaler Schichten auf electrische Sondierungen: Zeitschr. Geophysik, v. 21, no. 1, p. 10–24.

Orellana, Ernesto, and Mooney, H. M., 1966, Master tables and curves for vertical electrical sounding over layered structures: Madrid, Interciencia, 34 p., 125 tables, and supplement of theoretical curves. [English and Spanish]

Pitcher, G. G., 1957, Geology of the Jordan Narrows quadrangle, Utah: Brigham Young Univ. Research Studies Geology Ser., v. 4, no. 4, 46 p.

Vedrintsev, G. A., 1961, Problems in conducting and interpreting electrical sounding surveys in an area where there is sharp relief in the basement surface [In Russian]: Prikladnaya Geofizika, v. 29, p. 72–119. [English translation by G. V. Keller, *in* Dipole methods for measuring earth conductivity: New York, Plenum Press, 1966, p. 147–177.]

Zohdy, A. A. R., 1965, The auxiliary point method of electrical sounding interpretation and its relationship to the Dar Zarrouk parameters: Geophysics, v. 30, no. 4, p. 644–660.

INFRARED SURVEYS IN ICELAND—PRELIMINARY REPORT

By JULES D. FRIEDMAN, RICHARD S. WILLIAMS, JR.,[1]
GUÐMUNDUR PÁLMASON,[2] and CARL D. MILLER,[3]
Washington, D.C., Bedford, Mass., Reykjavík, Iceland, Ann Arbor, Mich.

Work done in cooperation with the Terrestrial Sciences Laboratory of the U.S. Air Force Cambridge Research Laboratories, and the Iceland National Energy Authority

Abstract.—Seven geothermal regions generally within the neovolcanic zone of Iceland were surveyed in August 1966 by means of an airborne line-scanning system that senses infrared radiation emitted from the earth's surface. The distribution, configuration, and relative intensity of thermal anomalies at Surtsey, Reykjanes, Krísuvík, Hekla, the Mývatn area, Askja, and the northern margin of Vatnajökull at Kverkfjöll were recorded by an infrared line-scanning system during the subarctic summer twilight and night. Imagery of the August 1966 olivine-basalt fissure eruption from the Surtur I crater, taken over a series of days that included the first day of the eruption, indicates that a complex pattern of thermal anomalies extended beyond the eruptive area. The effusive eruption was also detected by the Nimbus II High Resolution Infrared Radiometer system on at least seven orbits in August and September 1966. Hydrothermal anomalies within the main crater of the Surtsey satellite volcano, Jólnir, were detected by the airborne system after cessation in mid-August of an 8-month sequence of spasmodic pyroclastic eruptions. On the Reykjanes Peninsula the alinement of thermal areas along northeast-trending high-angle faults and the location of a sublacustrine thermal spring in Kleifarvatn were confirmed. At Askja and Hekla, infrared emission from fumaroles and solfataras, documented by the infrared surveys, is interpreted as posteruptive. A linear array of thermal points and an ice cauldron-subsidence feature, indicating subglacial thermal activity, were detected in the Kverkfjöll reentrant on the north side of Vatnajökull. In the Mývatn area where surface thermal anomalies also seem to be structurally controlled, several previously unreported points of thermal emission were recorded.

In the summer of 1966 the U.S. Air Force Cambridge Research Laboratories (AFCRL), in cooperation with the U.S. Geological Survey, the Infrared Physics Laboratory of the Institute of Science and Technology of the University of Michigan, and the Iceland State Electricity Authority (now the Iceland National Energy Authority), undertook a series of thermal infrared-imagery surveys of selected sites in Iceland. The purpose of the surveys was twofold: (1) to study the distribution, configuration, and intensity of known surface thermal anomalies related to linear structures and volcanism in the neovolcanic zone of Iceland; and (2) to determine whether previously unrecognized thermal patterns exist in this tectonically active and unique region. Additional ground investigation of areas surveyed was undertaken in the summer of 1967. This is a preliminary report of the findings from these surveys. Results of a second series of aerial infrared surveys made over several of the same sites in August 1968, utilizing a more sophisticated recording unit, have not yet been reported.

The neovolcanic zone has an area of 35,000 square kilometers, of which 12,000 km^2 is occupied by postglacial lavas. This belt of active volcanism appears to be a supramarine continuation of the crest of the Mid-Atlantic Ridge rift system across the aseismic Brito-Arctic province of Tertiary olivine basalts and tholeiitic lavas (fig. 1). Ward and others (1969) suggested that the neovolcanic zone of Iceland is indeed a segment of the rift system offset to the east and bounded on the south, as well as on the north, by transform faults. Moreover, crustal extension and upward movement of magma, consistent with transform-fault theory (Wilson, 1965), are a distinct possibility in the neovolcanic zone. The association of large-scale thermal and volcanic activity with postglacial and recent crustal movement

[1] U.S. Air Force Cambridge Research Laboratories.
[2] Iceland National Energy Authority.
[3] University of Michigan.

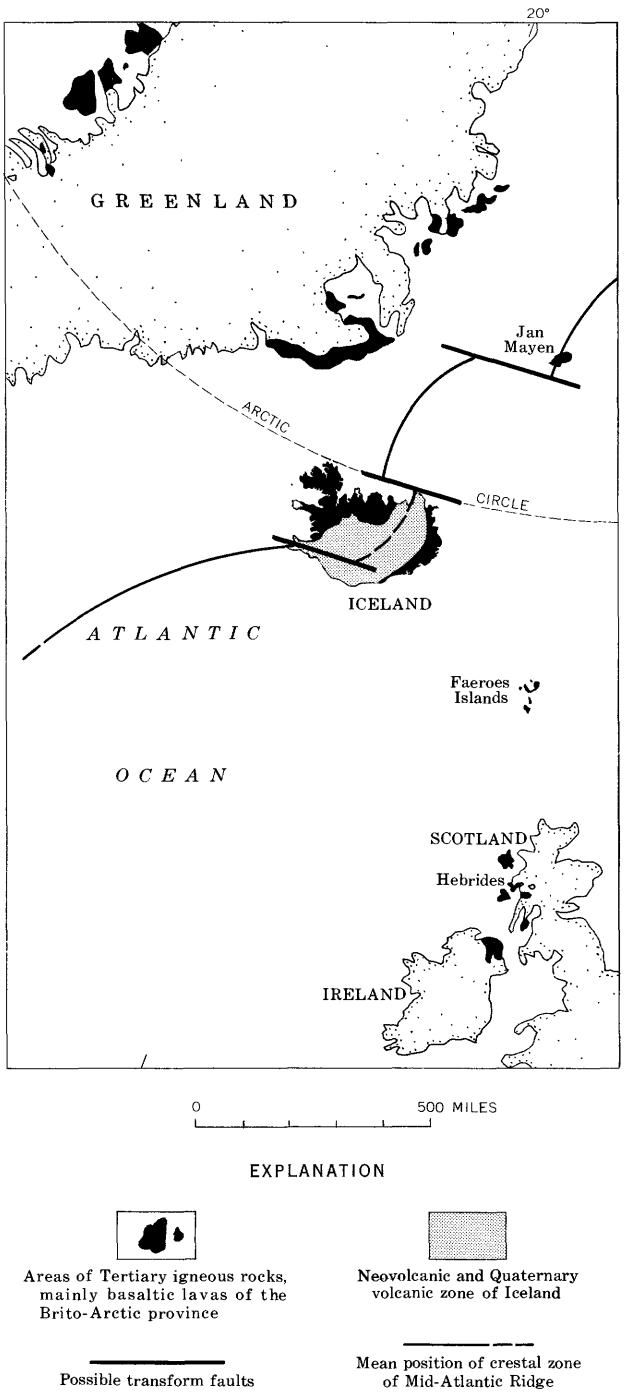

FIGURE 1.—Relationship of Iceland's neovolcanic and Quaternary volcanic zone to the mean position of the crestal zone of the Mid-Atlantic Ridge and to the Tertiary Brito-Arctic volcanic province. In part after Tyrrell (1949).

(expressed by eruptive and noneruptive dilation fissures known as gjár, normal faults and related graben strips, en echelon faults, and shallow-focus seismic activity in the zone) has been recognized for many years (Thórarinsson, 1960; Walker, 1965).

The en echelon array of northeast-trending dilation fissures and faults of the Reykjanes Peninsula suggests sinistral strike-slip movement along an east-west buried line of weakness, opposite to the direction of movement expected for a simple offset of the Mid-Atlantic Ridge. This direction of movement is consistent with the strike-slip focal mechanisms of earthquakes in fracture zones of the midoceanic ridges (Sykes, 1967) and is consistent with the transform-fault hypothesis as developed by Wilson (1965) and Ward, Pálmason, and Drake (1969). Einarsson (1968), however, points out that the fracture system of the Reykjanes Ridge can just as readily represent a shear plane with dextral shear without recourse to the transform-fault hypothesis. There is general agreement, however, that a striking correlation exists between high-temperature thermal-field activity in Iceland, regions of high seismicity (Ward and others, 1969), and linear structures of the neovolcanic zone.

On the basis of earlier estimates summarized by Karl Sapper, Rittman (1962, p. 156) estimated that 24 percent of the total outflow of lava from the earth's land surface since A.D. 1500 has been from the volcanoes and fissure eruptions of this Icelandic zone. More recent work suggests that the total quantity of lava erupted in Iceland during postglacial time is approximately 250 cubic kilometers, an average of about 0.025 km^3/year (Bövarðsson and Walker, 1964). In the neovolcanic zone itself, the heat flow in excess of the global average has been estimated by Böðvarsson to be about 100 calories/square centimeter/year. The subsurface movement of basaltic magma required for the maintenance of the excessively high conductive heat flow observed in the zone would have to amount to 0.1 km^3/year, about 4 times the material erupted at the surface (Böðvarsson and Walker, 1964). If we accept these estimates, the tectonic environment of the zone suggests almost continuous injection of dikes, great mobility of magma of low viscosity, and consequent rapid changes in thermal activity at the surface. Radiant emission associated with convective heat transfer at the earth's surface can be registered on thermal infrared imagery to document patterns of heat loss at a given point in time. This relation forms the basis for the present study.

Acknowledgments.—We are indebted to His Excellency, Mr. Pétur Thorsteinsson, Ambassador of Iceland, to Steingrímur Hermannsson, Director of the National Research Council of Iceland, to William A. Fischer, U.S. Geological Survey, and to Paul S. Bauer, formerly of American University, whose personal interest in this project made the infrared surveys and related field investigations in Iceland possible. The Surtsey Research Society provided transportation from Reykjavík to Vestmannaeyjar and Surtsey by light air-

craft and the Iceland Coast Guard vessel *Lóðsinn* in 1966; the NATO Iceland Defense Force base at Keflavík provided U.S. Navy H34 helicopter transportation to Surtsey in 1967. We were accompanied in the field on various occasions by the Icelandic scientists Thorbjörn Sigurgeirsson, of the University of Iceland; Jón Jónsson, Sveinbjörn Björnsson, and Gunnar Benediktsson, of the Iceland National Energy Authority; and by the American scientists Dana C. Parker, of the University of Michigan, and Hugo N. Swenson, of Queens College, University of the City of New York. Sigurður Thórarinsson, Museum of Natural History, Reykjavík, made many constructive suggestions on problems of volcanology in Iceland in relation to the infrared surveys and kindly reviewed parts of the manuscript. Kristján Saemundsson, National Energy Authority, provided a newly compiled geologic map of Iceland emphasizing volcanism and tectonics. Alonzo E. Stoddard, Pomona College, analyzed the physical basis for, and developed a method for checking, the blackbody-equivalent-temperature readout of the Nimbus II HRIR (High Resolution Infrared Radiometer) system from ground-temperature data specifically for this project. Lonnie Foshee, Larry McMillan, and Jack Conway of the National Aeronautics and Space Administration's Goddard Spaceflight Center kindly provided HRIR imagery prints and oscillograph records of the Nimbus II data. We wish to express our deep gratitude to all these men. All aerial infrared imagery presented in this report was obtained by the U.S. Air Force Cambridge Research Laboratories expressly for this cooperative project.

INSTRUMENTATION

The airborne infrared scanner used in the infrared surveys was designed and constructed by the University of Michigan as a geophysical research instrument. The system utilizes a photovoltaic indium antimonide (InSb) solid-state detector sensitive to radiation in the 1.0μ to 5.5μ wavelength region during nighttime surveys. The detector was filtered to the 4.5μ to 5.5μ band during daytime operation to take advantage of the atmospheric transmission window between 4.5μ and 5.0μ, thus rejecting reflected solar radiation at shorter wavelengths. Figure 2 indicates the infrared-system spectral response and shows its relation to the radiant emittance of ambient-temperature terrain features, incandescent basalt lava, and the reflected component of solar radiation. Blackbody curves of 300° K and 1,400° K approximate the emission from ambient-temperature terrain features and incandescent lava, respectively.

The optical elements of the infrared scanner (fig. 3) focus infrared radiation emitted from the earth's surface onto the detector, which transduces the radiation into wideband electrical signals and provides an input to an image recorder. The video signals from each scan modulate the intensity of a cathode-ray-tube spot as it sweeps across the face of the cathode ray tube. Film moving through a camera focused on the tube is exposed in relation to the intensity of the flying spot.

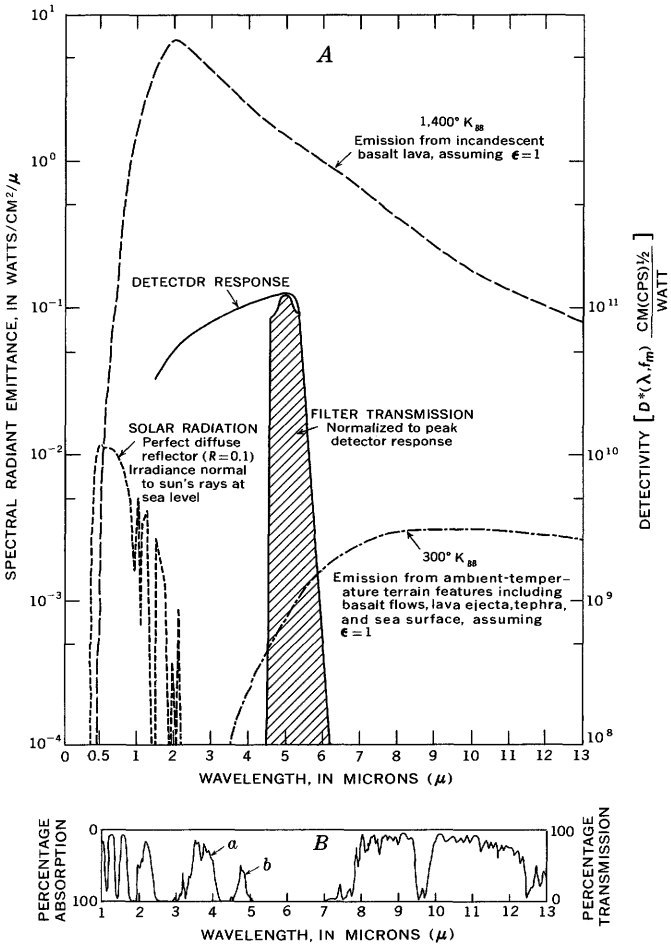

FIGURE 2.—Estimated radiant emittance from incandescent lava and infrared spectrum of solar irradiation of the earth's surface.

A, Estimated radiant emittance from incandescent lava of Surtur I effusive eruption, and ambient-temperature terrain features and surrounding ocean surface, based on the Stefan-Boltzmann function. Also shown are spectral solar radiation and the airborne M1A1 infrared scanner filter transmission normalized to peak InSb detector response.

B, Infrared spectrum of solar irradiation of the earth's surface, showing atmospheric transmission window utilized by Nimbus II HRIR (High Resolution Infrared Radiometer) system (*a*) and M1A1 airborne infrared scanner (*b*) over Iceland, August 1966. Note that spectral near-coincidence of the 3.4μ to 4.1μ transmission window, peak HRIR detector response, and peak radiant emission from incandescent olivine basalt lava (in *A*) account for the detection, from an orbiting satellite, of the Surtur I effusive fissure eruption. *B* from A. J. LaRocca, "Atmospheric phenomena," *in* "Fundamentals of infrared technology, University of Michigan Engineering Summer Conference, Ann Arbor, June 7–11, 1965," p. 6 (duplicated). ϵ, emissivity, a measure of how well a body can radiate energy as compared with a blackbody.

The film moves at a rate proportional to the ratio of ground speed to aircraft altitude, thus generating an image. The infrared scanner and image recorder were mounted in a U.S. Air Force C–130 aircraft assigned to the AFCRL Terrestrial Sciences Laboratory.

A portable fixed-field infrared radiometer (Barnes IT–3) and a digital multiprobe thermistor system (Digitec) were used for measuring changes in surface temperature on the ground simultaneously with overflights at several sites. Temperatures of incandescent lava were measured August 19–22, 1966, by Sigurgeirsson (1967) using a 10-m NiCr/NiAl-type Pyrotenax thermocouple. In 1967, thermistor systems (Yellow Springs telethermometer and Atkins thermistor probe) and a Rototherm thermocouple probe were used at Surtsey to obtain additional surface- and subsurface-temperature data from fractures in the basalt-flow crust.

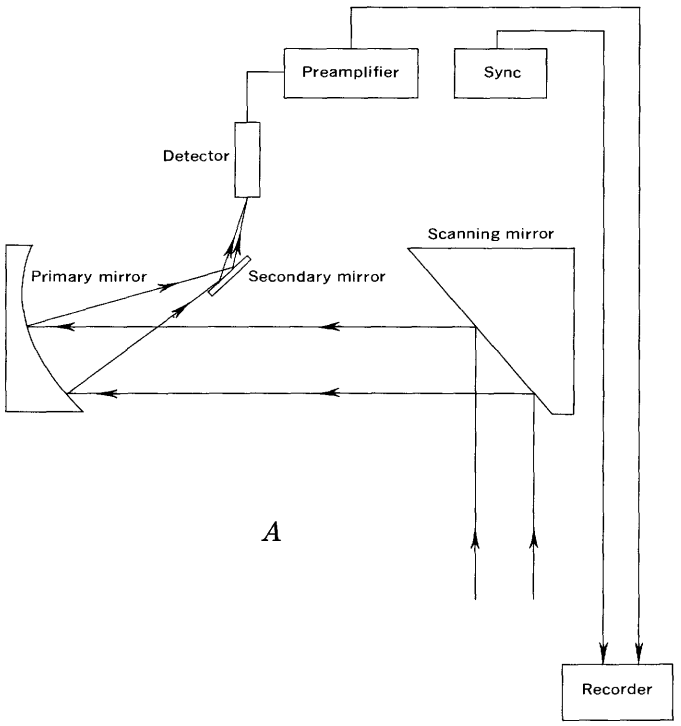

SITES SURVEYED

The sites surveyed were selected jointly by the U.S. Geological Survey and the National Energy Authority in Iceland. These included, among other sites, the volcanoes Surtsey, Katla, Hekla, Askja, and Kverkfjöll, as well as the Reykjanes, Krísuvík, Mývatn, and Theistareykir thermal fields (fig. 4). No thermal anomalies of volcanic origin were noted in the Mýrdalsjökull glacier, over the historical vent area of Katla. Summaries of the data from areas in which significant thermal anomalies were recorded on infrared imagery follow.

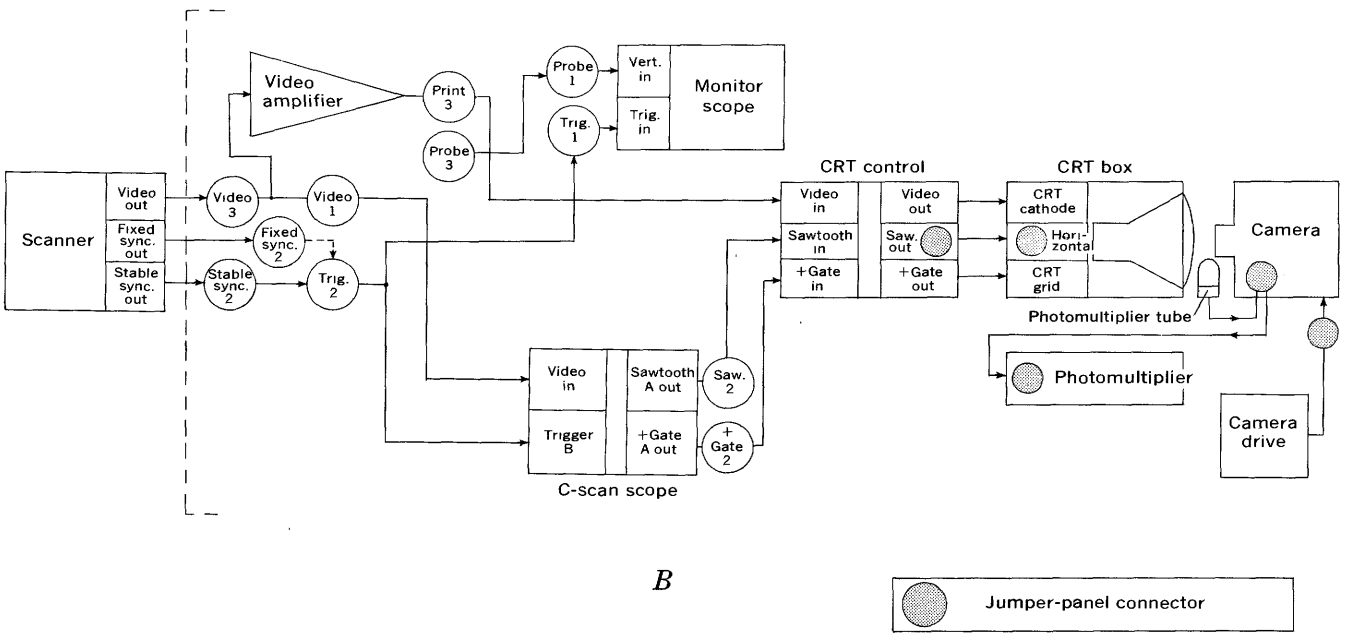

FIGURE 3.—Schematic diagram of the M1A1 line-scanning system, which electronically records a thermal image of the terrain over which it passes. The scanner can be separated into two major components, the scanning unit, *A*, and the recording unit, *B*. The scanning unit utilizes a Newtonian optical system coupled with a four-sided scanning mirror to produce continuous-strip infrared imagery. As shown in *B*, the infrared scanner provides three basic signals required in recording the data acquired, the video signal and two types of synchronizing pulses. The basic function of the image recording unit is to convert the electronic video amplitude variations from the scanner preamplifier into light variations of relative intensities on an intensity-modulated cathode-ray tube (CRT). The resulting images are then recorded on continuously moving film.

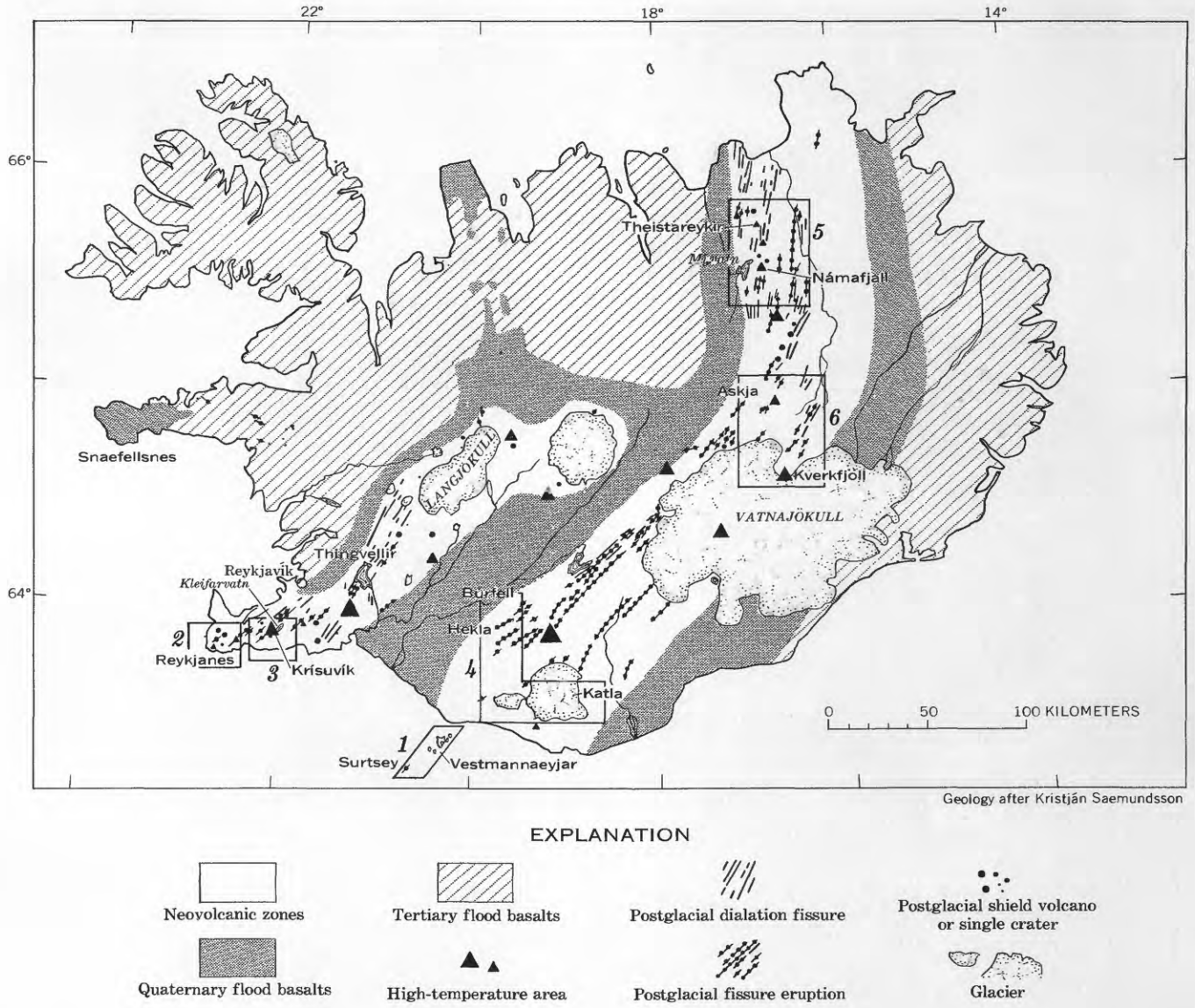

FIGURE 4.—Sites of airborne infrared surveys in Iceland, August 1966. The numbered areas are approximate areas of coverage by infrared imagery. These areas of coverage include the following regions described in the text: *1*, Surtsey; *2*, Reykjanes *3*, Krísuvík; *4*, Hekla; *5*, the Mývatn area; *6*, Askja (northern part of area *6*), and the northern margin of Vatnajökull at Kverkfjöll (southern part of area *6*). Size of triangles in high-temperature areas is proportional to heat flow. Geology after Kristján Saemundsson, Iceland National Energy Authority.

Surtsey (63°18′ N., 20°36′ W.)

On August 19, 1966, an effusive fissure eruption began at Surtsey (fig. 5), after more than 2½ years of inactivity in the Surtur I crater, and 1¼ years after the last effusive activity in the Surtur II crater (Thórarinsson, 1966). Explosive activity on Jólnir, a satellitic tephra cone that formed an ephemeral island 0.5 mile southwest of Surtsey, had ceased 9 days before. The August 1966 eruption fissure trends N. 10° E. and forms an en echelon pattern with the fault system that controlled earlier phases of Surtsey's 3-year eruptive activity. Three alined craters were simultaneously active along the fissure; the northeasternmost crater developed a spasmodic lava fountain and other symptoms of Hawaiian-type activity on the morning of August 20 (Thórarinsson, 1967a). Highly fluid olivine basalt lava at an estimated temperature of 1,140°C (Sigurgeirsson, 1967) was extruded at a rate of 4 cubic meters/second from 7:00 a.m. (0800 Universal Mean Time), August 19, until the morning of August 20, according to Thórarinsson (1967a); the lava flow reached the sea at 6:40 p.m. (1940 UMT), August 20. Thereafter, the eruption increased in intensity, yielding lava at 5 to 10 m^3/sec for several days. The average rate of extrusion was estimated as 3.0 to 3.5 m^3/sec between August 19 and December 31, 1966.

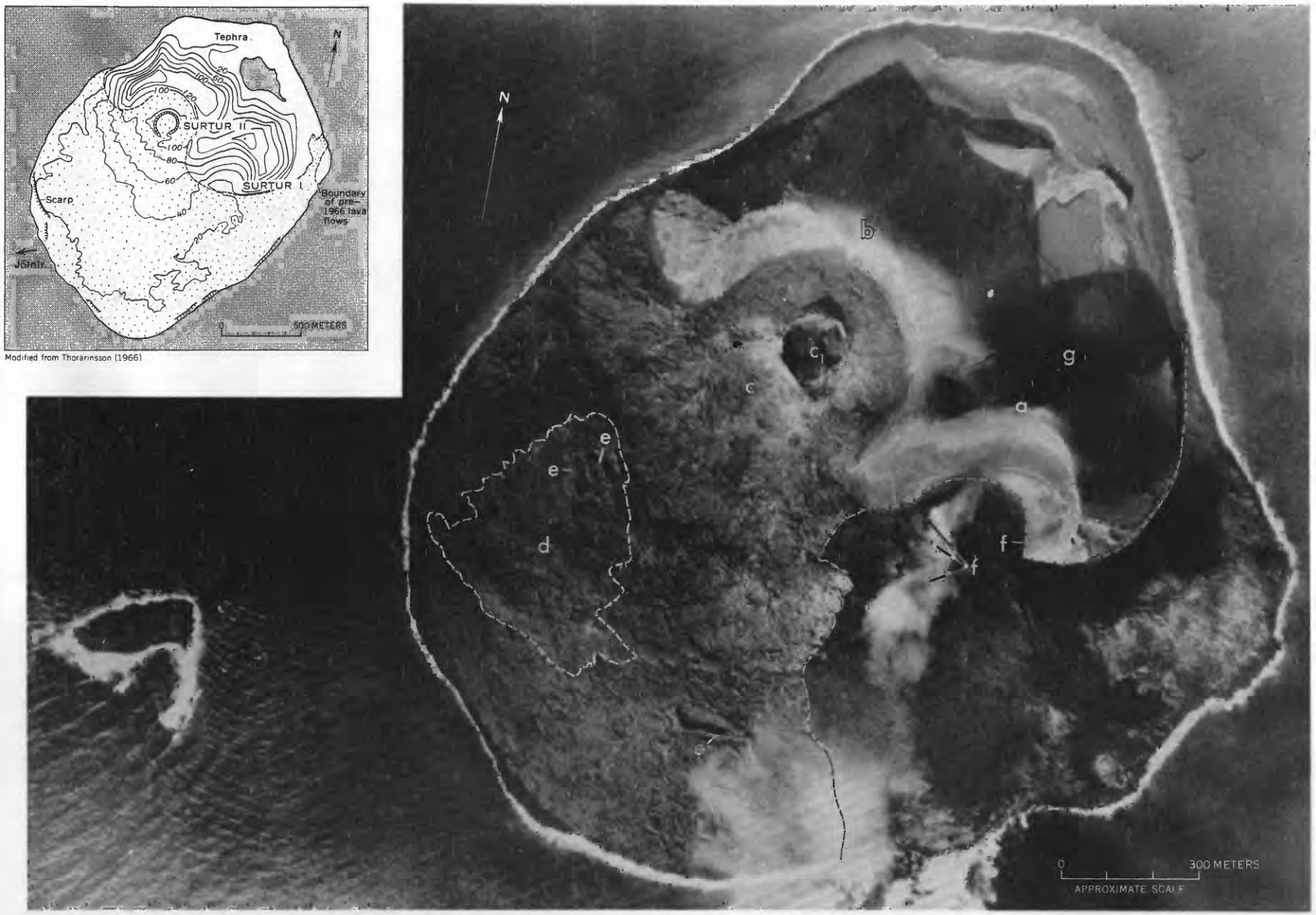

FIGURE 5.—Aerial photograph and topographic map of Surtsey. Aerial photograph taken October 2, 1966. *a*, tephra-rim remnant of Surtur I, 1963; *b*, tephra-rim remnant of Surtur II, 1964; *c*, lava shield; c_1, vent and congealed lava lake of Surtur II, 1964–65; *d*, approximate area of last great basalt flow from Surtur II, April–May 1965; *e*, pressure ridges in flows of 1964 and 1965; *f*, active crater row and effusive olivine basalt flow (bounded by dashed line) from fissure eruption, Surtur I, beginning August 19, 1966; *g*, area of last effusive outbreak from Surtur I fissure, January 3, 1967, after photograph was made. Locations of Surtla and Syrtlingur satellitic volcanic submarine eruptions are not shown. Eroded remnant of Jólnir appears on left side of photograph. Only Syrtlingur and Jólnir existed as ephemeral islands. Aerial photograph by Icelandic Survey Department. Note change in shoreline of Surtsey between August 1965 (map) and October 1966 (photograph) resulting from marine erosion and effusive volcanic activity.

Aerial surveys of infrared emission were begun the first day of the eruption and were repeated on three successive nights and again on August 29. On August 20 and again on the 22d, the Nimbus II meteorological satellite (Allied Research Associates, 1966; Allison and Kenney, 1967), with its High Resolution Infrared Radiometer (HRIR) system in operation, passed directly over Iceland in a near-polar orbit at an altitude of 1,114 km. These surveys were the first to provide confirmed concurrent airborne and earth-orbital observations of infrared emission from an erupting volcano.

Aerial surveys.—During the first four aerial surveys (August 19–22, 1966) the intensity of infrared radiation from the newly erupted lavas of Surtur I was so great that it saturated the detector and made it impossible to accurately delimit the new lava-flow area (fig. 6*A*). Figure 2*A* indicates that the emission from the incandescent lava was approximately three orders of magnitude greater than that from the ambient-temperature terrain features. By August 29, the lavas had developed a crust over much of their surface, and with the consequent reduction in radiation intensity, better imagery of the form of the lava flows was obtained (fig. 6*B*).

The imagery from these surveys reveals a complex pattern of thermal anomalies associated with features of the older lava shield of Surtur II, which formed between April 1964 and May 1965, contiguous to Surtur I on the west side of the island (fig. 6*A*). According to Thórarinsson, the more intense anomalies are related to gas and steam emission from scoriaceous material of the central crater walls which are warmer than the crater floor. An elongate anomaly south of Surtur II crater outlines the most likely subsurface course of the lava that flowed in April and May 1965—the last lava to flow from this crater. A spade-shaped anomaly farther south represents the last great exposure of that lava, which erupted near the end of April 1965 (Sigurður Thórarinsson, oral commun., 1967). Intense curvilinear anomalies represent convective venting from fractures along pressure ridges and collapsed lava tunnels, which were observed by the authors in 1967. One large curvilinear anomaly appears to mark pressure-ridge type fractures associated with an apalhraun (in Iceland, a flow which includes both aa and block lava) outflow channel, where flows emerged from below the Surtur II shield. Fractures parallel to this channel emitted vapors at temperatures above 100°C as recently as July 1967.

At the satellitic tephra volcano, Jólnir, posteruptive hydrothermal anomalies appeared in the main crater between August 19 and August 22, approximately 9 to 12 days after the last-reported explosive activity at Jólnir; anomalies were also detected in the semicircular structural lagoon of Jólnir on August 21 (fig. 7). A few days after the lagoon anomaly appeared, subsidence may have occurred along concentric fractures on the south side of the island. Heavy seas then destroyed the tephra cone and breached the rampart enclosing the lagoon. A warm area that indicated previously unrecorded hydrothermal activity at the breached end of the lagoon was recorded on August 29, although the main crater and its thermal anomaly were already gone. By October most of the island had been reduced to a shoal by wave erosion.

Satellite data.—The Surtsey anomaly appeared as a minute black spot on at least seven separate orbital swaths on Nimbus II infrared imagery (Friedman and others, 1967, p. 101); the first appearance was on orbit 1288, 12:27:29 UMT, August 20, 1966, 12 hours after the first extrusion from the eruption fissure, and the spot definitely was present as late as October 3. The anomaly, first identified by Williams and Friedman in December 1966, is clearly visible on imagery from the following orbits: 1288, August 20; 1315, August 22; 1541, September 8; 1648, September 16; 1701, September 20; 1774, September 21; and 1874, October 3 (Friedman and Williams, 1968). It was confirmed by the identification of a single sharp peak in the correct geographic position for Surtsey on scan-line analog profiles of maximum effective radiance ($\overline{N}$) [1] made from the original spacecraft interrogation records for several of these orbits (fig. 8).

Nimbus II oscillograph records of effective radiance ($\overline{N}$) permit accurate measurement of temperature as a function of time and sensor-scan angle (Foshee, 1966, p. 30). Oscillograph analog profiles for orbit 1315, August 22, require little or no angular correction for transmission path length because the subsatellite trace passed close to Surtsey; the nadir angle was 14° (Jack Conway, oral commun., 1967). In using HRIR data, corrections for atmospheric absorption, emission, and scattering between the ground and the Nimbus spacecraft are typically 2° to 4°K (Kunde, 1964), generally within the experimental error inherent in the ground-radiance estimates of the present study.

Comparison of the maximum effective radiant flux recorded by Nimbus II and the estimated thermal-energy yield of Surtsey based on volumetric rate of extrusion of olivine basalt lava of known thermal parameters and temperature (table 1) indicates that 3.4 percent of Surtsey's estimated total thermal-energy yield was transmitted through the earth's atmosphere as radiant emission. The effusive eruption on Surtsey was detectable from orbital altitude only because of the spectral coincidence of the Nimbus II HRIR detector sensitivity, the peak wavelength

[1] The effective radiance, $\overline{N}$, is that part of the radiance of the 64-km² target which passes the equivalent HRIR detector filter per second; $\overline{N}$ is measured in watts/m²·steradian by the Nimbus II from orbit; $\overline{N}$ may also be expressed as an equivalent temperature of a blackbody (T_{BB}) filling the field of view, which would cause the same response from the radiometer (Foshee, 1966, p. 35).

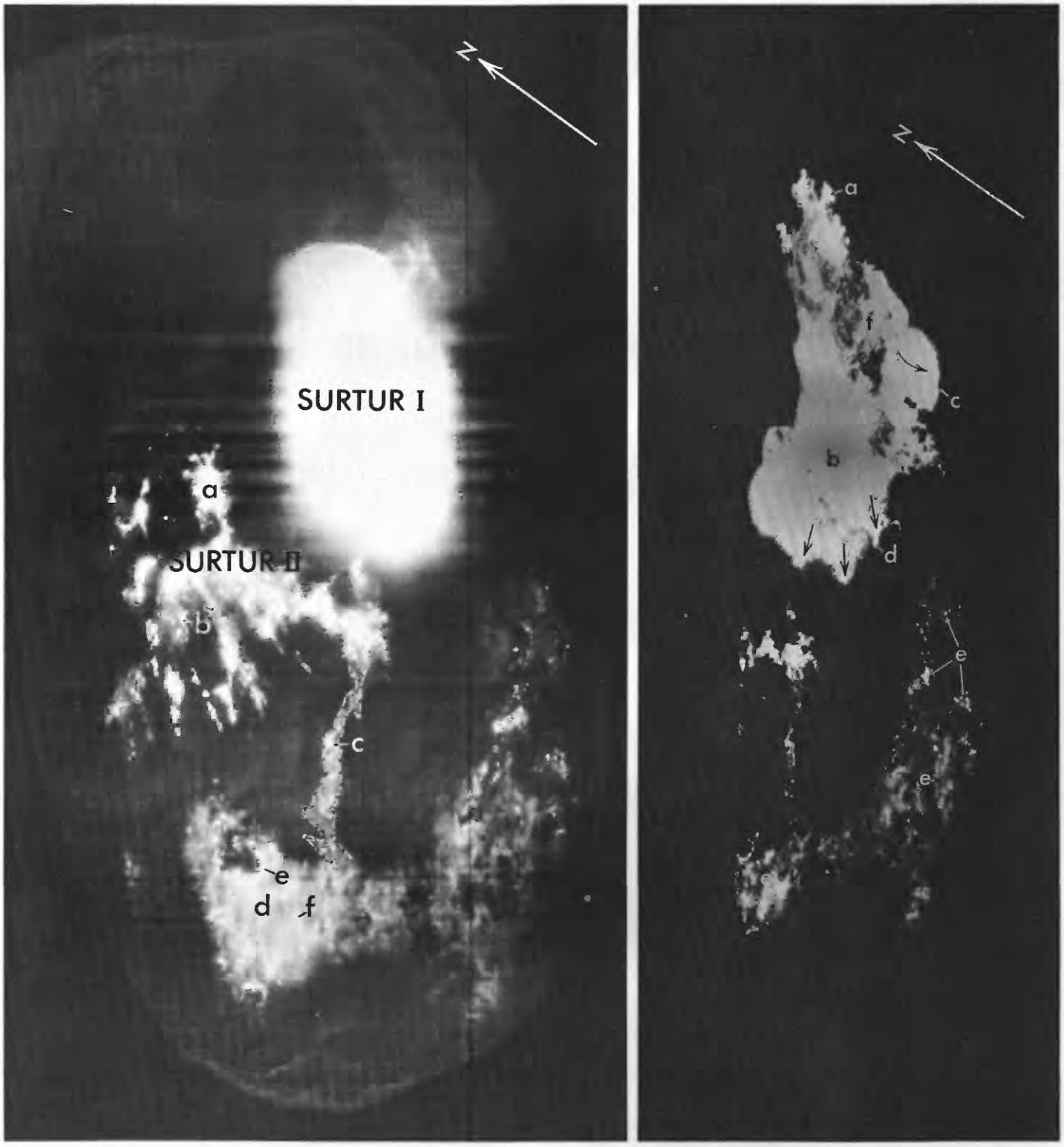

A *B*

emittance of the incandescent lava, and the 3.4μ to 4.1μ atmospheric transmission window (fig. 2).

Earlier work by Hédervári (1963) and Yokoyama (1956–57) on energy dissipation during effusive volcanism shows that the overwhelming proportion of energy dissipated during historical eruptions consisted of thermal (more than 90 percent of the total) rather than kinetic energy. It follows, then, that most energy dissipation resulting from the Surtur I effusive eruption must have occurred as convective, conductive, and other forms of nonradiant heat transfer to the atmosphere, ocean (table 1), and solid subsurface of the island. Nevertheless, repeated detection of the Surtsey anomaly on Nimbus II HRIR imagery demonstrates that radiation from effusive volcanic events of similar magnitude can undoubtedly be detected and monitored from earth or planetary orbit. It is significant that no record of the pyroclastic eruptions at Jólnir has been found on Nimbus II HRIR imagery.

Hekla (63°58′–64°01′ N., 19°36′–44′ W.)

Hekla is located within a short northeast-trending belt of active volcanoes along the northwest border of the eastern branch of the neovolcanic zone. It is a polygenetic volcano, representing an intermediate stage between a typical Icelandic crater row and a classical stratovolcano (Thórarinsson, 1967b, p. 9). Heklugjá crestal fissure trends N. 60° E., as do most fissures and faultlines in this part of the neovolcanic zone, and has built up the volcano by repeated eruptions along its entire length of 5.5 km. The Summit Crater (Toppgígur) and Shoulder Crater (Axlargígur) alined along Heklugjá were last active in the summer of 1947 when they erupted dacitic to andesitic tephra. Intense effusive activity also occurred in other parts of the volcano during the 1947–48 eruption (Thórarinsson, 1950). Northeast-trending thermal anomalies noted on 1966 infrared imagery coincide spatially with the linear crest of Hekla volcano, along which Heklugjá eruption fissure opened in 1947–48.

In 1966, infrared emission of the greatest intensity was recorded from several point sources along the inside walls of Heklugjá between the two main craters. Intense infrared emission was also recorded from the northeast and southwest flanks of Shoulder Crater and its subsidiary explosion crater to the northeast and from the southwest and northeast flanks of Summit Crater. Long-continuing posteruptive fumarolic activity probably accounts for most of these anomalies. This conclusion is supported by comparison of the configuration of Hekla's firn fields and glacierets as depicted on the 1966 infrared imagery with that shown on August 1960 aerial photographs (fig. 9*A*, *B*). Such a comparison indicates little change in firn pattern between 1960 and 1966. The long-continuing existence of the present posteruptive thermal anomalies follows the pattern noted after the eruptions of 1766 and 1845 (Thórarinsson, 1967b).

Mývatn area, including Námafjall (65°41′–43′ N., 16°48′–53′ W.) and Theistareykir (65°52′–53′ N., 16°58′–17°02′ W.)

North of Askja, in the Mývatn area, along the generally north-trending part of the neovolcanic zone, infrared imagery obtained in 1966 confirms the structural control of numerous hot springs, solfatara, and fumarole fields. Structural control can be inferred from the coincidence of alined thermal points and the local trend of faults, dilation fissures, and subsided graben strips, many of which are currently active. The Námafjall thermal field east of Mývatn and the strong lineaments of the thermal field at Theistareykir north of Mývatn are examples (Chaturvedi and Pálmason, 1967). At Námafjall the high-temperature thermal field has numerous solfataras, mud pots, fumaroles, and superheated steam vents. These features flank both sides and lie astride the serrate hyaloclastite ridge, Námafjall (trend N. 10° E.). The thermal field is very clear on the infrared imagery, as is an area to the west between the Námafjall thermal field and lake Mývatn, where warm ground water circulates through a recent lava field toward the lake. The Stóragjá (fissure), for example, appears as a faint linear anomaly, because the fissure contains warm (43°C) circulating ground water (July 1967). Points of seepage of warm ground water into the lake give rise to surface thermal anomalies in

FIGURE 6.—Aerial infrared images of Surtsey.

A, Surtsey, 1845 UMT, August 19, 1966. Survey made approximately 11 hours after first effusive activity from Surtur I eruption fissure. Excessively high infrared emission from lava fountains and incandescent flows at 1,130°C in the Surtur I area saturated the scanner detector, although the instrument gain setting was suitable for detection of secondary thermal anomalies of the Surtur II area. *a*, emission from scoriaceous walls of vent; *b*, emission from cooling lava rivulets which emerged from lava-tube outlets high on the lava shield; *c*, emission from extended subsurface lava channel; *d*, last great surface exposure of lava from Surtur II, April–May 1965; *e*, convective emission from fractures parallel to base of pressure ridges; *f*, circular collapse feature. Scale: 1 inch=266 m in northeast-southwest direction, 480 m in northwest-southeast direction.

B, Eastern half of Surtsey, 1825 UMT, August 29, 1966. Increased crustification of the active lava flow and a possible decrease in lava fountain activity reduced infrared emission sufficiently to make possible this record of the configuration of the Surtur I flow during the 10th day of its development. *a*, most active crater at northeast end of crater row; *b*, active flow; *c*, flow front entering the ocean; *d*, incandescent lobes indicating emergence of lava from tunnels and tubes; *e*, residual anomalies related to convection from fractures and secondary fumaroles in 1964 and 1965 flows from Surtur II; *f*, thick coherent slabs of helluhraun (pahoehoe) forming islands in the 1966 flows. Arrows show direction of flow of olivine basalt. Scale: 1 inch=282 m in northeast-southwest direction, 500 m in northwest-southeast direction.

TABLE 1.—*Comparison of thermal-energy yield and radiant emission, as estimated by two remote-sensing systems, from Surtsey, August, 22, 1966*

[Nimbus II HRIR data are from a scan-line oscillograph record, taken during orbit 1315, at 02:27:29 Universal Mean Time. The airborne M1A1 infrared data include an isodensitometric scan of imagery as well as surface-temperature measurements; in this method, sizes of areas at different temperatures are estimated. Volcanologic ground observations include measurements of maximum temperature of incandescent lava (by thermocouple; Sigurgeirsson, 1967), volumetric rate of outflow (Thórarinsson, 1967a), and temperature of ocean and tephra surface by radiometer]

	Radiant emission				Thermal-energy yield
	Spectral		Total		
Energy unit estimated.	Effective radiant flux, W_λ (watts/m²·steradian) (that part of the radiant flux of the 64-km² target which passes the equivalent HRIR detector filter[1] per second) $W_\lambda \cong \int A(T)\left\{\int_{3.45}^{4.07} B_\lambda(T_{BB})d\lambda\right\}dT$, where $A(T)$ = area at temperature T, and $B_\lambda(T_{BB})$ = Planck function.		Total hemispherical emission (W) (radiation emitted per second in all wavelengths, assuming emissivity = 1) $W = \int A(T)\left\{\int_0^\infty B_\lambda(T_{BB})d\lambda\right\}dT \cong \sigma \int A(T)\ T^4\ dT$, where $A(T)$ = area at temperature T, $B_\lambda(T_{BB})$ = Planck function, and σ = Stefan-Boltzmann constant ($5.679\times10^{-12}\ T^4$ watt cm^{-2}).		Thermal-energy yield (Eth) $Eth = V\rho\ (TC+B)J$,[2] where V = volumetric outflow of lava per second, ρ = mean density of olivine basalt lava, T = maximum temperature (°K) above ambient, C = specific heat of basalt at 800°C, B = latent heat of lava, and J = equivalent work of heat.
Method of obtaining data.	Nimbus II HRIR (orbital).	M1A1 infrared scanner (airborne) (emission estimated from spectral band comparable to that of Nimbus II HRIR).	Nimbus II HRIR (orbital) (scan-line oscillograph record equivalent blackbody radiation in all wavelengths).	M1A1 infrared scanner (airborne) (emission in all wavelengths estimated).	Volcanologic ground observations.
Energy (ergs/sec) from 64-km² elliptical area,[3] including Surtsey.	7.13×10^{14}	13.21×10^{14}	2.95×10^{17}	2.48×10^{17}	Not applicable.
Energy from active volcano (Surtur I) (ergs/sec).	Volcano emission alone not resolvable from Nimbus II record. See M1A1 value.	10.02×10^{14}	Volcano emission alone not resolvable from Nimbus II record. See M1A1 value.	0.09×10^{17}	2.67×10^{17}
Percentage of total.	Not available.	Not applicable.	Not available.	3.4	100

[1] The effective spectral response of the HRIR detector is such that greater than 50-percent perfect transmission occurs between 3.45μ and 4.07μ (Foshee, 1966, p. 34).

[2] From Hédervári (1963).

[3] Nimbus II HRIR system integrated radiation from 64-km² area of the earth's surface from an orbital altitude of 1,114 km above Iceland. Infrared imagery was obtained over the same area by the airborne M1A1 system.

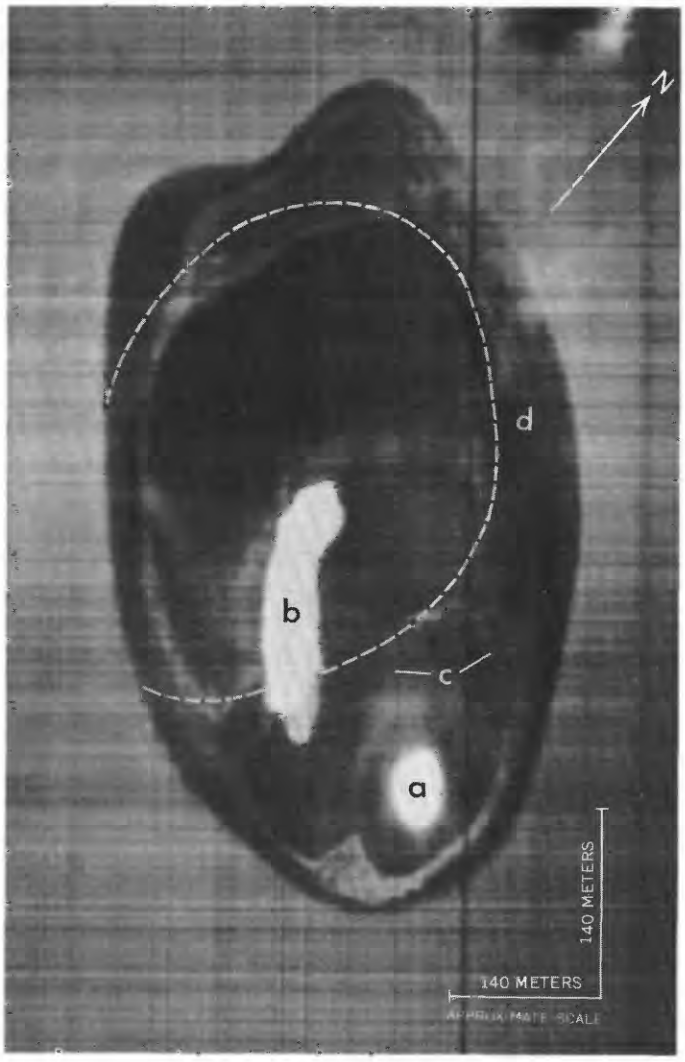

A

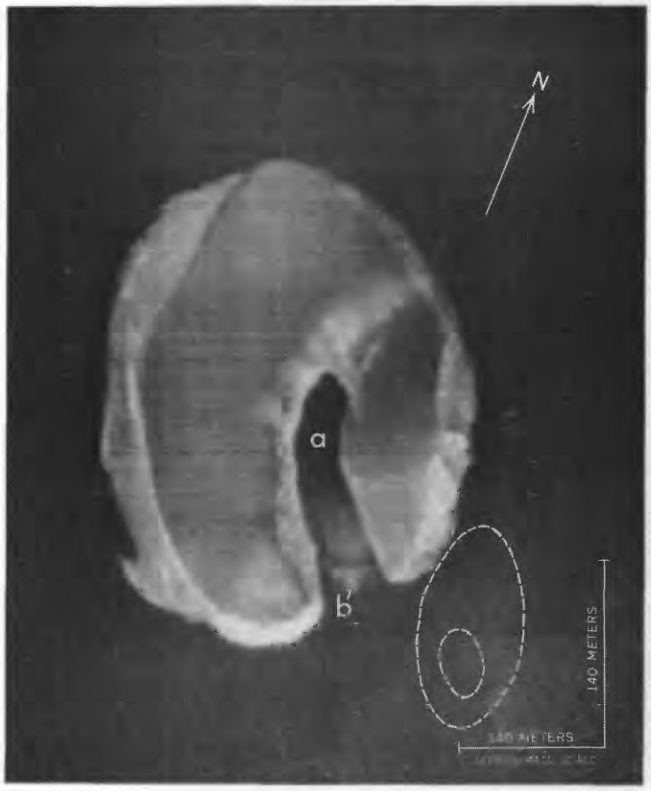

B

FIGURE 7.—Aerial infrared images of Jólnir volcano.

A, August 21, 1966, 2341 UMT, approximately 11 days after last explosive eruption. *a*, crater lake, water temperature at 40° to 50°C; *b*, thermal waters of structural lagoon; *c*, tephra rim of main crater; *d*, part of island (area beyond dashed line), including main crater, which was destroyed following crater subsidence and wave erosion.

B, August 29, 1966, 1721 UMT. Jólnir after partial destruction by wave erosion: *a*, remnant of structural lagoon; *b*, thermal anomaly; approximate position of former tephra crater rim and vent indicated by *c* and *a* on *A* shown by dashed lines.

northeastern Mývatn that appear, on the basis of the infrared imagery, to be generally similar to the lake-surface thermal pattern reported by Barth (1942).

On the western side of the shield volcano, Theistareykjabunga, north of Mývatn, thermal lineaments intersect the table mountain, Baejarfjall, on its northern and western margins. Comparison of the infrared imagery with conventional aerial photographs which are 6 years older shows that these thermal lineaments represent solfatara fields; associated solfataric ground alteration can also be identified on the aerial photographs. One elliptical anomaly depicted on the infrared imagery northwest of the solfatara fields is not discernible on the aerial photographs. Field investigation by the authors in 1967 revealed that this anomaly represents an area of fumaroles and steam vents in recent apalhraun lavas, which are not associated with altered ground but may be related to changes that have occurred in the surface thermal activity in this area during the last few years. Vent temperatures measured by thermistor systems in this new field ranged from 65°C to 92°C in July 1967. A similar fumarole field occurs at the toe of the Bóndhólsskarð lava flow on the northeast flank of Baejarfjall. Vapor temperatures at the vent apertures are generally below 70°C in both fumarole fields. In the solfataras, surface temperatures of 99°C are common.

In the area from Námafjall north to Theistareykir, moderately intense thermal anomalies are associated with margins of fine hyaloclastite breccia slopes of table mountains, probably of subglacial volcanic origin. These anomalies suggest warm air circulation between sliderock blocks of talus slopes and possible downslope seepage of warm ground water. In this area, the circulation of warm ground water appears to be controlled in part by fracture systems in the rhyolitic

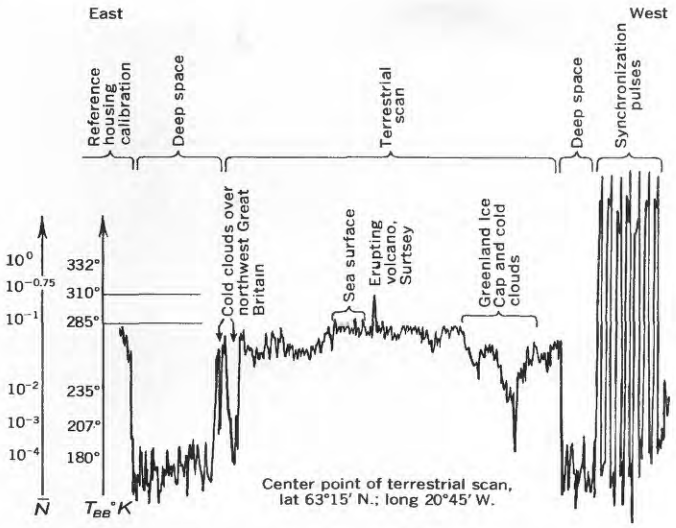

FIGURE 8.—Effective radiance ($\bar{N}$) from the earth's surface along a profile from Greenland to Great Britain, 02:27:29 UMT, August 22, 1966, recorded at an altitude of 1,114 km by Nimbus II HRIR system. This analog oscillograph record of one scan cycle, orbit 1315, was made from the original interrogation of the Nimbus II spacecraft. The highest positive spike represents infrared radiation in the 3.4μ- to 4.1μ-wavelength band emitted by lava craters and incandescent flows from Surtsey, integrated with infrared radiation from the surrounding 62-km² ocean surface. Effective radiance, $\bar{N}$, in watts/m²·steradian$=\int_0^\infty B_\lambda\ (T_{BB})\phi_\lambda d\lambda$, where B_λ=Planck function, T_{BB}=equivalent blackbody temperature in degrees K, and ϕ_λ=effective spectral response (about 3.4 to 4.1μ).

endogenous dome, Hlíðarfjall (Chaturvedi and Pálmason, 1967).

Askja (65°00′–07′ N., 16°40′–50′ W.)

Askja caldera, the most recently active volcanic area of the vast Ódáðahraun postglacial lava field north of the glacier, Vatnajökull, was surveyed from high altitude on August 22, 1966. Infrared imagery was obtained along a north-south and east-west grid traverse, covering much of the Dyngjufjöll volcanic massif, the ring remnant of a large Pleistocene stratovolcano, within which the 45-km² Askja basin is situated. A sizable effusive fissure eruption occurred within the caldera in 1961, forming the Vikraborgir crater row and 11-km-long lava flows to the east (Thórarinsson and Sigvaldason, 1962). The 1966 infrared imagery shows many thermal anomalies concentrated in a generally north-trending band that extends from the Vikraborgir crater row to the 1875 Víti explosion crater north of Öskjuvatn, and from there generally southeast along the east side of the lake.

Interpretation of the imagery and isodensitracer scans of the imagery, as well as field reconnaissance by the authors in July 1967, confirms that vapor emission from the Vikraborgir crater row was associated with 60°C surface temperatures. The strongest anomalies recorded indicate infrared emission from vigorous solfatara activity and near-boiling water temperatures in the Víti crater on the north shore of Öskjuvatn and from fumarolic activity along the eastern shore of the lake. Hydrothermal activity is also indicated at several points in the eastern part of the lake itself. Smaller punctate thermal anomalies may indicate fumarolic activity along the south and west banks of the lake and on the south side of the small volcanic island that appeared in 1926. The lava flows of 1961 appear outlined on the night imagery because of rather high infrared emission from the blocky and apalhraun basalt surfaces during night hours in comparison with relatively low emission from the surrounding rhyolitic pumiceous lapilli tephra deposited during the 1875 pyroclastic eruption. A probable explanation is a lower diurnal cooling rate for these basalt flows, because of their high total absorptivity coupled with high thermal inertia, in contrast with the more rapid diurnal cooling rate of the lower density ashfall materials.

Kverkfjöll (64°38′–41′ N., 16°40′–44′ W.)

The Kverkfjöll reentrant on the northern margin of the Vatnajökull is near the eastern border of the neovolcanic zone (fig. 4). Sapper (1927, p. 305) suggested that glacier outburst floods observed on the delta of the Jökulsá in the years 1655, 1685, 1717, 1726, and 1729, may have been caused by subglacial eruptions of the Kverkfjöll "vulkanreihe" which he located at 64°38′ N. and 16°30′ W. Thórarinsson (1965) added the years 1477 and 1711 to the list of eruptions in this general area but noted that the exact location of the points of eruption is uncertain.

A northeast-trending linear anomaly more than 2 km long, which represents infrared emission from the partly subglacial thermal field below the Kverkfjöll glacier on the northern margin of the Vatnajökull, was recorded on the west side of the Kverkfjöll reentrant (fig. 10). The thermal lineament extends from a point 2 km north of an ice cauldron-subsidence feature to within 2 km southwest of the Kverkjökull outlet lobe. The linear extent of the anomaly and the number of thermal points are greater than indicated on the current 1:100,000-scale topographic map (Blað 85, Kverkfjöll, 1954), and considerable ice melting over the thermal lineament is suggested. The Vatnajökull has a pronounced reentrant in the Kverkfjöll area. Volcanotectonic elements and associated geothermal emission in the Kverkfjöll area undoubtedly play a role in controlling the morphology of the northern margin of

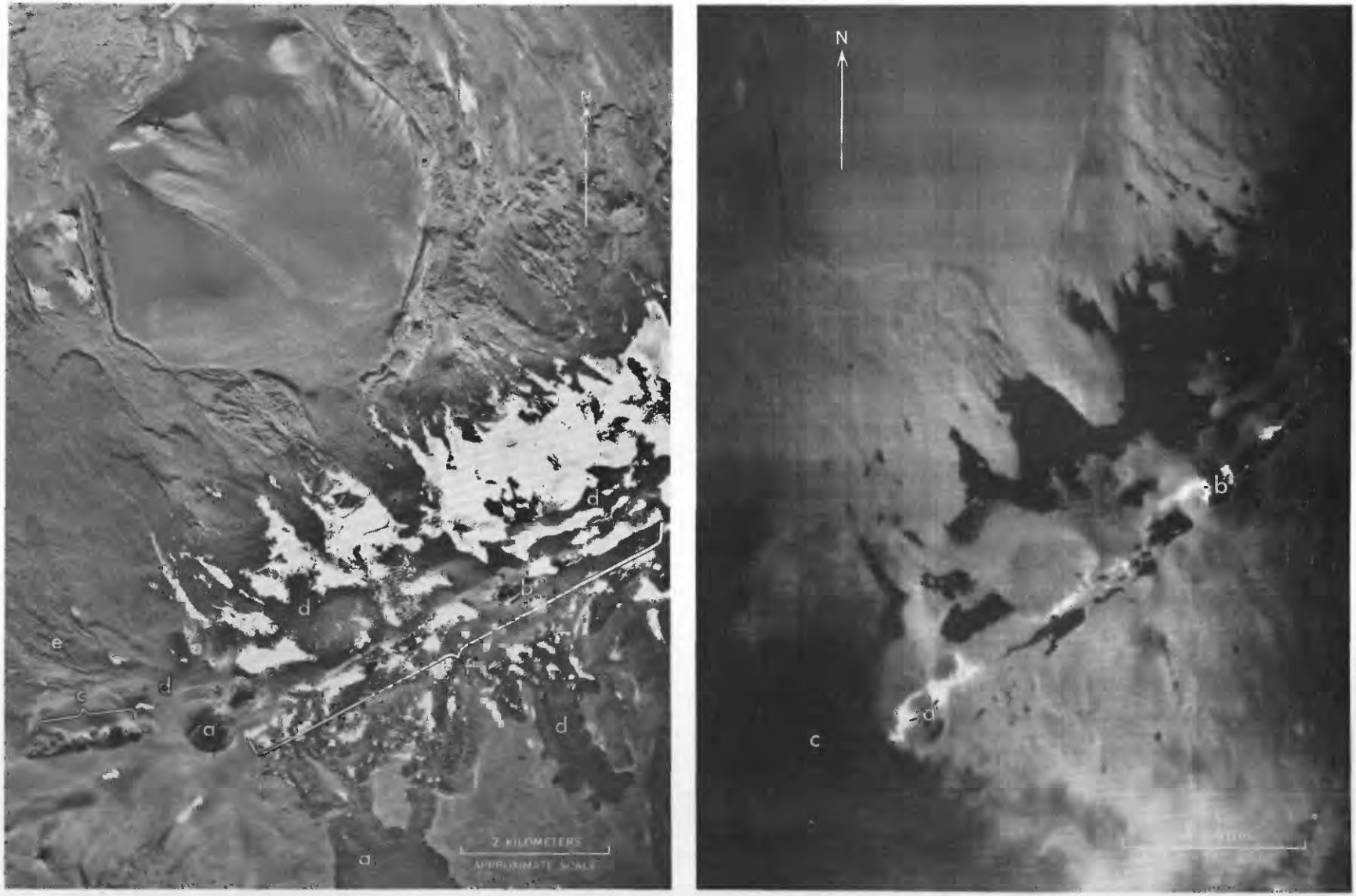

A *B*

FIGURE 9.—Aerial photograph and aerial infrared image of Hekla.

A, Aerial photograph of Hekla, August 13, 1960: *a*, Shoulder Crater; *b*, Summit Crater; *c*, southwest-flank eruption fissure; *d*, lava flows of 1947; *e*, lava flows of 1948; *f*, Heklugjá. White areas are perennial firn fields and glacierets. Aerial photography by U.S. Air Force.

B, Aerial infrared image (postsunset) of Hekla volcano, August 29, 1966. Light areas represent infrared emission from northeast-trending eruption fissure of 1947–48. Intense emission was recorded from the eruptive dilation fissure Heklugjá, Shoulder Crater (*a*) and subsidiary crater to the northeast, and Summit Crater (*b*). Dark areas are perennial firn fields and glacierets. Cool cloud (*c*) obscures extension of eruption fissure on southwestern shoulder of volcano.

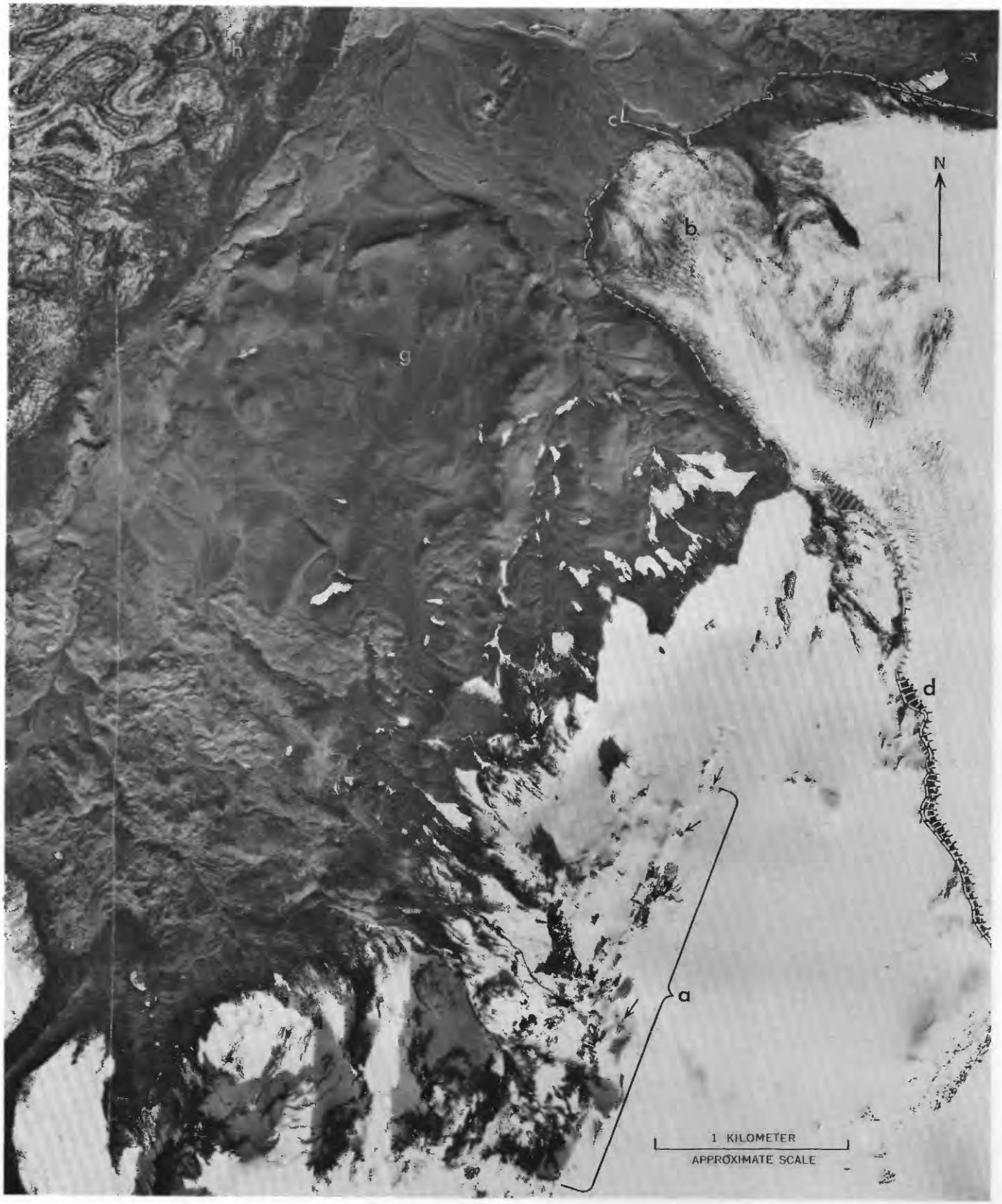

FIGURE 10.

the Vatnajökull at this point (fig. 10). Bright tones on the infrared imagery (fig. 11) also reveal northwest-flowing subglacial drainage from the thermal field and one point of emergence of distinctly warm melt water from the Kverkjökull outlet lobe.

Reykjanes (63°45′–50′ N., 22°40′–45′ W.) and Krísuvík (63°50′–57′ N., 22°10′–21°55′ W.)

At the Reykjanes thermal field in the southwestern part of the neovolcanic zone, the thermal area was found by infrared imagery (August 1966) to be, in part, localized and elongated along northeast-striking faults parallel to the trend of the rift system. Alinement of steam vents, warm ground, and other thermal features along several faultlines was noted.

On September 30, 1967, 16 strong earthquake shocks (reaching a magnitude of 4.4) were felt at the Reykjanes lighthouse, cracking the tower. Epicenters were within 4 km of 22°41.4′ W. and 63°49.4′ N. (Ward and others, 1969), probably within the thermal field. Ward, Pálmason, and Drake report that there had been an apparent progression of seismic activity from northeast to southwest culminating in these events, in visible fracturing, and in 5 to 8 cm of vertical movement on a northeast-trending fault across the Reykjanes thermal field. The thermal activity increased in intensity, producing new points of steam emission and increased activity at Stóri Geysir, which, during one period, erupted to a height of 15 m. The 1966 infrared imagery documents the thermal anomaly pattern in existence prior to these events. A 1968 infrared survey, not yet reported by the authors, provides data on changes in the thermal field following the seismic activity.

Sea-surface thermal currents noted in 1966 may represent a seaward continuation of the Reykjanes-trend thermal lineaments. These currents could be upwellings or vertical thermal currents arising from heat loss along fault traces on the Reykjanes submarine ridge (for inferred tectonic and (or) volcanic lineaments on this part of the sea floor, see Einarsson, 1968, fig. 5, p. 7569); more likely they result from known turbulent surface currents. Along the continuation of this line offshore, submarine eruptions occurred in the vicinity of Eldeyjar (the Fire Islands) in the years 1211, 1226, 1240, 1422, 1538, 1783, 1830, and 1879 (Thórarinsson, 1965).

The infrared imagery shows a sublacustrine thermal spring at the southwestern end of the lake Kleifarvatn near Krísuvík on the Reykjanes Peninsula. This imagery also shows the linear alinement of hot springs of the Krísuvík area.

FIGURE 10.—Aerial photograph of the northwest flank of Kverkfjöll subglacial volcanic ridge on the north margin of the glacier Vatnajökull. Photograph by U.S. Air Force, August 24, 1960. *a*, linear array of Hveradalur thermal features (note perforations in glacier, shown by arrows); *b*, Kverkjökull outlet lobe; *c*, active melt-water stream emerging from subglacial outflow tunnel; *d*, east-facing escarpment separating Kverkfjöll vestri from Kverkjökull outlet lobe; *g*, recent volcanic rocks; *h*, Dyngjujökull lobe.

SUMMARY

Infrared imagery obtained in 1966 by means of an airborne line-scanning system confirms that the major positive thermal anomalies of the terrestrial surface in Iceland are confined to the neovolcanic zone and are, in general, spatially related to known tectonic lineaments, especially high-angle normal faults and dilation fissures. The anomalies represent changing surface manifestations of hydrothermal circulation, fumarole and solfatara activity, gas and steam emission, and abnormally warm ground in areas of high convective heat loss where the total heat flow ranges from $<25 \times 10^6$ cal/sec in several high-temperature thermal fields to $6{,}370 \times 10^6$ cal/sec at Surtsey volcano during the 1966 effusive eruption (table 2). Changes have occurred in the configuration and intensity of the thermal fields during the general period of the infrared surveys and, at least at Reykjanes, these changes are related to seismic activity. Thermal emission representing interruptive- or posteruptive-stage activity was also recorded from the volcanoes Askja, Hekla, and Kverkfjöll. The thermal-anomaly pattern of 1966 at these volcanoes, as documented by infrared surveys, is undoubtedly not static. Subsequent changes in intensity and distribution of thermal emission can be judged by comparing future records to those obtained in 1966.

Radiometric data on infrared emission from ground measurements and Nimbus II satellite imagery indicate

TABLE 2.—*Total heat flow from selected geothermal and volcanic areas in which thermal anomalies were recorded on infrared imagery, August 1966*

[Data from Böðvarsson (1964) modified in part by more recent data]

Area	Approximate size (km²)	Maximum temperature (°C)	Total heat flow (10^6 cal/sec)
Surtsey volcano	2.54	1,140	6,370
Reykjanes	1.0	280	5 to 25
Krísuvík	10.0	230 [1]	5 to 25
Kverkfjöll	10.0	Boiling	25 to 125
Askja	5.0	do	5 to 25
Námafjall	4.5	280 [1]	25 to 125
Theistareykir	6.5	Boiling	5 to 25
Total Icelandic steam fields, including several steam fields for which infrared imagery is not available, and excluding Surtsey volcano.			1,000

[1] Drillhole temperatures.

that radiant emission from Surtsey, the largest of the group of thermal anomalies studied, was detected from an orbital platform beyond the bulk of the earth's atmosphere. The proportion of radiant emission recorded to total nonradiant heat loss from the August 1966 effusive volcanic event in Surtur I was low (about 3.4 percent). Taking into account earlier work that indicated a greater than 9:1 ratio of thermal-energy to kinetic-energy yields for a variety of volcanic eruptions, the authors estimate that more than 90 percent of the total energy yield of volcanic and geothermal surface activity is dissipated in or returned to the earth's atmosphere, hydrosphere, and lithosphere by convection, conduction, and absorption of radiation. Less than 10 percent is dissipated kinetically and, in effusive eruptions of the Surtsey type, a somewhat smaller percentage is transmitted through the earth's atmosphere as radiant emission.

REFERENCES

Allied Research Associates, 1966, The Nimbus II data catalog: U.S. Natl. Aeronautics and Space Adm. [Pub.], v. 2–4.

Allison, L. J., and Kenney, J. S., 1967, An evaluation of sea surface temperature as measured by the Nimbus I High Resolution Infrared Radiometer: U.S. Natl. Aeronautics and Space Adm. Tech. Note NASA TN–4078.

Barth, T. F. W., 1942, Some unusual ground-water phenomena in Iceland: Norsk Geogr. Tidsskr., v. 9, no. 4, p. 158–172.

Böðvarsson, Gunnar, 1964, Physical characteristics of natural heat resources in Iceland; Geothermal energy I: United Nations Conf. New Sources Energy, Rome, 1961, Proc., v. 2, p. 82–90.

Böðvarsson, Gunnar, and Walker, G. P. L., 1964, Crustal drift in Iceland: Geophys. Jour., v. 8, p. 285–300.

Chaturvedi, Lokesh, and Pálmason, Guðmundur, 1967, Interpretation of infrared imagery of Mývatn area: Reykjavík, Iceland Natl. Energy Authority, Dept. Natural Heat [Pub.], 21 p.

Einarsson, Trausti, 1968, Submarine ridges as an effect of stress fields: Jour. Geophys. Research, v. 73, no. 24, p. 7561–7576.

Foshee, Lonnie, 1966, High resolution infrared radiometer experiment, *in* Nimbus II user's guide: U.S. Natl. Aeronautics and Space Adm. [Pub.], sect. 3, p. 1–38.

Friedman, J. D., and Williams, R. S., Jr., 1968, Infrared sensing of active geologic processes, pt. II. Case history of volcanic activity on Surtsey, Vestmannaeyjar, Iceland: Proc. Fifth Symposium on Remote Sensing of Environment, 1968, Univ. Michigan, Ann Arbor. p. 795–819.

Friedman, J. D., Williams, R. S., Jr., Miller, C. D., Pálmason, Guðmundur, 1967, Infrared surveys in Iceland in 1966, *in* Surtsey research progress report 3: Reykjavík, Surtsey Research Soc., p. 99–103.

Hédervári, Péter, 1963, On the energy and magnitude of volcanic eruptions: Bull. Volcanol., v. 25, p. 373–385.

Kunde, V. G., 1964, Theoretical relationship between equivalent blackbody temperatures and surface temperatures measured by the Nimbus HRIR in observations from the Nimbus I meteorological satellite: U.S. Natl. Aeronautics and Space Adm. Spec. Paper NASA SP–89, p. 23–36.

Rittmann, Alfred, 1962, Volcanoes and their activity: New York, Interscience Publishers, 305 p. [Translated from 2d German edition by E. A. Vincent]

Sapper, Karl, 1927, Vulkankunde: Stuttgart, J. Engelhorns Nachf., 424 p.

Sigurgeirsson, Thorbjörn, 1967, Continued geophysical measurements in Surtsey, *in* Surtsey research progress report 3: Reykjavík, Surtsey Research Soc., p. 104–107.

Sykes, L. R., 1967, Mechanism of earthquakes and nature of faulting on the mid-oceanic ridges: Jour. Geophys. Research, v. 72, p. 2131–2153.

Thórarinsson, Sigurður, 1950, The eruption of Mt. Hekla 1947–1948: Bull. Volcanol., v. 10, p. 157–168.

——— 1960, The postglacial volcanism, *in* On the geology and geophysics of Iceland: Internatl. Geol. Cong., 21st, Copenhagen, 1960, Guide to excursion A2, p. 33–45.

——— 1965, Neðansjávargos vid Ísland—Submarine eruptions off the coasts of Iceland: Náttúrufraeðingurinn, v. 35, p. 49–74.

——— 1966, Sitt af hverju um Surtseyjargosið: Náttúrufraeðingurinn, v. 35, no. 4, p. 153–212.

——— 1967a, The Surtsey eruption, course of events during the year 1966, *in* Surtsey research progress report 3: Reykjavík, Surtsey Research Soc., p. 84–91.

——— 1967b, The eruptions of Hekla in historical times, *in* The eruption of Hekla 1947–1948: Reykjavík, Vísindafélag Íslendinga, Soc. Scientiarum Islandica, 182 p.

Thórarinsson, Sigurður, and Sigvaldason, G. E., 1962, The eruption in Askja, 1961—A preliminary report: Am. Jour. Sci., v. 26, p. 641–651.

Tyrrell, G. W., 1949, The Tertiary igneous geology of Scotland in relation to Iceland and Greenland: Meddelelser fra Dansk Geologisk Forening, v. 11, no. 4, p. 413–440.

Walker, G. P. L., 1965, Some aspects of Quaternary volcanism in Iceland: Leicester Literary and Philos. Soc. Trans., v. 59, p. 25–40.

Ward P. L., Pálmason, Guðmundur, and Drake, Charles, 1969, A microearthquake survey and the Mid-Atlantic Ridge in Iceland: Jour. Geophys. Research, v. 74, no. 2, p. 665–684.

Wilson, J. T., 1965, A new class of faults and their bearing on continental drift: Nature, v. 207, p. 343–347.

Yokoyama, Izumi, 1956–57, Energetics and active volcanoes: Tokyo Univ., Earthquake Research Inst. Bull., v. 35, pt. 1, p. 75–97.

FIGURE 11.—Aerial infrared image (2357 UMT) of north part of Kverkfjöll subglacial volcanic ridge (letters same as in fig. 10 where same features are shown), August 22, 1966. *a*, linear array of Hveradalur thermal features (limits shown by bracket) and possible northern extension of tectonic lineament (dashed line); a_1, surface drainage of thermal waters from Hveradalur; *b*, Kverkjökull outlet lobe; *c*, active melt-water stream emerging from subglacial outflow tunnel (bright tone of image indicates higher water temperatures near point of emergence from outlet glacier and lower temperature downstream; arrow indicates flow direction); *d*, east- and west-facing escarpments forming a couloir constricting flow of Kverkjökull outlet lobe; *e*, points of thermal emission around periphery of ice cauldron-subsidence feature; *f*, concentric pattern indicating thermal convection along fracture surfaces related to ice cauldron subsidence; *g*, recent volcanic rocks; *h*, Dyngjujökull lobe; *i*, thermal emission from steam vents, hot springs, and solfataras of Kverkfjöll eystri. Inset on left shows Hveradalur thermal area (*a*) in somewhat greater detail.

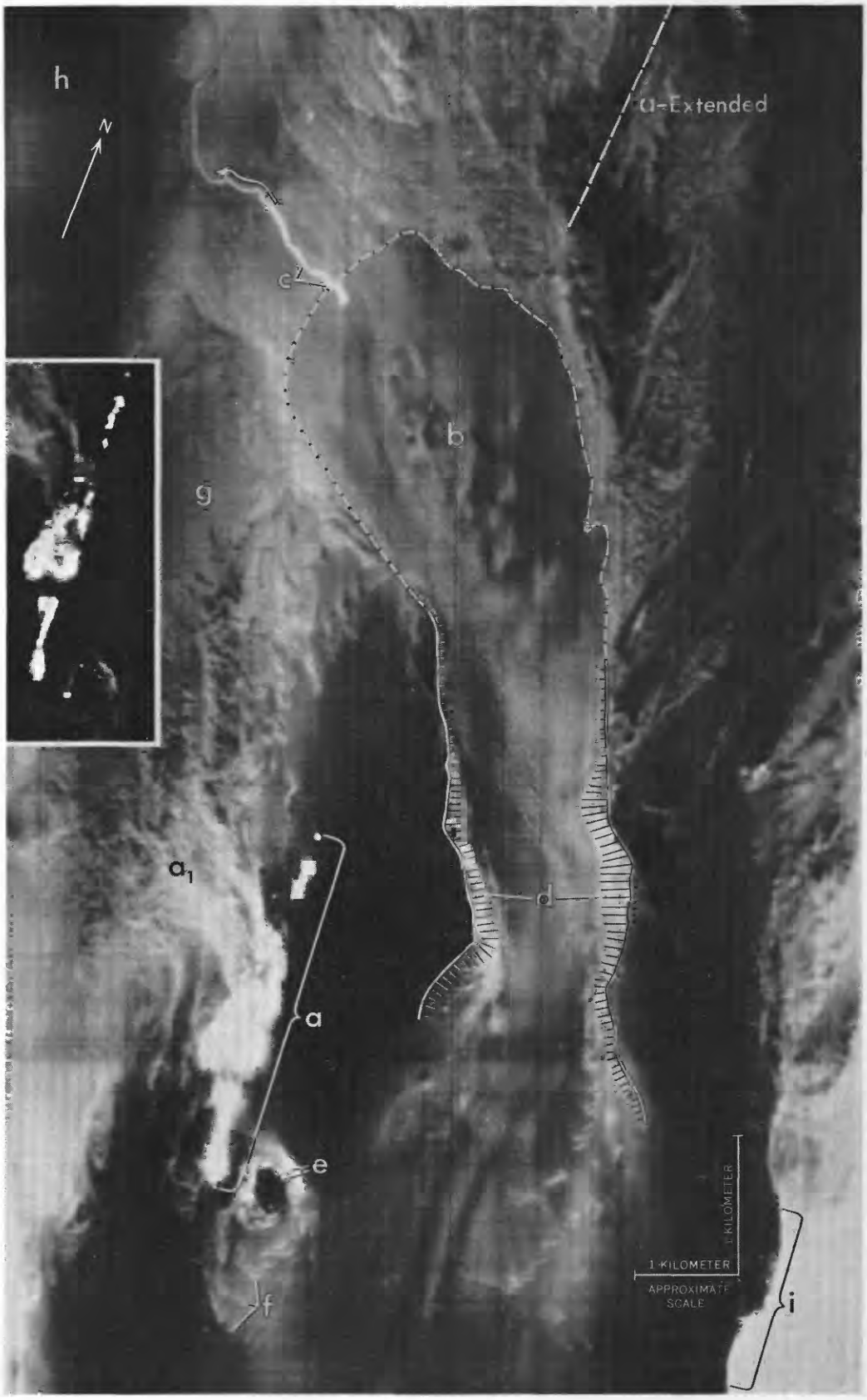
h
N
a-Extended
c
b
g
a_1
d
a
e
f
i
1 KILOMETER
1 KILOMETER
APPROXIMATE SCALE

FIGURE 11.

AERIAL INFRARED SURVEYS AT THE GEYSERS GEOTHERMAL STEAM FIELD, CALIFORNIA

By R. M. MOXHAM, Washington, D.C.

Work done in cooperation with the National Aeronautics and Space Administration

Abstract.—An infrared radiance pattern on aerial infrared images of The Geysers area extends beyond the present (1968) northwest limit of steam production, and suggests slightly elevated surface temperatures. The radiance zone seems to coincide in part with a mapped fault, across which a surface temperature difference was measured. The principal high-temperature zones are bounded at the surface on the southwest by thermal lineaments, suggesting some corresponding structural control. The abnormal radiance at The Geysers is restricted to hydrothermal alteration zones and other local features. No evidence was found of a regional geothermal anomaly at the surface in The Geysers area, within the detection limit of the equipment used in this survey.

The Geysers geothermal steam field, Sonoma County, Calif. (fig. 1) is the only site in the United States producing steam for electric power generation. Geothermal activity at The Geysers has been known for well over a century, and the hot springs have attracted visitors to a health resort that dates back to 1852. The first steam well was successfully completed in 1922, but commercial power production did not begin until 1960, when the Pacific Gas and Electric Co. put on a 12.5-kilowatt generator utilizing steam produced from four wells of the Magma and the Thermal Power Companies. This capacity was about doubled in 1963 and again in 1967; the present capacity is 55,000 kilowatthours. Construction for an additional 27,500 kwhr is under way, and future increases are being planned.

The Geysers area has many surface manifestations of abnormal geothermal conditions. Hot springs and steaming hydrothermally altered zones are well known. The high-temperature effluents, at about 80°–90°C, give rise locally to correspondingly high soil temperatures. But it is evident that, laterally from the high-temperature zones, values must decrease to some "normal" background level. It seemed conceivable that there might be areas where temperatures were above the background level, but yet not sufficiently high to produce any obvious manifestations. Aerial infrared surveys were undertaken to try to delineate the surface radiance and to see if the results bore any suggestive relation to the geology or to the subsurface geothermal regime.

Rocks are poor conductors of heat. Even in regions where the geothermal flux is 100-times normal (normal is $\approx 1.5 \times 10^{-6}$ cal $cm^{-2}sec^{-1}$), heat flow from the earth is about 50 times less than the incoming solar flux. A slight increase in heat flux from a subsurface source is not easy to detect because of local variations in the surface thermal regime resulting from differential solar heating and other meteorological factors. Heat transfer by convection, however, gives rise to abnormal surface temperatures where liquids and gases transfer heat to rocks along their path. Consequently, detectable surface-temperature anomalies most probably result from convective heat transfer, whereas direct detection of the underground thermal source by conductive heat transfer is not very likely.

GEOLOGIC SETTING

The Geysers area is in Sonoma County, about 70 miles north-northwest of San Francisco (fig. 1). Relief in the area is about 1,500 feet and is relatively rugged for aerial surveys. It was not possible to fly as low as was desired over some of the area because of steep valley walls.

A geologic map (scale 1:62,500), covering most of the report area, was published by Bailey (1946). The area in the vicinity of the steam field has been mapped on a larger scale by McNitt (1963, 1968). A detailed study of the fumaroles and hot springs is given in an excellent report by Allen and Day (1927). I have

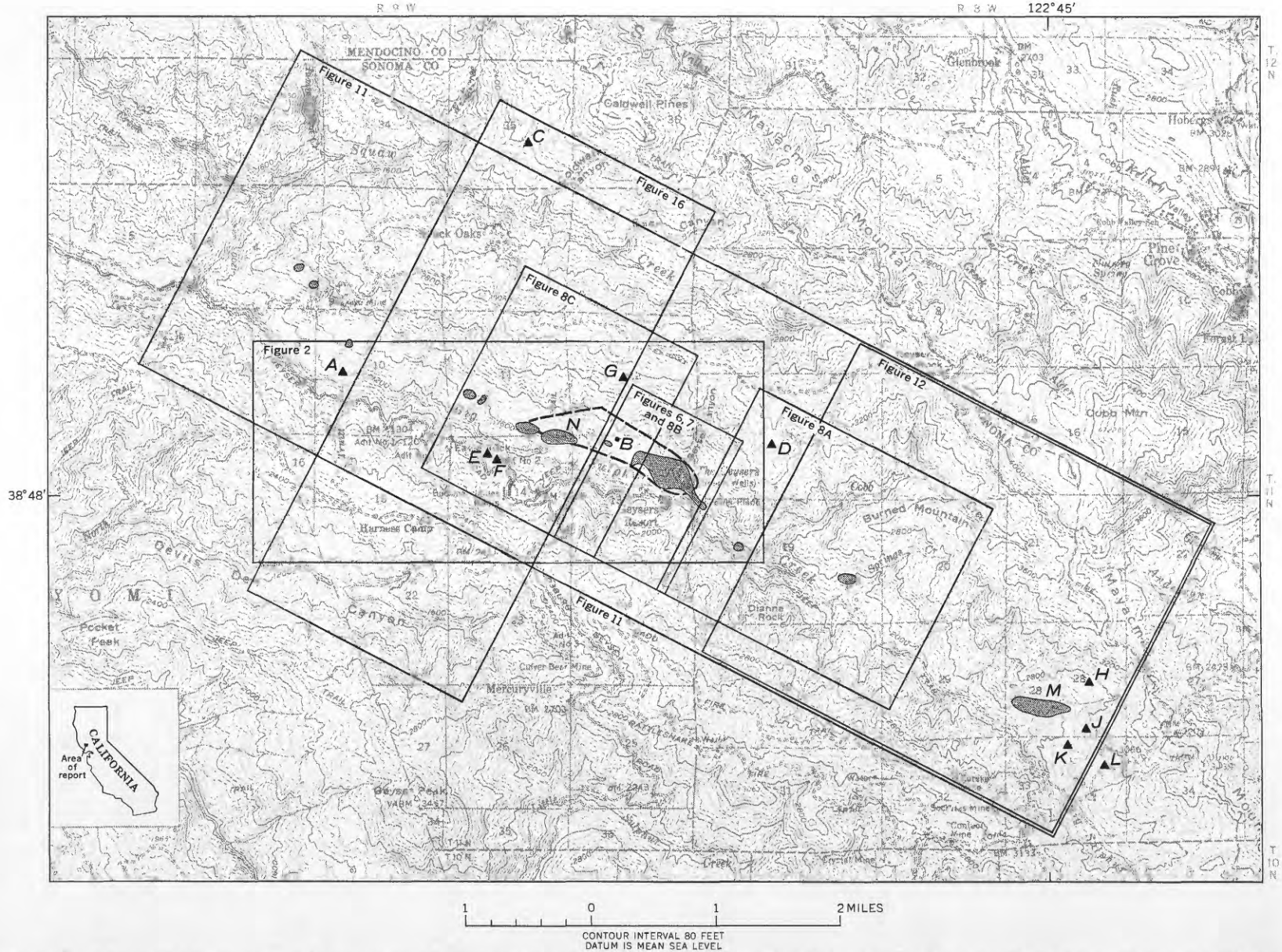

FIGURE 1.—Topographic map of The Geysers area, showing approximate boundaries of figures 2, 6–8, 11, 12, and 16. Areas of hydrothermal alteration (from Bailey, 1946) are shaded. Dashed line bounds approximate area of producing wells in the steam field in December 1967. Triangles indicate other wells drilled for steam: *A*, Signal Oil and Gas Co., Wildhorse No. 2; *C*, Signal Oil and Gas Co., Wildhorse No. 1; *D*, Signal Oil and Gas Co., Cobb Mountain No. 1; *E*, Geothermal Resources Inc., No. 1; *F*, Geothermal Resources Inc., No. 2; *G*, Union Oil Co., Ottobani No. 1; *H*, Geothermal Development Co. 65–28; *J*, Little Geysers No. 2; *K*, Little Geysers No. 1; *L*, D and V 73–33 (started September 1968). *B*, Powerhouse 2; *M*, Little Geysers; *N*, Sulphur Banks.

337-735 O—69——8

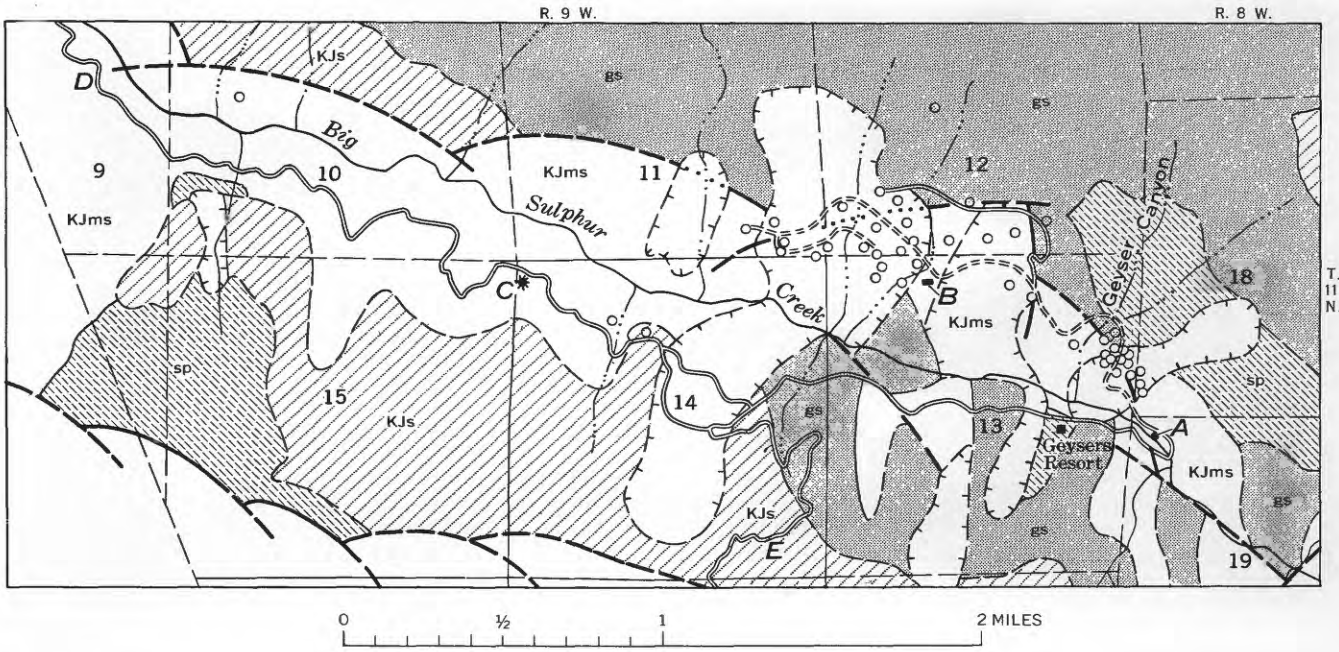

FIGURE 2.—Geologic map of The Geysers area (from McNitt, 1963). *A*, powerhouse 1; *B*, powerhouse 2; *C*, Eagle Rock; *D*, Geyser Road; *E*, Healdsburg-Geyser Road; geothermal steam wells (as of December 1967) are indicated by circles. Geologic units within the Franciscan Formation are indicated (ascending order) by the following symbols: (KJs) graywacke and shale; (gs) greenstone; (sp) serpentine; (KJms) micaceous graywacke and shale. Barbed lines enclose areas of landslides. Heavy dashed lines are approximately located faults.

used these papers extensively in the accompanying geologic descriptions and maps.

Figure 2 shows a part of The Geysers area as mapped by McNitt (1963). The area here is underlain by the Franciscan Formation (Jurassic-Cretaceous) which consists, from base upward, of the following: Massive graywacke and minor shale; several hundred feet of greenstone and associated chert beds, with serpentized peridotite at the upper and lower contacts; and poorly bedded micaceous graywacke and shale.

Cobb Mountain, near the northeast corner of the report area, is capped by rhyolite and other effusive rocks which Bailey (1946), citing earlier work, relates to the Sonoma Volcanics of Pliocene age, but which McNitt (1968) has designated as Pleistocene. During Pleistocene time, extensive eruptions northeast of the Mayacamas Mountains formed the Clear Lake volcanic field that extends to within 5 miles of the report area. No Tertiary or Quaternary volcanic rocks have been found at depth in The Geysers area.

The regional grain of the Franciscan rocks of the Mayacamas Mountains is northwest, resulting from a series of faulted structural blocks bounded by steeply dipping arcuate faults, according to McNitt's interpretation (fig. 2). Total vertical displacement along the major northeast-trending fault zones may exceed 15,000 feet. The Geysers area is on the northeast side of a downthrown block, flanked on the northeast by the Cobb Mountain horst.

A linear zone of hydrothermal activity, extending for perhaps 21 miles and including The Geysers, was recognized early in the exploration for quicksilver (Allen and Day, 1927, p. 11). This zone, which parallels the regional northwest strike, in places contains hot springs, fumaroles, and zones of hydrothermal alteration. The principal hot springs in the report area are associated with the hydrothermal alteration zones shown on figure 1. For a detailed description of the springs and fumaroles, see Allen and Day (1927). The most important hot-spring activity is in Geyser Canyon and extends for several hundred yards up the canyon from near the mouth at Big Surphur Creek. Most of the springs are above 60°C, and several are at the boiling point. The highest fumarole temperature reported by Allen and Day (1927, p. 25) in The Geysers area was 102°C at the "Safety Valve" in Geyser Canyon.

Another fumarole field, the Sulphur Banks, is about 1 mile west of Geyser Canyon. It is characterized by soft, steaming ground where temperatures at the numerous gas vents are in the 90°C range.

Upstream from The Geysers resort, several hot springs (80°–95°C) are found in the valley of Big Sulphur Creek and on Hot Springs Creek. At the Little Geysers, a group of hot springs occurs in a barren alteration zone.

On the basis of the Day and Allen measurements, McNitt (1963) assumes the total natural thermal spring discharge to be 5,000 gallons per hour, which represents

a minimum natural heat loss of about 4.2×10^5 calories per second. This amount does not include losses caused by evaporation and radiation.

Drilling for steam by the Magma and the Thermal Power Companies began in 1955 in the Geyser Canyon alteration zone. Superheated steam was produced from depths of 500 to 1,200 feet. Development of this locale continued, and drilling was later extended westward to the Sulphur Banks (fig. 2) where deeper steam production was found at pressures up to 500 pounds per square inch. By early 1968, 42 wells from 1,500 to 6,000 feet deep, had been drilled in an area of about 300 acres. Since 1967, the Union Oil Co. has undertaken drilling here in partnership with the Thermal Power Co.

Several wells have been drilled beyond the present (1968) productive area. Those that are generally regarded as successful (C. Otte and R. F. Dondanville, written commun., 1968; Koenig, 1968) are designated "S" in table 1. The other wells are either listed in State reports as plugged and abandoned, or are generally understood not to meet present commercial requirements. The D and V 73–33 well had not been completed at the time this report was written.

The amount of steam on line and proved by drilling is capable of producing about 200 megawatts (J. R. McNitt, oral commun., 1968).

TABLE 1.—*Status of wells beyond the present (1968) productive area*

Well	Designation (fig. 1)	Location			Status[1]
		Section	Township (north)	Range (west)	
Union Oil Co., Ottobani No. 1	*G*	12	11	9	S
Geothermal Resources Inc., No. 1	*E*	14	11	9	S
Geothermal Resources Inc., No. 2	*F*	14	11	9	S
Signal Oil and Gas Co., Cobb Mtn., No. 1	*D*	18	11	8	S
Little Geysers No. 1	*K*	33	11	8	S
Geysers Development Co., 65–28	*H*	28	11	8	S
Signal Oil and Gas Co., Wildhorse No. 1	*C*	35	12	9	
Signal Oil and Gas Co., Wildhorse No. 2	*A*	10	11	9	
Little Geysers No. 2	*J*	28	11	8	
D and V 73–33	*L*	33	11	8	Drilling, 12/19/68

[1] S, successful well.

Temperature-depth measurements were made in 1960 in eight steam wells of the Thermal Power Co. at Geyser Canyon. In each, a constant temperature interval was recorded in the upper part of the well, which McNitt (1963, p. 18) suggests is caused by ground water overlying the steam reservoir. Furthermore, hydrostatic equilibrium exists between the two phases whereby the expansive pressure of the steam is balanced by the hydrostatic pressure of the overlying water body. Calculation of the hydrostatic head leads to the conclusion that the steam-water interface slopes roughly parallel to the topographic surface in this vicinity.

Information on drilling techniques, steam production, and power generation at The Geysers is given by English (1964), Bruce (1964), and Hansen (1964). Koenig (1968) gives a geologic summary accompanied by the most recent drilling developments.

EQUIPMENT AND TECHNIQUES

The aerial infrared (IR) equipment used in this survey was a conventional line scanner. The terrain is scanned along a line normal to the flight path by means of a rotating 45° mirror. The IR emission from the earth is reflected through the optical system onto a solid-state detector. The detecting element converts the IR signal to electrical form which, after amplification, modulates a light source focused on a film strip. The light source is deflected across the film in synchronization with the scanning mirror, and the film strip advances in proportion to the aircraft velocity. This combined light deflection and film motion creates an image whose gray scale is related to the IR energy emitted from the terrain. The line scanner used in this work, however, is not a radiometer. That is, the scanner output signal (and therefore the image tone) is not a direct measure of the incoming IR energy, mainly because of the lack of d–c restoration and the a–c characteristics of the amplifiers (see Lowe, 1968, for a detailed discussion).

The scanner was equipped with a mercury-doped germanium (Ge:Hg) detector, generally termed a "long wavelength" detector as it has peak sensitivity at about 10 micrometers (μm). The sensitivity range, however, extends well beyond the 8–13 μm atmospheric window so that if no filter is used noticeable atmospheric absorption will result from the water vapor bands adjacent to the 8–13 μm window.

As the atmospheric absorption increases with path length, the terrain signal correspondingly decreases as the scan angle sweeps from the vertical toward the horizon. Inasmuch as the atmosphere itself emits IR along the scan path, the reverse effect operates at the same time. Atmospheric absorption, however, is evidently the more effective mechanism at the terrain and atmospheric temperatures encountered in these surveys (see Moxham, 1968).

A band-pass filter to restrict the incoming signal to one of the more transparent parts of the 8–13 μm

window tends to reduce the atmospheric losses, but also reduces the effective radiance sensitivity.

The film used by the scanner is a conventional Tri-X Aerecon whose negatives record high radiance from the terrain as dark image tones, that is, with greater film density. Consequently, in this report, greater film densities on the original negative refer to the higher radiance terrains. All images reproduced in this report are positive prints from the original negatives; hence, the lighter tones correspond to higher radiance terrain; darker tones correspond to lower radiance terrain.

The scanner was carried in a twin-engine D–18 Beechcraft operated by the U.S. Geological Survey. Portable rotating beacons were placed at strategic locations on ridgetops to assist night navigation. All aerial photographs are by the U.S. Geological Survey except figure 6.

During the survey period, soil and water temperatures were monitored at selected localities. Yellow Springs Instrument Co. series 400 thermistors were used. The sensing element is disk shaped and the several varieties used had $\frac{3}{16}$- to $\frac{5}{8}$-inch diameters. At each site, the thermistor was implanted so that the perimeter was just beneath the surface of the ground. The depth variation (to the center of the thermistors) probably did not exceed 3 millimeters. In this report, all surface temperatures refer to a depth of about 3 mm. Thermistor resistance was measured with an automatic sequencing bridge, and the results were recorded on an Esterline-Angus strip-chart recorder. The temperature-monitoring equipment is described in detail by Moxham and others (1968).

AERIAL SURVEYS

Aerial surveys were made during August 15–19, 1966. Nine lines, about 4 miles long and spaced at about 1-mile intervals, were flown north-northeast, approximately normal to Big Sulphur Creek valley. The grid was centered on the steam-producing area. Another line was flown west-northwest, along Big Sulphur Creek from about the Sonoma-Lake County line to Squaw Creek.

One afternoon IR flight was made, using an 8–14 μm band-pass filter over the detector. All other IR surveys were made from 0230 to 0500 hours (PDT), with the detector open (unfiltered) or with an 8–14, 8.9–10, or 10–15 μm filter.

Aerial panchromatic 70-mm photographs along the survey lines were made on one flight.

It is a matter of some interest in aerial IR surveying to know the time at which the onset of solar heating at sunrise will begin to have a detectable effect on surface temperature. The first light of dawn is sometimes desirable, if not mandatory for low-level aerial navigation over rugged terrain. But as the sun rises, the surface temperature at some point in time begins to increase and to obscure some predawn thermal features. Moxham, Greene, Friedman, and Gawarecki (1968, p. 9) have shown in an earlier experiment at Tonopah, Nev., that there is roughly a 1-hour lag between the first light of dawn and the onset of a detectable surface-temperature rise at Tonopah's latitude (fig. 3). The surface temperature evidently responds quickly (a few minutes) to direct solar radiation, but not to the presunrise sky radiation, that is, within the limits of our measurements.

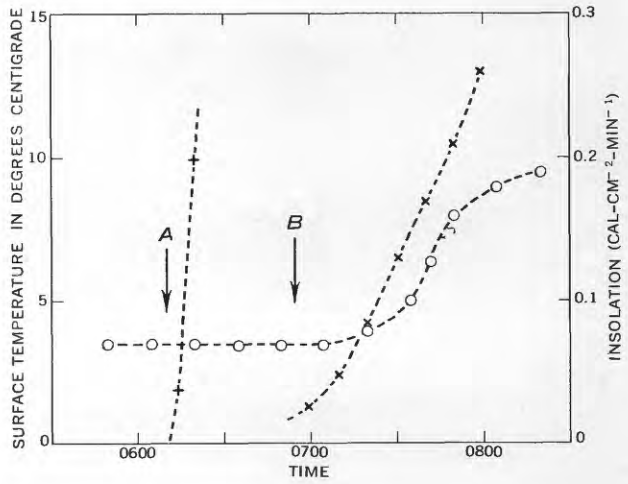

FIGURE 3.—Relation between insolation and surface temperature. Insolation was measured with an Eppley 180° pyranometer (x). Between the first light of dawn (*A*) and local sunrise (*B*), sky radiation was less than the detection limit of the pyranometer. First light was detected with an uncalibrated cadmium sulfide cell (+) which recorded a full-scale deflection from 0610 to 0630 hours PDT, and is shown here on an arbitrary scale. Surface temperature (open circles) was measured with a thermistor buried about 3 mm beneath the ground surface. Experiment conducted at Tonopah, Nev., October 13, 1967.

DATA ANALYSIS

Film density

In the treatment of data from the IR surveys, analysis of film density in terms of terrain temperature has for the most part been deliberately avoided. The instrument used in this work does not yield quantitative data for several reasons, but the principal cause is the lack of d–c restoration. Where the scanner "sees" an infinite target of constant temperature over the entire scan line, the average d–c signal level establishes a given gray tone (density) on the film. Now, if two targets of unequal width and temperature are scanned, the average d–c level will shift in response to the magnitude and polarity of the two target signals, and the film density will change accordingly. This effect is most noticeable where large, uniform-temperature

targets (such as bodies of water) are bordered by a target of different temperature (land). Variations in the land temperature give rise to light and dark streaks across the water on the image (fig. 4). In figure 5, if we assume the temperature of Clear Lake to be uniform (27°C, indicated by X), the horizontal solid bracket through the point at a density of 0.75 indicates the density variation over the lake along the flight path on the image. This density variation corresponds to about 1.5°C on this image, but of course the error could be much larger were the contrast between lake and land temperatures much greater.

FIGURE 4.—IR image of Clear Lake, 0345 hours PDT, August 17. Lake and adjacent shore surface temperatures (station 4) were measured at *A*. Horizontal white line indicates flight path. Dark streaks in the water are caused by lack of d–c restoration in scanner circuitry.

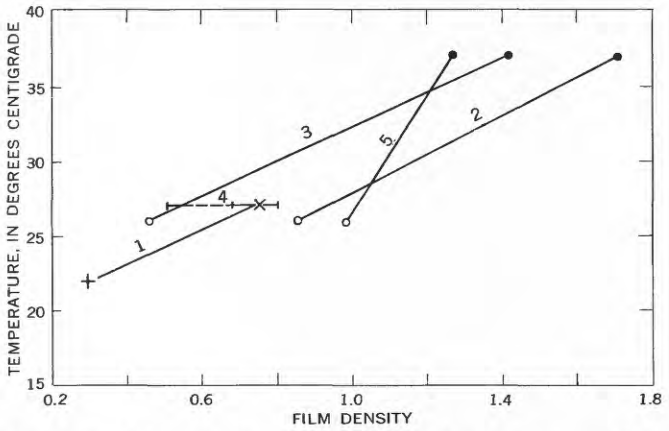

FIGURE 5.—Film density versus ground temperature. Film density was measured with a Joyce-Loebl microdensitometer at points corresponding to ground (or water) observation stations. Densitometer aperture, 100μm. Solid circles, station 1; open circles, station 2; X, station 4 (water); +, station 4 (beach). Bracket, labeled as 4, indicates density range along film axis (solid) and across film axis (solid plus dashed), across Clear Lake. Each numbered curve represents an individual flight over the observation stations, using an unfiltered detector; altitude above terrain was about the same for 1, 2, and 3, but doubled for 5.

Curve	*Time (PDT)*	*Figure in this report*
1	0344	4
2	0337	8
3	0305	Not shown
5	0400	11

Film density along a given scan line normal to the flight path over a uniform-temperature infinite target tends to decrease toward the horizon (that is, from the center of the image toward the edges) owing to atmospheric absorption. A density profile was made parallel to the scan direction across the Clear Lake image. The density decrease from the center of the film to the edge was about 0.3 (solid plus dashed bracket) corresponding to about 3°C. In figure 5, each curve is drawn through two points, corresponding to observations at two ground stations. For a given pair, the two stations were separated at most by only 500 feet. Consequently, the terrain targets are nearly adjacent on the IR images. The slopes of curves 1–3 are nearly parallel, suggesting that relative temperatures between adjacent terrain features on a given image can probably be estimated ≈1°C. But the separation between the curves along the abscissa, probably caused by variation in location of the pairs with respect to the center of the film, shows that absolute temperatures may be in in error by as much as ≈5°C.

Density values for curve 5 (fig. 5) are from an image made at about twice the altitude (half the scale) as those of curves 1–3. The marked change in slope stems largely from the reduction in film speed through the film-transport system. At the higher altitude the decreased film speed leads to increased exposure which tends to increase the background gray level.

Many of the electronic deficiencies mentioned are being overcome by more recent technology. Some radiometric scanners are now available that yield quantitative data by means of d-c restored or d-c coupled amplifiers, internal black-body calibration, and tape recording to retain dynamic range. But in light of the quantitative limitations on the rather unsophisticated instrument used in this study, much of the following discussion will be in rather qualitative terms.

Film-density slicing is a useful technique for comparing relative densities at several places on an IR image. An Image Quantizer manufactured by the Tech/Ops Co. was used for this purpose. The film specimen to be analyzed is placed on a rotating drum and electronically scanned through a 300 μm aperture. The amount of light which passes through the film is sensed by a photocell, amplified, and impressed on a spark stylus in the recorder. The recording paper is rotated and translated in coordination with the specimen scanning. The Quantizer is used conventionally for contouring density. But by manipulating the threshold voltage to the stylus and by deliberately overexposing a photographic copy of the recording, a print was produced whereon only film densities that exceed a given value are shown and all lower densities are re-

jected. A new recording is made with a slightly lower threshold voltage, yielding a print which includes slightly lower densities as well as all previously selected higher densities. The process is repeated at successively lower thresholds, yielding a set of prints as in figure 13. The IR image used in this case was figure 8.

The density value obtained by any densitometric system represents the average for that part of the film which fills the field of view. The complex density patterns associated with terrain targets consequently present special problems. In order for small ground elements to fill the densitometer field of view, a small aperture is desired. The small aperture, on the other hand, yields a high noise level, increases the scan time perhaps to unreasonable duration, and makes it exceedingly difficult to pass the aperture precisely over a small target. A trade-off resulting in a 100–300 μm aperture has been found most useful

Diurnal temperature effects

One of the principal areas of interest is the present steam-production site on the north side of the valley of Big Sulphur Creek. This rather steeply sloping surface is largely grass covered with scattered trees. Along the drainageways, trees and brush are more abundant (fig. 6). The south valley slope, however, has a heavy growth of trees and brush. Figure 6 is an aerial photograph taken in 1955 before the extensive cultural changes resulting from the drilling for steam. The photograph shows the light-colored barren areas of hydrothermal alteration against the darker background of the grass-covered unaltered ground.

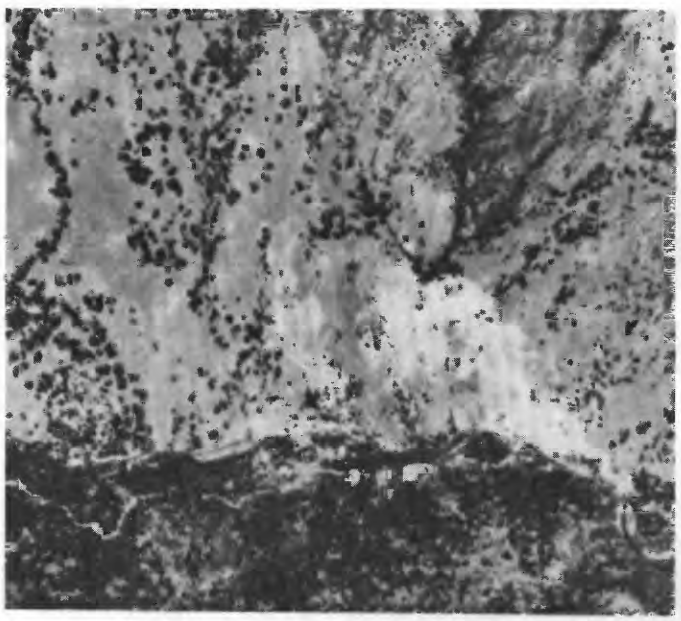

FIGURE 6.—Aerial photograph of the steam-production area at The Geysers, 1955. Lightest patches are areas of hydrothermal alteration. Figures 7 and 8*B* cover approximately the same area.

A daytime IR image of this area (fig. 7) shows only the highest anomalous surface temperatures in a doughnut-shaped pattern where copious steam is escaping around the drilling pad of a blown-out steam well. This pattern may result from steam being forced laterally by the grouting which was emplaced in attempts to seal off the well. The cool vegetation contrasts strongly with the hot, sunlit grass-covered slope. Many of the topographic features on the IR image resemble those on the aerial photograph because of differential solar heating.

A predawn image of the same area (fig. 8*B*) shows how the diurnal cooling of "normal" ground affects the IR emission. The lower temperature geothermal anomalies now contrast strongly against the cooler grassy slopes. The vegetation is apparently at about the same radiant temperature as the soil, though some mottling may be due to the plant material.

Cooler air has settled into topographic lows (fig. 8*C*) and, though I have no supporting data, it is assumed that the surface temperatures in the topographic lows are thereby diminished. I believe that these meteorological effects are more readily detected by the unfiltered detector because of the greater amount of radiation passed, whereas the same effects tend to be more subdued on narrow band-pass images which cut off part of the incoming energy. The open-detector images, however, tend to darken toward the horizon more than the filtered images. There is some supporting evidence (Moxham, 1968) that atmospheric transmission losses are the principal cause. Atmospheric attenuation is also probably responsible, in part, for the lower apparent radiance over topographic lows shown in the unfiltered images of figure 8. Though most of the dark mottling correlates with smaller topographic depressions, vegetation also contributes to this pattern.

The increase in temperature difference between anomaly and adjacent ground from afternoon to predawn is borne out by ground temperature measurements at the Sulphur Banks (figs. 9 and 10). Three thermistors were emplanted at random in a warm alteration zone at station 1. Another three-thermistor array was established at station 2 on a flat bare soil surface about 500 feet northwest of the anomaly at station 1. The bare soil at station 2 showed no alteration or thermal activity and appeared to be fairly uniform in texture and composition. The temperature spread among the three thermistors was on the order of 1.5°C. Though the unaltered area at station 2 was about 500 feet from the alteration zone at station 1, its surface temperature may be somewhat greater than the regional

FIGURE 7.—Daytime IR image of the steam-production area at The Geysers (1534 hours PDT, August 16, 1966). Arrow indicates doughnut-shaped thermal anomaly surrounding blown-out steam well. *A*, powerhouse 1; *B*, powerhouse 2.

background, as suggested by figure 13. In the alteration zone, there is a spread of as much as 17°C between the thermistors owing to the local percolation of warm gases through the soft ground and possibly to slight variations in thermistor depth. The results (fig. 10) show that during the day the average temperature at station 2 is about 4°C warmer than at the anomaly, whereas in the predawn hours, the average temperature at the anomaly is about 10°C greater than at station 2.

BIG SULPHUR CREEK VALLEY

An overall thermal view of the report area is shown in figure 11. Additional details are on figures 8 and 13. The most intense anomalies lie, for the most part, in the alteration zones shown in figure 1. The group of springs at the Little Geysers (fig. 12) is the southeasternmost conspicuous anomaly, though there seems to be a small thermal spot about a quarter of a mile farther upstream on Big Sulphur Creek. This area was not examined on the ground, and the small thermal feature could not be identified. Additional anomalies, apparently associated with hot springs, occur along Big Sulphur Creek between Little Geysers and powerhouse 1. The most noticeable is about 1 mile southeast of the mouth of Hot Springs Creek. In contrast, the springs on Hot Springs Creek are barely perceptible.

The two most intense anomalies lie between powerhouse 1 and Geyser Canyon (fig. 8*B*). They are in the eastern part of area's largest alteration zone, and it is here that steam development first began. Natural steam vents at temperatures near 90°C are common and, at the westernmost of the two anomalies, steam venting from the periphery of the grouted drilling pad of the wild-blowing well adds to the thermal signal. The southwest limit of the easternmost of the two anomalous zones is a thermal lineament which extends along the north bank of Big Sulphur Creek from near the powerhouse for a distance of about 700 feet downstream. A similar west-northwest linear thermal zone lies along the creek from near the mouth of Geyser Canyon and extends 700–800 feet downstream. This zone also forms the southern limit of a zone of thermal spots in the valley immediately west of Geyser Canyon. Figure 8*B* suggests, and field examination tends to confirm, that the linear thermal feature contains two steaming zones; one zone evidently follows fractures in bedrock at

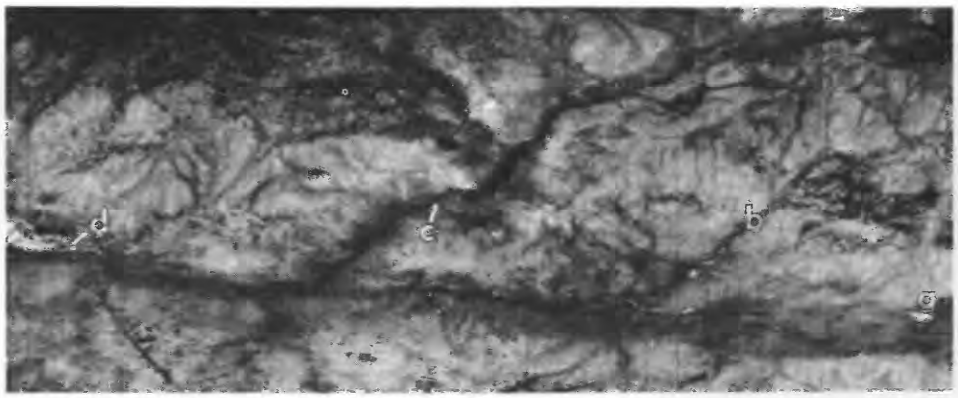

A

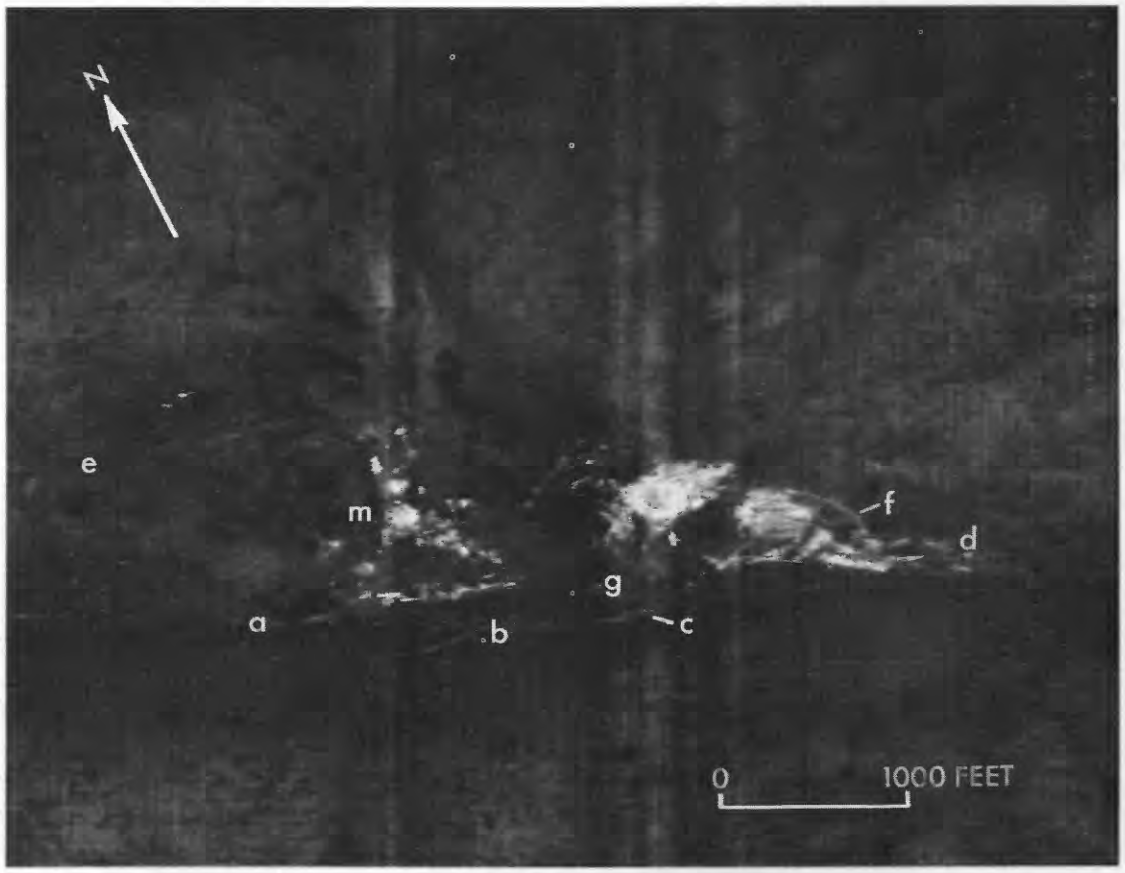

B

FIGURE 8.—Predawn IR image of Big Sulphur Creek valley in three overlapping views from southeast (part *A*) to northwest (part *C*) (0337 hours PDT, August 17, no filter). Part *A*: *a*, hot springs(?); *b*, Hot Springs Creek; *c*, Cobb Creek; *d*, powerhouse 1. Part *B*: *a*, Big Sulphur Creek; *b*, Geyser Road; *c*, The Geysers resort; *d*, powerhouse 1; *e*, powerhouse 2; *f*, steam pipeline; *g*, mouth of Geyser Canyon; *m*, common point shown on part *C*. Vertical streaks are caused by amplifier saturation over hot targets. Part *C*: *a*, temperature-monitoring station 1; *b*, station 2; *c*, station 5; *d*, Geyser Road; *e*, Healdsburg-Geyser Road; *f*, Big Sulphur Creek; *g*, jeep trail; *h*, Eagle Rock; *j*, Union Oil Co., Ottobani No. 1; *k*, Geothermal Resources, Inc. (GRI), No. 1; *l*, GRI No. 2; *m*, common point shown on part *B*. The last two wells had not been drilled at the time this image was made.

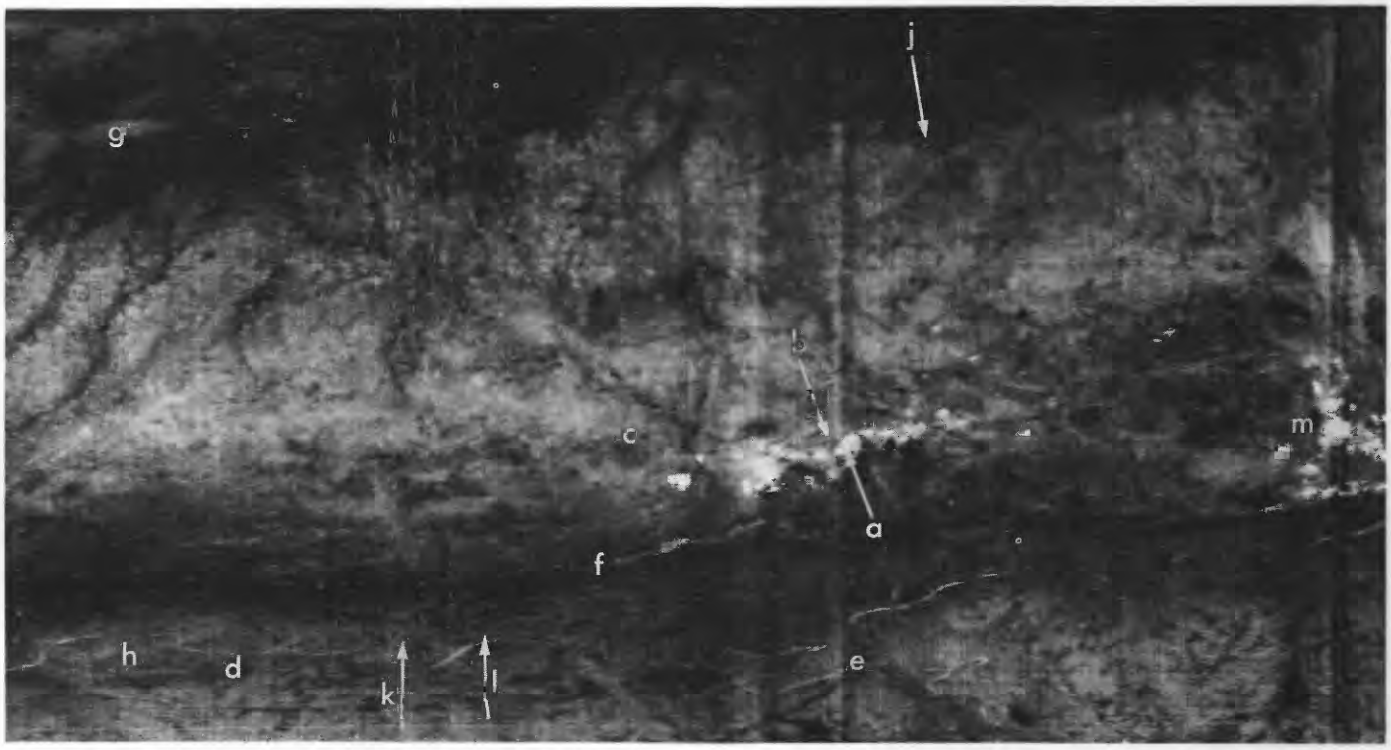

C

FIGURE 8.

about creek level, the other is about 20 feet above the creek in landslide debris.

Farther west (fig. 8*C*), the Sulphur Banks anomalies are in an area mantled by landslides. The hot patches form a line of interconnected thermal spots extending half a mile west-northwest from near powerhouse 2.

En echelon with the Sulphur Banks thermal zone is a straight reach of Big Sulphur Creek along which are several small thermal spots; they were not field checked, but are probably due to hot springs, as the creek brightness on the IR image is perceptibly greater along this reach.

It thus appears that the two most conspicuous mapped thermal zones are bounded on the south by linear features and that a third zone is itself also linear. Though the thermal alinements do not coincide with any of the faults mapped by McNitt (1968), an abnormally warm fracture system along parts of Big Sulphur Creek is strongly suggested. It is evidenced by locally steaming fractures in the bedrock at creek level. At least one of the linear steaming zones above creek level is in landslide debris, but the linearity suggests some underlying bedrock structural control.

The most intense thermal anomalies in The Geysers area coincide generally with hydrothermally altered steaming ground. IR maximums are recorded over active fumaroles and hot springs, but close inspection of figure 8*C* and figure 11 shows a barely perceptible, arcuate, low-intensity radiance feature extending northwest from the Sulphur Banks. In fact, I was unaware of this arcuate pattern until the film was analyzed with the Image Quantizer (fig. 13).

Figure 13 covers Big Sulphur Creek valley from about Hot Springs Creek to about 1 mile southeast of the Buckeye mine; maximum film densities in this area are shown in figure 13*A*. The highest density is in the main alteration zone at a point about midway between powerhouse 1 and Geyser Canyon. The hottest parts of the anomalies at the Sulphur Banks also fall in this density increment, which includes the site at station 1, thus suggesting that this slice includes temperatures $\geqq 38°C$, approximately. The next lower density increment (fig. 13*B*) increases the size of the Geyser Canyon thermal zone by perhaps a factor of two and the Sulphur Banks zone by about five. The alteration zone about midway between Geyser Canyon and powerhouse 2 now makes its appearance rather faintly. Perhaps more significant, however, is the appearance of an arcuate density zone extending west from the Sulphur Banks, and after a gap, an oval-shaped ring of density features still farther to the west, which will be discussed below.

By adding the next lower density increment (fig. 13*C*), a slight enlargement of the Sulphur Banks-Geyser Canyon suite of anomalies is obtained, but the area

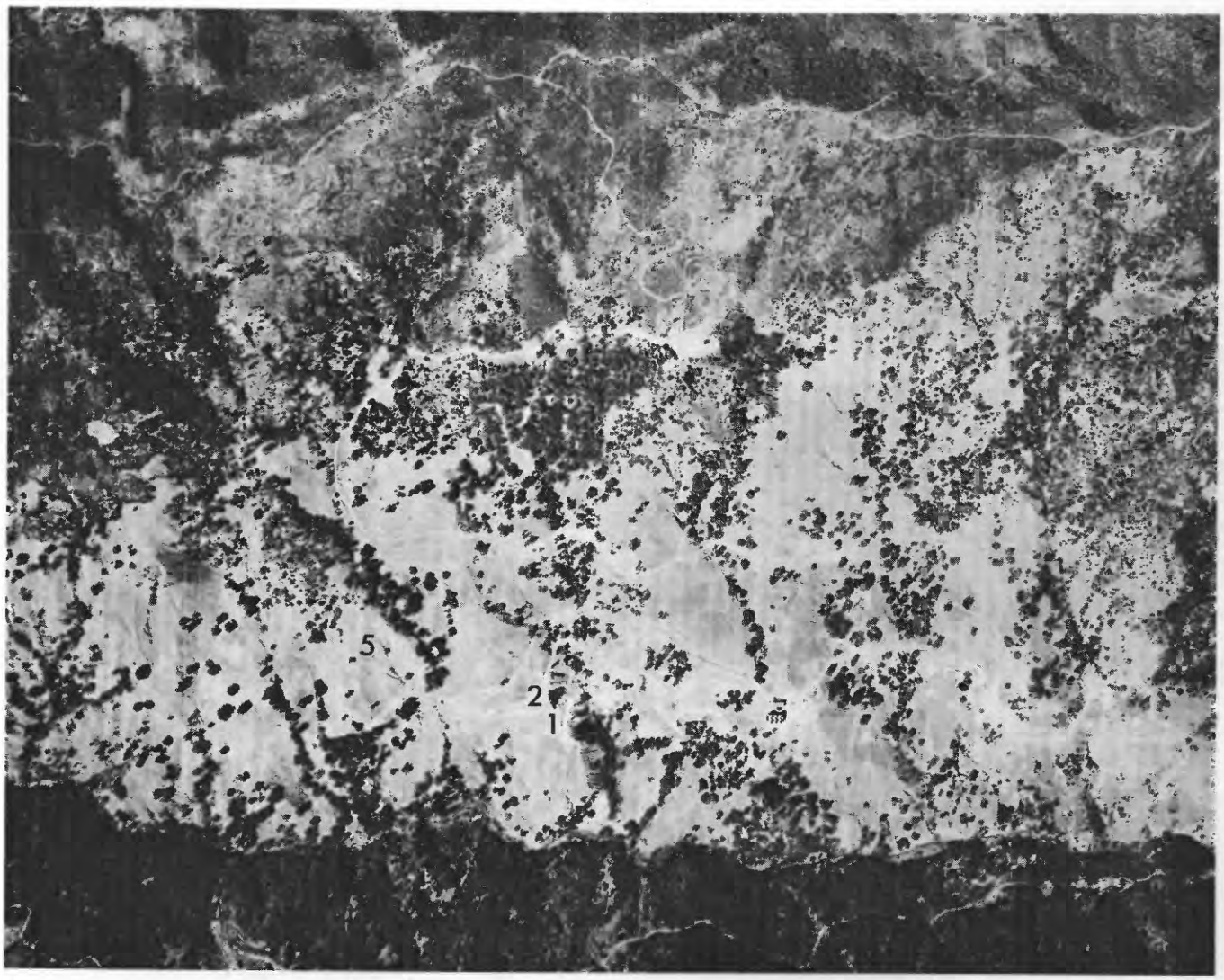

FIGURE 9.—Aerial photograph of the Sulphur Banks, 1966. Powerhouse 2 is in the lower center. Temperature-monitoring stations are indicated by *1*, *2*, and *5*.

west of Sulphur Banks is greatly enlarged and several spots are included southeast of The Geysers and south of Big Sulphur Creek. Station 2 at the Sulphur Banks is difficult to identify but I believe it is included in this density slice, suggesting that this increment includes temperatures $\geqq 27°C$, approximately.

The area south of Big Sulphur Creek including the Geothermal Resources, Inc., (GRI) well sites does not appear until the next density increment is added, which results in a printout roughly half the area of the IR image. Recall however, that atmospheric transmission losses no doubt reduce density toward the film edges, and would include the GRI sites.

It seems safe to say that figure 13*A* depicts only thermal anomalies, inasmuch as all the localities relate directly to known steaming ground. At the other extreme, figure 13*D* is believed to be well within the geologic noise level. We have no quantitative data to support this view, but density levels in the regions adjacent to Big Sulphur Creek valley (described below) suggest it. Consequently, the boundary between normal and abnormal surface temperatures ought to be at some intermediate density level between that of figures 13*A* and 13*D*. Most likely the boundary is at some level within the density increment covered by figure 13*B* because this slice includes known thermal anomalies immediately west of Geyser Canyon, as well as the low-level anomalies west of the Sulphur Banks where no known surface manifestations are evident.

In the density analyses, unfiltered images were used to take advantage of the maximum signal response. Unfiltered images suffer the greatest atmospheric transmission losses; these losses reduce the apparent radiance toward the image edges. This effect is illustrated in

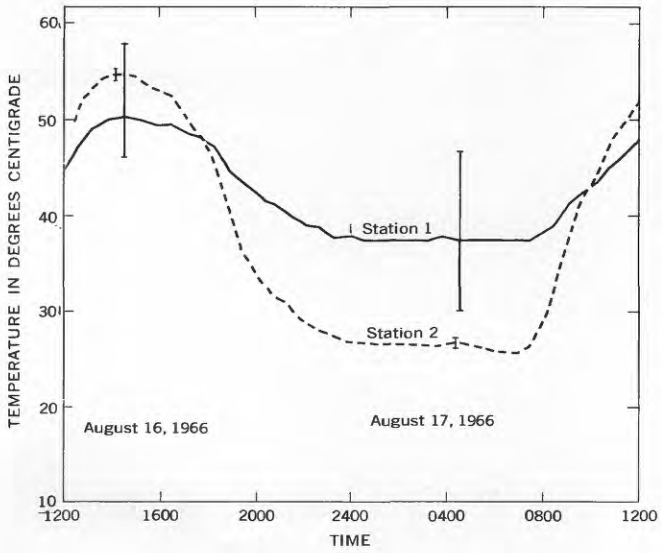

FIGURE 10.—Surface-temperature observations at the Sulphur Banks. Images shown in figures 7 and 8 were made during the infrared surveys on August 16 and 17, respectively. Station locations are shown on figure 8*C*. Brackets show temperature spread among the three thermistors at each station at time indicated.

figure 14, where the colder air in topographic depressions and the density rolloff with increased scan angle (that is, toward the image edges) are much more evident on the unfiltered image than on the 8.9–10 μm band pass. The density maps consequently are useful only for comparing relative densities in the central part of the image and on a local basis.

Immediately west of the Sulphur Banks, the low-intensity radiance zone shown on figures 8*C* and 13 is arcuate (concave to the southwest). Though I cannot identify enough landmarks on the IR image to be certain of its location, the feature seems nearly to coincide with the curved fault which McNitt (1968) has mapped in section 11 (see fig. 2). In December 1967, soil temperature measurements were made at this location. A linear array of five thermistors spaced at about 50-foot intervals was implanted on the south-sloping ridge between two landslides in the SE¼ sec. 11, T. 11 N., R. 9 W. (figs. 2 and 9). The array crossed the mapped location of the arcuate fault. At most of the thermistor sites, the bedrock evidently was at shallow depth (only inches below ground surface). The results (fig. 15) indicate a nighttime difference of about 7°C between the two thermistors on the south as opposed to the three on the north. A direct comparison of this temperature step, measured in December 1967, with the results obtained in the IR study of August 1966 would hardly be justified because of seasonal differences alone. The relatively large (7°C) ground-temperature variation measured at station 5 would surely give rise to a substantial density contrast on an IR image, much greater in fact than the very small density contrast associated with the arcuate radiance pattern on figure 8*C*. It seems evident that there is some anomalous soil temperature condition at this locality, but many more surface observations are required before one can draw any further conclusions.

REGIONAL ASPECTS

Density profiles were made of several northeast-oriented IR images that extend from Little Sulphur Creek to Squaw Creek. In all images, radiance levels in Big Sulphur Creek valley do not exceed those in the adjacent areas except in the immediate vicinity of the hydrothermal zones (fig. 16). The arcuate radiance zone west of the Sulphur Banks is (barely) visible on some of these regional images, but the absolute value of the radiance level is relatively low. The higher radiance levels elsewhere in the region can be ascribed locally to vegetation and to slope orientation with respect to sun angle, but there is not a great deal of consistency. Variation in emissivity may also be involved. Representative samples of several bedrock units in The Geysers area were examined in an emis-

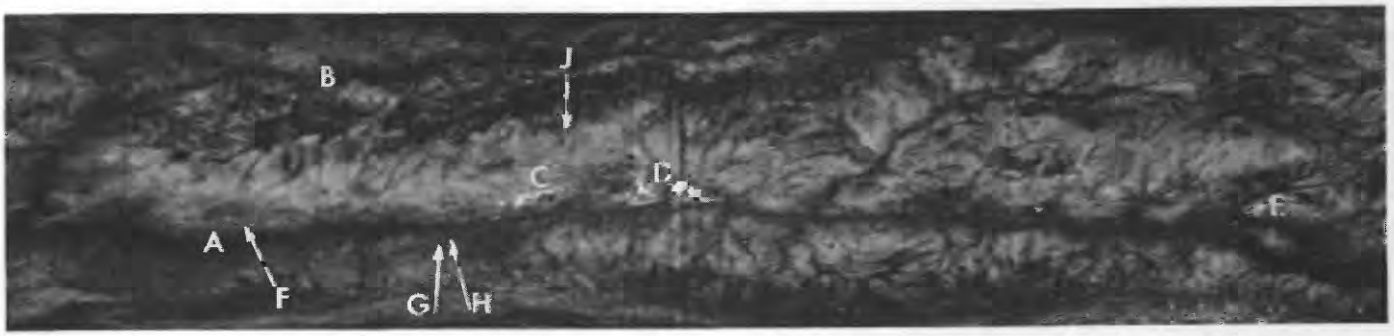

FIGURE 11.—IR image of Big Sulphur Creek valley (0400 hours PDT, August 17, 1966, no filter). *A*, Big Sulphur Creek; *B*, Squaw Creek; *C*, The Sulphur Banks; *D*, The Geysers; *E*, Little Geysers; *F*, Signal Oil and Gas Co., Wildhorse No. 2; *G*, Geothermal Resources, Inc. (GRI), No. 1; *H*, GRI No. 2; *J*, Union Oil Co., Ottobani No. 1. A row of white dots at the lower right of the image is caused by static electricity discharge.

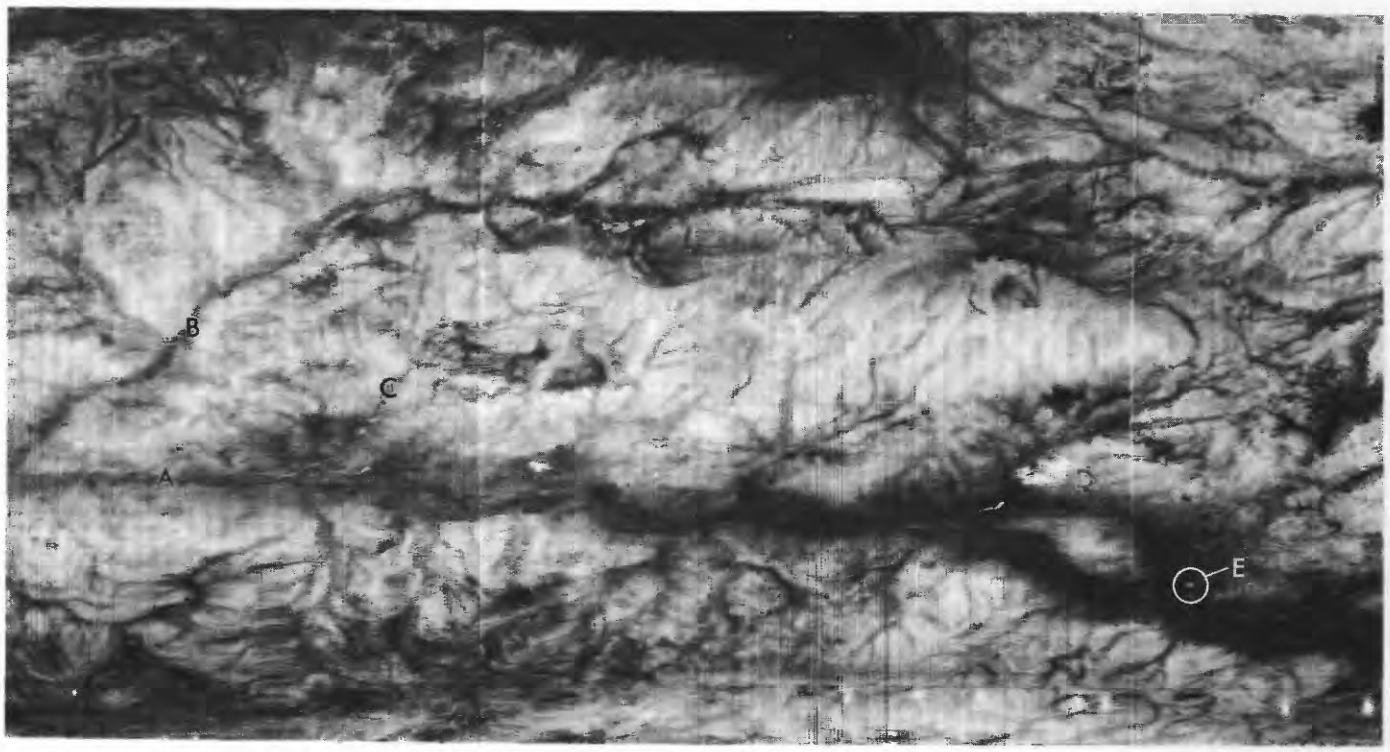

FIGURE 12.—IR image of the Little Geysers area (0400 hours PDT, August 17, no filter). *A*, Big Sulphur Creek; *B*, Cobb Creek; *C*, Hot Springs Creek; *D*, Little Geysers; *E*, unidentified anomaly. This figure is an enlargement of the southeast part of figure 11.

sivity box with a Barnes 8–14 μm radiometer. The results (table 2) show a spread in the 8–14 μm band from 0.91 to 0.98, but more commonly from 0.94 to 0.97 for weathered surfaces. This variation in emissivity amounts to about 3°C for a 25°C surface temperature. Soil development and generally rough surface textures, however, probably tend to increase the emissivity to a somewhat larger value than suggested by the bedrock samples.

CONCLUSIONS

Within the limits of detection of the instrument used in the aerial surveys, there seems to be little evidence for a regional geothermal anomaly associated with the known geothermal reservoirs in Big Sulphur Creek valley.

The first-order manifestations of geothermal activity—hot springs and fumaroles—can be rather easily and quickly depicted by IR surveys. Moreover, there is some evidence that lower temperature phenomena associated with the steam field and not immediately evident on the ground, were detected by the aerial survey. These more subtle radiance features occur beyond the limits of present steam production and surface alteration, and may be useful in guiding exploration.

TABLE 2.—*Emissivity (8–14 μm) of rocks in the The Geysers area, Sonoma County, Calif.*

[Abbreviations: f, fresh; w, weathered; fw, partly weathered]

Sample	Location (T. 11 N.; R. 9 W.)	Description [1]	Emissivity (8–14 μm)
1	SE¼ sec. 11; about 300 ft northwest of station 5.	Greenstone (gs)	0.96 fw
2	SE¼ sec. 14; about 0.4 mi east-southeast of Buckman mine headquarters.	Cherty shale (KJs)	.91 f
3	NW¼ sec. 14; adjacent to Geyser Road, 500 ft east-southeast of Eagle Rock.	Graywacke (KJms)	.93 f .94 w
4	NE¼ sec. 13; alteration zone about 500 ft north of powerhouse 1, on north side of main access road.	Altered graywacke (KJms)	.98
5	SE¼ sec. 11; station 5	Graywacke (KJms)	.97 w
6	SE¼ sec. 14; 600 ft east of sample 2 locality.	Greenstone (gs)	.96 f .96 w

[1] Letter symbols refer to map units on figure 2.

The aerial IR technique of mapping terrain radiance may find its principal application in preliminary regional assessment of undeveloped geothermal areas. Recent advancements in scanner technology toward quantitative radiometry will provide means for attacking more sophisticated problems in geothermal exploration.

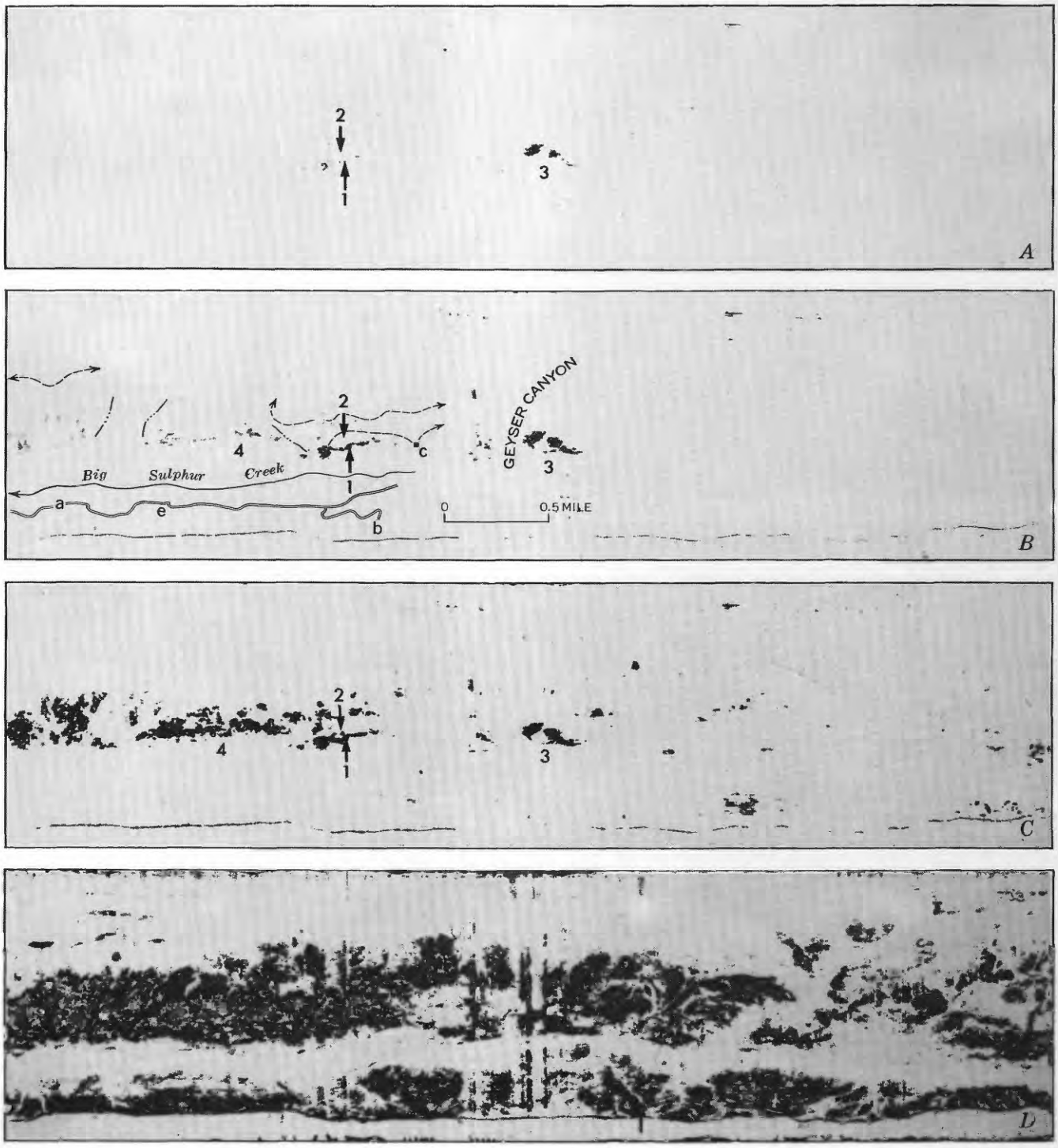

FIGURE 13.—Film-density map of part of figure 8. *A*, density slice showing only maximum densities. Lower densities are added by increments in *B*, *C*, and *D*. Parts *A–C*: *1* and *2*, ground observation stations at Sulphur Banks; *3*, alteration zone at Geyser Canyon; *4*, arcuate pattern west of Sulphur Banks. Part *B*: *a*, Geyser Road; *b*, Healdsburg-Geyser Road; *c*, powerhouse 2; *e*, Eagle Rock. Dashed lines are roads and jeep trails. Segments of stream valleys have been shown where they can be identified. Configuration of Healdsburg-Geyser Road is greatly distorted owing to its location on the edge of the IR image. West is to the left.

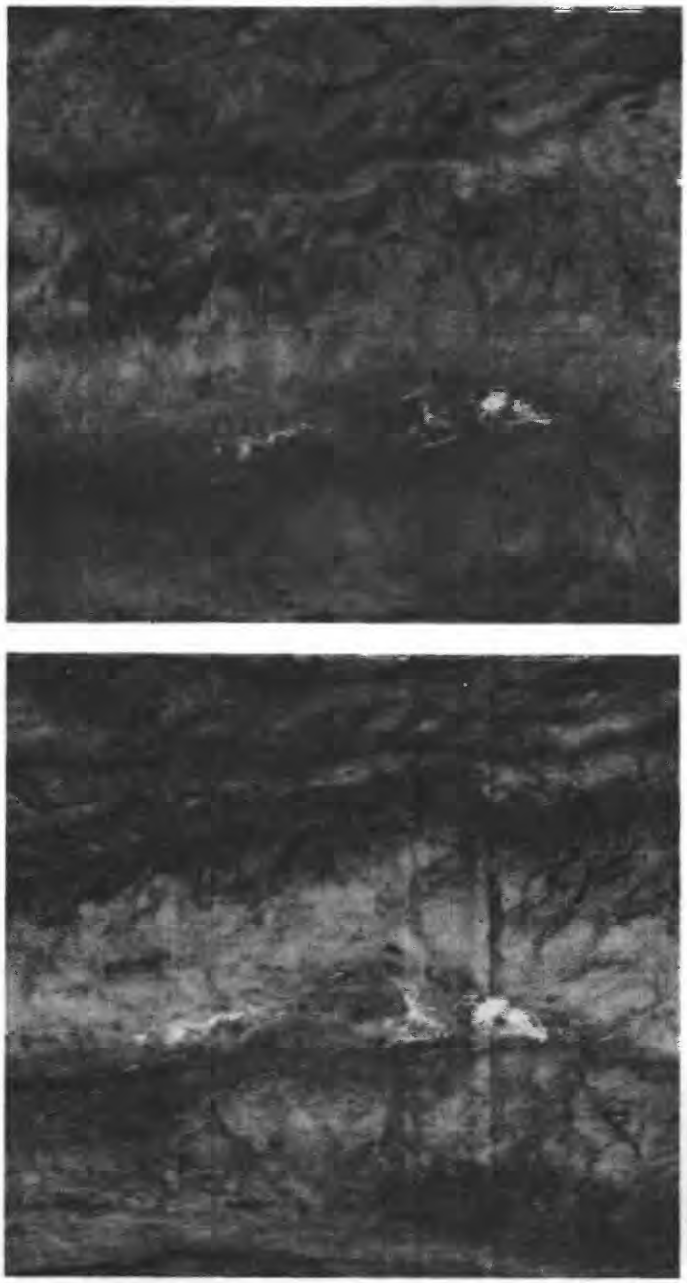

FIGURE 14.—IR images of the Geysers steam field, showing effects of band-pass filter. Top, 8.9–10 μm, 0350 hours PDT, August 18. Bottom, no filter, 0400 hours PDT, August 17.

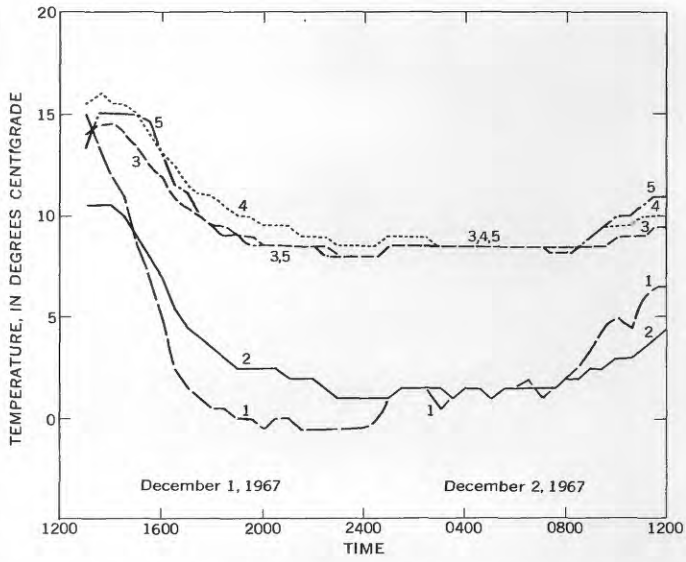

FIGURE 15.—Surface temperatures at station 5 across the fault west of the Sulphur Banks. Each curve, numbered consecutively from the southwest, represents the temperature recorded by one thermistor. The thermistors were placed in a northeast-southwest line at about 50-foot intervals. Curves 1 and 2 represent the two thermistors on the southwest. Only curve 3 is shown where curves 3, 4, and 5 coincide. The weather was clear on December 1st; there was fog and light drizzle on the 2d.

ACKNOWLEDGMENTS

Very competent assistance in the field was rendered by C. R. Fross who operated the infrared scanner, pilots Ray Rote, Howard Chapman, and William Myers, and technicians George Boynton, P. W. Philbin, and R. M. Turner, all of the U.S. Geological Survey.

The author thanks the Thermal Power Co. for many courtesies extended during this study. James Koenig, California Division of Mines and Geology, provided much useful information which is greatly appreciated.

Donald E. White and L. J. Patrick Muffler, of the U.S. Geological Survey, and James R. McNitt, of the California Division of Mines and Geology, reviewed the manuscript. Their constructive comments are gratefully acknowledged.

REFERENCES

Allen, E. T., and Day, A. L., 1927, Steam wells and other thermal activity at "The Geysers" California: Carnegie Inst. Washington pub. 378, 106 p.

Bailey, E. G., 1946, Quicksilver deposits of the western Mayacamas district, Sonoma County, California: California Jour. Mines and Geology, v. 42, no. 3, p. 199–230.

Bruce, A. W., 1964, Experience generating geothermal power at The Geysers powerplant, Sonoma County, California: United Nations Conf. on New Sources of Energy Proc., v. 3, p. 284–296.

English, E. F., 1964, Methods and equipment for harnessing geothermal energy at The Geysers, California: United Nations Conf. on New Sources of Energy Proc., v. 3, p. 142–153.

Hansen, Alf, 1964, Thermal cycles for geothermal sites and turbine installation at The Geysers powerplant, California: United Nations Conf. on New Sources of Energy Proc., v. 3, p. 365–377.

Koenig, J. B., 1968, Field trip guide to The Geysers, Sonoma County, California: California Div. Mines and Geology, 10 p.

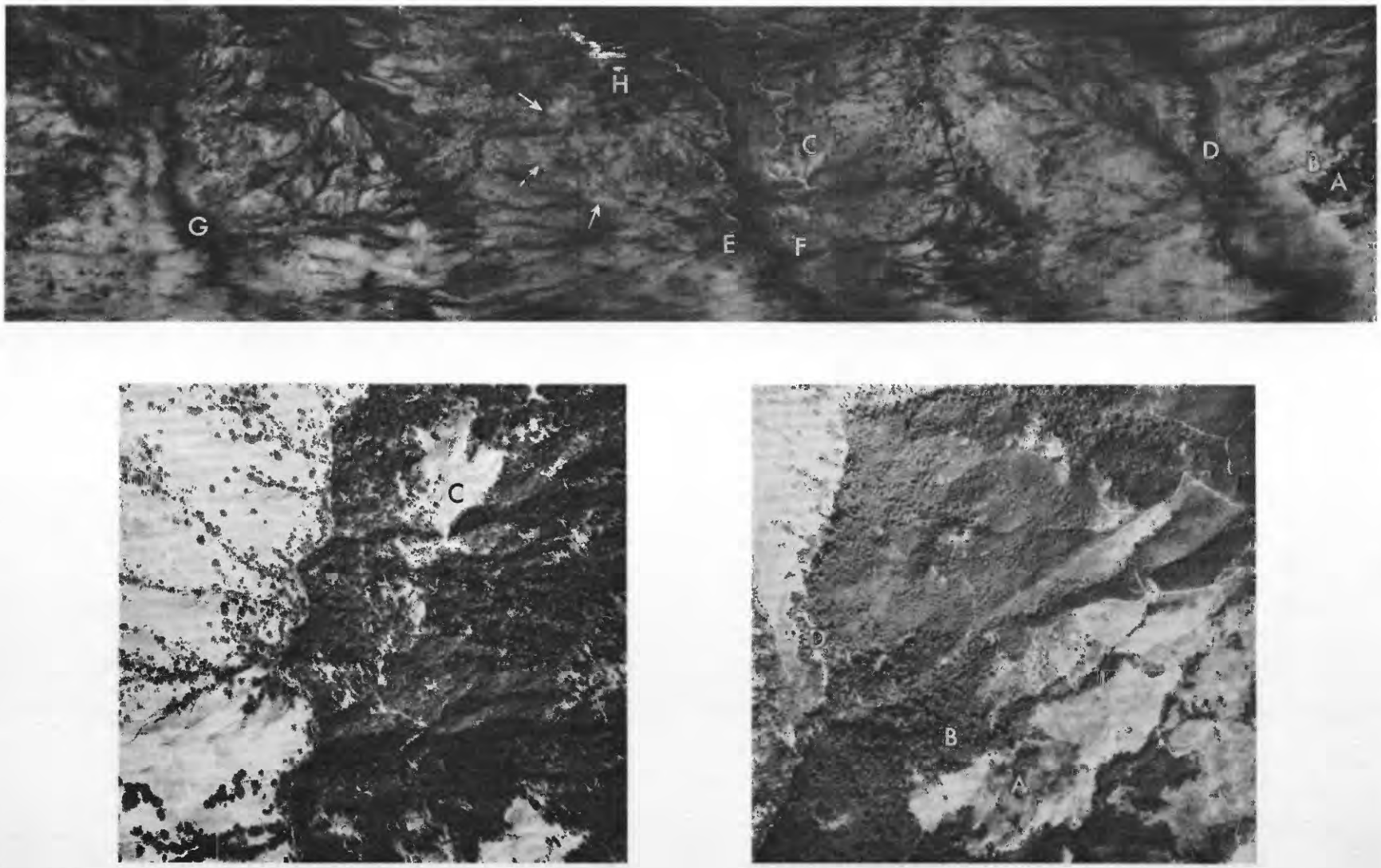

FIGURE 16.—Aerial photographs (bottom) and IR image (top), 0305 hours PDT, August 17 (no filter) across the regional structure. Some apparent contradictions are illustrated. A barren area (*A*) and an adjacent heavily forested area (*B*) west of the north branch of Little Sulphur Creek appear to have radiances reversed from a similar barren area (*C*) and its adjacent heavily forested area on the west slope of Big Sulphur Creek. *D*, North Branch of Little Sulphur Creek; *E*, Big Sulphur Creek; *F*, Geyser Road; *G*, Squaw Creek at the mouth of Coldwater Canyon; *H*, the Sulphur Banks. Arrows indicate position of arcuate radiance feature.

Lowe, D. C., 1968, Line scan devices and why use them: Fifth Remote Sensing Symposium Proc., Ann Arbor, Univ. Michigan, p. 77–101.

McNitt, J. R., 1963 (revised 1965), Exploration and development of geothermal power in California: California Div. Mines and Geology, Spec. Rept. 75, 45 p.

——— 1968, Geology of the Kelseyville quadrangle, California: California Div. Mines and Geology, Map Sheet 9.

Moxham, R. M., 1968, Aerial infrared surveys at The Geysers geothermal steam field, California: U.S. Geol. Survey open-file rept., 25 p.

Moxham, R. M., Greene, G. W., Friedman, J. D., and Gawarecki, S. J., 1968, Infrared imagery and radiometry—Summary report, December 1967: U.S. Geol. Survey open-file rept., 29 p.

A RAPID FILM-DENSITY ANALYZER

By G. R. BOYNTON and R. M. MOXHAM, Washington, D.C.

Work done in cooperation with the National Aeronautics and Space Administration

Abstract.—A commercially available electro-optical scan-type copying machine was modified to permit film-density slicing. The electrical circuit changes allow only densities greater than a selected level to be printed and lesser densities to be rejected. One useful application of the instrument is to relate film density, image gray scale, and terrain radiance in the analysis of images from infrared line scanners.

The output from most of the currently available infrared (IR) line scanners is a film negative whose gray tone (that is, film density) is related to terrain radiance. The relationship more often than not is only semiquantitative. Nevertheless, it is often desirable to compare the density of specific portrayed geologic features by some objective method. For features immediately adjacent to one another on the film, the eye is an excellent device. But where many widely separated targets are involved, an analytical machine is needed.

Experience with two commercial density analyzers, the Joyce-Loebl microdensitometer-isodensitracer and the Tech/Ops Image Quantizer, has been previously described (Turner and Boynton, 1968). Both of these instruments permit contouring of film density. For many film-density problems, we felt that a film-density slicing technique would be more useful than contouring. In film-density slicing, each density increment is portrayed separately, often yielding a less ambiguous presentation than a contour map.

For this purpose, we modified a Gestefax Model 451 electronic scanning machine originally designed primarily for conventional business-office use. In using this machine, the document to be copied (which we will hereafter refer to as the specimen) and the electrosensitive reproduction paper are placed side by side on a metal drum. A light beam scans the specimen as the drum rotates. The instantaneous amplitude of the reflected light beam is a function of the specimen's reflectivity at a given location. The reflected beam passes through a focusing lens and 0.005-inch (0.127 mm) aperture to a photocell, and a proportional voltage is fed to a spark stylus that traces a fine line on the copy paper. The instantaneous stylus voltage governs the "blackness" of the line at a given spot. The photocell and stylus are mechanically linked and are translated laterally at a rate adjustable to yield 200, 400, or 600 scan lines per inch (7.9, 15.7, or 23.6 lines per mm).

In conventional operation of this machine, an 18-kilohertz oscillator is modulated by the output of the photomultiplier tube. The modulated 18-kHz signal is amplified and fed through the tone contrast control (fig. 1). This control provides a d-c level that governs the minimum signal amplitude which will be passed to the next stage. The tone contrast control is used to eliminate undesired background tones. All signals passing the tone contrast control are fed to an amplifier whose gain is governed by the film-density control, thereby providing an adjustment of the gray scale of the reproduction. It is evident from figure 1 that at the amplifier output each signal has an amplitude proportional to the input signal amplitude. Thus, several shades of gray are reproduced on the printout.

Acknowledgments.—The authors are grateful to Gordon W. Greene and Howard A. Pohn for critical review of the manuscript.

MODIFICATIONS

Mechanical

We attempted to use paper prints of IR film in the reflection mode to avoid any mechanical or optical modifications. Unfortunately, the reflected light intensity was insufficient, but we found that an adequate signal could be attained by transmitting the light beam through a film negative or positive. To use the transmission mode, it was necessary to provide a transparent

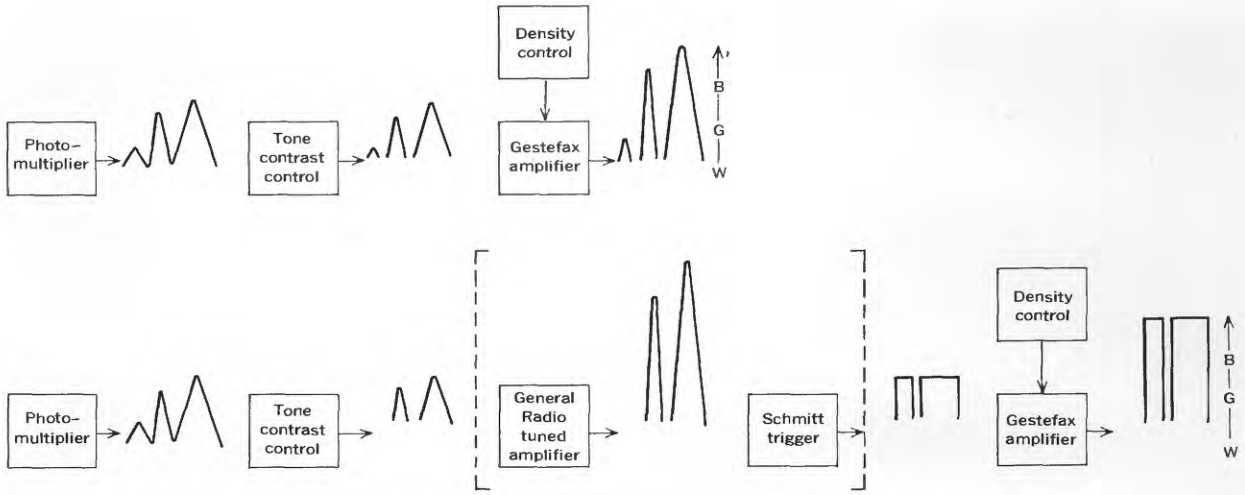

FIGURE 1.—Schematic diagram showing waveforms (modulation envelope of 18-kHz carrier) of unmodified (top) and modified (bottom) circuits. Components added in circuit modification are enclosed by dashed brackets. W–G–B, white-gray-black scale.

scanning drum and to relocate the optics. The outer face of the drum pulley was first trued on a lathe. An aluminum adapter was fabricated to form a support for the new scanning drum. The scanning drum was made of cast Lucite in the form of a cylinder 6 in. long and 5 in. O.D. with $\frac{3}{16}$ in. wall thickness. The 6 in. cylinder length is adequate for 70-mm film and an accompanying density step tablet. The Lucite drum was press fitted and expoxied to the aluminum adapter, and the entire drum assembly bolted to the trued pulley face. A heavy aluminum bar was bolted to the scanning carriage to extend the photomultiplier to the new scanning drum. (The end housing was cut out to accommodate the new components.)

One of the original light sources was relocated inside the scanning drum with the bulb filament fixed about ½ inch from the drum's inside surface. The projection optics were eliminated. The modified instrument is shown in figure 2.

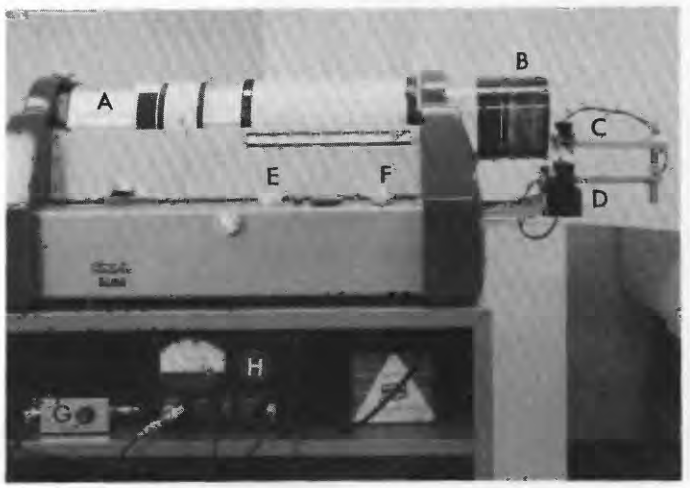

FIGURE 2.—The modified Gestefax electronic scanning machine. *A*, reproduction drum; *B*, specimen drum; *C*, light source; *D*, photomultiplier housing; *E*, contrast control; *F*, density control; *G*, Schmitt trigger; *H*, tuned logarithmic amplifier. *D* is attached to the new carriage extension bar. In this view, the carriage has been extended beyond its normal limit to show *C* and *D*.

Electrical

To achieve density slicing, it is necessary to control the electronics in such a way that all signals less than a selected level will be rejected, and all the remainder be printed. The output should be either black or white, with gray eliminated. This was accomplished by inserting a Schmitt trigger (fig. 3) after the tone contrast control. The trigger "fires" when the input voltage exceeds a specific value, and continues to fire until the input voltage drops below that value. The trigger must have zero hysteresis, that is, the same signal amplitude be required to turn on the trigger as to turn it off. The integrated circuit RCA CA–3001 was selected for this reason. In the circuitry shown, the firing level is about 3.2 volts.

The tone contrast control in the modified circuit determines the signal threshold for the Schmitt trigger. It was found that the output from T2 at low signal levels was insufficient to fire the Schmitt trigger. Consequently, a General Radio Co. tuned logarithmic amplifier was inserted to boost the low-level signals.

The Gestefax service manual discusses some additional modifications which we followed. These refer to the tone contrast control. Two resistors were changed; R10 was increased to 4.6K and R11 decreased to 11.9K, to increase the tone contrast. C22, a coupling condenser between V2A and V2B, was increased 200 picofarads to increase the signal amplitude.

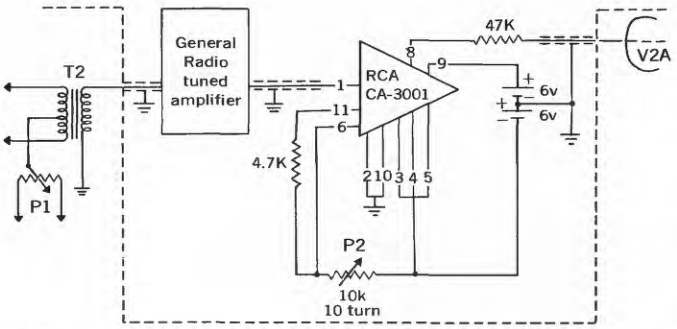

FIGURE 3.—Schematic diagram of electronic modifications. T2 and V2A are components of the Gestefax circuit. The output of T2 originally fed directly to the grid of V2A through a grid resistor. The tuned amplifier and Schmitt trigger replace the grid resistor. P1, tone contrast control; P2, Schmitt trigger firing-level control.

OPERATING PROCEDURES

The zero hysteresis point of the RCA CA–3001 is determined with a two-channel oscilloscope connected to the trigger input and output. A film-density wedge is placed on the specimen drum and the Schmitt trigger potentiometer (P2) is adjusted so that the trigger on-and-off occurs at the same density level when the density wedge is very slowly moved back and forth by hand. When the proper potentiometer setting is achieved, it should not be adjusted further.

It is useful to place a density step tablet permanently on the specimen drum so that on each run the density-level setting will be printed on the duplicating paper. Calibrated density step tablets are available from the major photo suppliers. We use a 21-step tablet ranging in density from 0.05 to 3.0. In order to identify the density values on the recording, we labeled each step with opaque ink.

It probably would be advisable to focus the optical system on a transparent film-resolution target, with emulsion toward the drum, and, subsequently, to run all specimens with emulsion toward the drum.

The following procedure has been used for this modified instrument:

1. Insert recording paper, place a calibrated density step tablet on the specimen drum, and turn on machine.
2. Set tone control to maximum and density control to about midrange.
3. Set tuned amplifier to logarithmic mode, 18 kHz, and minimum gain. Increase gain until printing meter flickers, indicating that a signal is present at the stylus.
4. The recording will now show the maximum density level which can be defined. All densities above this level will be printed.
5. Adjust density control to achieve desired "blackness."
6. Density slicing can now proceed, reducing the tone contrast control to reduce the threshold density level as desired.

RESULTS

The printout of an IR film negative will be a negative, in the sense that the maximum IR-negative densities correspond to maximum printed densities. Hotspots on the image will print black on high-density slices. If a film-positive specimen is used, this relationship will be reversed.

The results obtained by density slicing an IR negative (fig. 4) are shown in figure 5 (p. C126).

Experiments with the density step tablet and a resolution target indicate that density increments on the order of 0.04 can be achieved and that the resolution is on the order of five lines per millimeter.

REFERENCE

Turner, R. M., and Boynton, G. R., 1968, Film density analyzers for infrared investigations: U.S. Geol. Survey open-file report, 10 p.

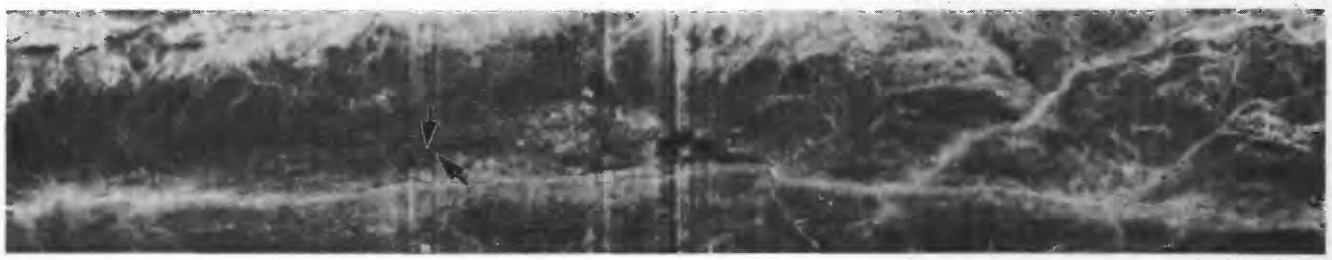

FIGURE 4.—Infrared image of the Geysers geothermal stream field, California. This is a negative print; black indicates high radiance, and white indicates low radiance. On the original negative, sliced as shown in figure 5, highest film densities (highest terrain radiance) correspond to the blackest spots shown here. Approximate scale is 1 inch=2,440 feet. The arrows are reference points explained in figure 5.

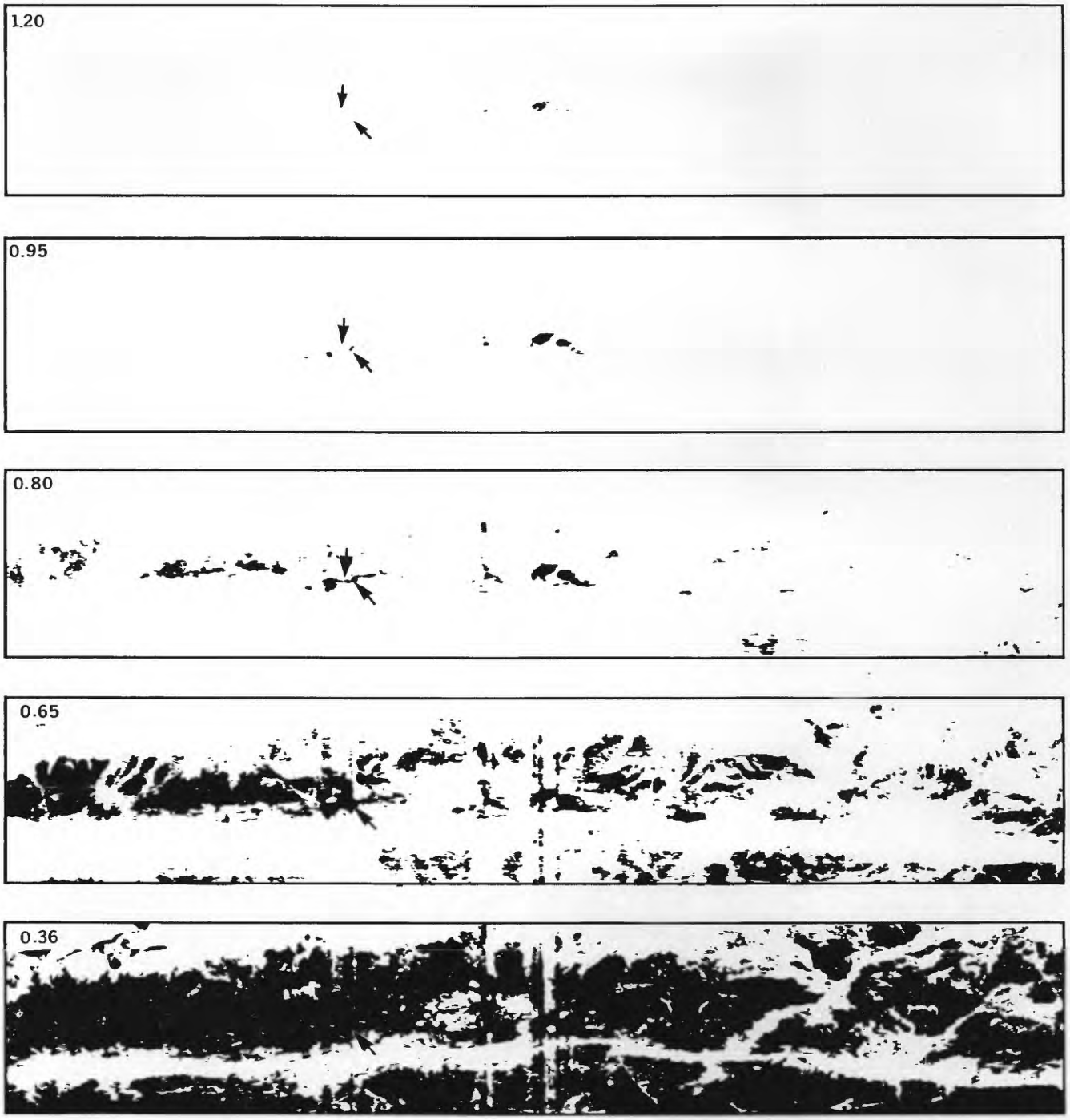

FIGURE 5.—Density slices of figure 4 made from the original film negative. For a given slice, those areas of the film having a density greater than the selected value (shown in upper left corner) are printed in black. Areas of lesser density have been eliminated. Arrows were fixed on the original negative so that their location is identical on each slice.

SOME RELATIONS BETWEEN STRESS, GEOLOGIC STRUCTURE, AND UNDERGROUND EXCAVATION IN A METAMORPHIC ROCK MASS WEST OF DENVER, COLORADO

By FITZHUGH T. LEE, THOMAS C. NICHOLS, JR., and JOHN F. ABEL, JR., Denver, Colo.

Abstract.—Field testing of a solid-inclusion probe that determines three-dimensional stress changes at one location in a borehole in a rock mass began in December 1966. Since then, 19 probes have been installed underground at two locations in the Front Range west of Denver. The stability of the probes and the reliability of the measurements have been good. Evaluation of results from the probes shows that major geologic structures such as faults, foliation, and conspicuous joint sets are major influences upon the redistribution of stresses around an actively excavated opening. The mining operations and preexcavation rock stresses also influence the redistribution of stresses, but usually not in a manner that can be explained by a simple elastic analysis. Anomalously high stresses are shown to be associated with local or regional geologic structures. The results of the investigation suggest that the high stresses are produced by the activation, through excavation, of strain energy that may have been stored in the rock by Laramide tectonic forces.

The accuracy with which the behavior of a large mass of rock can be forecast is increasingly important in determining the economic feasibility of large, costly, subsurface excavations. The exactness of predictions of underground support requirements, for example, is controlled by the accuracy and applicability of information concerning behavior of the rock mass. The relation between the geologic environment and the in-place stress conditions should be determined before an excavation is started. Also of concern are changes in the state of stress around an active underground opening and the influence of geological conditions—and associated stress fields—on excavating operations. Because rocks can store large amounts of energy at shallow depths for long periods of time, simple (elastic) overburden pressure calculations may yield grossly erroneous estimates of stress.

Many tools and techniques are available for studying subsurface rock behavior. However, a bonded solid-inclusion borehole instrument that determines three-dimensional stress changes approximately at a point in a rock mass should be one of the most useful tools to analyze the interactions among the in-place stress field, the geology, and the excavation. Such a borehole probe has been designed, fabricated, and tested in the laboratory and field by the U.S. Geological Survey as part of an applied rock-mechanics research project (Nichols and others, 1968). This report presents preliminary findings based on data from two of the borehole probes that were emplaced in a mass of metamorphic rock.

Acknowledgments.—We express our appreciation to the Department of Mining Engineering, Colorado School of Mines, for the use of their underground facilities at Idaho Springs, Colo. We are grateful for the comments of D. J. Varnes, U.S. Geological Survey, which contributed to our understanding of stress in rocks.

CAPABILITIES OF THE PROBE

The three-dimensional solid-inclusion borehole probe has been described and laboratory test results have been reported previously (Nichols and others, 1968). The instrument has been shown, on the basis of laboratory tests and the successful underground installation of 19 probes, to have the following desirable features:

1. Three-dimensional stress changes taking place in a stress field can be determined approximately at a point in one borehole. The absolute stress state at one location can be obtained in most rock by overcoring.
2. Long-term monitoring indicates that there is no creep of probe materials.
3. Instrument sensitivity can be increased or decreased by varying the elastic modulus of the sensing element, potentially extending its use to soft rocks and soils.

U.S. GEOL. SURVEY PROF. PAPER 650–C, PAGES C127–C132

4. The probe can be installed in a borehole that is wet or dry and at any inclination; borehole wall is better rough than smooth.
5. Dynamic strain changes having a frequency range of 0–20 kilocycles per second can be measured by continuously monitoring the gage output.

FIELD INSTALLATION

The probe as described by Nichols, Abel, and Lee (1968) was designed initially for laboratory experimentation. In order to extend its use to field locations, the instrument was encapsulated with epoxy, increasing the length and diameter so that it would fit properly in a 3-inch (NX) borehole. Figure 1 shows the field borehole probe and switching unit and the emplacement apparatus. The construction of the field probe is such that the stress-carrying epoxy member extends 7 inches each way from the center of the probe, eliminating end effects near the sensing element and affording proper (effectively infinite) confinement for the sensing element. Probe design is also intended to reduce or average out the effect of anisotropic rock stiffness variations that are caused, for example, by minor fractures across a borehole. Neoprene packers are installed at both ends of the probe to center the sensing element in the borehole and to contain the epoxy grout mixture until it sets. A square aluminum adapter bar is mounted on the end of the probe to facilitate orientation and to permit a positive coupling with the emplacement apparatus. The switching unit facilitates the readout of many gage wires and eliminates electrical resistance changes caused by repeated wire-to-terminal connections. The compensating (dummy) probe eliminates the effects of temperature-induced strain so that

FIGURE 1.—Field borehole probe with associated equipment, as described in text.

only changes in mechanical strain are measured. Emplacement rods have wedge-and-groove couplings so that the desired probe position can be maintained during installation. The transfer cylinder is used to hold the epoxy grout, the end plug, and the piston. The hand pump is used to supply compressed air. The epoxy grout in the cylinder is forced out by the piston through the short lengths of clear vinyl tubing (shown in center of fig. 1) and around the probe. After the grout is pumped into the borehole, the cylinder and rods are withdrawn. Grout hardening time is from 2 to 4 days, depending on grout composition and borehole temperatures.

FIELD RESULTS

The field experiments reported here were made at the Colorado School of Mines experimental mine at Idaho Springs, Colo.—28 miles west of Denver in the Front Range of the Rocky Mountains (fig. 2). The Precambrian regional geology of the mine has been

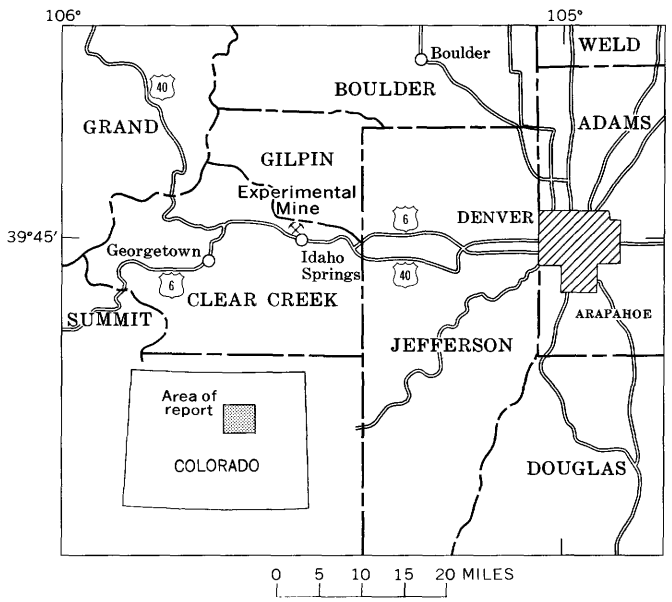

FIGURE 2.—Index map showing location of Colorado School of Mines experimental mine at Idaho Springs, Colo.

described by several writers. Structural geology and rock units were reported by Moench (1964), joint patterns by Harrison and Moench (1961), wallrock alteration by Tooker (1963), general economic geology by Moench and Drake (1966), and uranium deposits by Sims, Sheridan, King, Moore, Richter, and Schlottman (1964). Tertiary intrusive rocks were described by Wells (1960). The mine is in a generally conformable sequence of folded metasedimentary gneisses and metaigneous and igneous rocks of Precambrian age (Harrison and Moench, 1961). Most of the gneissic rocks were probably clastic sedimentary rocks that were deformed, recrystallized, and partly reconstituted at considerable depth and at high temperatures (Moench, 1964). The metaigneous and igneous rocks were intruded during Precambrian time—but are younger than the metasedimentary gneisses—and include granodiorite, quartz diorite, and biotite-muscovite granite.

The stress measurements were made at the site of a recent excavation of a room in the experimental mine (fig. 3). In this part of the mine most of the rock is biotite gneiss and granite or gneissic granite with lesser

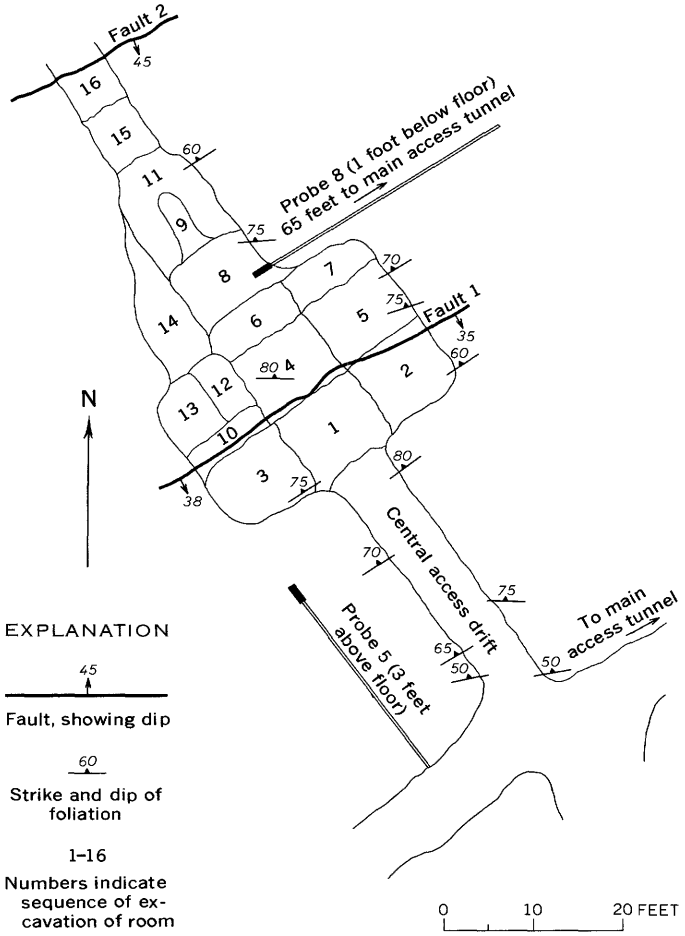

FIGURE 3.—Map of room in Colorado School of Mines experimental mine at Idaho Springs, showing major geologic structures, locations of probes, and mining sequence.

amounts of amphibolite and pegmatitic granite. Major joints, which have an average spacing of 0.5 foot, parallel the uniformly steeply dipping east-northeast-trending foliation. Two subparallel faults that trend northeast and dip to the southeast pass through the mapped area (fig. 3). The southernmost fault (fault 1) has as much as 0.1 foot of associated gouge and as much as 4 feet of moderately sheared mineralized rock. The northernmost fault (fault 2) has 0.05–0.4 foot of gouge

and is bordered by as much as 12 feet of sheared and altered rock—mainly in the hanging wall. Both faults are exposed in two mine openings that are as much as 100 feet apart, and the faults show little change in attitude from one of these exposures to the other. Thus, although these faults are relatively narrow, the discontinuities formed within the rock mass by them are through-going features that cut the foliation at nearly right angles.

Numbers within the small areas in figure 3 indicate the actual excavation sequence within the room, which was changed several times from the original plan. Two borehole probes were installed in the locations shown on figure 3—probe 5 in the southwest wall of the future room, approximately 3 feet above floor level; and probe 8 in the northeast wall, approximately 1 foot below floor level. Both installations were completed before room excavation began. The room—excavated for rock-bolt performance studies—was to have been 24 by 40 feet and unsupported. The overburden in this part of the mine is approximately 300 feet thick.

The relation of the hanging wall of fault 1 (containing probe 5) and the footwall (containing probe 8) to foliation is shown in figure 4. Excavation proceeded from left to right (southeast to northwest) beginning in the hanging wall of fault 1. When mining intersected the fault surface, rapid vertical decompression (that is, relative tension) occurred around probe 8. At the same time, probe 5 experienced moderate compression (a typical wall situation). A large decompression on probe 8 (fig. 5) coincided with the largest displacement on the fault as measured by a borehole extensometer located in the roof of the room and penetrating the fault surface. During this period, slabbing of rock from the roof and wall around probe 8 became serious and necessitated changes in the mining sequence. Remedial rock bolts and wire mesh were installed in the roof and east wall of the room but they were only partly effective in stabilizing the adjacent rock. Despite changes in the sequence and timing of excavation the room could not be completed as planned. The rock bolting and renewed central drift excavation (fig. 3) profoundly influenced the behavior of the stress field around probe 8 as shown on figure 5. The load-carrying ability of the rock was effectively increased by 3,100 pounds per square inch in compression in the rock (fig. 5). The rock bolts were probably too far away from probe 5 to noticeably affect the behavior of the rock there, and the rock gradually decompressed and expanded toward the opening.

When the central drift intersected fault 2, the largest recorded decompression was produced around probe 8 (fig. 5). Because of the difficulty presented by fault 1, it

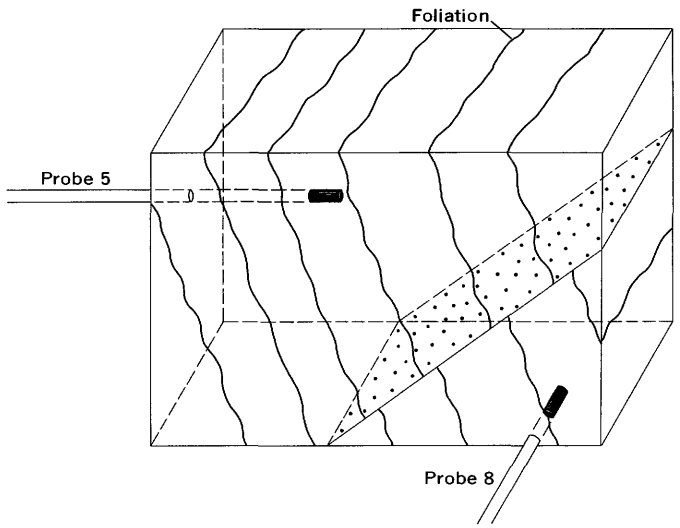

FIGURE 4.—Generalized diagram (facing west) showing relation of foliation and hanging wall and footwall of fault 1 (stippled) to probes 5 and 8.

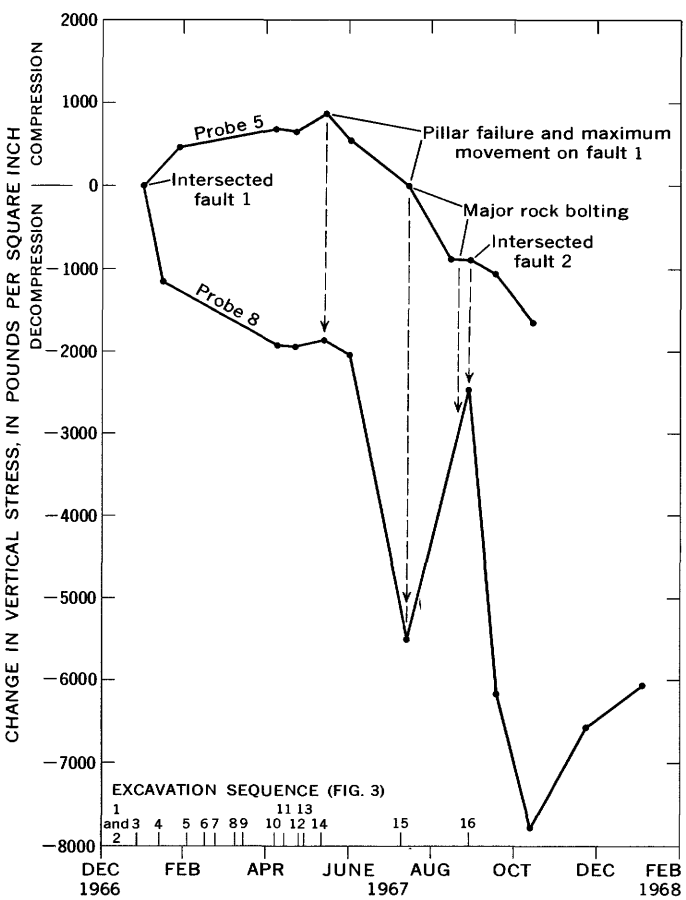

FIGURE 5.—Vertical normal stress changes in rock adjacent to probes 5 and 8 as excavation advanced. Each point represents several readings. Some data points have been removed for clarity.

is probably fortunate that the central drift was not widened near this fault.

Three-dimensional analysis generally is necessary for adequate evaluation of probe data. This can be done in several ways; one method uses the equal-area lower hemisphere projection which combines geologic data and stress-orientation data on one diagram. Figure 6

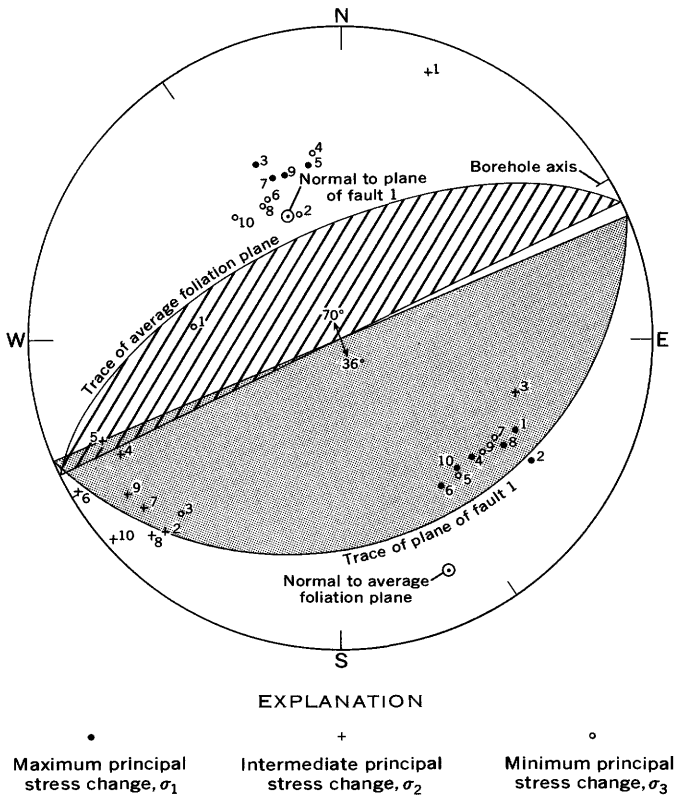

FIGURE 6.—Equal-area diagram (lower hemisphere) of poles of principal stress changes, as determined from probe 8. Shown are 10 readings taken over a 2-week period, beginning when mining intersected fault 1 (fig. 5).

shows the traces of the plane of fault 1 and the average foliation plane in the same vicinity, the poles of the fault, and foliation-plane normals. In such a diagram horizontal linear elements plot on the circumference of the circle and vertical linear elements plot at the center of the circle. The other poles on the figure represent 10 principal stress changes at probe 8 obtained from daily measurements over a 2-week period, beginning at the time mining intersected fault 1. The attitudes of the three principal stress-change vectors are shown by the indicated symbols. The data show that the intermediate principal stress-change vectors are oriented consistently nearly horizontally in a plane parallel to the fault and bear to the southwest, nearly at right angles to the dip of the fault and foliation planes. Both the maximum and the minimum principal stress-change vectors are oriented either approximately in the plane of the fault or approximately parallel to the fault normal. The poles of the maximum and minimum stress-change vectors exchange positions from time to time, as shown by their alternations in readings 4 through 10, figure 6. Later measurements (not on the figure) showed that the poles in the north half of the diagram migrated with time to form a maximum at the fault normal. All poles in the southeast sector (on or near the fault plane) represent the greatest absolute stress changes—changes of either maximum compression or maximum decompression. This indicates that, as excavation in the footwall continued, the rocks bordering the fault were expending strain energy—rebounding—in a series of contractions and dilations having an almost daily periodicity. These incremental stress changes, triggered in response to penetration of mining into fault 1, occurred in the initial 2-week period (fig. 5). Therefore, it appears that movement on the fault was gradually allowing stored (potential) energy to be expended, as indicated by the overall decompression in the rock around probe 8 during this 2-week period.

CONCLUSIONS

The fact that smaller stress changes were measured in the hanging wall (probe 5) of fault 1 than in the footwall (probe 8) suggests that the rock above the fault was able to store less strain energy than the rock below the fault. This interpretation is supported by the results of probe overcoring—a method that permits the total stresses acting at the probe location to be determined. For the overcoring, an additional probe was installed in the hanging wall and another in the footwall of fault 1. The maximum principal stress acting in the footwall was found to be three times greater in compression than the hanging-wall stress. When this strain energy was stored in the rock is uncertain. However, faults 1 and 2 are similar to others elsewhere in the Front Range that are interpreted to be of Laramide age (50–100 million years). For example, Tweto and Sims (1963, p. 998) believe that typical Laramide features—gouge, brecciation, and brittle (open) fractures—are products of a shallow environment, with relatively low temperature and pressure, whereas the Precambrian tectonic features—cataclasis, granulation, and mylonitization—were formed at considerable depth in an environment of relatively intense pressure and, in some cases, elevated temperature.

Although there are numerous previously published reports of abnormally high underground stresses at different places in the world (for example, Coates and Grant, 1966; Hast, 1967; Olsen, 1957) the possibility of past tectonic events influencing the presently exist-

ing stress field has not been thoroughly explored. We believe that rock may be capable of retaining strain energy, possibly related to an ancient tectonic episode, which is "mobilized" by mining or overcoring. Rather than storing a record of all previous episodes of deformation, the strain "memory" of the rock near fault 1 is probably associated with only the most recent tectonic episode—the Laramide orogeny.

The variation of stress magnitudes partly independent of the weight of the overlying rock has caused perplexing problems of rock behavior in shallow as well as deep underground excavations. Localized tectonic strain energy stored in rock for long periods of time at relatively high magnitudes and at shallow depths and independent of the potential energy derived from the overlying rock may explain some of the problems encountered during many mining and civil construction projects.

REFERENCES

Coates, D. F., and Grant, F., 1966, Stress measurements at Elliot Lake: Canadian Inst. Mining and Metallurgy Trans., v. 69, p. 182–192.

Harrison, J. E., and Moench, R. H., 1961, Joints in Precambrian rocks, Central City-Idaho Springs area, Colorado: U.S. Geol. Survey Prof. Paper 374–B, p. B1–B14.

Hast, Nils, 1967, The state of stresses in the upper part of the earth's crust: Eng. Geology—Internat. Jour., v. 2, no. 1, p. 5–17.

Moench, R. H., 1964, Geology of Precambrian rocks, Idaho Springs district, Colorado: U.S. Geol. Survey Bull. 1182–A, p. A1–A70 [1965].

Moench, R. H., and Drake, A. A., Jr., 1966, Economic geology of the Idaho Springs district, Clear Creek and Gilpin Counties, Colorado: U.S. Geol. Survey Bull. 1208, 91 p.

Nichols, T. C., Jr., Abel, J. F., Jr., and Lee, F. T., 1968, A solid-inclusion borehole probe to determine three-dimensional stress changes at a point in a rock mass: U.S. Geol. Survey Bull. 1258–C, p. C1–C28.

Olsen, O. J., 1957, Measurement of residual stress by the strain relief method: Colorado School Mines Quart., v. 52, no. 3, p. 183–204.

Sims, P. K., Sheridan, D. M., King, R. U., Moore, F. B., Richter, D. H., and Schlottman, J. D., 1964, Geology of the uranium deposits in the Front Range, Colorado: U.S. Geol. Survey Bull. 1159, 116 p.

Tooker, E. W., 1963, Altered wallrocks in the central part of the Front Range mineral belt, Gilpin and Clear Creek Counties, Colorado: U.S. Geol. Survey Prof. Paper 439, 102 p.

Tweto, Ogden, and Sims, P. K., 1963, Precambrian ancestry of the Colorado mineral belt: Geol. Soc. America Bull., v. 74, no. 8, p. 991–1014.

Wells, J. D., 1960, Petrography of radioactive Tertiary igneous rocks, Front Range mineral belt, Colorado: U.S. Geol. Survey Bull. 1032–E, p. 223–272 [1961].

Sr^{87}/Sr^{86} VARIATIONS WITHIN INDIVIDUAL ASH-FLOW SHEETS

By DONALD C. NOBLE[1] and CARL E. HEDGE, Cambridge, Mass., Denver, Colo.

Work done in part in cooperation with the U.S. Atomic Energy Commission

Abstract.—Vertical changes in initial strontium isotope composition within each of five upper Cenozoic ash-flow sheets of the Great Basin, U.S.A., indicate that the parent magmas were isotopically zoned prior to eruption. Such zonation, which cannot have resulted from differentiation, probably can be explained by the incorporation of radiogenic sialic material by the upper parts of less radiogenic magmas as they ascended through the earth's crust.

Initial Sr^{87}/Sr^{86} ratios have been determined on whole-rock material and (or) feldspar separates from both the upper and the lower parts of five upper Cenozoic ash-flow sheets (table 1) as part of a general isotopic study of Tertiary volcanic rocks in the southern Great Basin, U.S.A. (Hedge and Noble, 1967). Four of the sheets belong to the Miocene Paintbrush and Pliocene Timber Mountain Tuffs (Byers and others, 1968; Orkild, 1965), which crop out mainly within southern Nye County, Nev.; the fifth is the Pleistocene Bishop Tuff of east-central California (Gilbert, 1938).

We wish to thank P. W. Lipman and Robert L. Christiansen, who provided a number of the specimens used in the study.

GEOLOGIC RELATIONS

Each sheet is composed of many individual ash flows. Vertical variations in the degree of welding and in the character and distribution of zones of glassy, primarily devitrified, and vapor-phase altered tuff show that in each sheet the successive ash flows were deposited while underlying flows were still hot. Abnormalities in welding and crystallization zonation are present in most sections; these indicate brief depositional hiatuses and (or) differences in emplacement temperature between successive flows, but they are never of such magnitude that each sheet cannot everywhere be described in terms of a single cooling unit (Smith, 1960).

With the exception of the Bishop Tuff, all the sheets show a pronounced vertical zonation from rhyolite at the base to quartz latite at the top (table 2, fig. 1) (Byers and others, 1968; Lipman and others, 1966; Lipman, 1966). Within a given sheet the quartz latitic tuffs contain larger and more abundant phenocrysts than do the underlying rhyolitic tuffs. The quartz latites also have a higher proportion of mafic to felsic phenocrysts and, except for the Topopah Spring Member of the Paintbrush Tuff, a higher ratio of plagioclase to both quartz and sanidine. Numerous published (Lipman and others, 1966; Lipman, 1966) and unpublished (F. M. Byers, Jr.) chemical analyses show that the groundmass materials of the quartz latites are markedly less silicic and contain greater amounts of aluminum, iron, mangnesium, calcium, strontium, titanium, manganese, and phosphorus than do the groundmass materials of the rhyolitic rocks (tables 1, 2). In the Paintbrush sheets the transition from rhyolite to quartz latite tuff is more rapid than in the Timber Mountain sheets—taking place within several tens of feet. Although the Bishop Tuff is not obviously compositionally zoned, some vertical zonation is suggested by the difference in the strontium contents of the two sanidine separates and by a possible slight increase in total phenocryst content toward the top of the unit (Sheridan, 1965).

There seems to be general agreement that vertical compositional variations such as are seen within the several Paintbrush and Timber Mountain ash-flow sheets reflect vertical compositional zonation that existed within the parent magma (Williams, 1942; Ratté and Steven, 1964; Quinlivan and Lipman, 1965; Ewart, 1965; Martin, 1965; Smith and Bailey, 1966; Fisher, 1966; Lipman and others, 1966; Lipman, 1967; Noble and others, 1968; Giles and Cruft, 1968; Byers and others, 1968). The rapidity of eruption and the immense volumes of the tuff units (table 1), as well as the sys-

[1] Department of Geological Sciences, Harvard University.

TABLE 1.—*Analytical data on whole-rock and phenocryst samples from vertically zoned ash-flow tuff sheets*

[U, upper part of sheet; L, lower part of sheet; WR, whole rock; S, sanidine; F, sanidine, sodic plagioclase, and quartz; G, groundmass composition. Subscript $_o$ indicates isotopic ratio; subscript $_i$ indicates calculated isotopic ratio at time of eruption. Ages based on K-Ar determinations by R. W. Kistler (1968), J. D. Obradovich and H. H. Mehnert, of the U.S. Geological Survey, and data from Dalrymple and others (1965). Original volumes of the members of the Timber Mountain and Paintbrush Tuffs from P. P. Orkild (oral comm., 1966)]

Specimen No.	Material analyzed	Rb (ppm)	Sr (ppm)	Sr^{87}/Sr^{86}_o	Sr^{87}/Sr^{86}_i	$\pm(2\sigma)$	Weight percentage SiO_2 (whole rock)
TIMBER MOUNTAIN TUFF							
Ammonia Tanks Member, age 11 m.y., minimum original volume 200 cu miles							
63L–41C (U)	WR	116	293	0.7080	0.7078	0.0005	68.5
SCN–3–1B (L)	S	62.1	17.9	.7167	.7151	.0008	77.0
Rainier Mesa Member, age 11.3 m.y., minimum original volume 300 cu miles							
RM–4600 (U)	WR	102	295	0.7067	0.7065	0.0005	70.5
SJW–6 (L)	F	120	58.7	.7139	.7129	.0006	76.5±1.5
TP–TRL (L)	WR	149	51.3	.7127	.7113	.0006	76.5±1.5
PAINTBRUSH TUFF							
Tiva Canyon Member, age 12.4 m.y., minimum original volume 50 cu miles							
AGE–4 (U)	WR	127	120	0.7075	0.7070	0.0006	70.5
62L–50X (U)	WR	79.8	290	.7084	.7082	.0005	70.5±2
	F	31.0	645	.7088	.7088	.0005	7.5±2
	G				[1].7080		70.5±2
63L–110 (L)	S	55.7	142	.7135	.7133	.0005	76.0
Pah Canyon Member, minimum original volume <5 cu miles							
63L–50I	F	48.1	751	0.7101	0.7101	0.0005	70.0±1.5
Topopah Spring Member, age 13.2 m.y., minimum original volume 70 cu miles							
AGE–2 (U)	WR	112	143	0.7107	0.7103	0.0005	69.0
63L–17C (U)	WR	140	72.9	.7122	.7112	.0006	71.5
	F			.7129	.7128	.0008	71.5
	G				[2].7110		71.5
SC–1B (L)	WR (G) [3]	195	22.7	.7160	.7113	.0010	76.5
63L–17H [4] (L)	WR (G) [3]	194	21.2	.7179	.7128	.0010	77.5
63L–17I [4] (L)	F	56.8	262	.7166	.7165	.0005	77.5
BISHOP TUFF							
Age 0.7 m.y., minimum original volume 50 cu miles							
UB–1 (U)	S	107	150	0.7061	0.7061	0.0005	76.5±1.5
LB–1 (L)	S	117	24.3	.7078	.7075	.0005	77.0±1.5

[1] Calculated from modal data, assuming an average strontium content of the phenocryst fraction of 700 ppm.
[2] Calculated from modal data, assuming an average strontium content of the phenocryst fraction of 400 ppm.
[3] Phenocrysts make up less than 2 percent of these rocks, and groundmass Sr^{87}/Sr^{86} thus is effectively equal to that of the rock.
[4] Specimens are from the same ash flow and were collected from localities only several feet apart.

tematic nature of the vertical zonation and, in the Timber Mountain and Bishop Tuffs, the nature of the collapse calderas which formed during or immediately after eruption (Christiansen and others, 1965; Pakiser and others, 1964), strongly suggest that each sheet was erupted from a single geometrically simple magma chamber located high in the earth's crust. For the reason that magma from near the top of such a high-level magma chamber would tend to be erupted and deposited before magma located near the bottom of the chamber, a vertical section through an ash-flow sheet would thus provide an inverted sample—albeit one more or less homogenized by mixing during eruption and turbulent lateral movement of the ash flows—of the magma as it existed at various depths within the chamber immediately prior to eruption.

METHODS OF ANALYSIS

Strontium isotopic measurements were made on a 6-inch solid-source mass spectrometer utilizing a triple filament mode of ionization. Sr^{87}/Sr^{86} values were normalized to correspond to a Sr^{86}/Sr^{88} value of 0.1194. The Sr^{87}/Sr^{86} ratio of the M.I.T. Eimer and Amend

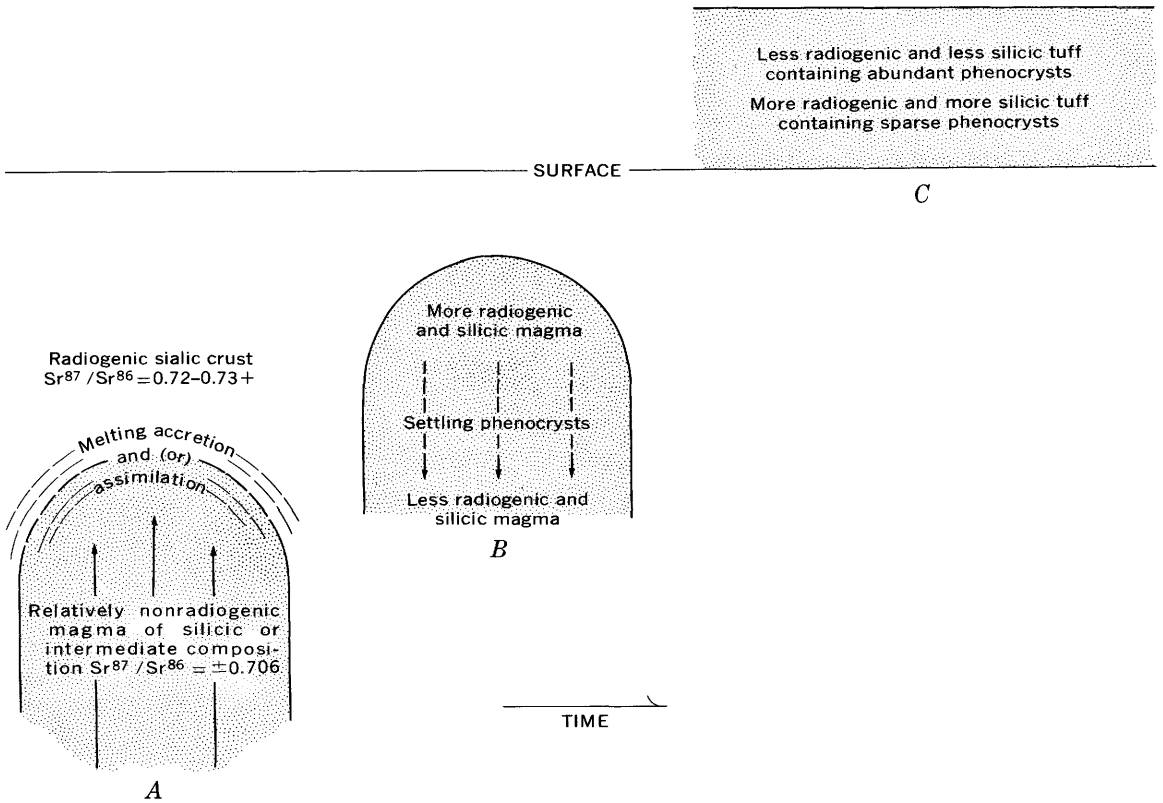

FIGURE 1.—Diagrammatic sketches (not to scale) showing possible evolution of isotopically and compositionally zoned magmas. *A*, ascension of magma through earth's crust; *B*, protracted crystal differentiation in high-level magma chamber; *C*, inversely zoned ash-flow sheet produced by eruption of zoned magma. The episodes of assimilation, and so forth, and crystal fractionation may overlap in time, and magma may have been compositionally and isotopically zoned to a greater or lesser degree prior to ascension.

TABLE 2.—*Average major-element compositions, in weight percent, of uppermost quartz latitic and lowermost rhyolitic zones of the several ash-flow sheets of the Paintbrush and Timber Mountain Tuffs*

	Paintbrush Tuff		Timber Mountain Tuff	
	Quartz latite	Rhyolite	Quartz latite	Rhyolite
SiO_2	70	77	69.5	77
Al_2O_3	15.7	12.7	16.0	12.5
Fe as FeO	1.8	.9	2.0	.8
MgO	.35	.15	.65	.3
CaO	.85	.3	1.6	.4
Na_2O	4.4	4.0	4.2	3.7
K_2O	5.8	4.7	5.2	4.7
TiO_2	.4	.12	.4	.14
P_2O_5	.07	.02	.2	.03
MnO	.1	.1	.1	.07

standard $SrCO_3$ was 0.7080. Two sigma values for the initial ratios are inferred from the results of replicate isotopic analyses made over the same period of time on shelf strontium and on several compositionally similar rocks and from the results of replicate analyses for Rb/Sr ratios. Rubidium and strontium concentrations were determined by X-ray fluorescence methods (Peterman and others, 1968) that have a precision of ±15 percent. Rb/Sr ratios, however, are precise to ±4 percent at the 95-percent confidence level.

MATERIALS ANALYZED

Both whole-rock samples and feldspar-phenocryst separates were analyzed. The whole-rock samples are from densely welded primarily devitrified specimens, which were carefully selected and collected by experienced geologists. Although all the specimens are very fresh appearing, both in hand specimen and thin section, the groundmass material of the tuffs may have acquired as much as 20 parts per million of strontium transported by foreign ground water. Such addition has been demonstrated (D. C. Noble, C. E. Hedge, and Joseph Haffty, unpub. data) by direct comparison of the strontium contents of paired crystallized and nonhydrated glassy specimens from several upper Tertiary ash-flow and lava units that are closely associated with the Timber Mountain and Paintbrush Tuffs. Nevertheless, it is unlikely that the isotopic ratios of the quartz latite specimens have been significantly affected. Although their lower strontium contents make the addition of foreign strontium potentially much more significant for rhyolites, the almost identical strontium contents of specimens 63L–17H and SC–1B tend to suggest that negligible amounts of strontium have been added to these two specimens.

Most of the ground-water-transported strontium which was added to the ash-flow sheets probably was derived from various Tertiary volcanic units. Some undoubtedly was from Paleozoic carbonate rocks, which are the dominant rock type of the pre-Tertiary basement of south-central Nevada. The average Sr^{87}/Sr^{86} of the carbonate rocks, 0.708–0.709 (Hedge and Walthall, 1963; Faure and others, 1965), is very close to the average Sr^{87}/Sr^{86}, about 0.707, of the Tertiary volcanic rocks (Hedge and Noble, 1967). The addition of ground-water-transported strontium thus will tend to make fairly nonradiogenic rocks more radiogenic and fairly radiogenic rocks less radiogenic.

The intratelluric crystals show no sign of alteration or any other feature that would suggest that they have either gained or lost rubidium or strontium subsequent to their deposition. Moreover, general crystallochemical considerations provide no reason to expect such changes.

Xenocrystic material, if present, also could affect the Sr^{87}/Sr^{86} ratios. Even though well over 95 percent of the intratelluric crystals in the rocks studied are unquestionably phenocrysts, the possibility of a small xenocrystic component is suggested by the presence in many of the rocks studied (for example, Lipman and others, 1966) of a few abnormally calcic plagioclase grains. Although morphology and the nature of the compositional zonation strongly suggest that many and probably most of these calcic grains are of magmatic origin, the heaviest feldspars have been separated from the feldspar concentrates in an attempt to reduce the percentage of xenocrysts. In summary, the percentages of the total strontium contributed by xenocrysts, both to the whole-rock samples and to the feldspar concentrates, is extremely small, and the effect on the Sr^{87}/Sr^{86} ratios is believed to be negligible.

ISOTOPIC DATA

The isotopic data (table 1) show significant to pronounced intrasheet differences in initial Sr^{87}/Sr^{86} within each of the five ash-flow sheets studied. Furthermore, samples from the lower parts of the individual ash-flow sheets are, with one exception, more radiogenic than samples from upper parts of the sheets, and feldspar phenocrysts tend to be more radiogenic than associated groundmass material.

The whole-rock specimens from the Topopah Spring Member are progressively, if irregularly, more radiogenic as silica content increases. The increase in Sr^{87}/Sr^{86} also is paralleled by a decrease in phenocryst content from 16 and 13 percent, respectively, for specimens AGE–2 and 63L–17C to less than 2 percent for the rhyolites. The feldspar phenocrysts separated from specimens 63L–17C and 63L–17I also are significantly more radiogenic than the associated groundmass materials.

The Pah Canyon Member of the Paintbrush Tuff (Orkild, 1965) is a small-volume ash-flow sheet of quartz latitic composition, which directly overlies the Topopah Spring Member. Stratigraphic position, chemical composition, and phenocryst mineralogy suggest that the Pah Canyon may represent a still lower level of the same magma from which the Topopah Spring Member was erupted. The isotopic composition of the phenocryst separate, similar to that of specimen AGE–2 (and very possibly more radiogenic than the associated groundmass material) is consistent with the possible genetic relationship between the two members and with the pattern of general upward increase in Sr^{87}/Sr^{86} values observed within the Topopah Spring Member.

Fewer data are available for the overlying Tiva Canyon Member. The two quartz latite specimens appear to have significantly different isotopic compositions; however, surprisingly, the specimen richer in strontium, and thus presumably less silicic, has the higher initial Sr^{87}/Sr^{86} ratio. The feldspar concentrate from rhyolite specimen 63L–110 is appreciably more radiogenic than any of the other specimens. Unfortunately, whole-rock data are not now available for rhyolites from the Tiva Canyon Member, in part because of problems associated with the very low original strontium content of the groundmass material. However, the disequilibrium observed in the rhyolitic Topopah Spring specimens and the rather high strontium contents of the phenocrysts from specimen 63L–110 suggest that the groundmass material of rhyolites from the Tiva Canyon may well be appreciably less radiogenic than the associated phenocrysts.

Rhyolitic tuffs from both members of the Timber Mountain Tuff are much more radiogenic than are the quartz latites. Whole-rock compositions of the rhyolite and quartz latite specimens from the Rainier Mesa Member differ in initial Sr^{87}/Sr^{86} ratios by almost 0.005. Unpublished optical emission spectrographic data on whole-rock material and glassy groundmass material from the same specimens, in conjunction with modal data, indicate that one-third or less of the strontium present in the quartz latites of the Timber Mountain Tuff is in the groundmass material. Thus, if isotopic disequilibrium exists between the phenocryst and groundmass fractions, the whole-rock Sr^{87}/Sr^{86} ratios more closely approximate the average isotopic compositions of the phenocryst fractions. The groundmass materials may have significantly different—presumably less radiogenic—isotopic compositions from those of the phenocrysts. Calculations based on spectrochemical and modal data similar to those described for the

quartz latites indicate that less than 50 percent of the strontium in the rhyolitic tuffs of the Rainier Mesa Member is present in the groundmass material and thus, similar to the quartz latites, the original isotopic composition of the groundmass material may deviate markedly both from that of the whole-rock material and from that of the phenocryst fraction.

Emission spectrographic analyses show that the groundmass material of the rhyolitic ash flow from which specimen SCN–3–1B was collected had an original strontium content of equal to or less than 10 ppm, indicating that, as with the rhyolitic tuffs of the Tiva Canyon Member, the groundmass material is the product of protracted fractional crystallization (compare Noble and others, 1969). Sanidine is by far the dominant phenocryst mineral in the rhyolitic tuffs of the Ammonia Tanks Member (Byers and others, 1968), being associated with smaller amounts of quartz and very small amounts of oligoclase and biotite. The very low strontium content of the sanidine (table 1) suggests that the phenocrysts in the rhyolitic tuffs of the Ammonia Tanks Member were effectively precipitated from the liquid with which they are now associated and thus suggests that the initial isotopic composition of the groundmass material is close to that of the sanidine.

The difference between the isotopic ratios of the two sanidine separates from the Bishop Tuff is significant and is suggestive of an upward increase in Sr^{87}/Sr^{86} within the Bishop magma.

INTERPRETATION AND CONCLUSIONS

Applying the eruption-inversion model discussed in the beginning of the report, we can infer that immediately prior to the onset of eruptive activity, magma bodies were zoned with respect to Sr^{87}/Sr^{86}, with the more radiogenic material overlying the less radiogenic (fig. 1).

Although very few direct isotopic data are available on the crystalline basement of southern Nevada, regional considerations (Engel, 1963; Goldich and others, 1966) suggest a crust 1,400–1,700 m.y. (million years) old. The upper part of this crust must have a strontium concentration of equal to or greater than 200 ppm and, because of its age, a Sr^{87}/Sr^{86} ratio equal to or greater than 0.720. Presently available data (Hedge and Noble, 1967; Hedge and Walthall, 1963; Hedge, 1966; Doe and others, 1966; Mauger and others, 1967) indicate that most Tertiary silicic volcanic rocks in the Western United States had initial Sr^{87}/Sr^{86} values of no more than 0.71. This shows that the magmas originated from relatively nonradiogenic—presumably intermediate, mafic, or ultramafic—material in the lower crust or mantle. Because of the marked difference between the initial Sr^{87}/Sr^{86} ratios of the magmas and the Sr^{87}/Sr^{86} values inferred for the Precambrian crystalline rocks that compose the upper part of the crust, it seems not unreasonable to hypothesize that much of the variation in initial Sr^{87}/Sr^{86} (0.704–0.715) observed for the silicic volcanic rocks is the result of the assimilation of varying amounts of Sr^{87}-enriched upper crustal material.

The observed intrasheet variations appear consistent with this model. Radiogenic crustal material would have been incorporated by the upper parts of the ascending bodies of relatively nonradiogenic parental magma (fig. 1). This could occur either by fusion and accretion or mixing or by assimilation through the reaction of solid rock with the rising melt. Subsequent turbulent flow or convective overturn apparently never completely mixed the composite bodies of magma. Heier and Brooks (1966) inferred a similar assimilation process to account for unusually high initial Sr^{87}/Sr^{86} ratios in granites from Tasmania. The necessity of incorporating large volumes of crustal rock is the major drawback of this mechanism.

Other mechanisms such as (a) the partial fusion of isotopically zoned columns of mantle and crustal or crustal material and (b) the separation of successive melt fractions produced by the partial melting of the progressively more refractory (and less radiogenic) portions of a rock mass cannot be ruled out by the isotopic data. In any case, the isotopic variations must have originated from initial isotopic variations within the parent rock material or from the bringing together of isotopically different melts and (or) rock material. As strontium isotopes do not fractionate geochemically, any differentiation—whether by crystal fractionation, volatile transport, diffusion, or some related process—could only have acted to subdue any isotopic variations present within a magma body.

Indeed, the greater concentration and the larger average size of the phenocrysts in the quartz latites suggest that the isotopic zonations had been modified prior to eruption by the settling of phenocrysts toward the bottoms of the chambers. The apparent isotopic disequilibrium between the feldspar phenocrysts and the whole-rock material in specimen 63L–17C, and possibly in specimen 62L–50X, is consistent with the settling of crystals into the lower, less radiogenic, parts of the magma bodies.

The isotopic disequilibrium observed in specimens 63L–17H and 63L–17I was unexpected, for we had assumed that the phenocrysts in tuffs from the lower parts of the ash-flow sheets would be associated with the groundmass material from which they crystallized. Although consistent with the other data and with the assimilation mechanism proposed to explain the origin

of isotopically inhomogeneous magmas, the data for the rhyolitic specimens from the Topopah Spring Member are intriguing. Perhaps much of the assimilated country rock was dissolved and subsequently reprecipitated as phenocrysts within a narrow marginal zone of necessarily relatively radiogenic magma. Subsequent settling of these radiogenic phenocrysts into both the upper rhyolitic and the lower quartz latitic parts of the magma would, along with settling of stoped blocks and mechanical admixture of radiogenic magma from the marginal zone, be an important means of transferring radiogenic strontium into the interior of the magma.

The rhyolitic rocks have significantly higher Rb/Sr ratios—in certain specimens approaching 15 (F. M. Byers, Jr., unpub. data; D. C. Noble, unpub. data)—than do the quartz latites. Because of this, some part of the observed intrasheet differences in initial Sr^{87}/Sr^{86} ratio may have developed within the magmas between the times the magmas became compositionally zoned and the times of their eruption. The short (1–2 m.y.) interval of time separating the eruption of the Paintbrush and Timber Mountain Tuffs from almost geographically coincident high-level magma chambers (Kistler, 1968; Byers and others, 1968; F. M. Byers, Jr., unpub. data; Christiansen and others, 1965), however, suggests that ascension, high-level differentiation, and eruption of the parent magmas took only several million years. If so, not nearly enough time appears to have been available for an important part of the isotopic variations to have developed in place within closed melt systems located in high-level magma chambers.

Strontium isotope studies provide an additional tool for the study of the origin and evolution of silicic magmas. Data from them, incorporated judiciously with chemical and modal data on phenocryst and groundmass constituents and with volume and other field data on the various rock types, should allow estimation of the original isotopic and chemical variations within a magma body—thus permitting more precise inferences to be drawn concerning parentage—and should allow estimation of the extent to which initial compositional zonations had subsequently been modified by crystal fractionation or other differentiative and mixing processes. Conversely, the demonstration of pronounced intrasheet variations obviously means that strontium isotope ratios can be used only with extreme caution as a correlation tool in working out the stratigraphic relations in ash-flow terranes.

REFERENCES

Byers, F. M., Jr., Orkild, P. P., Carr, W. J., and Quinlivan, W. D., 1968, Timber Mountain Tuff, southern Nevada, and its relation to cauldron subsidence, *in* Nevada Test Site. Studies in geology and hydrology: Geol. Soc. America Mem. 110, p. 87–99.

Christiansen, R. L., Lipman, P. W., Orkild, P. P., and Byers, F. M., Jr., 1965, Structure of the Timber Mountain caldera, southern Nevada, and its relation to basin-range structure, *in* Geological Survey Research 1965: U.S. Geol. Survey Prof. Paper 525–B, p. B43–B48.

Dalrymple, G. B., Cox, Allan, and Doell, R. R., 1965, Potassium-argon age and paleomagnetism of the Bishop Tuff, California: Geol. Soc. America Bull., v. 76, no. 6, p. 665–674.

Doe, B. R., Hedge, C. E., and White, D. E., 1966, Preliminary investigation of the source of lead and strontium in deep geothermal brines underlying the Salton Sea geothermal area: Econ. Geology, v. 61, no. 3, p. 462–483.

Engel, A. E. J., 1963, Geologic evolution of North America: Science, v. 140, p. 143–152.

Ewart, A., 1965, Mineralogy and petrogenesis of the Whakamaru ignimbrite in the Maraetai area of the Taupo volcanic zone, New Zealand: New Zealand Jour. Geology and Geophysics, v. 8, no. 4, p. 611–677.

Faure, G., Hurley, P. M., and Powell, J. L., 1965, The isotopic composition of strontium in surface water from the North Atlantic Ocean: Geochim. et Cosmochim. Acta, v. 29, no. 4, p. 209–220.

Fisher, R. V., 1966, Geology of a Miocene ignimbrite layer, John Day Formation, eastern Oregon: California Univ. Pubs. Geol. Sci., v. 67, 58 p.

Gilbert, C. M., 1938, Welded tuff in eastern California: Geol. Soc. America Bull., v. 49, no. 12, pt. 1, p. 1829–1862.

Giles, D. L., and Cruft, E. F., 1968, Major- and minor-element variations in zoned ash flows and their biotites [abs.], *in* Abstracts for 1966: Geol. Soc. America Spec. Paper 101, p. 78.

Goldich, S. S., Muehlberger, W. R., Lidiak, E. G., and Hedge, C. E., 1966, Geochronology of the midcontinent region, United States; 1. Scope, methods, and principles: Jour. Geophys. Research, v. 71, p. 5375–5388.

Hedge, C. E., 1966, Variations in radiogenic strontium found in volcanic rocks: Jour. Geophys. Research, v. 71, no. 24, p. 6119–6120.

Hedge, C. E., and Noble, D. C., 1967, A strontium isotopic study of magma origin and evolution in the southern Great Basin [abs.]: Am. Geophys. Union Trans., v. 48, p. 253–254.

Hedge, C. E., and Walthall, F. S., 1963, Radiogenic strontium-87 as an index of geologic process: Science, v. 140, no. 3572, p. 1214–1217.

Heier, K. S., and Brooks, C. K., 1966, Geochemistry and the genesis of the Heemskirk granite, West Tasmania: Geochim. et Cosmochim. Acta, v. 30, no. 6, p. 633–643.

Kistler, R. W., 1968, Potassium-argon ages of volcanic rocks in Nye and Esmeralda Counties, Nevada, *in* Nevada Test Site. Studies in geology and hydrology: Geol. Soc. America Mem. 110, p. 251–263.

Lipman, P. W., 1966, Water pressures during differentiation and crystallization of some ash-flow magmas from southern Nevada: Am. Jour. Sci., v. 264, no. 10, p. 810–826.

——— 1967, Mineral and chemical variations within an ash-flow sheet from Aso caldera, southwestern Japan: Beitr. Mineralogie u. Petrographie, v. 16, no. 4, p. 300–327.

Lipman, P. W., Christiansen, R. L., and O'Conner, J. T., 1966, A compositionally zoned ash-flow sheet in southern Nevada: U.S. Geol. Survey Prof. Paper 524–F, p. F1–F47.

Martin, R. C., 1965, Lithology and eruptive history of the Whakamaru ignimbrites in the Maraetai area of the Taupo

volcanic zone, New Zealand: New Zealand Jour. Geology and Geophysics, v. 8, p. 680–701.

Mauger, R. L., Livingston, D. E., Jensen, M. L., and Damon, P. E., 1967, Sulfur and initial strontium isotopic investigations of Basin and Range intermediate igneous rocks [abs.]: Am. Geophys. Union Trans., v. 48, p. 254.

Noble, D. C., Haffty, Joseph, and Hedge, C. E., 1969, Strontium and magnesium contents of some natural peralkaline silicic glasses and their petrogenetic significance: Am. Jour. Sci. v. 267, p. 598–608.

Noble, D. C., Sargent, K. A., Mehnert, H. H., Ekren, E. B., and Byers, F. M., Jr., 1968, Silent Canyon volcanic center, Nye County Nevada, *in* Nevada Test Site. Studies in geology and hydrology: Geol. Soc. America Mem. 110, p. 65–75.

Orkild, P. P., 1965, Paintbrush and Timber Mountain Tuff of Nye County, Nevada, *in* Cohee, G. V., and West, W. S., Changes in stratigraphic nomenclature by the U.S. Geological Survey, 1964: U.S. Geol. Survey Bull. 1224–A, p. A44–A51.

Pakiser, L. C., Kane, M. F., and Jackson, W. H., 1964, Structural geology and volcanism of Owens Valley region, California—A geophysical study: U.S. Geol. Survey Prof. Paper 438, 68 p.

Peterman, Z. E., Hedge, C. E., and Braddock, W. A., 1968, Age of Precambrian events in the northeastern Front Range, Colorado: Jour. Geophys. Research, v. 73, no. 6, p. 2277–2296.

Quinlivan, W. D., and Lipman, P. W., 1965, Compositional variations in some Cenozoic ash-flow tuffs, southern Nevada [abs.], *in* Abstracts for 1964: Geol. Soc. America Spec. Paper 82, p. 342.

Ratté, J. C., and Steven, T. A., 1964, Magmatic differentiation in a volcanic sequence related to the Creede caldera, Colorado: Art. 131 *in* U.S. Geol. Survey Prof. Paper 475–D, p. D49–D53.

Sheridan, M. F., 1965, The mineralogy and petrology of the Bishop Tuff: Stanford Univ. unpub. Ph. D. dissert, 193 p.

Smith, R. L., 1960, Zones and zonal variations in welded ash flows: U.S. Geol. Survey Prof. Paper 354–F, p. 149–159.

Smith, R. L., and Bailey, R. A., 1966, The Bandelier Tuff—A study of ash-flow eruption cycles from zoned magma chambers: Bull. Volcanol., v. 29, p. 83–104.

Williams, Howel, 1942, The geology of Crater Lake National Park, Oregon, with a reconnaissance of the Cascade Range southward to Mount Shasta: Carnegie Inst. Washington Pub. 540, 162 p.

337–735 O—69——10

OXYGEN AND CARBON ISOTOPIC COMPOSITION OF ORE AND HOST ROCK OF SELECTED MISSISSIPPI VALLEY DEPOSITS

By WAYNE E. HALL and IRVING FRIEDMAN
Menlo Park, Calif., Denver, Colo.

Abstract.—Variations in carbon and oxygen isotopic composition of ore and host rock around selected ore bodies in the Upper Mississippi Valley and Tri-State districts, were investigated. Systematic decreases in δO^{18} and δC^{13} values found in limestone and dolomite host rock toward ore are interpreted as diminishing isotopic fractionation with increasing temperature. Late-stage ore minerals have a broad scatter of δO^{18} and δC^{13}. Calculated δO^{18} of late-stage mineralization ore fluid is $+0.4$ to -1.6 per mil for the Upper Mississippi Valley district and -3 per mil for the Tri-State district. These values are considered reasonable for ore fluid of hot oil-field brine proposed to have mixed with meteoric water during late-stage mineralization. The δO^{18} and δC^{13} of carbonate host rocks of Mississippi Valley deposits do not seem practical as guides to ore because the area of limestone depleted in these isotopes is small.

This study of the variation in the isotopes of carbon and oxygen of ore and host rock of Mississippi Valley deposits was undertaken to investigate the feasibility of using these light stable isotopes as a guide to ore and to obtain the temperature of ore deposition from coexisting mineral pairs as was done at the Gilman mine, Colorado, by Engel, Clayton, and Epstein (1958).

The districts have been described in detail in many papers: for example, the southern Illinois fluorite district by Weller and others (1952), Heyl and Brock (1961), and Brecke (1962); the Upper Mississippi Valley district by Heyl, Agnew, Lyons, and Behre (1959); and the Tri-State district by Fowler and Lyden (1932). All the deposits occur in limestone or dolomite of Paleozoic age. Their mineralogy is simple; sphalerite and galena are the principal ore minerals, and calcite, dolomite, jasperoid, and quartz, the principal gangue. Fluorite is abundant only in the southern Illinois-Kentucky district. Wallrock alteration aureoles are present around each of the deposits, but the thickness of the alteration zones is generally less than 200 feet. Alteration consists of solution thinning, silicification, dolomitization, and clay-mineral alteration. Descriptions of the alteration of the Upper Mississippi Valley district have been given by Heyl, Hosterman, and Brock (1964) and of the southern Illinois district by Brecke (1962) and Hall and Heyl (1968).

Samples of ore and gangue minerals and of host rock were collected from the Thompson-Temperly mine and the Calumet and Hecla mine in the Upper Mississippi Valley district, Wisconsin and from the Webber and West Side mines in the Tri-State district, Kansas. Samples were collected of calcite and, where present, quartz and dolomite in ore and from host rock through the adjacent alteration zone to unaltered limestone or dolomite. As coexisting dolomite-calcite is much more abundant than coexisting quartz-calcite in the deposits sampled, isotopic work was done entirely on the former pair.

Friedman and Hall (1963) previously reported on the fractionation of O^{18}/O^{16} between coexisting calcite and dolomite from some of these samples. We found little fractionation of O^{18}/O^{16} between coexisting calcite and dolomite in this low-temperature environment. The maximum fractionation that was measured was a $\Delta_{\text{dolomite-calcite}}$ of 1.8 per mil, and many pairs had little or no fractionation.

In this paper we report the δO^{18} and δC^{13} values in 125 calcite and dolomite samples within ore bodies, and in samples of altered and unaltered host rock. Unaltered limestone is used here to mean unaltered by ore solutions. Excluded are diagenetic changes or isotopic exchange of O^{18} between ground water and carbonate rocks over long periods of time. Further study is being made of O^{18} of coexisting quartz and carbonate from these deposits and from the southern Illinois district.

U.S. GEOL. SURVEY PROF. PAPER 650–C, PAGES C140–C148

In a previous paper (Friedman and Hall, 1963) we assumed the kinetic fractionation factor associated with the H_3PO_4 reaction to be the same for both dolomite and calcite. Later work by Sharma and Clayton (1965) shows that this is not so, and the $\Delta_{\text{dolomite-calcite}}$ given in our paper must be reduced by 0.8 per mil.

Acknowledgments.—The writers wish to thank the many persons who made this investigation possible. Allen Heyl and D. M. Pinckney assisted in the collection of samples. J. L. Harris made most of the C^{13} and O^{18} mass spectrographic measurements. E. W. Tooker and R. O. Rye critically reviewed this paper and made many helpful suggestions. We especially wish to acknowledge the cooperation of the mining companies. Samples were collected with permission and extensive cooperation from the owners of the Dyer Hill and Oxford mines in the southern Illinois-Kentucky fluorite district, from the Calumet and Hecla mine and Thompson-Temperly mine in the Upper Mississippi Valley district, and from the Eagle-Picher Co. in the Tri-State district.

EXPERIMENTAL PROCEDURES

Samples were run of either calcite or dolomite, but not of their mixtures. Where the two occurred together, calcite was separated in bromoform, and dolomite was purified by leaching the calcite in diluted glacial acetic acid. The purity of all calcite and dolomite samples was checked by X-ray diffraction.

After separation the samples were finely ground, and the fine powder was reacted with 100-percent phosphoric acid at 25°C (McCrea, 1950) to liberate CO_2. The CO_2 produced was collected in a liquid-nitrogen-cooled trap in a vacuum line and was analyzed in a Nier-type double-collecting ratio mass spectrometer (McKinney and others, 1950).

As shown by Sharma and Clayton (1965), the isotopic fractionation factors of the various carbonates is not the same. We used the factors recommended by J. R. O'Neil (oral commun., 1969) of 1.01026 (calcite) and 1.01109 (dolomite) to relate the isotopic composition of acid-liberated CO_2 and total carbonate (modified after Sharma and Clayton, 1965). Our C^{13}/C^{12} analyses are given in per mil relative to the carbon from the Cretaceous belemnite (PDB) used by Urey and others (Craig, 1957). The O^{18}/O^{16} data are given in per mil relative to standard mean ocean water (SMOW) and are expressed by the formula:

$$\delta O^{18}{}_{\text{sample}}{}^{\circ}/_{\circ\circ} = \left[\frac{\left(O^{18}/O^{16}\right)_{\text{sample}}}{\left(O^{18}/O^{16}\right)^{\text{SMOW}}} - 1 \right] 1{,}000.$$

ISOTOPIC DATA

Upper Mississippi Valley district

The carbon and oxygen isotope compositions for ore and host rock for the Calumet and Hecla mine and the Thompson-Temperly mine are given in figures 1 through 4. δO^{18} is plotted versus δC^{13} in figures 1 and 2; the basic data are given in tables 1 and 2. Both figure 1 and 2 show that δO^{18} of host rock tends to increase with increase of δC^{13} values. Limestone outside the alteration aureole has a δO^{18} of +25.5 to +26. 0 per mil relative to SMOW and δC^{13} of approximately +1 per mil relative to PDB. At the Thompson-Temperly mine the δO^{18} and δC^{13} values of altered limestone are smaller than those outside the alteration halo, and they follow a linear trend to δO^{18} of +22.5 per mil and δC^{13} of −2.3 per mil (fig. 1). δC^{13} values for dolomite host rock show more scatter than limestone host rock at the Thompson-Temperly mine (fig. 1) and tend to be smaller than in the limestone. Vein calcite within the Thompson and Temperly ore bodies does not follow the linear trend line of δO^{18} versus δC^{13} of the host rock (fig. 1), and has a large scatter, particularly in δC^{13}, which ranges from −5.2 to −9.8 per mil.

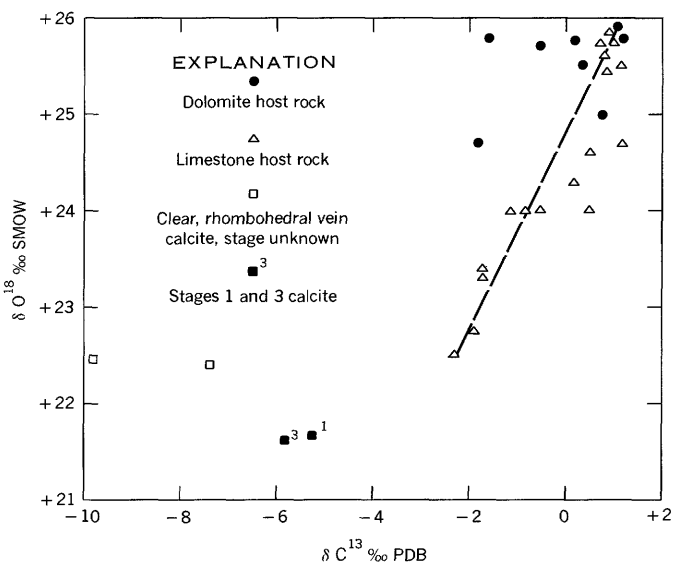

FIGURE 1.—Oxygen versus carbon isotopic compositions, Thompson-Temperly mine, Wisconsin.

The pattern of δO^{18} and δC^{13} values in host rock and ore calcite at the Calumet and Hecla mine (fig. 2) is similar to that at the Thompson-Temperly mine. The limestone outside the alteration aureole has a δO^{18} of approximately +26 per mil and δC^{13} of zero. The δO^{18} and δC^{13} values of the altered limestone change in a linear trend to δO^{18} of +23.7 per mil and δC^{13} of −2 per mil from the values in the unaltered rock (fig. 2). Dolomite values follow the same trend line as do

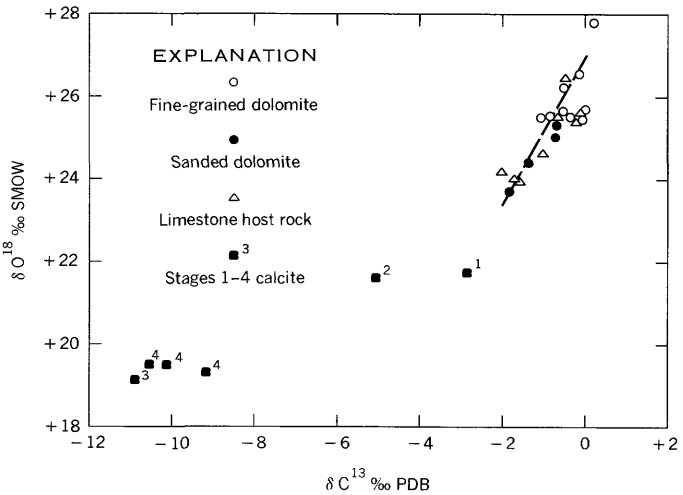

FIGURE 2.—Oxygen versus carbon isotopic compositions, Calumet and Hecla mine, Wisconsin.

those of limestone. δO^{18} and δC^{13} values in vein calcite, similar to those at the Thompson-Temperly mine, are lighter than values of the host rock. δO^{18} of the vein calcite ranges from +19 to +21.6 per mil and δC^{13} from −2.8 to −11 per mil. The early calcite is enriched in both O^{18} and C^{13} over the later ore calcites. Stage 1 calcite of Heyl, Agnew, Lyons, and Behre (1959, p. 100) has larger δO^{18} and δC^{13} values than stages 3 and 4 (fig. 2).

Figures 3 and 4 show δO^{18} and δC^{13} values plotted against distance from ore for the Thompson-Temperly mine and Calumet and Hecla mine. There is a trend from larger δO^{18} and δC^{13} values in limestone and dolomite host rock outside of alteration aureoles to compositions lighter in oxygen and carbon isotopes as ore is approached. In the alteration aureole there is a suggestion that dolomite coexisting with limestone has higher values in both δO^{18} and δC^{13} by +1 to +2 per mil (fig. 3).

Changes in isotopes of carbon and oxygen correlate with the changes in mineralogy from unaltered host rock through the alteration zone to ore at the Thompson-Temperly mine that were found by Heyl, Hosterman, and Brock (1964). The 1Md polymorph of illite that occurs in unaltered shaly limestone is altered successively to 1M and 2M illite in the altered rock and to the 2M illite polymorph within ore bodies. Accompanying this alteration, calcite decreases and dolomite and microcline increase toward the ore zone.

This trend toward lighter oxygen and carbon isotopic compositions in limestone as ore is approached suggests that (1) a large reservoir of water of uniform isotopic composition was present; and (2) an increase in temperature toward ore; that is, fractionation of the isotopes decreases with increase in temperature. The decrease of δO^{18} of about 3.2 per mil at the Thompson-Temperly mine can be explained by a temperature gradient of 20°C from ore to the outer limit of the alteration aureole.

Vein calcite does not show the same trend in carbon and oxygen isotopic compositions as the limestone and dolomite host rock. Four stages of calcite were deposited during the late stages of mineralization; stage 1 is the

TABLE 1.—*Isotopic composition of carbon and oxygen in host rock and ore, Thompson-Temperly mine, Wisconsin*

Sample No. (each prefixed by "BHTT-")	Mineral or rock type	Description	δO^{18}_{SMOW} (per mil)	δC^{13}_{PDB} (per mil)
BHTT-1	Dolomite	Fine grained, brownish gray; from Quimbys Mill Member of Platteville Formation, Temperly ore body.	+25.0	+0.8
2	Limestone	Fine to medium grained, brownish gray; 50 feet from ore	+24.0	−1.1
3	do	Fine grained, brownish gray; 100 feet from ore	+24.0	−.9
4	do	Fine grained, brownish gray; 150 feet from ore	+22.8	−1.9
5	do	Fine grained, brownish gray; 200 feet from ore	+24.3	+.2
6	do	Fine grained, brownish gray; 250 feet from ore	+25.5	+.6
7	do	Fine grained, brownish gray; 300 feet from ore	+24.6	+.5
8	do	Fine grained, brownish gray; 400 feet from ore	+24.0	+.5
9	do	Fine grained, brownish gray; 500 feet from ore	+25.4	+.8
10	do	Fine grained, brownish gray; 700 feet from ore	+25.9	+.9
11	do	Fine grained, gray; 700 feet from Thompson ore body	+25.6	+.8
12	do	Fine grained, brownish gray; 500 feet from ore	+25.8	+.9
13	do	Fine grained, brownish gray; 300 feet from ore	+24.7	+1.0
14A	do	Fine grained, brownish gray; 200 feet from ore	+24.0	−.6
14B	Dolomite	Rhombohedrons of dolomite, 0.1 mm long, separated from BHTT-14A in fine-grained, partly dolomitized limestone.	+25.8	+1.0
15	Limestone	Fine grained, brownish gray; 150 feet from ore	+25.7	+.7
16	do	Fine grained, brownish gray; 100 feet from ore	+22.5	−2.3
17A	do	Fine grained, brownish gray; 75 feet from ore	+23.4	−1.8
17B	Dolomite	Fine grained, gray; from fine-grained mixture of dolomite and calcite.	+24.7	−1.9
18	do	Fine grained, brownish gray; 60 feet from ore	+25.8	+.3
19	do	Sandy textured, brownish gray; 35 feet from ore	+25.7	−.5
20	Limestone	Fine grained, brownish gray; 5 feet from ore	+23.4	−1.7

TABLE 2.—*Isotopic composition of carbon and oxygen in host rock and ore, Calumet and Hecla mine, Wisconsin*

Sample No. (each prefixed by "CH-")	Mineral or rock type	Description	δO^{18}_{SMOW} (per mil)	δC^{13}_{PDB} (per mil)
CH-1	Calcite	Stage 4, clear, rhombohedral; 40 feet from ore	+19.5	−10.2
2	do	Stage 4, clear, rhombohedral; 100 feet from ore	+19.3	−9.2
3	do	Stage 4, clear, rhombohedral; in ore	+19.5	−10.6
4	Dolomite	Fine grained, light gray; from ore	+25.3	−.7
5	do	Sandy textured, mixed with fine-grained dolomite; light gray; 40 feet from ore.	+24.4	−1.5
7	do	Fine grained, light gray; 120 feet from ore	+26.1	−.6
8	do	Fine grained, light gray; 200 feet from ore	+25.6	−.5
9	do	Sandy textured, porous, light gray; 370 feet from ore	+23.8	−1.8
10	do	Fine grained, light gray; 290 feet from ore	+26.7	−.1
11	do	Fine grained, gray; 200 feet from ore	+27.8	+.2
12	do	Sandy textured, porous, light gray and brownish gray; 80 feet from ore.	+25.0	−.7
13	do	Medium grained, dense, gray; edge of ore body	+25.5	−1.1
14	do	Fine to medium grained, light gray; in ore	+25.4	−.3
15	Limestone	Fine-grained, brownish gray; in ore	+24.2	−2.0
17A	do	Fine grained, brownish gray; 120 feet from ore	+25.6	−.1
17B	Dolomite	Fine grained, gray; separated from CH-17A	+25.6	.0
18	Limestone	Fine grained, brownish gray; 200 feet from ore	+23.9	−1.7
19	do	Fine grained, brownish gray; 300 feet from ore	+24.7	−1.0
20A	do	Fine-grained, gray; 370 feet from ore	+25.4	−.2
20B	Dolomite	Fine grained, brownish gray; from ¼-inch vein cutting CH-20A	+25.6	−.1
21A	Limestone	Fine grained, light gray; 940 feet from ore	+25.3	−.8
21B	Dolomite	Fine grained, gray; separated from CH-21A	+25.5	−.9
22	Limestone	Fine grained, light gray; 1,100 feet from ore	+26.4	−.8
24A	Calcite	Stage 1, rhombohedral, pink	+21.7	−2.9
24B	do	Stage 2, scalenohedral, milky	+21.6	−5.0
24C	do	Stage 3, scalenohedral, clear	+19.1	−10.9
24D	do	Stage 4, rhombohedral, clear	+19.4	−10.1

earliest, and stage 4 is the last (Heyl and others, 1959). Vein calcite contains much less δC^{13} than does the limestone and dolomite host rock. At the Calumet and Hecla mine, stages 1 and 2 calcite have lower δO^{18} and δC^{13} values than those in stages 3 and 4 calcite (fig. 2). Two possible explanations for the low C^{13} values of vein calcite are suggested. The first is that organic carbon, which is light isotopically, was caught up in the late stages of ore fluid to produce the light carbon isotopic compositions. During this late stage, meteoric water mixed with the hot saline ore fluid identified by our earlier fluid inclusion studies (Hall and Friedman, 1963). Although we do not have data on the δC^{13} of local ground water, it is not uncommon for it to be in the range −7 to −18 per mil (J. R. O'Neil, oral commun., 1968) and mixing of ground water with the hot saline ore fluid alone may account for the spread of carbon-isotope compositions.

Another possible explanation for the light carbon in the vein calcites is that these calcites were produced from light (C^{13}-depleted) CO_2, resulting from the release of CO_2 from solutions supersaturated in CO_2 or bicarbonate ion and accompanied by a decrease in pressure. Work by Friedman in Yellowstone Park shows that travertine-depositing hot springs are releasing CO_2 depleted in C^{13}. Although the Yellowstone hot springs are not releasing CO_2 in isotopic equilibrium with the solution, experimental data (Malinin and others, 1967) support the conclusion that at temperatures below 150°C, CO_2 gas in equilibrium with HCO_3 ion will be depleted in C^{13} relative to HCO_3^{-1} in solution. The C^{13}-depleted CO^2 that is formed at depth may migrate until it meets descending water undersaturated with CO_2. The C^{13}-depleted CO_2 (aq.) that results can dissolve limestone, and the $CaHCO_3$-saturated water would precipitate calcite when it migrates to an area of lower pressure or higher temperature.

The vein calcite is also several per mil lighter in O^{18} than it is in altered limestone and dolomite, and presumably the calcite was deposited at a lower temperature than that attained by the altered sandy-textured dolomite and limestone adjacent to ore. Filling tempertures of vein calcite by Bailey and Cameron (1951, p. 635) indicate that stages 2 and 3 calcite were deposited in the range 50°–78°C, whereas sphalerite, deposited during the earlier main period of mineralization, was formed between 75° and 121°C. The wallrock alteration presumably also occurred early and at higher temperatures than those attained during deposition of the late vein calcite. If so, the calcite could not have been deposited from waters of the same oxygen isotopic composition as that of the water present during wallrock alteration because the fractionation of O^{18} would be greater at the lower

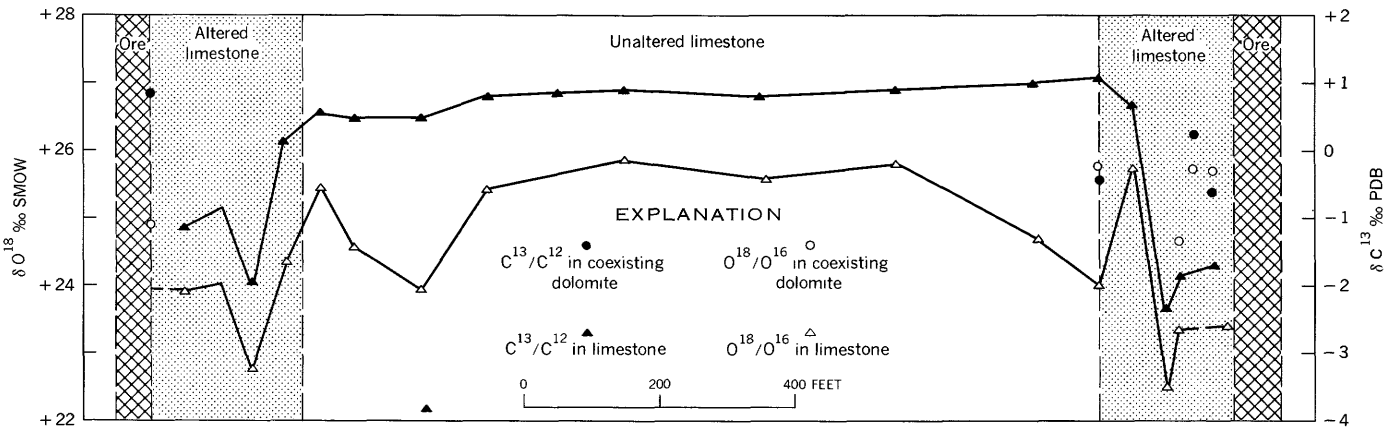

FIGURE 3.—Variation in carbon and oxygen isotopic compositions in carbonate host rock versus distance from ore, Thompson Temperly mine, Wisconsin.

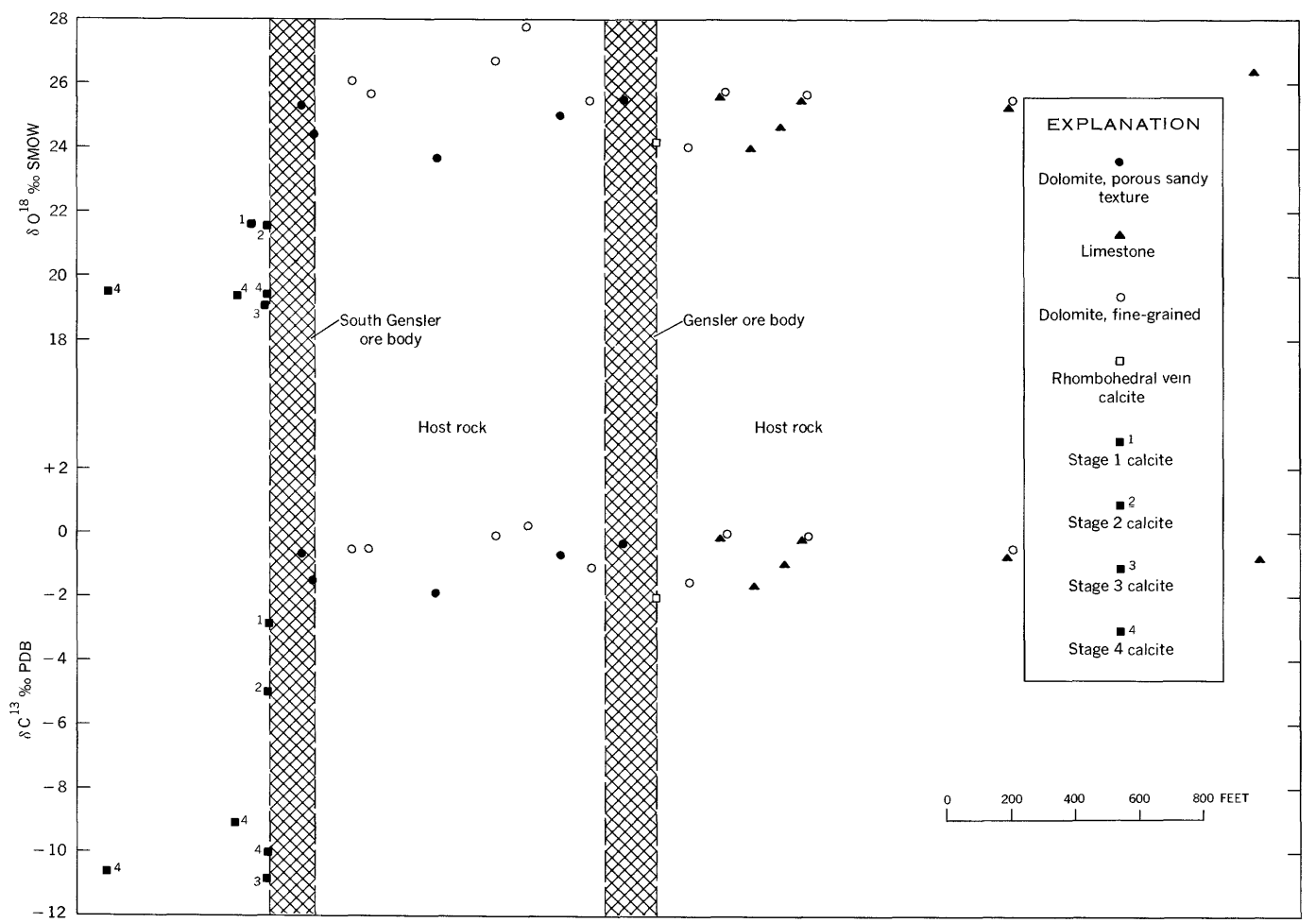

FIGURE 4.—Variation in carbon and oxygen isotopic compositions in carbonate host rock versus distance from ore, Calumet and Hecla mine, Wisconsin.

temperature, and the vein calcite should be higher in O^{18} than is the most altered carbonate host rock.

The oxygen isotopic composition of the late-stage ore fluid that deposited calcite can be calculated from the information given previously because the oxygen isotopic composition of calcite is a function of the temperature of deposition (obtained by filling temperature measurement of fluid inclusions), the isotopic fractionation factor for oxygen in the calcite-water system, and the oxygen isotopic composition of the water. The following formula was supplied by J. R. O'Neil (oral commun., 1969):

$$1{,}000 / \mathrm{n}\ \alpha_{c-w} = 2.80(10^6 T^{-2}) - 3.40,$$

where α is the calcite-water (c–w) fractionation factor and T is temperature in degrees Kelvin.

When we used a filling temperature of 70°C for both stages 2 and 3 calcite, a δO^{18} of +21.6 per mil for stage 2 calcite, and of +19.1 for stage 3 calcite, the δO^{18} of the ore fluid of stage 2 calcite was calculated to be +0.4 per mil, and the ore fluid of stage 3 calcite was calculated to be −1.6 per mil.

Fluid-inclusion studies by Hall and Friedman (1963) have shown the isotopic and chemical composition of the ore fluid during the late stages of mineralization was different from that of the ore fluid of the main period of ore mineralization. The ore fluid in the waning stages of mineralization had low relative deuterium values and approached the chemical composition of present-day meteoric water, whereas the ore fluid during the main period of ore mineralization was a hot water of the chemical and isotopic composition of oil-field brine.

Tri-State district

The limestone and dolomite host rocks in the Tri-State district and in the Upper Mississippi Valley district have the same trend in oxygen and carbon isotope compositions (tables 3 and 4). Figure 5 shows the δO^{18}_{SMOW} versus δC^{13}_{PDB} plot for the host rock and ore minerals from the Webber and West Side mines. It shows a crude correlation between δO^{18} and δC^{13} values. Limestone outside the alteration aureole has a δO^{18} of +24 to +25.6 per mil and a δC^{13} of +2 to +3 per mil; the limestone within the alteration aureole has lower δO^{18} and δC^{13} values that fall off to +22.3 and +1 per mil, respectively.

This decrease in the δO^{18} and δC^{13} values in the host rock, as in the Upper Mississippi Valley district, is interpreted in terms of the smaller fractionation of these isotopes with increasing temperature toward ore bodies.

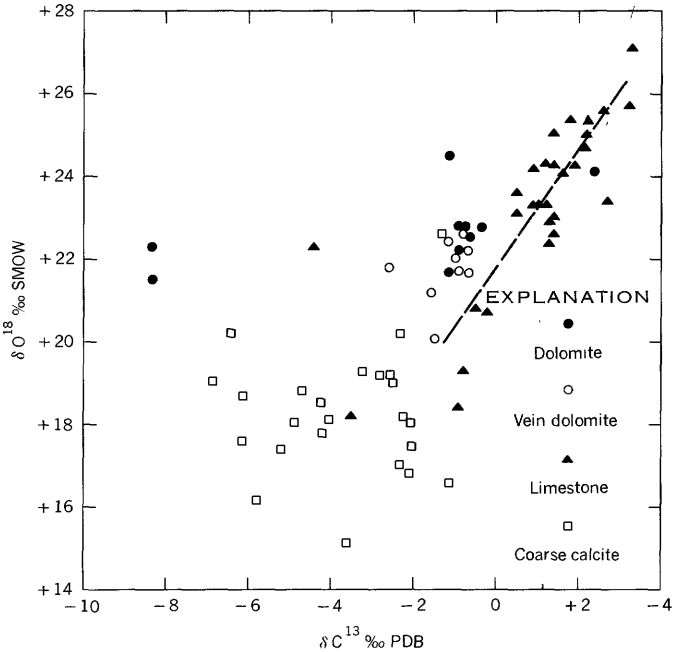

FIGURE 5.—Oxygen versus carbon isotopic compositions, Webber and West Side mines, Tri-State district, Kansas.

The dolomite isotope compositions are clustered at a δO^{18} of +22 per mil. This includes both dolomite crystals that are closely associated with ore and the dolomite host rock, suggesting a contemporaneity of the two dolomites. Two dolomite samples are depleted in C^{13}, with δ values less than −8 per mil (fig. 5). Both are medium-grained dolomite host rock. One contains disseminated sphalerite and galena. We suspect that both equilibrated with an ore fluid that had incorporated organic carbon.

Coarse rhombohedral and scalenohedral calcite is present both as a late gangue mineral in ore bodies and as a vug filling in chert near ore. The calcite has a wide range of isotopic compositions (fig. 5). Filling temperature of the late yellow scalenohedral calcite, as determined by J. Thomas Nash (written commun., 1968), is 71°C±3°. The δO^{18} of the calcite is +18. The calculated δO^{18} of the ore fluid from which the calcite deposited is about −3 per mil. As in the Upper Mississippi Valley district, the calcite was deposited in a late stage of mineralization from a dilute ore fluid, with low relative deuterium values, that probably was dominantly of meteoric origin.

Figures 6 and 7 (p. C147, C148) show variations in carbon and oxygen isotope compositions versus distance from ore for the Webber and West Side mines. No clear-cut pattern is shown by either δO^{18} or δC^{13} content versus distance to ore. Shattered limestone and dolomite host rock near ore may have permitted the ore fluid to per-

TABLE 3.—*Isotopic composition of carbon and oxygen in host rock and ore from the Webber mine, Tri-State district, Kansas*

Sample No.	Mineral or rock type	Description	δO^{18}_{SMOW} (per mil)	δC^{13}_{PDB} (per mil)
(Each No. prefixed by "Web")				
Web 1A	Dolomite	Coarse, pink crystals; from ore	+22.0	−1.1
6A	do	Medium grained, gray; in ore	+22.6	−.8
6B	do	Coarse, gray crystals; in ore	+22.6	−.8
6C	Calcite	Late scalenohedral calcite on pink dolomite; from ore	+22.6	−1.3
7	Dolomite	Medium grained, gray; at edge of ore body	+21.7	−.9
8	do	Medium grained, gray; 8 feet below ore	+24.5	−1.1
12	Limestone	Fine grained, light gray; 150 feet from ore	+23.0	+1.4
13	do	Fine grained, light gray; 200 feet from ore	+24.3	+1.4
16	Dolomite	Fine grained, light gray; 90 feet from ore	+23.2	+1.1
17	Limestone	Fine grained, brownish gray; 50 feet from ore	+25.6	+2.6
19	Calcite	Yellowish gray, rhombohedral; in ore	+19.0	−6.9
20	do	Yellow, clear, rhombohedral; in ore	+18.0	−4.9
21	do	Yellowish gray, rhombohedral; in ore	+16.8	−2.1
22	do	White, rhombohedral; in ore	+19.2	−2.8
25	Dolomite	Pink, coarse crystals; at edge of ore body	+20.1	−1.5
38C	Calcite	Coarse, white, rhombohedral	+16.6	−1.1
(Each No. prefixed by "WH 62-")				
WH 62-65A	Limestone	Medium grained, gray; 170 feet from ore	+22.2	−4.4
65B	Calcite	White, rhombohedral; veining WH 62-65A	+18.2	−2.2
66A	Dolomite	Coarse, pink crystals; 165 feet from ore	+21.7	−.7
66B	do	Fine grained, brownish gray; adjacent to WH 62-66A	+21.7	−1.1
67	Limestone	Fine grained, brownish gray; 140 feet from ore	+22.8	+.8
68	do	Fine grained, gray; 115 feet from ore	+19.3	−.8
69A	Dolomite	Pink, coarse crystals; 90 feet from ore	+22.2	−.7
69B	do	Medium grained, gray	+21.5	−8.3
70A	Limestone	Fine grained, gray; 60 feet from ore	+18.4	−.9
70C	Calcite	Coarse, brownish gray, rhombohedral	+17.3	−5.2
71A	do	Coarse, yellow, scalenohedral; 15 feet from ore	+18.7	−6.1
72	do	Coarse, white, rhombohedral; in ore	+18.8	−4.7
73	Dolomite	Coarse, pink crystals; in ore	+22.2	−1.4
74A	do	Coarse, pink crystals; in ore	+21.2	−1.5
74B	Calcite	Coarse, brown, rhombohedral; in ore	+17.7	−6.0
75A	Dolomite	Pink, coarse, from dolomitic core of ore body	+21.8	−2.6
75B	do	Medium grained, gray	+21.7	−1.5
82	Calcite	Coarse, yellow, rhombohedral; 300 feet from ore	+16.0	−5.8
83	do	Coarse, white, rhombohedral; 400 feet from ore	+17.8	−4.2
84	do	Coarse, clear, scalenohedral; 500 feet from ore	+17.0	−2.3
86	do	Scalenohedral, 2 inches long, yellowish gray; 480 feet from ore	+15.1	−3.6

meate the host rock and equilibrate with much of it, irrespective of distance to ore.

CONCLUSIONS

The changes in O^{18} and C^{13} content of altered limestone and dolomite around ore bodies is interpreted as a result of decreasing fractionation of these isotopes between ore fluid and carbonate host rock with the increase in temperature toward ore. The decrease in δO^{18} and δC^{13} toward ore is accompanied (1) by a change in mineralogy of the host rock at the Thompson-Temperly mine from illite of 1Md polymorph in the unaltered rock to 1M and 2M illite in the altered rock and to 2M illite and microcline in the ore zone, and (2) by changes in the minor-element content of the host rock (Hall and Heyl, 1968).

The wide range of O^{18} and C^{13} in the late-stage ore minerals is consistent with an origin for the ore fluid suggested in Hall and Friedman (1963), who proposed that hot oil-field brines mixed with meteoric water during late stages of mineralization. The calculated δO^{18} of the ore fluid during the late stages of mineralization in the Upper Mississippi Valley district of +0.4 to −1.6 and for the Tri-State district of −3 is reasonable for the suggested type of ore fluid.

However, the δO^{18} and δC^{13} of carbonate host rocks of Mississippi Valley-type deposits do not appear to provide a practical tool for a guide to ore in this low-

TABLE 4.—*Isotopic composition of carbon and oxygen in host rock and ore from the West Side mine, Tri-State district, Kansas*

Sample No. (each prefixed by "WH 62-")	Mineral or rock type	Description	δO^{18}_{SMOW} (per mil)	δC^{13}_{PDB} (per mil)
WH 62-3	Calcite	Coarse, white; in jasper	19.3	−3.2
4	do	Coarse, white; with calcite and chert	19.2	−2.5
5	do	Coarse, white; in chert breccia	+19.1	−2.4
7	do	Coarse, white; in ore	+18.1	−2.0
8	Limestone	Medium grained, brownish gray; 2½ feet from ore	+22.8	+1.3
9	do	Fine grained, brownish gray; with chert, 8 feet from ore	+24.7	+2.0
10	do	Medium grained, brownish gray; with chert, 18 feet from ore	+22.6	+1.4
11	do	Fine grained, brownish gray; with chert, 40 feet from ore	+23.4	+2.6
12	do	Medium grained, brownish gray; 65 feet from ore	+23.0	
13	do	Medium grained, brownish gray; 94 feet from ore	+24.7	+2.1
14	do	Medium grained, brownish gray; 110 feet from ore	+25.1	+1.4
15	do	Fine grained, brownish gray; adjacent to stylolite; 135 feet from ore.	+22.9	+1.3
16	do	Medium grained, brownish gray; 150 feet from ore	+27.1	+3.3
17	do	Medium grained, brownish gray; 135 feet from ore	+23.6	+.5
18	do	Medium grained, brownish gray; 120 feet from ore	+25.4	+1.8
20	do	Brownish gray, fine grained; 90 feet from ore	+23.3	+.9
21	do	Fine grained, gray; 70 feet from ore	+24.2	+.9
22	do	Fine grained, brownish gray; 40 feet from ore	+24.2	
23	do	Fine grained, brownish gray; contact with ore	+20.7	−.2
25	do	Light gray, fine grained; 5 feet within ore body	+20.8	−.5
26	Dolomite	Medium grained, gray; in ore body	+22.0	−1.2
52	Limestone	Fine grained, light gray; 100 feet from ore	+23.4	+.4
54	do	Fine grained, gray; 230 feet from ore	+25.7	+3.2
56	do	Fine grained, light gray; 120 feet from ore	+24.3	+1.9
57	Calcite	Coarse, white, rhombohedral; edge of ore body	+17.1	−2.1
59	do	Coarse, white, rhombohedral; in ore	+18.1	−4.0
60	Dolomite	Coarse, gray, crystals; in ore	+21.4	−1.2
61A	do	Coarse, gray, crystals	+21.2	−1.6
61B	Calcite	Clear, yellow, scalenohedral; late	+15.1	−6.2
61C	Dolomite	Fine grained, gray; under WH 62-61A	+22.7	−.9
62	do	Medium grained, brownish gray; in ore	+22.3	−8.3

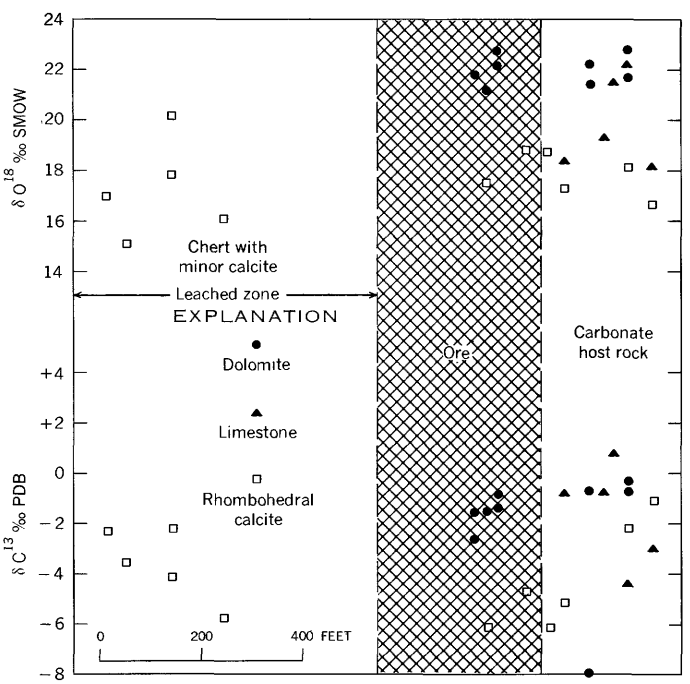

FIGURE 6.—Variation in carbon and oxygen isotopic compositions versus distance from ore, Webber mine, Kansas.

temperature environment. There is a difference of approximately 3 per mil in δO^{18} between altered and unaltered limestone, but the area of limestone depleted in δO^{18} does not extend beyond the area of visible rock alteration.

REFERENCES

Bailey, S. W., and Cameron, E. N., 1951, Temperatures of mineral formation in bottom-run lead-zinc deposits of the Upper Mississippi Valley, as indicated by liquid inclusions: Econ. Geology, v. 46, no. 6, p. 626–651.

Brecke, E. A., 1962, Ore genesis of the Cave-In-Rock fluorspar district, Hardin County, Illinois: Econ. Geology, v. 57, no. 4, p. 499–535.

Craig, Harmon, 1957, Isotopic standards for carbon and oxygen and correction factors for mass-spectrometric analysis of carbon dioxide: Geochim. et Cosmochim. Acta, v. 12, nos. 1–2, p. 133–149.

Engel, A. E. J., Clayton, R. N., and Epstein, Samuel, 1958, Variations in the isotopic composition of oxygen (and carbon) in the Leadville limestone (Mississippian, Colorado) and in its hydrothermal and metamorphic phases: Jour. Geology, v. 66 no. 4, p. 374–393.

Fowler, G. M., and Lyden, J. P., 1932, The ore deposits of the Tri-State district (Missouri-Kansas-Oklahoma): Am. Inst. Mining Metall. Engineers Trans., v. 102, p. 206–251.

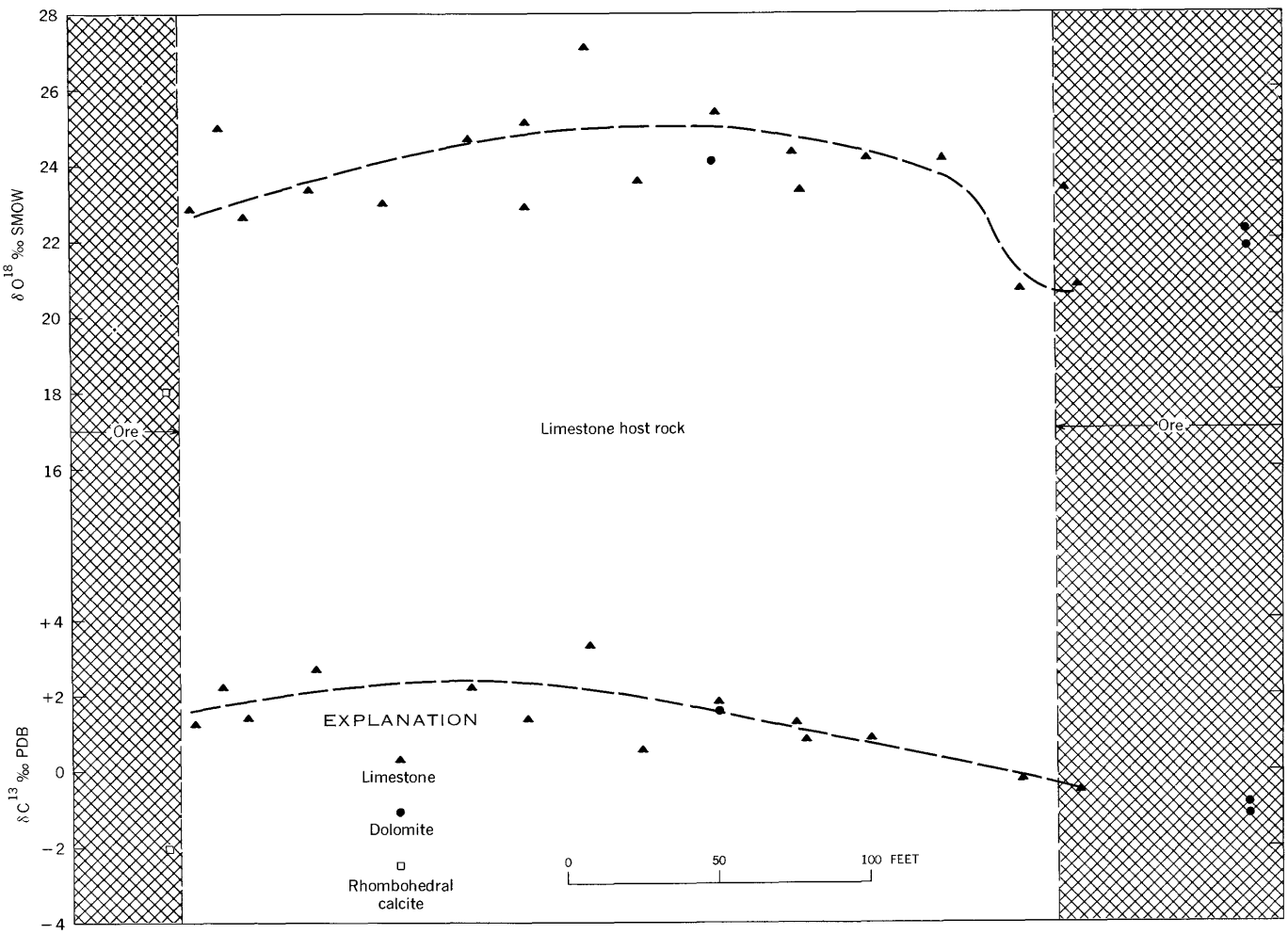

FIGURE 7.—Variation in carbon and oxygen isotopic compositions versus distance from ore, West Side mine, Kansas.

Friedman, Irving, and Hall, W. E., 1963, Fractionation of O^{18}/O^{16} between coexisting calcite and dolomite: Jour. Geology, v. 71, no. 2, p. 238–243.

Hall, W. E., and Friedman, Irving, 1963, Composition of fluid inclusions, Cave-in-Rock fluorite district, Illinois, and Upper Mississippi Valley zinc-lead district: Econ. Geology, v. 58, no. 6, p. 886–911.

Hall, W. E., and Heyl, A. V., Jr., 1968, Distribution of minor elements in ore and host rock, Illinois-Kentucky fluorite district and Upper Mississippi Valley zinc-lead district: Econ. Geology, v. 63, no. 6, p. 655–670.

Heyl, A. V., Jr., Agnew, A. F., Lyons, E. J., and Behre, C. H., Jr., 1959, The geology of the Upper Mississippi Valley zinc-lead district (Illinois-Iowa-Wisconsin): U.S. Geol. Survey Prof. Paper 309, 310 p.

Heyl, A. V., Jr., and Brock, M. R., 1961, Structural framework of the Illinois-Kentucky mining district and its relation to mineral deposits: Art. 294 *in* U.S. Geol. Survey Prof. Paper 424–D, p. D3–D6.

Heyl, A. V., Jr., Hosterman, J. W., and Brock, M. R., 1964, Clay-mineral alteration in the Upper Mississippi Valley zinc-lead district: Natl. Conf. on Clays and Clay Minerals, 12th, Atlanta, Ga., 1963, Proc., p. 445–453.

Malinin, S. D., Kropotova, O. L., and Grinenko, V. A., 1967, Experimental determination of carbon isotope exchange constants in CO_2 (g)$\rightleftarrows HCO_3^-$ (sol'n) system under hydrothermal conditions: Geochimiya, no. 8, p. 927–935 [In Russian].

McCrea, J. M., 1950, On the isotopic chemistry of carbonates and a paleotemperature scale: Jour. Chem. Physics, v. 18, p. 849–857.

McKinney, C. R., and others, 1950, Improvements in mass spectrometers for the measurement of small differences in isotope abundance ratios: Rev. Sci. Instruments, v. 21, no. 8, p. 724–730.

Sharma, Taleshwar, and Clayton, R. N., 1965, Measurement of O^{18}/O^{16} ratios of total oxygen of carbonates: Geochim. et Cosmochim. Acta, v. 29, no. 12, p. 1347–1353.

Weller, J. M., and others, 1952, Geology of the fluorspar deposits of Illinois: Illinois Geol. Survey Bull. 76, 147 p.

MODE OF OCCURRENCE OF PLATINUM, PALLADIUM, AND RHODIUM IN CHROMITITE

By F. S. GRIMALDI and MARIAN M. SCHNEPFE, Washington, D.C.

Abstract.—The fraction of total chromite decomposed by fusion with a deficiency of sodium peroxide is compared to the fraction of total platinum, palladium, or rhodium dissolved. From such data it is inferred that in the chromitite in the Stillwater Complex rhodium occurs almost entirely within, palladium almost entirely outside, and platinum both inside and outside the chromite lattice.

The mode of occurrence of platinum, palladium, and rhodium in chromitite is of obvious importance both from the geochemical and economic standpoint. This study is not concerned primarily with mineralogy but inquires into the problem of whether these elements occur outside the chromite as separate phases (without attempting to identify these phases), or inside the chromite either in solid solution or as inclusions. These questions are of concern in defining extractive processes; for example, in solid solution, the metals would be largely unavailable unless complete chemical decomposition of the chromite were made.

EXPERIMENTAL METHOD

Sample description and preparation

The sample was collected by Norman J Page, of the U.S. Geological Survey, who describes it as a chromitite from the "A" zone of the Stillwater Complex from Stillwater County, Mont. The chromitite consists of chromite admixed with a silicate phase. It contains 28.8 percent chromium and 81.3 percent chromite. The chromite content was determined by digesting a sample with HF and then evaporating the solution repeatedly with HCl to remove fluoride. The chromite was filtered off, ignited, and weighed. The filtrate was tested for chromium, and as only 0.25 percent was found, on the basis of the original sample, a satisfactory isolation of chromite is indicated. Petrographic examination showed the chromite to be pure.

Semiquantitative spectrographic analyses of the original chromitite and the isolated chromite were made by Claude Waring. The chromitite contains approximately 10 percent Fe, 7 percent Mg, >10 percent Cr, 3 percent Si, and 7 percent Al. Similarly, the isolated chromite shows 10 percent Fe, 5 percent Mg, >10 percent Cr, 0.1 percent Si, and 7 percent Al. These elements characterize the chromite.

The sample was ground to pass a 100-mesh sieve and then thoroughly mixed. A 50-gram portion was split and then quartered to yield 15 portions each weighing slightly more than 3 g. From these, 3-g portions were weighed for the analyses.

Procedure

Chromite is completely decomposed by fusion with excess sodium peroxide. If less sodium peroxide is used than is required for complete decomposition, the undecomposed chromite can be isolated by digesting the melt with HCl and filtering. The chromite residue can be purified by treatment with HF and HCl as described earlier, thus yielding a measure of the amount of chromite decomposed. The filtrate, containing the decomposed fraction, is used for the determination of platinum, palladium, and rhodium. We are then able to relate the fraction of the total chromite decomposed to the fraction of the total platinum, palladium, or rhodium dissolved. For the situation where these metals are present only in solid solution, a plot of these two fractions should yield a straight line passing through the origin with a slope of unity. Where a metal is partly in solid solution and partly outside as a separate phase, a plot of the dissolved metal concentration against the fraction of the chromite decomposed would be a straight line with a positive intercept on the y axis. Here the only assumption made is that the external phase is completely decomposed by the quantities of sodium peroxide used. The value of the intercept determines the amount of a given metal present in the external phase. This can

U.S. GEOL. SURVEY PROF. PAPER 650-C, PAGES C149-C151

then be subtracted from the amount dissolved to yield data for plotting the fraction of metal from solid solution against fraction of chromite decomposed, which again should be a straight line through the origin, with unit slope. For the situation where a given metal is all in the external phase, a constant total concentration would be found independent of the amount of chromite that was decomposed.

Methods used for the determination of platinum, palladium, and rhodium were developed by the writers. The precious metals are isolated from 2.5*N* HCl by coprecipitation with a few milligrams of tellurium formed by reducing tellurite with stannous chloride (Grimaldi and Schnepfe, 1967, 1968; Schnepfe and Grimaldi, 1968). The precipitate is dissolved in aqua regia, and the salts converted to chlorides by evaporation with HCl. Each of the elements is determined by atomic absorption. For platinum and palladium the determinations are made from solutions 10 percent by volume in HCl and strongly buffered with a mixture of $CdSO_4$ and $CuSO_4$ to eliminate interference of other elements (Schnepfe and Grimaldi, 1969). Rhodium is similarly determined except that $La_2(SO_4)_3$ instead of $CdSO_4$ and $CuSO_4$ is used to eliminate interferences (Schnepfe and Grimaldi, unpub. data).

RESULTS

Rhodium

A total of 11 sample splits was taken for the rhodium experiments. Five samples decomposed completely with excess sodium peroxide yielded a mean value for total rhodium of 2.70 parts per million, a standard deviation of 0.108, and a coefficient of variation of 4 percent. The fraction of rhodium recovered was based on this average, and the results on all samples were used to calculate a least-squares fit shown by the solid line plotted in figure 1. The slope of this line is 0.95; the intercept, 5.1; and the 2-sigma limits of the intercept, −0.451 and 10.7. Although the data do not exclude the possibility that all the rhodium occurs in solid solution or as uniformly distributed minute inclusions in the chromite, it would seem that a few percent of the rhodium is present in an external phase. Because the intercept is small and the slope almost unity, no further reworking of the data was thought necessary. In one experiment where the sample was leached with aqua regia, only 2.2 percent of the total rhodium was found in the extract.

Platinum

Platinum was determined on 12 samples, 11 of which were aliquots of the solutions prepared for determining rhodium. The mean for total platinum was 10.0 ppm,

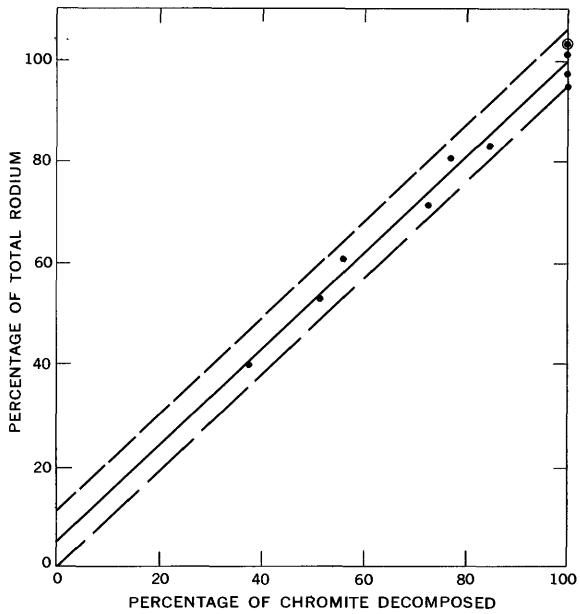

FIGURE 1.—Percentage of total rhodium extracted as a function of percentage of chromite decomposed. Circled dot denotes two samples with identical analyses.

with a standard deviation of 0.47 ppm and a coefficient of variation of 4.7 percent. The results are plotted in figure 2. The least-squares fit is shown by the solid line having a slope of 0.069 and an intercept of 3.0 ppm. The 2-sigma for the intercept is ±0.947. We infer from

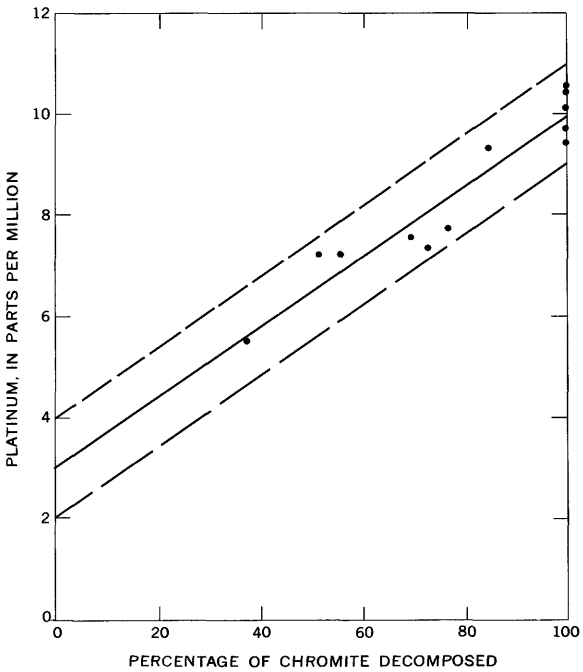

FIGURE 2.—Platinum extracted as a function of percentage of chromite decomposed.

these data that approximately 3 ppm of the platinum is in an external phase, a value supported by aqua-regia-soluble platinum which amounts to 2.8 ppm.

The data, corrected for platinum in the external phase, are replotted in another form in figure 3. The least-squares fit has a slope of 0.99 and an intercept of 0.46; the 2-sigma value for the intercept is ± 13.49. These data support the conclusion that 70 percent of the total platinum is within the chromite phase. The large scatter in results suggests that at least some of the platinum within the chromite is in the form of inclusions. This scatter could arise, for example, if inclusions were "large" or not uniformly distributed within the chromite.

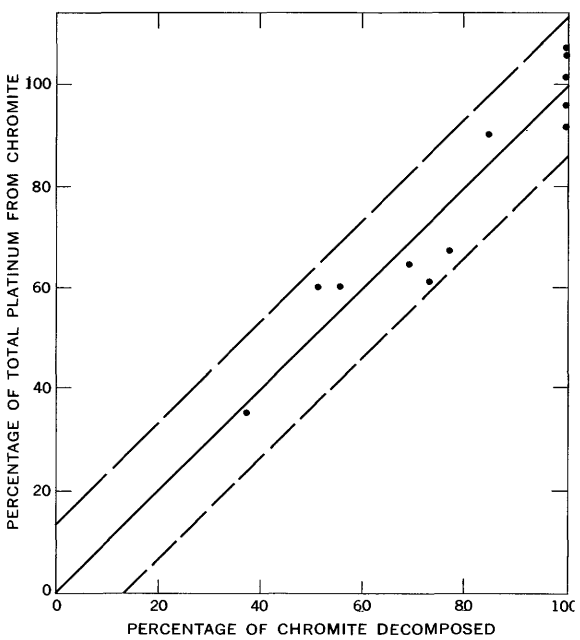

FIGURE 3.—Percentage of total platinum derived from chromite as a function of percentage of chromite decomposed.

Palladium

The solutions used for determining platinum were also used for determining palladium. Total palladium averaged 13.4 ppm with a standard deviation of 0.413 ppm and a coefficient of variation of 3.2 percent. Results for palladium on partly decomposed samples do not differ significantly from those that were completely decomposed. Thus, practically all the palladium occurs in the external phase. This is confirmed by the result of 13.6 ppm of Pd obtained for aqua regia soluble palladium.

DISCUSSION

In the Stillwater chromitite, therefore, rhodium occurs almost entirely within and palladium almost entirely outside the lattice, whereas platinum occurs both inside and outside. This distribution is in accord with the relevant ionic radii: Rh^{+3} and Cr^{+3} are very close in size, 0.68 and 0.63 A, respectively, whereas Pt^{+2} and Pd^{+2} are too large (0.80 A) to permit extensive substitution for chromium. On the other hand, Pt^{+4} (0.65 A) could occur in nature and could substitute for the chromium in chromite; this may account for the fraction of platinum found in the chromite lattice.

If the results found here are generally true, it seems that a complete chemical decomposition would be required for good recoveries of noble metals from chromite ores.

REFERENCES

Grimaldi, F. S. and Schnepfe, M. M., 1967, Determination of palladium in the parts-per-billion range in rocks, *in* Geological Survey Research 1967: U.S. Geol. Survey Prof. Paper 575–C, p. C141–C144.

——— 1968, Determination of palladium and platinum in rocks, *in* Geological Survey Research 1968: U.S. Geol. Survey Prof. Paper 600–B, p. B99–B103.

Schnepfe, M. M., and Grimaldi, F. S., 1968, Determination of rhodium in rocks, *in* Geological Survey Research 1968: U.S. Geol. Survey Prof. Paper 600–D, p. D210–D213.

——— 1969, Determination of palladium and platinum by atomic absorption: Talanta, v. 16. (In press)

DETERMINATION OF GERMANIUM IN SILICATES BY NEUTRON ACTIVATION ANALYSIS

By L. PAUL GREENLAND and J. E. McLANE,
Washington, D.C.

Abstract.—A neutron activation procedure with a detection limit of 0.2 nanogram of Ge has been devised for the analysis of germanium in rock samples. After a 5-minute irradiation, the sample is fused with $NaOH$-Na_2O_2 in the presence of a germanium carrier. The fusion cake is dissolved and made $9M$ in HCl. Germanium is extracted to carbon tetrachloride, washed, and back-extracted to water. The germanium separated in this way is radiochemically pure and may be counted by either β^- or γ techniques. After counting, the chemical yield of the procedure is determined by re-irradiation and counting. Determinations of eight U.S. Geological Survey standard rocks by this method are reported.

Germanium occurs in most rocks and minerals at about the 1-part-per-million concentration level. This is below the detection limit of common emission spectrographic methods, and thus, the geochemistry of germanium is poorly documented. Most of the existing data have been obtained by chemical spectrophotometric techniques (for example, Onishi, 1956; Burton and others, 1959). Although apparently reliable, these techniques require a gram of sample for analysis, a great disadvantage if the analysis of purified mineral separates and other small samples is contemplated. In our continuing investigations of tektites, meteorites, crater materials, and other terrestrial rocks, it became necessary to develop a method for the reliable determination of germanium in 10–100-milligram samples.

Neutron activation procedures for the determination of germanium in silicates have been described (Fouché and Smales, 1967; Morris and Batchelor, 1966). These are sensitive and accurate, but are tedious since elaborate radiochemical separations are required. Most of these procedures rely on repeated extractions of $GeCl_4$ from acid aqueous solution to CCl_4, interspersed with at least one distillation of germanium from HCl to obtain radiochemical purity. We have found (from decay curves and γ spectra) that a single extraction of $GeCl_4$ from 9–10M HCl with CCl_4 is sufficient to provide adequate purity. This simplified method is described below.

Neutron irradiation of natural germanium produces 82-minute Ge^{75} and 11-hour Ge^{77} as the only isotopes of interest to activation analysis. Decay of Ge^{77} produces 38-hour As^{77}; thus, As^{77} grows into a purified germanium sample and must be taken into account. For practical irradiation and counting times, Ge^{75} provides the most sensitive analysis.

Our procedure uses a short irradiation time to keep the Na^{24} activity (the predominant activity) of the sample low, and fast chemistry to yield the greatest sensitivity from Ge^{75}. With this procedure, a detection limit of 0.002 ppm of Ge in a 100-mg sample may be obtained.

REAGENTS AND APPARATUS

Germanium carrier: Fuse an accurately known amount of GeO_2 with KOH in a zirconium crucible. Dissolve the fusion cake with H_2O, and dilute to volume to give a known concentration of about 2 mg of Ge per milliliter.

Flux monitor: Just before use, dilute 1 ml of the carrier solution to 100 ml with H_2O.

Holdback carrier: Dissolve about 5 grams of NaCl, 9 g of $Ni(NO_3)_2 \cdot 6H_2O$, and 8 g of $MnCl_2 \cdot 4H_2O$ in 200 ml of H_2O. The exact concentration is unimportant.

γ counting system: The system used here consists of four 3- by 3-inch NaI(Tl) detectors connected through a mixer-router arrangement to a 1,024-channel analyzer. This arrangement permits the counting of four samples simultaneously, but any NaI(Tl) system may be used.

β^- counting system: A Geiger-Müller detector with an automatic sample changer was used here; shielding and anticoincidence circuitry reduce the background counting rate to 0.4 counts per minute. Any standard β^- counting system may be used, though a higher background necessarily raises the detection limit reported here.

ANALYTICAL PROCEDURE

Irradiation

Approximately 100 mg of each sample was accurately

weighed into a polyethylene vial. The vials were sealed and irradiated for 5–10 minutes in a thermal neutron flux of about 7×10^{12} n/cm²/sec at the reactor of the U.S. Naval Research Laboratory, Washington, D.C. Chemical separations were started about 30 minutes after the irradiation, thus permitting the intense Al^{28} activity to decay.

A flux monitor was irradiated simultaneously with each batch of samples. The flux monitor was prepared by transferring 0.050 ml of the diluted carrier solution (see the section "Reagents and Apparatus") to approximately 20 mg of NH_4NO_3 in a polyethylene irradiation vial. After evaporation overnight at 60°C, the vials were sealed and treated as the samples.

Radiochemical purification

1. Transfer the sample quantitatively to a 35-ml iron crucible in which 1.00 ml of the carrier solution has been evaporated with 1 g of NaOH. Add about 1 g of Na_2O_2 and fuse the mixture at a red heat until a clear melt is obtained. Place the crucible in a covered beaker on a hotplate; when the melt has solidified, cautiously add water, finally filling the crucible.

2. While the fusion cakes (step 1) are being decomposed, open the monitor vial and submerge it, with its contents, in a beaker containing 1.00 ml of the carrier solution and 30 ml of 1*M* NaOH. Stir vigorously and heat on a hotplate until the samples have been processed, then continue the monitor chemistry with step 3.

3. Acidify the solution with 1:1 H_2SO_4, dilute to 50 ml with H_2O, and transfer to a separatory funnel containing 70 ml of CCl_4. Add 150 ml of concentrated HCl and shake the funnel for 1 minute. The bulk of the radioactivity of the sample remains in the aqueous layer which may be discarded as radioactive waste.

4. Transfer the CCl_4 layer to a separatory funnel containing 30 ml of 9*M* HCl and 1 ml holdback carrier solution. Wash the CCl_4 by shaking for 1 minute.

5. Repeat step 4 except for the addition of holdback carrier.

6. Transfer the CCl_4 layer to a separatory funnel containing 10 ml of H_2O. Extract the germanium into the aqueous layer by shaking for 1 minute; discard the CCl_4.

7a. If γ counting is to be used, transfer the aqueous layer to a polyethylene counting vial containing 1 ml of HF. After counting, dilute this solution to 15.0 ml in a graduated cylinder and transfer 0.100 ml (with a micropipet) to an irradiation vial. The chemical yield of the procedure, relative to the monitor, is then determined by irradiating these vials for 2 minutes in the reactor and directly counting the Ge^{75} γ activity.

7b. If β^- counting is to be used, then transfer the aqueous layer to a beaker containing 1 g of $(NH_4)_2SO_4$, dilute to 50 ml with H_2O, and heat on a hotplate. To the hot solution, add 2 ml of 10-percent tannic acid and continue heating until the precipitate coagulates. Filter, with suction, through a 2.4-cm glass filter paper disk. Dry the precipitate at 120°C for 15 minutes. After counting, transfer the filter paper and precipitate to a polyethylene bag, irradiate in the reactor for 1 minute, and count the Ge^{75} γ activity to obtain the relative chemical yield.

Counting procedure

When the greatest sensitivity is required, β^- counting must be used. With the low-background instrument in use here, 0.01 ppm of Ge can be reliably determined (0.002 ppm of Ge detected) in 100-mg samples. Because no energy discrimination is available with this counting mode, radioactive decay of the sample must be followed for at least 3 hours; verification of radiochemical purity may then be obtained by comparison of the sample decay curves with that of the monitor.

For amounts of germanium exceeding 0.5 ppm of Ge in 100-mg samples, γ counting may be used. This procedure simplifies the chemical manipulations and avoids the necessity of following the radioactive decay; radiochemical purity is verified by comparison of the γ spectra. Because of the inherent lack of sensitivity of this counting mode, samples are counted for more than a half life of Ge^{75} (usually 100 minutes) and thus require correction for decay during the counting interval; the required correction is given graphically in Lyon (1964, p. 78).

The observed counting data must be extrapolated to obtain a counting rate at some standard time. The decay, however, is complicated because, in either counting mode, radiations from 82-minute Ge^{75}, 11-hour Ge^{77}, and 38-hour As^{77} (daughter of Ge^{77}) are all present; the observed decay curve, then, is a complex function which cannot be extrapolated by the usual simple techniques. Greenland (1969) gives decay constants and algebraic expressions for the total counting rate as a function of time. Alternatively, a semilogarithmic plot of the flux-monitor counting data may be made to obtain an empirical decay curve; interpolation then provides a monitor counting rate for each observed sample counting time.

Calculations

The concentration of Ge in the sample is found from the equation

$$X = \left(\frac{R_s}{R_m}\right)\left(\frac{R'_s}{R'_m}\right)\left(\frac{W_m}{W_s}\right),$$

where X is the concentration of Ge in the sample (in parts per million), R_s/R_m is the ratio of the sample counting rate to the monitor counting rate at a given time, R'_s/R'_m is the ratio of the sample-yield counting rate to the monitor-yield counting rate at a given time, and W_m/W_s is the ratio of the weight (in micrograms) of Ge in the monitor to the weight (in grams) of sample taken.

It may be noted that knowledge of the actual concentration of germanium in the carrier solution and of the absolute chemical yield of the procedure is not required. Furthermore, the sample (and sample yield) counting rates need not be extrapolated to the same time; if the graphical interpolation method of decay correction is used, the (R_s/R_m) and (R'_s/R'_m) ratios may be obtained for the midpoint of the sample counting interval.

ANALYTICAL RESULTS

Results of the neutron activation analysis for germanium (single analyses) in eight USGS standard rock samples are given in table 1. Analyses were made on separate portions by both β^- counting and γ counting techniques; these results are compared with each other and with previous determinations in table 1.

TABLE 1.—*Comparison of germanium content (ppm) of eight USGS standard rocks determined by different analytical methods*

USGS standard rock	Analytical method				
	Neutron activation (this report)		Chemical spectrophotometric [1]	Emission spectrographic [1]	Other [2]
	β^- counting	γ counting			
Granite, G–1	1.1	1.2			1.0
Diabase, W–1	1.0	1.4			1.6
Granite, G–2	.90	1.0	0.5	0.76	
Basalt, BCR–1	1.2	1.7	2.1	1.1	
Andesite, AGV–1	1.4	1.1	1.2	.85	
Granodiorite, GSP–1	.99	1.3	.9	.68	
Dunite, DTS–1	.77	.85		$<.5$	
Peridotite, PCC–1	.88	.79		$<.5$	

[1] Analyses quoted by Flanagan (1969).
[2] "Best" value given by Ahrens and Fleischer (1960).

The "best" values for standard rock samples G–1 and W–1 are averages of results from various analysts and methods. In view of this, the neutron activation results presented here appear to be reasonable. For the other six standard rocks, the chemical spectrophotometric and the emission spectrographic analyses cited by Flanagan (1969) show very poor agreement; furthermore, neither agrees very well with our analyses. Lack of information about the other methods makes it impossible to evaluate our results.

Many analytical techniques may be checked by analyzing artificial standards and (or) natural samples to which known amounts of the element of interest have been added. Unfortunately, neither of these procedures is appropriate to neutron activation analysis; the greatest source of error is radioactivity from an element incompletely separated from the element of interest. The contaminating element may be present from mechanical carryover as well as from incomplete chemical separation; the amount of interference will depend on the ratio of contaminating element to analysis element. It is not practical to make an artificial standard containing all elements producing radioactive isotopes in appropriate proportions, and spiking a natural sample alters the ratio of the contaminating element to the element of interest; thus, both methods tend to give unduly optimistic results. In practice, checking the half-life obtained from the decay curve and checking the γ spectrum for contaminating peaks gives a better estimate of the reliability of the data; a further advantage is that each sample can (and should) be checked individually. This check was routinely made here, and there is no apparent reason to doubt the reliability of these results; this conclusion is confirmed by the comparison of results for G–1 and W–1.

REFERENCES

Ahrens, L. H., and Fleischer, Michael, 1960, Report on trace constituents in granite G–1 and diabase W–1, *in* Stevens, R. E., and others, Second report on a cooperative investigation of the composition of two silicate rocks: U.S. Geol. Survey Bull. 1113, p. 83–111.

Burton, J. D., Culkin, F., and Riley, J. P., 1959, The abundance of gallium and germanium in terrestrial materials: Geochim. et Cosmochim. Acta. v. 16, p. 151–180.

Flanagan, F. J., 1969, U.S. Geological Survey standards, I. First compilation of data for the new U.S.G.S. rocks: Geochim. et Cosmochim. Acta, v. 33, p. 81–120.

Fouché, K. F., and Smales, A. A., 1967, The distribution of trace elements in chondritic meteorites, 1. Gallium, germanium, and indium: Chem. Geology, v. 2, p. 5–33.

Greenland, L. P., 1969, Decay equation for the neutron activation determination of germanium: Jour. Inorganic and Nuclear Chemistry. [In press]

Lyon, W. S., Jr., 1964, Guide to activation analysis: New York, D. Van Nostrand Co., Inc., 186 p.

Morris, D. F. C., and Batchelor, J. S. P., 1966, Germanium in the rocks G–1 and W–1 determined by neutron activation analysis: Geochim. et Cosmochim. Acta, v. 30, p. 737–738.

Onishi, Hiroshi, 1956, Notes on the geochemistry of germanium: Chem. Soc. Japan Bull., v. 29, p. 686–694.

THE POSSIBILITIES FOR USING DATA CENTERS IN GEOLOGIC MAPPING

By IVO LUCCHITTA, JOHN W. M'GONIGLE, and DAVID SCHLEICHER, Flagstaff, Ariz.

Abstract.—A data center similar in concept to that being developed for lunar exploration may increase the efficiency, thoroughness, and speed of geologic mapping. Basically, use of a center involves a fieldman or men radioing observations to a team of other geologists and technicians, who promptly record and compile the field data. The elaborateness of the data center depends on mapping requirements. Although equipment and procedures are more complex than those used in conventional geologic mapping, the use of a data center should (1) encourage speedy development of a comprehensive and regional perspective, (2) utilize people economically in functions commensurate with their training, (3) generally make for more efficient use of time, and (4) thus commonly reduce overall costs for certain field projects.

The National Aeronautics and Space Administration is sponsoring the U.S. Geological Survey in developing a data center whose function is to collaborate with astronauts exploring the lunar surface. The center comprises a well-coordinated team of scientists and technicians who will (1) record and compile data radioed by the astronauts; (2) process and analyze such data as they are received; and (3) on the basis of these data, serve as advisors, promptly answering questions from the astronauts and suggesting critical observations to be made or modifications of the traverse plan. The system presupposes the need for utmost efficiency in the field, for traverse time is limited and mobility of the astronauts is restricted. The data center offers a means of compensating for these restrictions in order to get a maximum of pertinent and accurate geologic information during each mission.

This emphasis on efficient use of field time suggests that the idea of a data center may be applied to certain kinds of terrestrial geologic mapping, particularly when field time is restricted or logistics are difficult. Under such conditions the possibility of doing a good job despite field restrictions might compensate for greater expense. Under other conditions, however, use of a data center offers a means for making an overall field project more economical, (1) by using a well-coordinated team of people whose duties are commensurate with their skills to plan and execute the project, and (2) by producing a near-final map and report by the end of the field season through editing and compiling concurrently with the fieldwork. The data-center technique would augment conventional mapping, and should be used only when the desired end results can be attained faster, more efficiently, or more economically than by conventional mapping.

The ideas presented in this report are based on various field exercises involving data centers, most particularly the exercise discussed in a companion report that appears elsewhere in this chapter (Lucchitta and others, 1969, p. C158). Systematic description, communication, and recording—essential to the proper functioning of the data center—are also discussed in the companion report.

OPERATION

The use of a data center typically involves a fieldman radioing his observations to the center, housed in a van or trailer, where they are tape recorded. A communicator keeps in radio contact with the fieldman, asks for clarifications, makes pertinent suggestions, and commonly takes notes as well. A plotter, possibly the communicator himself, enters geologic information on photographs, maps, and sketches. This basic arrangement can be expanded or contracted to meet specific needs.

Relatively large and complex data centers would probably be best used in conjunction with several field parties. They would seem ideal for reconnaissance work, particularly the kind involving use of helicopters, where the geology of a large—and commonly remote—area is mapped in a short time. They may also be useful for more detailed fieldwork that can be improved through immediate compilation and discussion. Detailed mapping could also be carried out by using the data center for an initial reconnaissance of the area, the details being filled in later by conventional mapping. Smaller data centers can probably be used with a single field

U.S. GEOL. SURVEY PROF. PAPER 650-C, PAGES C155-C157

337-735 O—69——11

party, while the smallest and simplest ones imply, in essence, more efficient utilization of field assistants.

TYPES

Three main conceptual types of data center are discussed below, but each type can have many configurations, each of them best suited to specific conditions.

1. *Large data center.*—This, the largest and most complex type, would be used only in conjunction with several field parties working simultaneously. With some imagination and optimism, one could envisage a fixed and permanent data center serving a whole region. A large data center requires communicators, recorders of verbal information, recorders of map information, typists, draftsmen, and a coordinator. Several of these functions can probably be fulfilled by the same individual, as time and rate of data flow permit. Since the electronic equipment used is likely to be complex, the services of an electronic technician would be desirable.

The basic equipment needed would consist of good two-way radios, a reliable source of electricity, drafting facilities, typewriters, and devices for filing and displaying information. The whole would be housed in one or more trailers. This type of data center could be associated with a mobile laboratory—of the type already in existence—to enable prompt microscopic and laboratory analysis of samples.

2. *Small data center.*—This type of data center would be similar to the large one but designed to serve only one field party; it would thus be much smaller and simpler. The required tasks would be the same, but two or more could be fulfilled by each man. Thus, the communicator could double as coordinator, the recorder of verbal information as typist, the recorder of map information as draftsman. If necessary, taped transcripts could be sent to the home office for typing. Similarly, the full-time services of a mobile laboratory would probably not be economical, but speedy processing and return of material and data could be arranged.

3. *Field man and two assistants.*—This type of data center would be best suited to small field operations akin to the conventional type. Special equipment needed would consist of two-way radios, tape recorders, an electric generator, and drafting tools. Sample analysis and most typing would be done at the home office and the results promptly returned to the field. One assistant would accompany the geologist in the field; the other would man the base station, recording and plotting the data radioed from the field. In addition to his conventional duties, the assistant in the field would keep track of location. There may be times during a field season when it would be more efficient for the geologist to record his field notes directly on magnetic tape rather than transmit them by radio. The recorded tapes would be given to the camp assistant at the end of each day; the assistant would transcribe the notes and transfer map information to the compilation sheet on the next day. The one-day time lag would not present a serious inconvenience.

ADVANTAGES

Use of a data center would yield the following advantages:

1. Field men would be freed from the chore of recording many of their data and would thereby be encouraged to report more. The resulting notes would be relatively complete and well edited.

2. Several field parties could map simultaneously in a given area and report to the same data center, resulting in the speedy development of a much more comprehensive and regional perspective than would be possible with the separate mapping of individual areas.

3. Compilation of geologic maps, cross sections, measured sections, and so forth, and the processing of data in general, would proceed simultaneously with the fieldwork, giving better direction to subsequent mapping, and eliminating much of the field checking that is so commonly required to rectify errors or omissions. The communicator or the data recorder could often point out inconsistencies, omissions, or inadequate information before a field party leaves a particular locality.

4. Many of the routine tasks that commonly must be done by the geologist or party chief in the office would be done in the field by field assistants or other less highly trained personnel. The geologist's office time would thus be released for activities that better utilize his training.

DISADVANTAGES

The data-center technique would have limitations, but many could be overcome by using proper equipment and suitable procedures. Potentially serious limitations follow:

1. The necessary equipment would generally be more expensive than ordinary field equipment. A compromise would have to be made between economy and excellence.

2. The equipment would be more complex than that normally used in fieldwork. This would require familiarization on the part of the users and would introduce a greater possibility of equipment malfunction or failure.

3. Adequate radio communication generally requires that no major topographic obstacles lie between transmitter and receiver. Possible solutions would be: (a) set up base camp in an open, unobstructed area; (b) elevate

the base station antenna (for example, by attaching it to a helium-filled balloon); (c) set up a self-powered repeater station on a prominence with line-of-sight transmission to the base station and most of the area to be mapped; and (d) transmit information from the field to the base station only when in a favorable position. In order to implement the last solution, the geologist would tape record his observations as he made them, transmitting them to the base station in one burst from the top of a hill; this could be done while he was otherwise engaged (looking at an outcrop, having lunch) by playing back the tape recorder at high speed and feeding its output into the transmitter.

4. Describing geologic features to people who are elsewhere is difficult and calls for systematic procedures, which are analyzed in the companion paper. Geometric information is particularly difficult to describe in words and can probably be transmitted adequately only by means of the line tracer. Such a device, which is now being studied by the U.S. Geological Survey, consists of a modified *X–Y* plotter which is carried by the fieldman and which can translate the two-dimensional movement of a writing pen into an appropriately modulated radio signal. This signal is detected by a similar device at the base camp (data center) and reconverted into two-dimensional movement of a recording pen. The geologist in the field can thus make a sketch, or draw a contact on a registered map, and have the sketch or contact reproduced simultaneously in camp. The line tracer must be accurate, portable, and relatively inexpensive.

SUMMARY AND CONCLUSIONS

The use of a data center should encourage speedy development of a comprehensive and regional perspective, utilize people economically in functions commensurate with their training, generally make for more efficient use of time, and reduce overall costs for some field projects. However, the use of any type of data center implies that the geologist in the field must describe his observations to people who cannot see what he is talking about but who must understand his descriptions and record them. This requires systematic and logical methods for describing, communicating, and recording. These methods are not spontaneous—that is, they must be learned—but, as was shown in a preliminary test (see Lucchitta and others, 1969; p. C158, this chapter), they do tend to encourage more complete and more comprehensible observations than those commonly made in conventional field mapping.

USE OF A DATA CENTER IN GEOLOGIC MAPPING—A TEST REPORT

By IVO LUCCHITTA, JOHN W. M'GONIGLE, DAVID SCHLEICHER, and MORTIMER H. HAIT, Flagstaff, Ariz.

Abstract.—A field test was held to study geologic exploration done in conjunction with a data-reduction center conceptually similar to that proposed for lunar exploration. A geologist in the field radioed his observations to a van, where they were recorded by three other geologists. Objectives were to test: a guide for describing geologic data, forms for systematically recording and retrieving the data, and procedures for effective communication. The test suggests that a data center can effectively record and organize geologic data. Use of a description guide focused and organized descriptions. The recording forms tested did not provide for recording interpretations or making corrections, but they did systematize the raw field data.

This report discusses a test of methods for geologic description and recording held in the Rainbow Gardens, just east of Frenchman Mountain, Clark County, Nev., from April 23 to April 28, 1967. The test was the first of a series whose purpose is to study the application of proposed lunar techniques, developed under National Aeronautics and Space Administration (NASA) contract, to terrestrial geologic exploration and mapping.

It is a pleasure to acknowledge Harry Smedes' collaboration during this test.

BACKGROUND AND OBJECTIVES OF THE TEST

Lunar geologic exploration must be as efficient as possible to compensate for the restrictions imposed on the astronauts. Accordingly, it has been suggested (E. N. Goddard and others, unpub. data; David Schleicher and J. M. Goldberg, unpub. data) that the astronauts radio their geologic observations to an Earth-based data center, which would edit the incoming data for clarity and completeness and would systematically record descriptive data as well as compile maps and sections. The resulting notes and compilations would be far more elaborate than any that could be made on the Moon. More fundamentally, they would be made available to a team of scientists for intensive study, thus enabling prompt answers to the astronauts' questions, and suggestions on how to deal with scientific contingencies. The hope was that such a system might be advantageously used for terrestrial geologic mapping in situations roughly analogous to those expected on the Moon, that is, where field time is restricted or logistics are difficult (see Lucchitta and others, 1969; p. C155, this chapter).

The problem of terrestrial geologic exploration in conjunction with a data center was approached by analyzing three activities considered to be basic to field mapping—description, communication, and recording—in an attempt to adapt them for use with a data center. The test was designed to evaluate equipment and procedures for carrying out these three activities. A geologist in the field was to radio his observations to the data center, where the information was to be recorded in several ways.

The general objective of the test was to compare the effectiveness of handling geologic data through the data center with the effectiveness of more conventional methods. Specific objectives were to test (1) the radio gear and the van serving as a data center; (2) a description guide and recording forms for geologic field data; and (3) the means for orally communicating the type of information commonly shown on a geologic map.

GEOLOGIC SETTING

Discussion of the geologic setting is superficial because we have deliberately avoided learning about the test-site geology so as not to vitiate test results by knowing too much about the geologic relations that were being described and recorded. For more complete information, see Longwell, Pampeyan, Bowyer, and Roberts (1965).

The test area covers several square miles. The underlying sedimentary rocks differ greatly in their resistance to erosion. The units are offset, tilted, and repeated by faults and are eroded into subparallel hogbacks. There is very little vegetation, and alluvium is confined to

narrow valleys between the hogback ridges. Relief is several hundred feet.

The area was selected for the test because its superb exposure of distinctive rock formations and its apparently straightforward structure aided photogeologic interpretation before the test and the subsequent field testing of techniques and equipment in a nearly ideal, yet geologically real, setting.

Map bases consisted of aerial photographs at scales of 1:47,200 and 1:23,600, and of 15-minute topographic maps at a scale of 1:62,500.

EQUIPMENT USED

The data center for the test was an air-conditioned van about 12 feet long, 8 feet wide, and 8 feet high, with tables built in along most of the two long sides. A 2.5-kilowatt generator and a 110-ampere-hour battery provided, respectively, 110-volt a-c and 12-volt d-c electric power.

The fieldman used a 5-watt walkie-talkie. (Most walkie-talkies have 1 or 2 watts of output power.) The data center used a 5-watt base station with an external 17-foot antenna. The radios operated on the AM frequency of 27.575 megahertz assigned to government use.

HANDLING GEOLOGIC DATA

Nature of geologic data

The use of radio communications has shown that some geologic data are relatively easy to convey in words, whereas others are not. In general, the easily conveyed (or "verbal") data are those for which there exist well-defined and clearly labeled conceptual models that are universally understood. The term "subrounded," for example, applies to a reasonably well-defined geometric form. Similarly, "granite" is the term applied to the model of a rock with certain widely accepted attributes. Any model is an idealization that conveys a certain amount of information. Because it is necessarily a generalization that considers only the attributes common to an entire class of objects (for example, folds), it neglects the features peculiar to any one of the objects within the class (for example, a specific anticline). Therefore, existing models often do not depict specific objects with sufficient accuracy; they are perhaps most commonly inadequate for depicting the details of complex geometric relations, because these relations are unique at each locality. Thus, although "nappe" suggests a general geometric model and "digitate nappe" a more refined model, accurate depiction of a specific digitate nappe requires the use of graphic devices, such as maps and cross sections.

Test preparation

As the aim of the test was to evaluate means of handling various types of geologic data, we prepared a description guide for use in the field, data recording forms for use in the data center, and photogeologic maps for both the field and the data center. The tentative description guide and data forms were checked against earlier description guides (H. H. Schmitt, unpub. data), descriptions given in previous tests, and stratigraphic and structural descriptions in the geologic literature. They were amended on the basis of these comparisons and finally were tried out before the test by describing outcrops of sedimentary and igneous rocks.

The description guide shown below was intended to be specific enough to encourage efficient description of routine geologic features, but still flexible enough to allow for describing unexpected but significant features or for disregarding irrelevant data:

Field description guide

GENERAL STATION INFORMATION

Station
Coordinates
Number of remote and local descriptions that will be made
Topics that will be discussed in the descriptions

SPECIFIC TARGET INFORMATION

Nature of individual description (remote or local)
Location of object described
Photograph numbers and identification of features portrayed

GEOLOGIC INFORMATION

General Introductory Description—Setting (transcurrent features—pertain to more than one unit)
- Topography
- Overall exposure
- Geomorphology
- Units
- Layering
- Fractures
- Folds
- Other geomorphic, stratigraphic, or structural features

Description of Individual Units ("internal" features—pertain to individual units)
- Unit
- Dimensions
- Colors
- Texture
- Composition
- Rock type
- Layering
- Contacts
- Fractures
- Folds
- Other internal structures

Conclusions, Hypotheses, Ideas

It was designed to be a simple mnemonic aid giving a sequence for describing geologic data, rather than a pigeonhole type of checklist, which tends to be restrictive, cumbersome, hard to remember—and an end in itself. The idea was to provide for a hierarchic presentation that logically links observations at different scales or levels (showing, for example, the relation of the grains to the bed and so to the member and to the formation). The guide thus encourages reporting the relations between facts as well as the facts themselves.

The forms shown by figures 1*A* and 2 provide for rapid and unambiguous recording of verbal data, as well as for easy reference to the data for correlation and interpretation; the forms thus represent a filing system that allows for cross indexing.

Two types of recording forms were developed. One (fig. 1*A*) is for general observations at the scale of whole outcrops and panoramas. The other (see fig. 2) is for single rock units; these data are generally more detailed and less interpretative than those recorded on the first form.

The main problem in designing a recording form was to provide a comprehensive and convenient format that would fit on a single sheet of paper about 8×10 inches in size. To achieve this format, we used the form as an underlay over which a blank subtransparent sheet was slid, so that the scheme for recording data (for example, "Color") within any descriptive category (such as "Unit") could be used as often as necessary: in this example, there would be as many descriptions as there are units observed at the station (see figs. 1*A* and *B*). As another example, the characteristics of each type of layering (for example, bedding or foliation) in a rock unit would be recorded in a definite sequence that would be repeated as many times as there were types of layering in the unit (see arrow, fig. 2). Use of the blank overlay sheet makes it possible to append marginal explanatory notes and to depart from the fixed format whenever necessary. Figures 1*B* and 2 show examples of data records obtained with the underlays.

Because experience had suggested that geometric data would be difficult to convey verbally (see section "Nature of geologic data," beginning on p. C159), the fieldman spent part of his time describing geometric relations in certain areas. These data were to be used during the traverses to annotate and amend the photogeologic base map and to compile cross sections, stratigraphic sections, and sketches, thus showing how well the data-center personnel could assimilate, interpret, and correlate such geometric relations.

To save field time and improve the quality of observation, we planned to use the "problem-solving method," that is, a field application of Chamberlin's (1897) ideas, in this case choosing in the field between alternative hypotheses defined before the traverse. To give a simple example, it was possible to determine from the photogeologic map that most of the faults in the test area were dip-slip rather than strike-slip, but it could not be decided whether they were high angle or low angle. Once these alternative hypotheses were defined, however, field inspection could quickly point to the correct one.

The method implies the definition of problems and the formulation of potential solutions before fieldwork begins. As much work as possible is done in the office, thus freeing field time for the activity to which it is especially well suited—the gathering of data. Efficiency is further increased by eliminating the need to describe the hypotheses themselves, by enabling the fieldman to select only those data most critical to the solution of a problem, and by encouraging him to follow the scientific method more rigorously than he otherwise would. Even unforeseen and unexpected problems will be easier to handle in the context of an established framework.

To implement the method, a detailed photogeologic map was used to outline localities where critical geologic relations could probably be observed in the field but could not be deciphered from the aerial photographs, partly because of limited resolution and (or) perspective and partly because of incomplete exposure or geologic complexity. The next steps would have been to formulate alternative hypotheses explaining the relations seen on the photographs at each problem locality, to label these hypotheses by letters or numbers, and finally, in the field, to select the correct hypotheses or formulate a new solution. Unfortunately, this program was a secondary objective of the test, so that lack of time prevented the compilation of a list of clearly stated and labeled hypotheses, even though the locations of the critical areas were known.

The main use of the photogeologic map was to define areas from which we needed field information and, accordingly, to plan traverses and stations for the test. Areas with apparently simple structure were selected to study the handling of "verbal" data (for example, stratigraphic descriptions), whereas areas whose geology appeared to be geometrically complex were chosen to study the handling of geometric data.

Test procedure

One geologist (the fieldman) followed planned traverses, visiting designated stations where he described lithology, contact relations, structures, and so forth. Instead of making notes, maps, or sketches, he radioed his observations to a team of three geologists in the data center. One member of the data-center

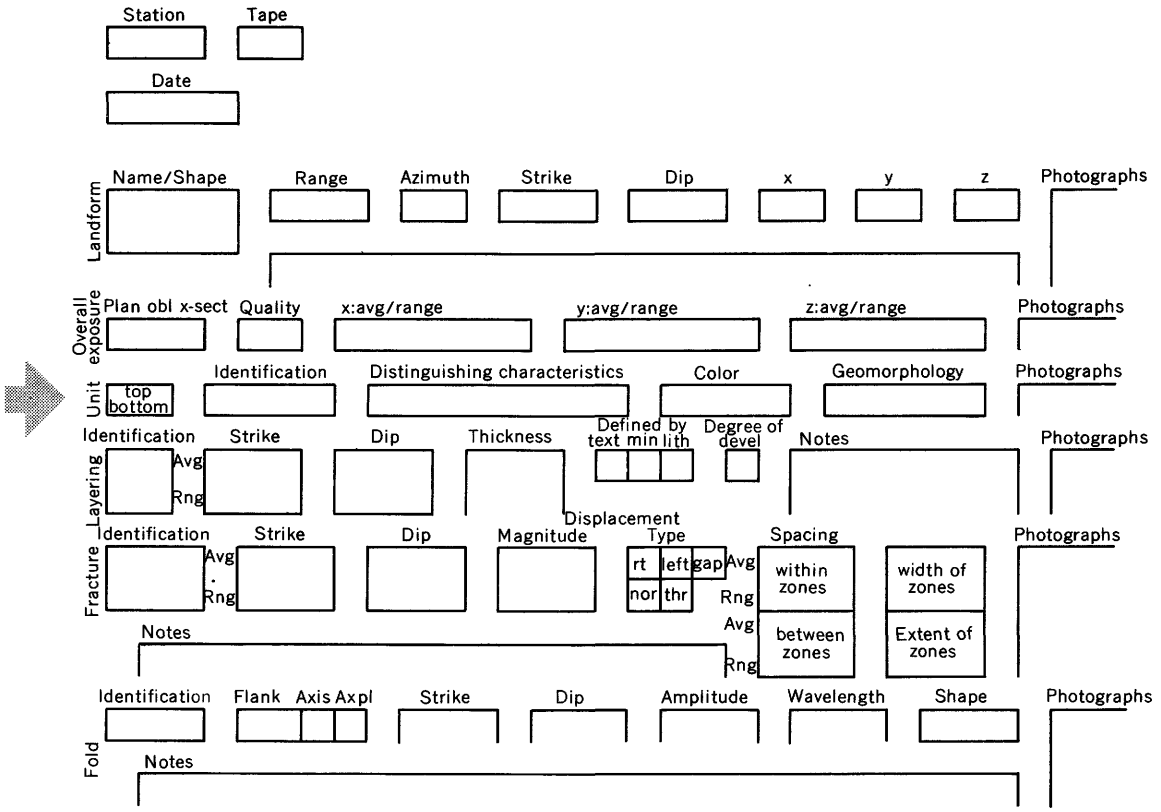

A

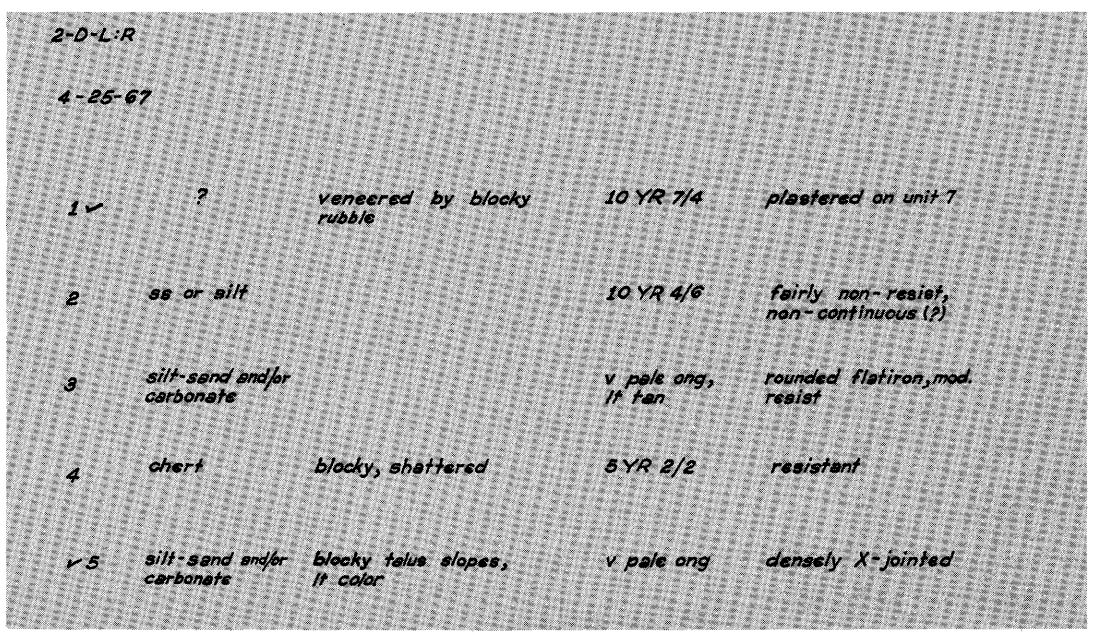

B

FIGURE 1.—Recording form for geologic setting (information pertaining to more than one map unit). *A*, blank form; *B*, data for a sequence of five lithologic units recorded on subtransparent overlay placed over format for "Unit" (indicated by arrow) on blank form *A*.

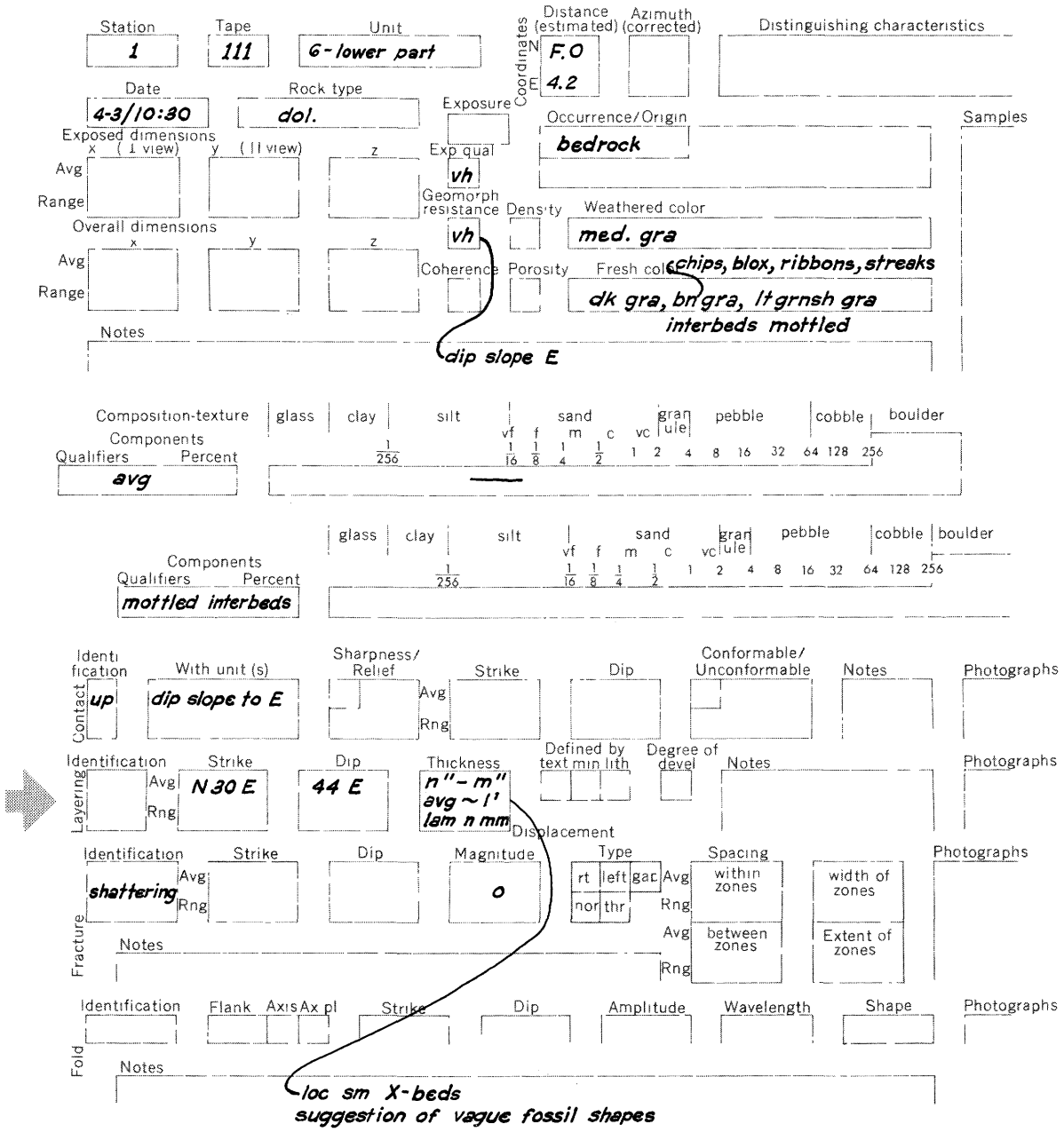

FIGURE 2.—Data as recorded for one map unit (for purposes of illustration, data are here superimposed on recording form). Note how marginal annotations impart flexibility to data recording. Arrow explained in test, p. C160.

team (the communicator) acknowledged the fieldman's transmissions and ensured their clarity and completeness, commonly making brief notes and sketches to aid his understanding of the field relations. A second man (the data recorder) entered incoming data on prepared forms, and the third man (the photogeologist) annotated and revised a photogeologic map on the basis of the incoming information; both occasionally asked the fieldman questions to resolve problems concerning their work. All radio conversation was tape recorded.

The fieldman generally used the description guide, but occasionally he substituted the recording form (fig. 2) as a description guide so that we could see how a more specific format affected his descriptions. He gave his position and that of features he described by means of coordinates on a grid overlay registered on the aerial photographs, but he referred some locations to topographic, geologic, or photographic features; to stations identified before the traverses; or to other annotations on the photographs.

Most traverses lasted several hours; afterward the team criticized the results and suggested modifications of technique for later traverses.

EVALUATION OF EQUIPMENT AND PROCEDURES

Equipment

The van was large enough for the three men, but sitting back to back was awkward. Coordination between communicator, data recorder, and photogeologist would be easier if they could all work around one table.

Air conditioning increased cleanliness and comfort.

The generator was disturbingly noisy and caused severe vibration because it was mounted directly on the truck bed. A generator trailer, or shock mounts and a good muffler, would eliminate both problems.

There was relatively little radio interference, even though in this area the assigned frequency is probably used a great deal by various government agencies. Transmission was clear and free of noise to a distance of several miles. Line-of-sight transmission was not necessary, although loss of signal occurred when the walkie-talkie was very near a steep slope, as, for example, in a steep-walled canyon.

The base station worked well, although the sound quality was rather poor. A single microphone and speaker in the van proved inadequate—members of the team could not hear the fieldman clearly, nor could they communicate with him conveniently. Background noise and the seating arrangement hampered communication between the members of the data-center team. A solution would be to provide each member of the team with earphones and a microphone, preferably built into a headset.

Performance of the walkie-talkie was excellent. Wind noise presented little problem because of the high-frequency rolloff of these units; under extremely windy conditions the microphone could easily be shielded from the wind. (Many walkie-talkies, however, are rather sensitive to the wind.) Each of the nickel-cadmium battery packs lasted about 4 hours in use and required about 18 hours for recharging.

The 5-watt walkie-talkie is larger and heavier than most walkie-talkies and consequently more awkward. A headset would make it possible to use a hammer, hand lens, rock color chart, and so forth, while transmitting descriptions. The 5-foot-long antenna could be a problem in brushy or timbered terrain.

Procedures

Description.—In general, descriptions made following the description guide were more complete and less wordy than those made without it. The guide helped the fieldman to organize his observations and descriptions and to focus on data relevant to the problems defined from the photogeologic map. Whenever the fieldman used the data-recording form in place of the description guide, the recording of data in the center was much easier, pointing up the need for correlation between description and recording formats.

Practice with the description guide greatly improved the description. The fieldman suggested that he could probably memorize the description-guide format in a few days at the beginning of a typical field season.

In general, verbal description of geometric relations was not successful. In most cases the fieldman could not convey information to the plotting crew without spending more time and energy than he would have spent mapping conventionally. Geometric information may be easier to describe and communicate with a more refined system of description and with more practice. Field annotation of Polaroid photographs also may help.

Recording.—The data forms made it possible to record "verbal" data quickly and to retrieve selected data with reasonable efficiency, but they did not lend themselves to depicting geometric relations. Although in general the data forms worked well for verbal data, they were not suitable for recording and filing interpretations, syntheses, and generalizations, nor for handling corrections. The idea of sliding overlays was apparently sound in that it made it possible to record data that could not easily be pigeonholed. Sliding the blank overlays over the master format sheet was awkward, but a simple mechanical holder might solve this problem. Considerable practice was required to become familiar with these forms—as with any other forms this complex.

Geometric data are best recorded on sketches or directly on the photogeologic map, and correlations are best done on sketch stratigraphic sections. Sketches made by the communicator on the basis of the incoming data helped the data-center team to understand the field relations and showed what was unclear or incomplete.

Problem solving.—Because we had not completely defined alternative hypotheses before the test, we could not often use the problem-solving method effectively. In the few instances when the fieldman was able to confirm or reject previously formulated hypotheses, however, efficiency was high. This was illustrated in a minor way by his accepting or rejecting tentative photogeologic contacts, faults, and so forth.

With rigorous preparation the problem-solving method can increase efficiency, for whenever potential solutions to a problem have not been anticipated and expressed, lengthy descriptions of geologic relations are unavoidable, and much thinking that would better have been done beforehand must be done in the field.

RECOMMENDATIONS FOR PROCEDURES

Some of the more general results of the test have already been presented. Specific conclusions and recommendations are summarized below under headings that correspond to the three primary test activities. Whenever activities overlap, making it difficult to decide whether a given point should be listed under, say, description or communication, similar conclusions are entered under more than one heading to indicate the interrelation.

Description

1. The description guide is a valuable mnemonic aid. Because it is deliberately concise—hence not comprehensive—practice is required for its proficient use.

2. Description should be systematic and should, in general, proceed from the system to the component, the general to the particular, the rule to the exception, the far to the near. This is necessary not only to ensure the satisfactory communication of information but to encourage the completeness and accuracy of the observation itself, in some cases bringing out details and relations otherwise unseen. Descriptions probably need not be rigidly systematized; certainly, though, an organized presentation aids recording. Because such a procedure is logical, it is relatively easy to learn and use.

3. In general, information should not be given between stations, because it is confusing and almost impossible to record systematically.

4. For each description, it is important to establish the geologic context against which information can be seen, understood, and evaluated. Accordingly, the fieldman should first present a generalized picture, indicating what information he will give and, in some cases, why. In general, geologic objectives should be planned before the traverses, and the data center should remind the fieldman of them at each station.

5. The fieldman should categorize or label information before giving it; he should, for example, indicate whether the information should go on a map or on a recording form, or whether it is an incidental note to appear only on magnetic tape. He should also indicate how detailed his description will be, thereby preparing the data team for recording the data in the most appropriate ways. If the fieldman plans to give information on a particular subject at a later time or at another station, he should say so.

6. Verbal description of geometric relations is difficult. Until an electromechanical line tracer or similar device becomes available, such description should be kept to a minimum, for example, by using the "problem-solving" method. Possibly, geometric information should be handled by conventional mapping, or by annotating Polaroid photographs in the field; the function of the data center during the traverse would then be to compile and coordinate only "verbal" data.

7. Frequent summarization of data by the data center for the fieldman enables the entire team to check the data for errors and to keep abreast of the compilations.

8. Whenever possible, the fieldman should describe objects by comparison with familiar objects or with objects that were described previously.

9. Distinctive, characteristic, and important features of any object should be mentioned even though they may seem obvious to the fieldman.

10. Topographic and photogeologic features should be labeled before the traverses to speed up description.

11. The fieldman should not waste time verbally describing features that are best portrayed by a photograph, but he should give enough information about each photograph to make its significance clear.

Communication

1. Practice is needed to speak proficiently on the radio.

2. In general, transmitting only a few sentences at a time makes recording easier and eliminates the need for lengthy repetitions owing to poor transmission.

3. A distinction should be made between a routine check back after transmitting a quantum of information ("Check?") and the end of the transmission ("Over."). This will ensure that the transmission is not interrupted by questions and comments that should be held until the end of the transmission.

Recording

1. Recording forms should probably be used to facilitate retrieval of selected data for study and ultimately for incorporation into a report. The forms should be flexible enough to enable recording of interpretations and syntheses, as well as of more routine descriptive data.

2. In any data record, it should be possible to correct mistakes and to judge the reliability of the data.

3 A complete record of the geologic field descriptions is essential; it should be on magnetic tape and probably also in printed transcript. Immediate access to the tape or a transcript allows the plotting crew to catch up if they fall behind.

4. Recording forms must be comprehensive, yet compact. The present underlay format to record repetitive information was awkward to use even though the idea is probably sound. A more efficient mechanism for sliding the overlay is needed.

5. Maps, sections, and sketches are probably the best means for recording geometric data. A system should be developed for filing sketches keyed to each station on the traverses, thus allowing for ready comparison.

REFERENCES

Chamberlin, T. C., 1897, Studies for students: Jour. Geology, v. 5, p. 837–848; reprinted in 1931 *as* The method of multiple working hypotheses: Jour. Geology, v. 39, no. 2, p. 155–165.

Longwell, C. R., Pampeyan, E. H., Bowyer, Ben, and Roberts, R. J., 1965, Geology and mineral deposits of Clark County, Nevada: Nevada Bur. Mines Bull. 62, 218 p.

METHODS OF STORING AND RETRIEVING CORE-LOG DATA ON COAL-BEARING ROCKS IN SOUTHWESTERN PENNSYLVANIA

By B. H. KENT, Denver, Colo.

Abstract.—Core-log data on Upper Pennsylvanian and Lower Permian coal-bearing strata in southwestern Pennsylvania are being stored and retrieved by computer methods by the U.S. Geological Survey. In the format for storage, a numerical code is applied to the named stratigraphic units and to all subordinate rock units in the lithologic column; data are then punched on cards. Both the code and the card-file system are expandable, to accommodate new data or further subdivision of rock units. Retrieval by specifying coded contacts instantly provides, for example, data on thickness of intervals and constituent coal, sandstone, and limestone, and on cumulative thicknesses. Utilization of this wide range of selective data, instantly available on demand, is illustrated by a coal-to-coal isopach map series. Comparisons between isopach maps in this series show recurring thickness patterns of possible environmental significance.

Upper Pennsylvanian and Lower Permian coal-bearing rocks in southwestern Pennsylvania were deposited in a large geosynclinal trough known as the Dunkard basin. The regional extent of the Dunkard basin as outlined by either the Pittsburgh coal bed or the base of the Upper Pennsylvanian Monongahela Group is shown on figure 1. As shown on figure 2, many of the coal beds and rock units present in southwestern Pennsylvania also occur in West Virginia and Ohio, and it is not difficult to correlate them across the northern part of the Dunkard basin even though stratigraphic nomenclature differs from place to place.

The Pittsburgh coal bed has been, and continues to be, a major source of bituminous coal. Thousands of test holes have been drilled, and coal companies are very generous in releasing core-log data for geologic study, but the volume of data has reached such proportions that the task of sorting and synthesizing it for specific geologic purposes requires prohibitive amounts of time.

Preliminary assessments of such core-log data have shown, for example, that comparisons among isopach maps of stratigraphic intervals, including isopach maps of individual beds, provide environmental, depositional,

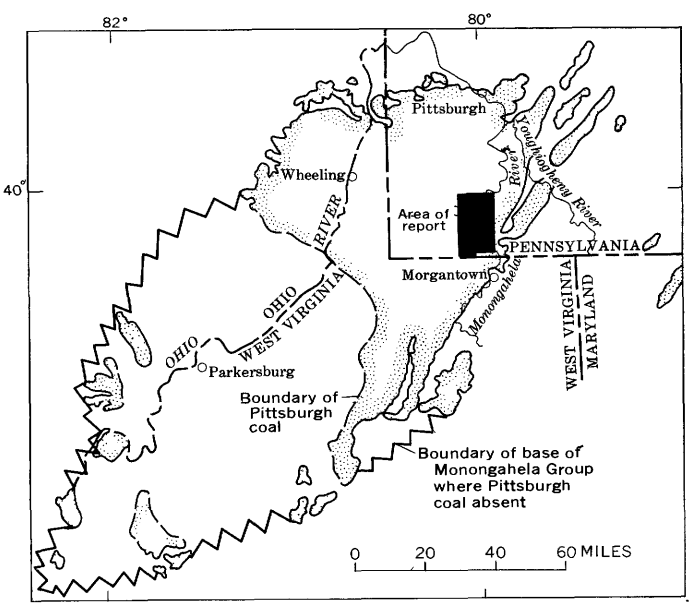

FIGURE 1.—Regional map of the Dunkard basin, incorporating the base of the Pittsburgh coal bed (stippled) and the base of the Monongahela Group.

and structural information which aids in reconstructing the geologic history of an area and in identifying some of the factors that influence the accumulation of coal. Compiling the thickness data required to make the isopach maps, however, is very time consuming. It has become apparent that if the geologic information contained in this vast reservoir of core-log data is to be adequately assessed, computer methods of data storage and retrieval will have to be used.

A current geologic study area in southwestern Pennsylvania, for which an unusually large number of core logs were available, was selected as a test area to see how computer methods might be applied.

Figure 3, an index map of the test area, shows the locations of core holes for which logs are available. Core

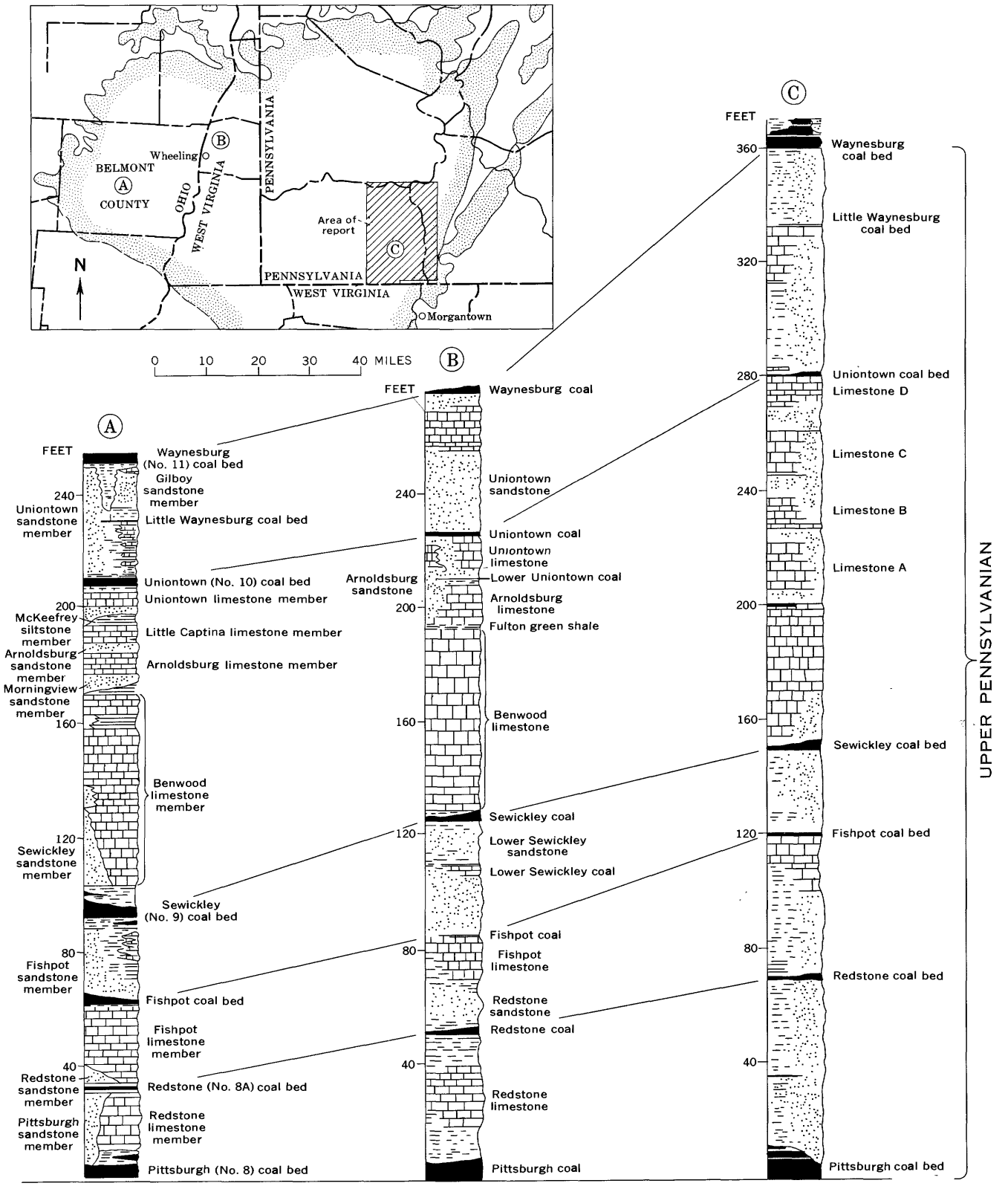

FIGURE 2.—Stratigraphic correlations of Upper Pennsylvanian rocks across the northern part of the Dunkard basin. Column A, Belmont County, Ohio, from Berryhill (1963, pl. 2); column B, Ohio River valley, from Cross and Schemel (1956, fig. 1–42, p. 54); column C, test area, southwestern Pennsylvania (this paper).

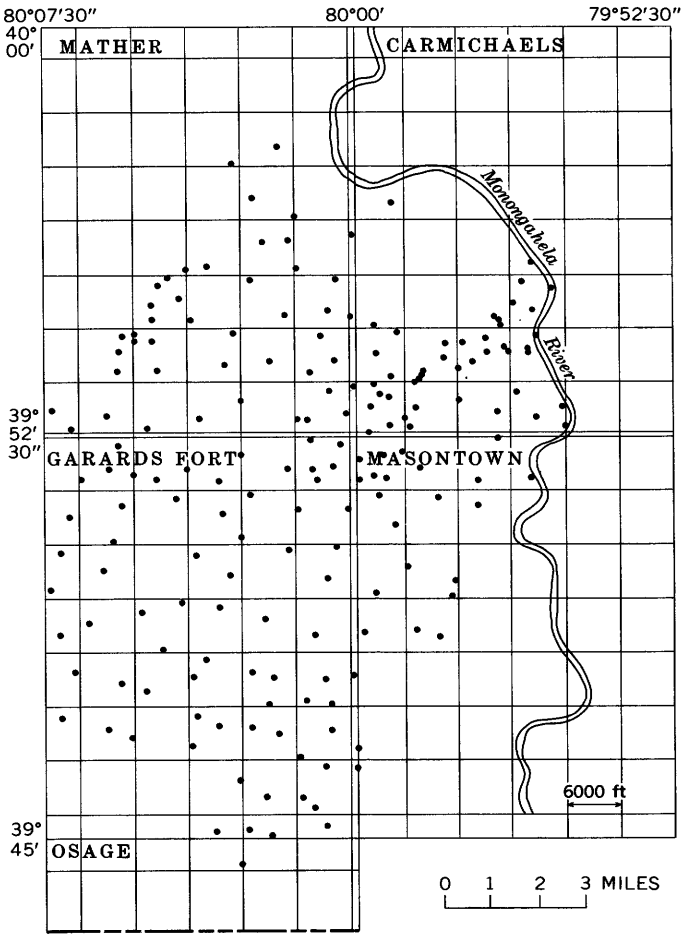

FIGURE 3.—Index map of test area, showing approximate locations of core holes plotted on a 6,000-foot grid.

holes are located with reference to a 6,000-foot grid system.

Although more than 800 feet of section above the Pittsburgh coal bed is exposed within the test area, for illustration purposes only the lower 400 feet is considered in this report. Figure 4, a generalized lithologic column, covers the stratigraphic interval from the base of the Pittsburgh coal bed up through the Waynesburg "A" coal bed. This part of the section includes the Pittsburgh, Sewickley, and Waynesburg coal beds, which are the principal coal beds in southwestern Pennsylvania.

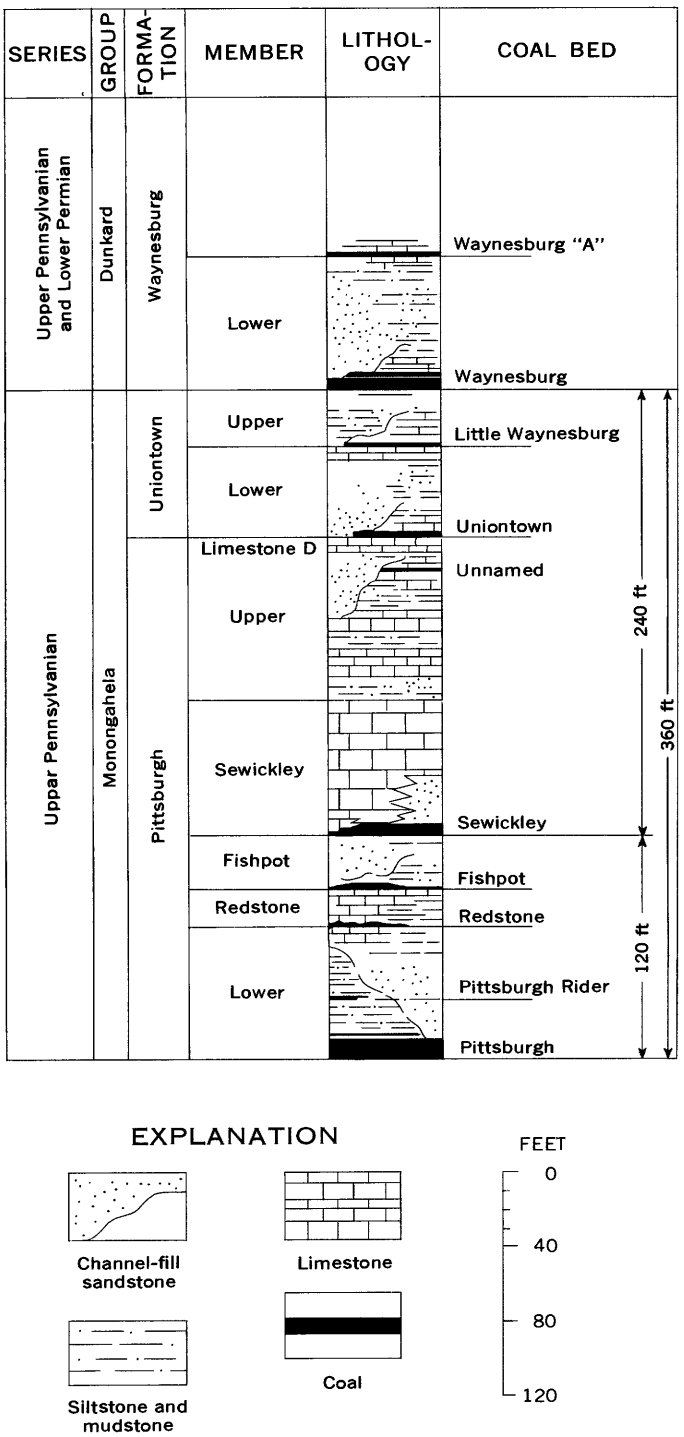

FIGURE 4.—Generalized lithologic column for the test area, from the Pittsburgh coal bed to the Waynesburg "A" coal bed.

PROCESSING CORE-LOG DATA FOR STORAGE

Numerically coded lithologic column

Current stratigraphic nomenclature used in southwestern Pennsylvania (that of Berryhill and Swanson, 1962) was selected as a basic reference, and a numerical code was applied to the lithologic column in the manner shown on figure 5.

Each identifiable rock unit is assigned a unique number that designates the base of the unit and a unique number that designates the top. For example, the base of the Waynesburg limestone of Piper (1933) is contact 430, the top is contact 420, and the 430–420 interval

CONTACT NO.	COAL BED	SANDSTONE UNIT	LIMESTONE UNIT	MEMBER	FORMATION
348				Middle	Waynesburg
349	Waynesburg "A"				
360				Lower	
370		Waynesburg			
380			Elm Grove		
385					
390					
399	Waynesburg				
405				Upper	Uniontown
407		Gilboy			
408					
409	Little Waynesburg				
420				Lower	
430					
438					
439	Unnamed				
440					
450		Uniontown			
490					
499	Uniontown				
510			Limestone D	Upper	Pittsburgh
513					
514		Arnoldsburg			
518					
519	Unnamed				
520					
525			Benwood	Sewickley	
528		Sewickley			
529	Sewickley				
530				Fishpot	
540		Fishpot			
548					
549	Fishpot				
550				Redstone	
555					
556					
557		Redstone			
558					
559	Redstone				
560				Lower	
565					
570					
578		Pittsburgh			
579	Pittsburgh Rider				
585					
590					
599	Pittsburgh				

FIGURE 5.—Numerically coded lithologic column, from the base of the Pittsburgh coal bed (contact 599) to the top of the Waynesburg "A" coal bed (contact 348).

delineates the Waynesburg limestone. Units of channel-fill massive sandstone occur locally at several levels within the column, and the bases of these sandstone units are very irregular. This circumstance does not introduce a coding problem, however, as there is no implication of stratigraphic thickness in the numerically coded lithologic column. Unique numbers can be used to designate the bases of these massive sandstone units. Coal beds are coded in sequence except that, for convenience, each number designating the base of a coal bed is chosen to end in the cipher "9", which serves as a reference to coal and which also keys the code to the stratigraphic nomenclature, inasmuch as the base of individual coal beds commonly marks the base of members or formations.

The 500 series is used to designate contacts within the Pittsburgh Formation, the 400 series is used for the Uniontown Formation, and the 300 series is used for the Waynesburg Formation. Numbers are in sequence but they are not consecutive; unused numbers that fall within intervals between established rock units are kept in reserve in case future mapping or recognition of regional or local facies changes leads to the establishment of new units.

Format for data storage

The next step is to select the types of core-log data to be stored and to design a format for storage. Figure 6 is a sample copy of a standard general-purpose form for computer input, as adapted for use in recording data obtained from hypothetical core log 236.

On figure 6, the information recorded on the top line (the A line) includes the hole number, location of the core hole, the surface elevation (altitude), and the number of B lines to follow. In the sample shown, the X and Y coordinates refer to the 6,000-foot grid system shown on figure 3, and the latitude and longitude coordinates are optional. In the future, however, the 1,000-meter Universal Transverse Mercator grid system will be used to locate core holes; 1,000-meter grid ticks are shown on all 7½-minute quadrangle maps published since 1957, and 10,000-meter grid ticks are shown on the Army Map Service 1:250,000 map series. Use of the Mercator grid system should standardize the location procedure.

Each of the B lines in the format refers to a specific coded contact. For example, line 1 of the B series indicates that contact 348 (the top of the Waynesburg "A" coal bed) occurs at a depth of 50.5 feet and that

Form 9-1506 (Mar.62) GENERAL PURPOSE FORM FOR COMPUTER INPUT

HOLE NO.	LATITUDE	LONGITUDE	X	Y	SURFACE ELEVATION	NO. LINES	
236			-60.0.2.0	345345.45	1102.97	18	A

CONTACT	DEPTH	COAL (inches)	DISCRETE SANDSTONE (feet)	DISCRETE LIMESTONE (feet)	CONTACT IDENTIFICATION	
348	50.5					B
349	51.8	15			WAYNESBURG A COAL	B
360	70.0					B
370	110.5		40		MASSIVE WAYNESBURG SANDSTONE	B
390	110.5					B
399	115.9	40			UPPER BENCH 12 IN. MAIN BENCH 28 IN	B
406	120.0					B
407	140.0		20		GILBOY SANDSTONE	B
420	140.0					B
430	150.0			10		B
510	185.0					B
525	335.0			80	150 FEET OF LIME AND SHALE	B
528	348.5					B
529	350.0	14			SEWICKLEY COAL	B
570	420.0			30		B
585	470.0		50		MASSIVE PITTSBURGH SANDSTONE	B
590	475.0					B
599	484.0	94			PITTSBURGH COAL	B

GPO 857-850

FIGURE 6.—Sample copy of a standard data form, showing format used and types of data stored.

this contact is the first identifiable contact on core log 236. On line 2, the base of the Waynesburg "A" coal bed (contact 349) occurs at a depth of 51.8 feet, the thickness of the coal is 15 inches, and there is no discrete sandstone or limestone in the 348–349 interval. Thicknesses (in feet) of discrete sandstone and limestone units are entered on the lines corresponding to the bases of these units. For example, on line 4, contact 370 designates the base of sandstone (fig. 5) in the lower member of the Waynesburg Formation; this sandstone is 40 feet thick at this core-hole location. The cumulative thickness of sandstone in the 348–370 interval is 40 feet, and the cumulative (or combined) thickness of sandstone in the 348–407 interval is 60 feet.

Lines 4 and 5 illustrate an important aspect of this type of coding. Contact 370 on line 4 designates the base of the Waynesburg sandstone at a depth of 110.5 feet below the surface, and contact 390 on line 5 designates the top of the Waynesburg coal bed also at a depth of 110.5 feet; this means that the base of the sandstone rests on the top of the coal bed at this locality. Both contact numbers need to be recorded in order to delineate both rock units involved. A similar situation is illustrated by lines 8 and 9.

Each core log is examined, and the appropriate code number is applied to the tops and bottoms of all identifiable coal, sandstone, and limestone beds; the code numbers, depths, and cumulative amounts of coal, sandstone, and limestone between the stratigraphic intervals are then posted on the work sheets and punched on cards. Information on the top line of the work sheet is punched on an A (index) card. A separate B card is used for each of the lines that follow. Any number of B cards can be added, as new rock units become established.

DATA RETRIEVAL

General advantages

The retrieval of basic data stored in the manner described above is a simple, rapid, and very flexible process. The elevations of specific contacts, thicknesses of specific intervals, thicknesses of constituent coal, sandstone, or limestone within specific intervals, cumulative thicknesses, and a variety of arrangements of data can all be retrieved automatically, on tape or on printout sheets. In addition, location of core holes with respect to a grid system would permit retrieval of computed data on thicknesses and elevations at any geographic (intersection) point in the grid system. Utilization of this computed information should result in more reliable resource estimates in the future, and serve to guide future fieldwork; however, this aspect of retrieval and analyses has not yet been explored.

Advantages in preparing isopach maps

In studying variations among sections of coal-bearing rocks, it is often advantageous to prepare isopach maps of stratigraphic intervals that do not fall conveniently within the framework of the stratigraphic nomenclature; nevertheless, compilation of the thickness data required is a tedious, time-consuming process. Consequently, the most immediate advantage in numerically coding stratigraphic columns for handling by a computer is the instant availability of thickness and lithologic data on any interval designated by two coded contacts—merely by specifying the two contact numbers involved. The interval for which this information is desired need not be restricted to stratigraphic units such as beds, members, or formations. This flexibility greatly increases the practicality, usefulness, and scope of isopach mapping as an aid to geologic investigations. By way of illustration, three isopach maps are shown on figure 7.

Map comparisons between isopachs of the Waynesburg coal (fig. 7*A*), of the underlying interval (fig. 7*B*), and of the combined sandstone within the upper part of this interval (fig. 7*C*) indicate certain relationships. In general, in areas where the Waynesburg coal is thickest, the underlying non-coal-bearing interval is thinnest; where the Waynesburg coal is thin, the underlying interval is thick; and where the underlying interval is unusually thick, the combined sandstone in the upper part of the underlying interval is also unusually thick.

These thickness relations require additional study for their explanation; and it is beyond the scope and purpose of this report to interpret the maps. It should be emphasized, however, that instant retrieval of data on other coal-to-coal intervals makes it practical to compare many isopach intervals, and that instant availability of a wide variety of data will facilitate the application of statistical tests of reliability. Such work will allow reconstruction of much of the environmental, depositional, and structural history of coal-bearing strata in the Dunkard basin and will help identify some of the factors that influenced the accumulation of coal.

CONCLUSIONS

The numerical code used for southwestern Pennsylvania to identify tops and bottoms of rock units and the punch-card system for storing stratigraphic data can be expanded to allow for new data or further subdivision of stratigraphic units. The same code and filing system should be equally useful elsewhere within the Dunkard

337-735 O—69——12

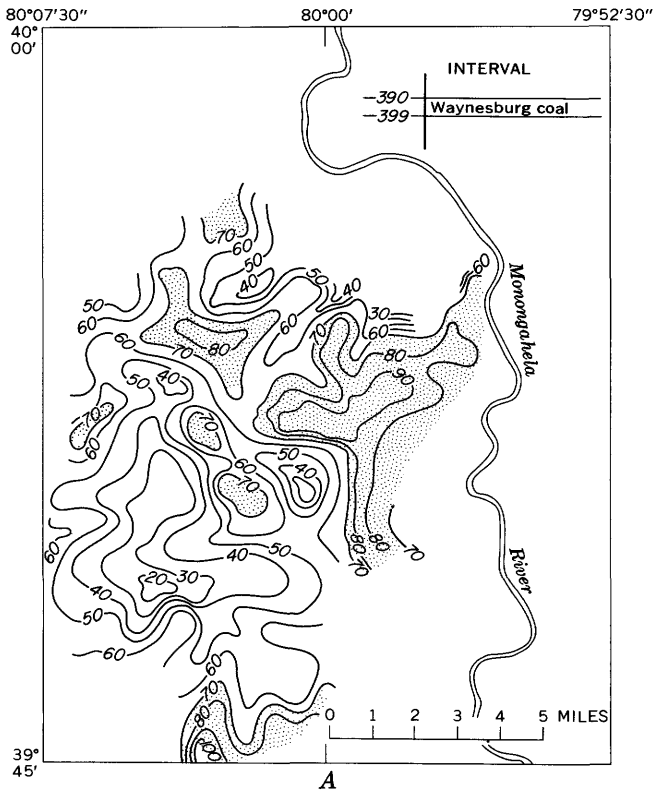

FIGURE 7.—Isopach map series. *A*, Isopach of Waynesburg coal; areas are shaded where the coal is more than 70 inches thick. *B*, Isopach of 529–399 interval, from base of Sewickley coal bed to base of Waynesburg coal bed; areas are shaded where this interval is more than 240 feet thick. *C*, Isopach of combined sandstone in the 510–399 interval; areas are shaded where combined thickness is more than 30 feet.

basin, as the occurrence of correlatable coal beds is basinwide.

In addition to the convenience of having a large volume of data safeguarded and stored in compact standardized form, a wide range of data can be selected and retrieved instantly, on demand. Time-consuming recompilations each time some specific type of data is required are eliminated. Isopach maps of a large number of stratigraphic intervals, or of several individual rock units, can be made and compared for significant relations or for leads to further, fruitful investigations.

REFERENCES

Berryhill, H. L., Jr., 1963, Geology and coal resources of Belmont County, Ohio: U.S. Geol. Survey Prof. Paper 380, 113 p.

Berryhill, H. L., Jr., and Swanson, V. E., 1962, Revised stratigraphic nomenclature for Upper Pennsylvanian and Lower Permian rocks, Washington County, Pennsylvania: Art. 75 *in* U.S. Geol. Survey Prof. Paper 450–C, p. C43–C46.

Cross, A. T., and Schemel, M. P., 1956, Geology and economic resources of the Ohio River Valley in West Virginia—pt. 1, Geology: West Virginia Geol. Survey [Rept.], v. 22, pt. 1, 149 p.

Piper, A. M., 1933, Ground water in southwestern Pennsylvania: Pennsylvania Geol. Survey, 4th ser., Bull. W1, 406 p.

GROUND-WATER INFLOW TOWARD JORDAN VALLEY THROUGH CHANNEL FILL IN SEVEN CANYONS IN THE WASATCH RANGE NEAR SALT LAKE CITY, UTAH

By R. W. MOWER, Salt Lake City, Utah

Work done in cooperation with the Utah Department of Natural Resources, Division of Water Rights

Abstract.—The estimated quantity of underflow moving toward the Jordan Valley in the channel fill of 7 major canyons in the Wasatch Range near Salt Lake City, Utah, is 3,400 acre-feet of water per year. About 2,000 acre-feet of this water is discharged by springs and wells before it reaches the principal ground-water reservoir in the valley, leaving about 1,400 acre-feet per year available for recharge. About 93 percent of the recharge is from Little Cottonwood Creek Canyon and 7 percent from the other 6 canyons.

The amount of ground water entering the Jordan Valley as underflow through unconsolidated fill in seven major canyons of the Wasatch Range was estimated as a part of an investigation of the water resources of Salt Lake County, Utah. The amount of underflow could not be measured directly; but an estimate was made using Darcy's law, $Q=KIA$. Q is the underflow—the amount of water flowing through a selected cross section of the saturated unconsolidated material in each canyon; K is the average hydraulic conductivity of the material, I is the hydraulic gradient, and A is the saturated area of the section. The locations of the canyons and points where underflow was computed are shown in figure 1.

The saturated part of each section consists principally of stream-laid deposits of silt, sand, and gravel; however, at some sections, there may be also glacial deposits, mudflows, and lake deposits. The lithology of the channel fill was determined from examination of exposures in excavations and streambanks, well drillers' logs, stratigraphic descriptions and sections by Morrison (1965), and a lithologic section by Richmond (1964, fig. 7).

The thickness of the fill in six canyons was determined by seismic-refraction methods (Mattick, 1968). (See fig. 2.) It was not possible to determine the thickness of fill in Mill Creek Canyon because of the narrowness of the canyon; however, R. E. Mattick (written commun., 1966) estimated that the fill is at least 50 feet thick. The maximum total thickness of fill in the 7 canyons ranges from about 250 feet in Little Cottonwood Canyon to about 8 feet in Big Cottonwood Canyon, and the maximum thickness of saturated fill ranges from about 170 feet in Little Cottonwood Canyon to about 6 feet in Big Cottonwood Canyon (fig. 2).

Water in channel fill at the sections is under water-table conditions and is moving toward the Jordan Valley. Some of the underflow is discharged as evapotranspiration in areas of streambank vegetation, some is discharged by springs and wells near the mouth of Little Cottonwood Canyon, and the remainder recharges the ground-water reservoir in the valley. Most of the water discharged by evapotranspiration is replenished by seepage from the creeks in lower reaches.

The hydraulic conductivity (K) as used in this report is defined as the amount of water, in cubic feet per day, that flows through a cross-sectional area of 1 square foot under a hydraulic gradient of 100 percent at the prevailing water temperature. Aquifer tests in Emigration and Little Cottonwood Canyons show that the hydraulic conductivities are 17 and 40 cubic feet per day per square foot, respectively. Aquifer tests in Emigration Canyon were made by pumping six 6-inch-diameter domestic wells, about ½ to 1 mile upstream from section A, and observing the amount of drawdown in each of the pumped wells. The hydraulic conductivity was determined by a method developed by Theis and modified by Brown and Meyer (Bentall, 1963, p. 331–340). The texture and sorting of the fill are fairly uniform in the reach of the canyon between the area tested and the section. Therefore, the hydraulic

U.S. GEOL. SURVEY PROF. PAPER 650-C, PAGES C174-C176

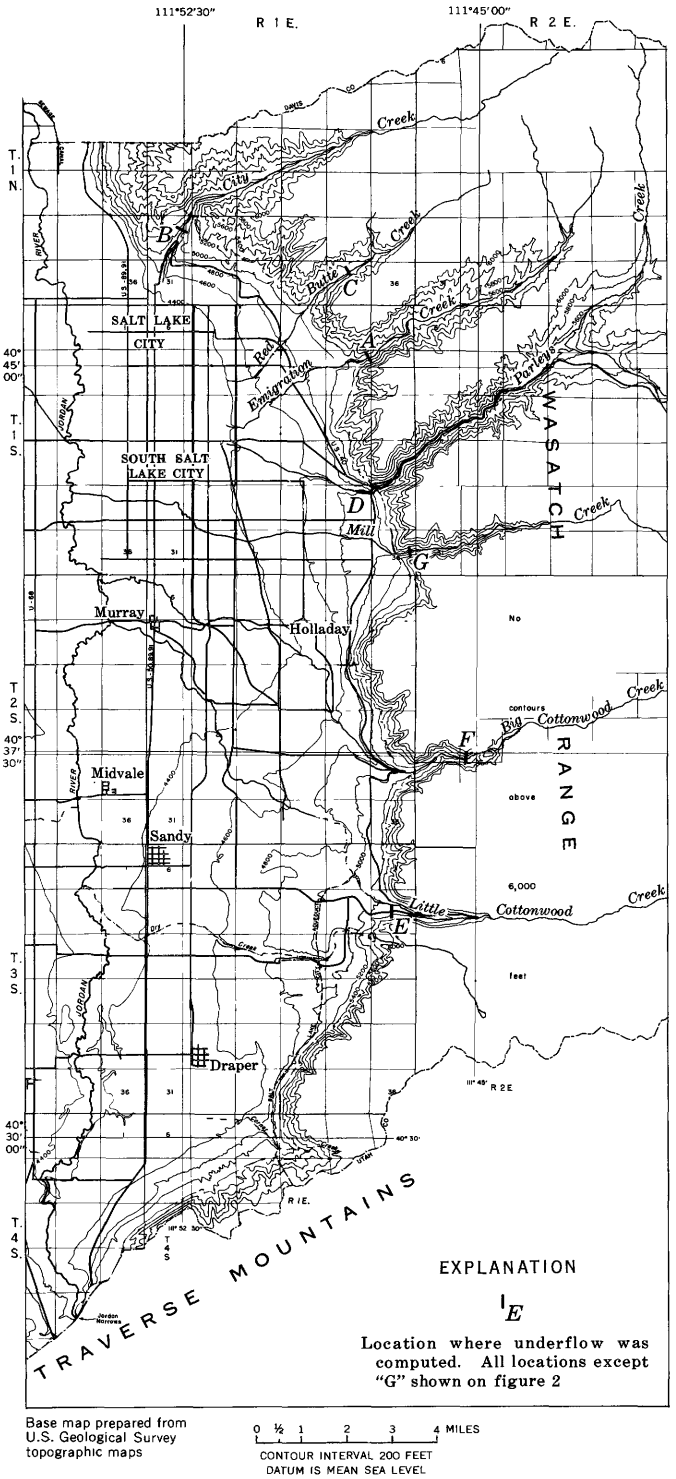

FIGURE 1.—Map of a part of Salt Lake County, showing locations where the amount of underflow was computed in seven canyons in the Wasatch Range near Salt Lake City, Utah.

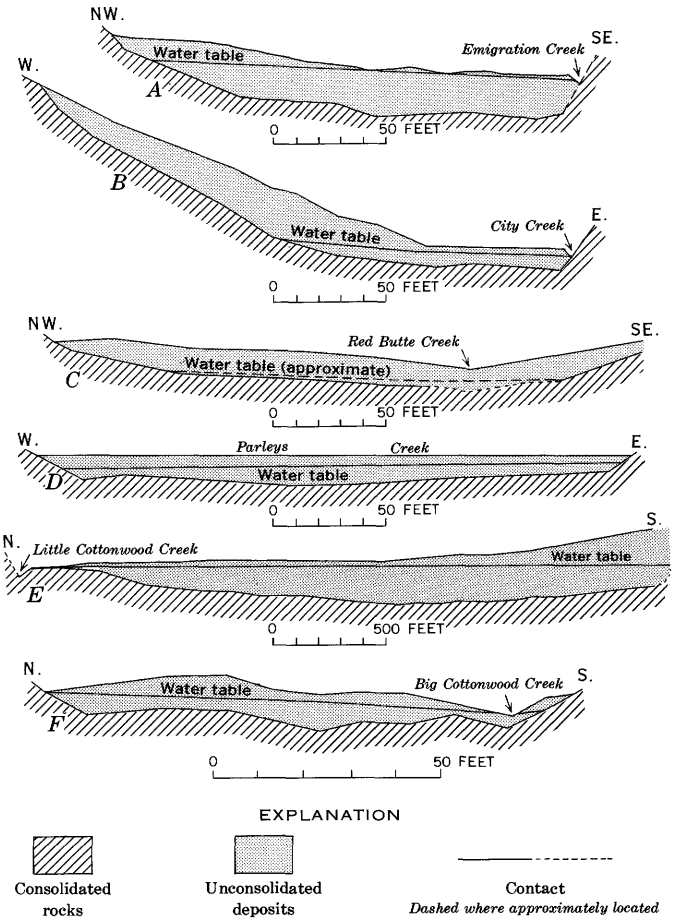

FIGURE 2.—Sections across (*A*) Emigration Canyon, (*B*) City Creek Canyon, (*C*) Red Butte Canyon, (*D*) Parleys Canyon, (*E*) Little Cottonwood Canyon, and (*F*) Big Cottonwood Canyon. The scale below each figure refers to both horizontal and vertical distances. Sections adapted from Mattick (1968, fig. 3).

conductivity calculated from the test data may be used to estimate underflow at the section.

In Little Cottonwood Canyon, one aquifer test was made at section *E* and another was made about half a mile upstream. A study of well logs in this half-mile reach of Little Cottonwood Canyon and of a profile across the canyon by Richmond (1964, fig. 7) indicates that in this reach the texture and sorting of the fill is uniform. Therefore, the average hydraulic conductivity (40 cubic feet per day per square foot) calculated from the 2 aquifer tests can be applied to the section with little error.

The fill in City Creek, Red Butte, Parleys, and Mill Creek Canyons has about the same texture and sorting as the fill in Emigration Canyon. For this reason, although there are no wells with which to test the hydraulic conductivity in these 4 canyons, the hydraulic conductivity is assumed to be the same as in Emigration Canyon, 17 cubic feet per day per square foot. The fill in Big Cottonwood Canyon is more like the fill in Little Cottonwood Canyon than it is like that in Emigration Canyon; therefore, the hydraulic conductivity of the fill in Big Cottonwood Canyon is estimated to be 40 cubic feet per day per square foot.

The average hydraulic gradient (I) of the underflow moving down each canyon is about the same as the average gradient of the streambed. The gradient of the streambed was computed by measuring on U.S. Geological Survey topographic maps, scale 1:24,000, the length of the stream channel between two contours (80 feet of change in altitude), one upstream and one downstream from the lithologic profile across each canyon. The gradients range from 140 feet per mile in Emigration Canyon to 330 feet per mile in Mill Creek Canyon.

The bottom of the saturated fill in the canyons was defined by Mattick's (1968) seismic explorations, but the location of the top or ground-water surface also was needed before the saturated cross-sectional area (A) could be computed. Several shallow holes were dug along most of the profiles in order to define the depth to the water table and the slope of the water table from the canyon walls toward the creek. All the creek beds, except those of Red Butte and Parleys Creeks, intersect the water table where the profiles cross them. The depth to the water table was known also at two wells along the profile across Little Cottonwood Canyon.

The amount of underflow ranges from 3 acre-feet a year in Red Butte Canyon to 3,300 acre-feet a year in Little Cottonwood Canyon and totals about 3,400 acre-feet a year in the 7 canyons (table 1). The saturated cross section is relatively constant throughout the year, thus, the rate of underflow is nearly constant. The amount of the underflow at each profile, except in Little Cottonwood Canyon, is the amount recharging the principal ground-water reservoir in the Jordan Valley. In Little Cottonwood Canyon, about 2,000 acre-feet of water a year is discharged by wells and springs between section E and the canyon mouth about half a mile downstream. The amount of underflow in Little Cottonwood Canyon available for recharge, therefore, is about 1,300 acre-feet a year. The total amount of underflow from the 7 canyons recharging the main ground-water reservoir in the Jordan Valley is estimated to be 1,400 acre-feet a year.

TABLE 1.—*Hydraulic conductivity, hydraulic gradient, saturated cross section, and underflow in unconsolidated fill in seven canyons in the Wasatch Range east of the Jordan Valley*

Canyon	Hydraulic conductivity (cu ft per day per sq ft)	Hydraulic gradient (ft per ft)	Saturated cross section (sq ft)	Underflow (acre-ft per yr)
City Creek	17	0.039	725	4
Red Butte	17	.052	385	3
Emigration	17	.026	2,700	10
Parleys	17	.034	1,475	7
Mill Creek	17	.063	7,500	67
Big Cottonwood	40	.043	400	6
Little Cottonwood	40	.028	350,000	[1] 3,300

[1] About 2,000 acre-feet of this underflow is discharged by wells or springs before it reaches the principal ground-water reservoir in the Jordan Valley.

REFERENCES

Bentall, Ray, compiler, 1963, Methods of determining permeability, transmissibility, and drawdown: U.S. Geol. Survey Water-Supply Paper 1536–I, p. 243–341.

Mattick, R. E., 1968, Seismic-refraction profiles across six canyons in the Wasatch Range near Salt Lake City, Utah, *in* Geological Survey Research 1968: U.S. Geol. Survey Prof. Paper 600–D, p. D255–D257.

Morrison, R. B., 1965, Lake Bonneville—Quaternary stratigraphy of eastern Jordan Valley, south of Salt Lake City, Utah: U.S. Geol. Survey Prof. Paper 477, 80 p.

Richmond, G. M., 1964, Glaciation of Little Cottonwood and Bells Canyons, Wasatch Mountains, Utah: U.S. Geol. Survey Prof. Paper 454–D, p. D1–D41.

DRAINAGE DENSITY AS AN INDICATOR OF BASE FLOW IN PART OF THE POTOMAC RIVER BASIN

By FRANK W. TRAINER, Washington, D.C.

Abstract.—The base flow from 10 stream basins in an area of 1,900 square miles in the Piedmont and Blue Ridge provinces in Pennsylvania, Maryland, and Virginia, as determined by hydrograph separation, is inversely proportional to drainage density. This relationship was used to estimate the base flow from ungaged basins in the area. Streamflow records from two gages on the Potomac River, also studied by hydrograph separation, define the contribution of the entire area to the discharge of the river and provide a check on the estimate made by drainage density. For a 1-year period the estimate of base flow from the ungaged basins, made by the use of drainage density, is within 45 percent of the estimate from hydrograph separation. This agreement suggests that drainage density will be useful in hydrogeologic mapping and in planning streamflow measurements for the study of base flow.

Stream-discharge records show that the dry-weather or base flow of some tributary streams in the Potomac River basin is much greater, per unit of drainage area, than that of others. Determination of the relative contributions of the various tributary basins to the base flow of the entire river system is a necessary first step in study of the relationships among geology, ground water, and streamflow, and hence in evaluation of methods for development of the water resource of the entire basin. An indirect method of estimating base flow of the tributary basins is needed because some streams, and the lower reaches of many others, are not gaged. This report describes the use of drainage density—the total length of streams in a basin divided by the area of the basin—as an indicator of base flow.

Since its definition by Horton (1932), drainage density has been recognized by geomorphologists as one of the important morphometric characteristics of drainage basins. Drainage density has been observed to be inversely related to the permeability of the terrain. (See, for example, Langbein and others, 1947, p. 133; Thornbury, 1954, p. 128; Ray and Fischer, 1960, p. 145.) Thus, streams tend to be more numerous where the land surface is underlain by relatively impermeable material, such as clay, and where most runoff of precipitation is therefore by surface channels. They tend to be less numerous where the surface is underlain by relatively permeable material, such as sand, and where much or most of the runoff is by ground-water discharge following the infiltration of precipitation. Carlston (1963) gave theoretical expression to these relationships, and showed quantitatively that base flow is inversely related, and flood flow directly related, to drainage density.

Acknowledgments.—Helpful discussions of this problem with R. R. Bennett, C. W. Carlston, H. H. Cooper, J. G. Ferris, R. L. Hanson, and M. T. Thomson, and the assistance of L. E. Burgess in the compilation of data, are gratefully acknowledged.

AREA OF STUDY

The Potomac River drains a region of diverse topography and geology covering about 14,700 square miles in Pennsylvania, Maryland, Virginia, and West Virginia. Its basin is underlain by unconsolidated sediments, by consolidated sedimentary rocks, and by metamorphic rocks. This report treats an area of about 1,900 square miles which is in the Piedmont and Blue Ridge physiographic provinces in Pennsylvania, Maryland, and Virginia, and which is underlain by fractured consolidated rocks. The area was selected for study because it is considered large enough to test the use of drainage density in estimating base flow; because its constituent basins present a wide range in base flow; and because it is entirely covered by topographic maps at the scale of 1:24,000, the largest scale in wide use in the United States.

The area studied is tributary to the reach of the Potomac River between two stream-gaging stations, one at Point of Rocks, Md., and the other near Washington, D.C. (fig. 1). This part of the Potomac River basin is made up of the basins of the Monocacy River in Pennsylvania and Maryland, of Goose Creek in Virginia, and of several smaller streams in Maryland

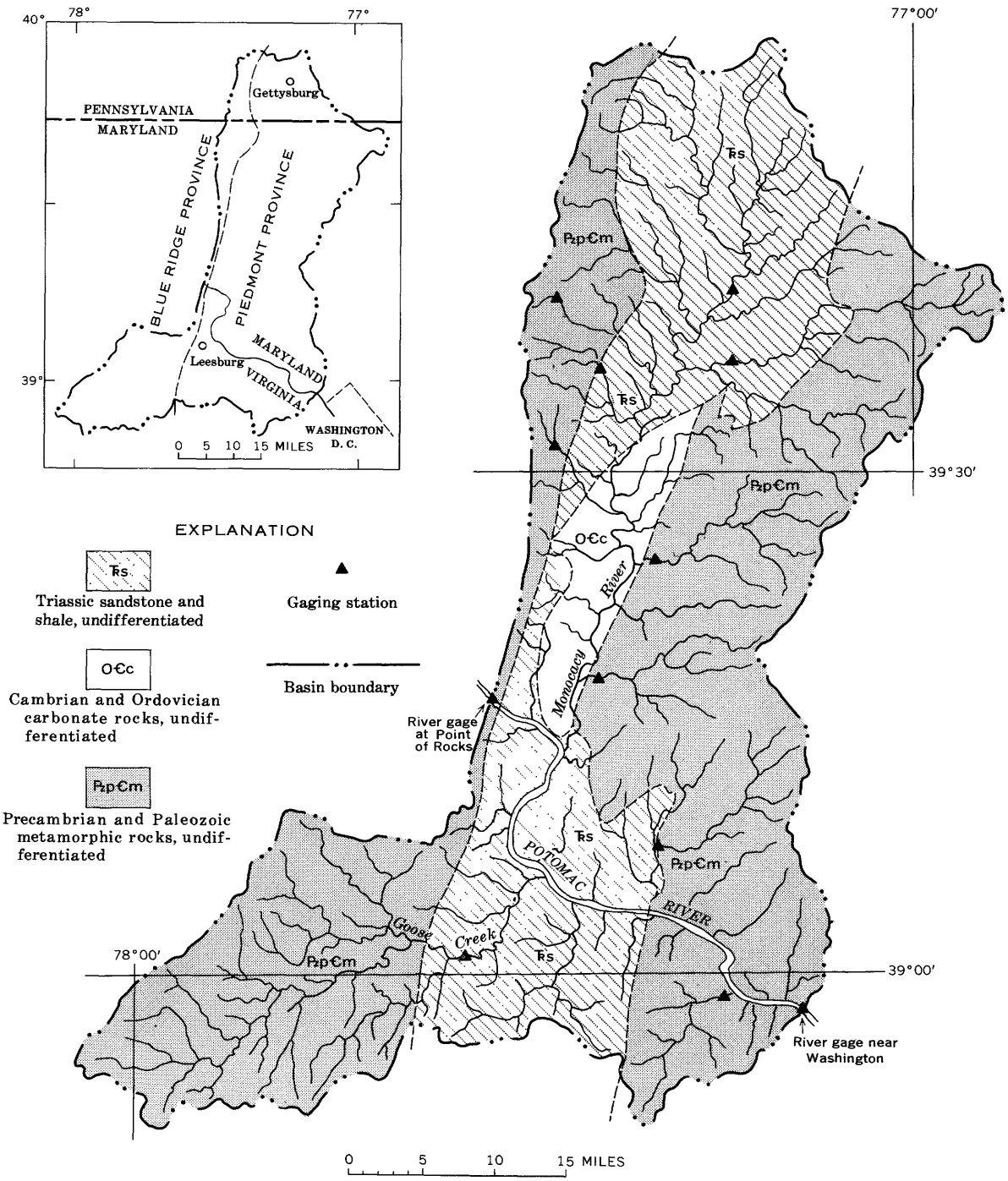

FIGURE 1.—Map of area described in this report, showing streams and generalized distribution of rock types. Gaging stations on tributary streams are identified in figure 4 and table 2. Inset map shows physiographic provinces. Geologic boundaries from Maryland Geological Survey (1968).

and in Virginia. Mean annual precipitation (for the period 1931–60) at 10 stations in the Piedmont part of the area ranges from 40.1 to 44.8 inches. Mean annual stream discharge ranges from 12.0 to 15.5 inches for 7 basins in the Piedmont and from 17.1 to 20.0 inches for 3 basins in the Blue Ridge (where precipitation is probably greater than in the Piedmont). Thus, about 30 to 40 percent of the annual precipitation becomes streamflow, and areal differences in total streamflow are relatively small. In contrast, base flow from some of these basins is as much as five times as great as that from others.

This area can be divided in three parts on the basis of broad groupings of rock types (fig. 1). First, to the

west, the Blue Ridge and part of the western Piedmont are underlain by metamorphic rocks, principally quartzite, greenstone (metabasalt), and gneissic rocks. Second, a belt which trends south-southwest through the center of the area is underlain by Triassic sedimentary and igneous rocks—shale and sandstone, with subordinate conglomerate and diabase—and, in Maryland, by Lower Paleozoic carbonate rocks. Third, the eastern part of the area is underlain by metamorphic rocks, chiefly schists and gneisses. The bedrock is commonly covered by a mantle of unconsolidated weathered material; in much of the area the thickness of this mantle reaches 50 to 75 feet. Alluvial deposits flank the streams.

DETERMINATION OF DRAINAGE DENSITY

Drainage density is the ratio of the total length of streams in a basin to the area of the basin. Of these two variables, area can be measured simply and fairly precisely; stream length is more difficult to measure, and there has been some disagreement among geomorphologists and hydrologists about how the measurement should be made. For this study the areas of gaged basins were taken from published compilations of streamflow records; areas of the remaining basins, and the lengths of all the streams, were measured on topographic maps published at the scale of 1:24,000. Stream lengths were measured directly as the lengths of blue lines on the maps. Measurements of length were also made in the field and on aerial photographs to test the adequacy of measurement of the blue lines.

Twenty-three streams in the Piedmont province in Maryland were examined in the field during a dry period in late February and early March 1968. At that time the water table was relatively high, streamflow was entirely base flow, and the streams were near the maximum lengths they attain during rainless periods. The lengths of 8 streams were found to be substantially as mapped, 4 were shorter (by 0.1 to 0.5 mile) than the blue lines, and 11 were longer (by 0.1 to 0.6 mile). On the average each stream was 0.1 mile longer than shown on the map. These streams were also examined on vertical aerial photographs (scale 1:21,000), and were found to average 0.1 mile longer than as mapped.

The lengths of the 23 streams were also estimated by extending the blue lines on the topographic maps up each valley to the highest contour line notched into a V shape by the channel. This is a procedure which has come into use in recent years (see, for example, Morisawa, 1957; Carlston, 1963, p. C3; Gregory, 1966, p. 328). By this method the streams were 0.0 to 0.7 mile (average 0.2 mile) longer than shown by the blue lines.

Increasing the length of each 1st-order stream in a basin by 0.1 or 0.2 mile could increase the total length of streams by an appreciable amount. Nonetheless, the length determined by measuring the blue lines was believed to be sufficiently precise for the purpose of this study. Field examination of even a substantial number of the streams in the area would have been impracticable because of the time required. Use of the V-contour method might have been desirable if the maps had been at a smaller scale such as 1:62,500, but at the larger scale used here it was not needed.

DETERMINATION OF BASE FLOW

Base flow is commonly considered to be the part of the streamflow provided by ground-water discharge. In this region, where rains are typically frequent throughout the year, base flow can be observed directly, as the total streamflow, only during occasional long rainless periods. In order to estimate the base flow at other times, when it is masked by surface runoff, the stream hydrograph must be separated into components. Numerous methods of hydrograph separation have been used. In this study the writer followed a graphical procedure described by Horton (1933, p. 449) and by Snyder (1939, p. 728–730).

Hydrographs extending over a period of several years were searched for segments which show the recession of streamflow during dry weather. These segments, when joined, form a recession curve or depletion curve which has long been believed (Horton, 1933, p. 449; and earlier workers cited by him) to represent the rate of ground-water discharge to the stream under the condition of no recharge. On the semilogarithmic plot in wide use for hydrographs this graphical recession curve commonly approximates a straight line. In analysis of a mathematical model, Rorabaugh (1964, p. 434) shows that once sufficient time has elapsed, after a period of recharge, for the shape of the water-table profile in a finite aquifer to stabilize, discharge from the aquifer can be represented on a semilogarithmic plot by a straight line. In the present study, therefore, the streamflow was assumed to consist of base flow wherever the falling limb of the hydrograph coincides with the base-flow recession curve. The contribution to streamflow in this area by water taken from channel storage is believed to be small during the later part of the recession from the flood peak, and in this study it was ignored.

The base-flow component of the hydrograph beneath a flood peak is believed by many hydrologists to take a form such as that shown by dotted line *3* in figure 2*B*. The shape of the dotted line implies that stream water moves into the banks during the flood, and that

ground-water discharge to the stream decreases or ceases temporarily. After passage of the flood peak the river level falls, water moves from bank storage back into the stream, and ground-water discharge to the stream increases. After a rainless period of some length the surface-runoff and bank-storage components of the streamflow largely or completely disappear. Various arbitrary procedures have been used to construct the base-flow hydrograph in this region beneath the flood peak. In one of these, used in this investigation, a straight line (*4* in figure 2*B*) is drawn from a point on the trend of the antecedent base-flow curve beneath the flood peak to the point on the falling limb of the hydrograph at which the hydrograph intersects the base-flow recession curve. This straight line is believed to yield a reasonable approximation to the total quantity of base flow beneath the flood peak.

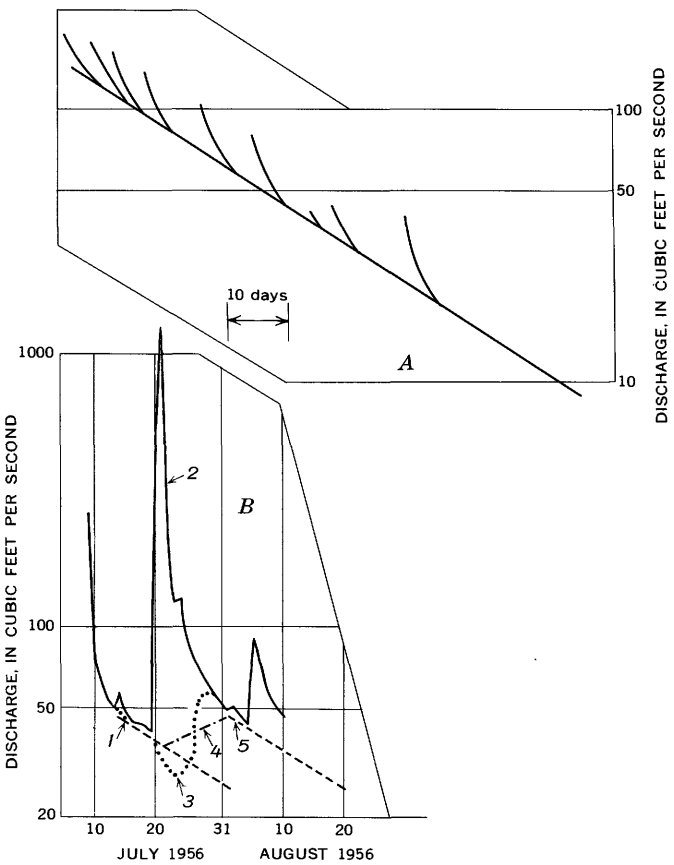

FIGURE 2.—Method of hydrograph separation used in this study. *A*, Example of base-flow recession curve (Big Pipe Creek at Bruceville, Md.); curved line segments are segments of stream hydrograph. *B*, Separation of hydrograph using recession curve: *1*, antecedent trend of base flow, with trace of recession curve (dashed line); *2*, surface runoff (flood); *3*, inferred general form of base-flow curve during flood event; *4*, arbitrarily constructed base-flow curve during flood event; *5*, trend of base flow after flood, with trace of recession curve (dashed line).

RELATION BETWEEN DRAINAGE DENSITY AND BASE FLOW

Using the procedure of separation described in the preceding paragraphs, the writer constructed a base-flow hydrograph for each of the 10 gaging stations on tributary streams in the area investigated. Streamflow records for the 1-year period from December 1949 through November 1950 were used. An average daily base flow for this period was determined from each hydrograph, and each average was recalculated in terms of discharge per mile of stream channel. Table 1 summarizes the data and calculated values. Figure 3 is a plot of these base-flow values against drainage density. The grouping of points confirms the conclusion of earlier workers that base flow is inversely related to drainage density; and it suggests that a quantitative expression for this relationship, such as that found by Carlston (1963, p. C6) in his study of monolithologic basins, can be developed for basins of diverse geology such as those in the Potomac River basin.

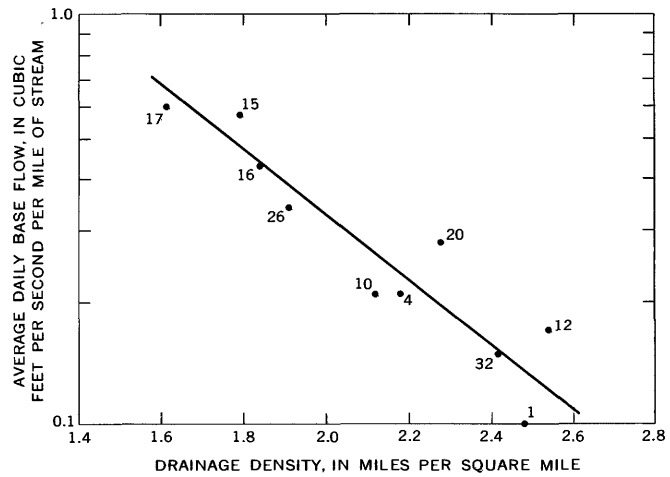

FIGURE 3.—Graph showing the relation of base flow to drainage density in 10 drainage basins. Data from table 1. Numbered drainage basins shown on figure 4.

BASE FLOW FROM UNGAGED BASINS

The two gages on the Potomac River, at Point of Rocks and near Washington (fig. 1), provide data for an estimate of the total base-flow discharge from the area of investigation. Hydrograph separations were constructed for the period December 1949–November 1950. The total base flow at Point of Rocks was 1,646,000 cfs (cubic feet per second)-days, and the total near Washington, including diversions for the Washington metropolitan area, was 2,056,100 cfs-days. The difference, 410,100 cfs-days, represents the total

TABLE 1.—*Base flow from 10 gaged basins, December 1949–November 1950, as determined by hydrograph separation*

Basin and station name (fig. 4)	Drainage density[1] (mi per sq mi)	Total annual base flow (cfs-days)	Total annual base flow (cfs-day per mi)[2]	Average daily base flow (cfs)	Average daily base flow (cfs per mi)[3]
1. Monocacy River at Bridgeport, Md	2.48	15,470	37	42.4	0.10
4. Big Pipe Creek at Bruceville, Md	2.18	17,250	78	47.3	.21
10. Linganore Creek near Frederick, Md	2.12	13,290	76	36.4	.21
12. Bennett Creek at Park Mills, Md	2.54	9,980	62	27.3	.17
15. Fishing Creek near Lewistown, Md	1.79	2,640	208	7.2	.57
16. Hunting Creek at Jimtown, Md	1.84	5,410	160	14.8	.43
17. Owens Creek at Lantz, Md	1.61	2,000	217	5.5	.60
20. Seneca Creek at Dawsonville, Md	2.28	22,630	98	64.7	.28
26. Difficult Run near Great Falls, Va	1.91	12,690	114	37.5	.34
32. Goose Creek near Leesburg, Va	2.42	44,296	57	121.3	.15
Total		145,700			

[1] Miles of stream per square mile of drainage basin.
[2] Cfs-days per mile of stream.
[3] Cfs per mile of stream.

TABLE 2.—*Base flow from ungaged basins and areas, December 1949–November 1950, as determined from drainage density, total length of streams, and graph in figure 3*

[See footnotes, table 1, for abbreviations]

Basin or area	Drainage density (mi per sq mi)	Stream length (mi)	Average daily base flow (cfs per mi)	Average daily base flow (cfs)	Total annual base flow (cfs-days)	Total annual base flow (cfs-days per mi)
2	2.03	268	0.31	83	30,300	101
3	2.00	71	.33	23	8,400	118
5	2.38	18	.16	3	1,100	61
6	2.14	167	.25	42	15,330	92
7	2.12	59	.26	15	5,480	99
8	2.09	192	.28	54	19,710	103
9	2.48	77	.14	11	4,020	52
11	2.88	114	.065	7	2,560	22
13	2.79	94	.077	7	2,560	27
14	2.40	65	.16	10	3,650	56
18	2.76	92	.081	7	2,560	28
19	2.44	77	.15	12	4,380	57
21	2.55	54	.12	6	2,190	41
22	1.81	40	.47	19	6,940	173
23	1.86	71	.42	30	10,950	154
24	3.04	26	.049	1	360	14
25	1.92	24	.38	9	3,280	137
27	2.74	21	.084	2	730	35
28	2.52	69	.13	9	3,280	48
29	2.24	179	.21	38	13,870	78
30	2.56	88	.12	11	4,020	46
31	3.28	162	.031	5	1,820	11
Total					147,490	

base flow from this area. The total base flow from the 10 gaged basins, also determined by hydrograph separation (table 1) is 145,700 cfs-days. From these data the base flow from the ungaged part of the area is estimated to have been 410,100 minus 145,700, or 264,400 cfs-days.

The total base flow from the ungaged part of the area was also estimated by the use of drainage density and the graph (fig. 3) constructed from data for the 10 gaged basins. This second total was compared with the total obtained from hydrograph separations, as a test of the use of drainage density in estimating base flow. The procedure was as follows:

The ungaged part of the area was divided into 22 units—basins or groups of basins—whose areas range from 8 to 146 square miles. The boundaries of most of these units follow lithologic or topographic (basin) boundaries; the remainder are arbitrary. The drainage density of each unit was used with the graph in figure 3 to estimate the base flow from the unit. The data and derived values are given in table 2. The total base flow estimated in this way is 147,500 cfs-days (rounded to nearest hundred). This total is 116,900 cfs-days, or 44 percent, less than the check value of 264,400 cfs-days obtained as the difference of totals of separations of Potomac River hydrographs.

Although the difference in these estimates is large, the two values are of the same order of magnitude, and the writer believes that drainage density can be used in a gross way to estimate the base flow from a group of basins in this area. Further work is needed to determine the reliability of estimates for individual basins in the group, and especially for the smaller basins.

AREAL DISTRIBUTION OF BASE FLOW

The areal pattern of base-flow values is shown on figure 4. Basins and groups of basins with similar base-flow discharge tend to cluster, and despite some gaps and apparent inconsistencies their pattern bears a credible relation to the distribution of rock types. For example, basins 15, 16, and 17 (fig. 4), in metamorphic rocks in the Blue Ridge, have relatively high base-flow yields. Several basins or units with relatively low yields (1, 13, 31) are largely underlain by Triassic sedimentary rocks. Intermediate yields of units in the western part of the area (such as 2, 14, and 30) probably reflect the combined effect of these metamorphic and sedimentary rocks on ground-water discharge and streamflow. Basins in metamorphic rocks in the eastern part of the area have intermediate or relatively high base-flow yields. Among questions which arise from study of figure 4, the relatively low yields of some units (for example, 11, 24, and 27) are not explained by the available data.

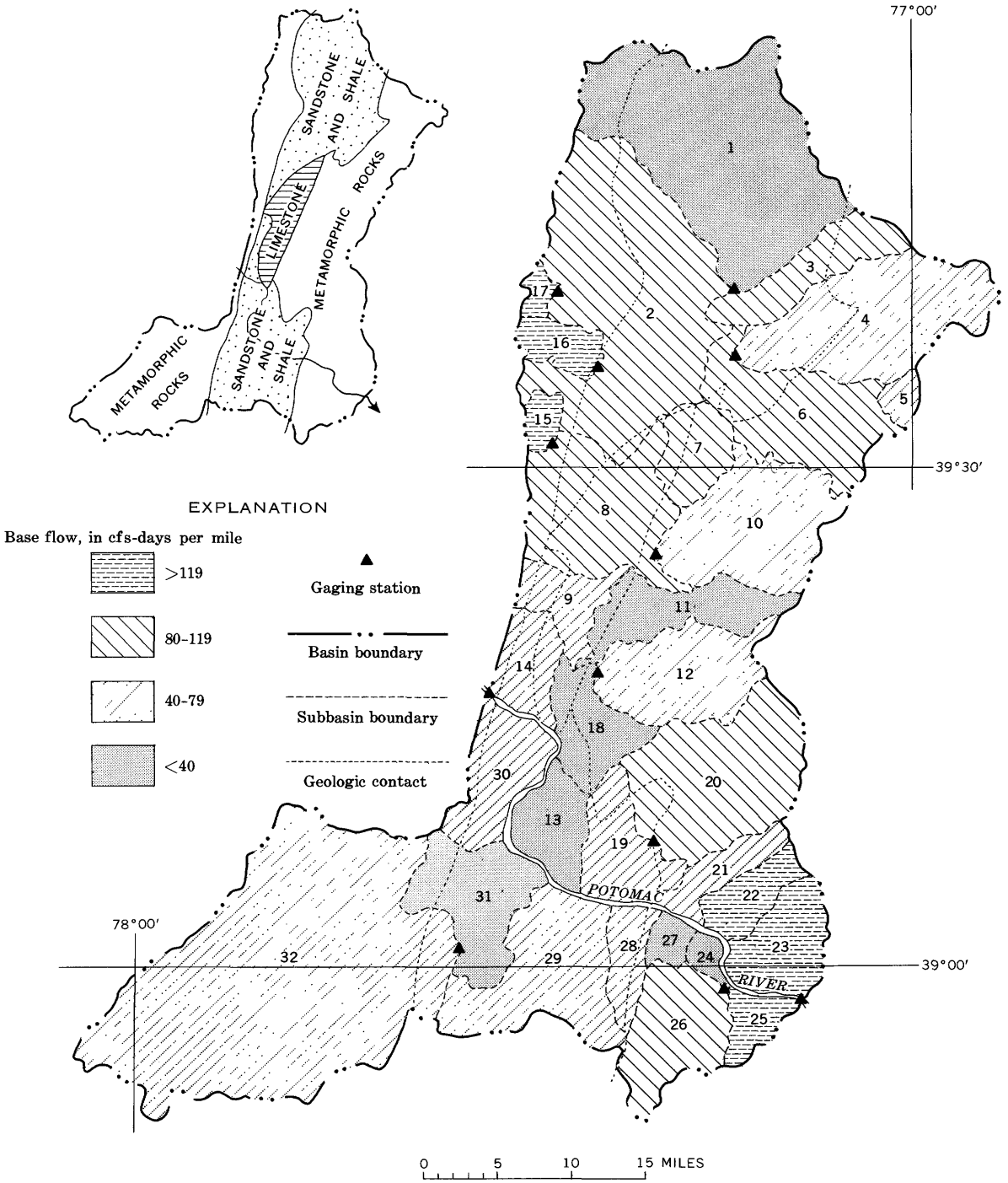

FIGURE 4.—Areal distribution of base flow. Inset map (upper left) shows distribution of major rock types; rock boundaries also shown (dotted lines) on large map. Hydrologic data and identifying numbers of basins and groups of basins given in tables 1 and 2. Geologic boundaries from Maryland Geological Survey (1968).

Mapping of the base flow of streams in terms of tributary basins or groups of tributary basins, as in figure 4, appears to offer a valuable approach to study of the geologic control of base flow. Revision of the map is being carried out by means of stream-discharge measurements at localities selected on the basis of drainage density, study of geologic maps, and review of streamflow records.

CONCLUSIONS

Base flow from a basin is inversely proportional to drainage density. This relationship can be used to estimate base flow, even in an area of rather diverse geology such as the Piedmont and Blue Ridge provinces in the Potomac River basin. The estimates are believed adequate to serve in hydrogeologic mapping and in the planning of stream-discharge measurements for the study of base flow.

Extension of the use of drainage density to other fractured-rock terrains will require careful evaluation. It seems likely that a fundamental factor to be considered is the degree of adjustment of streams to terrain. The Potomac River basin has a long span of history (although recent in the perspective of the geologist) under the influence of one group of geologic processes, without serious interruptions such as those caused by glaciation in some regions. The streams are undoubtedly well adjusted to the terrain, and should be reliable indicators of the geohydrologic character of the terrain. This may not be true of some other regions where two or more unlike groups of geologic processes have been active so recently that adjustment by the streams may not yet reflect the character of the terrain.

REFERENCES

Carlston, C. W., 1963, Drainage density and streamflow: U.S. Geol. Survey Prof. Paper 422–C, p. C1–C8.

Gregory, K. J., 1966, Dry valleys and the composition of the drainage net: Jour. Hydrology, v. 4, p. 327–340.

Horton, R. E., 1932, Drainage basin characteristics: Am. Geophys. Union Trans., v. 13, p. 350–361.

——— 1933, The role of infiltration in the hydrologic cycle: Am. Geophys. Union Trans., v. 14, p. 446–460.

Langbein, W. B., and others, 1947, Topographic characteristics of drainage basins: U.S. Geol. Survey Water-Supply Paper 968–C, p. 125–157.

Maryland Geological Survey, 1968, Geologic map of Maryland: Maryland Geological Survey, scale 1:250,000.

Morisawa, Marie, 1957, Accuracy of determination of stream lengths from topographic maps: Am. Geophys. Union Trans., v. 38, p. 86–88.

Ray, R. G., and Fischer, W. A., 1960, Quantitative photography—A geologic research tool: Photogramm. Engineering, v. 26, p. 143–150:

Rorabaugh, M. I., 1964, Estimating changes in bank storage and ground-water contribution to streamflow: Internat. Assoc. Sci. Hydrology, Pub. 63, p. 432–441.

Snyder, F. F., 1939, A conception of runoff-phenomena: Am. Geophys. Union Trans., v. 20, p. 725–738.

Thornbury, W. D., 1954, Principles of geomorphology: New York, John Wiley & Sons, Inc., 618 p.

COMPARATIVE RESULTS OF SEDIMENT SAMPLING WITH A SURFACE SAMPLER AND DEPTH-INTEGRATING SAMPLERS

By CLARENCE T. WELBORN, Austin, Tex.

Work done in cooperation with the Texas Water Development Board

Abstract.—An investigation was made to determine the possibility of correlating sediment data from samples collected with a surface sampler with data from samples collected with depth-integrating samplers. The results of the investigation show that a coefficient can be computed for sediment concentrations collected with a surface sampler from streams that carry small amounts of sand. It was not possible to compute a single coefficient that could be applied to the samples collected with a surface sampler from streams carrying a significant sand load.

Historically, the first sediment samples were taken from the Rhone River, France, in 1808 (U.S. Inter-Agency Committee on Water Resources, Subcommittee on Sedimentation, 1952, p. 13). Some 65 samplers, embodying a number of different designs, have been used since the first sediment samples were collected. After years of investigations with various samplers, it is generally considered that the depth-integrating sampler is the one that can collect a sample that most nearly defines the mean concentration of sediment in a stream.

Vertical distribution of suspended sediment should be understood before comparing the results obtained with a depth-integrating sampler and a surface sampler. The concentration of suspended sediment increases from the water surface to the streambed. The upward components of turbulent currents tend to lift the sediment particles into suspension; thus, the concentration of sediment at any given depth will depend on the individual grain size of the sediment and the force of the upward currents.

The mean sediment concentration is best determined by collection of an integrated sample of sediment and water throughout a vertical. When the quantity of sediment in the sample, expressed as concentration, is multiplied by the product of mean velocity of the stream at, and the depth of, the vertical, the result is the suspended-sediment discharge per unit width. The U.S. Inter-Agency Committee on Water Resources, Subcommittee on Sedimentation (1941, p. 77) stated: "A sampler which fills at a rate equal to the velocity at every point in the vertical and which will traverse 95 percent of the depth, or more, gives the most accurate results." As an alternative procedure, the mean sediment concentration may be approximated by collecting a sediment sample at one point in the vertical and applying the proper coefficient. However, the selection of the proper coefficient is difficult because it will vary according to the stream characteristics and the particle-size distribution of the sediment.

Data on the amounts of suspended sediment transported by streams in Texas have been collected for a number of years by both the U.S. Geological Survey and the Texas Water Development Board. The Texas Water Development Board has used the Texas (surface) sampler since the beginning of a cooperative program with the Department of Agriculture in 1924. The Geological Survey uses U.S. standard depth-integrating samplers. This investigation was made to obtain comparative data with both types of samplers to determine if past and future sediment records obtained by the two methods can be correlated.

EQUIPMENT

The surface (Texas) sampler used in this investigation consists of a ⅛- by ¾- by 15-inch hanger bar to which a sheet metal bottle holder is fastened. The hanger bar is fastened to a 15-pound lead current-meter weight (fig. 1). An 8-ounce small-mouth bottle is placed in a vertical position in the bottle holder and is lowered 1 foot below the surface of the stream. The sampler is brought to the surface when air bubbles cease to come from the bottle.

The depth-integrating samplers used in this study ranged in weight from 24 to 100 pounds (fig. 1). These samplers have a cast bronze steamlined body in which the sample container (round pint milk bottle) is enclosed. The nose of the sampler is drilled and tapped for intake nozzles of ⅛-, 3/16-, and ¼-inch diameters. An air-exhaust port is located on the side of the sampler head. Integrally cast tail vanes orient the sampler in the streamflow. The depth-integrating sampler continuously accumulates a sample of the water-sediment mixture by moving vertically at a constant rate and by admitting the water-sediment mixture at a velocity equal to that of the stream. The nozzle is oriented upstream. Some depth-integrating samplers collect a water-sediment mixture within 0.3 foot of the streambed; others collect samples within 0.5 foot of the streambed. The depth-integrating samplers used in this study were the U.S. D–43, U.S. D–49, U.S. P–46, and U.S. DH–59. For information on other samplers of this type see U.S. Inter-Agency Committee on Water Resources, Subcommittee on Sedimentation (1959.)

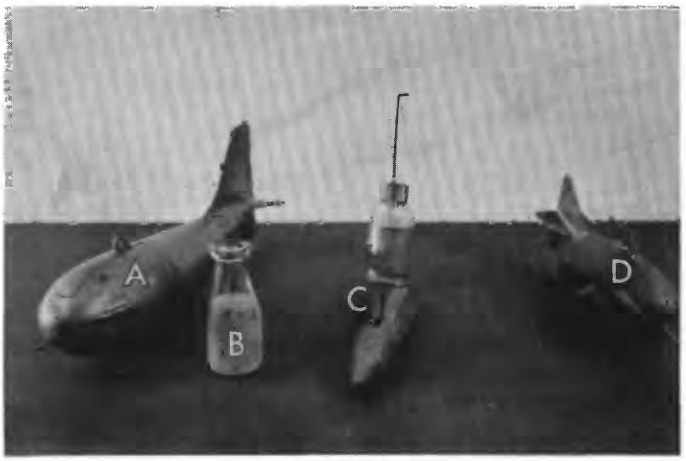

FIGURE 1.—Depth-integrating samplers and surface (Texas) sampler. *A*, U.S. D–49 depth-integrating sampler; *B*, sample bottle used with *A* and *D*; *C*, Texas (surface) sampler; *D*, U.S. DH–49 depth-integrating sampler.

PROCEDURE

On the basis of a study by Faris (1933), the Texas Water Development Board uses a coefficient of 1.102 to correct the sediment data collected with the Texas (surface) sampler. Faris concluded that the mean suspended-sediment concentration generally occurs at the 0.6 depth, and that if the concentration of a sample collected near the surface is multiplied by the factor 1.102, the results will equal the mean concentration for the vertical.

To compare results obtained with the surface sampler with those obtained with the depth-integrating sampler, 25 sampling sites were selected in a wide geographic area of Texas, including all major river basins except the Red River and the Rio Grande. Using both types of samplers, two or more samplings were made at each site to cover as wide a range of water discharge as possible. Coefficients were computed for each sampling by dividing depth-integrated concentrations by surface-sampler concentrations. Particle-size analyses were also made on many of the samples.

RESULTS

The coefficients required to make surface-sampler concentrations comparable to depth-integrated concentrations ranged from 0.96 to 3.41. They were highest for the streams that carry high percentages of sand and nearer unity for streams carrying high percentages of silt and clay in suspension.

In streams where sand makes up large percentages of the sediment load, concentrations of sediment are much greater near the streambed. Figure 2 shows the vertical distribution of suspended-sediment concentrations at two places in the cross section of the Trinity River at Romayor—a typical sand-bearing stream. The uppermost point on each part of the figure represents the concentration of sediment in a sample collected with the surface sampler. The particle-size distribution of suspended sediment collected by the two samplers from the Trinity River is shown in figure 3. The integrated samples contained about 35 percent sand (particles larger than 0.062 millimeters in diameter) and the surface samples only 8 percent.

For one sampling of the Trinity River, the depth-integrated sediment sample contained 1,230 miligrams per liter and the surface sample contained 397 mg/l. A

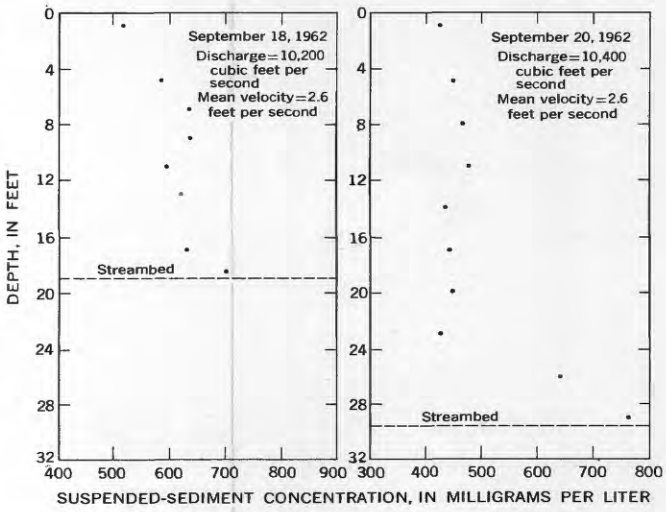

FIGURE 2.—Vertical distribution of suspended-sediment concentration of the Trinity River at Romayor, Tex., September 18 and 20, 1962.

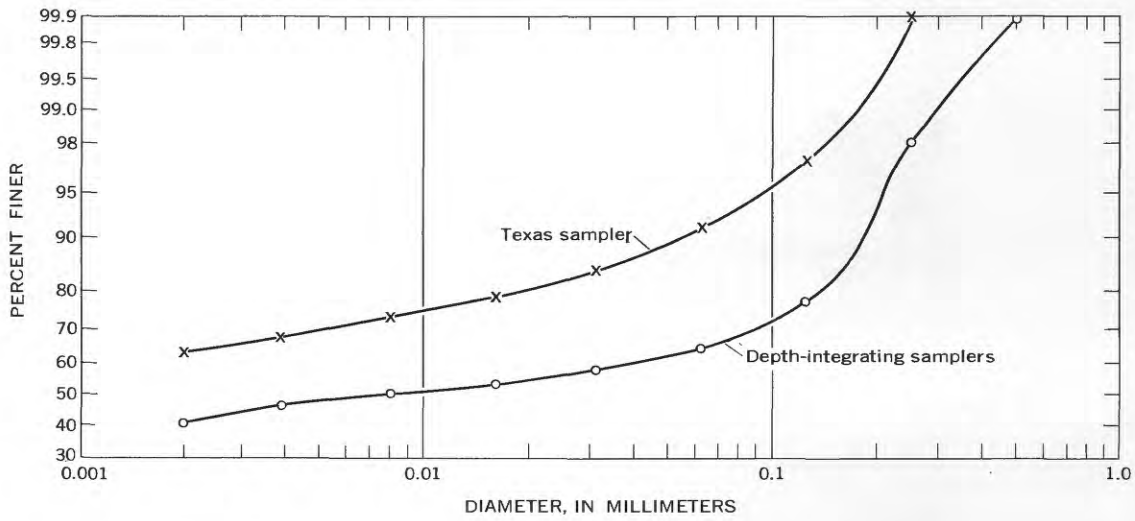

FIGURE 3.—Particle-size distribution of suspended-sediment samples collected by the surface (Texas) sampler and by the depth-integrating samplers, Trinity River at Romayor, Tex. Each curve is average of 11 particle-size analyses.

coefficient of 3.10 is required to relate the surface-sample data to the mean sediment concentration of the vertical. A depth-integrated sample from the Sabine River contained 150 mg/l sediment, compared to 44 mg/l in a surface sample. A coefficient of 3.41 is required to correlate the data.

To illustrate further how the data collected with a surface sampler are affected by sand in suspension, the sand percentages of depth-integrated sediment samples are plotted against the ratio of sediment concentrations of the depth-integrated samples to the sediment concentrations of samples collected near the surface (fig. 4). The points on the graph correlate fairly well up to about 40 percent sand in suspension. A coefficient of 0.8 to 1.6 must be applied to the sediment concentration of a sample collected with a surface sampler to obtain the mean sediment concentration of the vertical. Above 40 percent sand in suspension, the points were widely scattered and the ratios of the two samplers ranged from 1.26 to 3.10.

For streams carrying high percentages of silt and clay in suspension, the coefficients for correcting the suspended-sediment concentrations of samples collected with a surface sampler are nearer unity than those for sandy streams. West Texas streams often carry a large suspended-sediment load, but the percentage of sand is less than that of either of the silt and clay fractions. Because the suspended-sediment load of these streams consists largely of silt and clay, the suspended-sediment concentration is nearly uniform throughout the vertical and the concentration of a sediment sample collected near the surface approximates the mean sediment concentration. Figure 5 represents a stream that carries

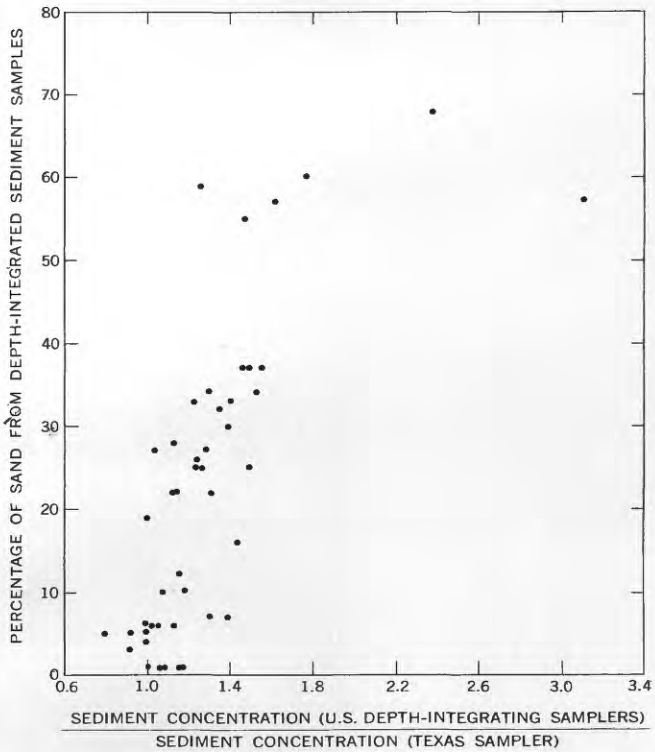

FIGURE 4.—Ratio of sediment concentration from depth-integrated samples to sediment concentration from surface samples (Texas sampler) plotted against percentage of sand from depth-integrated sediment samplers.

less than 10 percent sand. The sediment concentrations collected by each sampler are almost the same. Figure 6 shows that the particle-size distribution of the sediment samples collected with each sampler agrees very closely.

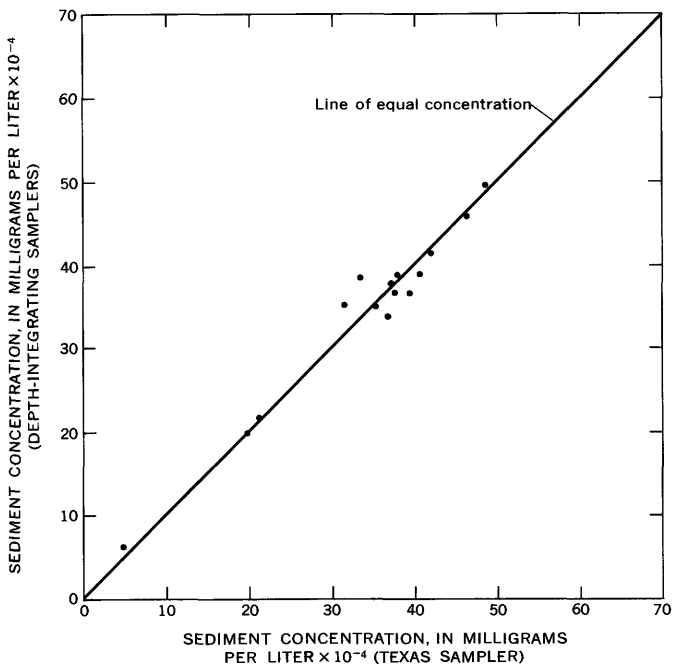

FIGURE 5.—Comparison of sediment concentration from a surface (Texas) sampler and from the depth-integrating samplers, Double Mountain Fork Brazos River near Aspermont, Tex.

SUMMARY AND CONCLUSIONS

Suspended-sediment samples were collected with a surface (Texas) sampler and depth-integrating samplers in all the major river basins in Texas except the Red River and Rio Grande. Results showed that suspended-sediment samples collected with a surface sampler from streams that carried a high percentage of sand were not representative of the mean suspended-sediment concentration. Furthermore, the ratio of the suspended-sediment concentration of samples collected by the depth-integrating samplers and a surface sampler varied over such a wide range on sandy streams that no single coefficient could be applied to the concentrations collected by a surface sampler to obtain a mean concentration. On streams where sand is less than 10 percent of the suspended sediment, the difference between the sediment concentrations collected by the two types of samplers is not large; a single coefficient can be computed for these streams to apply to the sediment concentration collected by a surface sampler to obtain the mean sediment concentration of the stream. The depth-integrating samplers should be used on streams in which 10 percent or more of the suspended sediment is sand.

REFERENCES

Faris, O. A., 1933, The silt load of Texas streams: U.S. Dept. Agriculture Tech. Bull. 382, 71 p.

U.S. Inter-Agency Committee on Water Resources, Subcommittee on Sedimentation, 1941, Analytical study of methods of sampling suspended sediment: U.S. Inter-Agency Committee on Water Resources, Subcommittee on Sedimentation Rept. 3, Iowa City, Iowa, 82 p.

——— 1952, The design of improved types of suspended-sediment samplers: U.S. Inter-Agency Committee on Water Resources, Subcommittee on Sedimentation Rept. 6, Minneapolis, Minn., 103 p.

——— 1959, Federal Inter-Agency sedimentation instruments and reports: U.S. Inter-Agency Committee on Water Resources, Subcommittee on Sedimentation Rept. AA, Minneapolis, Minn., 38 p.

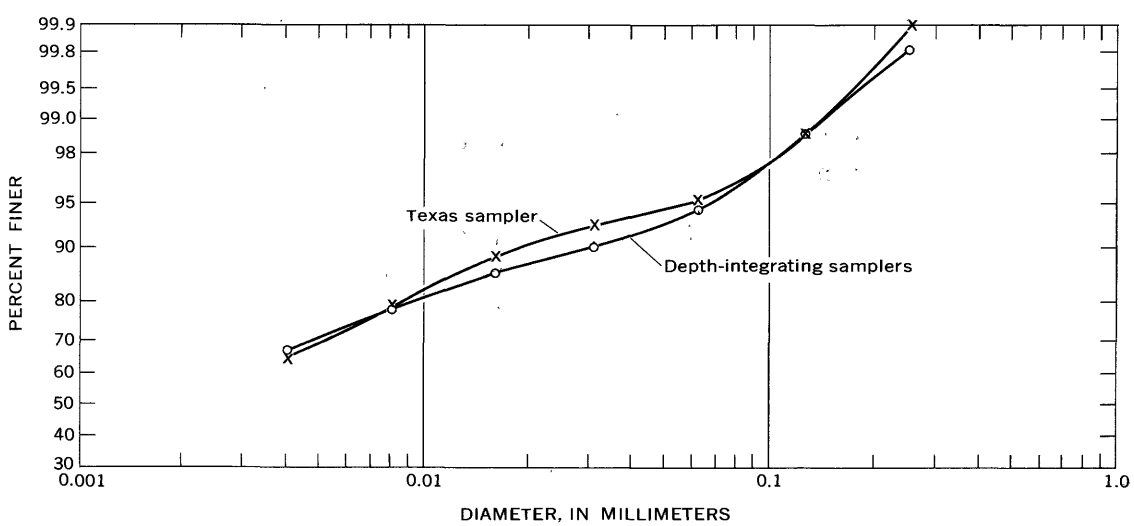

FIGURE 6.—Particle-size distribution of suspended-sediment samples collected by a surface (Texas) sampler and by depth-integrating samplers, Double Mountain Fork Brazos River near Aspermont, Tex. Each curve is average of five particle-size analyses.

AN ANALYSIS OF SOME DATA FROM NATURAL ALLUVIAL CHANNELS

By GEORGE H. CADDIE, Dunedin, New Zealand [1]

Abstract.—Recent work on the geometry of stream channels has resulted in a hypothesis that the friction factor of any stream flowing in alluvium is virtually indeterminate because friction is the result of specific constraints placed upon the stream. The relationships between velocity, unit discharge, and slope for several locations on the Colorado River below Glen Canyon Dam are different from those of channels in which depth, velocity, and discharge all vary with changes in load and discharge. Apparently this is so because the stream is degrading its bed at these locations. Some natural streams, unaffected by man-made reservoirs, are shown to have the same characteristics.

For many generations men have interfered with the natural flow in sediment-laden streams or diverted the waters of these streams through canals and ditches. For numerous reasons these efforts have sometimes had unexpected and undesired consequences. As a result, engineers and others have long struggled for a better understanding of the relationship between sediment loads, sediment characteristics, and flow parameters.

Maddock (1969) has analyzed many data from numerous flume experiments by other researchers. This paper describes an initial extension of his results to some natural streams. The data are mainly from Colorado River records.

As this paper relies upon Maddock's analysis of laboratory data, some of his results (written commun., 1966) are summarized. The natural stream data have been analyzed within this framework to see if similar relationships exist in rivers.

A list of the symbols used in equations and discussion follows:

A = cross-sectional area,
C = sediment concentration in parts per million,
d = mean particle diameter of sediment,
D = depth,
g = acceleration due to gravity,
L = load per unit width,
L_e = an effective load,
N = a number; for example, sample size,
q = discharge per unit width,
Q = discharge,
r = sample correlation coefficient,
S = slope,
V = mean velocity,
w = fall velocity,
W = width,
γ = weight per unit volume of water,
$\Delta\gamma$ = submerged weight per unit volume of sediment particles,
ρ = density, and
$\frac{(\rho w^2)}{(\Delta\gamma d)}$ = drag coefficient of particle diameter d.

[1] Design Engineer, Otago Catchment Board. Formerly hydrologist, U.S. Geological Survey, Tucson, Ariz.

VELOCITY-LOAD RELATIONSHIPS

For unigranular sediment, Maddock distinguishes three velocity ranges with different relationships between velocity and load. Equilibrium conditions are assumed.

In the low-velocity range,

$$V \propto L_e^{1/9}, \tag{1}$$

where V is mean velocity and L_e is a modification of L, the actual load per unit width; L_e accounts for the fact that at no load ($L=0$) there is a velocity greater than zero ($V>0$).

In the midvelocity range,

$$V \propto L^{1/4} \tag{2}$$

or, with a correction for q, discharge per foot width,

$$V \propto q^{1/16} L^{1/4}. \tag{3}$$

The high-velocity range is considered to be an unstable condition, especially for unigranular sediments, so there is no discernible relationship between velocity and load. This leads to the postulation of an upper limiting velocity.

Figure 1 is a schematic diagram showing these relationships. The position of the lines depends upon bed-material diameters, fall velocities, slopes, depths, and other related factors. The dashed line suggests the probable modification of these relationships when the sediments are mixtures or contain a wide range of sizes.

U.S. GEOL. SURVEY PROF. PAPER 650–C, PAGES C188–C194

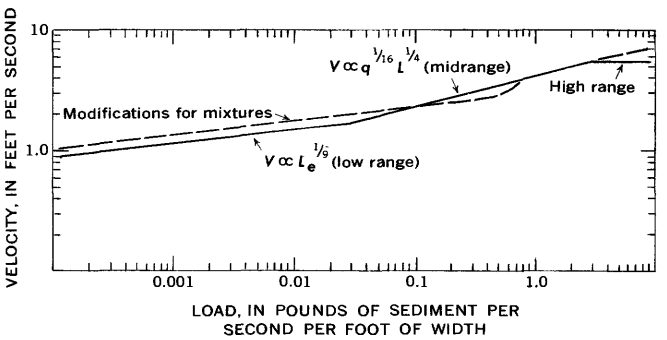

FIGURE 1.—Relationships of load to velocity. Dashed line shows probable variations caused by mixtures of grain sizes of load.

The range of velocities for each sediment size and velocity to load range is an implicit function and depends on other factors such as depth or unit discharge. For 0.25-mm sand and some typical values of unit discharge the velocities are:

Velocity-to-load relationship	*Velocity (feet per second)*
Cessation of movement	About 0.7.
Intersection of low- and mid-velocity ranges	About 2.
Limiting velocity	About 4.5.

VELOCITY-qS RELATIONSHIPS

The product of unit discharge, q, and slope, S, is a measure of the power per unit area. By assuming the velocity to load relationships described above, and through an analysis of variance and minimizations, Maddock concludes that there should be velocity-qS relationships as follows:

$$V \propto (qS)^{0.5} \tag{4}$$

when q and L are independent variables, and combined variance of friction factor and shear is minimized;

$$V \propto (qS)^{0.4} \tag{5}$$

when q and S are independent variables, and combined variance of friction factor and shear is minimized; and

$$V \propto (qS)^{0.3} \tag{6}$$

when q and S are independent variables, and combined variance of velocity and friction factor is minimized.

For other situations, other relationships can be derived.

Laboratory experiments conforming to the above constraints show the behavior predicted. Size parameters are included in the proportionality. For equation 5 enough data were available to determine the most probable form of the full equation for unigranular sediments, namely

$$V = 5.5\left[\frac{\gamma}{(\rho\Delta\gamma)^{1/2}}\right]^{0.4}\left[qS\left(\frac{w}{d}\right)^{1/2}\right]^{0.4} \tag{7}$$

or

$$V = 10\left[qS\left(\frac{w}{d}\right)^{1/2}\right]^{0.4} \tag{8}$$

for usual values of γ, and others.

Similarly, for the $V \propto (qS)^{0.5}$ relationship the equation becomes

$$V = 4.7\left(\frac{g\gamma}{\Delta\gamma d}\right)^{1/4}\left(\frac{\rho w^2}{\Delta\gamma d}\right)^{1/8}(qS)^{1/2}. \tag{9}$$

By substituting VD for q, and rearranging the relationship,

$$\frac{V}{(DS)^{1/2}} \propto \left(\frac{\gamma DS}{\Delta\gamma d}\right)^{1/2} \tag{10}$$

emerges. This is the form of the Einstein-Barbarossa (1952) relationship. A similar relationship can be derived from the formulas presented by Engelund (1966).

ANALYSIS OF DATA FROM NATURAL STREAMS

Most of the data were taken from records available in U.S. Geological Survey files in Tucson, Ariz. The rest came from published reports and from records supplied by the Ministry of Works, New Zealand. Sites investigated were at Lees Ferry, downstream from the Glen Canyon Dam, and near Grand Canyon, Ariz., both on the Colorado River; also, data from the lower Colorado River between Davis and Imperial Dams (U.S. Bureau of Reclamation, 1958) and from the Middle Loup River at Dunning, Nebr. (Hubbell and Matejka, 1959) were used. Data from the New Zealand rivers are shown in figure 5.

At Lees Ferry, data from the discharge-measurement notes made at the upper cableway, water years 1959–65, were used. Data on suspended sediment size, bed-material size, and distribution were collected periodically; these show variations, but for most purposes an average value of 0.1 mm can be assumed for suspended sediment and 0.25 mm for bed material. Slopes are calculated from the fall through the 5,000-foot reach between the upper cableway and the recorder. Large percentage errors are possible in these slope data because differences in elevation were sometimes as low as 0.01 feet in 5,000 feet, and may not even be the true slope at the cableway. In 1962 the staff gage at the upper cableway washed out; thus from then on slope data are scant. At Grand Canyon, slopes are calculated from the fall through the 700-foot reach between two recorders and are available only for measurements made at higher stages.

In the lower Colorado reaches, however, powerplant operations create unsteady flow conditions at some

stations. Since Glen Canyon Dam has been operating, Lees Ferry and Grand Canyon have also been affected by unsteady flow conditions.

VELOCITY-qS PLOTS

Figures 2, 3, 4, and 5 show the velocity-qS product plots for the sites investigated.

In figure 2 the Lees Ferry data cover the widest range of values for a single station and the points fall within enveloping lines where (equation 6) $V \propto (qS)^{0.3}$. This corresponds to the relationship where q and S are independent variables and the combined variance of velocity and friction factor is minimized. Also plotted is equation 8 for $d=0.25$ mm, the equation predicted for minimization of combined variance of shear stress and friction factor. In the middle range of values the points also lie close to this line but definitely diverge from it at the upper and lower ends.

Data from the other stations plot substantially within the enveloping lines for Lees Ferry.

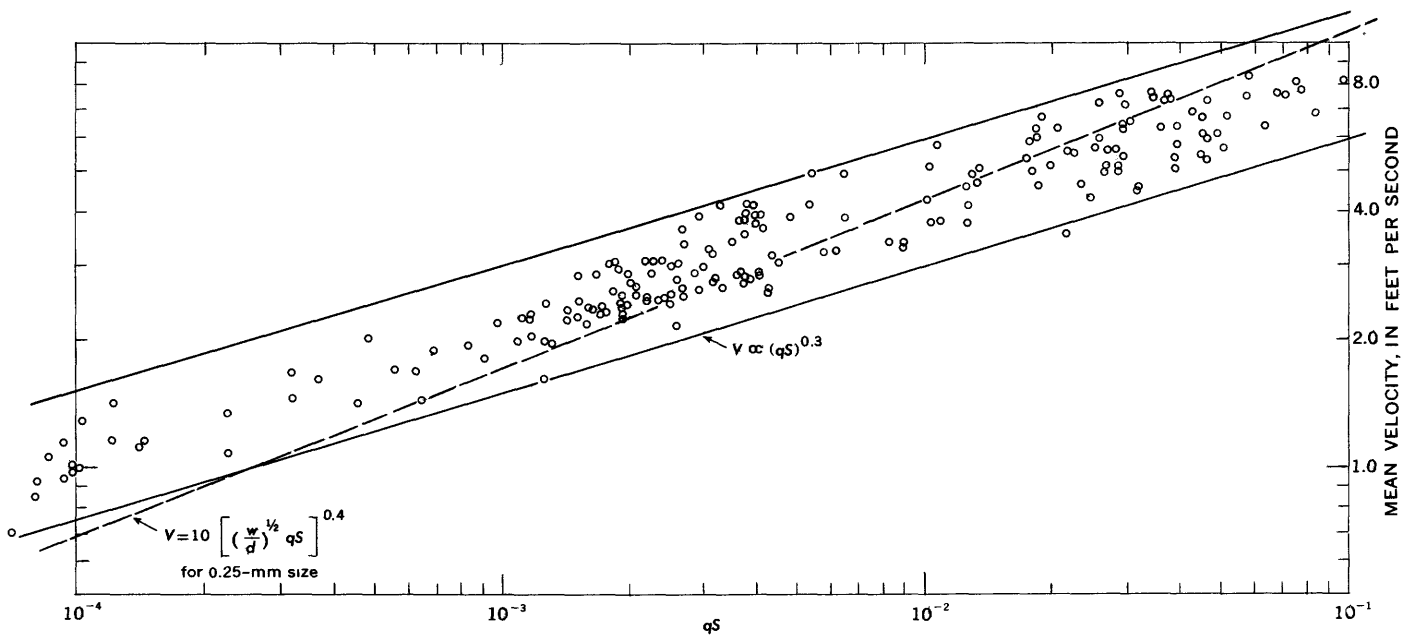

FIGURE 2.—Velocity-qS plot for Colorado River at Lees Ferry, Ariz., water years 1959–1962.

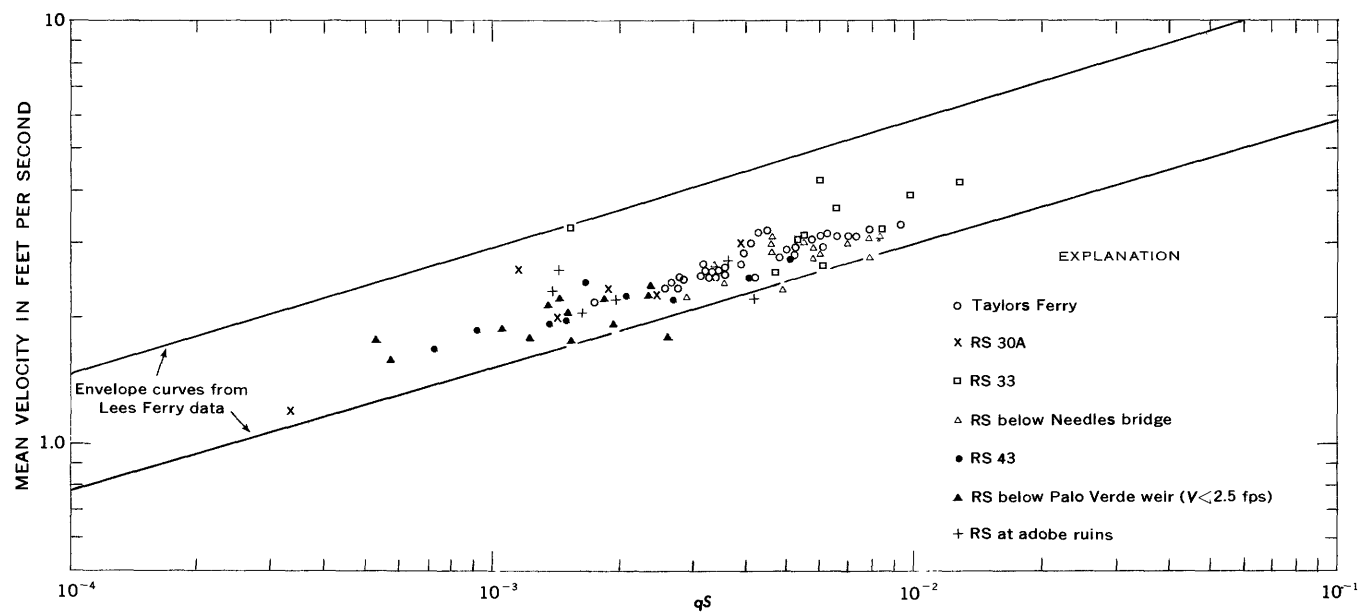

FIGURE 3.—Velocity-qS plot of data from lower Colorado River. Data from U.S. Bureau of Reclamation (1958).

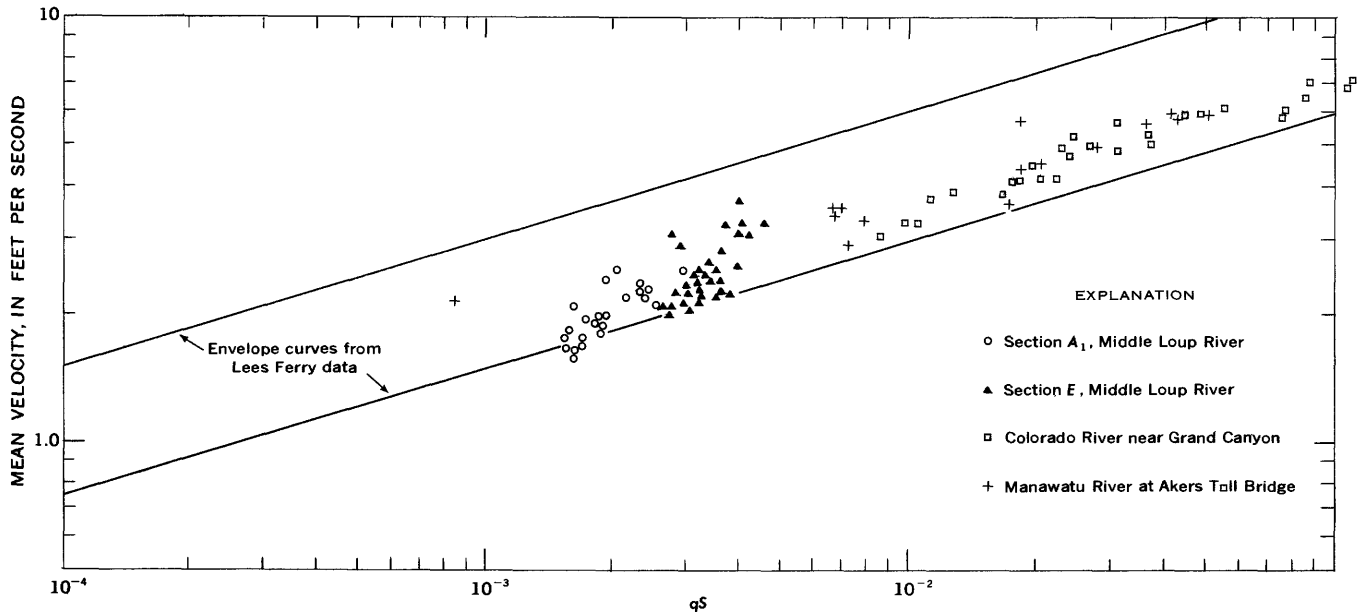

FIGURE 4.—Velocity-qS plot of limited data from four sites—two on Middle Loup River, Nebr.; one on Colorado River, Ariz.; and one on Manawatu River, New Zealand.

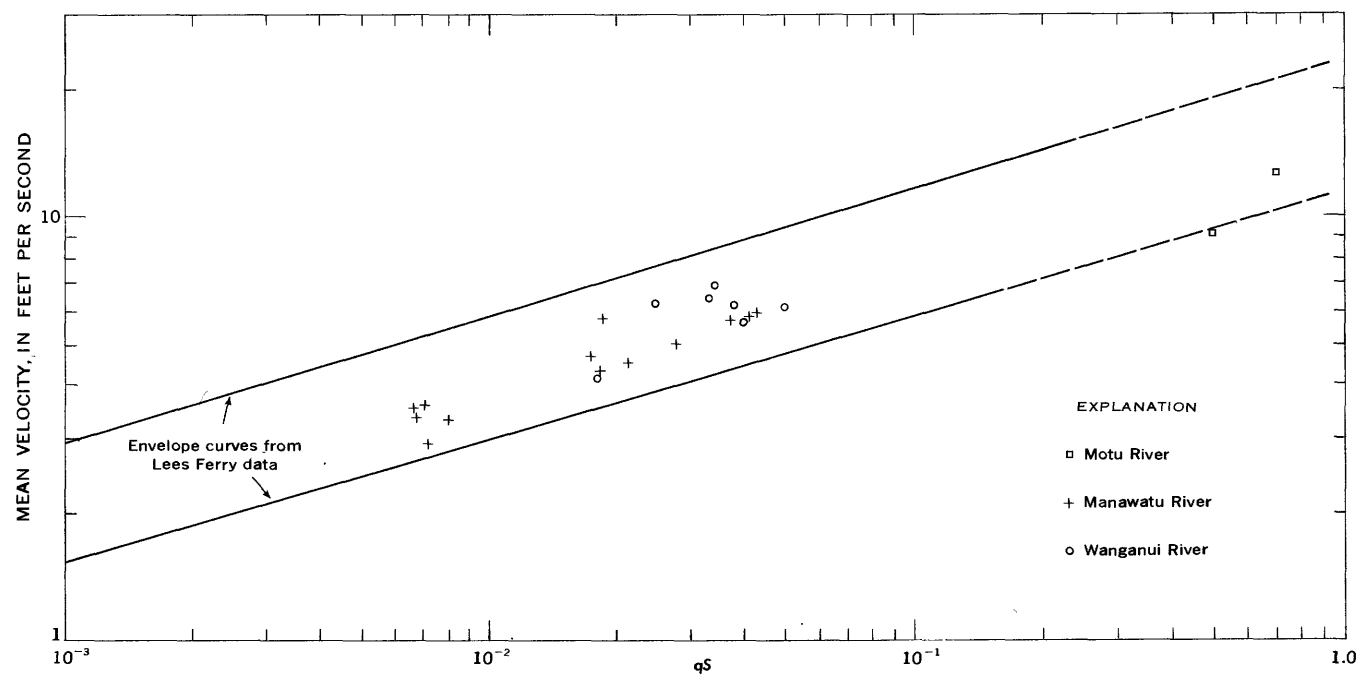

FIGURE 5.—Velocity-qS plot of data from New Zealand rivers.

VELOCITY-LOAD RELATIONSHIPS

Equation 3 can be modified to

$$V^{15/4} \propto LD^{1/4}, \quad (11)$$

where D is the mean depth and L has been calculated from the suspended sediment concentration C such that $L=\gamma qC\times 10^{-6}$ pounds per second per foot width.

When the Lee's Ferry data were plotted together they showed a large scatter but did show a trend such that

$$V \propto (LD^{1/4})^{4/5}. \quad (12)$$

However, it was possible, on the basis of suspended sediment size analyses, to separate the data into four groups. These are shown in figure 6.

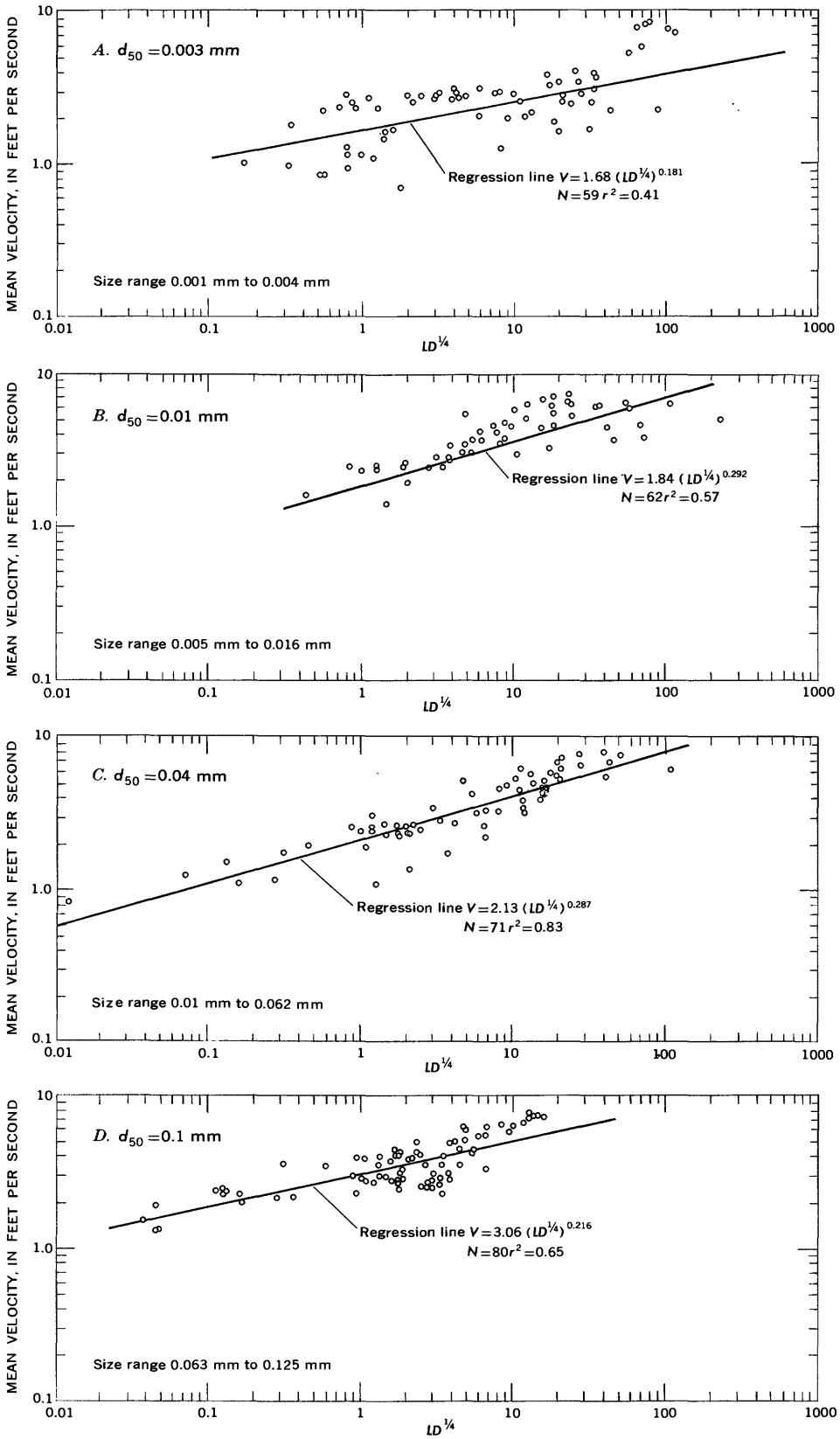

FIGURE 6.—Particle size. *A*, estimated d_{50}=0.003 mm; *B*, estimated d_{50}=0.01 mm; *C*, estimated d_{50}=0.04 mm; *D*, estimated d_{50}=0.1 mm. d_{50} is mean size; 50 percent of particles are finer and 50 percent are coarser than the given size.

Regression equations derived by computer are:

for 0.003 mm; $V = 1.68(LD^{1/4})^{0.8}$, $N=59, r=0.64$
.01 mm; $V=1.84(LD^{1/4})^{0.29}$, $N=62, r=0.75$
.04 mm; $V=2.13(LD^{1/4})^{0.29}$, $N=71, r=0.91$
.1 mm; $V=3.06(LD^{1/4})^{0.22}$, $N=80, r=0.81$

Besides changes in suspended sediment size, other reasons could be advanced for the observed scatter. Nonequilibrium conditions prevail as demonstrated in figure 7, which shows the mean bed elevations and monthly mean discharges at Lees Ferry, thus invalidating the assumption of equilibrium. Temperature variations may be another factor.

DISCUSSION

The analysis shows that natural stream data to some extent confirm the laboratory data and that, for streams which have a deficiency of sediment, that is, a tendency to scour their beds and banks, the usual relationship is $V \propto (qS)^{0.3}$ (equation 6) and, in fact, for sand sizes common in natural streams

$$V=14.4\ (qS)^{0.3}. \qquad (13)$$

The data analyzed to date all follow this relationship, but there seems to be no reason why rivers should not follow some of the other $V=qS$ relationships found in laboratory experiments. Sometimes, in fact, when plotting the data, successive points would appear to plot along a line corresponding to one of the other relationships and then break back with some change in concentration or flow.

The velocity-load data permit only a few tentative conclusions. The most important observation is of velocities greater than $V=250\left(\frac{d^2}{w}\right)^{1/3}=4.5$ feet per second for 0.25-mm sand. Maddock is careful to qualify his remarks by saying that the largest sizes making up at least 10 percent of the bed material should be used to calculate this limiting velocity, but even if $d=1.0$ mm, then $V=250\left(\frac{d^2}{w}\right)^{1/3}=6.0$ feet per second.

At Lees Ferry, particles larger than 1.0 mm are rarely observed in bed material or suspended sediment samples. The highest mean velocity for the whole section is more than 8 feet per second, and the highest observed mean velocity in any vertical is more than 11 feet per second. In his work, Stein (1965) indicates some variation in "breakway" velocity as depth increases, but his range of depths from 0.3 feet to 1.0 feet is too small for extrapolation of any "depth correction" to 10 or 20 feet.

The comparatively good correlation coefficients in the V versus $LD^{1/4}$ plots is encouraging, and it seems that with more size data available the correlation could have been improved. Also note that for the 0.01-mm, 0.04-mm, and 0.1-mm classes, the slope of the line is near the predicted value of 0.265.

RECOMMENDATION FOR ADDITIONAL DATA COLLECTION

The majority of data used in this discussion have been from U.S. Geological Survey gaging stations. The

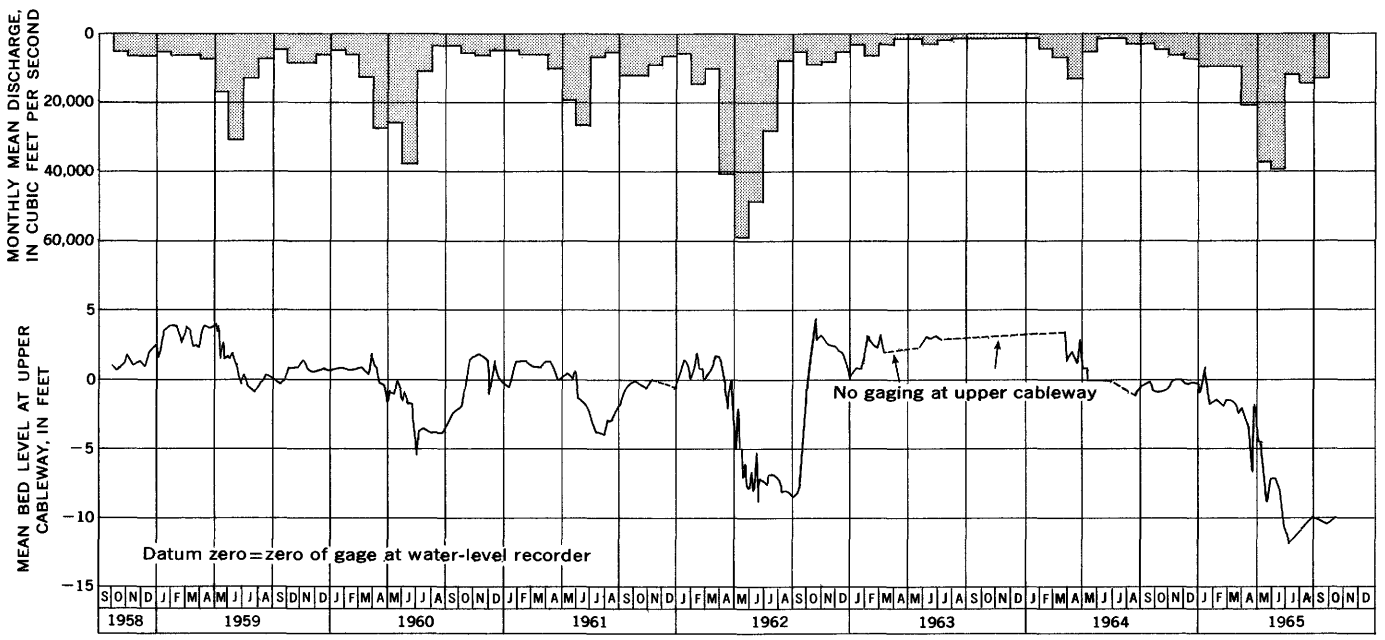

FIGURE 7.—Mean bed level for gagings at Lees Ferry upper cableway compared with monthly mean discharges.

only data that were not collected during a normal stream gaging were the slope data available at Lees Ferry.

Slope data are unnecessary when the requirement is merely to meter the water and sediment flowing past the section. However, as soon as the channel itself comes under scrutiny, then slope data become of major importance. Slopes could be easily obtained at many sites by installing staff gages at suitable places and observing differences in elevation whenever a discharge measurement is made. This would render the measurements potentially much more useful.

Also, sediment concentration, size samples, and discharge measurements could be taken as near together as practicable. This would give many of the data more internal consistency.

REFERENCES

Einstein, H. A., Barbarossa, H. L., 1952, River channel roughness: Am. Soc. Civil Eng. Trans., v. 117, no. 2528, p. 1121–1132.

Engelund, Frank, 1966, Hydraulic resistance of alluvial streams: Am. Soc. Civil Engineers Proc., Jour. Hydraulic Div., v. 92, HY2.

Hubbell, D. W., Matejka, D. Q., 1959, Investigations of sediment transportation, Middle Loup River at Dunning, Nebraska: U.S. Geol. Survey Water-Supply Paper 1476, 123 p.

Maddock, Thomas, Jr., 1969, The behavior of straight open channels with movable beds: U.S. Geol. Survey Prof. Paper 622–A. [In press]

Stein, R. A., 1965, Laboratory studies of total load and apparent bed loads: Jour. Geophys. Research, v. 70, no. 8.

U.S. Bureau of Reclamation, 1958, Interim report—Total sediment transport program, Lower Colorado River Basin: U.S. Bureau of Reclamation, 175 p.

A MUDFLOW IN THE SECOND CREEK DRAINAGE, LAKE TAHOE BASIN, NEVADA, AND ITS RELATION TO SEDIMENTATION AND URBANIZATION

By PATRICK A. GLANCY, Carson City, Nev.

Abstract.—A mudflow of more than 50,000 cubic yards occurred in the 1.5-square-mile Second Creek basin on August 25, 1967, after an intense thundershower. Although the mudflow originated naturally, its path was affected by manmade features. It damaged real estate and roadways in the lower part of the drainage, and also polluted Lake Tahoe. The mudflow probably is typical of one erosional process believed common throughout the area. The sequence includes sheet and rill erosion of nonforested uplands, severe downstream channel erosion that flushes out alluvium previously accumulated as a result of normal runoff and mass wasting, and extensive deposition along the flatter and lower part of the drainage. Estimates suggest that sheet and rill erosion of the upper basin contributed 60 to 80 percent of the debris, with the rest derived from the main channel. The event caused landscape denudation that averaged about 0.02 foot over the entire basin. Results of this reconnaissance influenced design of drainage structures for a new highway route through the area.

Rainfall was widespread throughout the Lake Tahoe region and adjacent areas during the late afternoon of August 25, 1967, as a result of regional thundershower activity (Dick Hambidge, U.S. Weather Bureau, Reno, oral commun., 1969). Precipitation recorded at several U.S. Weather Bureau stations in or adjacent to the area on August 25 is summarized in table 1.

TABLE 1.—*Precipitation in Lake Tahoe basin and adjacent areas, August 25, 1967*

Station	Altitude (feet)	Approximate location with respect to report area	Precipitation (inches)
Angora Lookout	About 7,200	26 miles south	1.31
Bower's Mansion	About 5,100	7½ miles east	.64
Meyers	About 6,400	27 miles south	.51
Mt. Rose Highway	7,360	8 miles northeast	.10
Truckee	5,995	12 miles northwest	.63
Stateline Lookout	6,900	1½ miles southwest	.10

Although the intensity of precipitation was moderate in most parts of the area, erosional evidence suggests that rainfall was exceptionally intense in the upper part of the Second Creek drainage (fig. 1). The precipitation stations listed in table 1 are at altitudes considerably lower than the upper parts of Second Creek drainage. According to Dick Hambidge (oral commun., 1969) precipitation from thunderstorms like those of August 25, 1967, is generally most intense on the high peaks of mountainous areas.

A reconnaissance investigation of flooding caused by runoff in the Second Creek drainage was made on August 26 and 28. According to newspaper accounts and reports of local residents, the runoff in the inhabited area occurred as a mudflow. It affected the western part of Incline Village near the mouth of Second Creek at Lake Tahoe. The mudflow caused extensive damage to one home and parts of the Crystal Shores Villas (an apartment-house complex), as well as damage to roads and their associated drainage structures. Some facts, observations, and interpretations of the event are as follows.

EROSION AND MUDFLOW CHARACTERISTICS

Although heavy precipitation fell throughout the 1.5-square-mile Second Creek basin, precipitation appeared to be most intense in the upper part of the basin, as indicated by extensive sheet and rill erosion in that area (fig. 1*C*). However, the erosion may have resulted partly from the lack of protective forest cover (fig. 1*B*). The basin land-surface altitude ranges from about 6,230 feet to about 9,450 feet, giving an overall topographic relief of about 3,220 feet (fig. 1*A*). Figure 1*A* also shows generalized geology (after Thompson and White, 1964). According to Mathews (1968, p. 7), the Tertiary volcanic mudflows and tuff breccias are readily affected by weathering and erosion forces. The volcanic unit that includes these flows and breccias is the dominant areally exposed geologic unit in the area of intense sheet

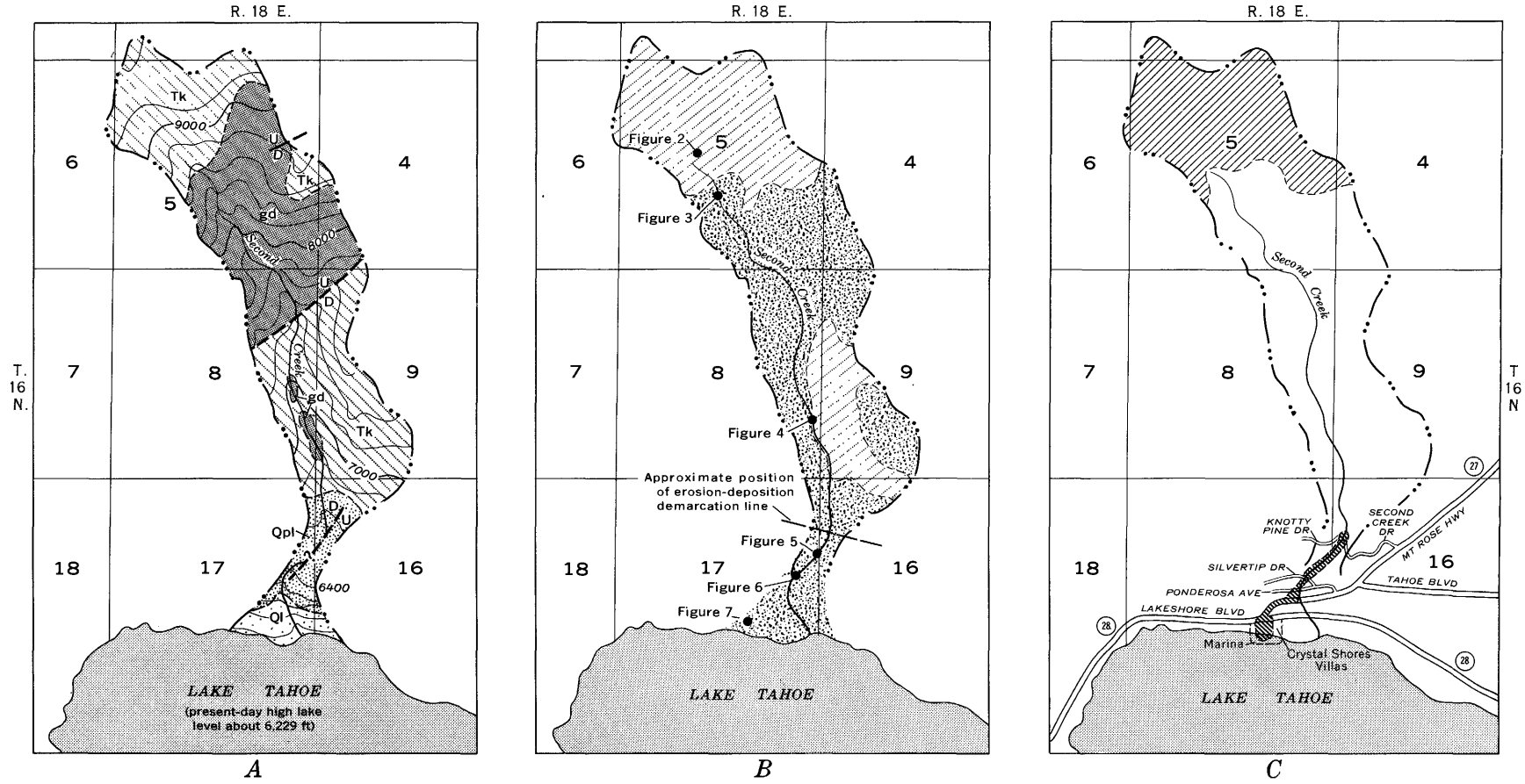

EXPLANATION

Ql — Quaternary lake deposits of gravel, sand, and silt

Qpl — Quaternary older alluvium characterized by mature soil cover

Tk — Tertiary volcanic flows, mainly Kate Peak Formation. *May include mudflow breccia and tuff breccia, mainly andesite*

gd — Cretaceous granodiorite

Approximate contact

U/D — Fault *Approximately located; U, upthrown side; D, downthrown side; queried where doubtful*

Drainage basin outline

Approximate area of natural forest cover

Approximate nonforested area

Approximate area of sediment deposition

Estimated area of intense precipitation

1 ½ 0 1 MILE

CONTOUR INTERVAL 200 FEET ABOVE 6,400 FEET, AND 40 FEET BELOW 6400 FEET
DATUM IS MEAN SEA LEVEL

FIGURE 1.—Sketch maps of the Second Creek basin showing: *A*, topography and geology (Thompson and White, 1964); *B*, natural forested areas and locations of photograph sites; and *C*, manmade features, and areas of intense precipitation and sediment deposition during the storm of August 25, 1967.

and rill erosion and, presumably, of intense precipitation (figs. 1 and 2). Field reconnaissance indicated that overland runoff from the storm caused sheet and rill erosion mainly above 8,600 feet, or in the upper 0.44 square mile of drainage. The general character and intensity of this erosion, as well as the characteristically steep land-surface slope in the eroded area, are shown in figure 2. Photograph locations are shown in figure 1*B*.

FIGURE 2.—Sheet and rill erosion of steep slopes in the unforested upper part of the drainage.

The overland runoff gathered sediment as it traversed the nonforested slopes, and the mixture finally flushed into the main channel at an altitude of about 9,000 feet. The abrasive water-sediment mixture eroded the main channel down to bedrock, as shown in figures 3 and 4. Figure 3 also shows freshly exposed tree roots and a distinct high-water line caused by the fine-grained mud plaster of the water-sediment mixture.

Below the 9,000-foot altitude, evidence of sheet and rill erosion is generally absent, which suggests either that precipitation intensity was considerably less or that forest cover attenuated erosive overland runoff. Therefore, below that altitude, erosion in the main stream channel was the dominant type. The channel was scoured to bedrock throughout most of its length, and some lateral cutting also occurred; however, the effectiveness of lateral cutting was restricted by steep channel walls.

The channel configuration and geometry before the flood are unknown, and a detailed survey of the channel after the flood was not within the reconnaissance scope of the study. However, photographic evidence and isolated field observations suggest that the average area of eroded channel cross section can be assumed to range between 25 and 50 square feet. On that basis it is estimated that main-stem channel erosion probably contributed somewhere between 20 and 40 percent of the total eroded material.

FIGURE 3.—Channel erosion to bedrock, and the high-mud-water line. Flow was from right to left.

Figure 4 shows a typical channel reach in the zone of dominant channel erosion; the only deposited sediment is a fine-grained mud plaster above the heavily scoured part of the channel, plus scattered large fragments such as the boulder lodged between the bank and tree. The large boulders, which apparently were carried along several feet above the channel floor, indicate that the transporting fluid was extremely turbulent or highly viscous, or both. A high viscosity, such as that associated with mudflows, may account for these erratic deposits, although large boulder movement may also occur during catastrophic stream floods (R. W. Janda, U.S. Geol. Survey, written commun., 1969).

The gradient along the main-stem channel, as shown by the U.S. Geological Survey Mt. Rose topographic map, scale 1:62,500, is a generally uniform 1,600 feet per mile between the altitudes of 9,200 and 7,200 feet. The gradient flattens to an average of about 670 feet per mile between 7,200 and 6,600 feet, and it then flattens to about 480 feet per mile between 6,600 and

FIGURE 4.—Example of severe channel erosion and deposition. The 2-foot diameter boulder was lodged between tree and slope. View is downstream.

6,230 feet (approximate lake level). The altitude of demarcation between areas of erosion and deposition is about 6,540 feet; therefore, deposition occurred in the area of gentlest channel gradient. The uphill edge of real-estate development also begins at about, and is prevalent below, the 6,540-foot altitude.

Second Creek channel is bridged by Second Creek Drive at about the 6,540-foot altitude, and the streamflow normally passes through a culvert. The combined effects of reduced channel gradient and the inability of the culvert to convey the entire viscous flow apparently triggered sediment deposition. The sediment effectively backfilled the channel and gully upstream from Second Creek Drive until it overtopped Second Creek Drive and continued downstream. Similar deposition occurred along the main channel gully downstream from Second Creek Drive.

A residence downstream from Second Creek Drive, and located in the main gully that also contains the main-channel flood plain, was severely damaged by mud and debris. Sediment deposition was heavy throughout this area; the character of deposits, and

FIGURE 5.—Severely damaged dwelling in mudflow's path.

some of the damage to the dwelling, are shown in figure 5. The dwelling was damaged because the normal mainstem channel overflowed, and the mud spread over the narrow flood plain on which the house is located. The house was damaged by mud that entered and flowed through the lower levels, and apparently also by the impact of trees being moved by the flow.

Farther downstream, culverts bridging Silvertip Drive also impeded the mudflow, and helped spread it over the relatively flat terrain below. Additional evidence of the ability of the viscous high-energy mudflow to transport large boulders is indicated by figure 6, which shows a boulder having an estimated mean diameter of about 7 feet deposited on the downstream shoulder of the roadway at Silvertip Drive crossing (culvert diameters are 3 feet). Note also the uprooted tree deposited by the flow (fig. 6).

When mud and debris reached State Route 27 (Mt. Rose Highway) the flow was diverted down the road-

FIGURE 6.—Granitic boulder (diameter 7 feet) deposited atop road culvert by mudflow.

way through the roadcut because drainage structures there and at Silvertip Drive and Ponderosa Avenue were unable to contain and transmit it through the normal stream channel. The mudflow therefore used the highway cut as the much larger and alternate channel, and was thereby diverted away from the natural stream course.

At the intersection of Nevada State Routes 27 and 28 (Mt. Rose Highway and Lakeshore Boulevard), the mudflow left its artificial channel (Route 27) at the roadcut terminus, crossed Route 28, and continued downslope through Crystal Shores Villas. Deposits of mud and debris were extensive in the villa area, and they damaged several buildings. Some parked cars were partly covered, and a few garages were invaded by mud. The lobate border of the deposit shown in figure 7 indicates that the runoff in this general area was in the form of a mudflow, rather than merely a debris-charged flash flood. However, the runoff probably began as a debris-charged flash flood in the upper part of the basin, and subsequently evolved into a mudflow downstream because of progressive debris pickup.

The land surface in the Crystal Shores Villas area slopes generally toward Lake Tahoe. An unknown quantity of the mudflow passed through the area and terminated in the lake near the marina area.

Mudflow deposition was significant below the Second Creek Drive crossing. The area of aggradation, not including the lake itself, was about 16 acres. Thickness of the deposits ranged from zero to probably more than 20 feet. Mean depth of deposits throughout the area, at the time effective downslope flow ceased, was an estimated 2 feet. Therefore, the deposits amounted to about 32 acre-feet, or about 50,000 cubic yards. Additional deposits in the lake, although sufficient to muddy the water of the marina and cause lake pollution, were probably somewhat less in volume than those remaining on land.

Assuming a porosity of 30 percent for the deposits, the estimated debris volume is about 35,000 cubic yards. Therefore, denudation of the landscape, averaged throughout the 1.5-square-mile basin, is about 0.02 foot. According to R. W. Janda and Edward Helley, of the U.S. Geological Survey (written commun., 1969), denudation at that rate suggests a frequency recurrence interval probably greater than 50 years for an erosive event of this magnitude in a high-altitude stream basin in this geographic area.

SUGGESTED EROSIONAL SEQUENCE

The Second Creek flood and mudflow of 1967 suggests one type of erosion in this general area of Nevada

FIGURE 7.—Apartment-house complex invaded by mudflow.

that may be characterized as follows: Mass wasting and runoff from low-intensity rainfall and snowmelt moves sediment into main stream channels, and part of the sediment (an unknown percentage) accumulates and is temporarily stored. Subsequently, periodic torrential runoff, caused mainly by summer thundershowers, subjects the land surface and stream channels to extreme erosive forces. If storm intensity is particularly great in the uppermost headwaters, especially where land slopes are steep and vegetation is sparse, rapid sheet and rill erosion results from the subsequent sudden runoff. The water converges rapidly on mainstem channels and, aided by its sediment load, severely erodes them. Sediment stored along the main channels is thereby set in motion. As the runoff moves down the channel, increased quantities of the readily available channel sediment are thus mobilized, and the sediment content of the mixture increases faster than the water content. As a result, the viscosity of the mixture also increases rapidly, and the abrasive character of the mixture may also increase. The increasing viscosity multiplies the capacity to incorporate larger sediment particles in the mixture, which further intensifies channel erosion. The mixture continues downgradient, increasing in volume and destructive capacity. Finally, a point is reached where stream gradient and channel walls flatten, the channel becomes shallow, and the mudflow leaves the channel and inundates the adjacent gently sloping parts of the drainage. Unfortunately, the flatter depositional area in many drainages is also the area in which most development has taken place, an area prone to costly damage. Many manmade stream-channel and land-surface structures retard efficient passage of the debris, and therefore increase the chances of costly damage. Furthermore, debris reaching Lake Tahoe probably contributes materially to pollution of the lake.

Results of extreme floods have been observed elsewhere in this general area. Thompson and White (1964, p. A43–A44) mentioned a similar event in the summer of 1952 on Galena Creek, which drains the east flanks of Mt. Rose. A similar flood occurred in Galena Creek on July 30, 1960, and another in the Third Creek drainage in August 1965, about 2 miles east of Second Creek. A flash flood and mudflow also occurred in Kings Canyon, on the east slopes of the Sierras just west of Carson City, Nev., on July 30, 1960 (R. D. Lamke, U.S. Geol. Survey, oral commun., 1969). Although the erosive event of the magnitude described on Second Creek is presently believed to have a recurrence interval of greater than 50 years in that particular drainage, evidence of several similar events in nearby drainages during recent years suggests that this general type of erosion and flooding is common throughout the area.

RELATIONSHIP OF MUDFLOW TO MANMADE STRUCTURES

The described mudflow originated naturally—its occurrence was not related to urbanization in the area. However, the mudflow's ultimate disposition was influenced by man's alteration of the landscape. The mudflow, in turn, also affected the landscape and its manmade structures.

The timely occurrence of the mudflow during design stages of a new Nevada State highway through the area emphasized the need for large highway-drainage structures. Accordingly, on the basis of the reconnaissance data reported here, structures were redesigned to allow more efficient transport of the naturally occurring floods and mudflows (Harry Green, Nevada State Highway Department, oral commun., 1969).

REFERENCES

Mathews, R. A., 1968, Geologic map of the Lake Tahoe Basin, northern half: California Div. Mines and Geology open-file rept., 9 p., 1 pl.

Thompson, G. A., and White, D. E., 1964, Regional geology of the Steamboat Springs area, Washoe County, Nev.: U.S. Geol. Survey Prof. Paper 458–A, 52 p., 2 pls.

HYDROGEOLOGIC RECONNAISSANCE OF THE CANARY ISLANDS, SPAIN

By ROBERT J. DINGMAN and JOSÉ NÚÑEZ,[1]
Lawrence, Kans., Canary Islands, Spain

Prepared in cooperation with the Consejo Superior de Investigaciónes Cientificas and the Instituto de Hidrología under the auspices of the International Hydrologic Decade of UNESCO

Abstract.—The Canary Islands are a group of volcanic islands off the west coast of Africa. Rainfall is sparse, and ground water is used to support an agricultural economy. On the major islands overpumpage occurs and water levels are lowering rapidly.

This article is based on data collected during a UNESCO-financed assignment to the Canary Islands during April and May 1967. The objective of the assignment was to study the feasibility of establishing a project in the Canary Islands to define the hydrologic system as a basis for managing or solving the water problems of the islands.

Acknowledgments.—The staff of the Instituto de Hidrología was very helpful while Mr. Dingman was in Madrid in providing reference material and in establishing a general background. Special appreciation is due Sr. Alonso Vega, Ingeniero Jefe del Servicio Hidráulico, for making available office space, secretarial and staff assistance, and, in general, offering every possible aid to Mr. Dingman.

[1] Ministry of Public Works, Canary Islands.

GEOGRAPHY

The Canary Islands (fig. 1) are approximately 160 kilometers off the west coast of Africa. The areas of the seven major islands range from 2,058 square kilometers for Tenerife to 278 km² for Hierro (table 1). The population ranges from 500,000 at Gran Canaria to 6,000 at Hierro.

The economy of the islands has always been based on agriculture, although tourism is becoming an increasingly important source of income. The principal agricultural products have changed through the years in response to changing world economic conditions. Production of wine, growing of sugar cane, and harvesting cochineal insects for dye were very important in the past but now have been almost entirely abandoned. During the last 100 years bananas have become the

TABLE 1.—*Precipitation and water use in the Canary Islands (1966)*

[Data from the Servicio Meteorologico Nacional, Ministerio del Aire, Spain]

Island	Area (km²)	Population	Average annual precipitation			Water use (m³/s)					Percentage of annual precipitation used
			mm/yr	10⁶m³/yr	m³/s	Agriculture	Municipal	Industrial	Other	Total	
Gran Canaria	1,551	500,000	[1] 400	[1] 620	19.66	5.64	0.5	0.3	[2] 0.03	6.5	34
Lanzarote	796	40,000	160	130	4.1	--------	.006	.003	--------	[3] .009	.22
Fuerteventura	2,017	17,000	100	200	6.3	.229	.004	----------		.233	3.7
Tenerife	2,058	400,000	445	915	29	[4]	[4]	[4]	[4]	8.43	29
La Palma	750	75,000	530	400	12.7	[4]	[4]	[4]	[4]	2.31	18
Gomera	378	10,000	[4]	[4]	[4]	[4]	[4]	[4]	[4]	.62	[4]
Hierro	278	6,000	[4]	[4]	[4]	[4]	[4]	[4]	[4]	.12	[4]

Abbreviations: km², square kilometers; mm/yr, millimeters per year; m³/yr, cubic meters per year; m³/s, cubic meters per second.
[1] Ranges from an average of 130 mm/yr (200×10⁶m³/yr) at low altitudes to 800 mm/yr (1,200×10⁶m³/yr) at altitudes of more than 1,500 meters.
[2] Harbor supply.
[3] Desalinization plant yield of 0.027 m³/s not included.
[4] Data not obtained.

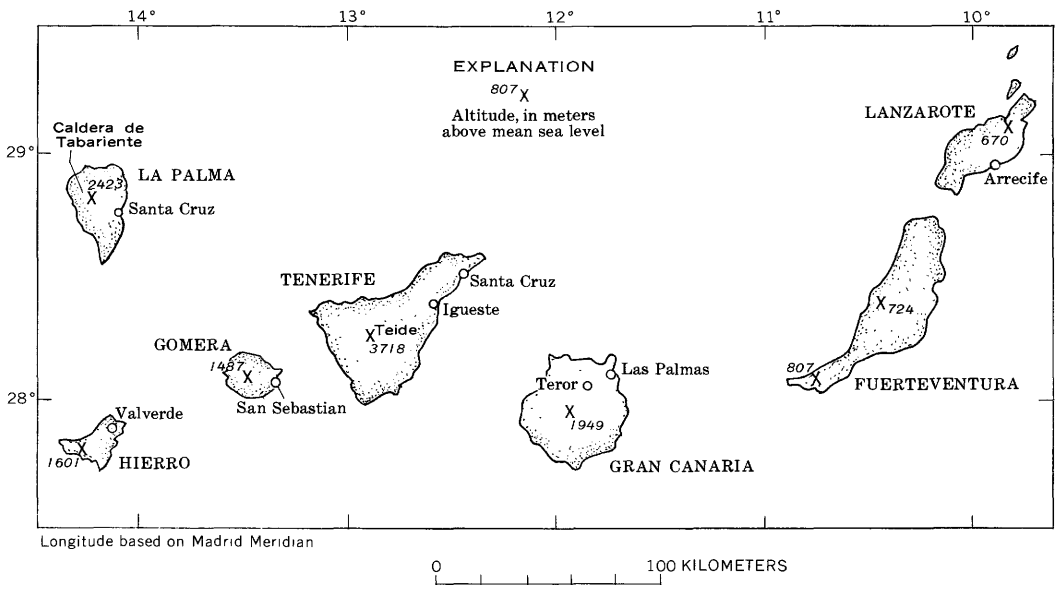

FIGURE 1.—Index map of the Canary Islands. Longitude based on Madrid meridian, which is 3°41'14.55" W. long. Greenwich.

most important product. Rapidly developing water shortages, accentuated by ever increasing demands for water by municipalities, may cause a decline in banana production and a change to intensively cultivated crops of high value. Tomato production has now become very important on Gran Canaria. Many small areas are now completely enclosed in plastic sheeting to produce truck garden crops under controlled climatic conditions. The scarcity of rainfall requires that crops be irrigated in order to obtain a cash return sufficient to support the heavy population of the islands.

The surface water trapped by the extensive system of dams is completely inadequate to irrigate the cultivated land. Therefore, more than 100 years ago the islanders began the development of ground water for irrigation. On Gran Canaria and to some extent on Tenerife the ground-water aquifers are seriously overdeveloped, and water levels are falling as much as 10 meters per year. Average pumping levels on Gran Canaria are approaching 150 m and in some localities are at 250 to 300 m.

A "water market" exists in which water is sold at a cost established by a supply and demand situation. The cost of water for irrigation ranges from 5 to 17 cents U.S. per cubic meter. Water in the upper part of this cost range is completely uneconomical for irrigation. As a result, the banana plantations that were formerly irrigated every 20 days are now irrigated every 60 days. Irrigation at 60-day intervals is sufficient to keep the plants alive but is not adequate to produce crops.

The seriousness of the situation is extreme. If new sources of water cannot be found, the economy faces a complete collapse. This has occurred twice in the islands during the past century—once when the world sugar market became dominated by the Central American countries, and again when the invention of analine dyes made the use of cochineal insect dyes uneconomical.

A thorough investigation of the hydrology of the islands must be made to determine if any untapped water resources exist. If significant sources are not discovered, the knowledge of the hydrology of the islands, gained by the study, can be used to manage existing water in the most economical way and in such a manner as to limit the use of water to the average quantity of water available annually.

The climate of the Canary Islands is typical of islands in this general latitude. Rainfall is sparse, 100 millimeters per year or less at low altitudes, increasing at higher altitudes to a maximum of 915 mm/yr on the upper slopes of Teide volcano on Tenerife. Temperatures are moderate except for rare periods of strong east winds bringing hot air from the Sahara Desert. During these times temperatures soar to above 40° C.

GEOLOGY

The geology of the area has been studied by many geologists in the past 160 years. The earliest investigator was Leopold Von Buch (1825). Of particular interest are the works of Hausen (1958, 1961, 1962), and the series of recent papers by Macau (1957, 1959, 1963). The islands were mapped by students and professional staff of the Instituto de Geologia, Madrid. Map compilation is on 1:25,000-scale base maps and publication scale is 1:50,000. As of October 1968, mapping and compilation were complete, many of the maps were

printed, and the rest were expected to be published in a few months.

The Canary Islands are underlain almost entirely by volcanic rocks or by sediments derived from volcanic rocks. Sediments of marine origin are exposed in a few low marine terraces. The oldest rocks exposed (age unknown) are basalts and trachytes. On Gran Canaria the trachytes dip steeply toward the northwest. The older beds are disconformably and in some areas unconformably overlain by a thick series of basalt flows and related pyroclastic rock. The composition of the rocks became more silicic with decreasing age until rhyolite or trachyrhyolite flows occurred. The more recent deposits are mafic, with basalt and olivine basalt the most common modern rock types.

The islands are studded with hundreds of volcanic cones ranging in size from small hills to the huge volcano of Teide, which reaches an altitude of 3,718 m. Volcanic activity has continued into historic time with the last eruption occurring on La Palma in 1949. Periods of relatively intense volcanism occurred in the late 15th century and near the end of the 18th century. The topography of Lanzarote and La Palma consists in large part of volcanic cones and flows of late Pleistocene or Holocene age. Many of the cones have been formed by eruptions that occurred in historic time.

The geology of the islands is simple in the sense that almost all the rocks exposed are volcanic in origin and have suffered very little folding or faulting. In detail the geology is complex because of the overlapping of deposits, the similarity of lithology of rocks of different ages, and in some localities because of the many dikes that have intruded the country rock.

As previously mentioned, faulting of major importance is rare. Bourcart (unpublished data, 1933) postulates the existence of a major fault oriented northwest that divides Gran Canaria in to two parts having somewhat different characteristics with regard to Pleistocene or Holocene volcanism. The existence of this fault has been accepted by most of the recent investigators. Minor faults with displacements from a few centimeters up to 30 m occur in several localities on Gran Canaria.

The geology of each of the major islands may be summarized as follows:

Gran Canaria.—The oldest rocks, exposed in the deep canyons and ocean cliffs of the western part of the island, are steeply dipping trachytes and flat-lying basalts (age unknown). The older rocks are overlain disconformably and, in some areas, unconformably by a thick series of basalt flows and related pyroclastic rocks. As is common throughout the islands, the volcanic rocks are progressively more silicic with decreasing age, reaching a rhyolitic or trachyrhyolitic composition. A thick bed of agglomerate (mud flow?) deposits exposed in many localities in Gran Canaria has been named the Roque Nublo Formation. The youngest deposits are mafic, consisting of basalts and olivine basalts with related pyroclastic material. Marine terraces (Miocene) are exposed in the northeast part of the island. The area of the terraces is small, and salt-water encroachment occurs in areas of groundwater development.

Lanzarote.—Lanzarote is a basaltic island. Except for exposures of the relatively older, flat-lying basalts in the northern one-fourth and the southern one-tenth of the island, the rest of the area is covered by more than 100 young volcanic cones, many of them dating from the 18th century.

Fuerteventura.—A basement complex of mafic rocks in near-vertical position is exposed in the western one-fourth of the island. This complex is intruded by ultramafic (pyroxenite, peridotite, and gabbro) and silicic (syenite) bodies. The southern and eastern parts of the island are covered by a basaltic tableland series with a constant dip of approximately 5° SE.

Modern volcanoes and their eruptive materials (lava streams, pyroclasts) cover the north and northeastern sectors of the island.

Gomerá.—Gomera is a volcanic shield, greatly destroyed by a long erosive cycle. The sequence of the volcanic material is as follows:

1. Basement of holocrystalline ultramafic rocks (gabbros and peridotites).
2. Thick layer of volcanic agglomerates.
3. Series of basalt flows ("old basalts").
4. Series of horizontal basalts unconformable with the underlying series.
5. Holocene basaltic series.

The entire sequence is intruded by thousands of vertical basaltic dikes and plugs of phonolites and trachytes.

Gomera is the only one of the Canary Islands having no indication of recent volcanic activity.

Hierro.—Hierro is a basaltic island with its surface covered by more than 200 pre-Holocene and Holocene volcanoes and their products: lava streams, lapilli, and ash. Hierro has 200 volcanoes in an area of 278 km^2 (1 volcano per 1.4 km^2), whereas Lanzarote, "the island of the volcanoes," has approximately 140 in an area of 796 km^2 (1 volcano per 5.5 km^2).

La Palma.—Basaltic lava of Holocene age is exposed in the northern half of the island. The southern half is covered by basalts from recent volcanoes, mostly of historic age. Volcan de San Juan, the youngest volcano in the islands was formed in 1949. Caldera de Tabariente, an erosional caldera developed from an

337-735 O—69——14

older caldera of explosive origin, has a crater approximately 80 km² in area and more than 1,500 m deep. Good exposures of the plutonic basement of the island occur in the caldera.

Tenerife.—The older rocks, basalts and agglomerates with phonolitic intrusions, are exposed in the northeastern and northwestern peninsulas. Trachyphonolitic rocks exposed in the central slope are remnants of the great pre-Teide volcano, destroyed during the formation of Las Canadas, a subsidence caldera. The old crater has been filled partly with lavas and ejecta of the new volcanoes. The present caldera has a diameter of about 15 km, a surface of 125 km², and a depth of 300 m. Pozzolan and pumice agglomerates from the pre-Teide crater cover most of the southern part of Tenerife. Recent volcanoes are scattered over most of the island.

HYDROLOGY

Surface water

There are no perennial streams in the Canary Islands. The combination of very steep gradients, sporadic rainfall, poor recharge conditions, and relatively high transmissibility has resulted in the establishment of a water table that in most areas is far below streambeds. Therefore, low streamflows cannot be maintained by ground-water seepage. There has been no attempt to measure flow during the short periods when heavy showers cause surface runoff. Relatively small amounts of water are discharged to the ocean as streamflow. In Gran Canaria in May of 1967, water flowed in the Barranco del Guiniguada to the sea for the first time in several years. The flow that passed under the bridge at Las Palmas was only a few (10 to 20) liters per second. Surface runoff was undoubtedly much greater in the past before the numerous dams and diversion system were created.

Many major dams (15 m or more high) have been constructed in the islands (table 2). Typically these dams are high and narrow, constructed of local rock with a cement-lime mortar, and have very small storage capacity in relation to their height. A few of the most recent high dams in Gran Canaria have been constructed of reinforced concrete.

Although the complete lack of streamflow data makes any exact determination impossible, the impression is that the storage capacity developed in some of the drainage basins is excessive in relation to the quantity of water likely to reach the dams during periods of heavy rain. On the other hand, the scarcity of water and its resultant high value to the economy may justify what would be considered overdevelopment of storage capacity in other areas.

TABLE 2.—*Surface-water development in the Canary Islands (as of May 1967)*

[Dams tabulated are more than 15 meters high]

Province and island	Dams existing		Dams planned or under construction		Total storage ($10^6 m^3$)
	Number	Storage capacity ($10^6 m^3$)	Number	Additional storage ($10^6 m^3$)	
Las Palmas:					
Gran Canaria [1]	54	52	12	30	82
Lanzarote	0	0	1	.2	.2
Fuerteventura	3	2.5	2	3	5.5
Santa Cruz de Tenerife:					
Tenerife	9	1.8	3	.7	2.5
La Palma	1	.045	0	0	.045
Gomera	9	1.1	3	1.2	2.3
Hierro	0	0	1	.045	.045

[1] Thousands of small reservoirs, with estimated storage capacity of 20 × $10^6 m^3$, exist in Gran Canaria.

Hundreds of small dams and impoundments have been constructed. Some of these small structures are used for temporary storage of water obtained from major dams or from ground-water sources. The majority of the small dams are used to trap surface runoff from small basins.

Virtually no water-quality data are available in the Canary Islands. The only analysis the authors were able to locate was on a bottle of mineral water. A few water analyses may have been made at the Universidad de la Laguna, Tenerife; however, local officials of Obras Publicas (Public Works) had no knowledge of any analyses, and time was too short to visit the university.

GROUND WATER

Ground-water resources are being developed, and in some areas greatly overdeveloped, throughout the islands (table 3).

Ground water exists under water-table conditions in most areas of the islands. In some localities high artesian pressures exist and, in local areas, pressure differentials of as much as 300 feet (90 m) exist across basalt dikes.

Wells, springs, and galleries obtain water from most of the rock formations of the islands. The following list of formations and rock types is arranged in an approximate order of decreasing permeability.

Modern basalts.—Very highly permeable, moderate to low storage coefficient, high yields temporarily obtained.

Terrace deposits.—Low-lying sedimentary deposits, high permeability, high porosity. Low topographic position results in rapid salt-water encroachment.

Roque Nublo Formation.—Thick series of agglomerate (mud flow deposits ?) and interbedded basalts, the

TABLE 3.—*Ground-water development in the Canary Islands*

[Data compiled by Servicio Hidráulico de Las Palmas for UNESCO appraisal report, May 17, 1967]

Province and island	Source of water and yield (m^3/s)								Total yield (m^3/s)
	Wells		Galleries		Springs		Desalinization plants		
	Number	Yield	Number	Yield	Number	Yield	Number	Yield	
Las Palmas:									
Gran Canaria	[1] 2,830	[2] 4–5.2	360	1.0	[3] 10	0.2	([4])	0.23	6.43
Lanzarote	3	0.003	2	.006	None	----	1	.027	.036
Fuerteventura	[5] 650	.227	2	0	6	.006	None	----	.233
Santa Cruz de Tenerife:									
Tenerife	73	.85	485	7.4	54	.18	None	----	8.43
La Palma	[6] 30	[6] .46	102	1.2	125	.65	None	----	2.31
Gomera	36	.17	3	.07	36	.38	None	----	.62
Hierro	3	.12	8	----	None	----	None	----	.12

[1] Includes 510 shallow wells in the alluvium of Aldea Valley.
[2] Yield reached 6.2 m^3/s during the drought of the middle 1960's.
[3] More than 1,000 small springs with yields of a fraction of a liter per second are used for domestic water or for irrigation of a very small plot of land.
[4] A desalinization plant is planned for Las Palmas.
[5] All wells produce brackish water, salinity 2,000 mg/l or higher.
[6] Incomplete data.

most extensively developed aquifer on Gran Canaria. Permeability is moderate, but the storage coefficient is very low, resulting in rapid decline of water levels. Water is commonly obtained in weathered zones at upper surface of interbedded basalt flows.

Older basalts.—Low permeability and low storage coefficients. Source of many small water supplies.

Phonolite.—Characteristics similar to those of older basalts, but permeability may be lower.

Rhyolites and trachytes.—Very low permeability. May be the source of a few small supplies.

A calculation was made to determine the approximate storage coefficient in an area of rapidly declining water levels in the northern part of Gran Canaria. This area, located near Teror, is greatly overdeveloped, and wells are now being hand dug in basalts to 160 m. Static and pumping levels are near 160 m. Over an area of 27 km^2, water levels have dropped 50 m. in the last 10 years.

During 1966, 3.15×10^6 cubic meters of ground water was pumped. Recharge probably is relatively small owing to the very steep surface relief and the impermeable nature of the exposed rocks. As a rough approximation, recharge could be considered as 15 percent of the local rainfall of 600 mm/yr. The storage coefficient was calculated by computing the ratio of the volume of water pumped to the volume of aquifer dewatered. If no recharge is assumed, the storage coefficient (S) is approximately 2.3×10^{-2}. If 15 percent of the rainfall is used as recharge, the value of $S=5.3\times10^{-3}$. The value of 2.3×10^{-2} is a maximum, and increased recharge would reduce the calculated value of the storage coefficient.

If it is assumed that all the ground water pumped in this area in 1967 (3.5×10^6 m^3) was derived from recharge, the quantity would represent only 19 percent of the 600 mm/yr of local rainfall. The actual recharge, however, must be much smaller than the annual pumpage because the continuing decline in water levels indicates some withdrawal from storage. If no recharge is assumed, the maximum possible storage coefficient would be 2.3×10^{-2} for an average decline of 5 m over an area of 27 km^2. The low storage coefficient is an indication of the low porosity of the aquifers. The basalt is of the ropy pahoehoe type and does not contain the blocky zones of high porosity and permeability usually associated with basalt of the aa type.

Water levels are declining very rapidly in Gran Canaria in the area of ground-water development, or roughly the northeast half of the island. In some areas the decline over the past 40 years has been 120 m. The rate of decline has accelerated recently owing to the increased number of wells and, also, to the fact that the zones of good production in the Roque Nublo formation have been drained and production is now from igneous rocks with lower storage coefficients. Near Arucas mountain the decline is now 10 meters per year and declines of 7 m/yr have occurred over most of the area of exploitation.

The recent prolonged dry period prior to 1967 was probably of minor importance in the lowering of water levels. The area is severely overdeveloped, and rainfall and surface-water supplies are seldom, if ever, adequate to irrigate the cultivated land that is normally under irrigation.

Water levels recover slowly when the wells are shut off. Maximum recovery is on the order of 30 m, leaving the present static level 100 m or more below the bottom of the wells that existed 40 years ago.

Yields have declined in spite of the deepening of the wells. As an example, one well that 24 years ago produced 35 l/s at 60 m now produces only 5 l/s at 200 m.

Macau (1960, p. 307) calculated that, as of 1960, the average rainfall was 700×10^6 m^3, and that approximately 150×10^6 m^3 of water was being pumped from aquifers in Gran Canaria. Recent data indicate a somewhat smaller annual rainfall (620×10^6 m^3/yr) and an

increased use of ground water (196×10^6 m³/yr). On the basis of these data, the use of ground water as related to precipitation has increased in 7 years from 23 percent to 32.5 percent (table 1). The latest figure is extremely high as the result of the large quantities of water being withdrawn from storage. These data may be used to make a crude approximation of average annual recharge. If in 1960 the discharge of 150×10^6 m³/yr was causing a decline of approximately 3.5 m/yr in the water table, and in 1967 the increase in discharge to 196×10^6 m³/yr caused a doubling of the rate of decline, then it follows that the water withdrawn from storage (Q_s) is twice the difference in discharge at these two dates. Thus:

$$\frac{(196\times10^6)-(150\times10^6)}{Qs}=\frac{3.5}{7.0},$$

Pumpage from storage $=92\times10^6$ m³/yr $=2.9$ m³/s,

Recharge $=104\times10^6$ m³/yr $=3.3$ m³/s,

Total pumpage $=196\times10^6$ m³/yr $=6.2$ m³/s.

This is obviously an approximation, but a rate of recharge in Gran Canaria of approximately 3 m³/s seems to agree with most of the available data. Groundwater use of 196×10^6 m³/yr is approximately 6 m³/s, so approximately 3 m³/s is being withdrawn from storage.

METHODS OF DEVELOPMENT

The preferred method of ground-water development varies from one island to another. As indicated in table 3, most of the ground water used in Gran Canaria is obtained from wells, whereas in Tenerife the gallery is the preferred method of development.

Wells

The wells in the island are all, or almost all, hand dug. The deepest of these wells is 318 m but many are between 150 and 200 m. The wells are typically 3 m in diameter and are rock-and-cement cribbed for the first few meters of their depth. Below the cribbing the wells are open shafts in the rock. At or near the bottom of the well there are usually a number of radiating galleries that roughly conform to the surface area of land owned by the man for whom the well was dug (fig. 2). At least in theory the galleries do not extend under the property of the neighbor. In fact, however, there is good reason to believe that many galleries have been dug to deliberately cross property lines and pass near a neighbor's well to steal his water. Needless to say visitors, official or not, are not welcome at wells of this type. On some occasions officials of Obras Publicas have needed police escort to visit wells and obtain data. How common is the practice of deliberately stealing water is very difficult to determine, but it certainly is not rare. During 1968 many wells on Gran Canaria were inspected by officials of Obras Publicas, and a number of illegal radial galleries and drains were cemented shut.

In addition to the galleries, vertical holes, 3 to 4 inches (7.5 to 10 cm) in diameter, are drilled downward for 20–30 m below the bottom of many wells.

Extraction of water was formerly by means of piston pumps. The most common method now is a diesel-electric generating system at the surface with a turbine or submersible electric-motor-driven pump down in the well.

Water is obtained either from the zones of weathering between lava flows or from rock fractures. A number of wells were reportedly dry for their total depth and obtained water only after one or more of the horizontal galleries intercepted a dike of intrusive rock. The existence of such impermeable vertical barriers causes one to suspect that horizontal water movement is restricted, and for this reason, submarine discharge of ground water may be small.

Pumping levels vary from one locality to another but in Gran Canaria probably average 150 m. The cost of digging a well is approximately 3,000 pesetas (US $50) per meter at shallow depths and increases to 4,000 pesetas (US $67) per meter at depths of over 200 m. The cost of the horizontal galleries at the bottom of the well is approximately 3,000 pesetas per meter.

Galleries

Galleries are commonly used in Tenerife, Gran Canaria, and La Palma to develop ground-water supplies. These galleries are approximately horizontal, usually with a slight upward slope away from the gallery mouth. Average length of the galleries in Tenerife, where they are most successful, is 2,000 m, but a few are 4,000 m or longer. The galleries are roughly symmetrical and are about 1.5 m wide by 1.5 to 2 m high. Usually only the entrance is lined with concrete; the rest of the gallery is open with exposed rock surfaces. In a few galleries water is obtained by infiltration from a number of permeable zones, but this unusual. In a typical gallery (fig. 3) the work progresses in dry rock until a vertical dike is encountered. When the dike is drilled, water rushes forth with very high pressure, sometimes as high as 12 atmospheres. This may not be the maximum as in some places it has been impossible to measure the pressure. In several instances dikes have ruptured, and the resulting rush of water has killed the workers in the gallery.

The authors visited one of these galleries near Igueste, Tenerife. This gallery was excavated in dry rock for 2,000 m to a point where the gallery penetrated

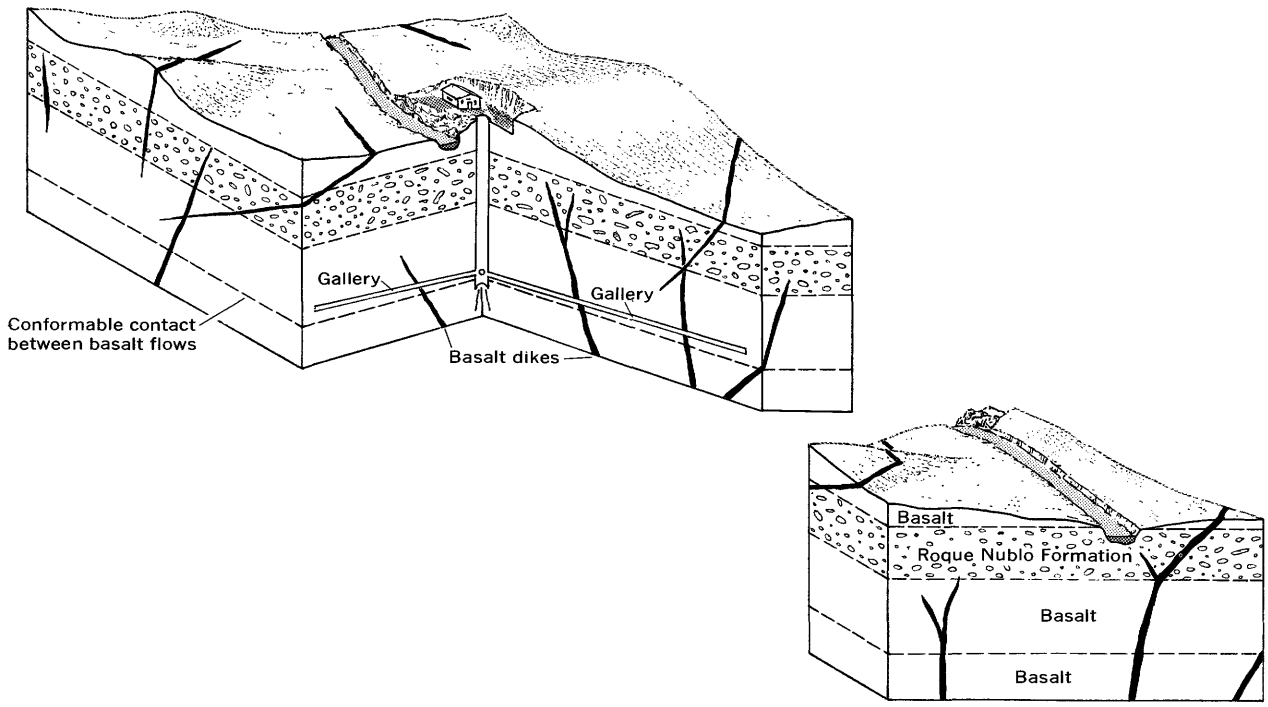

FIGURE 2.—Block diagram showing typical well on Gran Canaria.

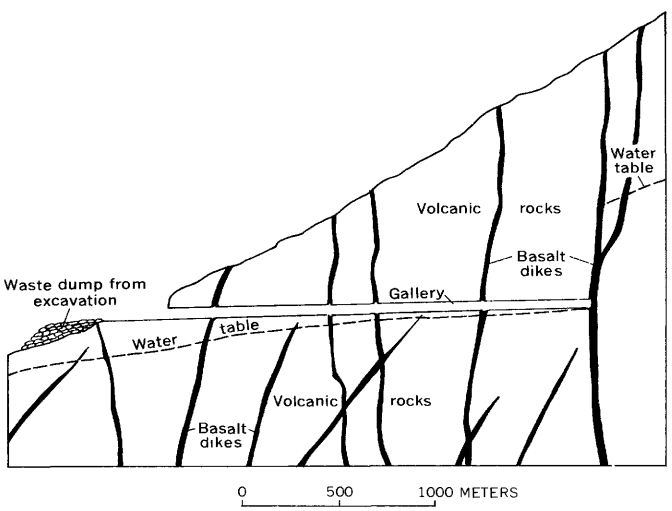

FIGURE 3.—Sketch of typical gallery. Gallery height exaggerated.

a dike. A small flow was obtained at the dike but rapidly declined as the saturated rock was drained. At 2,190 m a near-vertical dike was reached and water spurted out under high pressure when the dike was drilled. When the authors examined this gallery 4 years after its completion, it was completely dry up to the last mentioned dike. There, jets of water spurted out of several holes drilled through the dike and made up the entire flow. At the time of observation the flow from this gallery was 61 l/s. Maximum flow obtained from a gallery in Tenerife was reported to be approximately 160 l/s.

The hydrologic conditions observed and reported in these galleries led to the previous comment regarding the existence of vertical hydraulic gradients and the limitation of horizontal flow. With a pressure of 12 atmospheres, a change in pressure equal to approximately 100 m of water exists across the dike. Truly impermeable beds are seldom found in nature, but it would appear that the dikes of Tenerife approach this classification.

The relative impermeability of the basaltic dikes also leads to the conclusion that there has been so little tectonic movement since intrusion by the dikes that fractures are very widely spaced and faults are almost nonexistent.

The dikes in Gran Canaria would seem to be slightly more permeable. This may be an indication of greater tectonic activity as evidenced by the well-developed fracture systems and the fairly common faulting.

The cost of excavating horizontal galleries is reported to be 2,000 pesetas (US$33) per meter, with the equivalent of an additional 500 pesetas of services, air compressor, and so forth being furnished by the owner.

WATER LAW

In broad terms, ground-water law in the Canary Islands is based on private ownership of the water

beneath the land. The landowner has the right to develop and use the water beneath his land. However, he must apply for permission to dig a well or construct a gallery. In theory there is no legal way to refuse to grant permission. In practice, if it appears that the new construction may damage the yield of a neighbor's well, the applicant may be required to post a bond guaranteeing that the yield of the neighbor's well will not decrease. In some cases the amount of the bond is so high as to virtually prohibit well construction. On an island such as Gran Canaria, where the water table is declining rapidly, it is obviously impossible to guarantee a neighbor's well. The well is likely to go dry whether or not any new wells are constructed. In some instances, bonds have been posted and the guaranteed wells have gone dry, but the bonds have not been paid to the injured party.

One result of a water management study might well be the recommendation for a change in the water rights law.

REFERENCES

Hausen, Hans, 1958, On the geology of Fuerteventura (Canary Islands): Soc. Sci. Fennica (Helsinki), Commentationes Physico-Mathematicae, v. 22, no. 1, p. 1–211.

——— 1961, Canarian calderas—a short review based on personal impressions, 1947–1957: Suomen Géol Seura (Geol. Soc. Finland, Helsinki), Bull. 196, p. 179–211.

——— 1962, New contributions to the geology of Grand Canary: Soc. Sci. Fennica (Helsinki), Commentationes Physico-Mathematicae, v. 27, no. 1, p. 1–418.

Macau Vilar, Federico, 1957, Los tubos volcánicos originarios de manantiales, *in* Volcanología del Cenozoico, Sec. 1: Internat. Geol. Cong., 20th, Mexico 1956, Trabajos, p. 425–437.

——— 1959, Las calderas de Gran Canaria: Anuario de Estudios Atlanticos, Madrid-Las Palmas, no. 5, 47 p.

——— 1963, Sobre el origen y edad de las Islas Canarias—El Archipiélago equivalente: Anuario de Estudios Atlanticos, Madrid-Las Palmas, no. 9, 52 p.

Von Buch, Leopold, 1825, Physikalische beschreibung de Canarischen Inseln: Royal Acad. Sci., Berlin (with atlas). 427 p.

FLOW-THROUGH SAMPLING SYSTEM FOR SMALL BOATS OR ICE SHELTER

By JOHN F. FICKE and ROBERT G. LIPSCOMB,
Washington, D.C., Fort Wayne, Ind.

Abstract.—A simple pumping sampler and flow-through system have been assembled for making rapid nonrecording temperature, conductance, dissolved-oxygen, and pH measurements on lakes. The set of observations at a point can be completed in about 3 minutes. Measurements to a depth of 30 meters can be made from a small boat or a portable ice shelter. Tests show that the pumping system does not affect the concentration of dissolved gases in the water.

Pumping-type sampling systems have been used for several years to collect water samples for chemical and biological analyses. They are able to remove large volumes of water with minimal effort and adapt well to flow-through analysis systems. Pumping samplers often have been avoided because of the bulk and weight of sampler and hose, the need for a power supply, the time required to flush the hose system, the possibility of disturbing dissolved gases in the sample, and the uncertainty of intake geometry.

The pumping-sampler and flow-through system described here was assembled to make frequent and rapid nonrecording measurements of temperature, conductance, dissolved oxygen, pH, and alkalinity at different depths in several verticals in a small lake. It works equally well either in a small boat or in a portable ice shelter, and offers the advantages of nominal cost, lightweight, rapid flushing, and little loss of accuracy.

Pictured in figures 1 and 2, the pumping assembly consists of a 12-volt submersible pump (Little giant Corp., Model V–12), powered by wet-cell automotive batteries, pumping through rubber hose mounted on an ordinary garden-hose reel. The dissolved-oxygen analyzer (Jarrell Ash Co., Model 26–601) electrode and conductivity cell are mounted against the boat gunwale. After passing through the cell chambers, water can be directed overboard or routed through a simple bath, in which buffer solutions and titrants can be kept

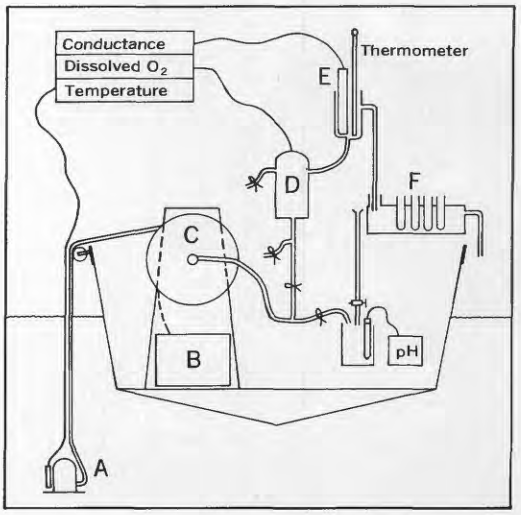

FIGURE 1.—Sampling pump and flow-through assembly mounted in a small boat. *A*, 12-volt submersible pump; *B*, wet-cell automotive batteries; *C*, garden-hose reel; *D*, dissolved-oxygen analyzer electrode; *E*, conductivity cell; *F*, temperature bath.

FIGURE 2.—A fiberglass shelter houses equipment for winter operation. *A*, 12-volt submersible pump; *B*, wet-cell automotive batteries; *C*, garden-hose reel; *F*, temperature bath.

near the sample temperature. Several taps are provided in the system so that samples for biological or chemical analysis may be withdrawn, or part of the system can be bypassed, drained, or flushed. Normally, samples are withdrawn for pH measurement and alkalinity titration. Electrodes to measure pH can be mounted in the flow system, but all flow past the electrodes must be stopped to eliminate streaming potential when pH readings are made.

With 30 meters of electrical wire (AWG 18, 2-conductor) there is about a 3-volt line loss between the batteries and the pump. To compensate for the loss, a 12-volt and a 6-volt automotive battery are connected in series. A 2-ohm rheostat reduces the potential to 15 volts. As the batteries discharge, the resistance of the rheostat is decreased to maintain a steady pumping rate of about 6 liters per minute. Under good conditions it has been found that about 3 minutes is required per observation, including flushing, taking instrument readings of temperature, pH, conductance, and dissolved oxygen, and making a simple titration of bicarbonate alkalinity (Rainwater and Thatcher, 1960, p. 93–95). More accurate two-buffer measurements of alkalinity (Barnes, 1964) require considerably more time, especially if time is allowed for the buffers to come to sample temperature.

A series of simple comparative tests was made to determine the effects of the pump and the flow system on the concentration of dissolved gases. Concentration of dissolved oxygen, as determined by the modified Winkler method (Rainwater and Thatcher, 1960, p. 233–236) was determined for samples drawn from one of the outlets of the flow system. At the same time, dissolved oxygen was determined on samples captured by a Kemerrer-type sampler from the same depth as the pump. Some sample pairs of data are listed in table 1. The tests of the pumping system seem to confirm that the concentration of dissolved gases, when not supersaturated, are unchanged by passage through the centrifugal pump and by flow through the system.

TABLE 1.—*Dissolved-oxygen concentration, in milligrams per liter, of sample pairs*

Pumped samples	*Captured samples*
8.4	8.4
7.7	7.5
6.8	6.8
4.3	4.4
0.2	.1
0	0

Hypolimnetic waters may be warmed as much as 2°C as they pass through the zone of warmer water and then through the coil of black hose on the boat deck. Accuracy of data is assured by measuring temperature near the pump intake with a thermistor for comparison with the temperature of water at the flow cells. With the particular instruments shown (figs. 1 and 2), this check is provided by the temperature-measuring feature of the dissolved-oxygen analyzer. A large, tractor umbrella will provide shade to reduce the

effect of radiant heating of the sample, buffers, pH electrodes, and instruments.

For winter operation the equipment is mounted inside a 3- × 6-foot (0.9- × 1.8-meter) portable shelter (fig. 2) made of translucent fiberglass attached to a wood frame. The shelter, which is disassembled into panels for transportation or summer storage, must be equipped with outriggers to prevent its being turned over by high winds. Sunlight through the walls provides light and heat, but an alcohol heater is used to keep the temperature above freezing on dark or extremely cold days. The shelter is light enough for two men to move by hand, although a towing vehicle of the type shown in figure 2 is needed to move it great distances.

REFERENCES

Barnes, Ivan, 1964, Field measurement of alkalinity and pH: U.S. Geol. Survey Water-Supply Paper 1535–H, 17 p.

Rainwater, F. H., and Thatcher, L. L., 1960, Methods for collection and analysis of water samples: U.S. Geol. Survey Water-Supply Paper 1454, 301 p.

SIMPLIFIED PUMPING SAMPLER FOR SUSPENDED SEDIMENT

By BENJAMIN L. JONES, Sacramento, Calif.

Work done in cooperation with the California Department of Water Resources

Abstract.—A simplified pumping sampler was developed for the collection of suspended-sediment samples from streams. The sampler has a capacity of 20 containers, and the interval between samples can be varied from 2 minutes to several hundred hours. The sampler consists of a pump, electronic controls, and a bottling mechanism. The low initial cost, small size, and ease of installation of the device make it suitable for incorporation into present data-collection programs.

Samples of suspended sediment are difficult and expensive to obtain. During high-flow periods, suspended-sediment concentration changes rapidly with discharge, and unless an observer or field engineer is present to obtain frequent samples it is impossible to define the concentration graph. Technical personnel generally are not available to collect the needed samples at all stations during a flood period, and it is a rare observer who will sample around the clock.

Some form of remote monitoring device eventually will be developed to complement conventional sampling methods, but this system is still several years away. Even when developed, such a system may be too expensive for immediate incorporation into most data-collection programs. Several pumping samplers have been developed (U.S. Inter-Agency Committee on Water Resources, Subcommittee on Sedimentation, 1962), but manufacturing and installation costs preclude their use except in special applications.

A simplified pumping sampler, developed by Mr. William G. Shope, Jr., and the author, is suitable for immediate use in most data-collection programs. The hydraulic system in this sampler is similar to that in previous pumping samplers, but the mechanism offers several advantages in cost, size, and ease of installation. Capacity of the sampler is twenty 1-pint glass milk bottles in a case or twenty 1-liter polyethylene bottles without a case.

The sampler is powered by a 12-volt battery. Where line power is available, it is used to recharge the batteries.

DESCRIPTION OF MECHANISM AND ELECTRONIC CONTROLS

The simplified pumping sampler is basically a rotary distribution system for bottling a sample of water-sediment mixture pumped from a point in a stream. An offset funnel, in the center of the sampler (fig. 1), is positioned by a cam and motor combination so that a one-bottle sample is obtained during each sampling cycle. The sample is collected by diverting water through the splitter mechanism into the offset funnel and through a tube into the sample bottle. Sample size is governed by the timing of the splitter cycle.

A screw-type positive-displacement pump is normally used to lift water from the stream to the sampler unit. This pump will lift to heads greater than 100 feet and will pump moderate quantities of sand-size materials without significant damage. A small centrifugal pump may be used for small quantities of sand and for heads of less than 30 feet. External contacts control the pump motor, so either 12-volt direct current or 115-volt line current can be used.

The electronic control consists of two parts: (1) A timer clock which determines the interval between samples, and (2) motor-driven cam switches which control the various operations in the sampling cycle. A standard digital-recorder timer is used where a sampling interval of 1 hour or less is desired. A clock from a circular-chart recorder with cycle times from 1 to 30 days is used to provide longer sampling intervals. The shaft on the clock is fitted with cams to operate miniature switches at the desired time intervals. Almost any sampling frequency can be provided from 2 minutes to

U.S. GEOL. SURVEY PROF. PAPER 650–C, PAGES C212–C214

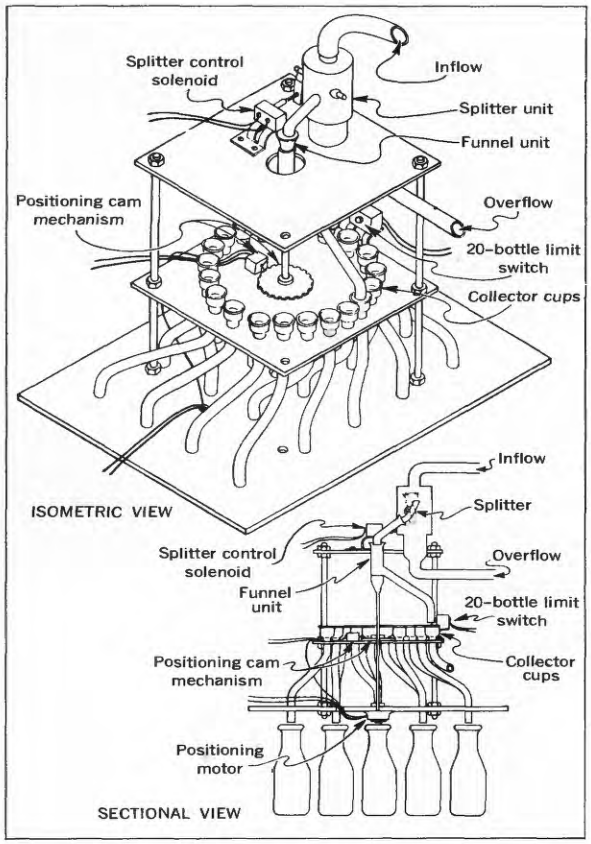

FIGURE 1.—The 20-bottle pumping sampler.

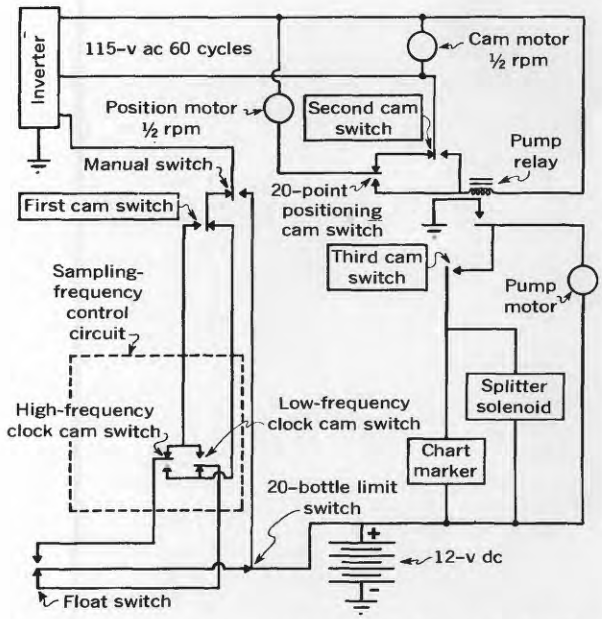

Notes: 1. Sampling frequency is controlled by an electrically wound circular chart clock with two timing cams attached to the drive shaft.
2. The switch for manual operation is a single-pole, double-throw, spring-return switch wired as shown.

FIGURE 2.—Schematic diagram of electronic controls.

several hundred hours. A water-level switch can provide several sampling frequencies at a single installation. In the schematic diagram of the control system presented in figure 2, a two-frequency system is shown.

Upon receiving an impulse from the timer, motor-driven cams in the control unit open and close a series of three switches (fig. 2). All cams are adjustable for both length of time of each function and timing of one function in relation to the others. Each cam switch operates a circuit that performs a part of the sampling cycle. The first cam switch provides a cutoff at the end of the cycle. A new cycle is initiated only when another impulse is received from the timer. The second cam switch controls the pump motor and positions the funnel unit. The third cam switch activates the splitter, diverting flow to the sample container, and at the same time operates a time marker on the water-stage recorder. A limit switch (fig. 1) deactivates the entire system after the 20th bottle is filled.

INSTALLATION AND OPERATION OF SAMPLER

The sampler and its shelter form a compact unit about 18 × 20 × 48 inches in size. In its shelter, as shown in figure 3, the sampler is virtually self-contained. A ½-inch plastic pipe carries water from the stream, and a 1-inch plastic pipe returns waste water. The only external electrical components are the water-level switch and the chart marker.

In operation, the device begins sampling when a rising water level reaches a preset stage; it continues sampling at selected intervals until the water level recedes below the sampling stage, or until all the bottles are filled.

The engineer services the sampler by removing and capping the bottles and recording the date and time the samples were removed from the sampler unit. A case of empty bottles is numbered in sampling order and inserted in the sampler, and the date and time of installation are recorded on the first bottle. The sampler is reset by manually rotating the funnel just past the 20-bottle limit switch and closing the switch. A manual switch is provided so that a pumped sample may be obtained for comparison with a simultaneous sample collected by conventional methods.

PRESENT STATE OF USE AND DEVELOPMENT

Prototypes of the simplified sampler are now in use in the California, Pennsylvania, and Maryland districts of the Water Resources Division of the U.S. Geological Survey. Recently, samplers constructed of plastic sheet and tubing have been built for use in Hawaii and California districts.

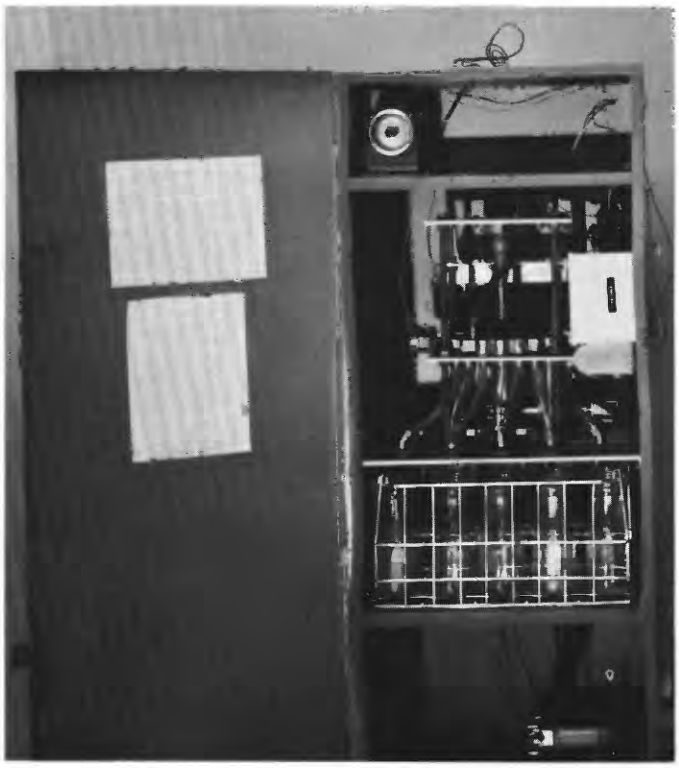

FIGURE 3.—Simplified pumping sampler mounted in shelter.

A modification of the sampler, with a capacity of 48 sample containers, has been built by the Federal Inter-Agency Sedimentation Laboratory for testing by the U.S. Forest Service. The 48-sample model probably will be the production prototype.

CONCLUSIONS

A simplified pumping sampler can serve as a valuable supplement to conventional sampling programs. The ease of construction and installation and the relatively low cost make the sampler a device which can be included in most data-collection programs. Although primarily designed to collect samples for determination of suspended-sediment concentration, the sampler also can be used to collect samples for determination of other water-quality parameters.

Use of the automatic sampler makes the data-collection program more compatible with the present trend toward automation of record processing. The frequent sampling possible with the device virtually eliminates the need for estimating or supplying synthetic values for computer operations.

REFERENCE

U.S. Inter-Agency Committee on Water Resources, Subcommittee on Sedimentation, 1962, Investigation of a pumping sampler with alternate suspended-sediment handling systems, Progress Rept. Q *of* A study of methods used in measurement and analysis of sediment loads in streams: Federal Inter-Agency Sedimentation Proj., Minneapolis, Minn., St. Anthony Falls Hydraulic Lab., 90 p.

CARBON-14 DATES OF GROUND WATER FROM A PALEOZOIC CARBONATE AQUIFER, SOUTH-CENTRAL NEVADA

By D. B. GROVE,[1] MEYER RUBIN,[2] B. B. HANSHAW,[2] and W. A. BEETEM,[1]
[1] Denver, Colo., [2] Washington, D.C.

Work done in cooperation with the U.S. Atomic Energy Commission

Abstract.—Radiocarbon determinations were used to estimate the ages of ground water from the Paleozoic aquifer underlying the Nevada Test Site and adjacent areas. A generally good correlation exists between the carbon-14 dates and the current hydraulic interpretations; but the aquifer is heterogeneous and is insufficiently defined to permit detailed predictions of ground-water velocities or flow patterns.

Hydraulic properties of the major ground-water system at the U.S. Atomic Energy Commission's Nevada Test Site have been difficult to measure because of the fractured carbonate rocks, quartzite, and shale through which the ground-water moves and the great depth to this aquifer. Recent successes in interpreting ground-water movement through the use of carbon-14 (Hanshaw and others, 1965; Pearson and White, 1967) prompted a similar study for this area.

GEOLOGIC SETTING

The Nevada Test Site lies in the Great Basin section of the Basin and Range physiographic province. The site consists of three major valleys: Yucca Flat to the north, Frenchman Flat to the south, and Jackass Flats to the southwest. Hills and ridges of moderate relief border these valleys. Carbonate rocks, quartzite, and shale of Paleozoic age, having a composite thickness of 37,000 feet, underlie the entire area. Tertiary rocks underlying the valleys consist mainly of ash flow and ash fall; this sequence of rocks, described as welded to semiwelded tuffs, overlies the Paleozoic carbonate rocks and is as much as 2,000 feet thick. A heterogeneous mixture of detritus derived from the adjacent bedrock area makes up the valley fill. The depth of this fill of Quaternary age may be as much as 2,000 feet in the central valleys (Johnson and Hibbard, 1957).

The Nevada Test Site and area adjacent to the site make up part of the Ash Meadow ground-water basin. This basin consists of parts of at least 10 valleys which are hydraulically connected at depth by highly permeable, fractured carbonate rocks. Winograd (1962) postulated that ground water in the valley fill and the tuffs beneath the bolsons of the Nevada Test Site moves vertically downward into and laterally through the Paleozoic carbonate rocks. He also postulated an underflow through the consolidated rocks flanking and underlying the valley fill. Potentiometric levels, measured in test holes drilled in 1962–65, supported this hypothesis of interbasin movement of ground water. The discharge from the Nevada Test Site valleys is to the south and west along a fault-controlled spring line in the Amargosa Desert.

Figure 1 is a map of the Nevada Test Site and adjacent areas. This map shows the locations of some of the major features of the area. These features include major springs in the Amargosa Desert, wells and springs sampled for this study, important valleys, and some of the higher mountain ranges.

SAMPLING SITES

Sampling sites were chosen in areas of known recharge to the aquifer, areas of lateral flow in the aquifer, and areas of known discharge from the aquifer. Cold Creek Spring, high on the Spring Mountains, is the base reference, as it produces water of recent origin not more than a few hundred years old. Point of Rocks Springs (King Springs) and Fairbanks Springs in the Amargosa Desert are two in the network of fault-controlled springs in the principal discharge area deriving their water from the complexly fractured

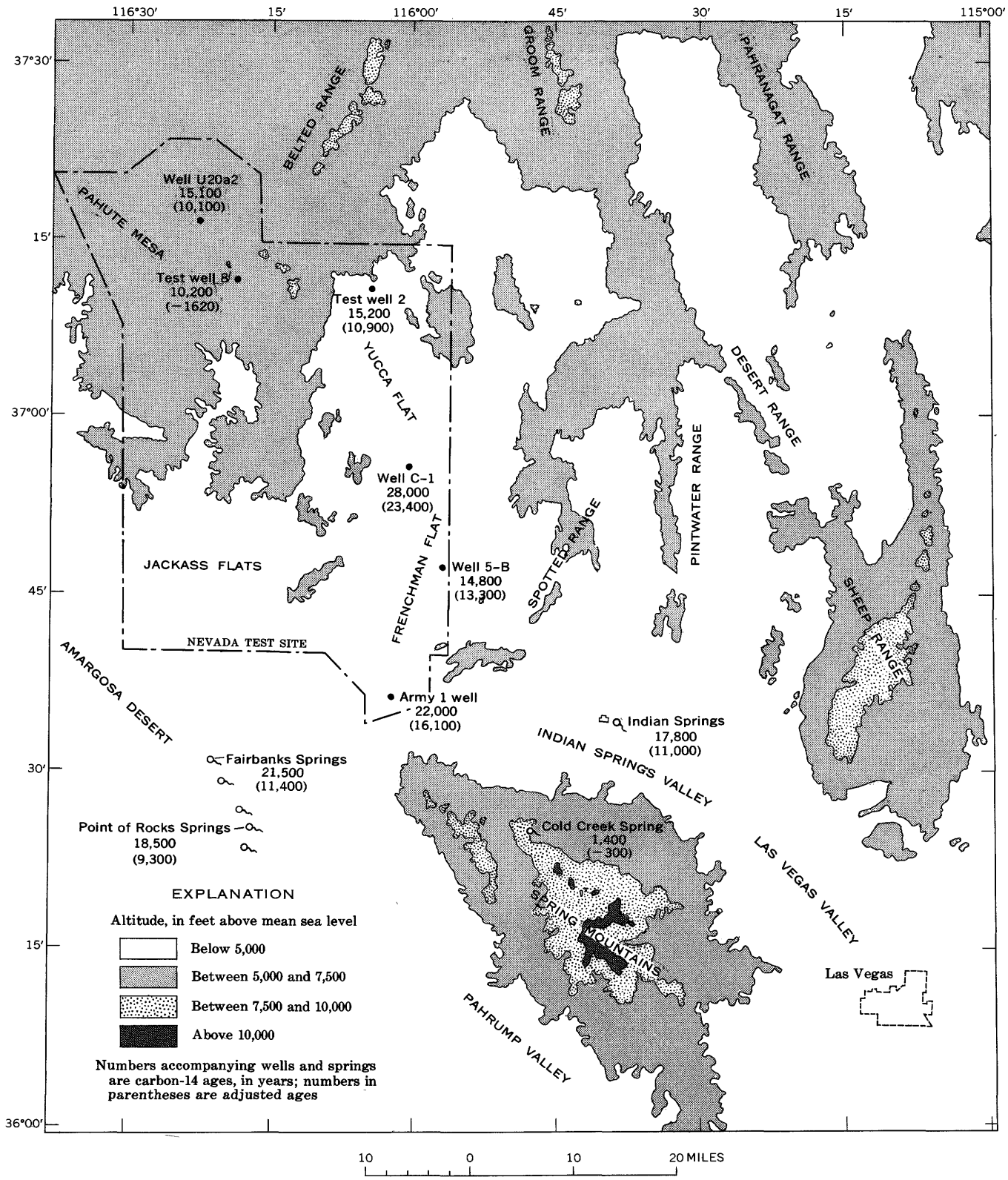

FIGURE 1.—Locations of wells and springs sampled for age determinations of water, and topographic features contributing to the hydrology of the Nevada Test Site and adjacent area, Nye County, Nev.

Paleozoic rocks, the principal aquifer in the region. Indian Springs in Indian Springs Valley, which is between the recharge area and the principal discharge area, discharges water at a constant rate and temperature regardless of season. Test well 2, well C–1, and Army 1 well on the Nevada Test Site supply water from the fractured carbonate rocks of Paleozoic age. Although well 5–B taps valley-fill deposits and cannot be regarded as a point in the flow net, it supports the use of carbon-14 to determine ground-water ages; the lakes that contributed this water probably existed 12,000 to 20,000 years ago. The surface water disappeared long ago; part of the water evaporated and part drained downward to the present depth (Johnson and Hibbard, 1957). Test well 8 and well U20–a2 are in upland areas above the valley floor and tap Tertiary volcanic rocks; they were not used in interpretation of ground-water flow patterns.

Whereas part of the Amargosa Desert is a known discharge area, the location of principal recharge areas and the amount contributed by these areas can only be estimated. Using geologic, geochemical, and hydraulic data, I. J. Winograd (written commun., 1968) has estimated flow patterns for these areas. The ground-water age data are correlated with Winograd's estimates.

METHODS AND DATA

Water samples were collected from each of the areas and transported to a field laboratory where the bicarbonate ion was precipitated as strontium carbonate. After filtering and drying, the strontium carbonate precipitates were shipped to the U.S. Geological Survey's radiocarbon laboratory in Washington, D.C., for determination of carbon-14 content. Irving G. Friedman, of the Survey's isotopic laboratory in Denver, Colo., determined carbon-13 content of the water samples. To calculate adjusted ages of the water samples, the authors applied carbon-13 data (Ingerson and Pearson, 1964) to the apparent ages calculated from the carbon-14 data. This adjustment takes into account the "dead" carbon dissolved by the water during its contact with carbonate-containing rock. Table 1 lists unadjusted and adjusted ground-water ages calculated by these methods, and bicarbonate content of the sampled water.

The equation used for the adjustment (after Pearson and White, 1967) is

$$C^{14}(‰ \text{ mod., adjusted}) = \frac{\delta C^{13}_{soil} - \delta C^{13}_{ls}}{\delta C^{13}_{water} - \delta C^{13}_{ls}} \times C^{14} (‰ \text{ mod. lab.})$$

where $C^{14}(‰$ mod., adjusted) is the new adjusted value of carbon-14 as referred to the NBS contemporary standard. δC^{13}_{soil} is the initial ratio of carbon-13 to carbon-12 in the soil during the introduction of the water, expressed in parts per thousand (‰) in relation to a particular standard and was assumed to be −25‰ for the adjustments calculated here. The δC^{13}_{ls} is the deviation from a standard of the carbon-13 content in the limestone or aquifer matrix and was assumed to be zero. The δC^{13}_{water} and $\delta C^{14}(‰$ mod. lab.) were the laboratory values determined for carbon-13 content and carbon-14 content, respectively

DISCUSSION AND CONCLUSIONS

The use of δC^{13}_{soil} equal to −25‰ for all adjusted values may not be valid. Sparsely vegetated recharge areas in semi-arid regions such as south-central Nevada may not contain the soil environment to produce initial δC^{13} values of −25‰. Test well 8 would be suspect, as an increase in δC^{13} from −25‰ to −5.76‰ is unlikely for this particular area.

Ground-water ages at the selected sampling locations correlate well with the estimated flow patterns for the area. Cold Creek Spring, in a recharge area high up in the Spring Mountains, produces water of a young age. The flow of water from Indian Springs is uniform with

TABLE 1.—*Carbon-14 age data of water at selected wells and springs, Nevada Test Site, Nevada*

Well or spring	Laboratory No.	δC^{14} (‰)	Unadjusted age (yrs)	δC^{13} (‰ relative to PDB standard)	Adjusted age (yrs)	Bicarbonate (mg/l)
Cold Creek Spring	W–1854	−164	1,400	−20.14	[1] −300	282
Indian Springs	W–1841	−890	17,800	−10.96	11,000	239
Point of Rocks Springs (King Springs)	W–1836	−900	18,500	−7.93	9,300	308
Fairbanks Spring	W–1858	−931	21,500	−7.19	11,400	304
Test well 2	W–1843	−850	15,200	−14.52	10,900	190
Well C–1	W–1849	−970	28,000	−13.84	23,400	576
Army 1 well	W–1838	−935	22,000	−11.99	16,100	256
Well 5–B	W–1852	−840	14,800	−20.89	13,300	178
Test well 8	W–1860	−718	10,200	−5.76	[1] −1,600	78
Well U20–a2	W–1861	−847	15,100	−13.47	10,100	108

[1] These ages are after present, a result of adjusted δC^{14} values being greater than contemporary.

respect to discharge and temperature and unaffected by seasonal variation in precipitation. This capacity of the spring to damp out cyclic input changes may be due to a large volume of water in storage or the lateral flow of water of such volumes from a long distance. The older age of this water supports this line of reasoning. Ground water probably moves very slowly through Yucca Flat, Frenchman Flat, and Jackass Flats before discharging at the springs in the Amargosa Desert. Ground-water velocity calculated from relative carbon-14 ages is about 7 feet per year between test well 2 at the north end of Yucca Flat and well C–1 at the south end. Water from well C–1 is the oldest in this study.

A good correlation of the data for test well 2 and well C–1 is not possible without additional data. In the Yucca Flat area, the water drains downward through the Quaternary and Tertiary rocks and tends to dilute the water in the Paleozoic carbonate rocks with water of a different age. The amount and the age of this entering water must be known before water from test well 2 and well C–1 can be accurately compared. Downward drainage occurs elsewhere in the system but only beneath Yucca Flat is the leakage likely to be a significant fraction of the total volume of water moving through the carbonate aquifer.

Some interesting conjectures can be drawn from the relative ages of the water from Indian Springs, Army 1 well, and the springs in the Amargosa Desert. Previous speculations assumed that most of the water issuing from the springs in the Amargosa Desert comes from the northwestern part of the Spring Mountains. Recent studies by I. J. Winograd (written commun., 1968) suggest that ground water from southern Indian Springs Valley (including that sampled from Army 1 well and Indian Springs) contributes only a fraction of the discharge of the springs in the Amargosa Desert. Extensive geochemical, geologic, and hydraulic interpretive studies support this suggestion by Winograd. The radiocarbon ages of water from Army 1 well and Indian Springs also support this thesis, as these ages are older than those of the water from the springs in the Amargosa Desert. This is not considered feasible if they were in the flow net which contributed a significant amount of water to the discharge of the springs in the Amargosa Desert.

Adjusted ages obtained by applying carbon-13 data to the carbon-14 ages of water indicate no significant changes in the flow pattern. The adjusted ages of water from Cold Creek Spring, Indian Springs, and all the wells on the Nevada Test Site correlate well with their assumed ages. However, adjusted ages for the water of Fairbanks Springs and Point of Rocks Springs are somewhat younger than expected. Although no adequate explanation is presently available for this anomaly, it may be due to the erroneous use of $-25^{o}/_{oo}$ for δC^{13}_{soil} in making the age adjustment.

This preliminary study indicates that radiocarbon age dating of water can be used to corroborate existing hydrologic views held for Nevada Test Site and adjacent areas, and with more detailed information possibly to predict flow patterns of ground-water movement. However, the large area studied and the complex hydrologic and geologic setting preclude its use to construct adequate flow nets for the area or to calculate ground-water velocities.

REFERENCES

Hanshaw, B. B., Back, William, and Rubin, Meyer, 1965, Radiocarbon determinations for estimating ground-water flow velocities in central Florida: Science, v. 148, no. 3669, p. 494–495.

Ingerson, Earl, and Pearson, F. J., Jr., 1964, Estimation of age and rate of motion of ground-water by the ^{14}C-method, *in* Recent researches in the fields of hydrosphere, atmosphere and nuclear geochemistry: Sugawara Festival Volume, Maruzen Co., Ltd., Tokyo, Japan, p. 263–283.

Johnson, M. S., and Hibbard, D. E., 1957, Geology of the Atomic Energy Commission Nevada proving grounds area, Nevada: U.S. Geol. Survey Bull. 1021–K, p. 333–384.

Pearson, F. J., Jr., and White, D. E., 1967, Carbon-14 ages and flow rates of water in Carrizo sand, Atascosa County, Texas: Water Resources Research, v. 3, no. 1, p. 251–261.

Winograd, I. J., 1962, Interbasin movement of ground water at the Nevada Test Site, Nevada: Art. 104 *in* U.S. Geol. Survey Prof. Paper 450–C, p. C108–C111.

THE INFILTRATION OF ALDRIN THROUGH OTTAWA SAND COLUMNS

By JOHN B. ROBERTSON and LLOYD KAHN,[1] Idaho Falls, Idaho

Abstract.—The penetrability of chlorinated hydrocarbon insecticides through soils is dependent upon the type of formulation applied, frequency of its application, soil conditions, and the frequency and rate of rainfall or irrigation. Aldrin, a representative member of the chlorinated hydrocarbon insecticide group, was infiltrated through columns of Ottawa sand in four experiments. Results of the experiments indicate that: (1) Most of the eluted aldrin in organic solvent systems was eluted during the passage of the first liter of water. (2) The aldrin distributed itself in a characteristic manner through each column, depending upon the composition and stability of the emulsion and rate of water infiltration. (3) The concentration of HHDN (active ingredient in aldrin) in the effluent from the columns reached a "steady state" condition of 0.5 to 2 micrograms per liter of water. (4) A commercial emulsible concentrate mixture transmitted more aldrin to the effluent than did a synthetic solution containing no emulsifier.

Surveys of the nation's major river basins have shown that many streams are polluted by organic insecticides that are members of the chlorinated hydrocarbon group (Breidenbach and Lichtenberg, 1963; Weaver and others, 1965). In time this pollution could also extend into ground water. The fate of a pesticide in a groundwater environment is affected by the chemical and biological stability of the compound, its method of application to the soil, the abundance of soil organic matter, the solubility of the compound in water, and the sorptive properties of the environmental system.

This study was initiated to investigate the mechanics of movement of chlorinated hydrocarbons through soil. Aldrin was selected as the representative of the chlorinated hydrocarbon insecticide group, which also includes dieldrin, endrin, DDT, heptachlor, heptachlor epoxide, and BHC or lindane. This group of compounds is nonpolar, nonionic, and has a solubility of the order of micrograms per liter in water (Richardson and Miller, 1960; Robeck and others, 1965), and is widely used to combat agricultural insects. All the compounds, except aldrin and heptachlor, which are degraded in the soil to dieldrin and heptachlor epoxide, respectively, (Gannon and Bigger, 1958; Lichtenstein and Schulz, 1959a, 1959b, 1960, 1961) are chemically and biologically stable (Robeck and others, 1965).

The persistence in the soil and effectiveness as an insecticide of a given compound is influenced by its volatility and by soil type, soil temperature, soil moisture, rainfall or irrigation, microorganisms, application rates, and soil cultivation (Chisholm and Koblitsky, 1959; Lichtenstein and Schulz, 1961; Lichtenstein, 1965; Schechter and others, 1964; Wheatley and others, 1963). Aldrin and predominantly dieldrin, its metabolite, have been found to persist in soils for more than 10 years (Alexander, 1965).

This study evaluates the mass transfer of aldrin formulations through the simple system, Ottawa quartz sand. This is a relatively pure and uniform natural sand which is easily available and commonly used in studies of this type. Two aldrin formulations were used: (1) a commercial emulsible concentrate, and (2) a synthetic solution containing no emulsifier. In each of the four experiments, the quartz sand in columns was wetted with water before adding the emulsible concentrate. Water was then applied to simulate a total of 40 inches of rainfall—as constant drizzle, lasting between 11 and 23 days—in 3 of the experiments, and as cloudbursts, equivalent to 2 inches of rainfall each, occurring approximately 3 hours apart in the fourth experiment. In the third experiment, which was designed to reflect another field condition, the emulsible concentrate applied to a column was allowed to dry before the addition of water. The amount of insecticide applied to each column corresponded to a field application of 50 pounds of aldrin per acre, which is 5 to 10 times the normal amount used in agriculture.

The data are reported in terms of HHDN, 1,2,3,4,10,10 - hexachloro - 1,4,4a,5,8,8a - hexahydro - 1,4-endo-exo-5,8-dimethanonaphthalene, the active ingredient in aldrin. Aldrin in this report, is the technical grade product defined as containing 95 percent HHDN.

Acknowledgments.—The authors wish to express their appreciation to Shell Chemical Co. and to Woodbury

[1] Present address: of Lloyd Kahn Federal Water Pollution Control Administration. Edison, N.J.

Chemical Co. who supplied the HHDN reference standard and the commercial formulation, respectively. Mention of products and manufacturers is for identification only and does not imply endorsement by the U.S. Geological Survey.

EQUIPMENT AND SOLUTIONS

Sand columns

Four specially made Pyrex glass cylinders (fig. 1) were filled with 20–30 mesh Ottawa quartz sand to a height of 44 inches. The dry sand was added over a ¾-inch layer of 3-mm gravel with tapping until no more settling was observed. Each cylinder contained 29.2 pounds of sand and had a porosity of 36.6 percent. The sand columns were washed with distilled water and ethanol, and dried by air drawn through them.

Gas chromatograph

A Wilkens Aerograph Hi-Fy Model 610–D gas chromatograph equipped with an electron-capture detector was used with a 5-foot-long × ⅛-inch outside diameter Pyrex glass tube packed with 5 percent Dow 11 silicone grease and 0.5 percent Carbowax 20M on 60–80 mesh Gas Chrom Q. The tube was conditioned for 3 days at 250°C prior to use. The detector, tube, and injection-port temperatures were maintained at 180°C, 150°C, and 200°C, respectively, during the analyses, and a carrier gas-flow rate of 120 milliliters per minute of nitrogen was used.

Solutions

Formulation A. Commercial aldrin emulsible concentrate containing 21 percent (2 pounds per gallon) technical grade aldrin, 69 percent heavy aromatic naphtha, 7 percent Emcol H–83–A, and 0.5 percent epichlorohydrin. Emcol H–83–A is an emulsifier composed of a blend of polyoxyethylene ethers and oil-soluble sulfonates. The HHDN content of the concentrate was found to be 20 percent as determined by infrared analysis using analytical standard HHDN.

Suspension A. A 1-milliliter aliquot of formulation A was diluted to 100 ml with water. This solution thus contained 2.1 milligrams of aldrin per milliliter, or 2 mg of HHDN.

Suspension B. A 1-ml aliquot of a solution containing 20 grams of HHDN per 100 ml of xylene was dispersed in 100 ml of water. This solution thus contained 2 mg of HHDN per milliliter.

HHDN. Analytical standard grade of greater than 99 percent purity.

PROCEDURE

The variables in the four experiments are given in table 1. After the uniform addition of the suspension to the top surface of each sand column, the surface was

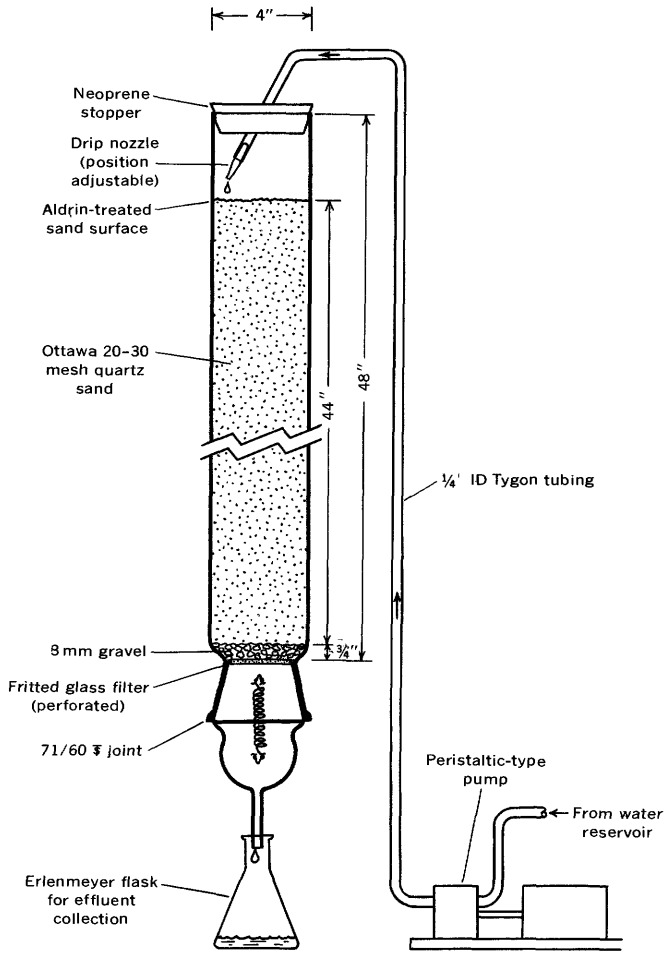

FIGURE 1.—Diagram of sand-packed column and pump setup for slow-drip infiltration studies.

covered with a 1-inch layer of ¼-inch-diameter gravel. The infiltrating water, pumped by a peristaltic-type pump, was dispersed onto the gravel layer by changing the position of the drip nozzle periodically. Effluent-water samples were collected in 100-ml fractions at the bottom of the column. The fractions were collected periodically throughout each experiment, but not continuously.

At the end of each experiment, consecutive horizontal layers of the column sand, ranging from 1 to 10 inches in thickness, were removed. The location and thickness of the individual layers in the columns are indicated in figure 2 by the horizontal brackets. Column 1 was segmented immediately at the end of the experiment, whereas the other columns were allowed to drain overnight to facilitate separation of the segments of the column. After segmentation, each layer of sand was extracted three times by agitation in acetone and the solvent extract analyzed for residual HHDN content.

Each water fraction was extracted three times with 25-ml quantities of hexane. The combined extracts were

TABLE 1.—*Variables in aldrin (HHDN) infiltration experiments*

[HHDN, 32.4 mg in each column; temperature range, 20°–26°C]

Variables	Column 1	Column 2	Column 3	Column 4
Suspension solution [1]	A	B	A	A
Water:				
Start of flow	Immediate	Immediate	After drying formulation	Immediate
Method of addition	Continuous	Continuous	Continuous	Intermittent [2]
Flowrate (average)—ml/min	12	13	24	
Timespan of addition—days	23	27	11	12
Effluent (total volume)—ml	6, 640	8, 368	6, 437	5, 935

[1] Refer to "Solutions" section in text.
[2] Individual 350-ml quantities were added; the first, immediately after application of suspension solution A, the others at approximately 3-hour intervals thereafter.

dehydrated with anhydrous sodium sulfate, concentrated in a Kuderna-Danish evaporative concentrator to volumes which contained 100 to 800 nanograms (10^{-9} grams) of aldrin per milliliter of solution, and analyzed by gas chromatography using the conditions described above.

RESULTS AND DISCUSSION

The distribution of HHDN in the sand columns at the end of the experiments is shown in figure 2. The sum totals of HHDN in all fractions (effluent and residuals in column) gave 110, 60, 65, and 68 percent recoveries of the HHDN for columns 1, 2, 3, and 4, respectively. The variation of the recoveries from 100 percent may be attributable to analytical errors to some degree, but most of it to losses from the top of the column by water-vapor (steam) distillation at the operating temperatures of 20°–26° C. This latter effect has been noted in natural systems by others (Bowman and others, 1965; Harris and Lichtenstein, 1961; Lichtenstein and others, 1962; Lichtenstein and Schulz, 1961; Richardson and Miller, 1960). The HHDN concentrations shown in figure 2 were, therefore, normalized to provide a complete accountability of the insecticide.

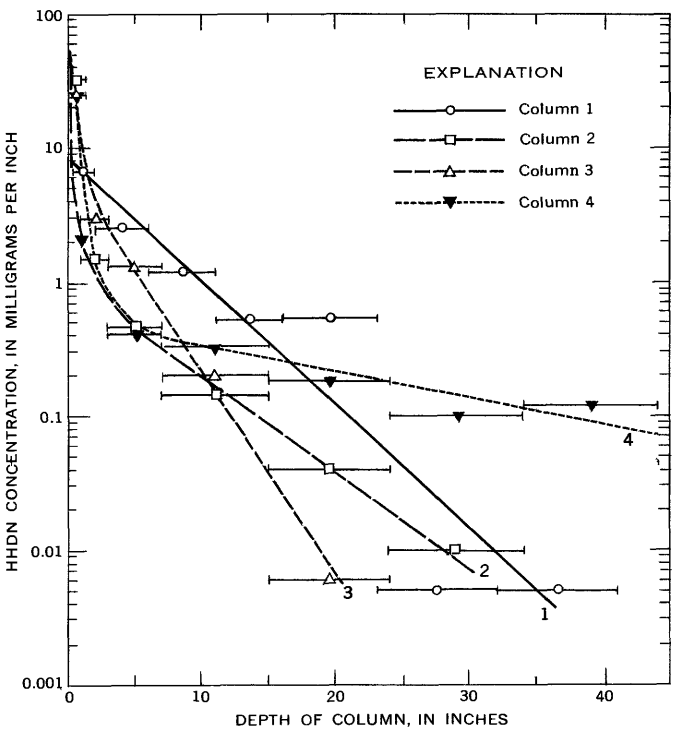

FIGURE 2.—Distribution of aldrin (HHDN) in the sand of the four columns. Brackets on data points indicate the part of the column sampled.

An examination of the "best-fit" curves drawn from the analytical data engenders the following interpretations: For column 1, in which a continuous water spray was started immediately after the commercial emulsion was applied, a linear relationship was obtained between the log of the HHDN concentration and its distribution through the column. This may be indicative of the relatively high stability of the formulation. However, curves of varying shapes characterized the distribution of HHDN in columns 2, 3, and 4. Each of these curves may be considered to consist of two straight-line segments in which (1) the upper segment probably reflects the displacement of the relatively "intact" emulsions through the upper layer of the columns, and (2) the lower segment reflects a phenomenon which may have been caused by the following factors, in sequence: 1. The addition of water to the formulation at the top of the column initiates a separation of the components of the emulsion. 2. Some of the more polar components migrate through the column at a greater rate than the insecticide and coat the sand particles with an organic layer which is characteristic of a particular formulation. 3. The nonpolar phase containing the insecticide moves down the column, and the insecticide is partitioned between the stationary organic coating on the sand and the mobile aqueous phase in a process which is analogous to liquid-liquid partition chromatography. The distribution coefficient, or the ratio of the amount of HHDN

which will partition into the organic coating on the sand to the amount remaining in the aqueous phase, is a function of the concentration and composition of the organic coating on the sand and the amount of HHDN in the aqueous phase.

The area under the upper segment of the curves may be considered to indicate the stability of the respective emulsions under similar experimental conditions. Thus, if one uses the mass transport of HHDN through the top 5 inches as the criterion, the stability of the emulsion apparently increases as one considers, in turn, columns 2, 3, and 1. The probable reason for the higher HHDN concentration found at the bottom of column 4 is that the heavy initial water addition prevents the separation of the aldrin emulsion to the same degree as in the other columns.

The concentration of HHDN in the effluent as a function of water flowing from the bottom of the columns is presented in figure 3. It is noteworthy that the HHDN composition reaches a virtually constant value (steady state) in each column after the passage of one to two liters of water. Despite the different conditions for each column, all the "steady-state" concentrations of HHDN in the effluents are approximately the same, and have values of 0.5 to 2 micrograms per liter. Because a "steady state" is reached during the passage of approximately 1 liter of water, it may be inferred that the final distribution of HHDN in the columns was achieved during this time. This view is supported by the fact that the effluent from column 4, which contains several orders of magnitude more HHDN at the bottom of the column, contains nearly the same HHDN concentration as the effluent at the "steady-state" condition.

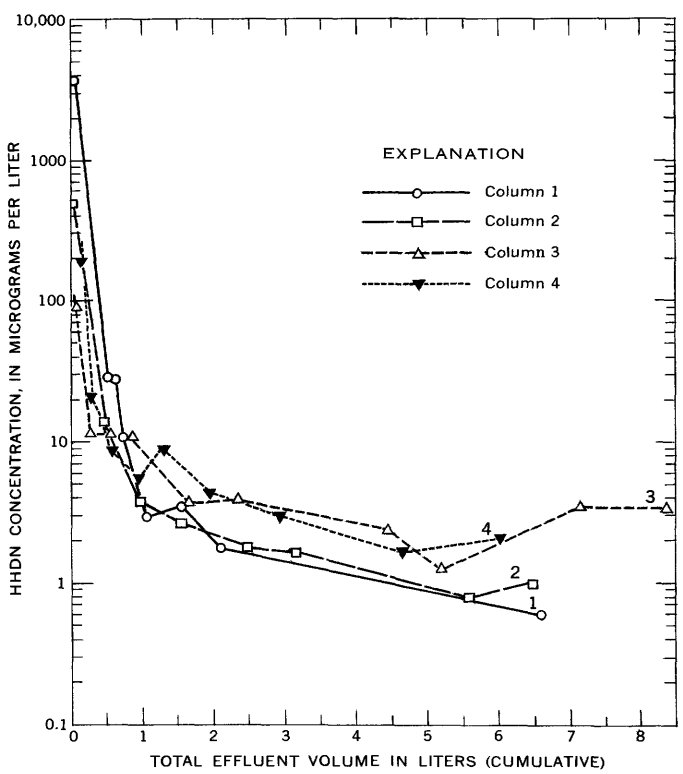

FIGURE 3.—Aldrin concentrations carried in the effluent water in relation to total volume of water infiltrated through each column. See table 1 for descriptions of the four columns.

CONCLUSIONS

This study engenders the following conclusions:

1. Most of the eluted aldrin in organic solvent systems applied to Ottawa sand columns is eluted during the passage of the first liter of water.
2. The aldrin distributes itself in a characteristic manner through each column, depending upon the composition and stability of the emulsion and rate of infiltration of the water.
3. The concentration of HHDN in the effluent from the columns reach a "steady-state" condition of 0.5 to 2 micrograms per liter of water. This concentration is independent of the aldrin concentration in the sand at the bottom of the column and of the nature of the applied emulsion.
4. The total amount of aldrin transmitted to the effluent was highest for the commercial emulsible concentrate mixture. Any factors which tend to destroy or decrease the emulsion properties, such as evaporation of some of the emulsible concentrate components, lack of an emulsifier, or an intermittent heavy flow of water through the column, result in a reduction of insecticide transported into the effluent water phase.

The data obtained in this study suggest that the type of formulation applied, the interval between its application, and the frequency and rate of rainfall, or irrigation, have an important bearing on the penetrability of chlorinated hydrocarbon insecticides through soils.

REFERENCES

Alexander, Martin, 1965, Persistence and biological reactions of pesticides in soils: Soil Sci. Soc. America Proc., v. 29, p. 1–7.

Bowman, M. D., Schechter, M. S., and Carter, R. L., 1965, Behavior of chlorinated insecticides in a broad spectrum of soil types: Jour. Agriculture and Food Chemistry, v. 13, p. 360–365.

Breidenbach, A. W., and Lichtenberg, J. J., 1963, DDT and dieldrin in rivers—A report of a national water quality network: Science, v. 141, p. 899–901.

Chisholm, R. D., and Koblitsky, Louis, 1959, Accumulation and dissipation of pesticide residues in soils: North American Wildlife Conf., 24th, New York, March 2–4, 1959, Trans., p. 118–123.

Gannon, Norman, and Bigger, J. H., 1958, The conversion of aldrin and heptachlor to their epoxides in soil: Jour. Econ. Entomology, v. 51, p. 1–2.

Harris, C. R., and Lichtenstein, E. P., 1961, Factors affecting the volatilization of insecticidal residues from soils: Jour. Econ. Entomology, v. 54, p. 1038–1045.

Lichtenstein, E. P., 1965, Persistence and behavior of pesticidal residues in soils—Their trans-location into crops: Archives of Environmental Health, v. 10, p. 825–826.

Lichtenstein, E. P., Mueller, C. H., Myridal, G. R., and Schulz, K. R., 1962, Distribution and persistence of insecticidal residues in soils as influenced by mode of application and a cover crop: Jour. Econ. Entomology, v. 55, p. 215–219.

Lichtenstein, E. P., and Schulz, K. R., 1959a, Breakdown of lindane and aldrin in soils: Jour. Econ. Entomology, v. 52, p. 118–123.

——— 1959b, Persistence of some chlorinated hydrocarbon insecticides as influenced by soil types, rate of application and temperature: Jour. Econ. Entomology, v. 52, p. 124–131.

——— 1960, Epoxidation of aldrin and heptachlor in soils as influenced by autoclaving moisture, and soil types: Jour. Econ. Entomology, v. 53, p. 192–197.

——— 1961, Effect of soil cultivation, soil surface and water on the persistence of insecticidal residues in soils: Jour. Econ. Entomology, v. 54, p. 517–522.

Richardson, L. T., and Miller, Q. M., 1960, Fungi-toxicity of chlorinated hydrocarbon insecticides in relation to water solubility and vapor pressure: Canadian Jour. Botany, v. 38, p. 163–176.

Robeck, G. G., Dostal, K. A., Cohen, J. M., and Kreissl, J. A., 1965, Effectiveness of water treatment processes in pesticide removal: Am. Water Works Assoc. Jour., v. 57, p. 181–199.

Schechter, M. S., Busbey, R. L., and Hall, S. A., 1964, Persistence of a pesticide: Chem. Eng. News, v. 42, p. 5–7.

Weaver, Leo, Gunnerson, C. G., Breidenbach, A. W., and Lichtenberg, J. J., 1965, Chlorinated hydrocarbon pesticides in major U.S. river basins: U.S. Public Health Reports, v. 80, no. 6, p. 481–493.

Wheatley, G. A., Hardman, T. A., and Strickland, A. H., 1963, Residues of chlorinated hydrocarbon insecticides in some farm soils in England: Plant Pathology, v. 11, p. 81–90.

GEOCHEMISTRY OF IRON IN A COASTAL-PLAIN GROUND WATER OF THE CAMDEN, NEW JERSEY, AREA

By DONALD LANGMUIR, Trenton, N.J.[1]

Work done in cooperation with the New Jersey Department of Conservation and Economic Development

Abstract.—In northern Camden and northwestern Burlington Counties, N.J., the pH of ground water in the Potomac Group and the Raritan and Magothy Formations of Cretaceous age ranges from 5–6 in the outcrop area to 8 several miles downdip to the southeast. Iron is present in the ground water as dissolved Fe^{+2} and $FeOH^{+1}$, and as suspended ferric oxyhydroxides, presumably formed by oxidation of ferrous species already in solution. The oxyhydroxides are probably a mixture of amorphous material and goethite with small amounts of hematite. In the outcrop area the concentration of dissolved ferrous or suspended ferric species is less than 0.5 milligrams per liter in unpolluted waters. Just downdip from the outcrop area, ferrous and ferric iron species increase abruptly to about 6–7 mg/l and 6–11 mg/l, respectively. Farther downdip at pH's above 6.5, both forms of iron decrease gradually to less than 0.5 mg/l. The decrease in ferrous species is not due to siderite precipitation, but may reflect an increase in the stability of suspended amorphous material owing to aging, coupled with adsorption of ferrous iron by the oxyhydroxides and partial conversion of the amorphous phase to goethite. The decrease in suspended ferric species is probably caused by cation adsorption, aging, coagulation, and settling.

Most of the potable water used in the coastal plain part of New Jersey is ground water pumped from the aquifer system in the Potomac Group and the Raritan and Magothy Formations of Cretaceous age. In northern Camden County and northwestern Burlington County, the area considered by this report (fig. 1), ground water in the aquifer system is generally of good quality, except for the common occurrence of total iron in amounts greater than the maximum of 0.3 milligrams per liter recommended by the U.S. Public Health Service (1962) for potable supplies. A detailed description of the occurrence of iron in this ground water written from the point of view of New Jersey water resources, has been published elsewhere (Langmuir, 1969a). This paper describes some geochemical implications of that study.

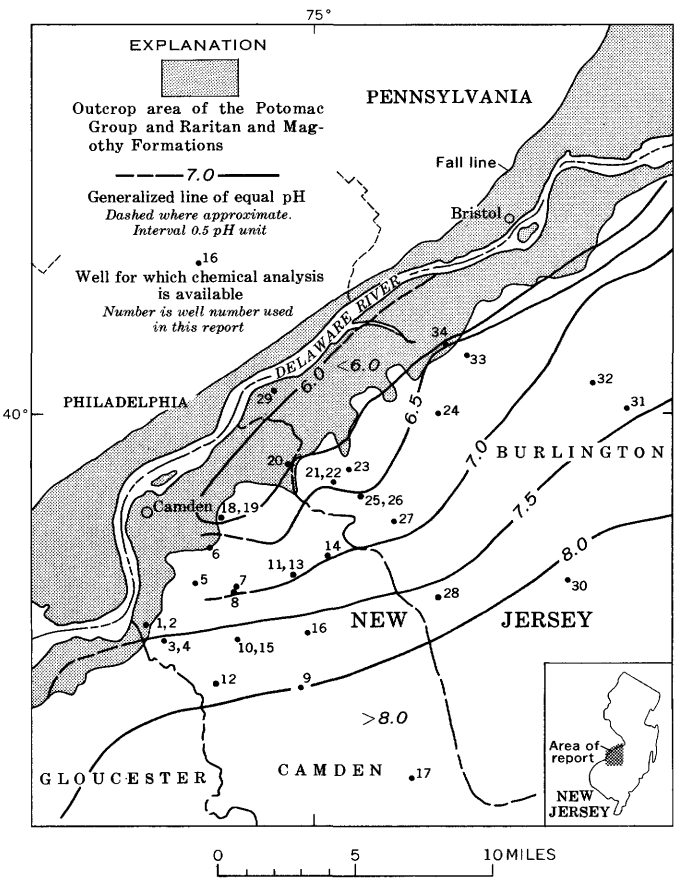

FIGURE 1.—Location of the study area and of wells for which chemical analyses are given in table 1. Generalized pH values of ground water in the Potomac-Raritan-Magothy aquifer system, 1966–67, are shown by contours.

[1] Present address: Department of Geochemistry and Mineralogy, and Mineral Conservation Section, The Pennsylvania State University, University Park, Pa.

GEOLOGY AND GEOHYDROLOGY

Coastal plain geology in New Jersey is characterized by a wedge of unconsolidated and semiconsolidated sediments of Cretaceous through Quaternary age that thickens downdip toward the Atlantic Ocean. The oldest of these sediments, known in New Jersey as the Potomac Group and the Raritan and Magothy Formations, rest unconformably upon an early Paleozoic and Precambrian crystalline basement which crops out at the surface northwest of the Fall Line (fig. 1). These three Cretaceous units, which make up approximately the lower half of the coastal plain sequence in New Jersey, are composed of unconsolidated sand, clay and silt, and small amounts of gravel. The units are predominantly fluvial, although the Magothy has been described also as transitional beach-lagoonal deposit (Owens and Minard, 1964, p. C317). All three units are relatively coarse grained in outcrop and become finer grained downdip, where they grade ultimately into sediments of an offshore marine character.

In outcrop and a few miles downdip in Burlington and Camden Counties, the sands of the three units are predominantly quartz with minor amounts of feldspar and muscovite; the clays are mixtures of kaolinite and muscovite. Marine fossils are occasionally found in the Magothy Formation; however none are present in the Raritan Formation or formations of the Potomac Group. The fossils are commonly pyritized. Pyrite and marcasite are relatively common in all three units, but are most abundant in the Magothy. The sulfide minerals are most often found as concretions and irregular masses associated with lignite in beds of carbonaceous clays. Pellets and concretions of siderite are also abundant and widespread in all three units. Limonite- and hematite-stained beds are common in Magothy and upper Raritan sediments.

In the outcrop area south of Trenton, the Potomac and Raritan sequence is about 200 feet thick and the Magothy ranges in thickness from 0 to 45 feet (H. E. Gill, oral commun., 1967). The formations dip from 40 to 100 feet per mile toward the southeast, with the lower dips assigned to the overlying Magothy Formation (Johnson and Richards, 1952, p. 2152). In the Delaware Valley south of Trenton, the outcrop area of all three units is almost completely covered by permeable sand and gravel, and semipermeable silt and clay deposits of Pleistocene age. Southeast of the outcrop area, aquifers within the Potomac-Raritan-Magothy sequence are effectively confined above by marine silts and clays of the Merchantville Formation and Woodbury Clay of Late Cretaceous age, which collectively are about 100 feet thick or more in the study area. Conformably above the Woodbury Clay is the Englishtown Formation of Late Cretaceous age. The hydrogeology and chemistry of ground water in the Englishtown have been discussed in detail by Seaber (1965).

The geohydrology of the aquifer system in Burlington County has been described by Rush (1968), and in Camden and Burlington Counties by Langmuir (1969a). Although predominant ground-water flow within the study area is now updip toward centers of heavy pumpage in and adjacent to the outcrop area, principal controls on the geochemistry of iron in the ground water now present in confined parts of the aquifer system were established at a time when most of this water was being emplaced by flow downdip toward the southeast. This conclusion is supported by the observation that pH (fig. 1), total dissolved-solids content (fig. 2), and bicarbonate concentrations increase downdip to the southeast in confined parts of the aquifer system. Emplacement of this older ground water downdip probably occurred during later stages of the Pleistocene glaciation when the ocean stood several hundred feet lower than present levels.

GROUND-WATER CHEMISTRY

Chemical data

The discussion of ground-water chemistry, and figures 1 through 4, are based on partial and complete chemical analyses of water samples collected between June 1965 and July 1967 from 120 wells in the study area. These analyses are presented in their entirety elsewhere (Langmuir, 1969a). Only the partial analyses of ground water samples from 34 wells used in calculations of iron equilibria are tabulated in this report (table 1). Locations of the wells listed in table 1 are shown in figure 1.

Methods of analysis

The pH values in table 1 are based on field pH measurements made in the spring of 1966. Measurements were conducted with a Coleman Model-37 battery-operated pH meter and a combination glass pH and silver-silver chloride reference electrode. The electrode was standardized against pH 4 and pH 7 buffers brought to within 0.5°C of ground-water temperature. Buffer checks in the field were always within ± 0.05 pH units based on a comparison of the two buffers. Most field pH values were also determined with a JNL Model-100–P battery-operated pH meter. Agreement between the two meters in the field was generally within ± 0.05 pH units. The bicarbonate concentrations listed in table 1 were determined in the field along with pH by titration to pH=4.50 with standard sulfuric acid (Rainwater and Thatcher, 1960).

In the pH range (5–8) normally found in ground water within the study area, iron is present in dis-

TABLE 1.—*Description of wells and chemical data for well-water samples from the Potomac Group and the Raritan and Magothy Formations in Camden and Burlington Counties, N.J.*

[WD, water department; WC, water company; MPWC, Merchantville-Pennsauken Water Commission; DRWC, Delaware River Water Company; WMUA, Willingboro Municipal Utility Authority]

Well No.	Owner and location	Altitude above sea level (feet)	Screen setting (interval in feet)	Date of measurement	Temperature (°C)	pH	Ferrous iron (mg/l, Fe^{+2} plus $FeOH^{+1}$)	Bicarbonate (mg/l as HCO_3^{-1})	Specific conductance (micromhos at 25°C)
1	Brooklawn WD, No. 2	5	133–166	3–31–66	14. 0	6. 97	4. 4	220	369
2	Brooklawn WD, No. 3	5	307–328	3–31–66	14. 2	7. 52	. 52	89	210
3	Bellmawr WD, No. 1	31	111–160	3–31–66	14. 0	7. 64	. 26	92	203
4	Bellmawr WD, No. 3	31	334–359	3–31–66	15. 0	7. 63	. 14	85	192
5	Collingswood Boro WD, well B	10	224–256 295–315	3–17–66	14. 5	7. 39	. 69	89	214
6	Collingswood Boro WD, No. 3	10	257–287	3–17–66	14. 0	6. 40	. 32	68	162
7	Haddon Twp. WD, No. 1	56	436–468	3–17–66	14. 0	6. 86	4. 6	92	219
8	Haddon Twp. WD, No. 2	50	439–470	3–17–66	15. 0	6. 99	2. 7	97	225
9	New Jersey WC, No. 14	85	389–441	5–11–66	15. 9	8. 01	. 11	87	181
10	New Jersey WC, No. 15	65	452–473 541–594	4– 6–66	15. 8	7. 63	. 67	81	191
11	New Jersey WC, No. 16	25	193–220	3–30–66	14. 4	6. 77	3. 9	90	213
12	New Jersey WC, No. 19	130	301–338	4– 6–66	15. 2	7. 94	. 19	84	178
13	New Jersey WC, No. 23	28	312–375	3–30–66	14. 9	6. 73	4. 0	87	203
14	New Jersey WC, No. 25	44	309–367	4– 6–66	15. 0	7. 00	2. 57	90	223
15	New Jersey WC, No. 30	65	224–275	4– 6–66	14. 4	7. 62	. 53	96	222
16	Hussman Refrigerator Co	67	276–307	5–12–66	14. 9	7. 75	. 37	106	228
17	Berlin Boro WD, No. 9	150	650–713	5–13–66	19. 8	8. 03	. 13	110	214
18	MPWC Browning Rd., No. 1	19	118–148	3–16–66	13. 2	5. 79	. 25	13	54
19	MPWC Browning Rd., No. 2A	19	204–224	3–16–66	13. 2	5. 72	. 33	13	59
20	MPWC Park Ave., No. 2	10	115–145	4– 7–66	13. 4	5. 84	. 55	15	75
21	Maple Shade Twp. WD, No. 2	10	91–121	3– 9–66	14. 3	6. 35	6. 4	72	122
22	Maple Shade Twp. WD, No. 4	10	211–272	3– 9–66	13. 5	6. 62	6. 6	94	149
23	Layne-New York Co., No. 1	65	266–286	3–15–66	14. 3	6. 35	6. 2	73	130
24	Moorestown Twp. WD, No. 4	59	298–338	3– 8–66	14. 0	6. 71	6. 5	95	170
25	Moorestown Twp. WD, No. 5	45	248–288	3– 8–66	13. 9	6. 46	6. 5	73	123
26	Moorestown Twp. WD, No. 6	47	262–312	3– 8–66	14. 2	6. 52	6. 5	70	144
27	Mt. Laurel WC, No. 1	30	558–589	3–10–66	16. 3	6. 85	3. 0	75	158
28	Evesham Twp. WD, No. 2	100	435	4– 6–66	17. 0	7. 86	. 29	110	264
29	DRWC, Riverton-Palmyra Div. No. 11	10	72–98	4–14–66	14. 1	6. 20	. 05	48	212
30	Medford WC, No. 3	48	506–536	4–13–66	17. 3	7. 96	. 25	106	209
31	Mt. Holly WC, No. 3	11	316–346	4–14–66	15. 0	7. 40	. 61	100	189
32	Mt. Holly WC, No. 5	55	500	4–14–66	15. 3	7. 17	1. 98	96	206
33	WMUA, No. 3	28	203–238 283–303	4–15–66	13. 4	6. 79	4. 77	81	188
34	WMUA, No. 4	28	196–279	4–15–66	13. 5	6. 56	4. 69	32	82

solved form chiefly as uncomplexed ferrous ion (Fe^{+2}), but also as monohydroxy ferrous ion ($FeOH^{+1}$). The ferrous iron analyses in table 1 represent the sum of Fe^{+2} and $FeOH^{+1}$. Filtration studies and a comparison of the total iron and ferrous iron analyses for individual ground-water samples show that substantial amounts of iron are also present as suspended ferric oxyhydroxides.

Most samples for ferrous-iron analysis were force filtered through a 0.01-micron filter using well-pump pressure prior to collection. A Kreuger Model-A–400 stainless steel (120-cubic-centimeter) vacuum and pressure filter and filter pads of combination paper and asbestos material were used for this purpose. The ferrous iron was immediately complexed in the field with 0.2-percent bipyridine solution, and laboratory analysis was made within 48 hours to preclude oxidation of the colored ferrous-bipyridine complex. Filtration was found necessary to remove most of the suspended ferric oxyhydroxides from the sample. Although these materials are not visible to the naked eye, they scatter and attenuate the spectrophotometer light beam during analysis and can lead to a substantial overestimate of the ferrous iron content in the sample.

Total iron concentrations are not listed in table 1; however, they are discussed in this article and are shown in figure 4. Samples for total-iron analysis were generally collected after force filtering through a 5-micron filter using well-pump pressure. Filtration was practiced to exclude from the samples fragments of iron-oxide rust which are sometimes dislodged from the casing or distribution lines as a result of pumping. Samples for total-iron analysis were always acidified in the field with hydrochloric acid prior to capping.

All iron analyses were performed in the laboratory with a Bausch and Lomb Model-20 spectrophotometer and 1-inch test tubes using methods described by Rainwater and Thatcher (1960). With the instrumentation and techniques described above, a precision of measurement of better than about 5 percent was

possible for samples containing between 0.3 and 3.2 mg/l ferrous iron, or between 0.3 and 3.7 mg/l total iron. Samples containing less than 0.05 mg/l iron could not be analyzed with any confidence using these techniques. Concentrations are reported to one significant figure between 0.05 and 0.10 mg/l and two significant figures above 0.10 mg/l.

The specific-conductance values in table 1 were measured in the laboratory within 48 hours after sample collection, using a Serfass conductance bridge and a dipping conductivity cell with a cell constant of 1.00 reciprocal centimeters. Measurements were corrected to 25°C and are probably accurate to about 2 percent (Rainwater and Thatcher, 1960).

Individual ion activities

Individual ion activities are used in subsequent calculations of iron equilibria. For the ionic species in table 1, these were determined as follows: Complete analyses of water samples from 26 wells in the study area were used to calculate the ionic strength, I, of each sample through the definition

$$I=1/2\,\Sigma m_i z_i^2, \tag{1}$$

where m_i is the molality, and z_i is the charge of ionic species "i". A plot of I versus the measured specific conductance, μ, of these samples in micromhos corrected to 25°C, closely obeyed the empirical equation

$$I=1.50\times10^{-5}\mu. \tag{2}$$

Accordingly, μ values of the samples in table 1 were used to estimate their ionic strength.

Individual ion-activity coefficients, γ_i, for such species as Fe^{+2} and HCO_3^{-1} in tables 1 and 4 were calculated from I using the expanded Debye-Hückel equation (see Klotz, 1964). Individual ion activities, a_i, were then determined through the definition $a_i=\gamma_i m_i$. At 15±3°C, the temperature of nearly all the ground-water samples in tables 1 and 4, γ_i values computed with the Debye-Hückel equation differ by less than 1 percent from their values at 25°C. Thus the 25°C values will be used throughout this discussion. Activity-coefficient data are not available for $FeOH^{+1}$, however the assumption that $\gamma FeOH^{+1}=\gamma HCO_3^{-1}$ which is made here, is probably accurate enough for the following discussion.

Gibbs free-energy data

Subsequent calculations of equilibria involving iron and related species are based on the Gibbs free-energy data in table 2. These data are taken from Langmuir (1969b). Methods of calculating equilibrium relations from free-energy data are explained in detail by Garrels and Christ (1965).

TABLE 2.—*The Gibbs free energy of formation from the elements, $\Delta G_f°$, of certain substances at 25°C and 1 atmosphere total pressure*

[*Italicized* values are for metastable phases. g, gas; l, liquid; and aq, aqueous]

Substance	$\Delta G_f°$ (cal/mole)
CO_2(g)	−94, 257±40
H_2O(l)	−56, 688±20
OH^{-1}(aq)	−37, 594±10
H_2CO_3(aq)	−148, 948±55
HCO_3^{-1}(aq)	−140, 285±60
CO_3^{-2}(aq)	−126, 196±70
Fe^{+2}(aq)	−21, 800±500
$FeOH^{+1}$(aq)	−67, 168±570
Fe^{+3}(aq)	−4, 020±500
$FeCO_3$(siderite)	−162, 390±510
α-Fe_2O_3(hematite)	−177, 728±310
α-FeOOH(goethite)	−116, 375±160
$Fe(OH)_3$(amorphous)	≦ *−167, 460±600*

The ferrous monohydroxy complex ($FeOH^{+1}$)

The Gibbs free-energy data in table 2 for the reaction,

$$Fe^{+2}+H_2O=FeOH^{+1}+H^{+1} \tag{3}$$

lead to

$$K=[FeOH^{+1}][H^{+1}]/[Fe^{+2}]=10^{-8.30}, \tag{4}$$

where the brackets denote activities. Thus, at 25°C, Fe^{+2} is the only significant dissolved ferrous iron species present below pH=6.30. The activity of $FeOH^{+1}$ increases in relative importance at higher pH's, equaling that of Fe^{+2} at pH=8.30.

No measurements have been made of K for reaction 3 at temperatures below 25°C, nor are enthalpy or heat-capacity data available which would permit its estimation at ground-water temperatures. However, the change in K with temperature can be evaluated differently. On the basis of the free-energy data in table 2, the dissociation constant for the reaction

$$FeOH^{+1}=Fe^{+2}+OH^{-1} \tag{5}$$

is $10^{-5.70}$ at 25°C. Constants for the analogous dissociation reactions involving $ZnOH^{+1}$, $MnOH^{+1}$, and $SrOH^{+1}$ have been measured at 15° and 25°C (Sillén, 1964). At 15°C these constants differ by no more than 0.05 log units from their values at 25°C. The same behavior probably also applies to the dissociation constant for $FeOH^{+1}$. The reverse of reaction 5, summed with ($H_2O=H^{+1}+OH^{-1}$), yields reaction 3. Thus

$$\log K\text{ (reaction 3)}=\log Kw+5.70, \tag{6}$$

where $Kw=[H^{+1}][OH^{-1}]$. Log Kw values as a function of temperature are given by Sillén (1964). A plot of log K (reaction 3) versus degrees Celsius permits the rapid estimation of this quantity at ground-water temperatures.

Water-quality zones

In order to characterize better the occurrence and behavior of iron in the ground water, it is useful to define four water-quality zones in the study area. These zones are shown in figure 2 and are described in table 3 in terms of their dissolved-solids content, pH, prevalent chemical character, and iron content. The high dissolved-solids content in zone 1 is primarily a consequence of induced flow of contaminated ground water beneath the Delaware River into New Jersey from the Greater Philadelphia area (Barksdale and others, 1958; Greenman and others, 1961), and to a less extent is due to ground-water contamination from local New Jersey sources. Also, at times of low flow, recharge from the Delaware River contributes dissolved solids in excess of 100 mg/l at Trenton and 200 mg/l at South Philadelphia (Durfor and Keighton, 1954). The low dissolved-solids content of zone 2 ground water reflects the good quality of local recharge from precipitation and streamflow, and the general absence of unstable minerals or soluble salts among the well-leached materials present in the outcrop area. In zone 3, dissolved solids are due primarily to reactions of the ground water with geologic materials. Dissolved-solids content in this zone increases downdip in the direction of flow at the time of emplacement. Ground water in shallow parts of zone 4 was probably introduced by flow downdip from zone 3. The calcium in the ground water of zone 4 has been replaced by sodium through ion-exchange reactions with clays and other exchange materials (Foster, 1950). South of the 500-mg/l line, dissolved-solids content increases rapidly as mixing occurs with residual saline water high in sodium chloride. This saline water may be what remains of sea water, trapped in the sediment when it was deposited over 70 million years ago.

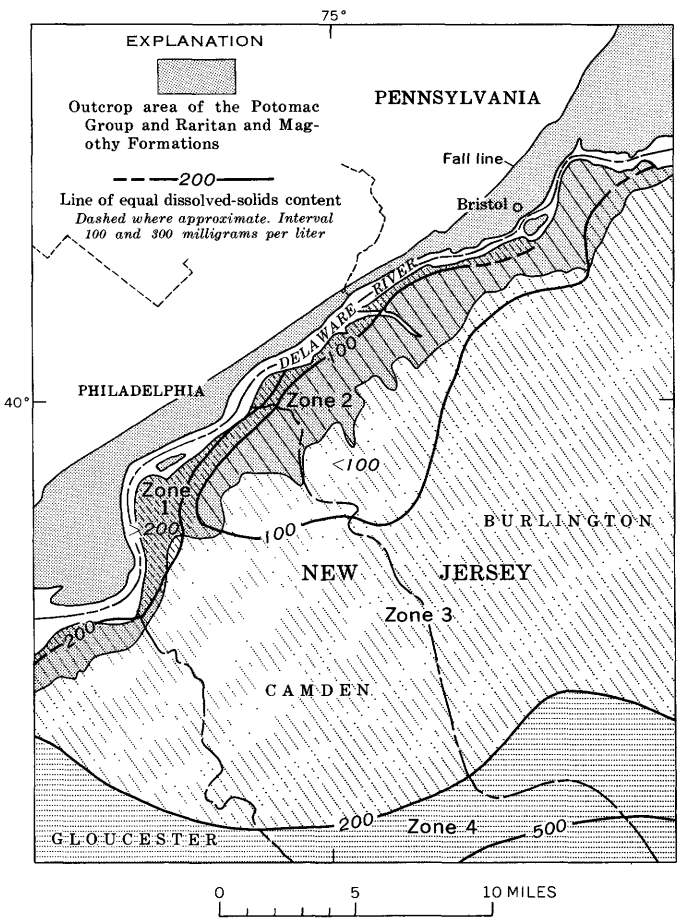

FIGURE 2.—Generalized dissolved-solids content in ground water of the aquifer system, and location of water-quality zones, 1966–67.

General iron geochemistry

The greatest concentrations of ferrous iron occur in zones 1 and 3 under confined or semiconfined conditions, where the ground water is prevented from mixing with oxygen-rich surface recharge. The smallest amounts of ferrous iron are found in zone 2 under water-table conditions in the presence of oxygenated water, and in zone 3 where pH values are above 8.0. A comparison of figures 3 and 4, and detailed chemical measurement during pumping tests of several wells, show that wherever the ground water contains ferrous iron species, particulate ferric species are also present in characteristic amounts. The converse is also generally true.

Numerous filtration studies in the field have demonstrated that the oxyhydroxides range in size from less than 0.01 micron to greater than 5 microns, and average about 1 micron in size. Repeated analyses of the iron content in the water from several shallow artesian wells in Camden County (zone 3), has shown that induced oxygen-rich recharge can seasonally lower the concentration of aqueous ferrous species, and proportionately increase the amount of ferric oxyhydroxides without significantly changing the total iron content of the ground water (Langmuir, 1969a). This implies a substantial reactivity for the oxyhydroxides, and is consistent with their predominantly colloidal size.

Probably most of the iron in the ground water has been derived ultimately from the solution and reduction of ferric oxyhydroxide minerals which are common in aquifer sediments. At present, however, relatively more soluble and less stable suspended ferric oxyhydroxides, denoted for simplicity as $Fe(OH)_3$, are almost always found in the ground water along with dissolved ferrous iron. Thus the reaction

$$2Fe(OH)_3+4H^{+1}=2Fe^{+2}+5H_2O+1/2O_2 \qquad (7)$$

TABLE 3.—*Prevalent chemical character and iron content in ground water from the Potomac Group and the Magothy and Raritan Formations in Camden and Burlington Counties, N.J.*

[Based on Langmuir (1969a)]

Water-quality zone No.	Location and dissolved-solids content (location on fig. 2)	Normal range of pH values	Principal cations and anions in decreasing order of abundance	Iron content [1]	Remarks
1	Areas in and adjacent to outcrop with dissolved solids >100 mg/l.	6. 0–7. 0	Ca, Na, Mg, K; HCO_3, SO_4, Cl, NO_3	Total iron and ferrous iron usually >0.5 mg/l. Total iron as much as 20 mg/l; ferrous iron as much as 5 mg/l.	Ground water polluted or vulnerable to pollution in and adjacent to these areas. Dissolved solids may exceed 400 mg/l.
2	Outcrop areas with dissolved solids <100 mg/l.	5. 0–6. 0	Ca, Na, Mg, K; $HCO_3 \approx$ Cl, SO_4, NO_3	Generally both total iron and ferrous iron <0.5 mg/l.	Principal areas of high-quality recharge; from the Delaware River, precipitation, and streams.
3	Downdip from outcrop areas, with dissolved solids <200 mg/l or outcrop areas with dissolved solids 100–200 mg/l.	6. 0–8. 0	Ca, Na, K, Mg; HCO_3, SO_4, Cl	Total iron <0.05 to 16 mg/l; ferrous iron <0.05 to 6.6 mg/l.	Quality due to natural geohydrologic environment and reactions with geologic materials.
4	Downdip from outcrop areas with dissolved solids >200 mg/l.	>8. 0	Na≫Ca, K, Mg; HCO_3≫Cl, SO_4	Both total iron and ferrous iron probably <0.3 mg/l throughout.	Quality deteriorates south of the 200-mg/l contour owing to mixing with residual saline water. Chloride increases rapidly south of 500-mg/l contour.

[1] At pH values above 6.3, ferrous iron includes Fe^{+2} and $FeOH^{+1}$.

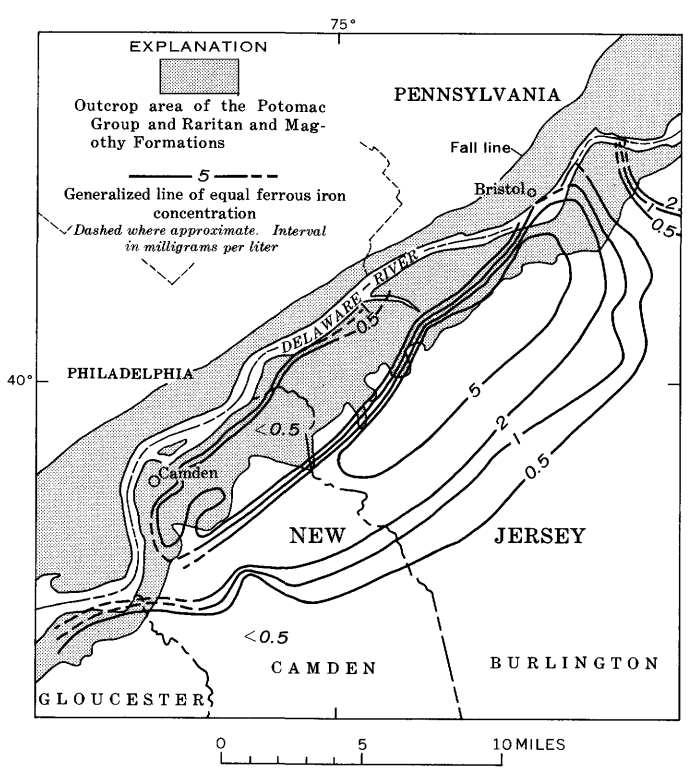

FIGURE 3.—Generalized ferrous iron concentration in ground water of the aquifer system, 1965.

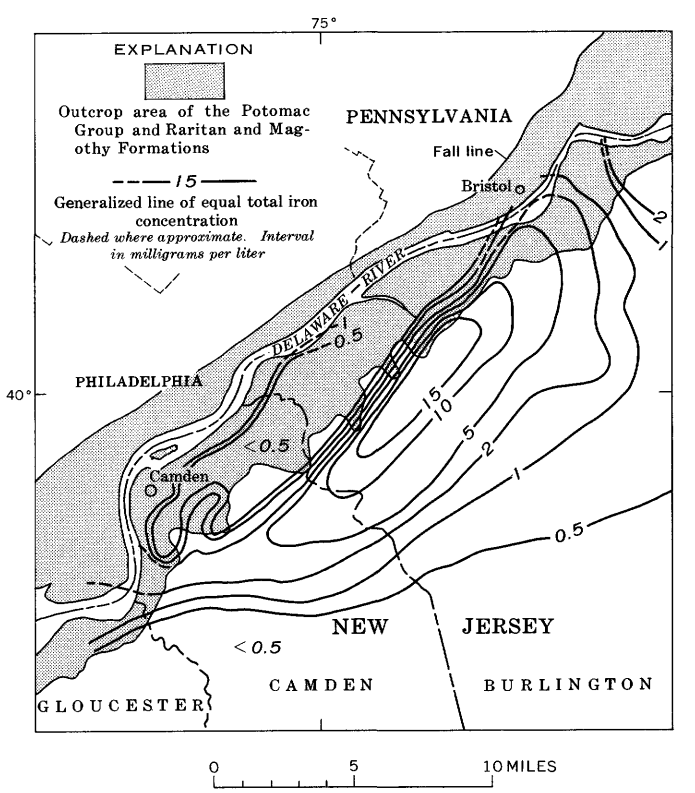

FIGURE 4.—Generalized total iron concentration in ground water of the aquifer system, 1965.

is probably an important control on iron concentration throughout the study area. Reaction 7 indicates that an increase in H^{+1} or a decrease in DO (dissolved oxygen) leads to solution of $Fe(OH)_3$ and reduction of the ferric iron to Fe^{+2}. Conversely, an increase in pH or DO may cause precipitation of $Fe(OH)_3$. The occurrence of ferrous and ferric iron species in the ground water thus depends on the concentration of H^{+1} ions and DO.

Ground water in zone 1 normally contains more than 0.5 mg/l and in some instances as much as 20 mg/l total iron (table 3). Considerably higher amounts have been reported in ground water under Philadelphia (Greenman and others, 1961). Ground water beneath Philadelphia and adjacent parts of New Jersey in zone 1 is cut off locally from mixing with DO-rich recharge or atmospheric oxygen, by intraformational clay beds, city pavements and buildings, and by clays beneath the Delaware River. Appreciable quantities of organic waste materials are introduced into the ground water in zone 1 from such sources as leaky sewers and storm drains, and municipal and industrial waste-disposal practices. Hence, even where surface water does percolate down to the water table, microbial oxidation of organic wastes probably depletes the oxygen in this water before much mixing with ground water can occur. Important organic waste-decomposition processes such as

$$CH_2O+O_2=H_2CO_3=H^{+1}+HCO_3^{-1} \qquad (8)$$

use up oxygen and produce hydrogen ions, thus driving reaction 7 to the right. Small amounts of the iron disulfides, pyrite, and marcasite, are present in the aquifer sediments of zone 1, as well as in other parts of the study area. Oxidation of these minerals according to the reaction

$$FeS_2+H_2O+7/2\ O_2=Fe^{+2}+2H^{+1}+SO_4^{-2} \qquad (9)$$

is a minor source of ferrous iron in zone 1, and at the same time produces H^{+1} ions and uses up DO, facilitating the solution of ferric oxyhydroxides.

The land surface in zone 2 is less urbanized than in zone 1. Zone 2 ground water receives most of its recharge from the infiltration of unpolluted DO-rich surface water. An active soil horizon is usually present in this zone, so that plant-root respiration and bacterial oxidation of organic material in the soil produces important amounts of CO_2. The low pH values in zone 2 reflect the solution of this CO_2 by infiltrating groundwater recharge. Oxidation of traces of the ferrous disulfides according to reaction 9 may also be important locally. Although the acidity of ground water in zone 2 favors an increase in ferrous iron, the repeated mixing of the ground water with oxygenated recharge evidently prevents any major buildup of ferrous iron and hence also of suspended oxyhydroxides.

The Merchantville Formation and Woodbury Clay are an effective aquiclude above the Magothy Formation in most of zone 3. In addition, small amounts of lignitic material, ferrous-iron minerals such as the sulfides and siderite in the sediments, and organic substances in the ground water, tend to deplete DO in the ground water. Most important acidity-producing reactions require oxygenated water, and so they become less significant in confined parts of the aquifer system. Thus, pH increases downdip in zone 3 as the initial H^{+1} concentration has been depleted by hydrolysis reactions with aquifer materials. Bacterial reduction of sulfate also tends to raise the pH downdip according to reactions, such as

$$SO_4^{-2}+2CH_2O+2H^{+1}=H_2S+2H_2CO_3. \qquad (10)$$

Within the study area, pH values do not exceed about 8.0 in zone 3. This may be due to the release of carbonic acid through physical and or biological decomposition of lignite and other organic materials in the sediments (Foster, 1950).

The pH increase in zone 3 favors the precipitation of ferric oxyhydroxides; however, the rapid depletion of DO just southeast of the zone-2–zone-3 boundary is evidently the controlling factor which causes an abrupt increase in dissolved ferrous iron in this area. The suspended ferric oxyhydroxides in shallow parts of zone 3 are apparently precipitated by periodic mixing of the ground water with small amounts of oxygen-bearing recharge.

Iron decrease in zone-3 ground water

Of particular geochemical interest are reversals in the concentration trends of both ferrous iron and suspended ferric iron, with both forms decreasing to less than 0.05 mg/l a few miles downdip in zone 3. A chief purpose of subsequent discussion is to explain these reversals.

Siderite saturation

A similar reversal in total-iron concentration downdip occurs in the Englishtown Formation (Seaber, 1965). Chemical analyses of several Englishtown water samples, and calculations by the author (unpub. data), show that these samples are supersaturated with siderite, so that the ferrous iron reversal in this case is probably due to siderite precipitation downdip. Siderite is also common (but less so) in underlying Potomac Group, Raritan, and Magothy sediments, and both pH, and bicarbonate concentrations increase downdip in zone 3. This suggests that precipitation of siderite

might also account for the ferrous iron reversal in the study area.

The activity product of siderite expressed as $Ks = [Fe^{+2}][CO_3^{-2}]$ is $10^{-10.65}$ at 30°C and $10^{-10.55}$ at 25°C (Langmuir, 1969b). On the basis of these values Ks may be computed at temperatures near 25°C using the equation

$$-\log Ks = 10.55 + (0.02)(t - 25.0), \qquad (12)$$

where t is in degrees Celsius. With the analyses in table 1 and dissociation constants for carbonic acid at temperatures below 25°C (Garrels and Christ, 1965), we can calculate the ion-activity product, $IAPs = [Fe^{+2}][CO_3^{-2}]$, for each ground-water sample. The degree of saturation may be expressed in terms of a saturation index, $SI = \log(IAPs/Ks)$, which is negative for undersaturated samples, zero for saturated samples, and positive for samples supersaturated with siderite. Sample 1 in zone 1 is slightly supersaturated, with $SI = +0.14$; however, the other 28 water samples from confined parts of the aquifer system are undersaturated. Their SI values range from -0.26 to -1.06, and average -0.54. In addition, there is no correlation between $[Fe^{+2}]$ and SI downdip in zone 3. Thus, precipitation of siderite is not the cause of the ferrous iron reversal.

Mineralogy and stability of the suspended ferric oxyhydroxides

Because of the usual coexistence and similarity of behavior of dissolved ferrous- and suspended ferric-iron species, it is clear that whatever reason is given for the ferrous-iron reversal in zone-3 ground water should be consistent with the parallel decrease in suspended ferric oxyhydroxides. The explanation for both reversals seems to be tied to the nature and properties of the oxyhydroxides.

The suspended oxyhydroxides are generally formed in the ground water at pH values between 6 and 8 by the reaction of aqueous ferrous ion with dissolved oxygen in the presence of bicarbonate ion. The reaction may be written

$$2Fe^{+2} + 4HCO_3^{-1} + H_2O + 1/2O_2 = 2Fe(OH)_3 + 4CO_2. \qquad (12)$$

Experimental studies which duplicate these conditions have been described by Baudisch and Albrecht (1932), and Schwertman (1959). On the basis on X-ray methods, these workers noted that goethite forms as a result of ferrous-iron oxidation in the presence of HCO_3^{-1} and carbonic acid. Work with the electron microscope (Lengweiler and others, 1961; Feitknecht and Michaelis, 1962) reveals that freshly precipitated goethite is usually mixed with substantial amounts of amorphous material which cannot be detected by X-ray analysis.

Fresh precipitates of both phases increase in stability with time by aging, which involves such processes as the splitting off of excess water, particle-size growth, and crystallization. When amorphous material is precipitated in the presence of ferrous iron, the ferrous iron can accelerate its crystallization into goethite (Feitknecht and Michaelis, 1962), although such crystallization often takes many years at low temperatures (Welo and Baudisch, 1934; Garrels, 1959). After several years of aging in suspension or under water, amorphous material may also partially crystallize into hematite (Welo and Baudisch, 1934; Schindler and others, 1963; Schwertman, 1965).

Thus, the initial precipitate in the ground water is probably a mixture of goethite and amorphous material. Aging of this precipitate probably leads to a mixture containing reduced amounts of amorphous material, additional goethite, and small amounts of hematite. At the same time, aging must also cause an increase in the stability of the initial goethite precipitate and remaining amorphous material.

If a mixture of oxyhydroxides is subject to increased acidity or to more reducing conditions, there will be a tendency for the more soluble oxyhydroxides to dissolve. In this way, Lengweiler and others (1961) removed amorphous material from a mixture with goethite by acid leaching. Leaching can also be expected to occur in some ground water, with the result that relatively soluble oxyhydroxides are preferentially removed, and the more stable species remain behind and so control iron equilibria in the ground water.

The stability or solubility of the oxyhydroxides can be described in terms of pK, the negative common logarithm of the activity product, $[Fe^{+3}][OH^{-1}]^3$. Langmuir (1969b) estimated that at 25°C, pK values for the amorphous phase range from 37.1 ± 0.6 for a fresh precipitate to roughly 39.3 for long-aged material. For goethite the range is from roughly 39.7 for a fresh precipitate to 41.2 ± 0.4 for the stable phase. The range for hematite may be from about 40.8 for relatively young material to 41.9 ± 0.4 for the stable phase. The pK's for fresh amorphous material and stable goethite and hematite are based on the free-energy data in table 2. The pK values for long-aged amorphous material and the least-stable forms of goethite and hematite are largely conjectural.

Surface properties of the suspended ferric oxyhydroxides

The surface properties of the oxyhydroxides are probably of key importance in zone-3 ground water. We have noted that the conversion of amorphous material into goethite is accelerated by the adsorption of ferrous iron onto the surface of the amorphous particles. Adsorption can only occur at pH's above the isoelectric

point of the amorphous phase; that is when the surface of the particles is negatively charged. When so charged, the particles will adsorb cations, and especially small multivalent ones such as Fe^{+2}. The adsorption of Fe^{+2} not only facilitates goethite formation from amorphous material, but along with adsorption of such ions as Ca^{+2} and Mg^{+2} neutralizes the negative charge on both suspended phases causing their coagulation and precipitation. The precipitation may be enhanced by the fact that goethite crystals are usually larger than particles of the amorphous phase (Feitknecht and Michaelis, 1962).

No detailed studies have been made of Fe^{+2} adsorption on ferric oxyhydroxides; however, the adsorption of several other transition metals on the oxyhydroxides has been examined. Hem and Skougstad (1960) found that Cu^{+2} ions were adsorbed on a ferric-oxyhydroxide precipitate at pH's above 5.5 to 6.0. Mn^{+2} is similarly adsorbed at pH's above 7.3 (Morgan and Stumm, 1965), and Co^{+2} at pH's above 4 (Tanaka, 1965). These studies were apparently done with freshly precipitated material; however, the specific oxyhydroxide phases involved were not identified. The isoelectric point of amorphous material is somewhat higher than that of goethite (Parks, 1965). Unfortunately the exact isoelectric points of the suspended oxyhydroxides depend on their physical and chemical properties, and on the concentrations and types of cations and anions in the ground water. In any case the studies described above are consistent with the possiblity that adsorption of Fe^{+2} by the suspended oxyhydroxides is taking place at pH's above 6.0 to 6.5 in zone 3.

Eh calculations

Equilibrium between Fe^{+2} and the suspended ferric oxyhydroxides can be written

$$Fe(OH)_3+3H^{+1}+e^{-1}=Fe^{+2}+3H_2O. \quad (13)$$

The Eh due to this reaction is

$$Eh=E^\circ-1.984\times10^{-4}\ T\ \log\ ([Fe^{+2}]/[H^{+1}]^3) \quad (14)$$

where T is in degrees Kelvin. The value of E° depends on the stability of the particular ferric oxyhydroxide involved.

For freshly precipitated amorphous material at 25° C

$$E^\circ=-\Delta G^\circ/23.06=1.058 \text{ volts}, \quad (15)$$

where ΔG° is the Gibbs free energy of reaction 13 in kilocalories per mole. The change in E° with temperature may be estimated using the van't Hoff equation and enthalpy data for the species involved (Barnes and Back, 1964; Garrels and Christ, 1965). Based on this approach, at ground-water temperatures (about 15° C), E° differs from its value at 25°C by less than 0.005 volts, so that the effect of temperature on E° may be ignored. The temperature dependence of Eh is chiefly due to changes in the Nernst factor ($1.984\times10^{-4}\ T$), which is 0.0592 volts at 25°C and 0.0572 volts at 15°C. Thus, at 15°C for freshly precipitated amorphous material, expression 14 may be written

$$Eh=1.058-0.172\ pH-0.0572\ \log\ [Fe^{+2}]. \quad (16)$$

As is evident from equation 14, if the stability of the oxyhydroxide, and pH and $[Fe^{+2}]$ are known, one can calculate the Eh of the ground water. The computed Eh will be the true Eh if reaction 14 is readily reversible and also the only important redox reaction taking place; that is if the system is adequately poised (Nightingale, 1958) and the true Eh is not a mixed potential (Stumm, 1966). These conditions are probably satisfied in most ground water within the study area.

Accordingly, Eh values have been computed for each water sample described in table 1, assuming that the suspended phase is fresh, amorphous material. These Eh's are plotted against measured pH values in figure 5. Because the oxyhydroxides in the ground water must be somewhat more stable than fresh, amorphous ma-

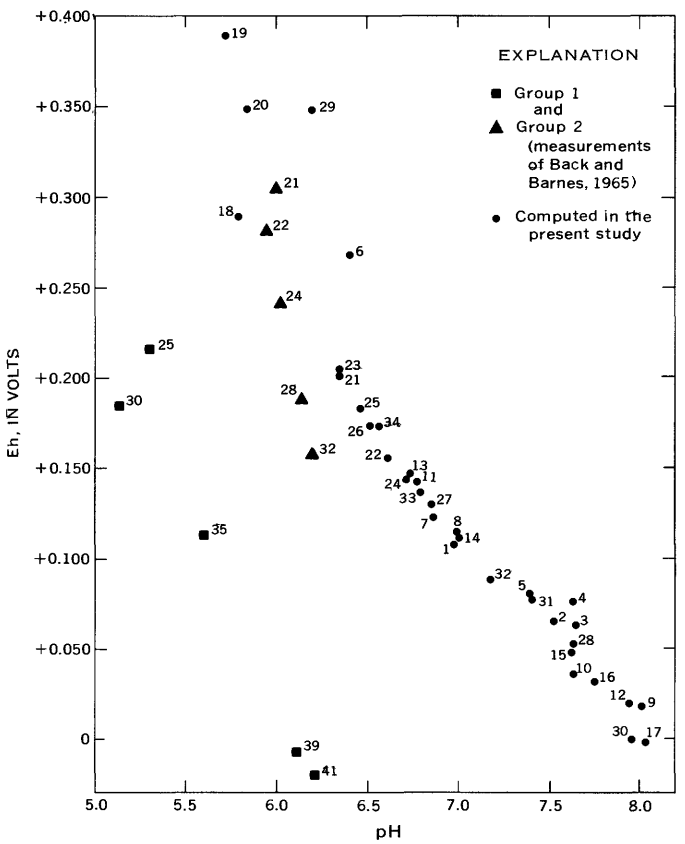

FIGURE 5.—Eh and pH values in well water from the Raritan and Magothy Formations in Maryland, measured by Back and Barnes (1965), compared to computed Eh and measured pH values in well water from the present study.

terial, owing to aging and (or) leaching, true Eh values should lie below the plotted values.

In general, the flow of ground water from the outcrop area zone 2, downdip into zone 3, corresponds to the trend of calculated points toward lower Eh and higher pH values. Ground water with higher Eh's than about +0.200 volts is in or adjacent to the outcrop area and zone 2. The other samples are from artesian parts of the aquifer system in zone 3, or from beneath confining clays in zone 1 (wells 1 and 2).

On the basis of the foregoing, the decrease in ferrous iron with Eh in zone-3 ground water is probably related to the aging of suspended amorphous material downdip, coupled with adsorption of Fe^{+2} by this phase and its partial conversion to goethite. As already noted, the decrease in the concentration of suspended oxyhydroxides may be caused by cation adsorption, aging, coagulation, and settling. If the ferrous iron decrease is due to aging of the oxyhydroxides, then above a pH of 6.3, measured Eh values should be increasingly less than the computed values plotted in figure 5. For example, if pK for the aged precipitate in sample 30 is 39.3, then sample Eh should be −0.044 volts. Unfortunately, this explanation for the ferrous iron decrease cannot be confirmed until field Eh measurements are made of ground water in the study area.

Comparison with similar ground water in Maryland

Although aging of the suspended oxyhydroxides is probably an important control on dissolved ferrous-iron concentration in ground water in New Jersey and elsewhere, no quantitative studies of the aging process have been made in natural water. However, the effect of leaching, combined with possible aging of the oxyhydroxides, on ferrous-iron concentration in similar ground water can be inferred from the work of Back and Barnes (1965). These authors made field Eh and pH measurements, and ferrous-iron analyses of several well-water samples from the Raritan and Magothy Formations in southern Maryland. Their analyses with pH values greater than 5 are summarized in table 4 (except for sample 36 which differs from the others in that it is saturated with siderite). Ionic strengths in the table were provided by William Back (written commun., 1969). The typically lower Eh and pH values and higher ferrous iron contents given in table 4 than in table 1 reflect relatively higher abundances of pyritic lignite in the Maryland sediments, and the fact that all the Maryland wells tap the aquifer system under water-table or, at most, semiconfined conditions.

Before calculating pK values for the oxyhydroxides from the data in table 4 and equation 14, it is important to examine the reliability of the Eh measurements in the table. For such measurements to represent the Eh due to reaction 14, several conditions must be met. Reaction 14 should be readily reversible. Stumm (1967, p. 448) has found this to be the case as long as Fe^{+2} concentration is greater than about 10^{-5} molal (0.6 mg/l). The lowest ferrous iron concentration in table 4 is 5.5 mg/l. Doyle (1968) concluded that the reversibility of reaction 14 is catalyzed by a layer of oxyhydroxide forming on the platinum-electrode surface during an Eh measurement. The presence of suspended oxyhydroxides in every sample in table 4 suggests that similar catalysis probably occurred during the Eh measurements of Back and Barnes. The published analyses of these water samples (Back and Barnes, 1965) and other chemical data provided by William Back (written commun., 1969) indicate that dissolved ferrous iron and suspended ferric oxyhydroxides are the only important redox-sensitive species present, so that mixed potentials should not have interfered with the Eh measurements (Charlot and others, 1962). However, these ground water samples are not well poised, and so the Eh values in table 4 are probably accurate to about ±0.030 volts (author's estimate).

TABLE 4.—*Selected chemical data for well-water samples from the Raritan and Magothy Formations in Anne Arundel County, Md.*

[After Back and Barnes (1965) and Back (written commun., 1969)]

Well No.	Temperature (°C)	pH	Ferrous iron (mg/l as Fe)	Eh (volts)	Ionic strength
21	14.7	6.00	5.5	+0.306	2.4×10^{-3}
22	14.7	5.94	6.6	+.282	2.4×10^{-3}
24	14.5	6.02	6.5	+.242	2.4×10^{-3}
25	13.9	5.31	12	+.216	2.2×10^{-3}
28	14.7	6.14	8.7	+.189	2.4×10^{-3}
30	13.8	5.14	13	+.185	8.5×10^{-4}
32	15.5	6.20	14	+.158	3.2×10^{-3}
35	14.5	5.60	24	+.113	2.4×10^{-3}
39	14.5	6.11	23	−.007	2.4×10^{-3}
41	14.4	6.20	26	−.020	2.6×10^{-3}

The Eh and pH values in table 4 are plotted in figure 5. It is evident that there are two groups of water samples of different general character. Group 1 includes samples 25, 30, 35, 39, and 41; group 2, samples 21, 22, 24, 28, and 32. Using the Eh, pH, and ferrous-iron values in table 4, we can calculate E° and therefore pK for the suspended oxyhydroxides present in each sample. These computed pK values are plotted against Eh in figure 6. Within the probable uncertainty of the Eh measurements, the pK values of group 1 samples correspond to the range of stability of goethite or hematite. Group 2 samples are within the range of stability of the amorphous phase. The data in table 4 and figure 6 show that a general increase in dissolved ferrous iron accompanies the increase in pK and decrease in Eh for both sample groups. Thus, in both

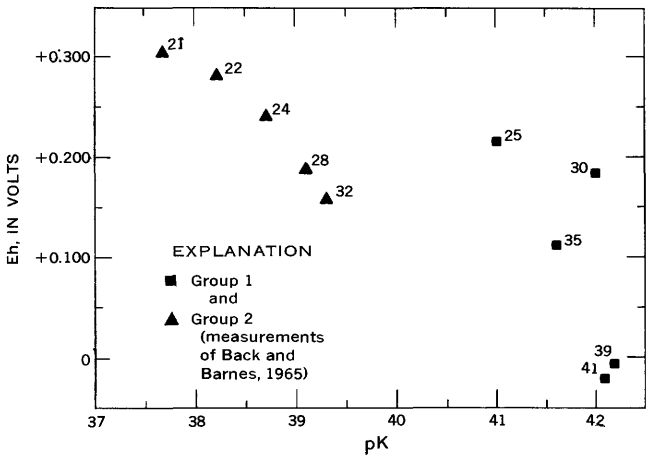

FIGURE 6.—Plot of Eh versus pK for the suspended ferric oxyhydroxides in well water described by Back and Barnes (1965) from the Raritan and Magothy Formations in Maryland.

instances the pK increase probably reflects chiefly a removal of the more soluble oxyhydroxides by leaching. The predominantly lower Eh and pH values of group 1 as compared with group 2 samples, may have led to removal of any amorphous material initially present in the group-1 samples, thus explaining why these ground water samples are now in apparent equilibrium with goethite or hematite. Group-2 samples are roughly similar in composition to those in table 1. This suggests that, as was assumed, amorphous material is the oxyhydroxide controlling reaction 14 in zone-3 ground water.

The New Jersey and Maryland studies described above show that variations in the physical and chemical properties of the suspended ferric oxyhydroxides can be a major control on the concentration of both dissolved and suspended iron species in the ground water. In this report the nature of the oxyhydroxides has been inferred from laboratory measurements and calculations based on ground water analyses. It would be most useful if the oxyhydroxides could also be directly identified by such techniques as X-ray diffraction and electron microscopy.

SUMMARY

In northern Camden and northwestern Burlington Counties, N.J., the pH of ground waters in the Potomac Group and the Raritan and Magothy Formations of Cretaceous age ranges from 5–6 in the outcrop area to 8 several miles downdip to the southeast. Iron is present in the ground water as dissolved Fe^{+2} and $FeOH^{+1}$, and as suspended ferric oxyhydroxides, presumably formed by oxidation of ferrous species already in solution. The oxyhydroxides are probably a mixture of amorphous material and goethite with small amounts of hematite.

In the outcrop area of the formations the concentration of dissolved ferrous or suspended ferric species is less than 0.5 mg/l in unpolluted waters, reflecting high DO (dissolved oxygen) concentrations. Just southeast of the outcrop area, the formations dip beneath silts and clays of the Merchantville Formation and Woodbury Clay, and ferrous species increase abruptly to about 6–7 mg/l as a result of DO depletion by microbial activity and reactions with ferrous iron minerals such as pyrite and siderite. The parallel increase in ferric species to 6–11 mg/l may be caused by partial oxidation of Fe^{+2} and $FeOH^{+1}$. Farther downdip at pH's above 6.5, both dissolved and suspended iron decrease gradually to less than 0.5 mg/l. The decrease in ferrous iron values is not due to siderite precipitation, but may reflect an increase in the stability of the suspended amorphous material owing to aging, coupled with adsorption of ferrous iron by the oxyhydroxides and partial conversion of the amorphous phase to goethite. The decrease in the concentration of suspended oxyhydroxides is probably caused by cation adsorption, aging, coagulation, and settling.

Computed Eh values, which range from about +0.400 to 0.0 volts, and measured pH values are compared with Eh and pH values measured in similar ground waters in Maryland by Barnes and Back (1964). The stability of the suspended oxyhydroxides generally increases with decreasing Eh and increasing dissolved ferrous iron in the Maryland study, owing probably to a leaching away of the more soluble oxyhydroxides.

REFERENCES

Back, William, and Barnes, Ivan, 1965, Relation of electrochemical potentials and iron content to ground-water flow patterns: U.S. Geol. Survey Prof. Paper 498–C, p. C1–C16.

Barksdale, H. C., Greenman, D. W., Lang, S. M., Hilton, G. S., and Outlaw, D. E., 1958, Ground-water resources in the tri-state region adjacent to the lower Delaware River: New Jersey Dept. Conserv. and Econ. Devel. Spec. Rept. 13, 190 p.

Barnes, Ivan, and Back, William, 1964, Geochemistry of iron-rich ground water of southern Maryland: Jour. Geology, v. 72, p. 435–447.

Baudisch, Oskar, and Albrecht, W. H., 1932, Gamma-ferric oxide hydrate: Am. Chem. Soc. Jour., v. 54, p. 943–947.

Charlot, Gaston, Badoz-Lambling, Janine, and Tremillon, Bernard, 1962, Electrochemical reactions: New York, Elsevier Pub. Co., 376 p.

Doyle, R. W., 1968, The origin of the ferrous ion-ferric oxide Nernst potential in environments containing dissolved ferrous iron: Am. Jour. Sci., v. 266, p. 840–859.

Durfor, C. N., and Keighton, W. B., 1954, Chemical characteristics of Delaware River water, Trenton, N.J., to Marcus Hook, Pennsylvania: U.S. Geol. Survey Water-Supply Paper 1262, 173 p.

Feitknecht, Walter, and Michaelis, W., 1962, Hydrolysis of iron (III) perchlorate solutions: Helvetica Chim. Acta, v. 45, p. 212–224.

Foster, M. D., 1950, The origin of high sodium bicarbonate waters in the Atlantic and Gulf Coastal Plains: Geochim. et Cosmochim. Acta: v. 1, p. 33–48.

Garrels, R. M., 1959, Rates of geochemical reactions at low temperatures and pressures, *in* Abelson, P. H., Researches in geochemistry: New York, John Wiley and Sons, Inc., p. 25–37.

Garrels, R. M., and Christ, C. L., 1965, Solutions, minerals, and equilibria: New York, Harper and Row, 450 p.

Greenman, D. W., Rima, D. R., Lockwood, W. N., Meisler, Harold, 1961, Ground-water resources of the Coastal Plain area of southeastern Pennsylvania: Pennsylvania Geol. Survey, 4th Ser., Bull. W–13, 375 p.

Hem, J. D., and Skougstad, M. W., 1960, Coprecipitation effects in solutions containing ferrous, ferric, and cupric ions: U.S. Geol. Survey Water-Supply Paper 1459–E, p. 95–110.

Johnson, M. E., and Richards, H. G., 1952, Stratigraphy of coastal plain of New Jersey: Am. Assoc. Petroleum Geologists Bull., v. 36, no. 11, p. 2150–2160.

Klotz, I. M., 1964, Chemical thermodynamics, revised ed.: New York, W. A. Benjamin Inc., 468 p.

Langmuir, Donald, 1969a, Iron in ground waters of the Magothy and Raritan Formations in Camden and Burlington Counties, New Jersey: New Jersey Dept. Conserv. and Econ. Devel., New Jersey Water Resources Circ. [In press]

——— 1969b, The Gibbs free energies of substances in the system $Fe–O_2–H_2O–CO_2$ at 25°C, *in* Geological Survey Research 1969: U.S. Geol. Survey Prof. Paper 650–B, p. B180–B184.

Lengweiler, H., Buser, W., und Feitknecht, Walter, 1961, Die Ermittlung der Löslichkeit von Eisen (III) -hydroxiden mit ^{59} Fe I, Fällungsund Auflösungsversuch: Helvetica Chim. Acta, v. 44, p. 796–805.

Morgan, J. J., and Stumm, Werner, 1965, The role of multivalent metal oxides in limnological transformations as exemplified by iron and manganese, *in* Proceedings of Second International Water Pollution Research Conference, Tokyo, 1964: New York, Pergamon Press, p. 103–118.

Nightingale, E. R., Jr., 1958, Poised oxidation-reduction systems. Quantitative evaluation of redox poising capacity and its relation to feasibility of redox titrations: Anal. Chemistry, v. 30, p. 267.

Owens, J. P., and Minard, J. P., 1964, Pre-Quaternary geology of the Bristol quadrangle, New Jersey-Pennsylvania: U.S. Geol. Survey, Geol. Quad. Map GQ–342.

Parks, G. A., 1965, The isoelectric points of solid oxides, solid hydroxides, and aqueous hydroxo complex systems: Chem. Rev., v. 65, p. 177–198.

Rainwater, F. H., and Thatcher, L. L., 1960, Methods for collection and analysis of water samples: U.S. Geol. Survey Water Supply Paper 1454, 301 p.

Rush, F. E., 1968, Geology and ground water resources of Burlington County, New Jersey: New Jersey Dept. Conserv. and Econ. Devel. Spec. Rept. 26, 65 p.

Schindler, P. W., Michaelis, W., and Feitknecht, Walter, 1963, Löslichkeits-produkte von Metalloxiden und -hydroxiden. VIII. Die Löslichkeit gealterter Eisen (III)-hydroxid-Fällungen: Helvetica Chim. Acta, v. 46, p. 444–449.

Schwertman, Udo, 1959, Synthesis of definite iron oxides under various conditions: Zeitschr. anorg. u. allg. Chemie, v. 298, p. 337–348.

——— 1965, The formation of geothite and hematite from amorphous ferric hydroxide. II: Zeitschr. Pflanzenernährung, Düngung Bodenkunde, v. 108, no. 1, p. 37–45.

Seaber, P. R., 1965, Variations in chemical character of water in the Englishtown Formation, New Jersey: U.S. Geol. Survey Prof. Paper 498–B, p. B1–B35.

Sillén, L. G., 1964, Stability constants of metal-ion complexes, sect. I. Inorganic ligands: London, The Chem. Soc., Spec. Pub. 17, 754 p.

Stumm, Werner, 1966, Redox potential as an environmental parameter; conceptual significance and operational limitation: Third Internat. Conf. on Water Pollution Research, sec. 1, no. 13, Washington, D.C., Water Pollution Control Federation, 15 p.

——— 1967, Discussion of "Chemical oxidation and reduction of metals and ions in solution," by Larson, T. E., *in* Faust, S. D., and Hunter, J. V., eds., Principles and applications of water chemistry: New York, John Wiley and Sons., Inc., p. 448.

Tanaka, Motoharu, 1965, The role of multivalent metal oxides in limnological transformations as exemplified by iron and manganese; formal discussions *in* Proceedings of Second International Water Pollution Research Conference, Tokyo, 1964: New York, Pergamon Press, p. 118–123.

U.S. Public Health Service, 1962, Drinking water standards: Pub. 956.

Welo, L. A., and Baudisch, Oskar, 1934, Active iron. II. Relationships among the oxide hydrates and oxides of iron and some of their properties: Chem. Rev., v. 15, p. 1–43.

337-735 O - 69 - 16

LABORATORY CALIBRATION OF FIELD SURVEYING INSTRUMENTS

By CLIFTON J. FRY, JR., Washington, D.C.

Abstract.—A system of precisely positioned and oriented collimators for testing and evaluating field surveying instruments has been installed in the U.S. Geological Survey Topographic Division research center. The system can be used to simulate field observations in the laboratory without the adverse effects of inclement weather and unstable setups and without the bias effect of atmospheric conditions. The collimator system (1) permits detailed analysis and evaluation of observing procedures and study of instrumental errors and (2) allows techniques to be effectively matched with instruments. Although intended primarily for studies with theodolites, the system is also suitable for studies with levels and alidades and can be adapted to evaluate other advanced instruments and techniques for surveying and mapping.

Production of new topographic maps by the U.S. Geological Survey totals approximately 100,000 square miles of mapping annually. This mapping requires a large amount of horizontal and vertical control, part of which is incorporated into the national geodetic network. Establishing this control reliably and efficiently depends on effective use of modern electronic and optical surveying instruments. As in many other technologies, measuring instruments and techniques are being improved to meet the requirements of greater accuracy and more rapid data acquisition. The precision of angle-measuring instruments has kept pace quite adequately with accuracy requirements; however, their data-acquisition rate has shown little improvement through the years. Manufacturers and users of surveying instruments have recognized this problem and have proposed solutions which range from revised angulation requirements to new laser devices.

To assist in evaluating proposed new instruments and techniques, the U.S. Geological Survey has installed a unique system of collimators which simulates, in the laboratory, basic field conditions for angle observations. The system was designed to calibrate, or check calibration of, optical surveying instruments and to permit detailed analysis of observing procedures. Although the components are not new, the composite structure is an original design adaptable to most optical surveying instruments.

The collimators, the essential components of the system, allow various target distances and infinity to be simulated in a minimum amount of space. Furthermore they are adaptable to both calibration and procedural tests.

Stability is extremely critical for testing and calibrating optical surveying instruments, and therefore the construction of the support pillars and the collimator mountings is described here in detail.

SYSTEM CONFIGURATION

The system has five collimators positioned to form a cross. Three of the five collimators are in a horizontal plane, separated by 45 degrees of arc, at the same height as the instrument stand (fig. 1). These are fixed on the circumference of a 5-foot-radius circle with the instrument stand at the center. The two remaining collimators are positioned vertically, one 20 degrees of arc above and the other 20 degrees of arc below the center collimator (fig. 2). There are four support stands (fig. 3), one large stand to hold the top, center, and bottom collimators, one each to hold the right and left collimators, and the fourth to hold the instrument to be tested.

The center collimator is a straightness-of-line-of-sight model which contains seven reticles positioned to simulate distances of 0, 4, 10, 25, 50, and 100 feet and infinity. The distance between this collimator and the test instrument is a constant which is added to the reticle-distance value to give the correct simulated distances for the system. The optical axis is adjusted to horizontal by means of a striding level with a coincidence-type reading system which is accurate within 1 second of arc.

The infinity target is graduated at 20-second intervals for a distance of 2 minutes 20 seconds of arc in four directions from zero (fig. 4*A*). Paired lines mark the 0.3, 0.6, and 1:100 stadia intercepts. The 10-foot reticle target contains 10 graduations for a distance of about 2 minutes of arc in four directions from zero (fig. 4*B*).

U.S. GEOL. SURVEY PROF. PAPER 650–C, PAGES C236–C239

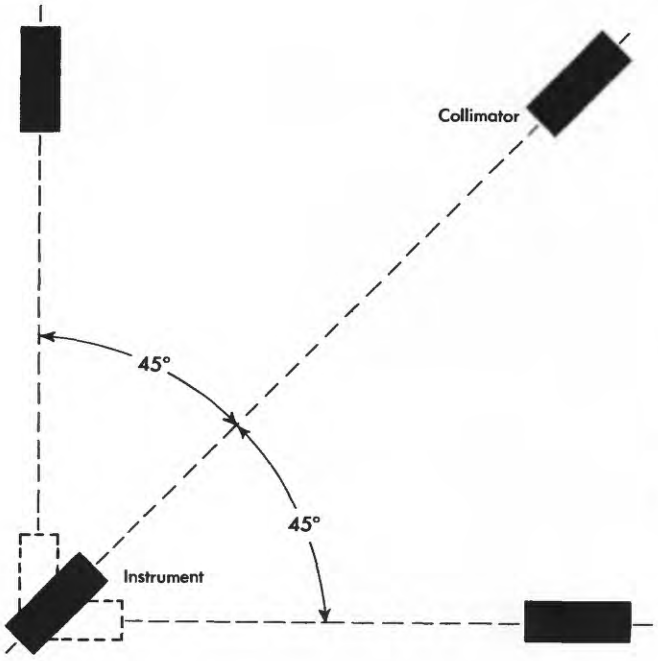

FIGURE 1.—Configuration of collimators in horizontal plane.

FIGURE 3.—The laboratory collimator system.

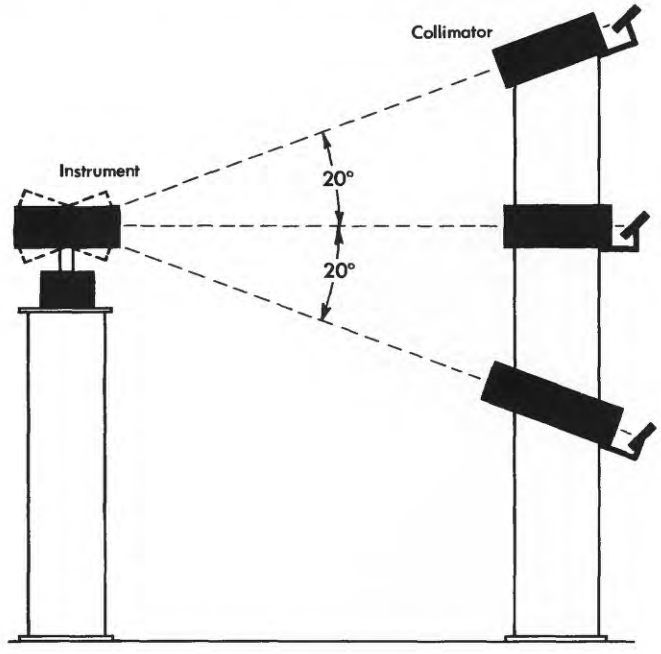

FIGURE 2.—Configuration of collimators in vertical plane.

A paired-line cross target with supplemental displacement graduations is mounted on the objective lens to represent the simulated zero distance. The four remaining targets are marked with paired lines in one direction only. Consequently, in addition to serving as a target for observing horizontal and vertical angles, this collimator can be used for the following:

1. Checking the straightness of the line of sight of a telescope, which may deviate with changes in focus.
2. Rapidly checking and adjusting the level sight of an instrument.
3. Checking stadia intercepts.

Top and bottom collimators are identical. Each has an infinity target graduated at 30-second intervals for a distance of 18 minutes in four directions from zero (fig. 5). In addition, a paired-line target is centered on the objective lens to aid in alining the collimator and to use as a short-focus target. The optical axis of each collimator is inclined 20 degrees from the horizontal. The right and left collimators are equipped with reticle targets identical with the infinity target in the center collimator. Focal length is 16 inches, and lens diameter is 2 inches.

The collimator targets are illuminated by reflected light from overhead fluorescent tubes. This arrangement furnishes even illumination and avoids the use of lamps which would transmit their heat to the collimators and cause them to move.

CONSTRUCTION OF SUPPORTING STANDS

Stability of the supporting stands is particularly important for long-period studies. Although infinite distances are simulated, the actual distance between the instrument stands and the collimators is only 5 feet, so that a 0.0003-inch displacement causes a discernible angular difference. Therefore, an adequately stable

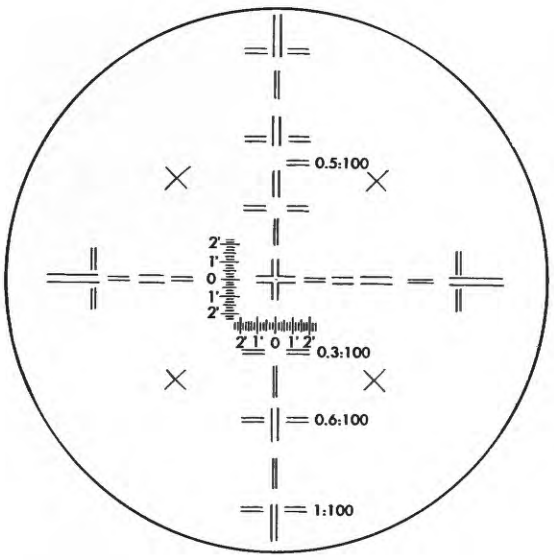

A

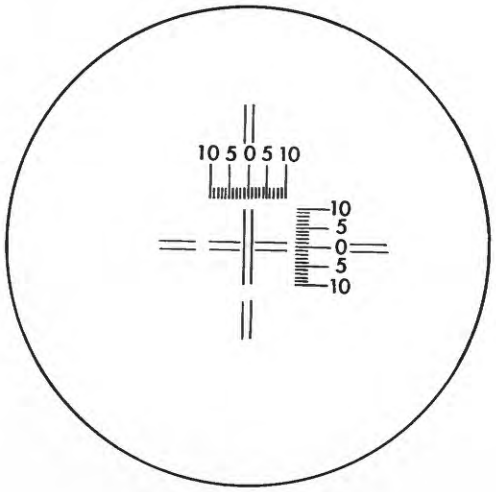

B

FIGURE 4.—Graduation patterns of distance-simulating reticles in center collimator. *A*, Infinity reticle target; *B*, 10-foot reticle target.

system depends largely on proper location and construction.

The system is located in a bottom-floor room, away from vibrating machinery and fluctuating temperatures. Concrete support piers beneath each stand were included in the building construction (fig. 6). These piers are 2 feet square at the top and flush with the concrete floor. A 1-inch cork filler separates the piers from the floor and isolates them from vibration. Each pier extends 3 feet below the surface and has a a 4-foot base which rests on an 8-inch-thick paved surface. A $16 \times 18 \times \frac{5}{8}$-inch steel plate was bolted to the top of each pier after the surface was grouted.

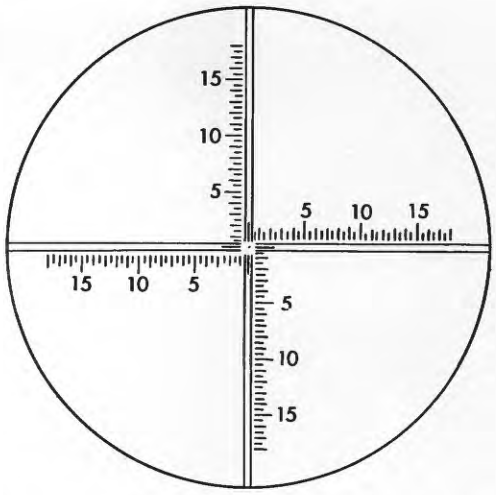

FIGURE 5.—Reticle graduation pattern for 20-degree inclined collimators.

The center stand is a 12-inch-diameter pipe 77 inches high made of $\frac{3}{8}$-inch low-carbon steel. A 15-inch-diameter plate of $\frac{1}{2}$-inch steel was welded to the bottom of the pipe. The pipe was then mounted vertically on the center pier and bolted in place. The two wing stands and the instrument stand are 8-inch-diameter pipes made of $\frac{3}{8}$-inch steel. Each has a 12-inch-diameter plate of $\frac{1}{2}$-inch steel welded to its base. Each stand is mounted vertically on its pier and bolted in place.

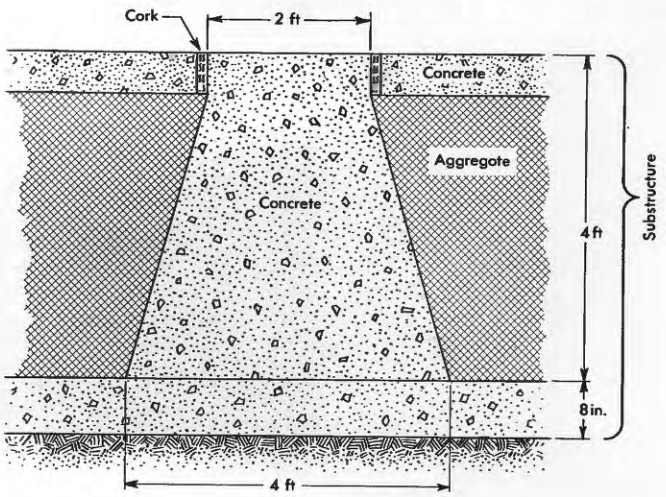

FIGURE 6.—Construction of collimator-stand support piers.

Adjustable supports were designed for each of the collimators. Mounting plates of $8 \times 20 \times \frac{1}{2}$-inch steel were welded to the top of each wing stand, the top of the center stand, and in the two parts of the center stand. A T-slotted base plate was bolted to each of these mounting plates. These base plates are specifically designed to adapt to adjustable cone-type V-block assemblies, which support each end of a collimator.

The two cone assemblies are used in combination so that the optical axis of the supported collimator can be adjusted horizontally or vertically.

Interchangeable spacer blocks are used on the instrument stand to compensate for the height difference of various instruments. Each block is a 6-inch-diameter cylinder of anodized aluminum. This method of height adjustment is not as flexible as the conventional screw-adjusting instrument stands, but the spacer blocks are more stable. The height of instrument need not be exact, except in tests of the straightness of line of sight, but the deviation is kept to a minimum to avoid abnormal lens distortions.

The collimator system has proved to be very satisfactory. A fixed vertical angle has been maintained between the top and bottom collimators, with a maximum deviation not exceeding ± 3 seconds of arc. Horizontal angles have indicated no instability of the stands during periods of observation.

SYSTEM USE

Testing procedures have been adapted to the instrument or application being evaluated. Each test is executed on a sampling basis, since no economic justification has been found for testing every circle graduation. The result is a statistical measure of quality of the instrument combined with a user. It was an appreciation of this combined instrumental and human measure of quality which led to collimation as the choice of system design rather than autocollimation, autoreflection, or mechanical stop tables. These methods limit the simulation of observer conditions, which are important in the determination of total instrument accuracy.

Acceptance tests of new and reconditioned instruments are completed rapidly and with greater precision than was previously possible. The source and extent of instrument malfunction can be readily isolated and recognized from the results obtained with the collimator system, and corrective adjustments can be made rapidly and accurately. Indicated repairs are made in the Geological Survey instrument shop, or by the manufacturer if the instrument is a new purchase.

Performance of a recently developed product can be conveniently evaluated with minimum time loss to the seller. Gyrotheodolites, digital-readout theodolites, and electronic-plate theodolites are examples of instruments which have been or will be evaluated as potential cost-saving replacements for conventional equipment.

Suggested modifications to existing instruments are laboratory tested before they are adopted or field tested. Such a modification is the five-wire theodolite reticle, which offers much time-saving advantage in searching for targets and in eliminating notekeeping errors. A part of our test compared 2 sets of 5-wire readings with 6 sets of conventional single-wire readings obtained with the same instrument. Results verified the logical deduction that inherent inaccuracy should not be greater than that of the graduated circle. Field setups are rarely as stable as those in the laboratory; therefore, the theoretical advantage of increased circle sampling is often offset by increased observation time. Selected field tests were recommended on this basis. Preliminary results are encouraging. Observation timesaving is more than 50 percent, and angular deviations from single-wire, multiset values have been insignificant.

Thus, in addition to evaluations of optical equipment, standard surveying procedures are examined for efficient matching with instrument precision. If this is carried a step further into the adjustment of computations, factors for observer error and instrument precision are derived from the collimator observations. These are combined with results of analyses of field records and used in standard propagation-of-error formulas to predict angular precision or to refine mathematical adjustments.

The design of the system is such that advanced techniques and equipment may be tested. The reflected-light feature, for example, may be useful in testing the reliability of angulation by optical-tracking devices. Under consideration, although not yet implemented, is the adaptation of this system for holographic experiments, which require the near-absolute stability provided by the construction of the supporting stands. Holograms are expected to be useful in determining lens distortions, studying refraction and air turbulence, and correlating images.

CONCLUSION

Demands for greater accuracy in all types of control surveys have been increasing. As components change or improve, it is desirable to assess the accuracy and efficiency of any procedure in relation to its intended purpose. A properly designed collimator system can be an important tool for determining these basic facts about optical surveying instruments.

ORTHOPHOTOSCOPE MODIFICATIONS

By HERBERT M. NEYLAND, Washington, D.C.

Abstract.—The orthophotograph, the principal product of the Orthophotoscope, is widely used for urban planning, geologic studies, map revision, and orthophotomapping. Improved resolution in orthophotographs has resulted from recent modifications to the T–64 Orthophotoscope which permit the accommodation of a full-size 9- × 9-inch diapositive plate. Besides sharper resolution, the new design makes possible the use of color photographs in the instrument.

The orthophotograph, the principal product of the Orthophotoscope, has long been recognized as a mapping tool of great potential, not just because it is a photographic representation of the ground but because it is a photograph which has been restituted to remove scalar error due to the displacement of imagery caused by relief and tilt. As a map substitute, it offers many advantages over the traditional line map which, for the sake of clarity and cost, must restrict the amount of terrain detail delineated. As the orthophotograph contains the full range of imagery recorded by the camera, it can be used directly, in single or mosaic form, for geologic studies, field classification and completion of mapworthy detail, highway and urban planning, and similar projects. With a suitable amount of cartographic treatment which varies according to the area portrayed, an orthophotomosaic becomes an inherent part of a new type of map, the orthophotomap (Scher, 1964).

THE ORTHOPHOTOSCOPE

The U.S. Geological Survey Orthophotoscope has evolved from the first experimental model designed in 1953. The latest model, the T–64 (fig. 1), retains the important features of earlier models, such as (1) the optical projection system, (2) the motorized drives for transmitting x, y, and z motions to the scanning assembly, and (3) the adaptability to simultaneous or subsequent use of profile data from each scan, for operating other image-restitution equipment or for extracting hypsometric information in digital or analog form.

In the T–64 Orthophotoscope, the stereomodel is scanned in the y direction over a 24- × 30-inch flat film-supporting platform rather than in the x direction over a cylindrical drum, as in the U–60 Orthophotoscope (Scher, 1962). The principal objective of the cylindrical design was to provide the operator with a better view of the stereomodel and to reduce fatigue. However, operational experience indicated that the drum-type instrument requires several critical mechanical adjustments that are not necessary when a flat platform is used as the film support. Because the geometric fidelity of the orthophotograph depends on the precision with which the scanning aperture is kept in contact with the apparent model surface, the comfort and convenience of viewing remain primary design considerations. For these reasons, the flat film-supporting platform of the T–64 Orthophotoscope is tilted toward the operator, approximately 40° from the horizontal plane. The projector system is, of course, tilted correspondingly. As originally produced, the model T–64 incorporated three ER–55 (known commercially as Balplex) projectors to provide coverage of a double stereomodel.

In the scanning operation, the film is exposed through the scanning aperture to small differential areas of the stereomodel surface as the platen carriage moves along its track. Although the film is exposed to both the red and blue rays that form the anaglyphic model, only the blue rays have an actinic effect on the blue-sensitive film. The scanning progresses at constant horizontal speed in a series of systematically stepped-over parallel bands. The aperture is kept in contact with the model surface by means of the z-motion control. Any scanning errors cause mismatches of imagery between adjacent scans and, because these mismatches cannot be concealed, the resulting orthophotograph has a built-in indicator of its fidelity.

IMPROVEMENT SOUGHT IN RESOLUTION

Although the orthophotographs produced with the Orthophotoscope have been acceptable for most requirements, the reduction of the original aerial negative

FIGURE 1.—Modified T–64 Orthophotoscope.

from its 230- × 230-millimeter format to the 83- × 83-mm ER–55 diapositive format and subsequent enlargement through projection to model scale caused a loss in resolution. Three projectors for 230- × 230-mm diapositives cannot be fitted to the T–64 Orthophotoscope for two reasons. First, the minimum base allowable with projectors for 230- × 230-mm plates would give an undesirably large scale in the plane of projection; second, to retain the economical double-model coverage would require a much larger instrument and therefore an entirely new physical design.

DIFFERENT PROJECTORS INTERCHANGED

An unorthodox approach circumvented these two difficulties. Experimentation showed that an ER–55 projector and a Kelsh-type projector with a correspondingly short projection distance could be used together to project anaglyphic stereomodels. There was no detectable parallax even though the projected diapositives differed in size by a ratio of nearly 3:1. That this is possible becomes obvious when one considers that each projector, of whatever design, must project essentially the same cone of rays if one is to obtain the precise model geometry required for accurate mapping.

Therefore, it was decided to replace the center (blue-filtered) ER–55 projector on the T–64 with a Kelsh-type projector and retain the left and right (red-filtered) ER–55 projectors. This change did not rerequire any basic redesign, but only an adaption of a new component to instruments already in operational use.

The Kelsh K–100 projector was ideally suited to the purpose because this projector and the ER–55 projector are coupled to their y slides by similar y-tilt (phi) spindles. It was easy to design an adaptor for fitting the K–100 y-tilt spindle to the ER–55 slide.

Consequently, K–100 projectors with a variable principal distance and Hypergon lenses of 115-mm focal length were ordered for installation on all T–64 Orthophotoscopes owned by the U.S. Geological Survey.

Because the configuration of the left and right ER–55 projectors permits them to nestle under the cone of the Kelsh K–100, the model base is just as small as that obtained with the group of three ER–55 projectors previously used. A 12-volt circuit was added to the power supply to control the Kelsh lamp, and a stiffening bracket was attached to the support bar to compensate the additional weight of the new projector. Because the Kelsh projector needs a guide arm for the lamp, a new exposure platen (fig. 2) was designed, with the guide-arm pivot situated as close to the film plane as possible so that the cone of light rays will remain in the platen area when the entire double model is scanned. The new platen is equipped with a removable center disk which can accommodate exposure slits of various sizes.

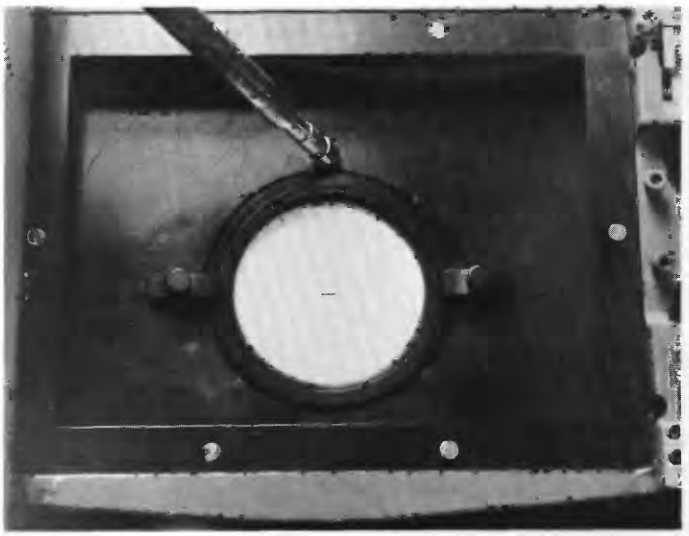

FIGURE 2.—Closeup view of redesigned platen.

RESULTS OF MODIFICATIONS

Several advantages have been gained by the replacement of the center (exposing) projector. Of primary importance is the increase in resolution obtained by the use of unreduced photographs for exposure of orthophotographs. Moreover it is now possible to use original negatives in the center projector and thereby obtain a positive orthophotograph as the direct product of scanning.

The variable principal distance of the K–100 projector permits a greater flexibility in operation. The scale of the exposed orthophotograph can be rigidly controlled by removing the new platen and scaling the models to established control.

It is now also possible to make color orthophotographs with the modified model T–64, by placing the two ER–55 projectors to one side and the Kelsh projector on the end, installing a lightproof curtain between the two types of projectors, and placing a color plate in the Kelsh projector. In this way, the ER–55 projectors form an anaglyphic model for the operator, and the Kelsh projector exposes a color orthophotograph. This mode of operation depends on the use of color negative aerial photographs from which both black-and-white and color materials can be processed. Initial tests have been successful, and practical tests are underway.

The servomotor powering of the motions on the Orthophotoscope provides a ready means for encoding these motions in either analog or digital form. Moreover, the flow of data can be either positive or negative. Hence the instrument can be used to generate data for other uses, or data generated by other machines can be used to control it. At present these possibilities are in the early experimental stage and will be reported on later.

REFERENCES

Scher, M. B., 1962, Research activity with the U–60 Orthophotoscope: Art. 57 *in* U.S. Geol. Survey Prof. Paper 450–B, p B135–B137.

——— 1964, Mapmaking applications of orthophotography, *in* Geological Survey Research 1964: U.S. Geol. Survey Prof. Paper 501–D, p D138–D140.

SUBJECT INDEX

[For major headings such as "Mineralogy," "Structural geology," "Ground water," see under State names or refer to table of contents]

AUTHOR INDEX

U.S. GOVERNMENT PRINTING OFFICE: 1969 O—337—735